Advances in Clinical and Experimental Medicine

MONTHLY ISSN 1899-5276 (PRINT) ISSN 2451-2680 (ONLINE) advances.umw.edu.pl

2025, Vol. 34, No. 8 (August)

Impact Factor (IF) – 1.9
Ministry of Science and Higher Education – 70 pts
Index Copernicus (ICV) – 171.00 pts



Wroclaw Medical University

Advances
in Clinical and Experimental
Medicine



Advances
in Clinical and Experimental Medicine

ISSN 1899-5276 (PRINT) ISSN 2451-2680 (ONLINE) advances.umw.edu.pl

MONTHLY 2025
Vol. 34, No. 8
(August)

Advances in Clinical and Experimental Medicine (*Adv Clin Exp Med*) publishes high-quality original articles, research-in-progress, research letters and systematic reviews and meta-analyses of recognized scientists that deal with all clinical and experimental medicine.

Editorial Office
ul. Marcinkowskiego 2–6
50-368 Wrocław, Poland
Tel.: +48 71 784 12 05
E-mail: redakcja@umw.edu.pl

Publisher
Wroclaw Medical University
Wybrzeże L. Pasteura 1
50-367 Wrocław, Poland

Online edition is the original version of the journal

Editor-in-Chief
Prof. Donata Kurpas

Deputy Editor
Prof. Robert Śmigiel

Managing Editor
Marek Misiak, MA

Statistical Editors
Wojciech Bombała, MSc
Anna Kopszak, MSc
Dr. Krzysztof Kujawa
Jakub Wronowicz, MSc
Maciej Wuczyński, MSc

Manuscript editing
Marek Misiak, MA
Paulina Piątkowska, MA

Scientific Committee
Prof. Sandra Maria Barbalho
Prof. Antonio Cano
Prof. Chong Chen
Prof. Breno Diniz
Prof. Erwan Donal
Prof. Chris Fox
Prof. Yuko Hakamata
Prof. Carol Holland
Prof. Sabine Bährer-Kohler
Prof. Markku Kurkinen
Prof. Christopher S. Lee
Prof. Christos Lionis
Prof. Leszek Lisowski
Prof. Raimundo Mateos
Prof. Zbigniew W. Raś
Prof. Dorota Religa
Prof. Jerzy W. Rozenblit
Prof. Silvina Santana
Prof. Sajee Sattayut
Prof. Barbara Schneider
Prof. James Sharman
Prof. Jamil Shibli
Prof. Luca Testarelli
Prof. Michał J. Toborek
Prof. László Vécsei
Prof. Cristiana Vitale
Prof. Ming Yi
Prof. Hao Zhang

Section Editors

Basic Sciences
Prof. Iwona Bil-Lula
Prof. Dorota Danuta Diakowska
Prof. Paweł Andrzej Karpiński
Prof. Bartosz Kempisty
Dr. Wiesława Kranc
Dr. Anna Lebedeva
Dr. Piotr Chmielewski
Dr. Phuc Van Pham
Dr. Sławomir Woźniak

Bioinformatics and Genetics
Assoc. Prof. Izabela Łaczmańska
Prof. Łukasz Łaczmański

Clinical Anatomy, Legal Medicine, Innovative Technologies
Prof. Rafael Boscolo-Berto

Dentistry
Prof. Marzena Dominiak
Prof. Tomasz Gedrange
Prof. Jamil Shibli
Prof. Luca Testarelli

Laser Dentistry
Prof. Kinga Grzech-Leśniak

Dermatology
Prof. Jacek Szepietowski
Assoc. Prof. Marek Konop

Emergency Medicine, Innovative Technologies
Prof. Jacek Smereka

Evidence-Based Healthcare
Assoc. Prof. Aleksandra Królikowska
Dr. Robert Prill

Gynecology and Obstetrics
Assoc. Prof. Tomasz Fuchs
Dr. Christopher Kobierzycki
Dr. Jakub Staniczek

Histology and Embryology
Dr. Mateusz Olbromski

Internal Medicine

Angiology
Dr. Angelika Chachaj

Cardiology
Dr. Daniel Morris
Assoc. Prof. Joanna Popiołek-Kalisz
Prof. Pierre François Sabouret

Endocrinology
Prof. Marek Bolanowski

Gastroenterology
Assoc. Prof. Katarzyna Neubauer

Hematology
Prof. Andrzej Deptała
Prof. Dariusz Wołowiec

Nephrology and Transplantology
Prof. Mirosław Banasik
Prof. Krzysztof Letachowicz
Assoc. Prof. Tomasz Gołębiowski

Rheumatology
Assoc. Prof. Agata Sebastian
Dr. Sylwia Szafraniec-Buryło

Lifestyle Medicine, Nutrition and Health Promotion
Assoc. Prof. Michał Czapla
Prof. Raúl Juárez-Vela
Dr. Anthony Dissen

Microbiology
Assoc. Prof. Adam Junka

Molecular Biology
Dr. Monika Bielecka
Prof. Dorota Danuta Diakowska
Dr. Phuc Van Pham

Neurology
Assoc. Prof. Magdalena Koszewicz
Dr. Nasrollah Moradikor
Assoc. Prof. Anna Pokryszko-Dragan
Dr. Masaru Tanaka

Neuroscience
Dr. Simone Battaglia
Dr. Francesco Di Gregorio
Dr. Nasrollah Moradikor

Omics
Prof. Mariusz Fleszar
Prof. Paweł Andrzej Karpiński

Oncology
Prof. Andrzej Deptała
Prof. Adam Maciejczyk
Prof. Hao Zhang

Gynecological Oncology
Dr. Marcin Jędryka

Ophthalmology
Dr. Małgorzata Gajdzis
Prof. Marta Misiuk-Hojło

Orthopedics
Prof. Paweł Reichert

Otolaryngology
Prof. Tomasz Zatoński

Pediatrics

Pediatrics, Metabolic Pediatrics, Clinical Genetics, Neonatology, Rare Disorders
Prof. Robert Śmigiel

Pediatric Nephrology
Prof. Katarzyna Kiliś-Pstrusińska

Pediatric Oncology and Hematology
Assoc. Prof. Marek Ussowicz

Pharmaceutical Sciences
Assoc. Prof. Marta Kepinska
Prof. Adam Matkowski

Pharmacoeconomics
Dr. Sylwia Szafraniec-Buryło

Psychiatry
Dr. Melike Küçükkarapınar
Prof. Jerzy Leszek
Assoc. Prof. Bartłomiej Stańczykiewicz

Public Health
Prof. Monika Sawhney
Prof. Izabella Uchmanowicz

Pulmonology
Prof. Anna Brzecka

Qualitative Studies, Quality of Care
Prof. Ludmiła Marcinowicz
Assoc. Prof. Anna Rozensztrauch

Radiology
Prof. Paweł Gać

Rehabilitation
Assoc. Prof. Aleksandra Królikowska
Dr. Robert Prill

Surgery
Assoc. Prof. Mariusz Chabowski

Telemedicine, Geriatrics, Multimorbidity
Assoc. Prof. Maria Magdalena Bujnowska-Fedak
Prof. Ferdinando Petrazzuoli

Editorial Policy

Advances in Clinical and Experimental Medicine (Adv Clin Exp Med) is an independent multidisciplinary forum for exchange of scientific and clinical information, publishing original research and news encompassing all aspects of medicine, including molecular biology, biochemistry, genetics, biotechnology and other areas. During the review process, the Editorial Board conforms to the "Uniform Requirements for Manuscripts Submitted to Biomedical Journals: Writing and Editing for Biomedical Publication" approved by the International Committee of Medical Journal Editors (www.ICMJE.org). The journal publishes (in English only) original papers and reviews. Short works considered original, novel and significant are given priority. Experimental studies must include a statement that the experimental protocol and informed consent procedure were in compliance with the Helsinki Convention and were approved by an ethics committee.

For all subscription-related queries please contact our Editorial Office: redakcja@umw.edu.pl
For more information visit the journal's website: advances.umw.edu.pl

Pursuant to the ordinance of the Rector of Wroclaw Medical University No. 37/XVI R/2024, from March 1, 2024, authors are required to pay a fee for each manuscript accepted for publication in the journal Advances in Clinical and Experimental Medicine. The fee amounts to 1600 EUR for all types of papers.

Indexed in: MEDLINE, Science Citation Index Expanded, Journal Citation Reports/Science Edition, Scopus, EMBASE/Excerpta Medica, Ulrich's™ International Periodicals Directory, Index Copernicus

Typographic design: Piotr Gil, Monika Kolęda
DTP: Wydawnictwo UMW
Cover: Monika Kolęda
Printing and binding: Drukarnia I-BiS Bierońscy Sp.k.

Advances
in Clinical and Experimental Medicine

MONTHLY 2025, Vol. 34, No. 8 (August)

ISSN 1899-5276 (PRINT)
ISSN 2451-2680 (ONLINE)
advances.umw.edu.pl

Contents

Editorials

1241 Marek Konop
Keratin biomaterials for wound healing and tissue regeneration: A promising approach in biomedical applications

1249 Marta Duda-Sikuła, Ole Jonas Boeken, Víctor Patricio, Chloe Buttard, Marie Benaiteau, Alvaro Mendes, Jerome Honnorat, Ava Easton, Josep Dalmau, Carsten Finke, Donata Kurpas
Caregivers' perspectives on long-term cognitive, psychiatric, psychological, and social outcomes in NMDAR encephalitis: Initial findings from the multi-center prospective SAPIENCE study

Meta-analysis

1255 Xin Lin, Yang Liu, Li Kong, Tejin Ba, Bagenna Bao, Shuanglin Zhang, Weihong Liu
Comorbidity-related risk factors for acute respiratory distress syndrome in sepsis patients: A systematic review and meta-analysis

1267 Chiqiong Liu, Fengying He
Systematic review and meta-analysis of randomized controlled trials comparing the clinical outcomes of SARS-CoV-2 and influenza in pediatric patients

Original papers

1277 Se-Kwon Kim, Venkatesan Jayachandran, Thanh Sang Vo, Isuru Wijesekara
Safety assessment of turmeric-boswellia-sesame formulation in healthy adult volunteers: An open-label prospective study

1289 Yasemin Yavuz, Sedef Kotanli, Mehmet S. Dogan, Zelal Almak
Examination of 6 and 12 month follow-up of calcium hydroxide and calcium silicate materials used in direct and indirect pulp capping

1299 Ting Zhang, Wei Zhuo, Wei-na Wang, Lu Zhao
Clinical analysis of 338 cases of dacryolithiasis

1307 Xiaotong He, Xiaoyue Lei, Yangxi Cheng, Huiyong Zhu
Neoadjuvant chemotherapy vs upfront surgery for resectable locally advanced oral squamous cell carcinoma: A retrospective single center study

1321 Piotr Morasiewicz, Marcin Pelc, Łukasz Tomczyk, Joanna Kochanska-Bieri, Andrzej Bobiński, Daniele Pili, Paweł Reichert
Clinical and radiological assessment of the Polish modification of the Ilizarov external fixator for the treatment of intra-articular calcaneal fractures

1331 Magdalena Kal, Michał Brzdęk, Elżbieta Cieśla, Piotr Rzymski, Izabella Karska-Basta, Antonio Pinna, Jerzy Mackiewicz, Mateusz Winiarczyk, Dominik Odrobina, Dorota Zarębska-Michaluk
Effect of reduced saturation and elevated D-dimer and interleukin 6 levels on vessel density and foveal avascular zone in patients with COVID-19 bilateral pneumonia

1343 Michał Chmielewski, Agnieszka Szeremet, Paula Jabłonowska-Babij, Maciej Majcherek, Anna Czyż, Natalia Bursiewicz, Tomasz Wróbel, Iwona Malicka
Assessment of the physical fitness status of patients with hematological malignancies qualified for hematopoietic stem cell transplantation

1353 Hangying Yu, Min Guo
Renal protection by acacetin in streptozotocin-induced diabetic nephropathy via TLR4/NF-κB pathway modulation in rats

1365 Weiqi Song, Rongyue Yao, Annamalai Vijayalakshmi, Yuan An
Eupatorin modulates BCPAP in thyroid cancer cell proliferation via suppressing the NF-κB/P13K/AKT signaling pathways

1375 Caihua Sun, Hongliang Yao, Jipan Liu, Shuai Wang
The effect of downregulation of ARL9 expression on the proliferation, metastasis and biological behavior of AGS gastric cancer cell lines

1383 Wei Ma, Hangyu Shi, Xinya Dong, Yongqiang Shi, Luyi Zhang, Bin Jiang
Umbelliferone inhibits proliferation and metastasis via modulating cadherin/β-catenin complex-aided cell-cell adhesion in glioblastoma cells

1393 Puyu Zhou, Jiazheng Duan, Jianqing Li
Improving sepsis mortality prediction with machine learning: A comparative study of advanced classifiers and performance metrics

Reviews

1403 Piotr Brzozowski, Piotr Niewiński, Stanisław Tubek, Krzysztof Nowak, Piotr Ponikowski
The consequences of cardiac autonomic nervous system modulation during pulmonary vein isolation: A review

Keratin biomaterials for wound healing and tissue regeneration: A promising approach in biomedical applications

Marek Konop[A–F]

Department of Experimental Physiology and Pathophysiology, Laboratory of Centre for Preclinical Research, Medical University of Warsaw, Poland

A – research concept and design; B – collection and/or assembly of data; C – data analysis and interpretation;
D – writing the article; E – critical revision of the article; F – final approval of the article

Advances in Clinical and Experimental Medicine, ISSN 1899–5276 (print), ISSN 2451–2680 (online) *Adv Clin Exp Med*. 2025;34(8):1241–1248

Address for correspondence
Marek Konop
E-mail: marek.konop@wum.edu.pl

Funding sources
None declared

Conflict of interest
None declared

Received on March 8, 2025
Reviewed on June 4, 2025
Accepted on June 6, 2025

Published online on June 17, 2025

Abstract

Keratin biomaterials, derived from natural sources, offer a promising, biocompatible solution for wound healing and tissue regeneration, though further clinical studies are needed to confirm their efficacy.

Key words: biomaterials, keratin, wound healing, wound dressing

Cite as
Konop M. Keratin biomaterials for wound healing and tissue regeneration: A promising approach in biomedical applications. *Adv Clin Exp Med*. 2025;34(8):1241–1248. doi:10.17219/acem/205998

DOI
10.17219/acem/205998

Copyright
Copyright by Author(s)
This is an article distributed under the terms of the Creative Commons Attribution 3.0 Unported (CC BY 3.0) (https://creativecommons.org/licenses/by/3.0/)

Highlights

- Keratin biomaterials accelerate wound healing and tissue regeneration, with preclinical studies confirming their safety and effectiveness.
- Natural keratin dressings deliver superior biocompatibility and biodegradability, positioning them as leading candidates in regenerative medicine.
- Keratin-based therapies enhance chronic wound repair, especially for diabetic ulcers, radiation dermatitis, and epidermolysis bullosa.
- Large-scale clinical trials are needed to validate keratin biomaterials' therapeutic efficacy, translating promising preclinical results into patient care.

Introduction

Impaired wound healing is a major medical problem, especially in diabetic patients. Among the numerous complications of diabetes, wound healing disorders are particularly noteworthy, severely impacting patients' quality of life and placing a considerable burden on healthcare resources.[1,2] Researchers worldwide are seeking new strategies for wound care, especially in diabetic conditions. Considering this, several natural biomaterials, including keratin, silk, chitosan, alginate, and collagen, have emerged as promising candidates due to their biomedical properties.[3–6] Among these, keratin-based biomaterials have emerged as promising candidates due to their biocompatibility, biodegradability and ability to promote cell growth.[3,4,7,8]

This editorial compiles insights from various preclinical and clinical studies on the use of keratin-based biomaterials for wound healing.

The biological effects and role of keratin

Keratins, a group of insoluble fiber-forming proteins, are found mainly in some vertebrate epithelial cells. It is formed through the copolymerization of 19 amino acids at the basic structural level.[9] Keratin is rich in cysteine (17.5%), serine (11.7%), glutamic acid (11.1%), threonine (6.9%), glycine (6.5%), arginine (5.6%) and proline (5.6%), but with low levels of lysine, histidine and methionine, with tryptophan barely present.[10] Keratin can be divided into 2 main types based on its molecular structure: α-keratin and β-keratin. α-keratin is mainly found in mammals and is a basic component of structures such as wool, hair, nails, hooves, and horns.[11] It has a helical (spiral) structure made up of α-helixes and is known for its elasticity and strength. On the other hand, β-keratin is found in reptiles and birds, including in feathers, beaks, claws, and scales.[12] Its β-sheet structure makes it stiffer and stronger than α-keratin. Additionally, keratins can be categorized as soft or hard based on their physical properties and sulfur content. Hard keratins are more rigid due to their higher sulfur levels.[12] Furthermore, keratins are proteins that form a protective layer for the epidermal appendages, thus playing an essential role in protection. Keratin genes account for the majority of intermediate filament genes in the human genome, forming the 2 largest groups of sequence homology: type I keratins (also known as acidic keratins, comprising KRT9–KRT40), and type II keratins (also known as neutral-base keratins, comprising KRT1–KRT8).[7,13–16]

Activated keratinocytes produce both types of keratin, which are encoded by 54 evolutionarily conserved genes: 28 type I and 26 type II. These genes are expressed in tightly regulated pairs, depending on tissue type, cellular differentiation and physiological context.[15,16] The specific combinations of keratin monomers vary depending on the epidermal layer. For example, the KRT14-KRT5 pair is expressed mainly in the basal layer of the epidermis, while the KRT10-KRT1 pair is more abundant in the suprabasal layers of the epidermis.[17] Following injury, stressed keratinocytes rapidly induce the de novo transcription of KRT16/17-KRT6. This is usually limited to the cells of the epidermis in smooth skin, the oral mucosa and several appendages.[18,19] KRT16/KRT17-KRT6 keratin pairs play a key role in wound healing. In the first few hours after injury, their expression is significantly increased. At the same time, a decrease in KRT10-KRT1 expression is observed. This change promotes keratinocyte proliferation over keratinocyte differentiation, thus facilitating rapid reepithelialization.[19,20] Studies using null mice have shown that a deficiency in KRT6a/KRT6b leads to fragile skin, imbalanced keratinocyte stability and defective wound healing. This is due to disrupted KRT6/KRT16 heteropolymer formation and reduced SRC kinase inhibition.[21–23] In case of KRT-17, it has been demonstrated that KRT-17 null keratinocytes are reduced in size and demonstrate a decreased protein translation rate, which correlates with reduced mTOR/AKT signaling and directly influences keratinocyte proliferation.[24]

Keratin and keratin-based biomaterials gain much attention in the biomaterials world due to their interesting set of properties, including excellent biocompatibility, biodegradability, bioactivity, and minimal immunogenic response (Fig. 1).[7,25,26] In addition, these materials present

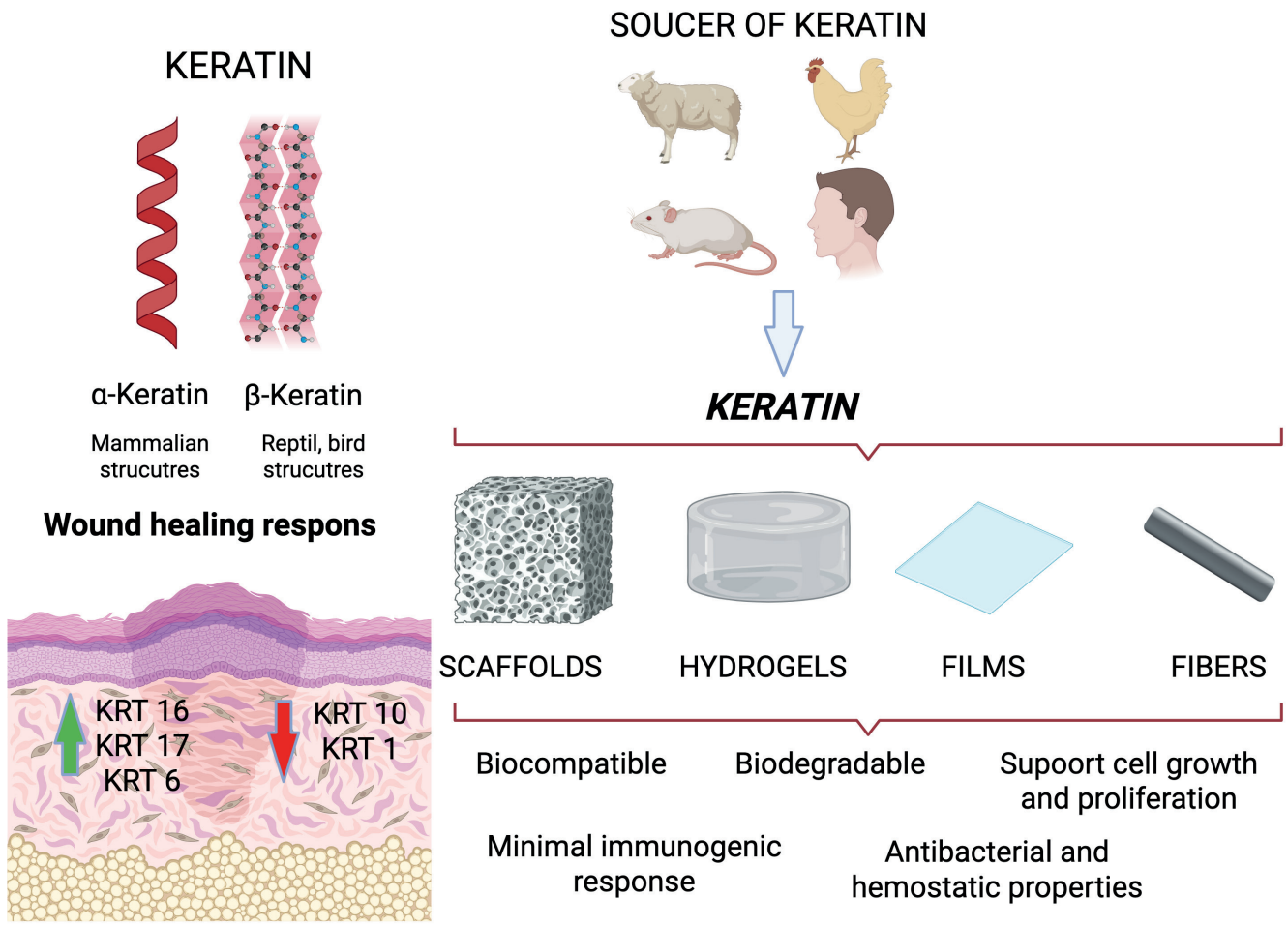


Fig. 1. Summary information on keratin materials. Created in BioRender. Konop, M. (2025). Available at: https://BioRender.com/nkugl2s

a hydrophilic surface, which is not commonly found in synthetic polymers.[27] Moreover, keratin-based biomaterials derived from wool and hair have been shown to facilitate cellular attachment, due to the presence of cell-binding motifs, including glutamic acid–aspartic acid–serine (EDS), arginine–glycine–aspartic acid (RGD), and leucine–aspartic acid–valine (LDV) residues.[28–31] On the other hand, the presence of RGD-binding residues acts as a binding motif for proteins such as fibronectin and fibrinogen. There are also studies describing the antibacterial and hemostatic properties of keratin biomaterials.[32–36] The aforementioned properties enable scientists to create various types of wound-healing materials that support the healing process.

Preclinical study

Naturally derived biomaterials, such as keratin, have recently garnered significant attention in dermatology and regenerative medicine. Researchers commonly use soluble or insoluble forms of keratin biomaterials as wound dressings in preclinical studies involving various animal models of wound healing. They have also used keratin-based biomaterials to create hydrogels, films, nanofibers, and scaffolds as wound dressings in wound care.[35,37–39]

Jelodari et al.[40] examined keratin-based hydrogel dressing and its impact on delivering LL-37 antimicrobial peptide using full-thickness rat wounds. The L-KO25:KN75 hydrogel, a 25:75% ratio of keratose/kerateine, demonstrated significant human dermal fibroblast proliferation (~85% on day 7) and high adhesion (~90 cells per high-power field). It promoted enhanced migration with nearly complete wound closure within 24 h in a "scratch assay". Microbiological examination showed effective antibacterial activity against *Escherichia coli* and *Streprococcus aureus*, reducing bacterial growth by over 70%. In vivo studies in Wistar rats indicated superior wound healing (~80% on day 14, >98% on day 21), outperforming other hydrogels. Histological analysis revealed increased angiogenesis, collagen deposition and skin regeneration. Increased mRNA expression of vascular endothelial growth factor (VEGF) and interleukin 6 (IL-6) further supported wound healing. The results summarize that LL-37-loaded keratin hydrogels can promote wound healing by enhancing tissue regeneration and reducing bacterial infections.

Han et al.[38] also investigated a hydrogel composed of strontium ranelate-loaded human hair keratin and

hyaluronic acid, utilized as a wound dressing in a full-thickness skin defect model in Sprague Dawley rats. In vitro examination revealed that incorporating strontium ranelate (SrR) into a hydrogel formulation significantly mitigated oxidative stress in murine fibroblasts (L929) and augmented the anti-inflammatory response in lipopolysaccharide-stimulated RAW264.7 macrophages. In vivo analyses further demonstrated that, relative to controls, the K/HA/0.5 mM SrR-treated group exhibited marked reductions in reactive oxygen species (ROS), IL-6 and tumor necrosis factor alpha (TNF-α), to 31.6%, 39.7%, and 61.1% of control levels, respectively. Moreover, in a full-thickness dermal wound defect model, the K/HA/0.5 mM SrR hydrogel significantly promoted wound closure by reducing oxidative injury, attenuating the inflammatory response and enhancing microangiogenesis.

Wang et al.[41] explored the wound-healing potential and biocompatibility of a hydrogel derived from chicken feather keratin. The hydrogel, created through the cross-linking of keratin with H_2O_2, demonstrated a high porosity range of 77–82% and exhibited solid-like rheological properties, particularly at a concentration of 20%. The full-thickness wound model in Sprague Dawley rats demonstrated accelerated wound closure (~90% by day 10 vs ~60% in controls). Complete reepithelialization was achieved within 21 days after injury. Histological examination showed enhanced collagen deposition and neovascularization in treated wounds. Subcutaneous implantation of hydrogel revealed no systemic toxicity, organ damage or inflammatory response. The hydrogel degraded fully within 4 weeks. In conclusion, these findings suggest that feather keratin hydrogel could be used as a bio-dressing to speed up wound healing.

Zhang et al.[42] developed and examined a novel bilayer wound dressing composed of poly(L-lactate-caprolactone) (PLCL) nanofibrous and keratin hydrogels, loaded with FGF-2 using a low-pressure filtration-assisted method. The keratin hydrogel mimicked the dermis with high porosity and a swelling ratio (874.09%), while the PLCL nanofibers simulated the epidermis due to their toughness and flexibility. In vitro examination using L929 cell line confirmed the biocompatibility and non-toxicity of the prepared dressing. In vivo studies on a full-thickness wound model in Sprague Dawley rats demonstrated accelerated wound healing in FGF-2-loaded dressings, with significantly higher re-epithelialization, collagen deposition, hair follicle regeneration, and angiogenesis compared to the control site ($p < 0.05$). The study concluded that the PLCL/keratin-FGF-2 bilayer dressing is a promising candidate for advanced wound care and tissue engineering applications.

In another study, Sun et al.[43] investigated a keratin-based hydrogel incorporating basic fibroblast growth factor (bFGF) for diabetic wound healing in a full-thickness skin defect model in type II diabetic rats. In vitro studies using L929 fibroblasts showed that the K31/bFGF hydrogel enhanced cell viability and migration compared to controls. In vivo application of the hydrogel significantly accelerated wound closure, with the K31/bFGF-treated group exhibiting improved healing rates by days 7 and 14 ($p < 0.001$), greater epidermal thickness, increased neovascularization, and more abundant skin appendages. Mechanistically, the hydrogel promoted epithelial–mesenchymal transition via upregulation of vimentin and downregulation of E-cadherin, and activated the PI3K/Akt signaling pathway. These findings suggest that the K31/bFGF hydrogel is a biocompatible and effective wound dressing for enhancing diabetic wound repair.

Chen et al.[44] created a glucose-triggered, in situ keratin hydrogel to treat diabetic wounds by employing a glucose oxidase-catalyzed disulfide shuffling approach. In vitro evaluations showed improved mechanical characteristics, low cytotoxicity using uman umbilical vein endothelial cells (HUVECs) and L929 mouse fibroblast cell line. In vivo experiments on streptozotocin-induced diabetic Sprague Dawley rats showed that the keratin-deferoxamine (DFO) hydrogel significantly accelerated wound closure on days 9 and 15 ($p < 0.01$). Moreover, keratin-DFO hydrogel facilitated reepithelialization, increased epidermal thickness and increased collagen formation/deposition. Additionally, immunofluorescence and immunohistochemical analyses indicated elevated angiogenesis through increased CD31 and VEGF labelling. In conclusion, the results obtained confirm that the keratin-DFO hydrogel is biocompatible, promotes the formation of new vessels and accelerates diabetic wound healing.

Khaliq et al.[45] examined multifunctional hydrogel membranes made from keratin-pullulan-polyvinyl alcohol (KR-PL-PVA) and infused with cefotaxime sodium (CTX) for diabetic wound healing. In vitro cytotoxicity assays performed using NIH3T3 fibroblast cells confirmed high biocompatibility, with cell viability exceeding 95%. In vivo experiments conducted on streptozotocin-induced diabetic rats revealed notably faster wound healing rates, with the CTX-KR-PL-PVA group achieving 89% wound closure by day 14 and over 99% by day 21 ($p < 0.05$). Histological evaluations showed improved reepithelialization, dense collagen formation, developed skin appendages, and reduced inflammation. These findings suggest that CTX-infused KR-PL-PVA membranes are effective, biocompatible wound dressings demonstrating strong antibacterial properties and significant potential for diabetic wound treatment.

Mirhaj et al.[46] prepared and examined mupirocin-loaded core-shell nanofibers using Pluronic F127, pectin, and keratin as an advanced wound dressing material. In vitro assays demonstrated that the sustained release of mupirocin from the core-shell fibers significantly improved human keratinocyte viability and proliferation compared to blended fibers, while also enhancing angiogenic activity in the CAM assay. In vivo tests using a full-thickness wound model in Wistar rats showed that wounds treated with the core-shell dressing achieved a 97.66% closure rate by day 14, significantly outperforming other formulations ($p < 0.05$). Histopathological and immunohistochemical examination confirmed accelerated reepithelialization, increased

skin appendage formation and greater collagen deposition and vascularization. In conclusion, the F127-Mup/Pec-Kr core-shell nanofibers exhibit excellent biocompatibility, antibacterial efficacy and enhanced regenerative properties, suggesting strong potential as an effective wound dressing for chronic and ischemic wounds.

Radu et al.[47] prepared and tested bacterial cellulose-keratin scaffolds, with and without adipose tissue-derived stem cells, as potential dressings for burn wounds. In vitro cytocompatibility tests using adipose tissue-derived stem cells showed increased cell viability (115%) after 72 h, indicating enhanced cell proliferation and biocompatibility. In vivo experiments on burn wounds in rabbits showed favorable healing progress at days 7, 14 and 21 after transplantation. In particular, wounds treated with the keratin-bacteria-cellulose scaffold with stem cells showed reduced inflammation, earlier regeneration of blood vessels and connective tissue, and more advanced re-epithelialization by day 21. In conclusion, the keratin-bacteria-cellulose scaffold promotes cell growth, accelerates tissue regeneration and significantly improves wound healing. Moreover, it is a promising dressing for treating burns when combined with stem cells.

Konop et al. examined keratin scaffolds as a wound dressing in healthy and diabetic conditions.[5,19,26,35] They showed that fur keratin-derived powder (FKDP) supports cell proliferation and migration. Moreover, they modified the obtained FKDP with antibacterial (AgNP)[35], anti-inflammatory (butyrate)[19] and analgesic substances (casomorphin).[48] In vivo experiments showed that wounds treated with different FKDP-wound dressings healed significantly faster than control wounds. Moreover, they found that the obtained variants of FKDP were naturally incorporated into regenerated tissue and exhibited tissue biocompatibility and biodegradability. Immunofluorescence examination revealed that in all wounds treated with the examined dressing, M2 macrophages were predominant.[19,48] This group's results showed the possible use of insoluble fractions of keratin biomaterials as wound dressings in clinical settings.

Rybka et al.[5] examined keratin scaffolds containing biphalin as a potential wound dressing in a full-thickness wound model in diabetic mice. In vitro examination using NIH/3T3 cells showed increased cell viability and upregulation of p-AKT/mTOR signaling. In vivo experiments on diabetic C57BL/6J mice demonstrated that wounds treated with the keratin-biphalin dressing healed faster on days 5 and 15 post-surgery ($p < 0.05$), showing improved reepithel-ialization, thicker epidermis and enhanced macrophage infiltration. In conclusion, keratin-biphaline fibers are biocompatible, promote cell growth and significantly accelerate wound healing, indicating their promising properties as a natural dressing for diabetic wounds. In another study Rybka et al.[25] examined keratin scaffolds containing trimethylamine N-oxide (TMAO) as a wound dressing in diabetic rats. They showed that keratin-TMAO wound dressing is safe, non-toxic and biocompatible in vitro and in vivo. In vivo examination showed that treated wounds healed significantly faster on days 4, 7, 14, and 21 post-injury ($p < 0.05$). Immunofluorescence and histopathological examinations showed that in dressed wounds predominant M2 macrophages, which are responsible for faster wound healing. Furthermore, the study revealed in vitro an enhanced activation of the PI3K/AKT/mTOR pathway, as indicated by a 2.6-fold increase in p-RPS6 expression ($p < 0.05$), which functions as a surrogate marker for the activation of the PI3K/AKT/mTOR pathway.

Clinical study

The clinical application of wound dressings made from keratin protein is still in development; however, the literature does contain single studies that employ these dressings in clinical practice. As mentioned below, the introduction of keratin dressings has had a positive effect on the healing of wounds of various etiologies.

Than et al.[49] investigated the use of keratin-based wound dressings in treating recalcitrant vascular wounds. This study presents 3 cases of patients with venous, arterial or mixed ulcers that had not healed with standard treatments, including compression therapy and traditional wound dressings. Each patient was treated with different formats of keratin dressings based on the wound's characteristics (Keraderm gel – for dry wounds, matrix for moderately exuding wounds and Kerafoam for highly exuding wounds). Results showed successful healing in all three cases, with complete wound closure occurring within 10–30 weeks. The study suggests that keratin-based wound dressings promote epithelialization, improve wound healing rates, and provide a new option for managing chronic wounds.

In another study, Than et al. [50] investigated keratin hydrogel – Keragel® (Keraplast Technologies LLC, San Antonio, USA) in treating an 11-year-old girl suffering from recessive dystrophic epidermolysis bullosa (RDEB). They applied Keragel® to the neck daily for 3 months, which resulted in stronger, more resilient skin, reduced blistering and effective wound healing. The patient no longer needed secondary dressings, greatly improving comfort, appearance and quality of life.

In another study, Kirsner et al.[51] used Keragel® (Keraplast Technologies, San Antonio, USA) to treat infant patient who experienced severe blistering, particularly on the hands and feet. Initially, the keratin-based dressing was applied only to one hand and one foot, while standard care was continued on the other hand and foot as a control. The study showed significant improvements in wound healing and skin strength, as well as reduced blister formation in the treated areas. Based on these promising results, treatment was extended to both hands and feet, leading to further improvements and eliminating the need for non-adherent silicone-based primary dressings.

Paulsen and Bygum[52] evaluated the use of a keratin-based gel – Keragel® (Keraplast Technologies LLC, Christchurch, New Zealand) as an adjuvant therapy for recalcitrant pyoderma gangrenosum (PG) ulcers in a 62-year-old patient who was unresponsive to conventional systemic treatments. Despite administering corticosteroids, cyclosporine, methotrexate, and infliximab, the ulcers expanded and failed to epithelialize. Following the introduction of keratin gel (Keragel®) as the primary topical treatment, a significant reduction in ulcer size was observed within 9 days. Continued use of this dressing led to full healing after 6 months. The authors concluded that keratin gel may enhance epithelialization and promote faster wound closure, especially when systemic therapies alone are insufficient, suggesting its potential as a valuable adjunct in treating pyoderma gangrenosum ulcers.

Davidson et al.[53] conducted a randomized control trial using a standard care dressing (alginate dressing (Algisite)) side by side with the experimental Keramatrix® (Keraplast) dressing for partial-thickness donor site wounds in 26 patients ("young" (≤50 y/o) and "old" (>50 y/o)). The results showed that keratin dressings significantly increased the rate of epithelialization in older patients (>50 years old), suggesting their clinical usefulness in cases where wound healing is delayed due to patient-related factors. However, in younger patients (≤50 years old), there was no significant difference in healing rates between keratin dressings and standard care.

Batzer et al.[54] examined a solid keratin matrix (Keramatrix®) and a liquid keratin gel (Keragel™) from the Replicine™ Functional Keratin® range from Keraplast Technologies, in the treatment of 45 refractory wounds in 31 patients with mixed etiologies, including diabetic ulcers, venous leg ulcers and surgical wounds. Treatments included either a solid keratin matrix or a liquid keratin gel, depending on wound exudate levels. Results showed that 37/45 wounds (82%) either healed completely or reduced in size by at least 50%. Among them, 29 wounds (64%) were fully healed, and 8 wounds showed significant size reduction. They showed that keratin dressings effectively promote wound epithelialization. However, 15 wounds required antimicrobial treatment during the treatment, suggesting that keratin dressing treatment should be interrupted briefly and then restarted when wound infection occurs. Overall, the products were found to be satisfactory for patients and easy to use across a wide range of wound etiologies, but further research and clinical experience with these products is warranted.

Hughes et al.[55] investigated the effectiveness of KeraStat® Cream (KeraNetics, Winston-Salem, USA), a keratin-based topical treatment, in managing radiation dermatitis (RD) in 24 patients undergoing radiotherapy (RT) for head and neck cancer (HNC). The patients were randomized to receive either KeraStat® Cream or standard care (SOC), with treatments applied at least twice daily during radiotherapy and for 1 month post-therapy. Adherence was high in both groups (KC 83% vs SOC 58% fully adherent), and while the cumulative incidence of grade 2+ RD did not differ significantly, the trial demonstrated good feasibility and patient compliance. KeraStat® Cream was well-tolerated and had good adherence, it did not significantly reduce the severity of radiation dermatitis compared to SOC. However, its anti-inflammatory properties and potential skin-protective effects warrant further investigation.

Conclusions

Keratin biomaterials represent a promising class of wound dressings that could transform routine treatment protocols for many types of wounds. Evidence from preclinical and clinical studies supports their safety, biocompatibility and ability to improve wound healing, even under diabetic conditions. However, while these results are promising, current research remains limited in scope and scale. The precise mechanisms by which keratin exerts its therapeutic effects are not yet fully understood. Moreover, although early clinical outcomes are positive, they are often derived from small-scale studies. Without large, multicenter randomized controlled trials, the translation of these results remains questionable. There is also a lack of comparative studies evaluating keratin dressings against standard treatments, which is essential for determining their relative clinical and economic value. Therefore, while keratin-based dressings demonstrate considerable potential, further rigorous investigation is essential. Future research should prioritize mechanistic studies, long-term safety evaluations and large-scale clinical trials. Through comprehensive research, keratin-based biomaterials have the potential to move beyond promising experimental studies and become a new clinical standard in wound treatment.

ORCID iDs

Marek Konop https://orcid.org/0000-0002-3914-6934

References

1. Rai V, Moellmer R, Agrawal DK. Clinically relevant experimental rodent models of diabetic foot ulcer. *Mol Cell Biochem*. 2022;477(4):1239–1247. doi:10.1007/s11010-022-04372-w
2. Kumbhar S, Bhatia M. Advancements and best practices in diabetic foot care: A comprehensive review of global progress. *Diabetes Res Clin Pract*. 2024;217:111845. doi:10.1016/j.diabres.2024.111845
3. Mazurek Ł, Szudzik M, Rybka M, Konop M. Silk fibroin biomaterials and their beneficial role in skin wound healing. *Biomolecules*. 2022;12(12):1852. doi:10.3390/biom12121852
4. Mazurek Ł, Rybka M, Jurak J, Frankowski J, Konop M. Silk sericin and its effect on skin wound healing: A state of the art. *Macromol Biosci*. 2024;24(10):2400145. doi:10.1002/mabi.202400145
5. Rybka M, Mazurek Ł, Czuwara J, et al. Biomedical potential of keratin-biphalin wound dressing in diabetic mice: In vitro and in vivo studies. *J Nat Fibers*. 2024;21(1):2287647. doi:10.1080/15440478.2023.2287647
6. Liu S, Yu JM, Gan YC, et al. Biomimetic natural biomaterials for tissue engineering and regenerative medicine: New biosynthesis methods, recent advances, and emerging applications. *Military Med Res*. 2023;10(1):16. doi:10.1186/s40779-023-00448-w

7. Konop M, Rybka M, Drapała A. Keratin biomaterials in skin wound healing, an old player in modern medicine: A mini review. *Pharmaceutics*. 2021;13(12):2029. doi:10.3390/pharmaceutics13122029
8. Bochynska-Czyz M, Redkiewicz P, Kozlowska H, Matalinska J, Konop M, Kosson P. Can keratin scaffolds be used for creating three-dimensional cell cultures? *Open Med*. 2020;15(1):249–253. doi:10.1515/med-2020-0031
9. Bertini F, Canetti M, Patrucco A, Zoccola M. Wool keratin-polypropylene composites: Properties and thermal degradation. *Polymer Degrad Stabil*. 2013;98(5):980–987. doi:10.1016/j.polymdegradstab.2013.02.011
10. Korniłłowicz-Kowalska T, Bohacz J. Biodegradation of keratin waste: Theory and practical aspects. *Waste Manag*. 2011;31(8):1689–1701. doi:10.1016/j.wasman.2011.03.024
11. Sarma A. Biological importance and pharmaceutical significance of keratin: A review. *Int J Biol Macromol*. 2022;219:395–413. doi:10.1016/j.ijbiomac.2022.08.002
12. Bragulla HH, Homberger DG. Structure and functions of keratin proteins in simple, stratified, keratinized and cornified epithelia. *J Anat*. 2009;214(4):516–559. doi:10.1111/j.1469-7580.2009.01066.x
13. Ehrlich F, Fischer H, Langbein L, et al. Differential evolution of the epidermal keratin cytoskeleton in terrestrial and aquatic mammals. *Mol Biol Evol*. 2019;36(2):328–340. doi:10.1093/molbev/msy214
14. Ehrlich F, Lachner J, Hermann M, Tschachler E, Eckhart L. Convergent evolution of cysteine-rich keratins in hard skin appendages of terrestrial vertebrates. *Mol Biol Evol*. 2020;37(4):982–993. doi:10.1093/molbev/msz279
15. Jacob JT, Coulombe PA, Kwan R, Omary MB. Types I and II keratin intermediate filaments. *Cold Spring Harb Perspect Biol*. 2018;10(4):a018275. doi:10.1101/cshperspect.a018275
16. Oshima RG. Apoptosis and keratin intermediate filaments. *Cell Death Differ*. 2002;9(5):486–492. doi:10.1038/sj.cdd.4400988
17. Zhang X, Yin M, Zhang L juan. Keratin 6, 16 and 17: Critical barrier alarmin molecules in skin wounds and psoriasis. *Cells*. 2019;8(8):807. doi:10.3390/cells8080807
18. Zhang LJ. Keratins in skin epidermal development and diseases. In: Blumenberg M, ed. *Keratin*. London, UK: IntechOpen; 2018. doi:10.5772/intechopen.79050
19. Konop M, Rybka M, Szudzik M, et al. Keratin-butyrate scaffolds promote skin wound healing in diabetic rats through down-regulation of IL-1β and up-regulation of keratins 16 and 17. *J Nat Fibers*. 2023;20(1):2136325. doi:10.1080/15440478.2022.2136325
20. Hobbs RP, Lessard JC, Coulombe PA. Keratin intermediate filament proteins: Novel regulators of inflammation and immunity in skin. *J Cell Sci*. 2012;125(22):5257–5258. doi:10.1242/jcs.122929
21. Wong P, Colucci-Guyon E, Takahashi K, Gu C, Babinet C, Coulombe PA. Introducing a null mutation in the mouse *K6α* and *K6β* genes reveals their essential structural role in the oral mucosa. *J Cell Biol*. 2000;150(4):921–928. doi:10.1083/jcb.150.4.921
22. Wong P, Coulombe PA. Loss of keratin 6 (K6) proteins reveals a function for intermediate filaments during wound repair. *J Cell Biol*. 2003;163(2):327–337. doi:10.1083/jcb.200305032
23. Rotty JD, Coulombe PA. A wound-induced keratin inhibits Src activity during keratinocyte migration and tissue repair. *J Cell Biol*. 2012;197(3):381–389. doi:10.1083/jcb.201107078
24. Kim S, Wong P, Coulombe PA. A keratin cytoskeletal protein regulates protein synthesis and epithelial cell growth. *Nature*. 2006;441(7091):362–365. doi:10.1038/nature04659
25. Rybka M, Mazurek Ł, Jurak J, et al. Keratin-TMAO dressing accelerates full-thickness skin wound healing in diabetic rats via M2-macrophage polarization and the activation of PI3K/AKT/mTOR signaling pathway. *Int J Biol Macromol*. 2025;310:143313. doi:10.1016/j.ijbiomac.2025.143313
26. Konop M, Czuwara J, Kłodzińska E, et al. Development of a novel keratin dressing which accelerates full-thickness skin wound healing in diabetic mice: In vitro and in vivo studies. *J Biomater Appl*. 2018;33(4):527–540. doi:10.1177/0885328218801114
27. Husain MSB, Gupta A, Alashwal BY. Development of keratin based hydrogels for biomedical applications. *IOP Conf Ser Mater Sci Eng*. 2019;702(1):012031. doi:10.1088/1757-899X/702/1/012031
28. Qin C, Wang Y, Gao H, Liu X, Nie Y, Ji X. Insight into the keratin ratio effect of the keratin/cellulose composite fiber. *ACS Appl Polym Mater*. 2024;6(1):265–276. doi:10.1021/acsapm.3c01912
29. Patrucco A, Visai L, Fassina L, Magenes G, Tonin C. Keratin-based matrices from wool fibers and human hair. *Mater Biomed Eng*. 2019;2019:375–403. doi:10.1016/B978-0-12-816872-1.00013-3
30. Lin C, Chen Y, Tang K, Yang K, Cheng N, Yu J. Keratin scaffolds with human adipose stem cells: Physical and biological effects toward wound healing. *J Tissue Eng Regen Med*. 2019;13(6):1044–1058. doi:10.1002/term.2855
31. Agarwal V, Panicker AG, Indrakumar S, Chatterjee K. Comparative study of keratin extraction from human hair. *Int J Biol Macromol*. 2019;133:382–390. doi:10.1016/j.ijbiomac.2019.04.098
32. Lei T, Fan J, Wang Y, et al. The fabrication and evaluation of silver nanoparticle-based keratin scaffolds. *J Biomater Appl*. 2023;37(6):1071–1085. doi:10.1177/08853282221150685
33. Serag E, El-Aziz AMA, El-Maghraby A, Taha NA. Electrospun nonwovens potential wound dressing material based on polyacrylonitrile/chicken feathers keratin nanofiber. *Sci Rep*. 2022;12(1):15460. doi:10.1038/s41598-022-19390-3
34. Vineis C, Cruz Maya I, Mowafi S, et al. Synergistic effect of sericin and keratin in gelatin based nanofibers for in vitro applications. *Int J Biol Macromol*. 2021;190:375–381. doi:10.1016/j.ijbiomac.2021.09.007
35. Konop M, Czuwara J, Kłodzińska E, et al. Evaluation of keratin biomaterial containing silver nanoparticles as a potential wound dressing in full-thickness skin wound model in diabetic mice. *J Tissue Eng Regen Med*. 2020;14(2):334–346. doi:10.1002/term.2998
36. Yan RR, Xue D, Su C, et al. A keratin/chitosan sponge with excellent hemostatic performance for uncontrolled bleeding. *Colloids Surf B Biointerfaces*. 2022;218:112770. doi:10.1016/j.colsurfb.2022.112770
37. Kelly R. Keratins in wound healing. *Wound Heal Biomater*. 2016;2016:353–365. doi:10.1016/B978-1-78242-456-7.00017-9
38. Han C, Zhang M, Xu S, Wang C, Li B, Zhao W. Strontium ranelate-loaded human hair keratin-hyaluronic acid hydrogel accelerates wound repair with anti-inflammatory and antioxidant properties. *Int J Biol Macromol*. 2024;281:136536. doi:10.1016/j.ijbiomac.2024.136536
39. Ye W, Qin M, Qiu R, Li J. Keratin-based wound dressings: From waste to wealth. *Int J Biol Macromol*. 2022;211:183–197. doi:10.1016/j.ijbiomac.2022.04.216
40. Jelodari S, Daemi H, Mohammadi P, et al. Assessment of the efficacy of an LL-37-encapsulated keratin hydrogel for the treatment of full-thickness wounds. *ACS Appl Bio Mater*. 2023;6(6):2122–2136. doi:10.1021/acsabm.2c01068
41. Wang J, Hao S, Luo T, et al. Feather keratin hydrogel for wound repair: Preparation, healing effect and biocompatibility evaluation. *Colloids Surf B Biointerfaces*. 2017;149:341–350. doi:10.1016/j.colsurfb.2016.10.038
42. Zhang M, Xu S, Du C, et al. Novel PLCL nanofibrous/keratin hydrogel bilayer wound dressing for skin wound repair. *Colloids Surf B Biointerfaces*. 2023;222:113119. doi:10.1016/j.colsurfb.2022.113119
43. Sun C, Huang Y, Wang L, et al. Engineered keratin/bFGF hydrogel to promote diabetic wound healing in rats. *Int J Biol Macromol*. 2024;261:129725. doi:10.1016/j.ijbiomac.2024.129725
44. Chen Y, Li Y, Yang X, et al. Glucose-triggered in situ forming keratin hydrogel for the treatment of diabetic wounds. *Acta Biomater*. 2021;125:208–218. doi:10.1016/j.actbio.2021.02.035
45. Khaliq T, Sohail M, Shah SA, Mahmood A, Kousar M, Jabeen N. Bioactive and multifunctional keratin-pullulan based hydrogel membranes facilitate re-epithelization in diabetic model. *Int J Biol Macromol*. 2022;209:1826–1836. doi:10.1016/j.ijbiomac.2022.04.156
46. Mirhaj M, Varshosaz J, Labbaf S, et al. Mupirocin loaded core-shell pluronic-pectin-keratin nanofibers improve human keratinocytes behavior, angiogenic activity and wound healing. *Int J Biol Macromol*. 2023;253:126700. doi:10.1016/j.ijbiomac.2023.126700
47. Radu CD, Verestiuc L, Ulea E, et al. Evaluation of keratin/bacterial cellulose based scaffolds as potential burned wound dressing. *Appl Sci*. 2021;11(5):1995. doi:10.3390/app11051995
48. Konop M, Laskowska AK, Rybka M, et al. Keratin scaffolds containing casomorphin stimulate macrophage infiltration and accelerate full-thickness cutaneous wound healing in diabetic mice. *Molecules*. 2021;26(9):2554. doi:10.3390/molecules26092554
49. Than MP, Smith RA, Hammond C, et al. Keratin-based wound care products for treatment of resistant vascular wounds. *J Clin Aesthet Dermatol*. 2012;5(12):31–35. PMID:23277802. PMCID:PMC3533319.

50. Than MP, Smith RA, Cassidy S, et al. Use of a keratin-based hydrogel in the management of recessive dystrophic epidermolysis bullosa. *J Dermatolog Treat*. 2013;24(4):290–291. doi:10.3109/09546634.2011.654108
51. Kirsner RS, Cassidy S, Marsh C, Vivas A, Kelly RJ. Use of a keratin-based wound dressing in the management of wounds in a patient with recessive dystrophic epidermolysis bullosa. *Adv Skin Wound Care*. 2012;25(9):400–403. doi:10.1097/01.ASW.0000419404.44947.de
52. Paulsen E, Bygum A. Keratin gel as an adjuvant in the treatment of recalcitrant pyoderma gangrenosum ulcers: A case report. *Acta Derm Venerol*. 2019;99(2):234–235. doi:10.2340/00015555-3081
53. Davidson A, Jina NH, Marsh C, Than M, Simcock JW. Do functional keratin dressings accelerate epithelialization in human partial thickness wounds? A randomized controlled trial on skin graft donor sites. *Eplasty*. 2013;13:e45. PMID:24058716. PMCID:PMC3767044.
54. Batzer AT, Marsh C, Kirsner RS. The use of keratin-based wound products on refractory wounds. *Int Wound J*. 2016;13(1):110–115. doi:10.1111/iwj.12245
55. Hughes RT, Levine BJ, Frizzell BA, et al. Keratin-based topical cream for radiation dermatitis during head and neck radiotherapy: A randomised, open-label pilot study. *J Radiother Pract*. 2024;23:e11. doi:10.1017/S1460396924000037

Caregivers' perspectives on long-term cognitive, psychiatric, psychological, and social outcomes in NMDAR encephalitis: Initial findings from the multi-center prospective SAPIENCE study

Marta Duda-Sikuła[1,A,C,D], Ole Jonas Boeken[2,A,B,F], Víctor Patricio[3,A,B], Chloe Buttard[4,B], Marie Benaiteau[4,B], Alvaro Mendes[5,A], Jerome Honnorat[4,A], Ava Easton[6,E], Josep Dalmau[3,A], Carsten Finke[2,A], Donata Kurpas[1,A,D–F]

[1] Department of Scientific Research Methodology, Wroclaw Medical University, Poland
[2] Department of Neurology, Charité – Universitätsmedizin Berlin, Germany
[3] Clinic Foundation for Biomedical Research (FCRB), Barcelona, Spain
[4] French Reference Center on Paraneoplastic Neurological Diseases and Autoimmune Encephalitis, Neurological Hospital, Bron, France
[5] Institute for Research and Innovation in Health, University of Porto, Portugal
[6] Encephalities International, Malton, UK

A – research concept and design; B – collection and/or assembly of data; C – data analysis and interpretation; D – writing the article; E – critical revision of the article; F – final approval of the article

Advances in Clinical and Experimental Medicine, ISSN 1899–5276 (print), ISSN 2451–2680 (online) *Adv Clin Exp Med*. 2025;34(8):1249–1253

Address for correspondence
Marta Duda-Sikula
E-mail: martadudasikula@gmail.com

Conflict of interest
None declared

Received on March 25, 2025
Reviewed on June 1, 2025
Accepted on June 23, 2025

Published online on August 1, 2025

Abstract

The SAPIENCE study explores the long-term psychological, social, and systemic challenges faced by caregivers of individuals with NMDAR encephalitis. It aims to inform patient- and caregiver-centered strategies that support recovery and wellbeing.

Key words: rare diseases, patient-centered care, multidisciplinary team, social & caregiver burden, autoimmune encephalities

Cite as
Duda-Sikula M, Boeken OJ, Patricio V, et al. Caregivers' perspectives on long-term cognitive, psychiatric, psychological, and social outcomes in NMDAR encephalitis: Initial findings from the multi-center prospective SAPIENCE study. *Adv Clin Exp Med*. 2025;34(8):1249–1253. doi:10.17219/acem/207434

DOI
10.17219/acem/207434

Copyright
Copyright by Author(s)
This is an article distributed under the terms of the Creative Commons Attribution 3.0 Unported (CC BY 3.0) (https://creativecommons.org/licenses/by/3.0/)

Funding sources
This work was supported by the European Joint Programme on Rare Diseases (EJPRD; grant No. EJPRD21-40 SAPIENCE). For the German site, funding was provided by the German Federal Ministry of Education and Research (BMBF) with grants No. 01GM210 (SAPIENCE) and 01GM1908D (CONNECT-GENERATE), as well as by the German Research Foundation (DFG) with grants No. 327654276 (SFB 1315), 504745852 (Clinical Research Unit KFO 5023 'BecauseY'), FI 2309/1–1 (Heisenberg Program), and FI 2309/2 – 1. For the Spanish site, funding was provided by the Instituto de Salud Carlos III (ISCIII) and the European Union (NextGenerationEU – Recovery and Resilience Facility), grant No. AC21 2/00053. The Polish part of the project is financed by the National Center for Research and Development under the European Joint Programme. The French partner of the project SAPIENCE is financed by the Agence Nationale de la Recherche (grant No. ANR-21-RAR4-0002).

Highlights

- High caregiver distress in N-methyl-D-aspartate receptor (NMDAR) encephalitis: The SAPIENCE study uncovers significant psychological burden among caregivers of anti-NMDAR encephalitis patients.
- Diagnostic delays exacerbate caregiver strain: Frequent misdiagnoses highlight the critical need for early NMDAR encephalitis recognition in neurology and emergency settings.
- Structured psychological support boosts caregiver and patient outcomes: Implementing formal mental health services within integrated care models promotes long-term wellbeing.
- Multidisciplinary care enhances recovery and social reintegration: Coordinated teams – neurologists, psychiatrists, rehabilitation specialists, and social workers – drive improved quality of life for patients and their families.

Introduction

N-methyl-D-aspartate receptor (NMDAR) encephalitis is a rare autoimmune disorder that affects the central nervous system, often leading to severe neuropsychiatric symptoms. It has an estimated annual incidence of 1.5 cases per million people and a prevalence of 0.6 per 100,000 individuals, primarily affecting young adults, with a median onset age of 21 years.[1] This disorder is characterized by a complex clinical presentation that can include psychiatric disturbances, cognitive impairment, movement disorders, autonomic instability, and seizures. Due to its heterogeneous and often initially misleading symptoms, NMDAR encephalitis is frequently misdiagnosed as a primary psychiatric disorder, leading to delays in appropriate treatment.[2]

The pathogenesis of NMDAR encephalitis is driven by autoantibodies directed against the NR1 subunit of the NMDA receptor, resulting in disrupted synaptic transmission and widespread neuroinflammation.[1] Standard first-line treatments typically include immunotherapy options such as corticosteroids, plasmapheresis or intravenous immunoglobulin (IVIG), with second-line agents like rituximab or cyclophosphamide considered when necessary. However, treatment responses can vary significantly between individuals. While early and intensive immunotherapy is linked to more favorable neurological outcomes, a considerable proportion of patients continue to struggle with persistent cognitive, psychiatric and functional impairments over the long term.[3]

Since its identification in 2007[4], extensive research has focused on characterizing the clinical presentation of the acute phase,[5–7] establishing diagnostic criteria,[8,9] exploring neuroimaging correlates,[10–14] and assessing treatment outcomes.[15–17] While these efforts have significantly advanced our understanding of the disease during its initial stages, research addressing the post-acute phase remains limited.

Although advancements in diagnostic techniques and treatment protocols have improved acute-phase clinical outcomes, the trajectory of recovery from NMDAR encephalitis extends far beyond symptom resolution. Many survivors continue to struggle with cognitive dysfunction, including deficits in working memory, executive function and information processing speed, which impact their ability to return to work, school and daily responsibilities.[15] Additionally, persistent psychiatric symptoms, such as anxiety, depression and psychotic episodes, may require ongoing psychiatric care and medication management. The protracted nature of recovery underscores the necessity of comprehensive long-term rehabilitation strategies.

Beyond its direct impact on patients, NMDAR encephalitis profoundly affects caregivers, who frequently undertake extensive responsibilities in supporting patient recovery. Caregivers frequently experience emotional distress, financial strain and social isolation as they navigate the challenges of supporting a loved one with a complex neurological disorder. The unpredictable course of the disease, combined with prolonged hospitalization and the need for continued rehabilitation, places immense psychological, financial and logistical burdens on family members. Many caregivers report experiencing symptoms of chronic stress, burnout, and even post-traumatic stress disorder (PTSD), reflecting the intense emotional toll of witnessing a loved one's deterioration and uncertain recovery trajectory.[16] The evolving caregiving role often requires individuals to become medical advocates, emotional support providers and financial coordinators, all while balancing personal and professional responsibilities.

Despite the crucial role caregivers play in the long-term outcomes of patients with NMDAR encephalitis, their experiences remain significantly underrepresented in the literature.[6] Previous research on rare neurological diseases suggests that informal caregivers frequently lack adequate psychological support and face systemic barriers when seeking assistance for themselves or their loved ones.[17] The lack of structured caregiver support programs and limited recognition of their needs within healthcare systems further exacerbates these challenges. Also, disparities in healthcare accessibility and inconsistencies in long-term follow-up care contribute to significant variability in patient and caregiver experiences across different healthcare settings.

Research increasingly emphasizes the importance of multidisciplinary approaches to treating NMDAR encephalitis that go beyond acute medical care. Incorporating neuropsychological rehabilitation, caregiver support programs and long-term social reintegration is crucial

for improving outcomes for patients and their families.[15] The SAPIENCE study addresses these gaps by investigating the long-term burden on caregivers, focusing on their psychological wellbeing, social adaptation and challenges navigating healthcare systems. By highlighting caregivers' lived experiences, the study aims to inform patient-centered interventions that address the difficulties faced by those caring for individuals with NMDAR encephalitis.

Ultimately, SAPIENCE underscores the need for integrative care models that support both patients and caregivers, promoting a more comprehensive approach to managing the long-term effects of NMDAR encephalitis.

Study overview and methodological framework

The SAPIENCE study is a multi-center European research initiative designed to evaluate long-term patient and caregiver outcomes. Level 1 participants were recruited from separate cohorts in Germany (Berlin), France (Lyon) and Spain (Barcelona), ensuring broad national representation.

Inclusion required a confirmed NMDAR encephalitis diagnosis,[8] age over 17, and fluency in a project language (German, French, Spanish, Catalan, or English). Individuals with preexisting neurological conditions or unable to give informed consent were excluded. The 1st phase of this study employed qualitative methods to capture in-depth narratives from 28 caregivers across 3 European study sites: Barcelona, Berlin and Lyon. Data were collected through semi-structured interviews and focus groups, allowing researchers to uncover recurring themes that shape the caregiving experience. A thorough inductive thematic analysis was conducted on the interview and focus group transcripts, following the methodology outlined by Braun and Clarke. This approach supports the development of themes directly from the data, rooted in participants' experiences rather than guided by existing theoretical frameworks.[18]

Caregivers offered valuable perspectives across 5 central themes: 1) their experiences during the initial diagnostic process, 2) the emotional and psychological impact of caregiving, 3) changes in social relationships and family dynamics, 4) interactions with healthcare professionals, and 5) the coping mechanisms they employed. A thematic analysis of these accounts revealed recurring patterns that contribute to a deeper understanding of the challenges encountered by those caring for individuals with NMDAR encephalitis.

Navigating the complexities of diagnosis

Many caregivers described the diagnostic journey as marked by confusion, frustration and emotional distress. Early symptoms often resembled psychiatric disorders, resulting in frequent misdiagnoses and significant delays in receiving appropriate treatment. The prolonged uncertainty surrounding the diagnosis exacerbated caregivers' emotional burden, often compelling them to advocate continuously for comprehensive neurological evaluations. The lack of prompt clinical recognition of NMDAR encephalitis highlights the urgent need to raise awareness among frontline healthcare professionals.

Emotional and psychological burden

The caregiving role was often marked by intense stress, heightened anxiety and emotional exhaustion. Numerous caregivers described experiencing symptoms similar to PTSD, stemming from the traumatic nature of the illness – witnessing seizures, aggressive behaviors, and enduring lengthy hospital stays. The ongoing demands of caregiving frequently resulted in burnout, highlighting the need for psychological support systems specifically designed for those caring for individuals with neuroimmune disorders.

Vaillant emphasized that extended caregiving responsibilities often necessitate the use of ego defense mechanisms to cope with emotional strain.[19,20] Many caregivers, often unconsciously, relied on strategies such as repression, dissociation and intellectualization to regulate their emotional reactions. Nevertheless, the cumulative psychological impact of caregiving remains substantial, underscoring the importance of structured interventions aimed at addressing both acute and long-term stress experienced by caregivers.

Social impact

Caregivers frequently described significant disruptions to family life, career paths, and personal relationships. The unpredictable course of the illness made it challenging to balance caregiving duties with professional obligations. In many instances, caregivers experienced financial hardship, often as a result of reducing their working hours or having to leave their jobs entirely. Social isolation was also commonly reported, as the intensive demands of caregiving left little time or energy for sustaining social connections or participating in leisure activities.

Coping strategies and resilience

Despite these challenges, caregivers developed various coping mechanisms, including reliance on patient advocacy groups, engagement in mindfulness-based stress reduction techniques and participation in caregiver support networks. Several caregivers emphasized the importance

of maintaining a structured routine to manage both their wellbeuing and that of the patient.[6] Humor, when appropriate, was cited as a crucial tool in mitigating stress and fostering resilience.

Enhancing holistic support in NMDAR encephalitis care

This qualitative analysis highlights the urgent need for a more holistic approach to managing NMDAR encephalitis – one that actively involves and supports caregivers alongside patients. The considerable emotional, financial and social strain placed on caregivers calls for a shift toward an integrated model of care that prioritizes both patient and caregiver wellbeing. Existing healthcare frameworks tend to focus primarily on acute treatment phases, often neglecting the long-term needs and challenges encountered during recovery. Bridging these gaps will require a comprehensive strategy that includes early intervention, ongoing psychological support, tailored rehabilitation services and broader policy reforms to ensure sustainable, long-term care solutions.

Improved diagnostic training

Early and accurate diagnosis and early treatment remains a fundamental challenge in NMDAR encephalitis management as in chronic diseases with poor prognosis with persistent cognitive impairments. Misdiagnosis or delayed recognition of the disease prolongs patient suffering and exacerbates caregiver stress.[2] Standardizing diagnostic protocols, increasing clinician awareness and incorporating NMDAR encephalitis into differential diagnosis training for psychiatrists, neurologists and emergency physicians are essential steps. Furthermore, the integration of biomarkers and imaging advancements, as described by Dalmau et al.,[1] may facilitate earlier and more precise detection, reducing the burden of uncertainty on caregivers.

Targeted psychological support

The psychological toll on caregivers is well-documented, with many experiencing symptoms of depression, anxiety and PTSD.[5] The unpredictability of patient recovery, coupled with the emotional strain of witnessing severe neuropsychiatric symptoms, necessitates structured mental health interventions. Vaillant highlighted that long-term caregiving responsibilities often require psychological defense mechanisms such as repression and intellectualization, yet these may not be sufficient to mitigate distress.[19,20] Implementing targeted psychological interventions, including structured counseling, peer support groups and stress-reduction programs, can significantly improve caregiver resilience and long-term wellbeing.

Long-term recovery and rehabilitation

While many patients recover from the acute phase of NMDAR encephalitis, persistent cognitive impairments – including deficits in memory, executive functioning, and attention – can hinder full reintegration into daily life.[3] These impairments, in turn, increase caregiving demands, often leading to chronic fatigue and emotional exhaustion. Establishing standardized rehabilitation programs, including neuropsychological therapy and cognitive training, can facilitate patient independence and alleviate caregiver burden.

Healthcare system – integrated multidisciplinary care

Fragmented healthcare pathways place considerable strain on caregivers, who often find themselves navigating complex and disjointed systems with little guidance. Participants in this study frequently reported challenges in securing consistent follow-up care and noted a lack of coordination between key healthcare providers, including neurologists, psychiatrists, rehabilitation specialists, and social workers. Establishing integrated multidisciplinary teams – consisting of neurologists, neuropsychiatrists, neuropsychologists, and social workers – can help ensure a more cohesive and continuous care experience, easing the transition from hospital to home. Such collaborative care models, successfully implemented in the management of other chronic neurological conditions, have been shown to enhance long-term patient outcomes while alleviating caregiver burden.[17]

Enhancing social reintegration strategies

The transition from acute hospitalization to community reintegration is a complex process that affects both patients and caregivers. Many caregivers in this study described challenges in facilitating social re-engagement, particularly for patients experiencing residual psychiatric symptoms or cognitive impairments. Public awareness campaigns, employer education programs, and community-based social integration initiatives can help mitigate stigma and promote a more inclusive environment for individuals recovering from NMDAR encephalitis.[17]

It is worth to highlight the vital work of patient organizations – such as Encephalitis International, which provides resources, advocacy, and peer support – can

further enhance public understanding (https://www.encephalitis.info/about-us/). Notably, initiatives like World Encephalitis Day play a crucial role in raising global awareness and promoting acceptance of those affected by encephalitis.

Limitations

A key strength of this study is its multicenter design, which enabled the inclusion of a diverse sample of patients and caregivers across various healthcare settings and cultural contexts, enhancing the generalizability of the findings. However, the sample size, while sufficient for qualitative analysis, may limit the broader applicability of the results. The analysis is limited to qualitative data without quantitative triangulation. Future project phases will include quantitative methods to validate and expand on these results.

Conclusions

Caregivers of individuals affected by NMDAR encephalitis are essential contributors to the recovery process, yet their roles and challenges often go unrecognized in clinical practice and health policy. The SAPIENCE study underscores the urgent need to address the multifaceted obstacles they encounter – ranging from diagnostic delays and psychological strain to gaps in rehabilitation services and systemic support. These findings emphasize the importance of developing comprehensive, integrated care models that prioritize the wellbeing of both patients and their caregivers. Future research should focus on creating and evaluating targeted interventions for caregivers, paving the way for more inclusive, patient- and caregiver-centered healthcare systems. Our findings align with the most recent World Health Organization (WHO) Technical Brief on Encephalities, which emphasizes that individuals recovering from encephalitis often require long-term care, placing significant emotional, financial and social burdens on caregivers.[21]

Use of AI and AI-assisted technologies

Not applicable.

ORCID iDs

Marta Duda-Sikuła https://orcid.org/0000-0003-1715-8958
Ole Jonas Boeken https://orcid.org/0000-0002-1727-3625
Víctor Patricio https://orcid.org/ 0009-0004-2636-4272
Marie Benaiteau https://orcid.org/0009-0005-2347-6006
Alvaro Mendes https://orcid.org/0000-0002-8766-7646
Jerome Honnorat https://orcid.org/0000-0002-4721-5952
Ava Easton https://orcid.org/0000-0002-1739-2915
Josep Dalmau https://orcid.org/0000-0001-5856-2813
Carsten Finke https://orcid.org/0000-0002-7665-1171
Donata Kurpas https://orcid.org/0000-0002-6996-8920

References

1. Dalmau J, Armangué T, Planagumà J, et al. An update on anti-NMDA receptor encephalitis for neurologists and psychiatrists: Mechanisms and models. *Lancet Neurol*. 2019;18(11):1045–1057. doi:10.1016/S1474-4422(19)30244-3
2. Tanguturi YC, Cundiff AW, Fuchs C. Anti-N-methyl d-aspartate receptor encephalitis and electroconvulsive therapy. *Child Adolesc Psychiatr Clin North Am*. 2019;28(1):79–89. doi:10.1016/j.chc.2018.07.005
3. Dubey D, Pittock SJ, Kelly CR, et al. Autoimmune encephalitis epidemiology and a comparison to infectious encephalitis. *Ann Neurol*. 2018;83(1):166–177. doi:10.1002/ana.25131
4. Dalmau J, Tüzün E, Wu H, et al. Paraneoplastic anti-N-methyl-D-aspartate receptor encephalitis associated with ovarian teratoma. *Ann Neurol*. 2007;61(1):25–36. doi:10.1002/ana.21050
5. Dalmau J, Gleichman AJ, Hughes EG, et al. Anti-NMDA-receptor encephalitis: Case series and analysis of the effects of antibodies. *Lancet Neurol*. 2008;7(12):1091–1098. doi:10.1016/S1474-4422(08)70224-2
6. Balu R, McCracken L, Lancaster E, Graus F, Dalmau J, Titulaer MJ. A score that predicts 1-year functional status in patients with anti-NMDA receptor encephalitis. *Neurology*. 2019;92(3):e244–e252. doi:10.1212/WNL.0000000000006783
7. Bartels F, Krohn S, Nikolaus M, et al. Clinical and magnetic resonance imaging outcome predictors in pediatric anti-N-methyl-D-aspartate receptor encephalitis. *Ann Neurol*. 2020;88(1):148–159. doi:10.1002/ana.25754
8. Graus F, Titulaer MJ, Balu R, et al. A clinical approach to diagnosis of autoimmune encephalitis. *Lancet Neurol*. 2016;15(4):391–404. doi:10.1016/S1474-4422(15)00401-9
9. Nguyen L, Wang C. Anti-NMDA receptor autoimmune encephalitis: Diagnosis and management strategies. *Int J Gen Med*. 2023;16:7–21. doi:10.2147/IJGM.S397429
10. Phillips OR, Joshi SH, Narr KL, et al. Superficial white matter damage in anti-NMDA receptor encephalitis. *J Neurol Neurosurg Psychiatry*. 2018;89(5):518–525. doi:10.1136/jnnp-2017-316822
11. Heine J, Prüss H, Bartsch T, Ploner CJ, Paul F, Finke C. Imaging of autoimmune encephalitis: Relevance for clinical practice and hippocampal function. *Neuroscience*. 2015;309:68–83. doi:10.1016/j.neuroscience.2015.05.037
12. Peer M, Prüss H, Ben-Dayan I, Paul F, Arzy S, Finke C. Functional connectivity of large-scale brain networks in patients with anti-NMDA receptor encephalitis: An observational study. *Lancet Psychiatry*. 2017;4(10):768–774. doi:10.1016/S2215-0366(17)30330-9
13. Finke C, Kopp UA, Pajkert A, et al. Structural hippocampal damage following anti-N-methyl-D-aspartate receptor encephalitis. *Biol Psychiatry*. 2016;79(9):727–734. doi:10.1016/j.biopsych.2015.02.024
14. Brier MR, Day GS, Snyder AZ, Tanenbaum AB, Ances BM. N-methyl-D-aspartate receptor encephalitis mediates loss of intrinsic activity measured by functional MRI. *J Neurol*. 2016;263(6):1083–1091. doi:10.1007/s00415-016-8083-6
15. Boeken OJ, Heine J, Duda-Sikula M, et al. Assessment of long-term psychosocial outcomes in N-methyl-D-aspartate receptor encephalitis: The SAPIENCE study protocol. *BMC Neurol*. 2024;24(1):322. doi:10.1186/s12883-024-03842-6
16. Cloitre M, Garvert DW, Weiss B, Carlson EB, Bryant RA. Distinguishing PTSD, complex PTSD, and borderline personality disorder: A latent class analysis. *Eur J Psychotraumatol*. 2014;5(1):25097. doi:10.3402/ejpt.v5.25097
17. McMullan J, Lohfeld L, McKnight AJ. Needs of informal caregivers of people with a rare disease: A rapid review of the literature. *BMJ Open*. 2022;12(12):e063263. doi:10.1136/bmjopen-2022-063263
18. Braun V, Clarke V. Using thematic analysis in psychology. *Qual Res Psychol*. 2006;3(2):77–101. doi:10.1191/1478088706qp063oa
19. Vaillant GE. Ego mechanisms of defense and personality psychopathology. *J Abnorm Psychol*. 1994;103(1):44–50. doi:10.1037/0021-843X.103.1.44
20. World Health Organization (WHO): Division of Mental Health and Prevention of Substance Abuse. WHOQOL: Measuring quality of life. Geneva, Switzerland: World Health Organization (WHO); 1997. https://iris.who.int/handle/10665/63482. Accessed March 15, 2025.
21. WHO Team: Mental Health, Brain Health and Substance Use (MSD). *Encephalitis: Global Threats, Trends and Public Health Implications. A Technical Brief*. Geneva, Switzerland: World Health Organization (WHO); 2025. ISBN:978-92-4-010647-5.

Comorbidity-related risk factors for acute respiratory distress syndrome in sepsis patients: A systematic review and meta-analysis

Xin Lin[1,A–F], Yang Liu[1,A–F], Li Kong[1,A–F], Tejin Ba[2,A–F], Bagenna Bao[2,A–F], Shuanglin Zhang[2,A–F], Weihong Liu[1,A–F]

[1] Emergency And Intensive Care Unit, The Affiliated Hospital of Shandong University of Traditional Chinese Medicine, Jinan, China
[2] Inner Mongolia Autonomous Region International Mongolian Medical Hospital, Hohhot, China

A – research concept and design; B – collection and/or assembly of data; C – data analysis and interpretation;
D – writing the article; E – critical revision of the article; F – final approval of the article

Advances in Clinical and Experimental Medicine, ISSN 1899–5276 (print), ISSN 2451–2680 (online) *Adv Clin Exp Med*. 2025;34(8):1255–1265

Address for correspondence
Weihong Liu
E-mail: 1312983352@qq.com

Funding sources
None declared

Conflict of interest
None declared

Received on January 18, 2024
Reviewed on June 15, 2024
Accepted on July 24, 2024

Published online on March 12, 2025

Abstract

Background. Acute respiratory distress syndrome (ARDS) presents a significant challenge in the management of sepsis, with various comorbidities potentially influencing its development. Understanding the impact of these comorbidities is crucial for improving patient outcomes.

Objectives. This meta-analysis was conducted to investigate the relationship between various comorbidities and the development of ARDS in patients with sepsis, with the aim of improving understanding and management of this condition.

Materials and methods. The study included adult sepsis patients from 8 studies, totaling 16,964 participants. Risk of bias was assessed using the Newcastle–Ottawa scale (NOS), and the data analysis was performed and reported as pooled odds ratios (ORs) computed using a random-effects model. Heterogeneity and publication bias were assessed using the I^2 statistic and Doi plots with the Luis Furuya-Kanamori (LFK) index, respectively.

Results. Chronic obstructive pulmonary disease was significantly associated with an increased risk of ARDS (OR: 1.43, 95% confidence interval (95% CI): 1.02–2.01). Other comorbidities showed no significant associations: diabetes mellitus (DM) (OR: 0.88, 95% CI: 0.69–1.11), hypertension (HTN) (OR: 0.86, 95% CI: 0.56 to 1.34), coronary artery disease (CAD) (OR: 0.95, 95% CI: 0.86–1.06), congestive heart failure (CHF) (OR: 1.08, 95% CI: 0.61 to 1.90), chronic kidney disease (CKD) (OR: 0.89, 95% CI: 0.65–1.22), chronic liver disease (CLD) (OR: 1.13, 95% CI: 0.61–2.09), and cancer (OR: 0.90, 95% CI: 0.59–1.35). Additional analyses indicated moderate-to-high heterogeneity and some evidence of publication bias.

Conclusions. Chronic obstructive pulmonary disease is a notable risk factor for ARDS in sepsis patients, suggesting the need for enhanced surveillance and management in this group. Further research is necessary to understand the mechanisms and explore other potential ARDS risk factors in sepsis.

Key words: COPD, ARDS, sepsis, meta-analysis

Cite as
Lin X, Liu Y, Kong L, et al. Comorbidity-related risk factors for acute respiratory distress syndrome in sepsis patients: A systematic review and meta-analysis. *Adv Clin Exp Med*. 2025;34(8):1255–1265. doi:10.17219/acem/191594

DOI
10.17219/acem/191594

Copyright
Copyright by Author(s)
This is an article distributed under the terms of the Creative Commons Attribution 3.0 Unported (CC BY 3.0) (https://creativecommons.org/licenses/by/3.0/)

Background

Acute respiratory distress syndrome (ARDS) is a severe, life-threatening medical condition characterized by rapid onset of widespread inflammation in the lungs.[1] This syndrome is a major cause of morbidity and mortality in critically ill patients, particularly in those with sepsis.[2] Sepsis, a systemic response to infection, can lead to multiple organ failure, including respiratory failure manifesting as ARDS.[3] The interplay between sepsis and ARDS is complex and multifaceted, with a variety of factors influencing the progression from sepsis to ARDS.

In recent years, the medical community has increasingly recognized the role of comorbidities in the development and outcome of ARDS among septic patients.[4] Comorbidities such as diabetes mellitus (DM), hypertension (HTN), chronic obstructive pulmonary disease (COPD), chronic kidney disease (CKD), coronary artery disease (CAD), chronic liver disease (CLD), congestive heart failure (CHF), and cancer have been identified as significant contributors to the susceptibility and severity of ARDS.[5] These comorbid conditions may alter the host response to infection and inflammation, potentially exacerbating the pathophysiological processes underlying ARDS.[4,5]

The pathogenesis of ARDS in septic patients is a subject of intense research. It is known to be dependent on a complex interplay of inflammatory mediators, endothelial and epithelial injury, and dysregulated immune responses.[6] In this milieu, comorbidities add another layer of complexity. For instance, DM can impair immune function, while chronic lung diseases like COPD alter baseline pulmonary function, potentially predisposing patients to more severe forms of ARDS when they develop sepsis.[7,8]

The presence of comorbidities can also influence the clinical management and outcomes of ARDS. These patients often require more intricate care strategies, balancing the management of their acute critical illness with the ongoing treatment of their chronic conditions. This intersection of acute and chronic diseases poses significant challenges in clinical decision-making and resource allocation in intensive care units (ICUs).

Additionally, an appreciation of the role of comorbidities in ARDS pathogenesis is essential for the development of targeted therapeutic strategies. The current management of ARDS is primarily supportive, with mechanical ventilation being a cornerstone of therapy.[9] However, patients with significant comorbidities may benefit from more tailored approaches that address both the acute and chronic aspects of their illness.

The intersection of ARDS and sepsis, compounded by the presence of comorbidities, represents a complex clinical challenge. Understanding the role of comorbidities in the development of ARDS among septic patients is not only crucial for elucidating the pathophysiology of this condition but also for improving its prognosis. A systematic review and meta-analysis of the existing literature on this topic should provide valuable insights into how these comorbidities influence the risk and outcomes of ARDS in sepsis. It will also enhance our understanding of the interactions between chronic health conditions and acute critical illnesses like ARDS. This understanding is vital for clinicians and researchers alike, as it has the potential to inform clinical practice and shape future research directions. A systematic analysis should also identify gaps in the current knowledge, guiding future research efforts. Hence, the purpose of this review is to synthesize the available evidence on the impact of various comorbidities on the risk of developing ARDS in patients with sepsis. We aim to provide a thorough and nuanced understanding of how comorbidities influence the risk and progression of ARDS in sepsis, ultimately contributing to better patient outcomes in this critically ill cohort.

Objectives

This review was done with an objective to determine the comorbidity related risk factors associated with ARDS in patients with sepsis.

Methods

Eligibility criteria

Study population

The inclusion criteria were as follows: adult participants (aged 18 years and older) who were diagnosed with sepsis and subsequently developed ARDS. The focus was specifically on populations with documented comorbidities such as DM, HTN, COPD, CKD, CAD, CLD, CHF, and cancer.

Exposure and comparison

This review analyzed studies that examined the impact of various comorbidities on the development of ARDS in sepsis patients. The comparison was made between patients with and without these specific comorbidities.

Outcome measures

The primary outcomes of interest were the incidence of ARDS in sepsis patients with comorbidities.

Study design

Included studies encompassed a range of designs: observational studies (prospective/retrospective cohort, case-control and cross-sectional analytical studies) relevant to the topic.

Information sources and search strategy

A thorough search strategy was implemented, utilizing databases such as PubMed, Scopus, Cochrane Library, Google Scholar, ScienceDirect, and Web of Science. Key search terms included combinations of "sepsis," "acute respiratory distress syndrome," "comorbidities," "diabetes mellitus," "hypertension," "COPD," "chronic kidney disease," "coronary artery disease," "chronic liver disease," "congestive heart failure," "cancer," and related terms. The search timeframe extended from January 1954 to December 2023, with no language restrictions.

Selection process

Two reviewers independently screened the studies, beginning with an assessment of titles, abstracts and key terms. Full-text articles were then reviewed for a more detailed assessment. Any disagreements were resolved through discussion and consensus. The selection process was documented in accordance with the Preferred Reporting Items for Systematic reviews and Meta-Analyses (PRISMA) guidelines.

Data collection process and data items

Data were extracted by the lead researcher, detailing study characteristics, participant demographics, study setting, and methodology. The data included the author, year of publication, country, study design, ARDS criteria, study participant details, mean age, gender distribution, quality assessment-related characteristics, number of participants with each comorbidity, outcomes measured, exposure details, and follow-up duration. A secondary reviewer verified the extracted data for accuracy.

Study risk of bias assessment

To ensure the credibility and reliability of the included studies, an assessment of the risk of bias was meticulously conducted using the Newcastle–Ottawa scale (NOS).[10] The NOS is a widely recognized tool specifically designed for evaluating the quality of observational studies.

Two independent researchers employed the NOS to evaluate the studies. Each researcher independently scored the studies, and discrepancies were resolved through discussion and consensus. This dual-assessment approach was adopted to enhance the objectivity and reduce the potential for bias in the review process. The NOS operates on 3 broad criteria:

Selection of the study groups: This criterion assesses the method of selecting the study participants, aiming to determine if the subjects and controls are representatively and appropriately chosen. It considers factors such as case definition, case representativeness, control selection, and control definition.

Comparability of the groups: This aspect of the NOS focuses on the comparability of the study groups, based on the design or analysis.

Ascertainment of the exposure or outcome: For case-control studies, this involves evaluating the method of ascertaining exposures, such as whether it was through secure records or self-reports. For cohort studies, it examines the method of ascertaining outcomes, including the independence of the outcome assessment and the length and adequacy of the follow-up.

Each study is judged in these categories using a star system, which indicates the quality of the study's methodology in each specific category. The maximum number of stars a study can receive is 9, with 4 stars allocated for "selection", 2 for "comparability" and 3 for "ascertainment of exposure or outcome". A study with a higher number of stars (7–9) is considered to have a lower risk of bias; 4–6 stars indicate a moderate risk of bias; and less than 4 indicates a higher risk of bias.

Effect measures and synthesis methods

Statistical software and version

Statistical analysis was conducted using Stata software v. 14.2 (Stata Corp., College Station, USA). This advanced statistical package allowed for detailed and accurate data analysis, crucial for the integrity of our study.

Methodology for analyzing binary outcomes

Given that all outcomes in this study were binary, we calculated the combined odds ratio (OR) along with a 95% confidence interval (95% CI). This was derived from the event frequencies observed in both the intervention and control groups, providing a comparative analysis of the efficacy of the interventions.

Model selection and variance method

A random-effects model was chosen for this analysis, incorporating the inverse variance method.[11] This approach was essential to account for the variability present across the studies included in our review.

Heterogeneity assessment techniques

To assess heterogeneity, or the degree of variation in the results among the different studies, a multifaceted approach was employed. The initial step involved a visual examination of forest plots to check for overlaps in confidence intervals. Then, χ^2 tests were used to detect the presence of heterogeneity. Finally, I^2 statistic was used to quantify the percentage of total variation across studies that is due to heterogeneity rather than chance.

Additionally, a sensitivity analysis was conducted to determine the influence of individual studies on the overall meta-analysis results. This step was crucial to ensure the stability and reliability of the meta-analysis.

Publication bias assessment tools

A funnel plot was created for all outcomes. Asymmetry of this plot was used as an indication of the presence of publication bias. We also utilized the Doi plot and the Luis Furuya-Kanamori (LFK) index to detect and quantify potential publication bias.[12] According to the LFK index, values ranging from –1 to +1 indicated an absence of publication bias (showing perfect symmetry). Values between –1 to –2 or +1 to +2 suggested minor asymmetry, while values less than –2 or greater than +2 signified major asymmetry, indicating a higher likelihood of publication bias.[12]

Results

Search results

In total, our search across the PubMed, Scopus, Cochrane Library, Google Scholar, ScienceDirect, and Web of Science databases yielded 1,632 potentially relevant studies. Upon an initial review of titles and abstracts, 78 studies were identified as potentially meeting our inclusion criteria. Subsequent in-depth examination of these full-text articles led to the final selection of 8 studies that were deemed suitable for inclusion in our analysis (Fig. 1).[8,13–19]

Characteristics of the studies included

The studies originated from multiple countries, including the USA, Japan, China, and South Korea, reflecting a global perspective on the issue. The sample size across these studies ranged considerably, from as few as 125 participants in the smallest study to as many as 11,566 participants in the largest. In total, we cumulatively analyzed data from 16,964 sepsis patients. Regarding the criteria for ARDS diagnosis, all included studies employed recognized definitions, with 7 studies using the Berlin definition and 1 study using the American European Consensus Conference criteria. The mean age of participants in these studies varied, ranging from 55 to 73 years. As for the assessment of study quality and risk of bias, 6 studies were categorized as having a low risk of bias, while 2 studies were determined to have a moderate risk of bias (Table 1).

Diabetes mellitus and the risk of ARDS in sepsis patients

Seven studies (including 16,953 sepsis patients) compared the risk of ARDS between DM and non-DM patients. Pooled OR was 0.88, with a 95% CI between 0.69 and 1.11

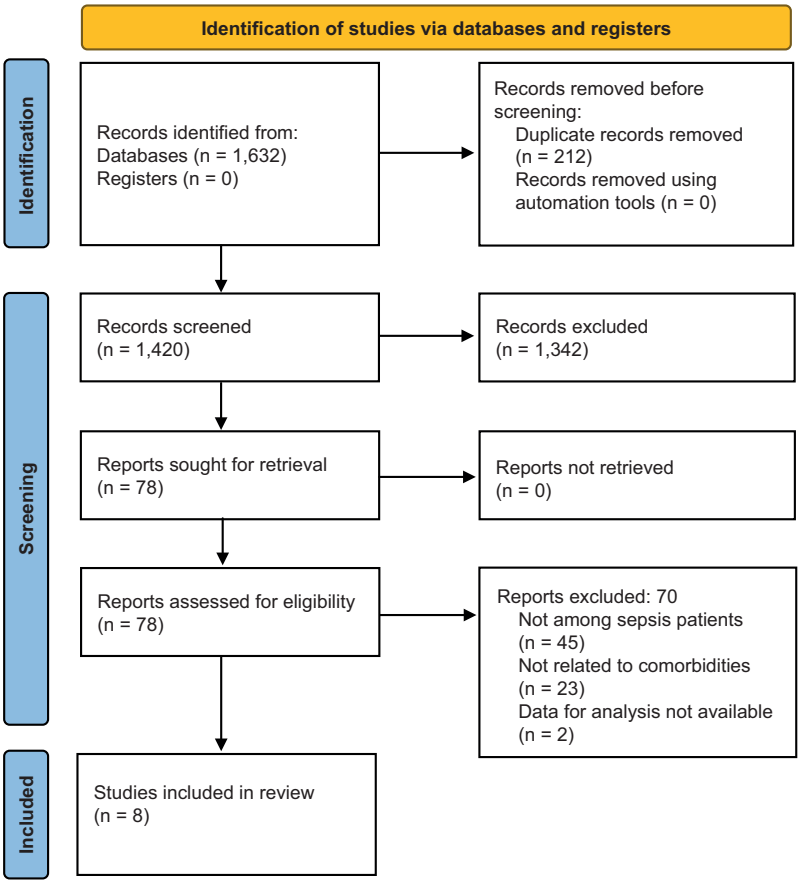


Fig. 1. Preferred Reporting Items for Systematic reviews and Meta-Analyses (PRISMA) flowchart

Table 1. Characteristics of the included studies (n = 8)

Study	Country	Study design	Sample size	Participants	ARDS criteria	Mean age [years]	Male/female (%)	Risk of bias
Shi et al., 2022[8]	China	retrospective	529	sepsis patients admitted to intensive care unit	meeting the Berlin definition of ARDS	ARDS = 66 no ARDS = 70	ARDS = 75/25 non-ARDS = 66/34	moderate
Iriyama et al., 2020[13]	Japan	secondary analysis of prospective	594	adult patients with severe sepsis caused by non-pulmonary infection	meeting the Berlin definition on the 1st or 4th day of screening	ARDS = 70 no ARDS = 72	ARDS = 60/40 non-ARDS = 56.8/43.2	low
Li et al., 2020[14]	China	prospective	150	patients with sepsis who attended Cangzhou Central Hospital	meeting the Berlin definition of ARDS	ARDS = 60.6 no ARDS = 55.5	ARDS = 66/34 non-ARDS = 65/35	low
Mikkelsen et al., 2013[15]	USA	retrospective	778	adults with severe sepsis presenting to emergency department	meeting the Berlin definition of ARDS	ARDS = 55 no ARDS = 57	ARDS = 50/50 non-ARDS = 54/46	low
Nam et al., 2019[16]	South Korea	retrospective	125	patients with septic bacteremia presenting to intensive care unit	meeting the Berlin definition of ARDS	ARDS = 65 no ARDS = 73	ARDS = 54.5/45.5 non-ARDS = 53.4/46.6	moderate
Seethala et al., 2017[17]	USA	prospective	2,534	septic adult patients presenting to the emergency department or being admitted for high-risk elective surgery	meeting the Berlin definition of ARDS	ARDS = 54.9 no ARDS = 58.8	ARDS = 60.3/39.7 non-ARDS = 50.6/49.4	low
Xu et al., 2023[18]	China	retrospective	11,566	sepsis patients admitted to intensive care unit	meeting the Berlin definition of ARDS	ARDS = 66.09 no ARDS = 63	ARDS = 59.9/40.1 non-ARDS = 60.2/39.8	low
Gong et al., 2005[19]	USA	prospective	688	sepsis patients admitted to intensive care unit	American-European Consensus Conference criteria for ARDS	ARDS = 65 no ARDS = 67	ARDS = 54/46 non-ARDS = 61/39	low

ARDS – acute respiratory distress syndrome.

(p = 0.27) among sepsis patients (Fig. 2). While heterogeneity was moderate with an I^2 value of 55.3%, a significant χ^2 p-value of 0.04 was obtained. The Doi plot (Supplementary Fig. 1) and funnel plot (Supplementary Fig. 2) showed major asymmetry, with the LFK index value equaling –2.22. This confirms the presence of publication bias.

Hypertension and the risk of ARDS in sepsis patients

Three studies (including 1,432 sepsis patients) compared the risk of ARDS between HTN and non-HTN patients. Pooled OR was 0.86, with a 95% CI of 0.56–1.34 (p = 0.52) (Fig. 3). The heterogeneity was moderate, with an I^2 value of 38.1% and a nonsignificant p-value of 0.20. The funnel plot (Supplementary Fig. 3) showed asymmetry, indicating the possibility of publication bias.

Chronic obstructive pulmonary disease and the risk of ARDS in sepsis patients

Six studies (including 13,742 sepsis patients) compared the risk of ARDS between COPD and non-COPD patients. Pooled OR was 1.43, with a 95% CI of 1.02–2.01, indicating the significant risk of ARDS among sepsis patients with COPD, compared to sepsis patients without COPD (p = 0.04) (Fig. 4). The heterogeneity was low, with an I^2 value of 23.6% and a nonsignificant χ^2 p-value of 0.26. The funnel plot (Supplementary Fig. 4) and Doi plot (Supplementary Fig. 5) showed major asymmetry, with an LFK index value equaling –4.39. This confirms the presence of publication bias.

Coronary artery disease and the risk of ARDS in sepsis patients

Five studies (including 13,592 sepsis patients) compared the risk of ARDS between CAD and non-CAD patients. Pooled OR was 0.89, with a 95% CI of 0.65–1.22 (p = 0.39) (Fig. 5) The heterogeneity was low, with an I^2 value of 31.6% and a nonsignificant χ^2 p-value of 0.19. The funnel plot (Supplementary Fig. 6) and Doi plot (Supplementary Fig. 7) showed major asymmetry, with an LFK index value equaling –6.15. This confirms the presence of publication bias.

Congestive heart failure and risk of ARDS in sepsis patients

Two studies with 1,372 sepsis patients have compared the risk of ARDS between CHF and non-CHF patients. Pooled OR was 1.08, with a 95% CI of 0.61–1.90 (p = 0.80;

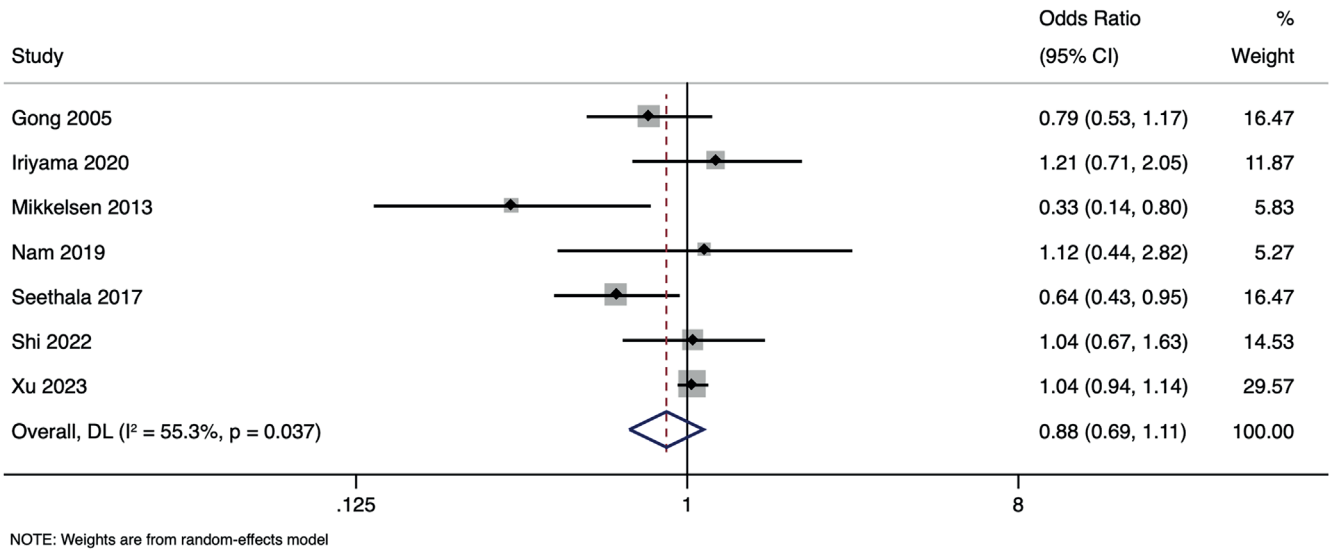


Fig. 2. Forest plot showing the association between diabetes mellitus and acute respiratory distress syndrome (ARDS) among sepsis patients

DL – DerSimonian and Laird approach; 95% CI – 95% confidence interval; OR – odds ratio.

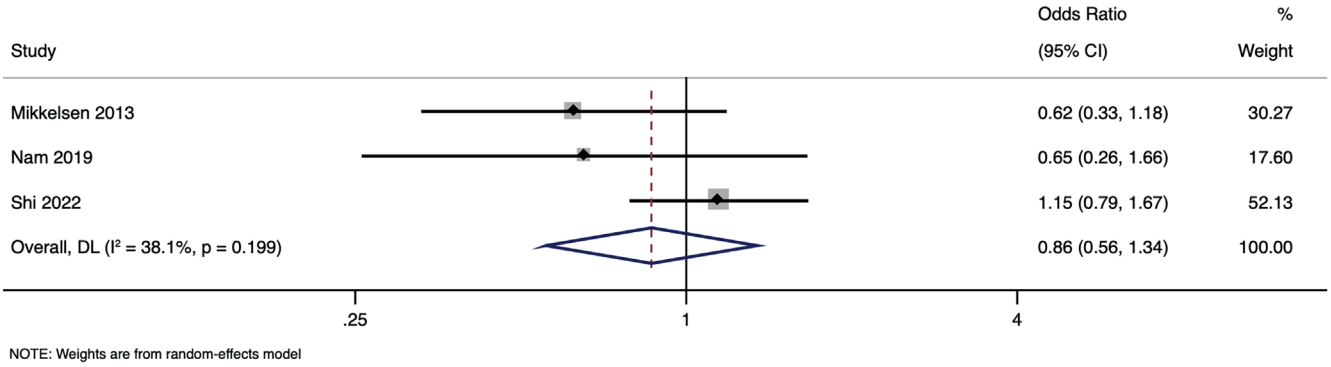


Fig. 3. Forest plot showing the association between hypertension and acute respiratory distress syndrome (ARDS) among sepsis patients

DL – DerSimonian and Laird approach; 95% CI – 95% confidence interval; OR – odds ratio.

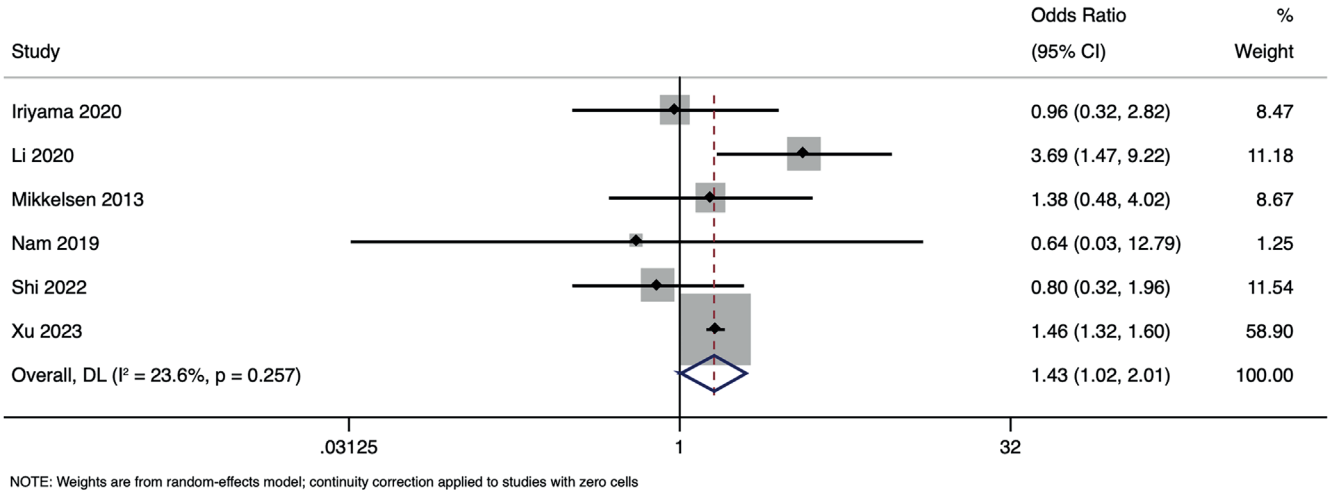


Fig. 4. Forest plot showing the association between chronic obstructive pulmonary disease and acute respiratory distress syndrome (ARDS) among sepsis patients

DL – DerSimonian and Laird approach; 95% CI – 95% confidence interval; OR – odds ratio.

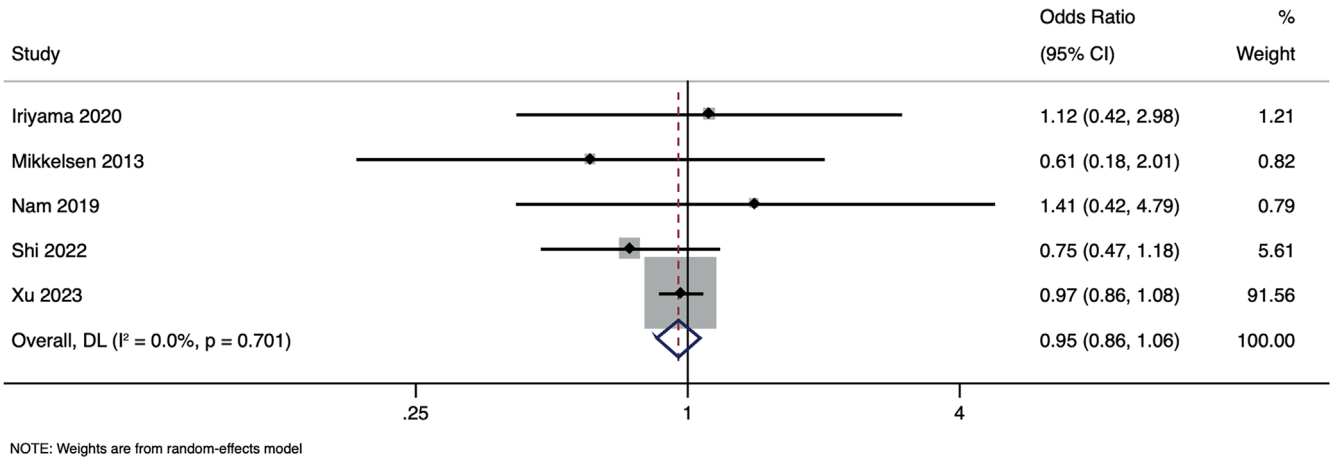


Fig. 5. Forest plot showing the association between coronary artery disease and acute respiratory distress syndrome (ARDS) among sepsis patients

DL – DerSimonian and Laird approach; 95% CI – 95% confidence interval; OR – odds ratio.

Fig. 6). No heterogeneity was found with an I^2 value of 0%. Funnel plot (Supplementary Fig. 8) showed major asymmetry during publication bias assessment.

CKD and risk of ARDS in sepsis patients

Seven studies with 14,430 sepsis patients have compared the risk of ARDS between CKD and non-CKD patients. Pooled OR was 0.89, with a 95% CI of 0.65 to 1.22 (p = 0.39; Fig. 7). Low heterogeneity was found with an I^2 value of 31.6%, with a nonsignificant χ^2 p-value of 0.19. Funnel plot (Supplementary Fig. 9) and Doi plot (Supplementary Fig. 10) showed major asymmetry with an LFK index value of –6.15. This confirms the presence of publication bias.

Chronic liver disease and the risk of ARDS in sepsis patients

Five studies (including 13,776 sepsis patients) compared the risk of ARDS between CLD and non-CLD patients. Pooled OR was 1.13, with a 95% CI of 0.61–2.09 (p = 0.70) among sepsis patients (Fig. 8). The heterogeneity was high, with an I^2 value of 73.7% and a significant χ^2 p-value of 0.004. The funnel plot (Supplementary Fig. 11) and Doi plot (Supplementary Fig. 12) showed major asymmetry, with an LFK index value equaling –7.35. This confirms the presence of publication bias.

Cancer and risk of ARDS in sepsis patients

Five studies (including 13,592 sepsis patients) compared the risk of ARDS between cancer and non-cancer patients. Pooled OR was 0.90, with a 95% CI of 0.59–1.35 (p = 0.70) (Fig. 9). The heterogeneity was moderate-to-high, with an I^2 value of 68.4% and a significant χ^2 p-value of 0.01. The funnel plot (Supplementary Fig. 13) and Doi plot (Supplementary Fig. 14) showed major asymmetry, with an LFK index value equaling –5.26. This confirms the presence of publication bias.

Additional sensitivity analysis

Leave-one-out sensitivity analysis did not demonstrate any notable alterations in terms of either the magnitude or the direction of the associations observed. This robustness check, which involved sequentially removing each study from the meta-analysis and reassessing the overall effect, showed consistent results. The absence of significant

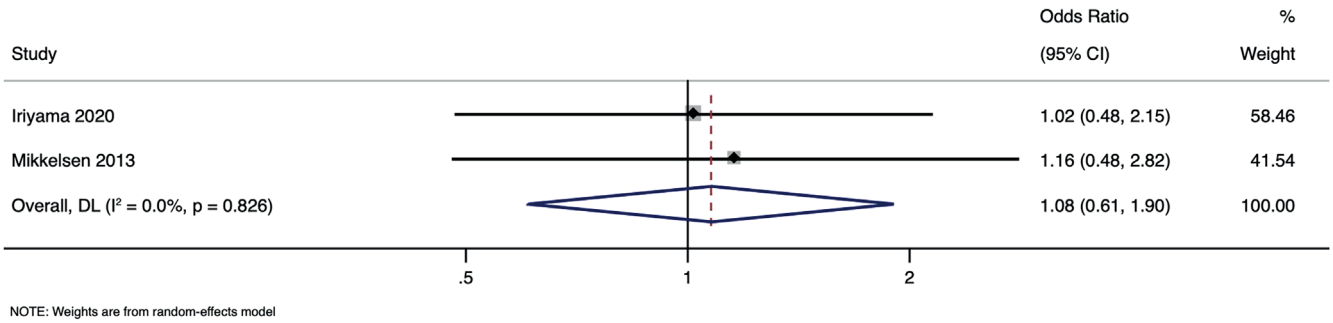


Fig. 6. Forest plot showing the association between congestive heart failure and acute respiratory distress syndrome (ARDS) among sepsis patients

DL – DerSimonian and Laird approach; 95% CI – 95% confidence interval; OR – odds ratio.

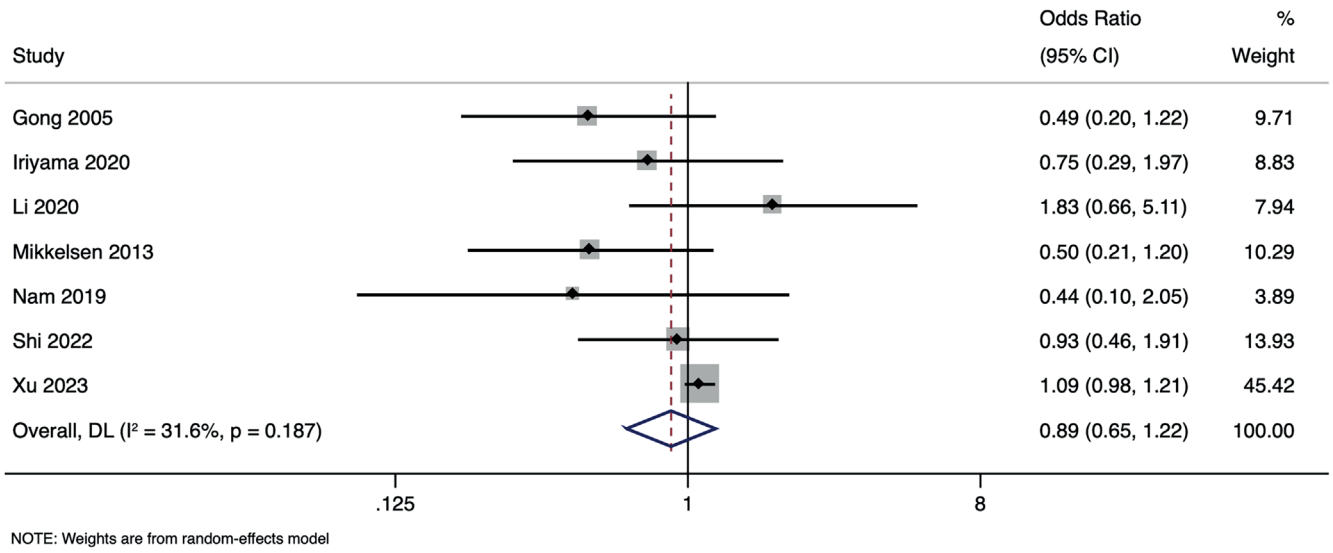


Fig. 7. Forest plot showing the association between chronic kidney disease and acute respiratory distress syndrome (ARDS) among sepsis patients

DL – DerSimonian and Laird approach; 95% CI – 95% confidence interval; OR – odds ratio.

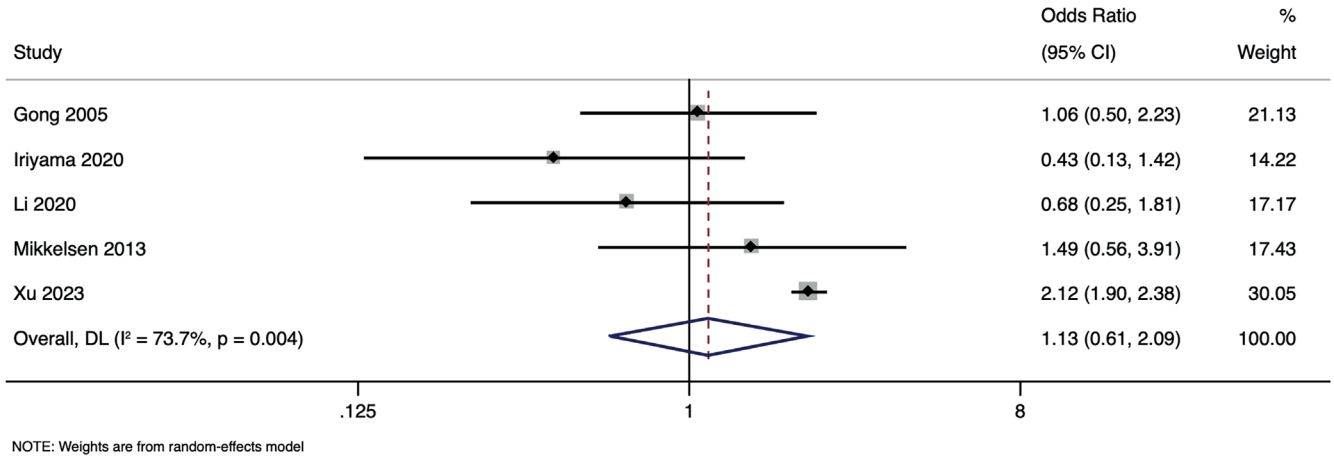


Fig. 8. Forest plot showing the association between chronic liver disease and acute respiratory distress syndrome (ARDS) among sepsis patients

DL – DerSimonian and Laird approach; 95% CI – 95% confidence interval; OR – odds ratio.

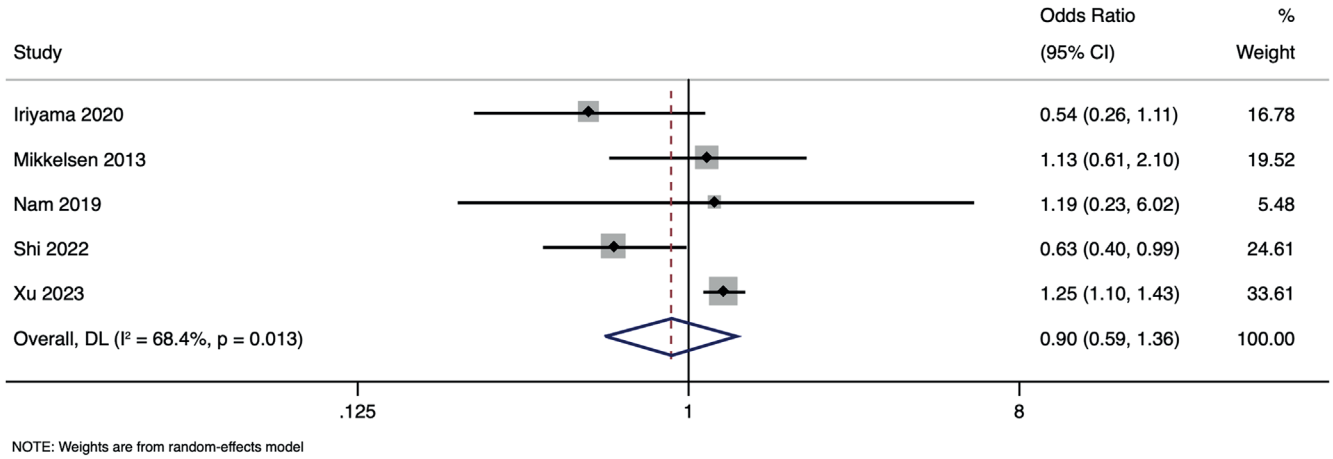


Fig. 9. Forest plot showing the association between cancer and acute respiratory distress syndrome (ARDS) among sepsis patients

DL – DerSimonian and Laird approach; 95% CI – 95% confidence interval; OR – odds ratio.

changes upon the exclusion of individual studies confirms the stability and reliability of the observed associations in our analysis.

Discussion

Our comprehensive review assessed the relationship between various comorbidities and the risk of developing ARDS in sepsis patients. The comorbidities evaluated included DM, HTN, COPD, CAD, CHF, CKD, CLD, and cancer. Among these, COPD was the only comorbidity that showed a significant association with an increased risk of ARDS in sepsis patients, with a pooled OR of 1.43. In contrast, other comorbidities such as DM, HTN, CAD, CHF, CKD, CLD, and cancer did not show a significant association with the development of ARDS in this patient population.

These findings add to the existing body of research on ARDS risk factors in sepsis patients. A previous review reported mixed results regarding the impact of comorbidities on ARDS development.[20] In fact, some studies have suggested that comorbidities like DM and HTN may be associated with a lower risk of ARDS,[15,17] potentially due to the protective effects of certain medications used in these conditions. However, our analysis did not find a statistically significant association, which may be attributed to variations in study designs, populations and methodologies.

The significant association between COPD and ARDS risk in sepsis patients aligns with previous research indicating that preexisting pulmonary diseases may predispose patients to more severe lung injury when faced with a systemic inflammatory condition like sepsis.[8,21] The differential impact of comorbidities on ARDS development in sepsis patients offers valuable insights into the complex pathophysiology of ARDS. Understanding these interactions is crucial for developing targeted therapeutic strategies. The absence of significant associations with certain comorbidities may also point to different underlying mechanisms of lung injury or protective factors that warrant further investigation.

The pathogenesis behind the increased risk of ARDS in sepsis patients with COPD could be attributed to several factors. Chronic obstructive pulmonary disease is characterized by chronic inflammation and structural changes in the lungs, which could exacerbate the pulmonary response to sepsis.[22] Additionally, COPD patients often have a compromised immune response, making them more susceptible to severe infections and complications.[22]

For other comorbidities, the lack of significant association might be influenced by various mechanisms. For instance, in DM, hyperglycemia-related immune dysfunction could potentially balance the risk of developing ARDS.[7] Similarly, in conditions like HTN and CAD, the chronic use of medications such as ACE inhibitors and statins might offer some protective effect against ARDS development.[23]

One of the main strengths of this study is its comprehensive approach, including a wide range of comorbidities and a large sample size. The use of rigorous statistical methods, such as the random-effects model and sensitivity analyses, also adds to the robustness of our findings. None of the studies had a higher risk of bias, further enhancing the credibility of the findings. The main limitation of the review is that a substantial amount of data was obtained from a single study.[18] However, our additional sensitivity analysis demonstrated no significant differences in the estimates for any of the outcomes.

The findings of this study have important clinical implications. Understanding the comorbidities associated with an increased risk of ARDS in sepsis patients can aid in risk stratification and personalized management strategies. Particularly, the identification of COPD as a significant risk factor highlights the need for careful monitoring and possibly more aggressive treatment in sepsis patients with this comorbidity. This result also calls for a multidisciplinary approach involving pulmonologists and intensivists to optimize patient outcomes. In contrast, for comorbidities where no significant association was found, such as DM and HTN, our findings suggest that the current standard of care in sepsis management remains appropriate, although overall, they do underscore the need for individualized patient care.

Future research should focus on further elucidating the mechanisms behind the relationship between different comorbidities and ARDS risk in sepsis patients. There is also a need for more standardized, large-scale studies to confirm these findings, and explore the impact of other potential risk factors. Longitudinal studies examining the long-term outcomes of ARDS in sepsis patients with various comorbidities would also be valuable. The integration of biomarkers that assess the risk of ARDS in sepsis patients is another promising area of research. Identifying specific biomarkers associated with ARDS risk in the presence of various comorbidities could enhance early diagnosis and allow for more targeted interventions. Therefore, prospective studies investigating the role of inflammatory, genetic and other biomarkers in predicting ARDS in sepsis patients are needed.

Limitations

There are several limitations to consider. The presence of publication bias, as indicated by the Doi plot and LFK index in some comorbidities, suggests that our results should be interpreted with caution. Additionally, the variability in study designs, populations and definitions of comorbidities across the included studies might have influenced the outcomes. The moderate-to-high heterogeneity observed in some analyses also underscores the need for more standardized research in this area.

Conclusions

Among the various comorbidities studied, only COPD significantly increased the risk of ARDS in sepsis patients. This underscores the complexity of ARDS pathogenesis and highlights the importance of considering individual patient characteristics, including comorbidities, in the management of sepsis. These findings provide valuable insights for clinicians in the risk assessment and treatment planning for sepsis patients.

Supplementary files

The Supplementary materials are available at https://doi.org/10.5281/zenodo.13203473. The package includes the following files:

Supplementary Fig. 1. Doi plot for DM and risk of ARDS in sepsis patients.

Supplementary Fig. 2. Funnel plot for DM and risk of ARDS in sepsis patients.

Supplementary Fig. 3. Funnel plot for HTN and risk of ARDS in sepsis patients.

Supplementary Fig. 4. Funnel plot for COPD and risk of ARDS in sepsis patients.

Supplementary Fig. 5. Doi plot for COPD and risk of ARDS in sepsis patients.

Supplementary Fig. 6. Funnel plot for CAD and risk of ARDS in sepsis patients.

Supplementary Fig. 7. Doi plot for CAD and risk of ARDS in sepsis patients.

Supplementary Fig. 8. Funnel plot for CHF and risk of ARDS in sepsis patients.

Supplementary Fig. 9. Funnel plot for CKD and risk of ARDS in sepsis patients.

Supplementary Fig. 10. Doi plot for CKD and risk of ARDS in sepsis patients.

Supplementary Fig. 11. Funnel plot for CLD and risk of ARDS in sepsis patients.

Supplementary Fig. 12. Doi plot for CLD and risk of ARDS in sepsis patients.

Supplementary Fig. 13. Funnel plot for Cancer and risk of ARDS in sepsis patients.

Supplementary Fig. 14. Doi plot for cancer and risk of ARDS in sepsis patients.

Data availability

The datasets generated and/or analyzed during the current study are available from the corresponding author on reasonable request.

Consent for publication

Not applicable.

Use of AI and AI-assisted technologies

Not applicable.

ORCID iDs

Xin Lin https://orcid.org/0000-0002-6066-5835
Yang Liu https://orcid.org/0009-0001-5355-9057
Li Kong https://orcid.org/0000-0002-1741-9655
Tejin Ba https://orcid.org/0009-0008-8792-3399
Bagenna Bao https://orcid.org/0009-0000-9386-7030
Shuanglin Zhang https://orcid.org/0009-0005-3942-3363
Weihong Liu https://orcid.org/0009-0004-5558-9921

References

1. Diamond M, Peniston HL, Sanghavi DK, Mahapatra S. Acute respiratory distress syndrome. In: *StatPearls*. Treasure Island, USA: StatPearls Publishing; 2024:Bookshelf ID: NBK436002. http://www.ncbi.nlm.nih.gov/books/NBK436002. Accessed August 19, 2024.
2. Wang Y, Zhang L, Xi X, Zhou JX; The China Critical Care Sepsis Trial (CCCST) Workgroup. The association between etiologies and mortality in acute respiratory distress syndrome: A multicenter observational cohort study. *Front Med (Lausanne)*. 2021;8:739596. doi:10.3389/fmed.2021.739596
3. Bellani G, Laffey JG, Pham T, et al. Epidemiology, patterns of care, and mortality for patients with acute respiratory distress syndrome in intensive care units in 50 countries. *JAMA*. 2016;315(8):788. doi:10.1001/jama.2016.0291
4. Rezoagli E, McNicholas BA, Madotto F, et al. Presence of comorbidities alters management and worsens outcome of patients with acute respiratory distress syndrome: Insights from the LUNG SAFE study. *Ann Intensive Care*. 2022;12(1):42. doi:10.1186/s13613-022-01015-7
5. Hoang T, Tran Thi Anh T. Comparison of comorbidities in relation to critical conditions among coronavirus disease 2019 patients: A network meta-analysis. *Infect Chemother*. 2021;53(1):13. doi:10.3947/ic.2020.0136
6. Xu H, Sheng S, Luo W, Xu X, Zhang Z. Acute respiratory distress syndrome heterogeneity and the septic ARDS subgroup. *Front Immunol*. 2023;14:1277161. doi:10.3389/fimmu.2023.1277161
7. Yu S, Christiani DC, Thompson BT, Bajwa EK, Gong MN. Role of diabetes in the development of acute respiratory distress syndrome. *Crit Care Med*. 2013;41(12):2720–2732. doi:10.1097/CCM.0b013e318298a2eb
8. Shi Y, Wang L, Yu S, Ma X, Li X. Risk factors for acute respiratory distress syndrome in sepsis patients: A retrospective study from a tertiary hospital in China. *BMC Pulm Med*. 2022;22(1):238. doi:10.1186/s12890-022-02015-w
9. Banavasi H, Nguyen P, Osman H, Soubani AO. Management of ARDS: What works and what does not. *Am J Med Sci*. 2021;362(1):13–23. doi:10.1016/j.amjms.2020.12.019
10. Lo CKL, Mertz D, Loeb M. Newcastle–Ottawa Scale: Comparing reviewers' to authors' assessments. *BMC Med Res Methodol*. 2014;14(1):45. doi:10.1186/1471-2288-14-45
11. Cumpston M, Li T, Page MJ, et al. Updated guidance for trusted systematic reviews: A new edition of the Cochrane Handbook for Systematic Reviews of Interventions. *Cochrane Database Syst Rev*. 2019;10(10):ED000142. doi:10.1002/14651858.ED000142
12. Furuya-Kanamori L, Barendregt JJ, Doi SAR. A new improved graphical and quantitative method for detecting bias in meta-analysis. *Int J Evid Based Healthc*. 2018;16(4):195–203. doi:10.1097/XEB.0000000000000141
13. Iriyama H, Abe T, Kushimoto S, et al; on behalf of JAAM FORECAST group. Risk modifiers of acute respiratory distress syndrome in patients with non-pulmonary sepsis: A retrospective analysis of the FORECAST study. *J Intensive Care*. 2020;8(1):7. doi:10.1186/s40560-020-0426-9
14. Li S, Zhao D, Cui J, Wang L, Ma X, Li Y. Prevalence, potential risk factors and mortality rates of acute respiratory distress syndrome in Chinese patients with sepsis. *J Int Med Res*. 2020;48(2):030006051989565. doi:10.1177/0300060519895659

15. Mikkelsen ME, Shah CV, Meyer NJ, et al. The epidemiology of acute respiratory distress syndrome in patients presenting to the emergency department with severe sepsis. *Shock*. 2013;40(5):375–381. doi:10.1097/SHK.0b013e3182a64682
16. Nam H, Jang SH, Hwang YI, Kim JH, Park JY, Park S. Nonpulmonary risk factors of acute respiratory distress syndrome in patients with septic bacteraemia. *Korean J Intern Med*. 2019;34(1):116–124. doi:10.3904/kjim.2017.204
17. Seethala RR, Hou PC, Aisiku IP, et al. Early risk factors and the role of fluid administration in developing acute respiratory distress syndrome in septic patients. *Ann Intensive Care*. 2017;7(1):11. doi:10.1186/s13613-017-0233-1
18. Xu C, Zheng L, Jiang Y, Jin L. A prediction model for predicting the risk of acute respiratory distress syndrome in sepsis patients: A retrospective cohort study. *BMC Pulm Med*. 2023;23(1):78. doi:10.1186/s12890-023-02365-z
19. Gong MN, Thompson BT, Williams P, Pothier L, Boyce PD, Christiani DC. Clinical predictors of and mortality in acute respiratory distress syndrome: Potential role of red cell transfusion. *Crit Care Med*. 2005;33(6):1191–1198. doi:10.1097/01.CCM.0000165566.82925.14
20. Mayow AH, Ahmad F, Afzal MS, et al. A systematic review and meta-analysis of independent predictors for acute respiratory distress syndrome in patients presenting with sepsis. *Cureus*. 2023;15(4):e37055. doi:10.7759/cureus.37055
21. Dvorščak MB, Lupis T, Adanić M, Šarić JP. Acute respiratory distress syndrome and other respiratory disorders in sepsis [in Croatian]. *Acta Med Croatica*. 2015;69(3):167–175. PMID:29077373.
22. Agarwal AK, Raja A, Brown BD. Chronic obstructive pulmonary disease. In: *StatPearls*. Treasure Island, USA: StatPearls Publishing; 2024:Bookshelf ID: NBK559281. http://www.ncbi.nlm.nih.gov/books/NBK559281. Accessed August 19, 2024.
23. Jeffery MM, Cummins NW, Dempsey TM, Limper AH, Shah ND, Bellolio F. Association of outpatient ACE inhibitors and angiotensin receptor blockers and outcomes of acute respiratory illness: A retrospective cohort study. *BMJ Open*. 2021;11(3):e044010. doi:10.1136/bmjopen-2020-044010

Systematic review and meta-analysis of randomized controlled trials comparing the clinical outcomes of SARS-CoV-2 and influenza in pediatric patients

Chiqiong Liu[A,B,E,F], Fengying He[A,C,D]

School of Medicine, Hunan Polytechnic College of Environment and Biology, Hengyang, China

A – research concept and design; B – collection and/or assembly of data; C – data analysis and interpretation;
D – writing the article; E – critical revision of the article; F – final approval of the article

Advances in Clinical and Experimental Medicine, ISSN 1899–5276 (print), ISSN 2451–2680 (online) *Adv Clin Exp Med*. 2025;34(8):1267–1276

Address for correspondence
Chiqiong Liu
E-mail: cliu03@outlook.com

Funding sources
None declared

Conflict of interest
None declared

Received on March 14, 2024
Reviewed on June 19, 2024
Accepted on August 11, 2024

Published online on January 3, 2025

Abstract

Only a few studies have examined the effects of coronavirus disease 2019 (COVID-19) and influenza on clinical outcomes in pediatric patients. Furthermore, no meta-analysis has assessed the impact of these diseases on adverse outcomes. This study aims to compare the clinical outcomes of COVID-19 and influenza in pediatric patients. Searches were conducted from December 2019 to February 2022 in databases including Embase, Scopus, PubMed Central (PMC), MEDLINE, Google Scholar, Cochrane Library, and ScienceDirect. Our meta-analysis used a random-effects model, reporting pooled odds ratios (ORs) or standardized mean differences with 95% confidence intervals (95% CIs). Thirteen studies meeting the inclusion criteria were analyzed. Most studies had poor quality. The pooled OR was 0.13 for oxygen requirement (95% CI: 0.04–0.45; $I^2 = 74\%$) and 0.03 for steroid requirement (95% CI: 0.01–0.19; $I^2 = 60.8\%$). No significant differences were found in outcomes such as intensive care unit (ICU) admission, duration of inpatient stay, invasive/non-invasive ventilation, death, acute respiratory distress syndrome (ARDS), and acute kidney injury (AKI). SARS-CoV-2 infection was comparable to influenza regarding mortality, pediatric intensive care unit (PICU) admissions, mechanical ventilation, and AKI incidence, but with notable differences in oxygen supplementation.

Key words: COVID-19, SARS-CoV, meta-analysis, pediatrics, influenza

Cite as
Liu C, Fengying He F. Systematic review and meta-analysis of randomized controlled trials comparing the clinical outcomes of SARS-CoV-2 and influenza in pediatric patients. *Adv Clin Exp Med*. 2025;34(8):1267–1276. doi:10.17219/acem/192224

DOI
10.17219/acem/192224

Copyright
Copyright by Author(s)
This is an article distributed under the terms of the Creative Commons Attribution 3.0 Unported (CC BY 3.0) (https://creativecommons.org/licenses/by/3.0/)

Introduction

In recent years, public health experts have been anticipating the potential emergence of a highly contagious respiratory virus with the capacity to cause a pandemic.[1] Upon the emergence of severe acute respiratory syndrome coronavirus 2 (SARS-CoV-2) in late 2019, a prompt comparison was made between this virus and both seasonal and pandemic influenza viruses due to the notable similarities exhibited by these viral entities. The disease conditions induced by both of these viruses exhibit comparable clinical manifestations, including symptoms such as fever and respiratory distress. These symptoms range from milder forms, such as cough and sore throat, to more severe manifestations, including lung infections.[2,3] Both SARS-CoV-2 and influenza viruses have comparable modes of transmission, as they can be spread through respiratory droplets, facilitating efficient human-to-human transmission.[3,4] SARS-CoV-2 and influenza are preventable through vaccination.[2] Although the vaccine may be less effective in older individuals, it can make the illness less severe and reduce the chance of complications and death.

The clinical manifestations of hospitalized patients with SARS-CoV-2 and seasonal influenza exhibit significant differences.[5] There is a high risk of SARS-CoV-2 infection in children of all ages, but the disease typically manifests in a mild manner and usually does not cause lasting consequences. Critical illness and death from SARS-CoV-2 in children are extremely rare.[6] Among SARS-CoV-2 patients, the primary mode of treatment is mostly supportive, although several experimental antiviral medications are currently being evaluated.[7] Prevention, timely judgment and adequate supervision of pediatric patients infected with influenza are crucial. In contrast, there is a lack of pediatric data comparing influenza and SARS-CoV-2. Newer and more severe forms of clinical expressions related to SARS-CoV-2 are continually developing in the pediatric age group. However, to the best of our knowledge, earlier published meta-analyses did not compare the clinical outcomes between SARS-CoV-2 and influenza, specifically in pediatric patients.

Objectives

The main objective of the current study was to compare the clinical outcomes between influenza and SARS-CoV-2 patients in the pediatric age group.

Materials and methods

Study participants

Studies containing both influenza and SARS-CoV-2 patients in the pediatric age group (<18 years) as a separate group were included.

Outcomes

The included outcomes were as follows: mortality,, intensive care unit (ICU) admission, necessity for mechanical ventilation (invasive and non-invasive), sepsis, oxygen requirement, acute kidney injury (AKI), steroid requirement, acute respiratory distress syndrome (ARDS), and duration of inpatient stay.

Study design

Prospective and retrospective observational study designs were eligible. Full-text studies were included. Research questions were framed in the PICO (P – patients, I – intervention; C – comparator; O – outcome) format as follows: P: influenza and SARS-CoV-2 patients in the pediatric age group; I: none; C: non-influenza and SARS-CoV-2 patients in the pediatric age group; O: mortality, ICU admission, necessity for mechanical ventilation (invasive and non-invasive), sepsis, oxygen requirement, AKI, steroid requirement, ARDS, and duration of inpatient stay.

Information sources and search strategy

A thorough and rigorous literature review was conducted by systematically searching multiple databases, including Embase, Scopus, PubMed Central, Cochrane Library, MEDLINE, Google Scholar, and ScienceDirect. Our search strategy included Medical Subject Headings and free-text terms with Boolean operators ("AND" & "OR"). An additional English-language filter and a time point restriction from December 2019 to February 2022 were applied. Terms referring to children and SARS-CoV-2 or influenza were used, with the complete list available in the Supplementary data.

Selection process

The initial phase of study selection was conducted by 2 independent investigators (C.L. and F.H.), who screened titles, keywords and abstracts. Duplicates (same study available in different databases) were identified and excluded. Both investigators collected the full-text studies and subsequently narrowed down the selection for the next round of screening, considering the predetermined eligibility criteria. Any inconsistencies during the initial phase were resolved through mutual agreement between these 2 investigators. During the 2nd phase, the same 2 investigators (C.L. and F.H.) reviewed the retrieved full texts. Only eligible studies were selected for further analysis. The review employed the Preferred Reporting Items for Systematic Reviews and Meta-Analyses (PRISMA) checklist 2020 for guidance.[8] Conflicting assessments were resolved after discussion among authors.

Data collection process and data items

Following the completion of the selection process for relevant full-text articles to be included and analyzed in the review, the 2 above authors actively participated in the manual extraction of data to obtain information such as authors' details, study title, publication year, study period and duration, design, setting, country, sample size, outcome details, and mean age of the participants.

Risk of bias assessment

Two authors (C.L. and F.H.) assessed the risk of bias using the Newcastle-Ottawa scale for observational studies, which includes selection, comparability and outcome domains. Studies with scores between 7–8 stars were considered of "good" quality, 5–6 stars indicated "satisfactory" quality and 0–4 stars indicated "unsatisfactory" quality.[9]

Statistical analyses (synthesis methods, effect measures, reporting bias assessment)

This meta-analysis was conducted using the Metafor R package (R Foundation for Statistical Computing, Vienna, Austria). The binary outcomes were assessed by inputting the number of events and sample size for each group, and the combined effect was presented as the pooled odds ratio (OR) with a 95% confidence interval (95% CI).

The model selection was based on the variation among the studies in terms of study design, sample size, type of participants, methodology, etc. The random effects model was applied. Heterogeneity was evaluated using a χ^2 test, and the level of inconsistency was quantified using the I^2 statistic. $I^2 < 25\%$ indicated mild heterogeneity, I^2 between 25% and 75% indicated moderate heterogeneity, and $I^2 > 75\%$ indicated substantial heterogeneity.[10] Forest plots showed the study-specific and pooled estimates. Sensitivity analysis was performed to determine whether the pooled estimate varied after removing studies one by one in the analysis. This ensured the robustness of the estimates and assessed the possibility of any small study effects. Publication bias was assessed for outcomes with at least 10 studies.

Results

Study selection

A total of 1,120 items were found. Of these, 801 studies were excluded for various reasons, such as not involving either SARS-CoV-2 or influenza patients, review articles, case reports, case series, systematic literature reviews, meta-analyses, formulation development for SARS-CoV-2 and influenza patients, as well as analytical studies. Finally, 99 studies were deemed relevant, and full texts were obtained. A final consensus was reached to include 13 studies with a total of 18,516 participants (Fig. 1 and Table 1) after screening against the eligibility criteria.[11–23]

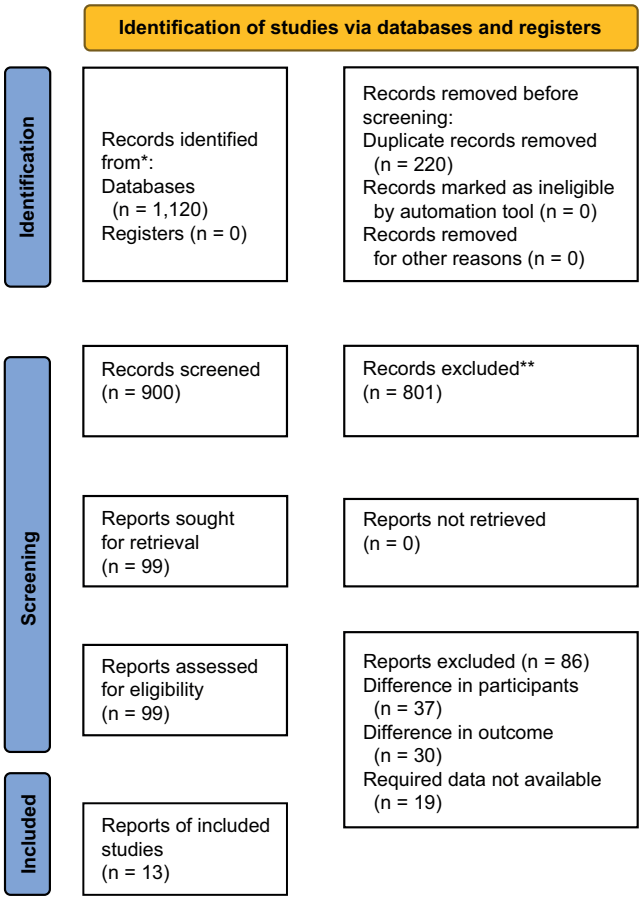


Fig. 1. Selection of studies according to the Preferred Reporting Items for Systematic Reviews and Meta-Analysis (PRISMA) guidelines

Characteristics of the included studies

Almost all analyzed studies (except Pokorska-Śpiewak et al.)[18] were retrospective. Most studies were conducted in China (3 studies) and Turkey (3 studies). Sample sizes varied from 47 to 10,169. The average age in the SARS-CoV-2 group ranged from 12 to 128 months, and in the influenza group from 16 to 112 months. Most studies involved both influenza A and B patients. All studies were found to be of fair and good quality, as indicated in Table 1.

Admission to Intensive Care Unit

Eight studies compared ICU admission rates between SARS-CoV-2 and influenza patients in the pediatric age group. The pooled OR was found to be 1.26 [0.86, 1.86], indicating no significant difference between pediatric patients with SARS-CoV-2 and those with influenza (Fig. 2A). However, heterogeneity among studies was high, as indicated by the I^2 statistic. Cochran's Q test ($p < 0.01$) and

Table 1. Newcastle-Ottawa Quality Assessment

Study & year	Selection	Comparability	Outcome	Total score	Quality of the study
Akkoc et al., 2021[11]	*	**	***	6	fair
Asseri et al., 2021[12]	**	*	***	6	fair
Hedberg et al., 2021[13]	***	**	**	7	good
Laris-Gonzaiez et al., 2021[14]	**	**	**	6	fair
Li et al., 2020[15]	***	**	**	7	good
Liu et al., 2021[16]	***	**	**	7	good
Piroth et al., 2021[17]	***	**	***	8	good
Pokorska et al., 2021[18]	***	**	***	8	good
Siddiqui et al., 2021[19]	***	**	***	8	good
Song et al., 2020[20]	**	**	***	7	good
Sousa et al., 2020[21]	**	**	**	6	fair
Yilmaz et al., 2021[22]	***	**	***	8	good
Zhao et al., 2020[23]	***	**	**	7	good

χ^2 test (p = 0.161) also indicated significant heterogeneity among the studies. Therefore, a sensitivity analysis was conducted.

The sensitivity analysis results showed the impact of high sample size studies on the outcome (Fig. 3A). The heterogeneity among studies was found to decrease. Furthermore, no significant difference between pediatric patients with SARS-CoV-2 and influenza was observed even after the removal of both high sample size studies,[17,21] as shown in Fig. 3. A symmetrical funnel plot and Begg's test (p = 0.322) (Supplementary Fig. 1) both indicated that there was no substantial publication bias.

Mechanical ventilation (invasive/non-invasive)

Four investigations revealed differences in the need for mechanical ventilation between children with SARS-CoV-2 and those with influenza. No significant difference was observed between pediatric patients with SARS-CoV-2 and those with influenza, as indicated by the pooled OR of 1.41 (95% CI: 0.74–2.67; I^2 = 84%) (Fig. 3A). The heterogeneity among studies decreased from 84% to 67%, as shown in Fig. 3A,B. The Cochran's Q and χ^2 tests (p = 0.303) also indicated significant heterogeneity among the studies. Sensitivity analysis results showed no impact on the conclusion (Fig. 3B). A symmetrical funnel plot and Begg's test (p = 0.497) (Supplementary Fig. 2) both indicated no substantial publication bias.

Invasive mechanical ventilation

Three studies compared the requirement for invasive mechanical ventilation between pediatric influenza and SARS-CoV-2 cases. The pooled OR was 1.34 (95% CI: 0.51–3.48), indicating no significant difference in the need for invasive mechanical ventilation between pediatric influenza and SARS-CoV-2 patients (Fig. 4). Cochran's Q test (p < 0.01) and χ^2 tests (p = 0.447) also indicated significant heterogeneity among the studies. Sensitivity analysis was not performed due to the availability of only 2 studies. The funnel plot indicated minimal publication bias (Supplementary Fig. 3).

Non-invasive mechanical ventilation

Two studies compared the requirement for noninvasive mechanical ventilation between SARS-CoV-2 and influenza patients in the pediatric age group. The pooled OR was 1.34 (95% CI: 0.51–3.48; I^2 = 93%), indicating no significant difference between pediatric patients with SARS-CoV-2 and those with influenza (Fig. 4). Cochran's Q test (p < 0.01) and χ^2 tests (p = 0.447) also indicated significant heterogeneity among the studies. Due to the limited number of studies, sensitivity analysis could not be performed. The funnel plot indicated minimal publication bias (Supplementary Fig. 4).

Oxygen requirement

Four investigations compared oxygen requirements between the 2 groups. The pooled OR was 0.34 (95% CI: 0.11–1.06; I^2 = 0%), showing no significant differences (Fig. 5A). Cochran's Q test (p = 0.61) and χ^2 test also indicated nonsignificant heterogeneity among studies. Sensitivity analysis results showed no impact of outliers on the study outcome, as shown in Fig. 5B. The funnel plot indicated minimal publication bias (Supplementary Fig. 5).

Steroid requirement

Two investigations examined the difference in steroid requirements between SARS-CoV-2 and influenza patients

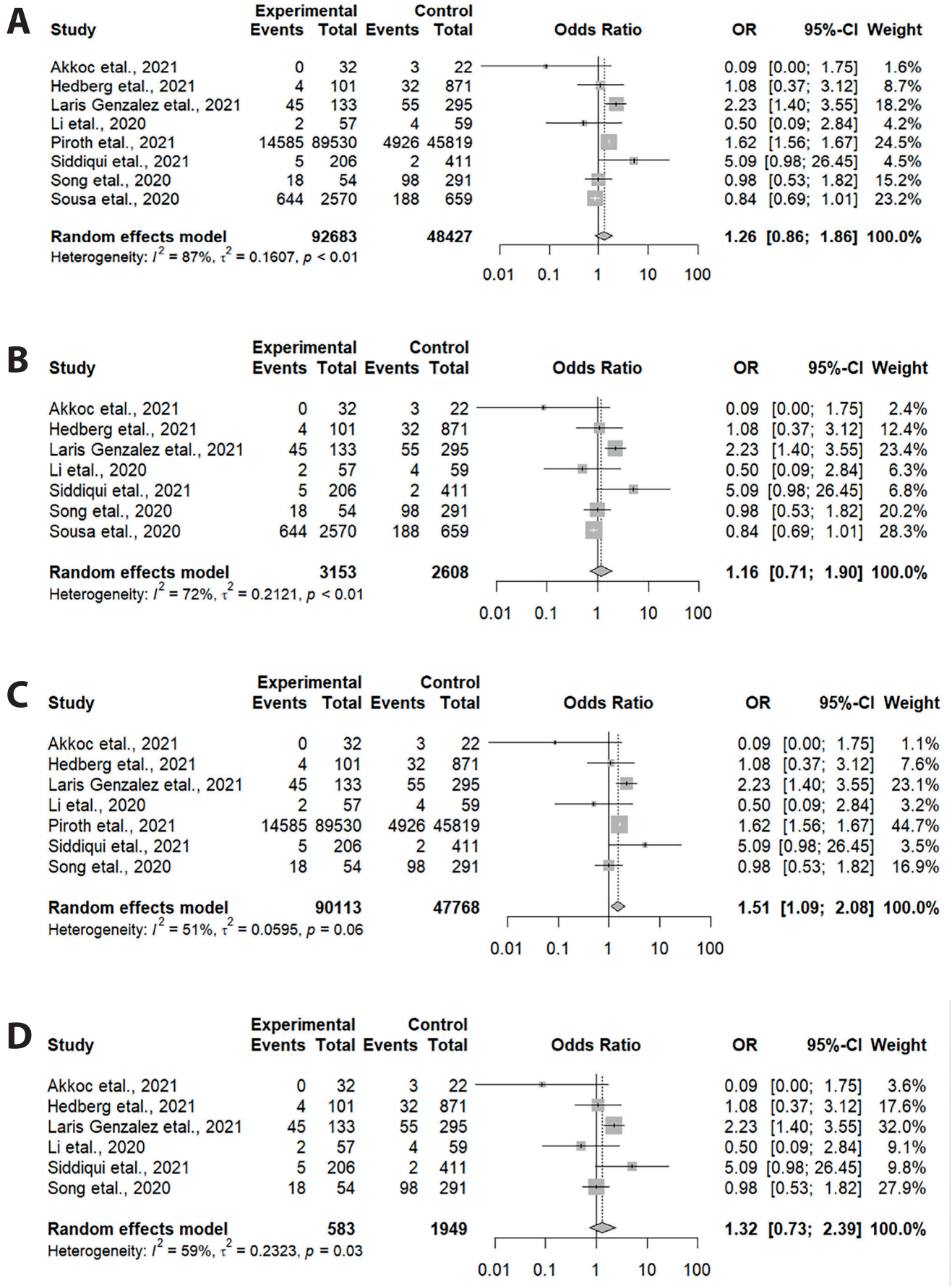


Fig. 2. Sensitivity analysis. A. Mechanical ventilation; B. After removal of Piroth et al.[17]; C. After removal of Sousa et al.[21]; D. After removal of Piroth et al.[17] and Sousa et al.[21]

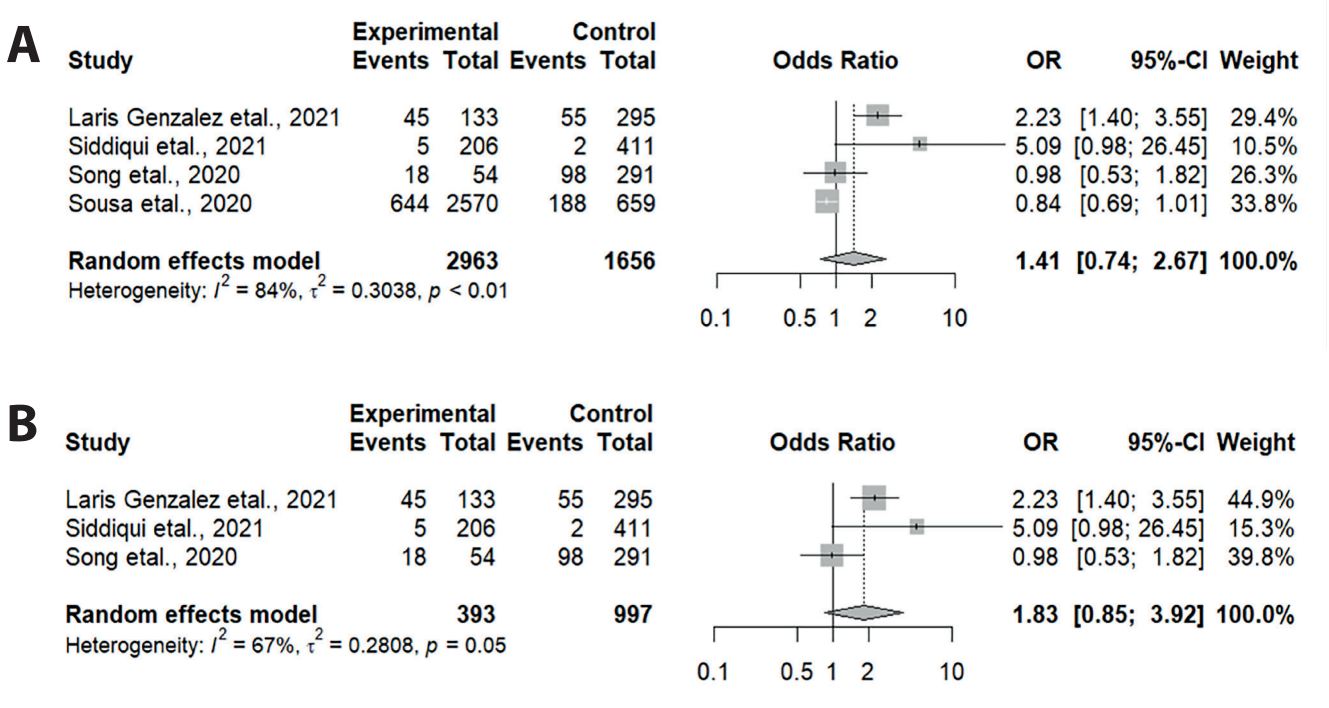


Fig. 3. Sensitivity analysis. A. Mechanical ventilation; B. After removal of Sousa et al.[21]

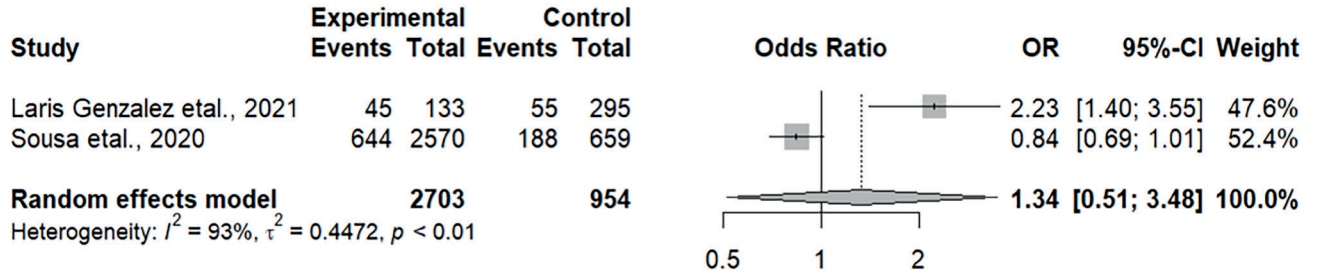


Fig. 4. Sensitivity analysis. A. Invasive mechanical ventilation; B. Non-invasive mechanical ventilation

in the pediatric age group. The pooled OR was 0.56 (95% CI: 0.06–5.31; I^2 = 92%), indicating no significant differences (Fig. 6A). Cochran's Q test ($p < 0.01$) and χ^2 test (2.451) also indicated significant heterogeneity among studies. Sensitivity analysis was not performed due to the limited number of studies.

Acute kidney injury

Four studies compared AKI between SARS-CoV-2 and influenza patients in the pediatric age group. The pooled OR was 1.31 (95% CI: 0.84–2.04; I^2 = 94%), indicating no significant difference between influenza and SARS-CoV-2 pediatric patients (Fig. 6B). Cochran's Q test ($p < 0.01$) and χ^2 test (0.168) also indicated significant heterogeneity among studies. Sensitivity analysis results showed no significant impact on the outcome, as shown in Fig. 7A–C. The symmetrical funnel plot and Begg's test ($p = 0.497$) (Supplementary Fig. 7) both indicated no substantial publication bias.

Mortality

Seven studies reported on the difference in mortality between influenza and SARS-CoV-2 pediatric patients. The pooled OR was 1.16 (95% CI: 0.71–1.90; I^2 = 72%), indicating no difference between pediatric patients with SARS-CoV-2 and those with influenza (Fig. 8A). Cochran's Q test ($p < 0.01$) and χ^2 test ($p = 0.212$) also indicated significant heterogeneity among studies. The symmetrical funnel plot (Supplementary Fig. 8) suggested significant publication bias (Begg's $p = 0.652$). Sensitivity analysis results showed no impact of outliers on the outcome, as shown in Fig. 8B.

Discussion

Coronavirus disease 2019 (COVID-19) is a novel disease caused by a newly identified virus, SARS-CoV-2. It is a positive-sense single-stranded RNA virus that mainly affects the respiratory system.[24,25] Influenza and

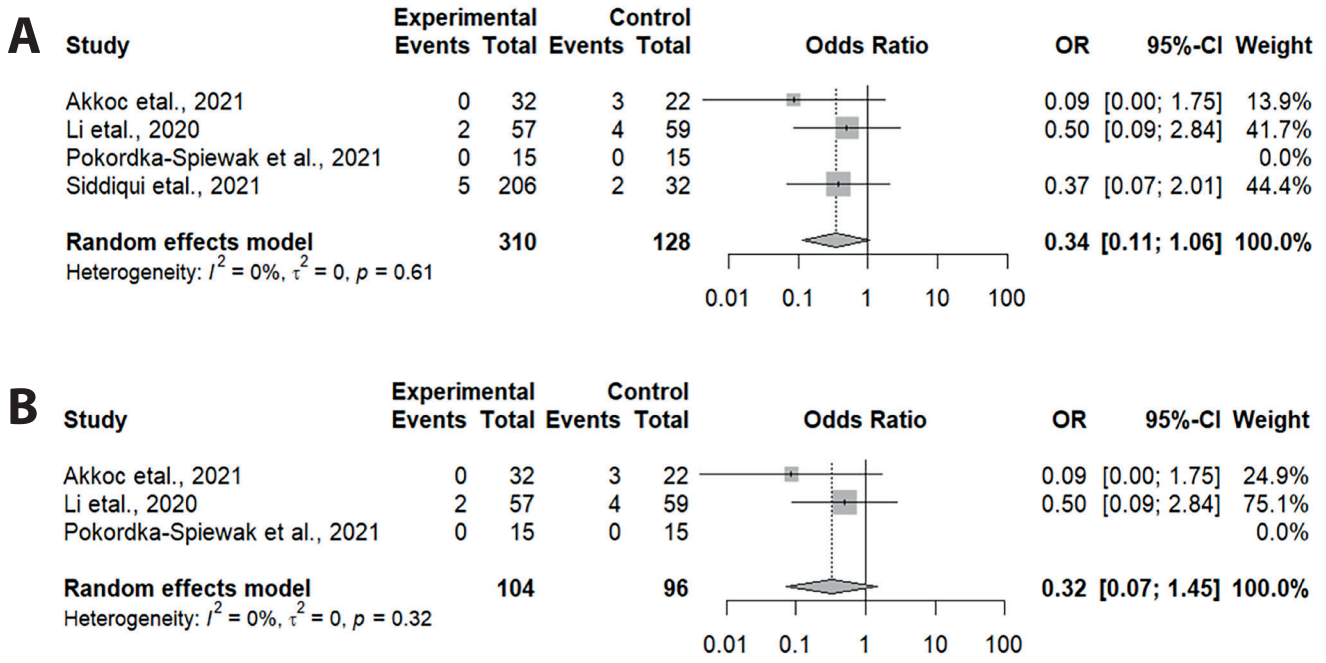


Fig. 5. Sensitivity analysis. A. Oxygen requirement; B. After removal of Siddiqui et al.[19]

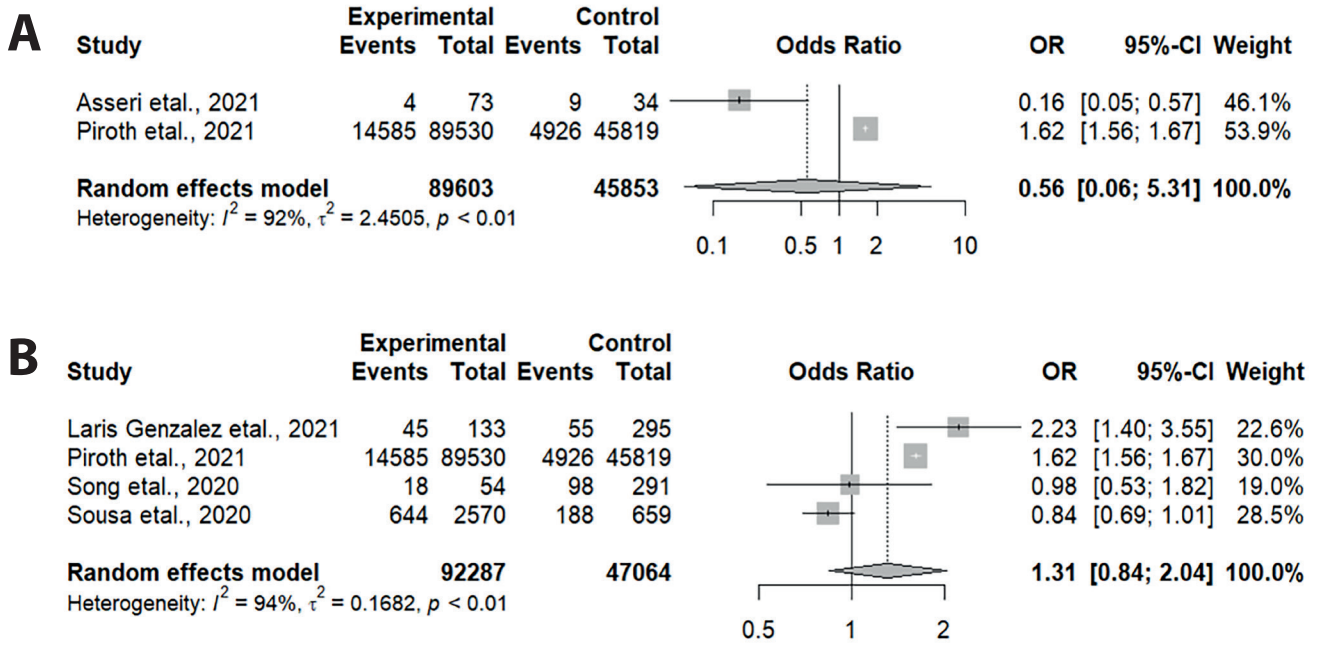


Fig. 6. Sensitivity analysis. A. Steroid requirement; B. Acute kidney injury (AKI)

SARS-CoV-2 are both preventable via vaccination.[26–28] While numerous experimental antiviral medications are presently undergoing assessment, supportive care remains the predominant approach for managing SARS-CoV-2 patients.[29] In this evaluation, we compared SARS-CoV-2 patients with influenza patients of all ages to assess the relative risk of several adverse clinical outcomes in terms of severity and complications. We have compiled 13 studies in total. China and Turkey topped the list of countries where these studies were performed, followed by Sweden, France and Poland. Except for the study by Pokorska-Śpiewak et al.,[18] all of the other research used a retrospective design, and the majority of them were highly at risk of bias.

A sensitivity analysis showed no significant change in effect magnitude. While no earlier pediatric case evaluations were available to compare with the present study, the reported results are consistent with previous pandemic

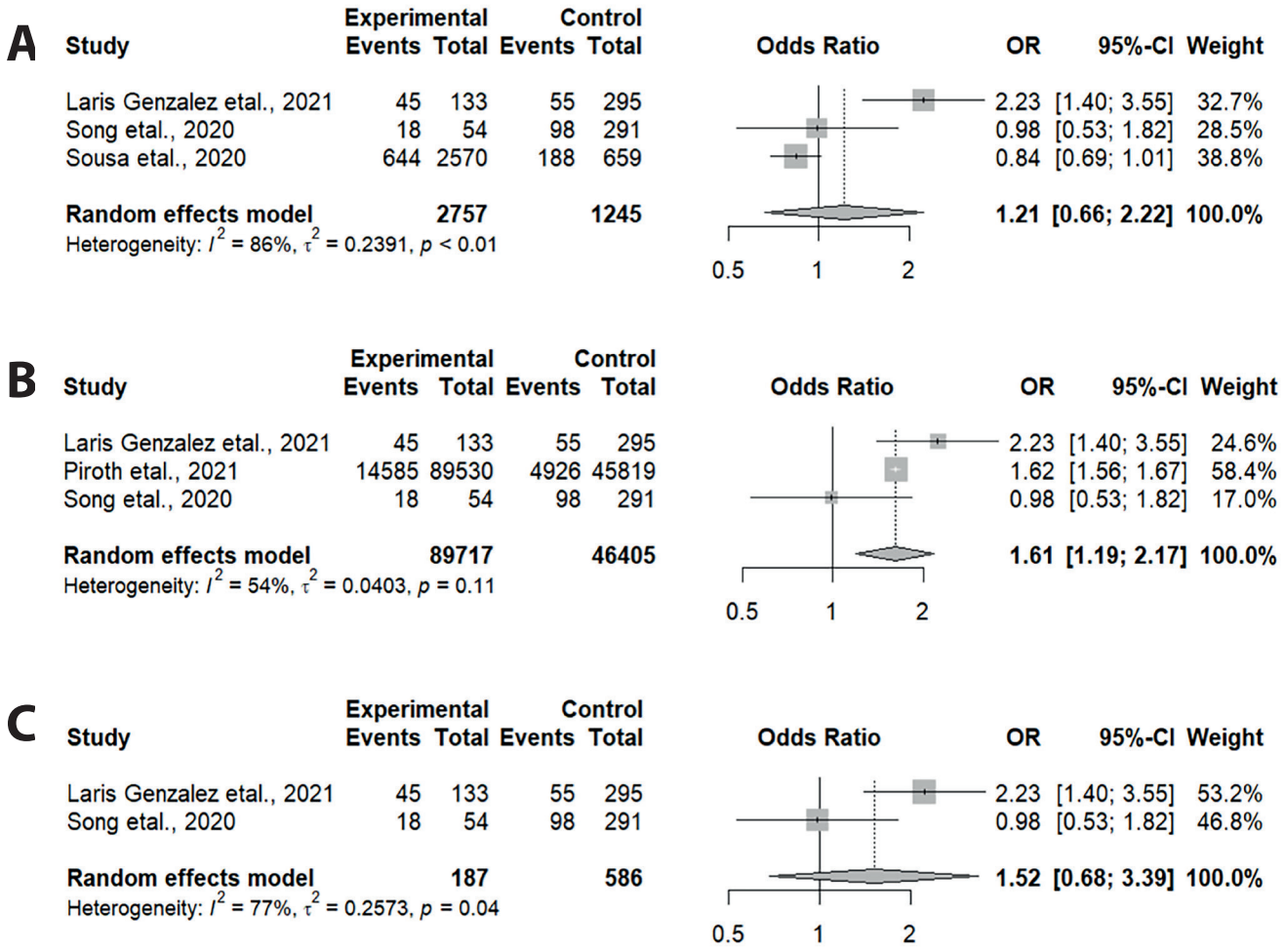


Fig. 7. Sensitivity analysis. A. After removal of Piroth et al.[17]; B. After removal of Sousa et al.[21]; C. After removal of Piroth et al.[17] and Sousa et al.[21]

infections.[29–30] The severity of the SARS-CoV-2 infection among pediatric patients was evidently different from that in adult patients.[31] This suggests that the pathogenicity of SARS-CoV-2 infection in children was similar to that of other severe respiratory illness-associated coronaviruses, such as Middle East Respiratory Syndrome Coronavirus (MERS-CoV) and SARS-CoV. Children with SARS/MERS coped better than adults with these illnesses.[32,33]

Other adverse clinical outcomes (death, ICU admission, mechanical ventilation, AKI, ARDS, and length of hospital stay) did not differ substantially between SARS-CoV-2 and influenza pediatric patients. However, previous studies on adult patients have found greater mortality and more frequent hospitalization and requirement for mechanical ventilation with late hospital discharge, particularly among individuals over the age of 50.[34–36] This could be due to related comorbidities such as diabetes, hypertension or heart disease among middle-aged and older adults, skewing the adverse outcome rates higher for SARS-CoV-2 patients. More longitudinal research into the outcomes of influenza and SARS-CoV-2 in pediatric patients is needed.

The review's major strengths are rigorous methodology and extensive investigation of the relevant literature. The evidence comparing the clinical outcomes of children with SARS-CoV-2 and children with influenza is scant, and this study fills a gap in that area. For any of the outcomes under evaluation, there was no discernible publication bias. The reliability of the findings may be enhanced as a result.

Limitations

The majority of the findings revealed a substantial amount of variation from one study to the next. This might influence the external validity (generalizability) of the study results. Virtually all of the studies were retrospective, making it challenging to establish a causal relationship. Therefore, longitudinal research is necessary for determining credible effect estimates and contributing to evidence-based recommendations for creating interventions in the hospital context. Most of the included studies lacked information about comorbidities, which play a substantial role in the outcomes of both infectious agents. Therefore, further studies are required to confirm the effects of comorbidities on clinical outcomes. We have considered only outcomes related to the respiratory system. Neurological

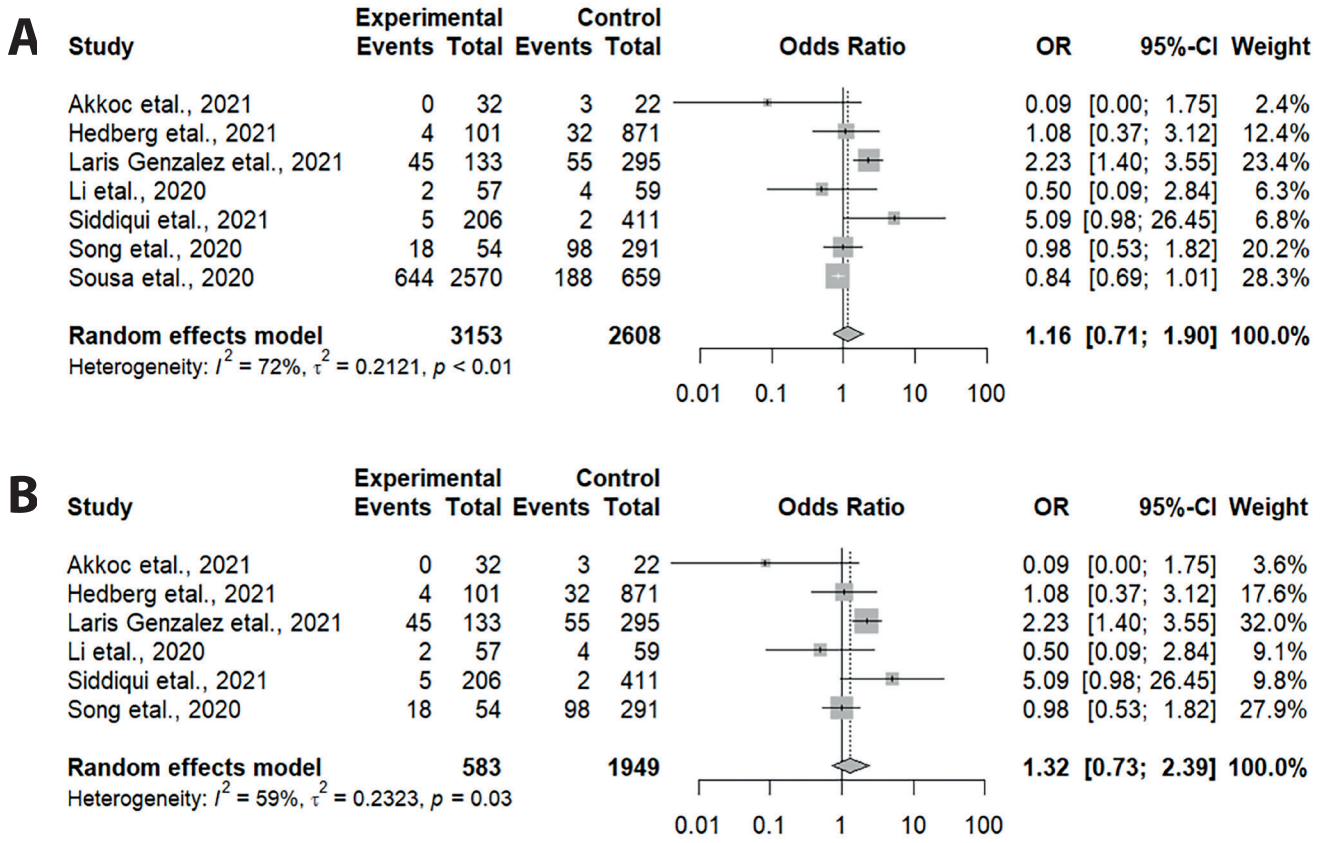


Fig. 8. Sensitivity analysis. A. Mortality; B. After removal of Sousa et al.[21]

outcomes, coagulation issues and other infection-related complications such as myocarditis, Guillain–Barré syndrome (GBS) or multisystem inflammatory syndrome in children (MIS-C) were not considered. There were differences in the results of studies including very young patients compared to older ones, which can produce predefined bias.

Conclusions

Based on our findings and experiences, SARS-CoV-2 infection is comparable to influenza in terms of mortality, pediatric intensive care unit (PICU) admissions, mechanical ventilation, and AKI incidence, with differences mainly observed in oxygen supplementation. Furthermore, the impact of influenza on specific age groups is influenced by the strain. The use of glucocorticoids also plays a significant role in the outcomes of both strains. Therefore, more large-scale and longitudinal studies are required to make a precise judgment on the severity of both of these diseases. The results of this investigation may provide preliminary evidence that SARS-CoV-2 infection may become permanently embedded in everyday life for many years to come (similar to influenza), particularly concerning the differences between these 2 conditions in terms of adverse clinical outcomes.

Supplementary data

The Supplementary materials are available at https://doi.org/10.5281/zenodo.13340768. The package includes the following files:

Supplementary Fig. 1. Symmetrical funnel plots and Begg's p = 0.322 show no publication bias.

Supplementary Fig. 2. Symmetrical funnel plots and Begg's p = 0.497 show no publication bias.

Supplementary Fig. 3. A funnel plot shows less publication bias for invasive mechanical ventilation.

Supplementary Fig. 4. A funnel plot shows less publication bias for noninvasive mechanical ventilation.

Supplementary Fig. 5. A funnel plot shows less publication bias for oxygen requirement.

Supplementary Fig. 6. A funnel plot shows less publication bias for steroid requirement.

Supplementary Fig. 7. A symmetrical funnel plot and Begg's p = 0.497 show no notable publication bias.

Supplementary Fig. 8. The symmetrical funnel plot indicated that there was significant publication bias (Begg's p = 0.652).

ORCID iDs

Chiqiong Liu https://orcid.org/0009-0009-7031-1553
Fengying He https://orcid.org/0009-0004-9411-9535

References

1. Mizumoto K, Kagaya K, Zarebski A, Chowell G. Estimating the asymptomatic proportion of coronavirus disease 2019 (COVID-19) cases on board the Diamond Princess cruise ship, Yokohama, Japan, 2020. *Euro Surveill*. 2020;25(10):2000180. doi:10.2807/1560-7917.ES.2020.25.10.2000180
2. Centers for Disease Control and Prevention (CDC). Similarities and differences between flu and COVID-19. Atlanta, USA: Centers for Disease Control and Prevention (CDC); 2021. https://www.cdc.gov/flu/symptoms/flu-vs-covid19.htm. Accessed January 3, 2022.
3. Bai Y, Yao L, Wei T, et al. Presumed asymptomatic carrier transmission of COVID-19. *JAMA*. 2020;323(14):1406. doi:10.1001/jama.2020.2565
4. Zhou F, Yu T, Du R, et al. Clinical course and risk factors for mortality of adult inpatients with COVID-19 in Wuhan, China: A retrospective cohort study [published correction appears in: *Lancet*. 2020;395(10229):1038]. *Lancet*. 2020;395(10229):1054–1062. doi:10.1016/S0140-6736(20)30566-3
5. Bai Y, Tao X. Comparison of COVID-19 and influenza characteristics. *J Zhejiang Univ Sci B*. 2021;22(2):87–98. doi:10.1631/jzus.B2000479
6. Liang H, Zhao L, Gong X, Hu M, Wang H. Virtual screening FDA approved drugs against multiple targets of SARS-CoV-2. *Clin Transl Sci*. 2021;14(3):1123–1132. doi:10.1111/cts.13007
7. He J, Hu L, Huang X, et al. Potential of coronavirus 3C-like protease inhibitors for the development of new anti-SARS-CoV-2 drugs: Insights from structures of protease and inhibitors. *Int J Antimicrob Agents*. 2020;56(2):106055. doi:10.1016/j.ijantimicag.2020.106055
8. Page MJ, McKenzie JE, Bossuyt PM, et al. The PRISMA 2020 statement: An updated guideline for reporting systematic reviews. *BMJ*. 2021;372:n71. doi:10.1136/bmj.n71
9. Wells GA, Shea B, O'Connell D, et al. The Newcastle-Ottawa Scale (NOS) for assessing the quality of nonrandomised studies in meta-analyses. Ottawa, Canada: Ottawa Hospital Research Institute; 2014. https://www.ohri.ca/programs/clinical_epidemiology/oxford.asp.
10. Cumpston M, Li T, Page MJ, et al. Updated guidance for trusted systematic reviews: A new edition of the Cochrane Handbook for Systematic Reviews of Interventions. *Cochrane Database Syst Rev*. 2019;10(10):ED000142. doi:10.1002/14651858.ED000142
11. Akkoç G, Ağbaş A, Selçuk Duru N. A comparison of clinical findings and laboratory test results between hospitalized children with COVID-19 and influenza. *J Pediatr Res*. 2021;8(4):432–437. doi:10.4274/jpr.galenos.2021.48751
12. Asseri AA, Shati AA, Al-Qahtani SM, et al. Distinctive clinical and laboratory features of COVID-19 and H1N1 influenza infections among hospitalized pediatric patients. *World J Pediatr*. 2021;17(3):272–279. doi:10.1007/s12519-021-00432-1
13. Hedberg P, Karlsson Valik J, Van Der Werff S, et al. Clinical phenotypes and outcomes of SARS-CoV-2, influenza, RSV and seven other respiratory viruses: A retrospective study using complete hospital data. *Thorax*. 2022;77(2):154–163. doi:10.1136/thoraxjnl-2021-216949
14. Laris-González A, Avilés-Robles M, Domínguez-Barrera C, et al. Influenza vs. COVID-19: Comparison of clinical characteristics and outcomes in pediatric patients in Mexico City. *Front Pediatr*. 2021;9:676611. doi:10.3389/fped.2021.676611
15. Li Y, Wang H, Wang F, et al. Comparison of hospitalized patients with pneumonia caused by COVID-19 and influenza A in children under 5 years. *Int J Infect Dis*. 2020;98:80–83. doi:10.1016/j.ijid.2020.06.026
16. Liu X, Li W, Zhang B, et al. Comparative study of hospitalized children with acute respiratory distress syndrome caused by SARS-CoV-2 and influenza virus. *BMC Infect Dis*. 2021;21(1):412. doi:10.1186/s12879-021-06068-w
17. Piroth L, Cottenet J, Mariet AS, et al. Comparison of the characteristics, morbidity, and mortality of COVID-19 and seasonal influenza: A nationwide, population-based retrospective cohort study. *Lancet Respir Med*. 2021;9(3):251–259. doi:10.1016/S2213-2600(20)30527-0
18. Pokorska-Śpiewak M, Talarek E, Popielska J, et al. Comparison of clinical severity and epidemiological spectrum between coronavirus disease 2019 and influenza in children. *Sci Rep*. 2021;11(1):5760. doi:10.1038/s41598-021-85340-0
19. Siddiqui M, Gültekingil A, Bakırcı O, Uslu N, Baskın E. Comparison of clinical features and laboratory findings of coronavirus disease 2019 and influenza A and B infections in children: A single-center study. *Clin Exp Pediatr*. 2021;64(7):364–369. doi:10.3345/cep.2021.00066
20. Song X, Delaney M, Shah RK, Campos JM, Wessel DL, DeBiasi RL. Comparison of clinical features of COVID-19 vs seasonal influenza A and B in US children. *JAMA Netw Open*. 2020;3(9):e2020495. doi:10.1001/jamanetworkopen.2020.20495
21. Sousa BLA, Sampaio-Carneiro M, De Carvalho WB, Silva CA, Ferraro AA. Differences among severe cases of SARS-CoV-2, influenza, and other respiratory viral infections in pediatric patients: Symptoms, outcomes and preexisting comorbidities. *Clinics (Sao Paulo)*. 2020;75:e2273. doi:10.6061/clinics/2020/e2273
22. Yılmaz K, Şen V, Aktar F, Onder C, Yılmaz ED, Yılmaz Z. Does COVID-19 in children have a milder course than influenza? *Int J Clin Pract*. 2021;75(9):e14466. doi:10.1111/ijcp.14466
23. Zhao Y, Sun DL, Bouchard HC, et al. Coronavirus disease 2019 versus influenza A in children: An observational control study in China. *Biomed Environ Sci*. 2020;33(8):614–619. doi:10.3967/bes2020.080
24. Kumar A, ed. *COVID-19 Current Challenges and Future Prospective*. Sharjah, UAE: Bentham Science Publishers; 2021. doi:10.2174/9789811 4986401210101
25. Vitalakumar D, Sharma A, Kumar A, Flora SJS. Neurological manifestations in COVID-19 patients: A meta-analysis. *ACS Chem Neurosci*. 2021;12(15):2776–2797. doi:10.1021/acschemneuro.1c00353
26. Rahman MdM, Masum MdHU, Wajed S, Talukder A. A comprehensive review on COVID-19 vaccines: Development, effectiveness, adverse effects, distribution and challenges. *Virusdisease*. 2022;33(1):1–22. doi:10.1007/s13337-022-00755-1
27. Kumar S, Thakur K, Sharma B, Bhardwaj TR, Prasad DN, Singh RK. Recent advances in vaccine development for the treatment of emerging infectious diseases. *Indian J Pharm Educ Res*. 2019;53(3):343–354. doi:10.5530/ijper.53.3.68
28. Rani M, Sharma AK, Chouhan RS, Sur S, Mansuri R, Singh RK. Natural flavonoid pectolinarin computationally targeted as a promising drug candidate against SARS-CoV-2. *Curr Res Struct Biol*. 2024;7:100120. doi:10.1016/j.crstbi.2023.100120
29. Al-Tawfiq JA, Kattan RF, Memish ZA. Middle East respiratory syndrome coronavirus disease is rare in children: An update from Saudi Arabia. *World J Clin Pediatr*. 2016;5(4):391. doi:10.5409/wjcp.v5.i4.391
30. Guan WJ, Ni ZY, Hu Y, et al. Clinical characteristics of coronavirus disease 2019 in China. *N Engl J Med*. 2020;382(18):1708–1720. doi:10.1056/NEJMoa2002032
31. Hon K, Leung C, Cheng W, et al. Clinical presentations and outcome of severe acute respiratory syndrome in children. *Lancet*. 2003;361(9370):1701–1703. doi:10.1016/S0140-6736(03)13364-8
32. Memish ZA, Al-Tawfiq JA, Assiri A, et al. Middle East respiratory syndrome coronavirus disease in children. *Pediatr Infect Dis J*. 2014;33(9):904–906. doi:10.1097/INF.0000000000000325
33. Thabet F, Chehab M, Bafaqih H, AlMohaimeed S. Middle East respiratory syndrome coronavirus in children. *Saudi Med J*. 2015;36(4):484–486. doi:10.15537/smj.2015.4.10243
34. Pormohammad A, Ghorbani S, Khatami A, et al. Comparison of influenza type A and B with COVID-19: A global systematic review and meta-analysis on clinical, laboratory and radiographic findings. *Rev Med Virol*. 2021;31(3):e2179. doi:10.1002/rmv.2179
35. Chong WH, Saha BK, Medarov BI. A systematic review and meta-analysis comparing the clinical characteristics and outcomes of COVID-19 and influenza patients on ECMO. *Respir Invest*. 2021;59(6):748–756. doi:10.1016/j.resinv.2021.07.006
36. Osman M, Klopfenstein T, Belfeki N, Gendrin V, Zayet S. A comparative systematic review of COVID-19 and influenza. *Viruses*. 2021;13(3):452. doi:10.3390/v13030452

Safety assessment of turmeric-boswellia-sesame formulation in healthy adult volunteers: An open-label prospective study

Se-Kwon Kim[1,A,B,D–F], Venkatesan Jayachandran[2,C–E], Thanh Sang Vo[3,C,D], Isuru Wijesekara[4,C,D]

[1] College of Science and Technology, Hanyang University, Ansan, South Korea
[2] Yenepoya Research Centre, Yenepoya (Deemed to be University), Mangalore, India
[3] Research and Development Institute of Advanced Agrobiology, Nguyen Tat Thanh University, Ho Chi Minh, Vietnam
[4] Department of Food Science and Technology, Faculty of Applied Sciences, University of Sri Jayewardenepura, Colombo, Sri Lanka

A – research concept and design; B – collection and/or assembly of data; C – data analysis and interpretation;
D – writing the article; E – critical revision of the article; F – final approval of the article

Advances in Clinical and Experimental Medicine, ISSN 1899–5276 (print), ISSN 2451–2680 (online) *Adv Clin Exp Med*. 2025;34(8):1277–1288

Address for correspondence
Se-Kwon Kim
E-mail: sknkim@pknu.ac.kr

Funding sources
None declared

Conflict of interest
None declared

Acknowledgements
The authors thank Arjuna Natural Pvt. Ltd., Kochi, India, for providing soft gels of the test product (Rhuleave-K) for this study.

Received on February 29, 2024
Reviewed on July 8, 2024
Accepted on September 6, 2024

Published online on January 8, 2025

Cite as
Kim S-K, Jayachandran V, Vo TS, Wijesekara I. Safety assessment of turmeric-boswellia-sesame formulation in healthy adult volunteers: An open label prospective study. *Adv Clin Exp Med*. 2025;34(8):1277–1288. doi:10.17219/acem/193023

DOI
10.17219/acem/193023

Copyright
Copyright by Author(s)
This is an article distributed under the terms of the Creative Commons Attribution 3.0 Unported (CC BY 3.0) (https://creativecommons.org/licenses/by/3.0/)

Abstract

Background. Turmeric and boswellia supplements have gained popularity for their anti-inflammatory and antioxidant properties. It is important to critically assess the safety of such supplements for prolonged use.

Objectives. To assess the safety and tolerability of turmeric-boswellia-sesame oil formulation (TBSF) in healthy human volunteers.

Materials and methods. Forty participants were supplemented with TBSF at a dose of 2,000 mg daily for 90 days. Safety assessments were performed at baseline, as well as on day 30, 60 and 90. Adverse events were monitored throughout the study period. Any evidence of hepatotoxicity injury or drug induced liver injury (DILI) was assessed using R value (R ratio/R factor), which is a relative pattern of liver enzymes. Additionally, Hy's law criteria, based on liver enzymes and bilirubin levels, were employed, along with an evaluation of drug-induced serious hepatotoxicity (eDISH) plot. The neutrophil-to-lymphocyte ratio (NLR) and platelet-to-lymphocyte ratio (PLR) were calculated, as these values are relevant to the safety of the intervention.

Results. The study found that TBSF supplementation did not cause any adverse effects or clinically significant variations in vital signs, hematological parameters, lipid profile, liver function enzymes, and renal function markers, and all were within the normal range after 90 days of TBSF supplementation. Platelet-to-lymphocyte ratio and NLR did not change significantly and were within the normal range. All the participants when plotted were in the normal range quadrant of the eDISH plot throughout the study period. No abnormal findings were observed in R value and Hy's law criteria, indicating that TBSF does not induce any hepatotoxicity. The present study showed a normal estimated glomerular filtration rate (eGFR), blood urea nitrogen (BUN), creatinine (Cr), Cr clearance, and BUN/Cr ratio throughout the study period. There was no significant change between these values at 4 abovementioned time points.

Conclusions. The study findings suggest that TBSF is a safe supplement for regular and long-term consumption.

Key words: safety, turmeric, dietary supplement, sesame, boswellia

Background

Nutraceuticals are bioactive compounds derived from plant sources that provide nutritional and medicinal benefits. The growing consciousness among consumers regarding potential health benefits and the necessity for enhanced wellness, especially in the post-pandemic era, highlights the importance of nutraceuticals. Furthermore, their safety, effectiveness and affordability contribute to their growing popularity. Nutraceuticals are easily accessible and widely available, making them attractive to a broad range of consumers. However, concerns regarding their safety and efficacy remain a topic of significant interest and investigation.

The use of natural products, such as turmeric and boswellia, for their anti-inflammatory properties has gained significant attention in musculoskeletal health.[1] While turmeric and boswellia have exhibited effectiveness in addressing these concerns over time, the challenge lies in the scarcity of natural products capable of delivering swift pain relief.[2–3] The experience of joint pain or muscle soreness is distressing and has a significant impact on a person's quality of life. Therefore, timely management and alleviation of inflammation is crucial to improving the overall wellbeing and quality of life of those affected. Promptly addressing the muscle or joint discomfort can minimize suffering, enable individuals to perform daily activities, and result a sense of comfort and wellbeing. Despite the growing popularity of natural products, more research and investigation is needed in this area. The unique formulation (Rhuleave-K) presented in this study combines turmeric, boswellia and sesame seed oil, and its integration with innovative technology represents a remarkable breakthrough in the field of natural products.

Turmeric and boswellia extract have been extensively researched for their effectiveness in managing inflammation, but the time required to see noticeable effects can be a challenge. However, the solubilization of turmeric and boswellia extracts in sesame seed oil sets Rhuleave-K apart from conventional physical blends. Given the significantly enhanced efficacy of Rhuleave-K, it is important to thoroughly evaluate its safety in humans, and this study is the first of its kind to address this aspect.

Objectives

The objective of the study was to assess the safety and tolerability of a novel formulation consisting of turmeric, boswellia and sesame oil (TBSF) integrated using SPEED-TECH technology (Rhuleave-K, Arjuna Natural Pvt. Ltd., Kochi, India), administered at a dosage of 2,000 mg per day over a 90-day period, in healthy adult volunteers. This objective of this study was to conduct comprehensive safety evaluations, including hematological, biochemical, radiological, and urine analyses, to provide a valuable insight into the potential for long-term clinical use of TBSF.

Materials and methods

The research protocol and associated documents underwent review and were approved by Royal Pune Independent Ethics Committee, Pune, India (date of approval: February 7, 2022; Drugs Controller General of India (DCGI) registration No. ECR/45/Indt/MH/2013/RR-19). The study was conducted in accordance with the declaration of Helsinki (52nd World Medical Association (WMA) General Assembly, Edinburgh, Scotland, October 2000) and the International Conference on Harmonization guidelines on Good Clinical Practice (GCP).

Study participants

The study population comprised healthy adult individuals of either gender, aged 18–55 years, without any clinically significant abnormalities as determined by the principal investigator based on the medical history, physical examination, chest X-ray, electrocardiogram (ECG), and routine laboratory evaluations. Additionally, all participants were required to demonstrate a willingness and ability to fully comply with the study procedures.

Individuals who tested positive for SARS-CoV-2 infection using reverse transcription quantitative polymerase chain reaction (RT-qPCR) or who had a history of comorbid medical conditions, including cardiovascular, endocrine, renal, hepatic, or other chronic diseases that may affect stress/anxiety levels, were excluded from participation in the study. Those with a history of anxiety disorders or other mental health conditions that may impact normal functioning, as well as those with a history of serious complications from diseases or any condition, including laboratory abnormalities, that in the opinion of the investigator posed an unacceptable risk or rendered the volunteer unfit to participate in the study, were excluded. Written informed consent was obtained from the participants by the investigator before initiating the screening process. There was no coercion of any kind and only those who voluntarily signed the consent form were included in the study.

Investigational product

The participants were instructed to take orally vegetarian reddish-brown soft gel capsules of TBSF 2,000 mg (500 mg × 2 soft gels, twice daily), containing 532 mg curcuminoids and 20 mg acetyl keto-boswellic acids, for a period of 90 days.

The TBSF contains turmeric extract (*Curcuma longa* L.), boswellia serrata extract and black sesame seed oil (*Sesamum indicum*). Cultivated variety of turmeric rhizomes from India were extracted with ethyl acetate and standardized to contain 26.6% curcuminoids. Wild variety of *Boswellia serrata* gum resin sourced from India was extracted using ethyl acetate and standardized to contain 1% acetyl-11-keto-β-boswellic acid (AKBA). The active

components from *Curcuma longa* and *Boswellia serrata* were uniformly solubilized in sesame seed oil sourced from India using proprietary technology. The investigational product was manufactured in compliance with applicable Good Manufacturing Practice (GMP) and Food Safety and Standards Authority of India (FSSAI) regulations, labelled and supplied by Arjuna Natural Pvt Ltd.

Participants received 3 bottles, each containing 128 "size 0" TBSF soft gel capsules. Bottle 1 was given at enrollment, bottle 2 at the 30-day follow-up visit and bottle 3 at the 60-day follow-up visit. Participants were instructed to take only 120 capsules from each bottle for 30 days (2 capsules twice daily), with 8 extra capsules for emergencies. Participants returned the bottles at the subsequent visit. The study coordinator maintained accurate records of the dates and amounts of capsules dispensed and consumed, and the percentage of treatment adherence was calculated.

Study procedure

This open-label study evaluated the safety and tolerability of TBSF in healthy adult volunteers. A total of 40 healthy volunteers were recruited in a single arm of the study. All the eligible participants were instructed to take TBSF at dose of 2 capsules (500 mg each) twice daily, in the morning and evening, for 90 days. The capsules could be ingested with or without food, according to the preferences of the participants, as instructed. The follow-up visits were at day 30, day 60 and day 90. Change in the safety parameters from baseline to endpoint compared at different time points were the primary outcomes of the study. The tolerability of the test product was determined by observing and evaluating the occurrence of adverse events throughout the treatment period up to the last dose. Averse events and serious adverse events reported by the participants were evaluated as secondary outcomes of the study.

Study assessments

Primary safety assessments of the repeated dose of TBSF included hematological and biochemical parameters. Hematological parameters included complete blood count (CBC) (hemoglobin (Hb), white blood cells count (WBC), platelet count (PLT), red blood cells count (RBC), hematocrit (HCT), neutrophil, eosinophil, lymphocytes, monocytes, basophil, and erythrocyte sedimentation rate (ESR)). Biochemical parameters included liver function test (total bilirubin, serum glutamate pyruvate transaminase (SGPT), serum glutamic oxaloacetic transaminase (SGOT)), renal function test (serum creatinine (CR), blood urea), lipid profile (low-density lipoprotein cholesterol (LDL-C), high-density lipoprotein cholesterol (HDL-C), very-low-density lipoprotein (VLDL), total cholesterol (TC), and triglycerides (TG)), fasting blood sugar, and urine analysis.

Glomerular filtration rate (GFR) is considered as an important test to determine the level of kidney function. It describes the flow rate of filtered fluid through the kidney and identifies the stage of renal disease. The GFR was estimated based on the Chronic Kidney Disease Epidemiology Collaboration (CKD-EPI) formula,[4] as detailed below:

For women with Cr <62 μmol/L:

$$\text{eGFR (mL/min/1.73 m}^2\text{)} = 144 \times (\text{Cr}/61.6)^{-0.329} \times (0.993)^{\text{age}}$$

1. For women with Cr >62 μmol/L:

$$\text{eGFR (mL/min/1.73 m}^2\text{)} = 144 \times (\text{Cr}/61.6)^{-1.209} \times (0.993)^{\text{age}}$$

2. For men with Cr <80 μmol/L:

$$\text{eGFR (mL/min/1.73 m}^2\text{)} = 141 \times (\text{Cr}/79.2)^{-0.411} \times (0.993)^{\text{age}}$$

3. For men with Cr >80 μmol/L:

$$\text{eGFR (mL/min/1.73 m}^2\text{)} = 141 \times (\text{Cr}/79.2)^{-1.209} \times (0.993)^{\text{age}}$$

where, "eGFR" is estimated glomerular filtration rate.

Hematology and biochemistry parameters were assessed at screening and on days 30, 60 and 90. Radiological parameters (ECG and X-ray) were assessed at screening and at the end of the study. Overall tolerability of the study medication was assessed by observing and evaluating the occurrence of adverse events and grading them as poor, fair, good, or excellent. Secondary safety assessments included vital signs and physical examination results at all visits and treatment-emergent adverse events reported by study participants throughout the treatment period. Participants were instructed to monitor themselves daily for any signs of adverse reactions throughout the study period. The investigator provided detailed guidelines for self-assessment of adverse reactions to ensure their consistent and accurate reporting, and each participant was provided with a standardized observation form that included sections to provide information on the date and time of the observation, the nature of the adverse event, and any other comments. Each participant's forms and responses were reviewed at each visit to assess for any adverse reactions during the study period.

Statistical analyses

As this research was conducted as a pilot study, an arbitrary sample size of 40 participants was selected for inclusion. Prior to statistical analysis, normality of the variables was assessed using the Shapiro–Wilk test (Supplementary Tables 1–5). Additionally, the assumption of sphericity was tested using Mauchly's sphericity test (Supplementary Table 6). The study data set was analyzed using repeated measures analysis of variance (rm-ANOVA) when normality and sphericity assumptions were met, as rm-ANOVA has greater statistical power. If the sphericity assumption was violated, the Greenhouse–Geisser correction was

applied. When the data did not meet the normality assumption, the nonparametric Friedman's rank test was used as the nonparametric analog of the one-way rm-ANOVA, with $\alpha = 0.05$. Pairwise multiple comparison of Hy's criteria was done using the McNemar's test, and Bonferroni correction was applied to account for multiple comparisons. To test for the differences in the binary R function outcomes, Cochran's Q test was used. All statistical tests were conducted using NCSS v. 20 (NCSS LLC, Kaysville, USA).

Results

Study participants and recruitment

Forty-six participants were screened after obtaining their written informed consent. Six participants were excluded from the study because they did not meet the eligibility criteria. Consequently, 40 study participants were enrolled according to the approved protocol and completed the study (Fig. 1). No amendments were made to the protocol and no instances of non-adherence to the protocol were observed during the study. The study had no missing data or dropouts. No adverse events or serious adverse events were reported.

Demographic characteristics and vital signs

The study participants were 22 men and 18 women with an average age of 32.38 years (Table 1). No significant variation was observed in the vital signs and weight of the participants over the course of the study (Table 2).

Safety assessment

Hematology

Complete blood count is an important tool in the safety assessment of a drug or substance. It count includes the measurement of several parameters, such as WBCs, PLT, RBCs, Hb, and HCT as well as RBC indices like mean corpuscular hemoglobin (MCH), mean corpuscular volume (MCV) and mean corpuscular hemoglobin concentration (MCHC). The neutrophil-to-lymphocyte ratio (NLR) is the ratio of absolute neutrophil count to the absolute lymphocyte count. The platelet-to-lymphocyte ratio (PLR) is the ratio of absolute platelet count to the absolute lymphocyte count. The study results showed that RBC indices, WBC, PLT, and differential count did not show any significant change at any time point. However, MCH and basophil absolute levels showed an increase at day 30 compared to baseline, which was not clinically significant. Furthermore, ESR values at day 60 and day 90 were decreased compared to the baseline. There were no significant changes in PLR and NLR, which remained within the normal range (Table 3).

Lipid profile

The lipid profile is an important component of safety assessment, particularly when evaluating the safety of an intervention that may affect lipid metabolism. The lipid profile typically includes measurements of LDL-C, HDL-C, TC, and TG. In this study, HDL-C increased significantly with nonsignificant decrease in TG and LDL-C, confirming no deterioration of renal function. The lipid profile data are shown in Table 4.

Table 1. Demographic profile of the study population

Participants	Number of participants	Age	Height [cm]	Weight [kg]
		mean ±SE	mean ±SE	mean ±SE
Total	40	32.38 ±1.53	159.83 ±1.36	73.23 ±0.83
Male	22	30.41 ±1.54	165.50 ±1.24	73.31 ±0.79
Female	18	34.78 ±2.77	152.89 ±1.39	73.13 ±1.59

SE – standard error.

Table 2. Vitals and weight

Parameters	Baseline	Day 30	Day 60	Day 90	ANOVA	Friedman
	mean ±SE	mean ±SE	mean ±SE	mean ±SE	p-value	p-value
Weight [kg]	73.23 ±0.83	73.255 ±0.83	73.2 ±0.81	73.375 ±0.83	–	0.939
Temperature [°C]	36.64 ±0.02	36.69 ±0.03	36.75 ±0.04	36.62 ±0.02	–	0.248
Systolic [mm Hg]	116.4 ±0.52	114.8 ±0.73	116.2 ±0.34	115.23 ±0.44	–	0.066
Diastolic [mm Hg]	77 ±0.43	77.18 ±0.62	77.5 ±0.58	77 ±0.43	–	0.574
Pulse_rate [bpm]	86.08 ±0.66	83.63 ±0.84	84.93 ±1.31	83.05 ±0.78	–	0.113
Respiratory rate [per min]	17.2 ±0.07	17.28 ±0.13	17.08 ±0.17	17.25 ±0.21	–	0.734

SE – standard error; ANOVA – analysis of variance.

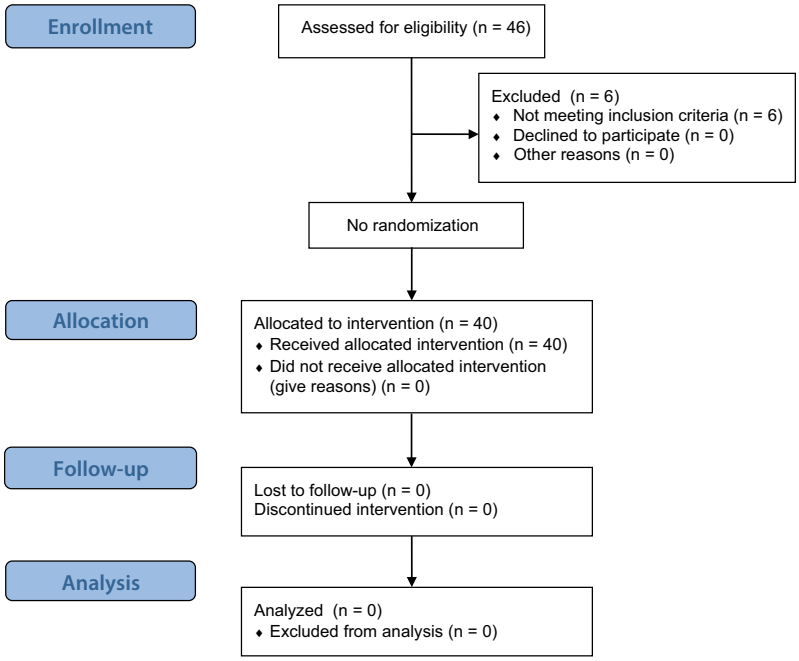


Fig. 1. Study flow diagram

Table 3. Assessment of hematology

Parameters	Baseline	Day 30	Day 60	Day 90	ANOVA	Friedman
	mean ±SE	mean ±SE	mean ±SE	mean ±SE	p-value	p-value
Hb [g/dL]	13.5 ±0.28	13.75 ±0.21	13.7 ±0.22	13.8 ±0.26	0.371	–
RBC [cells/µL]	4.61 ±0.09	4.56 ±0.07	4.57 ±0.07	4.61 ±0.09	–	0.283
HCT [%]	41.23 ±0.83	41.51 ±0.65	41.1 ±0.69	41.39 ±0.94	–	0.155
MCH [pg/cell]	29.31 ±0.16	30.2 ±0.31	29.97 ±0.1	29.94 ±0.1	–	0.001
MCHC [g/dL]	32.74 ±0.08	33.15 ±0.18	33.36 ±0.12	33 ±0.09	–	0.057
MCV [FL]	89.51 ±0.39	91.07 ±0.78	89.88 ±0.45	90.73 ±0.29	–	0.177
WBC [cells/µL]	7,768.5 ±307.94	7647.2 ±231.71	7,696.23 ±203.33	7,418.5 ±246.82	–	0.583
Platelets [cells/µL]	23,6725 ±12,932.22	23,9151.25 ±10,629.99	235,510.3 ±7817.73	235,529.18 ±6,750.68	–	0.060
Neutrophil absolute [cells/µL]	4,807.98 ±252.18	4,666.8 ±177.41	4,797.70 ±142.49	4,644 ±171.91	–	0.818
Lymphocyte absolute [cells/µL]	2,490.68 ±102.52	2,525.65 ±70.84	2,462.63 ±64.53	2,291.2 ±71.21	0.150	–
Monocyte absolute [cells/µL]	233.18 ±14.63	219.75 ±13.94	219 ±10.84	246.28 ±19.84	–	0.818
Eosinophil absolute [cells/µL]	236.63 ±11.11	220.78 ±15.22	209.08 ±16.34	230 ±12.75	0.433	–
Basophil absolute [cells/µL]	0 ±0	14.38 ±4.79	7.93 ±2.33	7.08 ±2.75	–	0.008
NLR	2.04 ±0.14	1.87 ±0.07	1.96 ±0.04	2.04 ±0.05	–	0.252
PLR	101.78 ±7.63	97.28 ±4.93	96.46 ±2.67	103.74 ±1.84	–	0.488
ESR [mm/h]	20.78 ±2.16	15.15 ±0.6	14.68 ±0.69	16.03 ±0.62	–	0.209

SE – standard error; ANOVA – analysis of variance; Hb – hemoglobin; RBC – red blood cells; HCT – hematocrit; MCH – mean corpuscular hemoglobin; MCHC – mean corpuscular hemoglobin concentration; MCV – mean corpuscular volume; WBC – white blood cells; NLR – neutrophil-to-lymphocyte ratio; PLR – platelet-to-lymphocyte ratio; ESR – erythrocyte sedimentation rate.

Liver function test

Liver function tests (LFTs) are a group of blood tests that are commonly used in safety assessment to evaluate liver function and to detect liver damage or disease. They typically include tests for liver enzymes such as aspartate aminotransferase (AST), alanine aminotransferase (ALT), alkaline phosphatase (ALP), and bilirubin levels. The study results showed that there was no significant difference in liver function test responses at baseline, day 30, day 60, and day 90 (Table 5).

The R value, also known as the R ratio or R factor, is a measure of the ratio of serum concentrations of 2 liver enzymes: ALP and ALT. It is used to define hepatotoxicity injury patterns. The R value can provide additional information about liver function and damage beyond individual enzyme levels. The relative pattern of ALT and/or ALP elevation indicates the type of drug-induced liver injury

Table 4. Lipid profile

Parameters	Baseline	Day 30	Day 60	Day 90	ANOVA	Friedman
	mean ±SE	mean ±SE	mean ±SE	mean ±SE	p-value	p-value
TC [mg/dL]	163.45 ±5.08	163.33 ±4.7	164.25 ±3.7	165.18 ±4.03	0.923	–
HDL [mg/dL]	45.13 ±0.76	45.78 ±1.17	45.93 ±1.39	50.05 ±1.46	–	0.024
LDL [mg/dL]	86.47 ±4.19	86.52 ±3.92	84.16 ±4.08	82.15 ±3.34	–	0.690
VLDL [mg/dL]	31.86 ±2.83	26.53 ±1.76	28.96 ±1.53	29.13 ±1.48	–	0.006
TG [mg/dL]	159.28 ±14.16	140.08 ±7.5	144.78 ±7.63	145.63 ±7.42	–	0.645
FBS [mg/dL]	86.38 ±1.97	86.43 ±1.35	86.3 ±1.48	88.9 ±1.23	–	0.079

SE – standard error; ANOVA – analysis of variance; TC – total cholesterol; HDL – high-density lipoprotein; LDL – low-density lipoprotein; VLDL – very low-density lipoprotein; TG – triglycerides; FBS – fasting blood sugar.

Table 5. Liver function test

Parameters	Baseline	Day 30	Day 60	Day 90	ANOVA	Friedman
	mean ±SE	mean ±SE	mean ±SE	mean ±SE	p-value	p-value
ALT (SGPT) [U/L]	34.73 ±4.27	32 ±1.61	31.85 ±1.55	32.93 ±1.2	–	0.075
AST (SGOT) [U/L]	33.33 ±1.86	34.13 ±1.15	33.8 ±1.14	36.1 ±1.19	–	0.067
ALP [U/L]	100.45 ±5.41	96.28 ±4.05	96.43 ±3.7	92.78 ±3.41	0.273524	–
Bilirubin [mg/dL]	0.67 ±0.04	0.68 ±0.03	0.66 ±0.06	0.73 ±0.03	–	0.509

SE – standard error; ANOVA – analysis of variance; ALT – alanine aminotransferase; AST – aspartate aminotransferase; ALP – alkaline phosphatase.

Table 6. R function analysis using Cochran's Q test

Time [min]	Condition		Percentage		Q	df	p-value	Significant at 0.05
	R not ≤ 2	R ≤ 2	R not ≤ 2	R ≤ 2				
0	6	34	15	85	4.5	3	0.212	no
30	2	38	5	95				
60	2	38	5	95				
90	2	38	5	95				

df – degrees of freedom; Q – quartile.

(DILI). A relatively elevated ALT compared to the ALP level indicates a hepatocellular pattern of DILI, whereas the opposite indicates a cholestatic pattern. In this study, none of the study participants experienced a hepatocellular injury or cholestasis or mixed injury at any time point (Table 6).

Hy's law criteria is a set of clinical criteria used to assess the likelihood of severe liver injury or liver failure in patients taking potentially hepatotoxic drugs. They are defined as the occurrence of elevated liver enzymes (ALT or AST greater than 3 times the upper limit of normal) and elevated bilirubin levels (greater than 2 times the upper limit of normal) without initial findings of cholestasis and absence of other explanation of liver injury (e.g., viral hepatitis, alcoholic hepatitis).[5] Meeting Hy's law criteria is associated with a high risk of severe liver injury or failure and can be an indication to discontinue the use of the potentially hepatotoxic drug. Therefore, Hy's law criteria are an important component of safety assessment for drugs that may potentially cause liver injury.

The primary graphical tool to evaluate a drug's liver safety profile and promptly identify cases of special concern is the evaluation of drug-induced serious hepatotoxicity plot (eDISH). This plot displays a log/log correlation between peak total bilirubin (TBL) and ALT, both measured in multiples of the ULN. Horizontal and vertical lines on the plot indicate the thresholds of Hy's law: ALT = 3 × ULN and total bilirubin = 2 × ULN. Study participants potentially meeting the Hy's law criteria are clearly visible in the upper right quadrant of the graph. Data points in the lower right quadrant, exceeding 3 × ULN for ALT, but remaining below 2 × ULN for total bilirubin, also suggest an increased risk for liver injury (Temple's Corollary range). According to the U.S. Food and Drug Administration (FDA) guidance on drug-induced liver injury, the identification of 1 case meeting Hy's law criteria in the clinical trial database is a cause for concern. However, the detection of 2 such cases is highly predictive that the drug has the potential to induce severe DILI when administered to a larger population.

Figure 2 illustrates the concept of the eDISH method. Each dot on the plane represents 1 subject in the clinical study. For each subject, the peak TBL multiplied by the upper limit of the reference range (ULRR) is plotted against

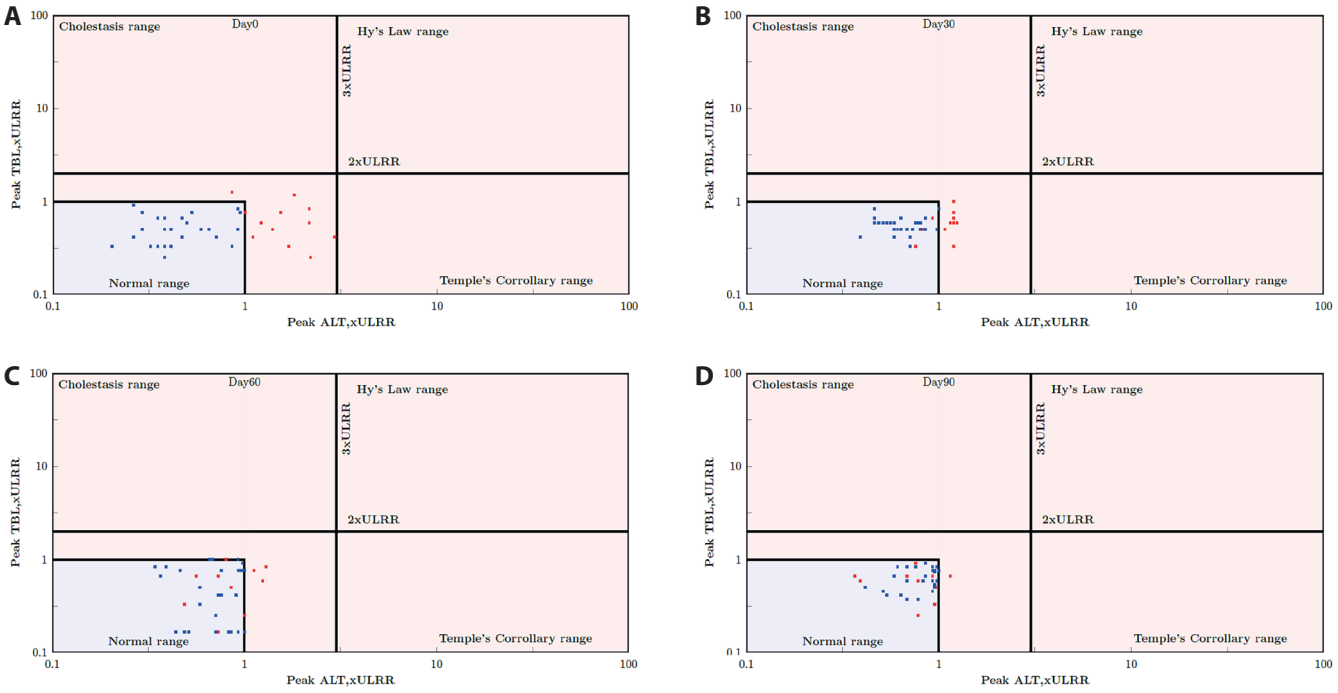


Fig. 2. Representation of evaluation of drug-induced serious hepatotoxicity (eDISH plot). A, B, C, and D represents the data of baseline, day 30, day 60, and day 90, respectively. Each dot on the plane represents individual participants in the clinical study. In the graph, for each participant, the peak total bilirubin (TBL) times the upper limit of the reference range (ULRR) is plotted against the peak alanine aminotransferase (ALT) times the upper limit of the reference range (ULRR), on a log10 scale. The 2 reference lines, 2 × ULRR for TBL × ULRR and 3 × ULRR for ALT × ULRR, are drawn to divide the plane into 4 quadrants – upper left (cholestasis quadrant), upper right (Hy's law quadrant), lower right (temple's corollary quadrant), and lower left (normal quadrants). Normal cases are in the lower left quadrant

Table 7. Evaluation of drug-induced serious hepatotoxicity (eDISH) plot quadrants

Quadrant	Condition	TBL	ALT
Upper left	cholestasis	>2 × ULN	<3 × ULN
Upper right	Hy's law	>2 × ULN	>3 × ULN
Lower right	temple's corollary	<2 × ULN	>3 × ULN
Lower left	normal	<2 × ULN	<3 × ULN

TBL – total bilirubin; ALT – alanine aminotransferase; ULN – upper limit of normal.

the peak ALT multiplied by the ULRR, utilizing a log10 scale. Figure 2 illustrates the approach proposed by Zimmerman[6] to use both the indicator of hepatocellular injury, i.e., ALT, and the measure of impaired liver function (TBL) together. Figure 2 includes 2 reference lines: 2 × ULRR for TBL × ULRR and 3 × ULRR for ALT × ULRR, dividing the plane into 4 quadrants (Table 7). Normal cases are situated in the lower left quadrant. Notably, the upper right quadrant is known as Hy's law quadrant, encompassing potentially DILI cases. Any subject falling within the Hy's law quadrant required additional investigation to adjudicate the case.

In our study, Fig. 2 shows that all study participants fall in the lower left quadrant (normal) at baseline, day 30, day 60, and day 90. None of the study participants were in the Hy's criteria range, the temples corollary range or the cholestasis range, which is a safe indication that the product does not induce any hepatotoxicity. Further analysis of the Hy's criteria using Cochran's Q test and McNemar's test showed that all study participants were in the normal first quadrant. However, there was a significant change in the proportion of study participants and study participants moving into the inner normal range when baseline was compared to day 60 and day 90 (Tables 8,9).

Renal function test

Renal function tests, including GFR and urine analysis, are important parameters in the safety assessment of any formulation.

Renal function assessment, involving measurements of Cr and/or blood urea nitrogen (BUN), is deemed essential for most clinical studies, alongside liver function tests such as serum glutamic oxaloacetic transaminase (SGOT), serum glutamic pyruvate transaminase (SGPT) and ALP. This assessment holds particular significance in the development of new drug or nutraceuticals. Renal

Table 8. Hy's criteria data

Time point	0 = within 1st quadrant but outside the inner normal range rectangle		1 = inner normal range	
	n	%	n	%
Hys_0	12	30	28	70
Hys_30	8	20	32	80
Hys_60	4	10	36	90
Hys_90	1	2.5	39	97.5

Table 9. Hy's criteria data using McNemar test

Multiple comparisons using the McNemar test						Significance
Comparison*	%	%	χ^2	df	p-value	α = 0.05†
Hys_0 vs Hys_30	70	80	4	1	0.046	no
Hys_0 vs Hys_60	70	90	8	1	0.005	yes
Hys_0 vs Hys_90	70	97.5	11	1	0.001	yes
Hys_30 vs Hys_60	80	90	4	1	0.046	no
Hys_30 vs Hys_90	80	97.5	7	1	0.008	yes
Hys_60 vs Hys_90	90	97.5	3	1	0.083	no

† individual comparison alpha = (overall alpha)/c = 0.05/6 = 0.00833; df – degrees of freedom.

function tests play a critical role in monitoring the kidney's response to treatment and measuring the progression of kidney disease. The BUN, a byproduct of liver function and protein digestion, serves as an indicator of renal function. Creatinine, derived from the creatine breakdown in muscle metabolism, is another waste product indicative of renal function. However, the Cr clearance may be influenced by patient muscle mass, diminishing with age despite serum Cr levels staying within the normal range due to age-related muscle mass reduction.

Glomerular filtration rate stands as the gold standard test for assessing kidney function, reflecting the rate at which fluid is filtered through the kidney and indicating the stage of renal disease. While serum Cr concentration is commonly interpreted as a measure of GFR and used as an index of renal function in clinical settings, it is important to note that glomerular filtration of Cr is only one determinant of its serum concentration. The GFR is estimated with serum Cr level using appropriate formula.

Glomerular filtration rate declines with age, even in people without kidney disease. The graph (Fig. 3) shows that the estimated GFR has never gone below the normal values at any time point for any individual.

The present study indicated a normal eGFR, BUN, Cr, Cr clearance, and BUN/Cr ratio throughout the study period and there was no significant change between these values at 4 time points (Table 10).

Urine analysis

Urine analysis can provide valuable information about kidney function and overall health. It includes a standard battery of tests of physical character (appearance, color, specific gravity), chemical analysis (pH, ketones, proteins, glucose, and bile) and microscopic evaluation of sediments (RBC, WBC, bacteria, and epithelial cells). The specific gravity measures the kidneys' capacity to reabsorb dissolved components of urine. Urine can vary widely in concentration. Table 10 shows that there was no significant change in the specific gravity and pH of urine throughout the study period and that these parameters were always within the normal range.

Ketones were absent in the urine at all time points. In a healthy individual, urine typically does not contain protein because protein molecules are too large to pass through the glomerular filtration barrier. Ketones, which are products of abnormal fat breakdown, are not typically present in urine of healthy individuals. Glucose enters the urine only when the serum glucose concentration surpasses the renal threshold for glucose reabsorption, which is typically around 180 mg/dL. In this study, since the serum glucose was well below the limit, glucose was absent in urine. The absence of bilirubin in the urine could indicate the efficient removal of breakdown products from RBCs by the liver, potentially suggesting a healthy liver. Likewise, the absence of blood in the urine suggests that the filtration barrier in the kidneys is functioning normally, effectively preventing blood from entering the urine.

Urine analysis is an effective screening tool for the assessment of an individual's health status. The results of this study demonstrated no abnormal findings, which corroborates the findings of the LFT, renal function test (RFT) and blood analysis.

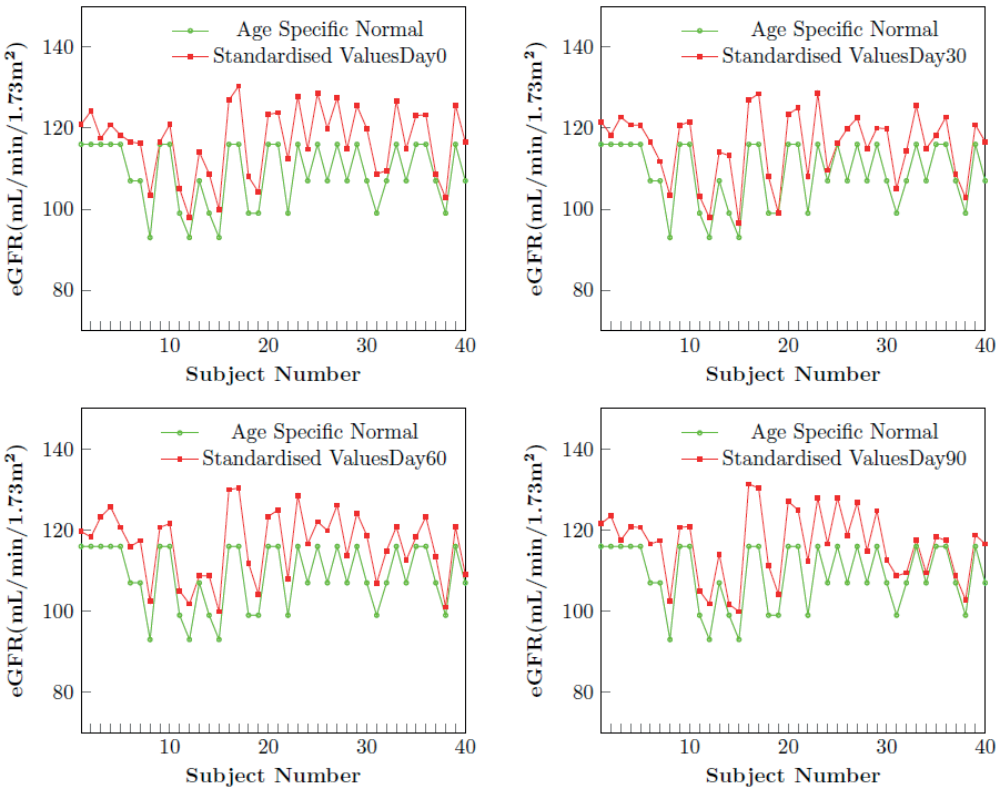


Fig. 3. Representation of estimated glomerular filtration rate (eGFR) of participants in the study. Each dot on the plane represents individual participant in the clinical study. Estimated standardized GFR is represented in red and average age specific normal value of GFR is represented in green. Estimated glomerular filtration rate has never gone below the normal values at any time point for any individual

Table 10. Renal function test and urine analysis

Parameter	Baseline	Day 30	Day 60	Day 90	ANOVA	Friedman
	mean ±SE	mean ±SE	mean ±SE	mean ±SE	p-value	p-value
pH	6.14 ±0.04	6.09 ±0.08	6.15 ±0.05	6.27 ±0.05	–	0.333
Specific gravity	1.02 ±0	1.02 ±0	1.02 ±0	1.02 ±0	–	0.281
Bun [mg/dL]	7.14 ±0.11	7.18 ±0.12	6.91 ±0.09	7.04 ±0.13	–	0.552
Creatinine [mg/dL]	0.76 ±0.01	0.77 ±0.01	0.76 ±0.01	0.76 ±0.02	–	0.461
Bun Cr ratio	9.47 ±0.09	9.36 ±0.1	9.17 ±0.11	9.28 ±0.1	–	0.209
GFR Std [mL/min/1.73 m^2]	116.73 ±1.36	115.59 ±1.35	116.35 ±1.33	116.12 ±1.36	–	0.461
Cr clearance [mL/min]	135.38 ±2.39	132.59 ±1.81	134.48 ±1.75	134.63 ±2.33	–	0.316
eGFR difference	7.91 ±0.55	6.76 ±0.57	7.53 ±0.53	7.29 ±0.62	0.234	–

SE – standard error; ANOVA – analysis of variance; pH – potential of hydrogen; BUN – blood urea nitrogen; Cr – creatinine; eGFR – estimated glomerular filtration rate.

Radiological assessment

Electrocardiography and radiography were performed during screening and at the end of the study, and were found to be clinically nonsignificant and safe. It is noteworthy that none of the study participants experienced symptoms such as anorexia, nausea, vomiting, fatigue, or abdominal pain. The absence of these symptoms highlights the favorable tolerability of the product and suggests that it did not cause any gastrointestinal or systemic discomfort. It is also important to note that no adverse events or serious adverse events were observed throughout the study, which indicates that the product has a favorable safety profile.

Discussion

The present study aimed to investigate the safety profile of TBSF with SPEEDTECH (Rhuleave-K). The integration of these natural compounds, known for their anti-inflammatory properties, represents a novel approach in addressing musculoskeletal health. Our findings indicated that TBSF, administered at a dosage of 2,000 mg per day over a 90-day period, demonstrated a favorable safety profile in humans. Notably, the incorporation of TBSF with SPEEDTECH (Rhuleave-K) in the solubilization process of turmeric and boswellia extract within sesame seed oil distinguishes this formulation from traditional blends.

This innovative approach not only enhances the efficacy of the product but also contributes to its safety. Comprehensive safety assessments, including monitoring for potential adverse effects, were conducted to ensure study participants' wellbeing.

Complete blood count provides information about the effects of the drug or substance on the blood cells, which can be used to assess the potential toxicity and adverse effects of the drug or substance on the hematological system. For example, a decrease in the RBC count, Hb or HCT may indicate anemia, which can be a side effect of certain drugs or substances. Similarly, an increase in the WBC count may indicate an immune response to the drug or substance. Platelet count is also important as it can indicate potential bleeding risks. In summary, CBC can help to detect potential toxicity and adverse effects on the hematological system.

The NLR and PLR are both calculated from values obtained in CBC. They are simple and cost-effective biomarkers that have been proposed as indicators of inflammation and immune status in various conditions. In the context of safety assessment, NLR and PLR can provide useful information about the immune response of an individual, which may be relevant to the safety of an intervention. For example, an increase in NLR or PLR may indicate a heightened inflammatory response, which could be indicative of adverse effects or toxicity. Additionally, PLR and NLR have been proposed as predictors of disease severity and prognosis in a variety of conditions, which could be useful in safety assessment.[7–11]

Lipids are an important class of biomolecules with diverse functions within the body, serving as an energy source, contributing to the structural integrity of cell membranes, and acting as precursors to hormones and other signaling molecules. However, abnormal lipid metabolism can lead to various health problems, including cardiovascular disease (CVD). Abnormalities in lipid profile can indicate a higher risk of CVD. For example, elevated levels of LDL-C are linked with an increased risk of coronary heart disease and atherosclerosis. Elevated levels of HDL-C correlate with a reduced risk of CVD. Assessing changes in lipid profile during drug development can help identify potential safety issues and inform dosing recommendations. The HDL-C has been linked to renal dysfunction in heart failure patients, but the apolipoprotein A1 (ApoA1) and apolipoprotein B (ApoB), TC, TG, and LDL-C exhibit no such association.[11,12] Some research indicated that low HDL-C levels are linked to a faster progression of kidney disease.[13] Moreover, a recent randomization analysis reported that genetically higher concentration of HDL-C were linked to improved kidney function, based on large samples form the largest lipid and chronic kidney disease (CKD) cohorts.[7] Visconti et al.[14] observed that lipid disorders in CKD are marked by decreased HDL-C, elevated triglycerides and LDL-C levels that are either normal or slightly reduced. Although the mechanism behind this association remains unclear, previous studies[15–18] have demonstrated that HDL-C possess antioxidant, anti-inflammatory and antithrombotic properties. These functions may mitigate atherosclerosis in renal and other arteries, suggesting a potential protective role for HDL-C in renal functions.[19]

Elevated liver enzymes can be an indicator of liver damage, inflammation or disease. Abnormal bilirubin levels can indicate liver or bile duct disease. Therefore, LFTs are an important component of safety assessment for drugs or other substances that may potentially cause liver damage or dysfunction. Alkaline phosphatase increases when there is injury to the bile ducts or obstruction of bile flow. Elevations in serum enzyme levels (ALP, ALT and AST) are indicators of liver injury, whereas rise in bilirubin levels may indicate the overall functioning of the liver.

The results of this study demonstrated that TBSF was well-tolerated and did not induce any adverse effects based on the assessments conducted.

Curcumin, the active compound in turmeric, has been extensively studied for its safety and therapeutic efficacy. Multiple clinical trials evaluating curcumin supplementation have consistently reported no major safety concerns or cases of DILI.[20,21] Similarly, boswellia, derived from the resin of *Boswellia serrata*, has been widely used in traditional medicine and clinical studies reported its safety without significant liver-related adverse events.[2]

In the context of herbal supplements, it is crucial to acknowledge the potential risks associated with certain products, particularly DILI. Some studies reported cases of liver injury or DILI associated with certain herbal products, highlighting the importance of thorough safety evaluations.[22,23] For example, a case-control study reported a correlation between the use of specific herbal supplements and liver injury, reinforcing the need for further investigation.[24] Caution is warranted as some studies reported potential hepatotoxicity associated with high doses of piperine.[25] However, TBSF evaluated in this study showed no evidence of hepatotoxicity.

In this study, results of liver function tests, including AST, ALT and bilirubin, were within normal limits at all time points, indicating the safety of the formulation. The R value and Hy's criteria were also evaluated to assess the risk of DILI. The R value was less than 5 in all participants, indicating a low risk of liver injury.

The lipid profile is an essential indicator of cardiovascular health and is often evaluated during safety assessments. Our study found no significant changes in the lipid profile of patients taking TBSF, indicating that it did not have any adverse effects on lipid metabolism. Renal function tests, including BUN and serum Cr, were evaluated in this study, and no significant changes were observed, indicating that TBSF did not have a negative effect on renal function.

Complete blood count is an essential test for evaluating the safety of any treatment or medication. The study found no significant changes in the CBC of patients taking TBSF, indicating its safety. The study results showed that TBSF was safe and had no adverse effects on liver function, lipid profile, renal function, CBC, radiological assessment, and urine analysis.

The study findings support the hypothesis that TBSF, when integrated with SPEEDTECH (Rhuleave-K), is a well-tolerated and safe option for long-term use. These findings provide a valuable insight into the safety profile of TBSF, paving the way for its potential clinical applications.

Limitations

The study included a small sample size of participants, which may limit the generalizability of the results, and a short 90-day observation period, which may be inadequate to detect long-term effects. In addition, the focus of the study was on healthy adults, which limited its applicability to a broader population. In addition, the study lacked a comparison group, making direct comparisons with alternative treatment options difficult. Another limitation of the study was that some of the key markers, such as cystatin C, kidney injury molecule 1 (KIM-1) and interleukin 6 (IL-6) levels were not included in the analysis. To confirm and extend the study results, further research and larger studies are warranted.

Conclusions

The results of the study demonstrated that TBSF (Rhuleave-K) is safe and has no adverse effects on liver function, lipid profile, renal function, CBC, radiological assessment, and urine analysis. The study provides a valuable insight into the safety profile of TBSF for long-term use.

Supplementary data

The Supplementary materials are available at https://zenodo.org/doi/10.5281/zenodo.13757433. The package includes the following files:

Supplementary Table 1. Results from Shapiro–Wilk test of normality for weight and vitals.

Supplementary Table 2. Results from Shapiro–Wilk test of normality for hematology parameters.

Supplementary Table 3. Results from Shapiro–Wilk test of normality for lipid test parameters.

Supplementary Table 4. Results from Shapiro–Wilk test of normality for LFT test parameters.

Supplementary Table 5. Results from Shapiro–Wilk test of normality for urine sample test parameters.

Supplementary Table 6. Results from Machuly's test of sphericity for normally distributed hematology, lipid, LFT, and urine sample test parameters.

Data availability

The datasets generated and/or analyzed during the current study are available from the corresponding author on reasonable request.

Consent for publication

Not applicable.

ORCID iDs

Se-Kwon Kim https://orcid.org/0000-0001-6507-9539
Venkatesan Jayachandran https://orcid.org/0000-0003-1716-8873
Thanh Sang Vo https://orcid.org/0000-0002-6726-3257
Isuru Wijesekara https://orcid.org/0000-0003-1688-8801

References

1. Rudrappa GH, Murthy M, Saklecha S, Kumar Kare S, Gupta A, Basu I. Fast pain relief in exercise-induced acute musculoskeletal pain by turmeric-boswellia formulation: A randomized placebo-controlled double-blinded multicentre study. *Medicine (Baltimore)*. 2022;101(35):e30144. doi:10.1097/MD.0000000000030144
2. Coppola C, Greco M, Munir A, et al. Osteoarthritis: Insights into diagnosis, pathophysiology, therapeutic avenues, and the potential of natural extracts. *Curr Issues Mol Biol*. 2024;46(5):4063–4105. doi:10.3390/cimb46050251
3. Hewlings S, Kalman D. Curcumin: A review of its effects on human health. *Foods*. 2017;6(10):92. doi:10.3390/foods6100092
4. Levey AS, Stevens LA, Schmid CH, et al. A new equation to estimate glomerular filtration rate. *Ann Intern Med*. 2009;150(9):604. doi:10.7326/0003-4819-150-9-200905050-00006
5. Davidson CS, Leevy CM, Chamberlayne EC. *Guidelines for Detection of Hepatotoxicity Due to Drugs and Chemicals*. Washington, D.C.-Bethesda, USA: U.S. Department of Health, Education, and Welfare, Public Health Service, National Institutes of Health (NIH); 1979. https://books.google.pl/books/about/Guidelines_for_detection_of_hepatotoxici.html?id=wEHn_Ee48vUC&redir_esc=y. Accessed October 15, 2023.
6. Zimmerman HJ. *Hepatotoxicity: The Adverse Effects of Drugs and Other Chemicals on the Liver*. 2nd ed. Philadelphia, USA: Lippincott Williams & Wilkins; 1999. ISBN:978-0-7817-1952-0.
7. Neuen BL, Leather N, Greenwood AM, Gunnarsson R, Cho Y, Mantha ML. Neutrophil-lymphocyte ratio predicts cardiovascular and all-cause mortality in hemodialysis patients. *Ren Fail*. 2016;38(1):70–76. doi:10.3109/0886022X.2015.1104990
8. Nakajima H, Kaneko S, Sato Y, Takano T, Hosino T. Optimum conditions for the efficacy and safety of cryofiltration apheresis: An analysis of circuit temperatures depending on plasma flow rate and cooling coil lengths/turns. *Ther Apher Dial*. 2015;19(4):324–329. doi:10.1111/1744-9987.12340
9. Ye M, Qian X, Guo X, et al. Neutrophil-lymphocyte ratio and platelet-lymphocyte ratio predict severity and prognosis of lower limb arteriosclerosis obliterans. *Ann Vasc Surg*. 2020;64:221–227. doi:10.1016/j.avsg.2019.09.005
10. Gasparyan AY, Ayvazyan L, Mukanova U, Yessirkepov M, Kitas GD. The platelet-to-lymphocyte ratio as an inflammatory marker in rheumatic diseases. *Ann Lab Med*. 2019;39(4):345–357. doi:10.3343/alm.2019.39.4.345
11. Vijayalekshmi Sujatha, Shukla H. Unilateral acute conjunctivitis due to *Oestrus ovis* in a veterinary doctor. *J Nat Sc Biol Med*. 2013;4(1):228. doi:10.4103/0976-9668.107304
12. Imle R, Tosev G, Behnisch W, et al. Intracardiac extension of Wilms tumor: A case of a 2.5-year-old girl presenting with upper venous congestion caused by tumor growth into the right cardiac ventricle. *Case Rep Oncol*. 2019;12(1):33–38. doi:10.1159/000496020
13. Kawachi K, Kataoka H, Manabe S, Mochizuki T, Nitta K. Low HDL cholesterol as a predictor of chronic kidney disease progression: A cross-classification approach and matched cohort analysis. *Heart Vessels*. 2019;34(9):1440–1455. doi:10.1007/s00380-019-01375-4

14. Visconti L, Benvenga S, Lacquaniti A, et al. Lipid disorders in patients with renal failure: Role in cardiovascular events and progression of chronic kidney disease. *J Clin Transl Endocrinol*. 2016;6:8–14. doi:10.1016/j.jcte.2016.08.002
15. Arora S, Patra SK, Saini R. HDL: A molecule with a multi-faceted role in coronary artery disease. *Clin Chim Acta*. 2016;452:66–81. doi:10.1016/j.cca.2015.10.021
16. Barter PJ, Nicholls S, Rye KA, Anantharamaiah GM, Navab M, Fogelman AM. Antiinflammatory properties of HDL. *Circ Res*. 2004;95(8):764–772. doi:10.1161/01.RES.0000146094.59640.13
17. Denimal D. Antioxidant and anti-inflammatory functions of high-density lipoprotein in type 1 and type 2 diabetes. *Antioxidants*. 2023;13(1):57. doi:10.3390/antiox13010057
18. Zuliani G, Vigna GB, Fellin R. The anti-atherogenic properties of HDL particles. *International Congress Series*. 2007;1303:103–110. doi:10.1016/j.ics.2007.04.003
19. Campbell CM, Edwards RR. Mind–body interactions in pain: The neurophysiology of anxious and catastrophic pain-related thoughts. *Transl Res*. 2009;153(3):97–101. doi:10.1016/j.trsl.2008.12.002
20. Pancholi V, Smina TP, Kunnumakkara AB, Maliakel B, Krishnakumar IM. Safety assessment of a highly bioavailable curcumin–galactomannoside complex (CurQfen) in healthy volunteers, with a special reference to the recent hepatotoxic reports of curcumin supplements: A 90-days prospective study. *Toxicol Rep*. 2021;8:1255–1264. doi:10.1016/j.toxrep.2021.06.008
21. Sahebkar A, Henrotin Y. Analgesic efficacy and safety of curcuminoids in clinical practice: A systematic review and meta-analysis of randomized controlled trials. *Pain Med*. 2016;17(6):1192–1202. doi:10.1093/pm/pnv024
22. Real M, Barnhill MS, Higley C, Rosenberg J, Lewis JH. Drug-induced liver injury: Highlights of the recent literature. *Drug Saf*. 2019;42(3):365–387. doi:10.1007/s40264-018-0743-2
23. Navarro VJ, Khan I, Björnsson E, Seeff LB, Serrano J, Hoofnagle JH. Liver injury from herbal and dietary supplements. *Hepatology*. 2017;65(1):363–373. doi:10.1002/hep.28813
24. Bessone F, García-Cortés M, Medina-Caliz I, et al. Herbal and dietary supplements-induced liver injury in Latin America: Experience from the LATINDILI network. *Clin Gastroenterol Hepatol*. 2022;20(3):e548–e563. doi:10.1016/j.cgh.2021.01.011
25. Mazzanti G, Di Sotto A, Vitalone A. Hepatotoxicity of green tea: An update. *Arch Toxicol*. 2015;89(8):1175–1191. doi:10.1007/s00204-015-1521-x

Examination of 6 and 12 month follow-up of calcium hydroxide and calcium silicate materials used in direct and indirect pulp capping

Yasemin Yavuz[1,A,D], Sedef Kotanli[2,C], Mehmet S. Dogan[3,E], Zelal Almak[1,B]

[1] Department of Restorative Dentistry, Harran University, Şanlıurfa, Turkey
[2] Department of Dentomaxillofacial Radiology, Harran University, Şanlıurfa, Turkey
[3] Department of Pediatric Dentistry, Harran University, Şanlıurfa, Turkey

A – research concept and design; B – collection and/or assembly of data; C – data analysis and interpretation; D – writing the article; E – critical revision of the article; F – final approval of the article

Advances in Clinical and Experimental Medicine, ISSN 1899–5276 (print), ISSN 2451–2680 (online) *Adv Clin Exp Med*. 2025;34(8):1289–1298

Address for correspondence
Yasemin Yavuz
E-mail: yyavuz-21@hotmail.com

Funding sources
The study was supported by the Harran University Scientific Research Project No. 21281.

Conflict of interest
None declared

Acknowledgements
We would like to thank the expert (Phd. M.E. Duken) who helped perform the statistical analysis in the results of the study.

Received on January 4, 2024
Reviewed on May 8, 2024
Accepted on October 11, 2024

Published online on February 11, 2025

Cite as
Yavuz Y, Kotanli S, Dogan MS, Almak Z. Examination of 6 and 12 month follow-up of calcium hydroxide and calcium silicate materials used in direct and indirect pulp capping. *Adv Clin Exp Med*. 2025;34(8):1289–1298. doi:10.17219/acem/194504

DOI
10.17219/acem/194504

Copyright
Copyright by Author(s)
This is an article distributed under the terms of the Creative Commons Attribution 3.0 Unported (CC BY 3.0) (https://creativecommons.org/licenses/by/3.0/)

Abstract

Background. Pulpal vitality is important for the tooth to maintain its physiological function and preserve its structure.

Objectives. The aim of this study was to evaluate the clinical and radiographic 6- and 12-month treatment success of calcium hydroxide (CH) and calcium silicate materials in indirect pulp treatment (IPT) and direct pulp capping (DPC) in teeth with deep dentin decay.

Materials and methods. The study included 143 teeth of patients aged 17–69 years with no systemic disease. The study is grouped under 3 main groups (Dycal, Biodentine, TheraCal PT). Direct pulp capping was applied to 65 teeth and IPT to 66 teeth. All teeth were restored with Universal adhesive system and Universal composite (G-Premio Bond; GC Corp., Tokyo, Japan).

Results. In the statistical evaluations of the data obtained, 0.05 was accepted as the level of statistical significance. The general success rate in the IPT group was found to be 95.2% for Biodentine (Septodont, SaintMaur-des-Fossés, France), 91.7% for Dycal (Dentsply/Caulk, International Inc. Milford, USA) and 90.1% for TheraCal PT (Bisco Inc., Schaumburg, USA) at both 6 and 12 months. When the clinical and radiographic success was compared at 6 months and 12 months, no statistically significant difference was determined between the materials ($p > 0.05$). In the clinical and radiographic evaluations at the end of 6-month follow-up in the DPC group, the success rates were determined to be 96.0% for Biodentine, 81.8% for Dycal and 63.2% for TheraCal PT. At 12 months, these rates were 96.0% for Biodentine, 68.2% for Dycal and 63.2% for TheraCal PT. DPC Biodentine was found to be the most successful material (96.0%).

Conclusions. At the end of the 12-month follow-up period, it was considered that the 3 materials (Biodentine, Dycal, TheraCal) can be selected for IPT. In DPC, Biodentine was found to be more successful than both calcium silicate containing resin and CH.

Key words: Biodentine, direct pulp capping, TheraCal PT, deep dentin decay, indirect pulp treatment

Introduction

In teeth with deep dentin decay which have formed cavitation, the aim is to maintain the vitality and function of the tooth in the mouth with appropriate decay management.[1–4] Irrespective of the method used to remove the decay, vital pulp treatment (VPT) is applied according to the status of the exposed pulp.[1,5,6] Vital pulp treatment includes a series of conservative procedures based on the internal repair mechanisms of the pulp–dentin complex.[7–12] These have attracted more interest with the utility of new bioactive materials.[1]

Pulp capping biomaterials are placed as a protective layer on the pulp exposed following trauma to the teeth or after removal of decay lesions.[13] These materials are found in live tissues and facilitate the survival and proliferation of stem cells which have the potential for repair.[14] Calcium hydroxide (CH) is the oldest and most commonly used amputation agent in clinical dental practice and is considered the gold standard. It is a low-cost, easily applied material which supports reparative dentin formation, and can be applied rapidly to the exposed pulp area.[15–18]

Calcium hydroxide is a basic salt ($Ca(OH)_2$) with low solubility in water with a high alkalic pH, which breaks down into calcium (Ca^{+2}) and hydroxyl (OH^-) ions within the solution. When applied to pulp tissue, it produces a caustic effect, and coagulation converts the reserve mesenchymal cells below the necrosis first to fibroblasts and then to odontoblasts, which will form a matrix. It is also known to induce the expression of bioactive molecules such as growth factor- β1 (TBF-β1) and bone morphogenic protein-7 (BMP-7), which stimulate pulp repair.[19,20] Despite these positive properties, CH is resorbed over time because of weak mechanical properties which do not show adhesion to dentin, and cannot provide long-term biological impermeability against bacterial infection.[21]

In recent years, calcium silicate cements, which are derivatives of Portland cement, have been developed as an alternative to CH. Calcium-silicate cements are hydrophylic materials able to tolerate moisture (hydraulic materials) and to polymerize and harden (setting) also in the presence of biological fluids (blood, plasma, saliva, dentinal fluid).[22] The hardening reaction alkalizes the environment by expressing calcium and hydroxyl ions to the tissues with which it is in contact, and creates the necessary alkaline environment for the formation of hydroxyapatite.[22,23] The hardeninng reaction of calcium silicate-based materials is hydration. When dicalcium silicate (C_2S) and tricalcium silicate (C_3S) enter into a reaction with water, OH^-, Ca^{+2} and Si^{+4} (silicate) ions emerge as the side product. The OH^- ion forms a thin necrotic layer by increasing the pH in the underlying vital tissue. The vital cells below this layer are protected from the alkaline pH of the material. By stimulating cells in the pulp, the Ca^{+2} ion contributes to mineralization. When the Si^{+4} ion remains free, it contributes to hard tissue formation by stimulating osteoblasts.[24–28]

Biodentine is a calcium silicate material that was first introduced to the market in 2010. The material comes in the form of a capsule with powder and a separate liquid. The powder is formed of tricalcium silicate (Ca_3SiO_5), dicalcium silicate (Ca_2SiO_4), calcium carbonate ($CaCO_3$), calcium oxide (CaO), iron oxide (Fe_2O_3), and zirconium oxide (ZrO_2). The liquid contains calcium chloride ($CaCl_2$), water and modified polycarboxylate. Biodentine hardens with the hydration reaction starting with the mixing of the liquid and powder and the hardening process takes 9–12 min. As in other calcium silicate materials, there is a calcium-silicate-hydrate (C-S-H) gel phase and CH is formed while hardening. Upon contact with phosphate-containing solutions, the CH formation and hardening reaction give rise to the generation of antigen-presenting cell (APC) precursors. This represents the initial phase in the development of hydroxyapatite.[29,30] Biodentine has many clinical uses such as dentin liner below composite, direct pulp capping (DPC), pulpotomy treatment, apexification, root filling material, and perforation repair.[31,32] It has provided significant clinical advantages over other pulp capping materials, such as being very successful in dentin bridge formation, dentin substitution, good sealing properties, and sufficient pressure resistance. It shares its indications with CH, but its main disadvantages include setting time and material cost.[33,34]

Light-curable resin-based calcium silicate cements have several advantages, including instant setting through light transmission and ease of use. However, these cements contain resin monomers, and incomplete polymerization during light curing is associated with the risk of pulp cell toxicity.[35]

TheraCal PT (Bisco Inc., Schaumburg, USA) is a calcium silicate-based material modified with dual-cured resin, designed for the use of VPT. According to the manufacturer's instructions for the material, which is in the form of a double pat ready for use, it is applied in 1-mm layers polymerized with light for 20 s. Although calcium silicate cements with resin content show high physicaal properties, low solubility and ease of clinical use, such material can be separated from dentin tissue due to polymerization shrinkage during the hardening with light. The bonding strength between calcium silicate cements and adhesive systems directly affects the success of VPT.[23,36]

Although CH is not accepted as the best possible material option today, CH is still widely used in direct and indirect pulp treatment (IPT) in many healthcare institutions due to the high cost of calcium silicate materials. Despite the superior properties of calcium silicate materials, can CH still be used in VPT?

Objectives

The null hypothesis of this study was that calcium silicate materials would show similar success rates when compared among themselves, and would present better clinical and radiographic results than CH material.

Materials and methods

To fulfil the research objectives, the authors planned a randomized, double-blind clinical trial, which was conducted in the Restorative Dental Treatment Department of the Dentistry Faculty of Harran University, Şanlıurfa, Turkey. The study was conducted in accordance with the Declaration of Helsinki, and the protocol was approved by the Ethics Committee of Harran University (decision No. HRU/21.15.31 dated September 6, 2021) . The risks and benefits related to the procedure were fully explained to all the patients included in the study, and written informed consent was provided by all the partcipants.

A total of 186 participants in the 17–69 age group were included in this study. Twenty-seven participants refused to take part in the study. Sixteen participants were excluded from the study according to exclusion criteria. As a result of clinical and radiographic examinations, the teeth included in the study were those with deep dentin decay where there was thought to be a possibility of pulp perforation resulting from the complete removal of the caries. Vital teeth were selected which had no history of spontaneous or long-lasting pain against thermal or chemical stimuli, no percussion sensitivity, pathological mobility, edema, fistula, or color change. In the radiological examination, premolar and molar teeth, in which the presence of deep decay approaching the pulp ICDAS 5, 6 (International Caries Detection and Assessment System) was observed, were selected when the lamina dura and periodontal gap were healthy, there was no loss of bone surrounding the root, no internal or external root resorption, and no calcified masses observed within the pulp.

Three main groups were formed as follows: CH Group (Dycal, Dentsply/Caulk, International Inc. Milford, USA): In the Dycal group (n : 48), IPT was applied to 25 teeth and DPC to 23 teeth. Following clinical and radiographic examinations, pulp vitality tests were applied (Pulp Tester; Foshan Adelson Medical Devices Co., Ltd., Foshan, China). After a local anaesthesia injection, rubber-dam isolation was performed. In the IPT procedure, the decayed enamel tissue was removed with a cooled high-speed handpiece and a sterile diamond round burr (Diamant GmbH, Schürenbreder Weg 27, Germany). Infected dentin was removed with low-speed, tungsten carbide round burrs (Meisinger Hager & Meisinger GmbH, Neuss, Germany). In accordance with the manufacturer's instructions for IPT, a thin layer of Ca(OH)2 (Dycal; Dentsply/Caulk) was applied to areas close (0.5 mm) to the pulp.

In the DPC procedure, a sterile cotton wad was applied with moderate pressure for 5 min to the bleeding pulp that was exposed after removal of the decay, and hemostasis was obtained. A thin layer of $Ca(OH)_2$ was applied to the exposed pulp area and areas close (0.5 mm) to the pulp in accordance with the manufacturer's instructions. Thus, DPC was performed.

Calcium silicate Group (Biodentine; Septodont, Saint-Maur-des-Fossés, France): In the Biodentine group (n = 48), IPT was applied to 22 teeth and DPC to 26 teeth. In the IPT procedure, the pulp capping material with tricalcium silicate content formed of powder and liquid components was mixed and then applied to areas close to the pulp (0.5 mm) in accordance with the manufacturer's instructions. In the DPT procedure, a sterile cotton wad was applied with moderate pressure for 5 min to the bleeding pulp that was exposed after removal of the decay, and hemostasis was obtained. A thin layer of Biodentine was applied to the exposed pulp area and areas close (0.5 mm) to the pulp in accordance with the manufacturer's instructions. A period of 12 min was waited for hardening of the material.

In the TheraCal PT group (n = 47), IPT was applied to 24 teeth and DPC to 23 teeth. In the IPT procedure, a thin layer of dual-cured resin-modified tricalcium silicate was applied at max. 1-mm thickness to areas close (0.5 mm) to the pulp in accordance with the manufacturer's instructions, and was then polymerized with light for 20 s (Valo LED, Ultradent Products Inc., South Jordan, USA). In the DPC procedure, a sterile cotton wad was applied with moderate pressure for 5 min to the bleeding pulp that was exposed after removal of the decay, and hemostasis was obtained. A thin layer of TheraCal PT was applied at a maximum thickness of 1 mm to the exposed pulp area and areas close (0.5 mm) to the pulp in accordance with the manufacturer's instructions; then, polymerization was applied with light for 20 s.

During the decay removal method, every effort was made not to expose the pulp tissue. After the pulp capping, the universal adhesive system G-Premio Bond (GC Corp., Tokyo, Japan), Filtek-Ultimate Flowable composite (3M ESPE, St Paul, USA) and 3M Filtek Universal composite (3M ESPE, St.Paul, USA) were placed over the pulp capping material in each of the 3 groups.

Before starting the study, power analysis was performed using G*Power v. 3.1 software. The sample size required was found to be 143 study participants at 0.05 error rate and in 0.80 confidence interval.

A total of 143 teeth with deep dentinal caries were numbered at random using Microsoft Excel 2013 (Microsoft Corp., Redmond, USA). It was planned to apply Dycal to the 1st tooth No. 1–48, Biodentine to tooth No. 49–96 and Therecal PT to tooth No. 97–143. Before the appointment, the randomization list was checked by the oral and dental technician, and the treating clinician was informed which application method should be used. Each group consisted of teeth randomly assigned by a blinded investigator according to the materials selected. All the clinical procedures in this study were performed by a single dentist (Y.Y.) The patients were instructed to call and inform the resarchers if they were in any pain or discomfort. All the patients were informed that if there were abnormal signs and symptoms, there could be a need for root canal treatment.

All clinical and radiographic follow-up evaluations were performed by the expert investigator (S.K.) who was blinded to the drugs used (not the operator). Patients were re-examined clinically and radiographically to evaluate pulp vitality 6 and 12 months after treatment. Among the clinical parameters used for evaluation, the presence of post-treatment pain, provoked pain, spontaneous pain, or night pain were used. In the clinical examination, the following aspects were investigated: percussion, palpation, mobility, edema, and the presence of a fistula. In radiographic evaluation, lamina dura continuity, periapical lesion, furcation lesion, and pathological root resorption were assessed. The presence of one or more of the clinical/radiographic findings was considered treatment failure.

Statistical analyses

The data obtained in the study were statistically analysed using IBM SPSS Statistics v. 23.0 (IBM Corp., Armonk, USA). Descriptive statistics were presented as mean ±standard deviation (mean ±SD) values for continuous variables and number (n) and percentage (%) for categorical variables. The suitability of the data for normal distribution was evaluated using the Shapiro–Wilk test. The χ^2 ttest was used to analyze the relationships between categorical variables. Bonferroni method was used in the pairwise comparisons of success rates at 6th and 12th month according to the groups. In this paper, we focused on the results for each group separately. Therefore, the McNemar test was used, for each group separately, for measurements made at 2 different times. Kruskal–Wallis test was used because the mean age data were not normally distributed. The χ^2 test was used to compare the distribution of genders between the groups. Comparisons in different groups are shown with letters in the tables. A p-value of less than 0.05 was deemed to be statistically significant.

Results

Figure 1 presents the flow diagram for patient recruitment and selection. The sample size of this study was 143. It was planned to apply Dycal to the first 48 teeth, Biodentine to the next 48 teeth and Therecal PT to the last 47 teeth. Twelve patients did not come to their appointments. Direct pulp capping was applied to 65 teeth and IPT to 66 teeth. Evaluation was made of 131 teeth of 50 men with a mean age of 34.26 ±12.86 years and 81 women with a mean age of 30.23 ±9.97 years (age range: 17–69 years). As a result of the statistical evaluations, age and gender distribution between the groups was not seen to be normal (Table 1) ($p > 0.05$). It was observed that there was no statistically significant difference between the mean ages of the individuals participating in the study in different groups groups ($p = 0.139$).

Evaluation of the success rates of indirect pulp treatment

At the end of month 6, there were 2 failures and 1 patient who did not attend the follow-up appointment in the Dycal IPT group, 1 failure and 1 patient who did not attend the follow-up appointment in the Biodentine IPT group, and 2 failures and 4 patients who did not attend the follow-up appointment in the TheraCal PT IPT group.

At the end of month 12, no clinical or radiographic failure was observed in any of the 3 groups (Dycal, Biodentine, TheraCal PT) applied with IPT. The success rates of IPT in the clinical and radiographic evaluations at 6 months and 12 months were determined to be 91.7% in the Dycal group, 95.2% in the Biodentine group and 90.0% in the TheraCal PT group. There was no difference between groups with the same letter (Table 2).

In the Biodentine IPT group, it was found that there was no statistically significant difference between the filling procedures performed at 2 different times ($p = 1.000$). In the Dycal IPT group, there was no statistically significant difference between the filling procedures performed at 2 different times ($p = 1.000$). In the TheraCal PT IPT group, there was no statistically significant difference between the filling procedures performed at 2 different times ($p = 1.000$) (Table 3).

Table 1. Comparison of mean age according to groups of patients

Groups	Mean ±SD	Median (Q1–Q3)	Skewness	Kurtosis	Shapiro–Wilk	Test statistic	p-value (Kruskal–Wallis test)
Biodentine DPC	32.44 ±11.44	46 (17–63)	0.809	0.574	0.161	1.703	0.139
Biodentine IPT	30.71 ±12.01	40 (18–58)	0.935	–0.323	0.007		
Dycal DPC	37.05 ±11.32	51 (18–69)	0.899	1.881	0.289		
Dycal IPT	32.04 ±11.04	41 (19–60)	1.107	0.462	0.009		
TheraCal PT DPC	30.00 ±9.72	28 (18–46)	0.400	–1.237	0.060		
TheraCal PT IPT	27.6 ±10.96	43 (17–60)	1.677	0.778	0.001		

DPC – direct pulp capping; IPT – indirect pulp treatment.

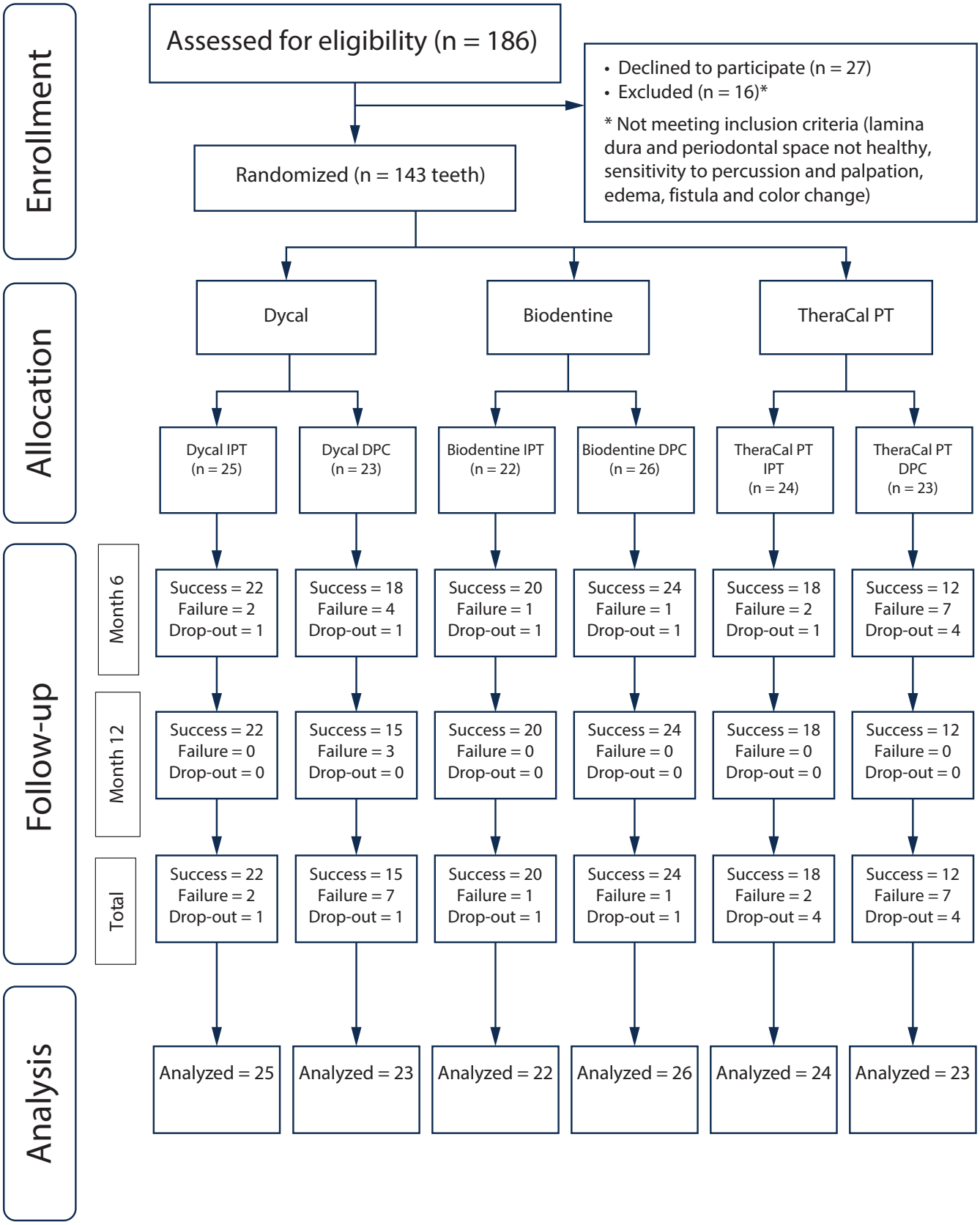


Fig. 1. Flow diagram of the study. DPC – direct pulp capping; IPT – indirect pulp treatment.

Table 2. The success rates of the different pulp capping materials applied in IPT

Groups	Success n (%)	Failure n (%)	Total n (%)	Test statistic	p-value
Month 6 IPT					
Biodentine IPT	20 (95.2)[a]	1 (4.8)[a]	21 (100.0)	$\chi^2 = 8.418$	0.811
Dycal IPT	22 (91.7)[a]	2 (8.3)[a]	24 (100.0)		
TheraCal PT IPT	18 (90.0)[a]	2 (10.0)[a]	20 (100.0)		
Month 12 IPT					
Biodentine IPT	20 (95.2)[a]	1 (4.8)[a]	21 (100.0)	$\chi^2 = 8.418$	0.811
Dycal IPT	22 (91.7)[a]	2 (8.3)[a]	24 (100.0)		
TheraCal PT IPT	18 (90.0)[a]	2 (10.0)[a]	20 (100.0)		

[a] no difference between groups with the same letter. IPT – indirect pulp treatment.

Evaluation of the success rates of direct pulp capping

At the end of month 6, there were 4 failures and 1 patient who did not attend the follow-up appointment in the Dycal DPC group, 1 failure and 1 patient who did not attend the follow-up appointment in the Biodentine DPC group, and 7 failures and 4 patients who did not attend the follow-up appointment in the TheraCal PT DPC group. In the clinical and radiographic evaluations at 6 months, the success rates of DPC were determined to be 81.8% in the Dycal group, 96.0% in the Biodentine group and 63.2% in the TheraCal PT group.

At the end of the 12-month follow-up period, there were 3 clinical and radiographic failures in the Dycal DPC group and none in the Biodentine DPC and TheraCal PT groups. In the clinical and radiographic evaluations at 12 months,

Table 3. Comparison of treatments applied to patients in 2 different time periods

Variable	Success status at month 6	Success at month 12		Failure at month 12		p-value
		n	%	n	%	
Biodentine DPC	success	24	100	0	0	1
	failure	0	0	1	100	
Biodentine IPT	success	20	100	0	0	1
	failure	0	0	1	100	
Dycal DPC	success	15	100	3	42.9	0.25
	failure	0	0	4	57.1	
Dycal IPT	success	22	100	0	0	1
	failure	0	0	2	100	
TheraCal PT DPC	success	12	100	0	0	1
	failure	0	0	7	100	
TheraCal PT IPT	success	18	100	0	0	1
	failure	0	0	2	100	

Table 4. Success rates of different pulp capping materials applied to DPC

Groups	Success n (%)	Failure n (%)	Total n (%)	Test statistic	p-value
Month 6 DPC					
Biodentine DPC	24 (96.0)[a]	1 (4.0)[a]	25 (100.0)	$\chi^2 = 7.827$	0.020*
Dycal DPC	18 (81.8)[ab]	4 (18.2)[ab]	22 (100.0)		
TheraCal PT DPC	12 (63.2)[b]	7 (36.8)[b]	19 (100.0)		
Month 12 DPC					
Biodentine DPC	24 (96.0)[a]	1 (4.0)[a]	25 (100.0)	$\chi^2 = 8.183$	0.017*
Dycal DPC	15 (68.2)[b]	7(31.8)[b]	22 (100.0)		
TheraCal PT DPC	12 (63.2)[b]	7 (36.8)[b]	19 (100.0)		

*$p < 0.05$; [a,b] no difference between groups with the same letter. DPC – direct pulp capping.

the success rates of DPC were determined to be 96.0% in the Biodentine group, 68.2% in the Dycal group and 63.2% in the TheraCal PT DPC group (p = 0.020; p = 0.017) (Table 4). In the Biodentine DPC group, it was found that there was no statistically significant difference between the filling procedures performed at 2 different times (p = 1.000). In the Dycal DPC, there was no statistically significant difference between the filling procedures performed at 2 different times (p = 0.250). In the TheraCal PT DPC, there was no statistically significant difference between the filling procedures performed at 2 different times (p = 1.000) (Table 3).

Discussion

The aim of VPT in teeth with decay lesions is to protect the vitality and integrity of dental tissues.[37]

This randomized clinical trial was conducted to evaluate the clinical and radiographic behavior of Dycal, Biodentine and TheraCal PT in VPT (direct and indirect) during a 1-year follow-up. The focus was on the use of dental materials to preserve the vitality of the pulp in teeth with deep dentin caries. The main findings of this study were that failures in IPT were low in all 3 groups (Dycal, Biodentine and TheraCal PT). It was found that there was no statistically significant difference between the filling processes of 3 materials at 2 different times in IPT. It was also observed that most of the failures occurred in the 1st follow-up period and the rate did not change in the 12th month. In DPC, clinical and radiographic failures were observed to be less frequent in the group treated with Biodentine compared to the groups treated with Dycal and TheraCal PT. Although failure rate in the Dycal group increased over time in the DPC, it was not found to be statistically significant at 2 different times.

Cho et al. reported that the material used in DPC was one of the most important factors affecting prognosis.[38] Calcium hydroxide, which has been used for many years as a vital pulp capping material, is still accepted as it is low-cost and easy to apply.[15–18] However, pulp capping materials containing tricalcium silicate have been recently reported to be more successful than CH.[7,17,39]

In their research on the effectiveness of Kusuma, Biodentine, $Ca(OH)_2$ and mineral trioxide aggregate (MTA) on the cellular response of pulp tissue; Biodentine showed activity with fewer neutrophils and macrophages and higher numbers of odontoblast-like cells and fibroblasts.[40]

In studies of pulpotomy, in which Biodentine and MTA were used, El Habashy et al. reported 100% clinical success of both materials.[41]

Hashem et al. compared the success of IPT using calcium silicate (Biodentine) and glass ionomer (Fuji IX™ GP; GC Corporation, Tokyo, Japan), and in a 2-year follow-up period, the clinical success rates were found to be 77.8% for Biodentine and 66.7% for Fuji IX.[42]

When clinicians are determining the biomaterial to be selected, the advantages of the material in clinical use should be evaluated. In hospitals providing oral and dental health services to the community, Dycal is the most frequently applied clinical material.[43]

In a study by Rahman et al., IPT was applied to young permanent teeth throughout 24 months, and the success rates were found to be 77.8% for CH, 94.4% for Biodentine, and 100% for TheraCal.[44]

In another study by Oğlakçıoğlu and Pamir, direct and indirect pulp capping was applied to teeth with deep dentin decay using CH (Dycal) as the coverage material. The 6-month follow-up results of the clinical examinations of the continued vitality of the teeth showed that vitality and functions were maintained in 92% of the teeth with no clinical or radiographic findings. The teeth in which failure was observed all had primary decay lesions and had been applied with Dycal and composite resin after preparation of the cavity.[10] The results of the current study support these findings, with success rates of 95.2% for Biodentine, 91.7% for Dycal and 90.1% for TheraCal PT at both 6 and 12 months in IPT applied to teeth with deep dentin decay. No statistically significant difference was determined between these rates. The main reason why the 3 pulp capping materials exhibit similar success rates may be that the pulp is not directly exposed and there is little dentin barrier.

In a study with a 2-year follow-up period, Mente et al. applied DPC using MTA and CH, and reported success rates of 80.5% in the teeth treated with MTA and 59% for those treated with CH.[45]

Biodentine has been shown to stimulate odontoblast-like differentiation and secretion of TGF-β1, an important growth factor. It has been shown to induce odontoblastic differentiation and increase mineralization in human dental pulp stem cells.[40,46]

In our study, the reason for the higher success rate in DPC of Biodentine compared to the other 2 materials (Dycal and TheraCal PT) may be that it increases repair dentin mineralization by inducing odontoblastic differentiation.

Light-hardened materials for VPT have been introduced by combining the superior use of resin with the desirable bioactive characteristics of calcium silicate cements. The fact that the hardening reaction occurs immediately and the restoration can be completed in a single session is seen as an advantage.[36]

Wassel et al. applied calcium silicate modified with dual-cured resin (TheraCal PT) and after a 12-month follow-up period of IPT, DPC, partial pulpotomy, and pulpotomy treatment, the success rates were found to be 93.87% in IPT, 80.4% in DPC, 96.15% in pulpotomy, and 57.4% in partial pulpotomy. The failure in partial pulpotomy was attributed to uncontrolled bleeding, the gap between TheraCal PT and the amputation region, and insufficient

disinfection before amputation, associated with misdiagnosis of the pulp status.[47]

Peskersoy et al. investigated the in vivo efficacy of different calcium silicate-based materials (Dycal, LC Calcihyd, Theracal LC, Biodentine, BioMTA) in DPC related to the pulp exposure status (<0.5 mm and 0.5–1 mm) and reported that the success rates of Biodentine and MTA were high at the end of 1 year and 3 years. The lowest success rate was seen in LC Calcihyd, and no statistically significant difference was determined between TheraCal LC and Dycal.[7]

Covaci et al. performed IPT and DPC to teeth with deep dentin decay using different materials (Life Kerr AC, TheraCal LC, Calcimol LC), and reported the survival rates to be 100% for Life Kerr AC, 92% for TheraCal LC and 83.87% for Calcimol LC, with no significant difference determined between the materials. Although self-hardening CH material showed better results than both CH and calcium silicate materials hardened with light, the difference between them was not significant.[3] Throughout a 9-year follow-up period of DPC applied with calcium silicate (MTA), Bogen et al. reported positive results in 97.96%. All the teeth in young patients with exposed apexes initially showed completed root formation (apexogenesis).[5] In a study by Harms et al., DPC using calcium silicate (Biodentine) was clinically evaluated after mean 2.3 years, and it was reported that patient age and gender, tooth type, arch type, and spontaneous pain before treatment did not affect the treatment results.[48] Therefore, the hypothesis that pulp capping should be avoided in elderly patients or in teeth with pain or discomfort was rejected.

The most recent data have shown the capacity of the pulp to respond by triggering dentin pulp regeneration with an inflammatory reaction. Materials containing resin, such as TheraCal, shift the response of the pulp towards an inflammatory reaction while changing the regeneration process.[24] In contrast, materials not containing resin, such as Biodentine, have anti-inflammatory potential and induce the pulp regeneration capacity. This information contradicts the recent tendency for the development of resin-based calcium silicate hybrid materials for pulp capping.[24] In the current study, the low success rate in DPC of TheraCal PT, which contains resin and has a dual-cure hardening reaction, could be attributed to the resin content and polymerization shrinkage. In contrast, materials not containing resin such as Biodentine have anti-inflammatory potential and induce the pulp regeneration capacity.[46]

Wang et al., in their study investigating the bioinductive effects of MTA and Biodentine on lipopolysaccharide-induced pulp cells with different severities of inflammation, showed that more Dentin sialophosphoprotein developed in both normal and lipopolysaccharide-induced pulp cells at 48 and 96 h. This may mean that Biodentine treatment is not affected by the duration of inflammation.[49]

Suhag et al. compared the pulp capping success rates and postoperative pain using CH and MTA in teeth with deep dentin decay and irreversible pulpitis. The results of thier study showed that treatment with DPC could be successful, and MTA was found to be better than CH in terms of success rates and pain severity.[50]

Ricucci et al. performed DPC on teeth clinically diagnosed with reversible pulpitis and exposed pulp due to advanced caries and reported long-term DPC success rates of 100% at 1 year, 95% at 5 and 10 years, 86% at 20 years, and 89% at 35 years. Especially in the first 10 years of follow-up of the treatment, a very high success rate was observed in DPC with CH. The main variable significantly affecting the treatment results in all the follow-up periods was found to be the quality of the coronal restoration.[51]

The follow-up period in the current study was 12 months, which seemed to be insufficient compared to the previous studies.[39,41,44,47] In parallel with other studies, the success rate was determined to be high in IPT when all the treated teeth were evaluated. In the clinical and radiographic evaluations of DPC at the end of 6-month follow-up, the success rates were seen to be 96.0% in the Biodentine group, 81.8% in the Dycal group and 63.2% in the TheraCal PT group, and after 12 months these rates were 96.0% for Biodentine, 68.2% for Dycal and 63.2% for TheraCal PT. However, the results at 2 different times were not statistically significant. The high success rate of Biodentine was believed to be due to the calcium silicate content, biocompatibility and the property of not showing microleakage of the material. The low success rate of Dycal with CH content at 6 months and the decrease over time was considered to be due to the absence of the property of excellent impermeability and that composite restoration was applied over the Dycal capping material in this study. The low success rate of TheraCal PT can be attributed to the fact that it does not show ideal impermeability because of the resin content and polymerization shrinkage.

Limitations

There are some limitations to this study. First, the post-treatment follow-up period was 12 months, which was insufficient for monitoring vital tooth functions. Second, the sample size was insufficient; therefore, larger sample sizes should be employed in future studies.

Conclusions

In IPT CH (Dycal), calcium silicate (Biodentine) and calcium silicate with resin content (TheraCal PT) showed high clinical and radiological success. Direct pulp capping, Biodentine containing calcium silicate was found to be more successful than CH (Dycal) and calcium silicate with resin content (TheraCal PT).

Data availability

The datasets generated and/or analyzed during the current study are available from the corresponding author on reasonable request.

Consent for publication

Not applicable.

Use of AI and AI-assisted technologies

Not applicable.

ORCID iDs

Yasemin Yavuz https://orcid.org/0000-0001-5961-4996
Sedef Kotanlı https://orcid.org/0000-0002-0827-0991
Mehmet S. Dogan https://orcid.org/0000-0002-3089-1305
Zelal Almak https://orcid.org/0000-0001-6031-427X

References

1. Llena C, Hernández M, Melo M, Sanz JL, Forner L. Follow-up of patients subjected to direct and indirect pulp capping of young permanent teeth: A retrospective study. *Clin Exp Dent Res*. 2021;7(4):429–435. doi:10.1002/cre2.362
2. Yazici AR, Başeren M, Dayangaç B. The effect of current-generation bonding systems on microleakage of resin composite restorations. *Quintessence Int*. 2002;33(10):763–769. PMID:12553620.
3. Covaci A, Ciocan LT, Gălbinaşu B, Bucur MV, Matei M, Didilescu AC. Dental pulp response to different types of calcium-based materials applied in deep carious lesion treatment: A clinical study. *J Funct Biomater*. 2022;13(2):51. doi:10.3390/jfb13020051
4. Duncan HF, Galler KM, Tomson PL, et al; European Society of Endodontology (ESE). European Society of Endodontology position statement: Management of deep caries and the exposed pulp. *Int Endod J*. 2019;52(7):923–934. doi:10.1111/iej.13080
5. Bogen G, Kim JS, Bakland LK. Direct pulp capping with mineral trioxide aggregate. *J Am Dent Assoc*. 2008;139(3):305–315. doi:10.14219/jada.archive.2008.0160
6. Schwendicke F, Brouwer F, Schwendicke A, Paris S. Different materials for direct pulp capping: Systematic review and meta-analysis and trial sequential analysis. *Clin Oral Invest*. 2016;20(6):1121–1132. doi:10.1007/s00784-016-1802-7
7. Peskersoy C, Lukarcanin J, Turkun M. Efficacy of different calcium silicate materials as pulp-capping agents: Randomized clinical trial. *J Dent Sci*. 2021;16(2):723–731. doi:10.1016/j.jds.2020.08.016
8. Sanz JL, Soler-Doria A, López-García S, et al. Comparative biological properties and mineralization potential of 3 endodontic materials for vital pulp therapy: Theracal PT, Theracal LC, and Biodentine on human dental pulp stem cells. *J Endod*. 2021;47(12):1896–1906. doi:10.1016/j.joen.2021.08.001
9. Pai S, Bhat V, Kini S, Purayil TP. Emergency pain management in symptomatic pulpo-periradicular pathosis: Case series. *J Int Dent Med Res*. 2018;11(1):339–341. https://www.jidmr.com/journal/wp-content/uploads/2018/04/65D17_493_Swathi_Pai.pdf.
10. Oğlakçıoğlu S, Pamir T. Direct and indirect pulp capping after complete caries removal: A preliminary study. *EÜ Dişhek Fak Derg*. 2020;41(2):91–98. doi:10.5505/eudfd.2020.20053
11. Kuhn E, Reis A, Chibinski AR, Wambier D. The influence of the lining material on the repair of the infected dentin in young permanent molars after restoration: A randomized clinical trial. *J Conserv Dent*. 2016;19(6):516. doi:10.4103/0972-0707.194026
12. Biçer H, Bayrak Ş. Evaluation of bond strength of restorative materials to calcium silicate-based biomaterials in vital pulp treatment [in Turkish]. *Selcuk Dent J*. 2019;6(3):271–279. doi:10.15311/selcukdentj.434762
13. Gandolfi MG, Siboni F, Botero T, Bossù M, Riccitiello F, Prati C. Calcium silicate and calcium hydroxide materials for pulp capping: Biointeractivity, porosity, solubility and bioactivity of current formulations. *J Appl Biomater Funct Mater*. 2015;13(1):43–60. doi:10.5301/jabfm.5000201
14. Spagnuolo G, Codispoti B, Marrelli M, Rengo C, Rengo S, Tatullo M. Commitment of oral-derived stem cells in dental and maxillofacial applications. *Dent J*. 2018;6(4):72. doi:10.3390/dj6040072
15. Hilton TJ. Keys to clinical success with pulp capping: A review of the literature. *Oper Dent*. 2009;34(5):615–625. doi:10.2341/09-132-0
16. Chatzidimitriou K, Vadiakas G, Koletsi D. Direct pulp capping in asymptomatic carious primary molars using three different pulp capping materials: A prospective clinical trial. *Eur Arch Paediatr Dent*. 2022;23(5):803–811. doi:10.1007/s40368-022-00720-y
17. Akçay M, Sarı Ş. Evaluation of efficacy of MTA and Ca(OH)2 on vital pulpotomy in primary teeth clinically and radiologically [in Turkish]. *Dent Sci Special Topics*. 2012;3(1):50–56. https://www.turkiyeklinikleri.com/article/tr-sut-disi-vital-pulpa-amputasyonlarinda-mta-ve-caoh2nin-etkinliginin-klinik-ve-radyolojik-olarak-degerlendirilmesi-62345.html.
18. Corralo DJ, Maltz M. Clinical and ultrastructural effects of different liners/restorative materials on deep carious dentin: A randomized clinical trial. *Caries Res*. 2013;47(3):243–250. doi:10.1159/000345648
19. Graham L, Cooper PR, Cassidy N, Nor JE, Sloan AJ, Smith AJ. The effect of calcium hydroxide on solubilisation of bio-active dentine matrix components. *Biomaterials*. 2006;27(14):2865–2873. doi:10.1016/j.biomaterials.2005.12.020
20. Charoenwongsawad C, Fuangtharnthip P, Tengrungsun T, Suddhasthira T, Tamura Y. Effect of capsaicin on proliferation and wound healing of dental pulp cells in vitro. *J Int Dent Med Res*. 2021;14(1):180–186. https://www.jidmr.com/journal/wp-content/uploads/2021/03/29-E-D20_1331_Pornpoj_Fuangtharnthip_Thailand.pdf.
21. Kitasako Y, Ikeda M, Tagami J. Pulpal responses to bacterial contamination following dentin bridging beneath hard-setting calcium hydroxide and self-etching adhesive resin system. *Dent Traumatol*. 2008;24(2):201–206. doi:10.1111/j.1600-9657.2007.00517.x
22. Gandolfi MG, Taddei P, Siboni F, Modena E, De Stefano ED, Prati C. Biomimetic remineralization of human dentin using promising innovative calcium-silicate hybrid "smart" materials. *Dent Mater*. 2011;27(11):1055–1069. doi:10.1016/j.dental.2011.07.007
23. Zakaria MN, Amalina SN, Seroja FB, Sidiqa AN, Cahyanto A. Calcium release and mechanical strength of calcium fluoride doped carbonate apatite cement as a novel pulp capping agent. *J Int Dent Med Res*. 2020;13(3):945–950. https://www.jidmr.com/journal/wp-content/uploads/2020/09/20-D20_1171_Arief_Cahyanto_Indonesia.pdf.
24. Giraud T, Jeanneau C, Rombouts C, Bakhtiar H, Laurent P, About I. Pulp capping materials modulate the balance between inflammation and regeneration. *Dent Mater*. 2019;35(1):24–35. doi:10.1016/j.dental.2018.09.008
25. Kunjan AP, Ballal NV. Calcium silicate based cements in endodontics. *J Int Dent Med Res*. 2020;13(3):1183–1190. https://www.jidmr.com/journal/wp-content/uploads/2020/09/61-D20_1097_Nidambur_Vasudev_Ballal_India.pdf.
26. Dogan MS, Rahardjo A, Wimardhani YS, Yavuz I. The rehabilitation of permanent teeth with complicated crown fracture by MTA pulpotomy and re-attachment: Case series report study and literature review. *J Dent Oral Dis Ther*. 2017;5(1):1–6. doi:10.15226/jdodt.2017.00172
27. Torabinejad M, Parirokh M. Mineral trioxide aggregate: A comprehensive literature review. Part II: Leakage and biocompatibility investigations. *J Endod*. 2010;36(2):190–202. doi:10.1016/j.joen.2009.09.010
28. Johari Y, Pungut NA, Yin VWX, Khamis MF, Yussof MNM. Sealing ability of injectable dental composites, biodentine and MTA in repairing furcal perforation of permanent molar teeth. *J Int Dent Med Res*. 2020;13(4):1428–1434. https://www.jidmr.com/journal/wp-content/uploads/2020/12/31-D20_1221_Yanti_Johari_Malaysia.pdf.
29. Kim JR, Nosrat A, Fouad AF. Interfacial characteristics of Biodentine and MTA with dentine in simulated body fluid. *J Dent*. 2015;43(2):241–247. doi:10.1016/j.jdent.2014.11.004
30. Megantoro A, Djauharie RN, Margono A. The effect of biodentineTM application in affected dentin remineralization after partial caries excavation in vivo. *J Int Dent Med Res*. 2019;12(3):1117–1122. https://www.jidmr.com/journal/wp-content/uploads/2019/10/48-D3_18390_Aryo-Megantoro.pdf.

31. Gandolfi MG, Taddei P, Siboni F, Modena E, Ciapetti G, Prati C. Development of the foremost light-curable calcium-silicate MTA cement as root-end in oral surgery: Chemical–physical properties, bioactivity and biological behavior. *Dent Mater*. 2011;27(7):e134–e157. doi:10.1016/j.dental.2011.03.011
32. Dania AR, Prisinda D. Biodentine as an apical plug material in immature teeth: A rapid review. *J Int Dent Med Res*. 2022;15(1):349–357. https://www.jidmr.com/journal/wp-content/uploads/2022/03/58-D21_1595_Ayu_Rahma_Dania_Indonesia.pdf.
33. Caruso S, Dinoi T, Marzo G, et al. Clinical and radiographic evaluation of biodentine versus calcium hydroxide in primary teeth pulpotomies: A retrospective study. *BMC Oral Health*. 2018;18(1):54. doi:10.1186/s12903-018-0522-6
34. Grewal N, Salhan R, Kaur N, Patel H. Comparative evaluation of calcium silicate-based dentin substitute (Biodentine) and calcium hydroxide (pulpdent) in the formation of reactive dentin bridge in regenerative pulpotomy of vital primary teeth: Triple blind, randomized clinical trial. *Contemp Clin Dent*. 2016;7(4):457. doi:10.4103/0976-237X.194116
35. Park SH, Ye JR, Asiri NM, Chae YK, Choi SC, Nam OH. Biocompatibility and bioactivity of a dual-cured resin-based calcium silicate cement: In vitro and in vivo evaluation. *J Endod*. 2024;50(2):235–242. doi:10.1016/j.joen.2023.11.009
36. Yavuz Y. Comparison of bond strength of biomaterials to universal adhesive systems: An in vitro study [in Turkish]. *Selcuk Dent J*. 2022;9(2):513–519. doi:10.15311/selcukdentj.1140867
37. Zero DT. Dental caries process. *Dent Clin North Am*. 1999;43(4):635–664. doi:10.1016/S0011-8532(22)00818-7
38. Cho SY, Seo DG, Lee SJ, Lee J, Lee SJ, Jung IY. Prognostic factors for clinical outcomes according to time after direct pulp capping. *J Endod*. 2013;39(3):327–331. doi:10.1016/j.joen.2012.11.034
39. Çalışkan MK, Güneri P. Prognostic factors in direct pulp capping with mineral trioxide aggregate or calcium hydroxide: 2- to 6-year follow-up. *Clin Oral Invest*. 2017;21(1):357–367. doi:10.1007/s00784-016-1798-z
40. Kusuma ARP. Efectivenesse of three pulp capping materials on cellular response of pulp tissue. *Odonto Dental Journal*. 2023;10(1):132–139. doi:10.30659/odj.10.1.132-139
41. El Habashy L. Biodentine versus MTA as pulpotomy agents in primary molars: Clinical and radiographic study. *Egypt Dent J*. 2020;66(3):1423–1434. doi:10.21608/edj.2020.26182.1079
42. Hashem D, Mannocci F, Patel S, Manoharan A, Watson TF, Banerjee A. Evaluation of the efficacy of calcium silicate vs. glass ionomer cement indirect pulp capping and restoration assessment criteria. A randomised controlled clinical trial: 2-year results. *Clin Oral Invest*. 2019;23(4):1931–1939. doi:10.1007/s00784-018-2638-0
43. Song W, Li S, Tang Q, Chen L, Yuan Z. In vitro biocompatibility and bioactivity of calcium silicate-based bioceramics in endodontics (Review). *Int J Mol Med*. 2021;48(1):128. doi:10.3892/ijmm.2021.4961
44. Rahman B, Goswami M. Comparative evaluation of indirect pulp therapy in young permanent teeth using Biodentine and Theracal: A randomized clinical trial. *J Clin Pediatr Dent*. 2021;45(3):158–164. doi:10.17796/1053-4625-45.3.3
45. Mente J, Hufnagel S, Leo M, et al. Treatment outcome of mineral trioxide aggregate or calcium hydroxide direct pulp capping: Long-term results. *J Endod*. 2014;40(11):1746–1751. doi:10.1016/j.joen.2014.07.019
46. Phang V, Malhotra R, Chen NN, et al. Specimen shape and elution time affect the mineralization and differentiation potential of dental pulp stem cells to Biodentine. *J Funct Biomater*. 2023;15(1):1. doi:10.3390/jfb15010001
47. Wassel M, Hamdy D, Elghazawy R. Evaluation of four vital pulp therapies for primary molars using a dual-cured tricalcium silicate (TheraCal PT): One-year results of a non-randomized clinical trial. *J Clin Pediatr Dent*. 2023;47(2):10–22. doi:10.22514/jocpd.2023.004
48. Harms CS, Schäfer E, Dammaschke T. Clinical evaluation of direct pulp capping using a calcium silicate cement: Treatment outcomes over an average period of 2.3 years. *Clin Oral Invest*. 2019;23(9):3491–3499. doi:10.1007/s00784-018-2767-5
49. Wang MC, Chang KW, Lin SC, Hung PS. Biodentine but not MTA induce DSPP expression of dental pulp cells with different severity of LPS-induced inflammation. *Clin Oral Invest*. 2022;27(3):1207–1214. doi:10.1007/s00784-022-04734-0
50. Suhag K, Duhan J, Tewari S, Sangwan P. Success of direct pulp capping using mineral trioxide aggregate and calcium hydroxide in mature permanent molars with pulps exposed during carious tissue removal: 1-year follow-up. *J Endod*. 2019;45(7):840–847. doi:10.1016/j.joen.2019.02.025
51. Ricucci D, Rôças IN, Alves FRF, Cabello PH, Siqueira JF. Outcome of direct pulp capping using calcium hydroxide: A long-term retrospective study. *J Endod*. 2023;49(1):45–54. doi:10.1016/j.joen.2022.11.005

Clinical analysis of 338 cases of dacryolithiasis

Ting Zhang[1,2,3,A,D,F], Wei Zhuo[1,2,3,B,C], Wei-na Wang[1,2,3,B,C], Lu Zhao[1,2,3,E,F]

[1] Eye Institute of Shandong First Medical University, Qingdao Eye Hospital of Shandong First Medical University, China
[2] State Key Laboratory Cultivation Base, Shandong Key Laboratory of Eye Diseases, Qingdao, China
[3] School of Ophthalmology, Shandong First Medical University, Qingdao, China

A – research concept and design; B – collection and/or assembly of data; C – data analysis and interpretation;
D – writing the article; E – critical revision of the article; F – final approval of the article

Advances in Clinical and Experimental Medicine, ISSN 1899–5276 (print), ISSN 2451–2680 (online) *Adv Clin Exp Med*. 2025;34(8):1299–1305

Address for correspondence
Lu Zhao
E-mail: zhaolueye2023@163.com

Funding sources
None declared

Conflict of interest
None declared

Received on December 6, 2023
Reviewed on April 18, 2024
Accepted on August 11, 2024

Published online on March 11, 2025

Abstract

Background. Dacryolithiasis can occur anywhere in the lacrimal drainage system and is frequently associated with microbial infections. The presence of dacryolithiasis is difficult to determine based on its clinical manifestations, which complicates clinical treatment.

Objectives. To analyze the clinical diagnosis, treatment and characteristics of dacryolithiasis, as well as surgical methods used to treat it and treatment effects over the past 5 years.

Materials and methods. A retrospective analysis was performed on the clinical data of 338 patients who were diagnosed with dacryolithiasis at our hospital from January 2017 to December 2021. Patients diagnosed with canaliculitis were treated with canaliculotomy. Dacryocystitis complicated by canaliculitis was treated with endoscopic dacryocystorhinostomy (En-DCR) combined with canaliculotomy. Dacryocystitis accompanied by dacryoliths was treated with En-DCR. Nasolacrimal duct stones were treated with lacrimal intubation. All patients were followed up for 6–12 months.

Results. All patients underwent successful surgery. Of 302 cases (89.35%) with canaliculitis, 297 (98.34%) were cured with canaliculotomy; 5 cases (1.66%) recurred within 1 year after surgery and were cured with canaliculotomy again. Four cases (1.18%) of dacryocystitis complicated by canaliculitis were treated with En-DCR combined with canaliculotomy. In addition, 30 patients (8.88%) had dacryolithiasis; 28 (93.33%) of them were cured, and 2 (6.67%) with common canalicular atresia were cured after lacrimal intubation. Furthermore, 2 patients (0.59%) with nasolacrimal duct stones underwent lacrimal intubation. In addition, 62 cases (20.53%) with canaliculitis tested positive for bacteria, and the top 2 common bacteria were *Staphylococcus epidermidis* and *Streptococcus mitis*.

Conclusions. Secretions are the main clinical characteristic of patients with dacryolithiasis, and surgery is the primary treatment method. In addition, different surgical methods correspond to different locations of stones.

Key words: dacryolithiasis, canaliculitis, dacryocystitis with dacryoliths, endoscopic dacryocystorhinostomy

Cite as
Zhang T, Zhuo W, Wang W, Zhao L. Clinical analysis of 338 cases of dacryolithiasis. *Adv Clin Exp Med*. 2025;34(8):1299–1305. doi:10.17219/acem/192223

DOI
10.17219/acem/192223

Copyright
Copyright by Author(s)
This is an article distributed under the terms of the Creative Commons Attribution 3.0 Unported (CC BY 3.0) (https://creativecommons.org/licenses/by/3.0/)

Background

Dacryolithiasis is a frequently occurring disorder of the lacrimal system, commonly linked with microbial infection and often underdiagnosed.[1,2] Dacryolithiasis is prone to occur in patients over 50 years old with a history of smoking, dacryocystitis, and facial and nasal trauma. Moreover, there is no significant difference in the incidence of dacryolithiasis between men and women.[3] Dacryoliths, first described in 1670, are stones that form in the lacrimal duct system. They can be found throughout the lacrimal drainage system, mainly consisting of lacrimal duct stones and lacrimal sac stones, and also involving a small part of the lacrimal duct system, such as nasolacrimal duct stones.[4] The lacrimal duct stones are mainly composed of lobulated and lamellar substances with amorphous nuclei. On the one hand, local necrotic tissue and calcification of mold or hypha can form stones. The formation of stones can be promoted by changes in tear rheology, mechanical stimulation, bacterial migration, and disruption of the balance between single mucin and trefoil factor peptides.[5] Although the specific pathogenesis of dacryolithiasis is not yet clear, some proteins and peptides play vital roles in the pathogenesis of lacrimal duct stones.[3] Moreover, Lew et al.[6] claimed that the concentration of lysozyme in tears of patients with dacryolithiasis was related to the pathogenesis of the condition.

Canaliculitis, one of the more common inflammatory diseases of the lacrimal duct, is mainly induced by lacrimal duct stones.[7] The presence of dacryolithiasis is difficult to determine based on its clinical manifestations, which complicates clinical treatment. Dacryolithiasis is mostly identified during dacryocystorhinostomy (DCR). Nasolacrimal duct stones are rare and lack typical manifestations, making them easily misdiagnosed as chronic conjunctivitis, chronic dacryocystitis or chalazion, which results in delays in effective treatment.[8] Recent studies revealed the role of tear rheology, mechanical stimulation and bacterial influences in dacryolith formation; however, these findings have not yet been sufficiently integrated into a comprehensive pathogenetic model. Given this context, the present study aims to bridge this gap by conducting a detailed biochemical analysis of lacrimal stones and correlating these findings with the clinical profiles of dacryolithiasis patients. This approach is anticipated to shed light on the specific molecular interactions involved in the pathogenesis of dacryolithiasis, offering a foundation for novel therapeutic strategies.

Objectives

This study was conducted to analyze the clinical diagnosis, treatment and characteristics of dacryolithiasis, as well as surgical methods used to treat it and treatment effects over the past 5 years, thereby providing a reference for the diagnosis and treatment of the disease.

Materials and methods

Study design and participants

This study was a retrospective analysis of cases. In total, 338 patients diagnosed with dacryolithiasis from 2017 to 2021 at Qingdao Eye Hospital of Shandong First Medical University (China) were enrolled. Among them, 71 were male and 267 were female, with an average age of 51.5 ±14.02 years. All patients were admitted to the hospital for a lacrimal duct irrigation examination, and dacryocystography was performed if the lacrimal duct was obstructed. The patients were divided into 4 groups based on the type of surgery. Specifically, 302 cases of dacryolithiasis diagnosed with canaliculitis underwent canaliculotomy; 4 cases of dacryocystitis complicated by canaliculitis were treated with endoscopic DCR (En-DCR) combined with canaliculotomy; 30 cases of dacryocystitis with dacryoliths were treated with En-DCR; and 2 cases of nasolacrimal duct stones were treated with lacrimal intubation. The definitive diagnosis was based on clinical manifestations and dacryocystography. This study was approved by the Ethics Committee of Qingdao Eye Hospital of Shandong First Medical University (approval No. 2022–48).

Types and surgical methods of dacryolithiasis

The clinical manifestations of canaliculitis (Fig. 1A) were as follows: 1) hyperemia and redness at the lacrimal punctum; 2) swelling of the lacrimal canaliculus area; 3) purulent and granular secretion upon pressure; and 4) unobstructed lacrimal duct flushing with secretion overflow. The surgical method was canaliculotomy. Specifically, the lacrimal punctum was dilated first, followed by a vertical incision on the lacrimal canaliculus. Next, lacrimal canaliculus stones were removed via curettage. Afterward, the lacrimal passage was flushed until the fluid coming out was transparent. A silicone drainage tube was inserted if the duct was not clear.

The main symptoms of dacryocystitis combined with canaliculitis were similar to those of canaliculitis alone, primarily involving tear overflow and secretion. In addition, dacryocystitis + canaliculitis was characterized by obstructed lacrimal duct flushing and secretion overflow, along with swelling and redness around the tear ducts, with granular secretions released upon pressure. The surgical method used was En-DCR combined with canaliculotomy.

The symptoms of dacryocystitis complicated by dacryoliths (Fig. 1B) were primarily lacrimation and secretion, with lacrimal sac stones observed during En-DCR. The surgical method involved removing calculi and granulation tissue from the lacrimal sac cavity via En-DCR.

Nasolacrimal duct stones (Fig. 1C), while similar to dacryocystitis, were characterized by low obstruction in the nasolacrimal duct and a short disease course (less than 4 months). The surgical method was removal



Fig. 1. Typical images of dacryolithiasis. A. Canaliculus stone in a case of canaliculitis; B. Lacrimal sac stone in a case of dacryocystitis complicated by dacryoliths; C. Nasolacrimal duct stone in a case of nasolacrimal duct stones

of the nasolacrimal duct stone through lacrimal duct probing with nasal endoscopy.

Postoperative medication and follow-up

The surgical eye was treated with antibiotic eye drops, 0.1% fluorometholone eye drops and antibiotic eye ointment. Patients undergoing En-DCR were given fluticasone propionate nasal spray twice a day and followed up at 1, 3, 6, and 12 months after surgery. Upon En-DCR, the patients underwent dressing changes and reexamination under a nasal endoscope. The secretion around the anastomosis was cleaned, and the lacrimal passage was washed. Subsequently, the epithelialization of the lacrimal sac, nasal cavity and anastomosis, as well as the recovery of lacrimal passage function, were observed.

Criteria for determining efficacy

Canaliculitis

The symptoms of lacrimation and secretion disappeared. The lacrimal punctum and lacrimal canaliculus had no redness and swelling. The lacrimal canaliculus had no secretion overflow after pressing the diseased lacrimal canaliculus, and the lacrimal passage was flushed unobstructedly and had no secretion.

Dacryocystitis combined with canaliculitis

The symptoms of lacrimation and secretion disappeared. The lacrimal punctum and lacrimal canaliculus did not exhibit redness and swelling. Upon pressing the diseased lacrimal canaliculus, there was no secretion overflow in the lacrimal canaliculus. In addition, the lacrimal passage was flushed unobstructedly and had no secretion. Nasal endoscopy showed that the mucosa of the anastomosis was epithelialized, the anastomosis was open and the lacrimal passage was flushed unobstructedly.

Dacryocystitis with dacryoliths

There were no symptoms of lacrimation and secretion. Nasal endoscopy displayed epithelialized anastomotic mucosa, with the anastomosis open and the lacrimal passage flushed unobstructedly.

Nasolacrimal duct stone

The symptoms of lacrimation and secretion disappeared. After pulling out the lacrimal drainage tube, the lacrimal duct was flushed unobstructedly and the secretion was absent.

Culture and identification of pathogenic bacteria

The secretions from the lacrimal punctum were extracted and sealed in sterile test tubes, and then bacterial culture and drug sensitivity tests were performed. In short, the collected specimens from the conjunctival sac and lacrimal duct were coated and scribed on a blood agar plate and cultured in a 35°C incubator for 24, 48 and 72 h to observe bacterial growth. If colony growth was observed, the bacteria were isolated and purified, followed by a drug sensitivity test.

Data presentation

For groups with less than 10 participants, the assumption of normal distribution was not checked; instead, data were reported using the median along with the minimum and maximum values. For larger groups exceeding 100 participants, the normality of distribution was not assessed; the central limit theorem was applied, and results were described using the mean and standard deviation (SD). For groups with sizes ranging from 10 to 100, the Shapiro–Wilk test was utilized to evaluate normality. If a statistically significant deviation from normal distribution was found,

the median and interquartile range (IQR) were reported. If there was no significant deviation, the mean and SD were used to present the data. Categorical data were consistently summarized as frequencies and percentages (n (%)).

Results

Clinical data characteristics

In this study, the clinical data of 338 patients with dacryolithiasis were analyzed, and the results are shown in Table 1. The 338 patients consisted of 71 (21%) men and 267 (79%) women, with a men-to-women ratio of 1:3.8. Their age ranged from 17 to 90 years (mean 61.40 ±14.02 years), and the disease duration ranged from 20 days to 20 years (mean 1.62 ±3.03 years). In addition, there were 76 cases (22.5%) of smokers and 302 cases (89.35%) of canaliculitis. Furthermore, 297 cases were cured, giving a cure rate of 98.34%; 5 cases (1.66%) recurred within 1 year after the operation and were cured by canaliculotomy again. Dacryocystitis combined with canaliculitis was found in 4 cases (1.18%) during the operation and was treated with En-DCR combined with canaliculotomy. Of the 30 patients (8.88%) with dacryolithiasis, 28 cases (93.33%) were cured, and 2 cases (6.67%) exhibited closed lacrimal ducts and were cured after re-catheterization. Two patients (0.59%) with nasolacrimal duct stones underwent lacrimal intubation; 1 case of nasolacrimal duct opening was examined by nasal endoscopy during the operation, and nasolacrimal duct stones were discharged. One case of stone-like secretion was removed from the nasal cavity after the operation, and all cases were cured. No recurrence was found within 1 year after the operation.

The location of canaliculitis

Subsequently, the location of canaliculitis was analyzed. The results showed that the first 4 locations of canaliculitis were the left inferior lacrimal canaliculus, the right inferior lacrimal canaliculus, the left superior lacrimal canaliculus, and the right superior lacrimal canaliculus, accounting for 34.44%, 26.49%, 14.9%, and 14.24%, respectively. Canaliculitis usually appeared in the inferior canaliculus, and there was no difference between the left and right eyes (Table 2).

Table 2. Location of canaliculitis lesions

Diseased region	Cases, n	Percentage (%)
Right superior lacrimal canaliculus	43	14.24
Right inferior lacrimal canaliculus	80	26.49
Right superior and inferior lacrimal canaliculi	13	4.30
Left superior lacrimal canaliculus	45	14.90
Left inferior lacrimal canaliculus	104	34.44
Light superior and inferior lacrimal canaliculi	11	3.64
Both superior lacrimal canaliculi	2	0.66
Both inferior lacrimal canaliculi	2	0.66
Both superior and inferior lacrimal canaliculi	2	0.66
Total	302	100

Etiology analysis

The samples from canaliculitis patients were sent for pathogen culture, and the distribution of pathogenic bacteria species in positive samples is shown in Table 3. Among the 302 cases with canaliculitis, 62 were positive for bacteria, with a culture positivity rate of 20.53%. In addition, a total of 17 bacterial strains were identified in these cultures, and the pathogenic bacteria were mostly Gram-positive cocci. *Staphylococcus epidermidis* was the most common pathogen, accounting for more than 51.61%.

The samples from dacryocystitis + dacryoliths patients were also subject to pathogen culture, and the distribution of pathogenic bacteria species in positive samples is presented in Table 4. Among the 30 cases with dacryocystitis + dacryoliths, 15 were positive for bacteria, with a culture positivity rate of 50%. Furthermore, a total of 6 bacterial strains were identified in these cultures, and the pathogenic bacteria were mostly Gram-positive cocci. *Staphylococcus aureus* and *S. epidermidis* were the most common pathogens, accounting for more than 66.67%.

Table 1. Clinical data of 338 patients with dacryolithiasis (mean ±SD, median (min, max), median (IQR), n (%))

Variables		Canaliculitis	Dacryocystitis complicated with canaliculitis	Dacryocystitis with dacryoliths	Nasolacrimal duct stone	Total
Cases, n (%)		302 (89.3)	4 (1.2)	30 (8.9)	2 (0.6)	338 (100)
Age [years]		61.60 ±13.91	74.5 (66, 82)	58.5 (45.70, 74.25)	45 (31, 59)	61.40 ±14.02
Gender, n (%)	male	65 (21.5)	0 (0)	4 (13.3)	2 (100)	71 (21.0)
	female	237 (78.5)	4 (100)	26 (86.7)	0 (0)	267 (79.0)
Smoking, n (%)	yes	68 (22.5)	1 (25)	5 (16.7)	2 (100)	76 (22.5)
	no	234 (77.5)	3 (75)	25 (83.3)	0 (0)	262 (77.5)
Duration [years]		1.35 ±2.29	1 (0.2, 10)	2.00 (0.50, 5.25)	0.3 (0.16, 0.44)	1.62 ±3.03

SD – standard deviation; IQR – interquartile range.

Table 3. Distribution of pathogenic bacteria in patients' positive samples with lacrimal canaliculitis

Genus of bacteria	Cases, n	Percentage (%)
Gram-positive cocci		
Staphylococcus epidermidis	32	51.61
Streptococcus anginosus	2	3.23
Staphylococcus haemolyticus	1	1.61
Staphylococcus aureus	3	4.84
Streptococcus mitis	10	16.13
Oral Streptococci	1	1.61
Staphylococcus hominis subsp	2	3.23
Staphylococcus cohnii	1	1.61
Staphylococcus intermedius	1	1.61
Staphylococcus suis	1	1.61
Gram-positive bacilli		
Corynebacterium spp.	2	3.23
Corynebacterium dried	1	1.61
Gram-positive coccus		
Neisseria cinerea	1	1.61
Gram-negative bacilli		
Yersinia enterocolitica	1	1.61
Sphingomonas paucimobilis	1	1.61
Acinetobacter lwoffii	1	1.61
Serratia marcescens	1	1.61
Total	62	100

Table 4. Distribution of pathogenic bacteria of dacryoliths in patients with positive samples

Genus of bacteria	Cases, n	Percentage (%)
Gram-positive cocci		
Staphylococcus aureus	5	33.33
Staphylococcus epidermidis	5	33.33
Streptococcus mitis	2	13.33
Gram-negative bacilli		
Pseudomonas aeruginosa	1	6.67
Enterobacter aerogenes	1	6.67
Klebsiella pneumoniae	1	6.67
Total	15	100

Discussion

Canaliculitis is one of the most common complications in dacryolithiasis. Due to similar clinical manifestations to a variety of ophthalmic diseases, lacrimal canaliculitis is an ophthalmic disease with a high misdiagnosis rate in outpatient settings.[9] Xiang et al.[10] reported that the misdiagnosis rate of canaliculitis was 77.8%. Non-lacrimal specialists often misdiagnose lacrimal canaliculitis as common infectious diseases in ophthalmology, such as conjunctivitis, meibomian gland inflammation or dacryocystitis, and long-term repeated medication often yields unsatisfactory results.[11] Some patients lose confidence and give up seeking medical treatment, which causes significant distress. When the patient exhibits conjunctival congestion and repeated drug treatments are ineffective, it should be differentiated from conjunctivitis. When the patient's eyelid is red and swollen, this should be differentiated from meibomian gland inflammation. In addition, many patients with exudate spillage from the lacrimal punctum are misdiagnosed as having dacryocystitis and may even undergo DCR, but the symptoms are not relieved after the operation. Patients with dacryocystitis typically exhibit normal lacrimal canaliculus and lacrimal punctum, with the main manifestation being purulent secretion overflow from the lacrimal punctum when pressing the lacrimal sac area. In contrast, purulent or granular secretion overflow can be seen in lacrimal canaliculitis when pressing the lesion lacrimal punctum area. Most of the lacrimal duct is flushed smoothly and can be identified based on different characteristics. Although some patients have an insidious onset, as long as the disease is recognized, patients with long-term recurrent secretion from the lacrimal canaliculus should be carefully examined, and the lacrimal duct should be rinsed in parallel. Based on symptoms and signs, the diagnosis is not difficult.

The incidence of female patients is significantly higher than that of male ones,[7] which our study also confirmed. The reason may be due to the decrease in estrogen levels in women during amenorrhea, leading to reduced tear secretion and decreased resistance to infection, making the lacrimal canaliculus more susceptible to microbial invasion. In addition, women's daily lifestyle, such as the use of cosmetics and exposure to oil fumes, may contribute to the blockage of lacrimal canaliculi by microparticles, facilitating the growth of microorganisms within the lacrimal passage.

Regarding the location of canaliculitis lesions, canaliculitis usually affects the inferior canaliculus, predominantly occurring in 1 eye, with no significant difference between the left and right eyes. Due to gravity, tear drainage is mainly achieved by the inferior lacrimal canaliculus, and bacteria on the ocular surface tend to accumulate mainly in the lower part. The diameter of the inferior lacrimal canaliculus is larger than that of the superior lacrimal canaliculus. Pathogenic microorganisms from the lacrimal sac or nasolacrimal duct are more likely to spread to the inferior lacrimal canaliculus, making inferior lacrimal canaliculitis more common.[12]

Previous studies believed that actinomycetes were the main pathogenic bacteria of lacrimal canaliculitis. However, recent studies have identified that the pathogenic bacteria of lacrimal canaliculitis have changed.[13] For instance, Alam et al.[14] reported *S. epidermidis* as the most common pathogen of canaliculitis. Zhang et al.[15] stated that the main pathogenic bacteria of lacrimal canaliculitis were Gram-positive bacteria, with common bacterial

genera including *Staphylococcus, Propionibacterium, Streptococcus*, etc. In this study, the top 2 most frequently identified bacteria were *S. epidermidis* and *Streptococcus mitis*, consistent with the distribution of the most common bacterial flora in the normal conjunctival sac reported by Wang et al.[16] A study[17] on the distribution and drug resistance of ocular bacterial culture-positive strains also pointed out that *S. epidermidis* was the primary pathogenic bacteria and the most important multi-drug resistant bacteria in the eye. The removal of stones is the major treatment of lacrimal canaliculitis. If lacrimal duct stones continue to block the lumen, only squeezing and scraping the stones can relieve the symptoms.

The prevalence of dacryolithiasis gradually increases after the age of 50 years.[18] Most of the pathogenic bacteria associated with dacryolithiasis are Gram-positive bacteria. However, dacryolithiasis is usually difficult to diagnose before operation. Given the inadequacies of imaging methods such as X-ray, dacryocystography and computed tomography (CT), dacryolithiasis often remains misdiagnosed or undetected. The overall incidence of dacryolithiasis is, therefore, difficult to assess. Dacryolithiasis is usually found when the lacrimal sac is opened during DCR, so intraoperative incision of the lacrimal sac is the only effective way to confirm the presence of dacryolithiasis. The DCR is often regarded as the gold standard for the treatment of dacryolithiasis.[4] For repeated secretion, the presence of dacryolithiasis should be highly suspected if drug control is ineffective. Pressing the lacrimal sac can show purulent secretion overflow, and lacrimal duct irrigation can vary in terms of its smoothness. Studies have revealed that lacrimal duct stones were diagnosed in 6–18% of patients during DCR,[2] and the proportion in this study was 6.68%, which is similar to literature reports.

Dacryocystitis complicated by canaliculitis is relatively easy to diagnose. Special attention should be paid to cases of canaliculitis combined with dacryolithiasis. In such patients, the lacrimal passage may sometimes be unobstructed, and secretion may spill, which is consistent with the symptoms of simple lacrimal canaliculus inflammation. If treatment of lacrimal canaliculitis alone does not resolve symptoms of secretion post-surgery and there is neither inflammation nor stone-like discharge upon compression of the lacrimal canaliculus, it is highly likely that the patient may have concurrent lacrimal sac stones. In such instances, DCR is required to incise the lacrimal sac for a definitive diagnosis. Two patients in our research were diagnosed with canaliculitis before the operation, but their symptoms were not relieved after the operation. Upon ineffective drug treatment, nasal En-DCR was performed. During the operation, large stones in the lacrimal sac cavity were found, granulation hyperplasia was present in the lacrimal sac cavity, and the inflammatory reaction was severe. If necessary, the treatments of such patients need to be combined with lacrimal intubation to prevent anastomotic adhesion and atresia.

Very few cases of dacryocystitis are not suitable for DCR as the first choice. Simple lacrimal duct probing combined with lacrimal intubation can dislodge intact lacrimal sac stones and sometimes nasolacrimal duct stones. This procedure is noninvasive, does not alter the natural anatomy and has a short operation time, making it a procedure that most patients are willing to undergo. This requires us to properly determine the surgical indications. For patients with a short duration of secretion symptoms and low-position of lacrimal duct obstruction as suggested by dacryocystography, which is generally located in the lower part of the nasolacrimal duct, we can attempt lacrimal duct probing combined with lacrimal duct intubation after communication with the patients and their families and obtaining their consent. Notably, if probing fails, En-DCR is performed.

Limitations

This study's retrospective design inherently introduced selection and information biases, potentially leading to skewed data due to non-random patient selection and variable data accuracy. In addition, the relatively small sample size of 338 patients limited the statistical power and generalizability of the findings to the broader population with dacryolithiasis. The absence of a control group further restricted our ability to distinguish between effects directly attributable to dacryolithiasis and those resulting from extraneous variables. To overcome these limitations and enhance the validity of future research, it is advisable to employ a prospective study design and conduct randomized controlled trials (RCTs), which would allow for systematic comparisons and more controlled conditions. Increasing the sample size and including multiple research centers would also help achieve a more representative population sample, thereby improving the generalizability of the results. Finally, applying advanced statistical techniques, such as multivariate analysis, can help control for potential confounders, ensuring a more accurate isolation of the effects being studied.

Conclusions

This study offers a comprehensive clinical analysis of dacryolithiasis, highlighting the essential role of diagnostic tools such as slit-lamp examination, lacrimal irrigation and dacryocystography. These tools are crucial not only for accurately diagnosing dacryolithiasis but also for determining the precise location of lacrimal stones, which guides the selection of appropriate surgical interventions. Clinicians are encouraged to integrate these diagnostic procedures into routine assessments to enhance detection and management, thereby ensuring that surgeries are minimally invasive, reduce complications and improve success rates. Future research should focus

on evaluating the long-term outcomes of surgical techniques, developing innovative diagnostic tools for more precise assessments, and exploring the pathophysiological underpinnings of dacryolithiasis to identify new therapeutic targets.

Data availability

The datasets generated and/or analyzed during the current study are available from the corresponding author on reasonable request.

Consent for publication

Not applicable.

Use of AI and AI-assisted technologies

Not applicable.

ORCID iDs

Ting Zhang https://orcid.org/0000-0002-4370-3692
Wei Zhuo https://orcid.org/0009-0001-0720-0326
Wei-na Wang https://orcid.org/0009-0002-7698-634X
Lu Zhao https://orcid.org/0000-0001-8845-4194

References

1. Andreou P, Rose GE. Clinical presentation of patients with dacryolithiasis. *Ophthalmology*. 2002;109(8):1573–1574. doi:10.1016/S0161-6420(02)01107-7
2. Kubo M, Sakuraba T, Wada R. Clinicopathological features of dacryolithiasis in Japanese patients: Frequent association with infection in aged patients. *ISRN Ophthalmology*. 2013;2013:406153. doi:10.1155/2013/406153
3. Mishra K, Hu KY, Kamal S, et al. Dacryolithiasis: A review. *Ophthalmic Plast Reconstr Surg*. 2017;33(2):83–89. doi:10.1097/IOP.0000000000000769
4. Khorrami Kashi A, Keilani C, Nguyen TH, Keller P, Elahi S, Piaton JM. Dacryolithiasis diagnosis and treatment: A 25-year experience using nasal endoscopy. *Br J Ophthalmol*. 2023;107(2):289–294. doi:10.1136/bjophthalmol-2021-319671
5. Martinez-Carrasco R, Argüeso P, Fini ME. Membrane-associated mucins of the human ocular surface in health and disease. *Ocul Surf*. 2021;21:313–330. doi:10.1016/j.jtos.2021.03.003
6. Lew H, Lee SY, Yun YS. Measurement of pH, electrolytes and electrophoretic studies of tear proteins in tears of patients with dacryoliths: A novel concept for dacryoliths. *Ophthalmologica*. 2004;218(2):130–135. doi:10.1159/000076149
7. Bayuk EG, Malkoç Şen E, Çorak Eroğlu F, Serbest Ceylanoğlu K, Evren E. Long-term follow-up results of primary canaliculitis patients. *Turk J Ophthalmol*. 2023;53(3):149–153. doi:10.4274/tjo.galenos.2022.37659
8. Wang Q, Sun S, Lu S, et al. Clinical diagnosis, treatment and microbiological profiles of primary canaliculitis. *Exp Ther Med*. 2023;25(4):157. doi:10.3892/etm.2023.11856
9. Bothra N, Sharma A, Bansal O, Ali MJ. Punctal dilatation and non-incisional canalicular curettage in the management of infectious canaliculitis. *Orbit*. 2020;39(6):408–412. doi:10.1080/01676830.2019.1704797
10. Xiang S, Lin B, Pan Q, et al. Clinical features and surgical outcomes of primary canaliculitis with concretions. *Medicine (Baltimore)*. 2017;96(9):e6188. doi:10.1097/MD.0000000000006188
11. Singh M, Gautam N, Agarwal A, Kaur M. Primary lacrimal canaliculitis: A clinical entity often misdiagnosed. *J Curr Ophthalmol*. 2018;30(1):87–90. doi:10.1016/j.joco.2017.06.010
12. Balıkoğlu Yılmaz M, Şen E, Evren E, Elgin U, Yılmazbaş P. Canaliculitis awareness. *Turk J Ophthalmol*. 2016;46(1):25–29. doi:10.4274/tjo.68916
13. Huang YY, Yu WK, Tsai CC, Kao SC, Kau HC, Liu CJL. Clinical features, microbiological profiles and treatment outcome of lacrimal plug-related canaliculitis compared with those of primary canaliculitis. *Br J Ophthalmol*. 2016;100(9):1285–1289. doi:10.1136/bjophthalmol-2015-307500
14. Alam MdS, Poonam NS, Mukherjee B. Outcomes of canaliculotomy in recalcitrant canaliculitis. *Saudi J Ophthalmol*. 2019;33(1):46–51. doi:10.1016/j.sjopt.2018.12.001
15. Zhang Y, Deng SJ, Wang ZQ, Ding JW, Sun XG. Etiological and drug sensitivity analysis of lacrimal canaliculitis [in Chinese]. *Chin J Ophthalmol*. 2018;54(2):111–114. https://med.wanfangdata.com.cn/Paper/Detail?id=PeriodicalPaper_zhyk201802009. Accessed August 15, 2024.
16. Wang J, Zhang HZ, Wang H, Zhang XY, Li L, Luo SW. Profiles and drug resistance of normal conjunctival bacterial flora [in Chinese]. *Chin J Pract Opthalmol*. 2017;35(8):790–794. https://caod.oriprobe.com/articles/53851677/Profiles_and_drug_resistance_of_normal_conjunctiva.htm. Accessed August 15, 2024.
17. Wang ZQ, Zhang Y, Sun XG. Distribution and drug resistance analysis of ocular bacterial culture positive strains from 2007 to 2013 [in Chinese]. *Ophthalmology*. 2015;24(4):262–267. https://d.wanfangdata.com.cn/periodical/yk201504011. Accessed August 15, 2024.
18. Komínek P, Doškářová Š, Švagera Z, et al. Lacrimal sac dacryoliths (86 samples): Chemical and mineralogic analyses. *Graefes Arch Clin Exp Ophthalmol*. 2014;252(3):523–529. doi:10.1007/s00417-013-2501-6

Neoadjuvant chemotherapy vs upfront surgery for resectable locally advanced oral squamous cell carcinoma: A retrospective single center study

*Xiaotong He[1,2,A–E], *Xiaoyue Lei[1,2,C,E], Yangxi Cheng[1,2,B,E], Huiyong Zhu[1,2,A,E,F]

[1] Department of Oral Maxillofacial Surgery, The First Affiliated Hospital of Zhejiang University School of Medicine, Hangzhou, China
[2] Clinical Research Center for Oral Diseases of Zhejiang Province, Hangzhou, China

A – research concept and design; B – collection and/or assembly of data; C – data analysis and interpretation;
D – writing the article; E – critical revision of the article; F – final approval of the article

Advances in Clinical and Experimental Medicine, ISSN 1899–5276 (print), ISSN 2451–2680 (online) *Adv Clin Exp Med*. 2025;34(8):1307–1319

Address for correspondence
Huiyong Zhu
E-mail: zhuhuiyong@zju.edu.cn

Funding sources
This project has received funding from the Zhejiang Provincial Clinical Research Center for Oral Diseases (grant No. 2022-KFKT-04). This research did not receive any specific grant from funding agencies in the commercial sectors.

Conflict of interest
None declared

Acknowledgements
We would like to thank all our patients who agreed to participate in our study.

*Xiaotong He and Xiaoyue Lei contributed equally to this work.

Received on February 21, 2024
Reviewed on August 3, 2024
Accepted on August 28, 2024

Published online on December 16, 2024

Cite as
He X, Lei X, Cheng Y, Zhu H. Neoadjuvant chemotherapy vs upfront surgery for resectable locally advanced oral squamous cell carcinoma: A retrospective single center study. *Adv Clin Exp Med*. 2025;34(8):1307–1319. doi:10.17219/acem/192623

DOI
10.17219/acem/192623

Copyright
Copyright by Author(s)
This is an article distributed under the terms of the Creative Commons Attribution 3.0 Unported (CC BY 3.0) (https://creativecommons.org/licenses/by/3.0/)

Abstract

Background. Oral squamous cell carcinoma (OSCC) is one of the most common cancers in humans. The role of neoadjuvant chemotherapy (NAC) in OSCC remains controversial.

Objectives. The study aimed to investigate the effect of NAC on locally advanced OSCC and identify prognostic factors varying is different therapies to ultimately guide the optimal selection of future treatment.

Materials and methods. A total of 156 patients with locally advanced OSCC were enrolled. The clinical characteristics and survival outcomes of patients with and without NAC were compared. The primary endpoint was overall survival (OS), and the secondary endpoint was disease-free survival (DFS).

Results. Among the 156 patients enrolled in this study, 81 patients received NAC followed by surgery and 75 patients received surgery alone. No significant difference in OS at 3 years was detected (78.3% vs 79.8%, $p = 0.76$). However, a significantly worse DFS was observed in the NAC group (42.4% vs 59.2%, $p = 0.048$). Within the NAC group, 50 patients (61.7%) had a favorable clinical response, and 12 patients (14.8%) had a complete pathological response. Better survival outcomes were observed in patients with favorable clinical responses. In stratified analysis, patients of pT3/4 OSCC after NAC showed worse DFS than those of the same stage who underwent surgery alone (40.2% vs 58%, $p = 0.033$). In Cox regression, clinical response and pathological stage were predictors of survival in the NAC group, while pathological stage was the only predictor of OS in the surgery group.

Conclusions. Patients with advanced pathological stages after NAC may be at a higher risk of treatment failure, and upfront surgery is recommended for locally advanced OSCC patients in current clinical practice.

Key words: prognosis, neoadjuvant chemotherapy, oral squamous cell carcinoma

Background

Oral cancer represents one of the most common malignancies. There were approx. 373,097 (95% uncertainty interval (95% UI): 340,884–403,865) incident cases and 199,379 (95% UI: 181,651–218,058) deaths worldwide in 2019, according to the national epidemiological profiles of cancer burden in the Global Burden of Disease Study (https://ghdx.healthdata.org/ihme_data). The mainstays of oral squamous cell carcinoma (OSCC) therapeutics are surgery, radiotherapy, chemotherapy, or a combination of these modalities, depending on the extent of the disease. Oral squamous cell carcinoma has long been regarded as a favorable indication for primary surgical intervention.[1] Advances in surgical techniques over the past 4 decades have resulted in significantly enhanced outcomes. Minimally invasive surgery is widely acknowledged as striking a favorable balance between cancer resection and functional restoration for early-stage OSCC.[2] Numerous clinical trials have demonstrated the efficacy of surgical interventions for early-stage OSCC, with ongoing research focusing on the impact of various surgical techniques and extent of resection on the local recurrence rates and preservation of tissue function in early-stage human papilloma virus (HPV)-negative OSCC.[3] Compared to non-surgical interventions, oral surgery resection in OSCC has been shown to increase the survival rate in oral cancer.[4,5] A large-scale, 10-year clinical study on borderline oral cavity cancers demonstrated a significant increase in the 10-year survival rate for patients who underwent surgery compared to those who did not. This finding strongly underscores the importance of surgical treatment.[6] However, the prognosis for locally advanced OSCC remains grim. The overall and long-term survival rates for patients with OSCC continue to be unsatisfactory, with a 5-year survival rate of approx. 60% across all stages.[7] A significant challenge lies in enhancing the survival outcomes of patients with advanced OSCC through the utilization of various chemotherapy regimens in conjunction with surgical interventions, a matter that remains unresolved.[8]

Neoadjuvant chemotherapy (NAC) has been routinely utilized for several cancers, with the goal of down-staging the primary tumor and controlling potential micrometastasis.[9,10] Neoadjuvant chemotherapy has been introduced for head and neck squamous cell carcinoma (HNSCC), with the goal of function preservation and better survival outcomes. However, several clinical trials have failed to prove the benefits in survival with the addition of chemotherapy prior to chemoradiotherapy or surgery in HNSCC patients.[11–13] Although the superiority of NAC remains controversial, there are some promising results. First, a reduction in the distant metastasis rate was reported in OSCC patients treated with NAC and surgery compared to those who received surgery directly.[14] Second, NAC was reported to be a strategy for selecting patients for conservative surgery. A retrospective study of small samples revealed that limited surgery without flap reconstruction was feasible in advanced OSCC patients who had a favorable clinical response to chemotherapy.[15] Similarly, another study identified that for patients needing mandibular resection for paramandibular disease without obvious bone erosion, NAC was also a feasible option for mandibular preservation with no compromise of survival.[16] Third, specific subsets of patients are likely to benefit from neoadjuvant treatment, especially those who respond well to preoperative chemotherapy.[13] A phase II clinical trial of 36 patients demonstrated the safety of pembrolizumab and a decrease in 1-year recurrence rate in patients with locally advanced, HPV-negative HNSCC.[17] However, there are still many patients who cannot benefit from NAC combined with immunotherapy, and its effect in oral cancer still needs to be supported by more clinical research data.

Objectives

This study aimed to investigate the effects of NAC and identify the potential clinicopathological risk factors in patients with different treatment regimens and thus guide reasonable therapeutic options in locally advanced OSCC patients for future practice.

Methods

Patients and study design

The clinical data for this retrospective study were collected at the First Affiliated Hospital of Zhejiang University School of Medicine (Hangzhou, China) from 2017 to 2020. The study was approved by the institutional review board and was conducted in accordance with the principles of the Declaration of Helsinki (approval No. IIT20220674A). Informed consent was obtained from all individual participants included in the study. The inclusion criteria were as follows: 1) pathological examination confirmed squamous cell carcinoma (SCC); 2) resectable clinical stage III–IV OSCC without metastasis; and 3) received surgery in our hospital. Patients with previous surgery involving a primary tumor or clinical evidence of metastasis were excluded. Patients who received preoperative chemotherapy were enrolled in the NAC group, while patients who received surgery directly were enrolled in the surgery alone group (Fig. 1). For the present study, a total of 294 patients with locally advanced resectable SCC from 2017 to 2020 were considered. After excluding 89 patients who did not meet the inclusion criteria and 49 patients who were lost to follow-up, 156 patients were ultimately included in the analysis. These patients were divided into 2 groups: the NAC plus surgery group (n = 81), who received neoadjuvant therapy followed by surgery, and the surgery group (n = 75), who underwent surgery alone.

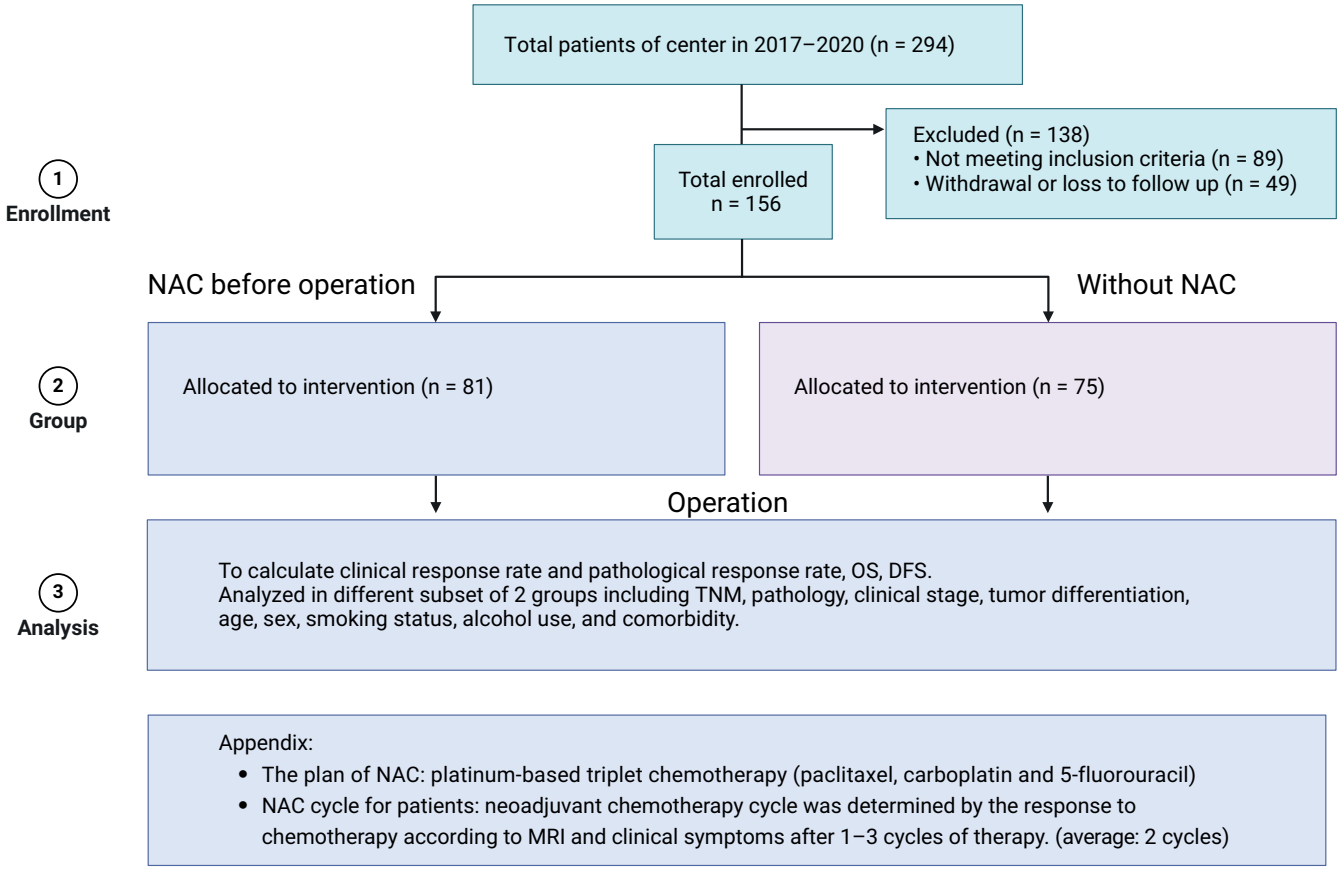


Fig. 1. Schematic diagram of the study design

Patient characteristics and treatment information, including age, sex, smoking status, alcohol use, comorbidity (collected using the ACE-27 index), NAC regimen, type of reconstruction, and postoperative adjuvant therapy, were recorded. Tumor characteristics, including the site of the primary lesion, pathological grade and clinical and pathological tumor-node-metastasis (TNM) stage, were also retrieved for each patient. The clinical and pathological TNM staging were determined according to the 8th edition of the American Joint Committee on Cancer (AJCC) classification.

Clinical management

For the patients in the NAC group, we mainly used platinum-based triplet chemotherapy (paclitaxel, carboplatin and 5-fluorouracil) for preoperative treatment. There is currently no unified standard for the number of cycles of NAC. In this study, the number of NAC cycles was determined by the response to chemotherapy according to magnetic resonance imaging (MRI) and clinical symptoms after 1–3 cycles of therapy. Patients who do not respond to NAC should be discontinued early for surgery, and for those who respond to NAC, the number of chemotherapy cycles should be determined according to the adverse effects and the degree of remission. The duration of neoadjuvant therapy may be appropriately prolonged if the patient's physical condition permits. Magnetic resonance imaging of patients with mandibular gingival disease in the NAC group revealed the absence of medullary infiltration. The average number of preoperative chemotherapy cycles was 2 (1–3). Before chemotherapy, the palpable edge of the primary tumor was marked by at least 4 points in patients who were assigned to the NAC group to determine the extent of radical surgery. During the 3–4 weeks after NAC completion, they proceeded to radical resection, with 1 cm resection extension to the markers and the proper type of neck dissection. In the surgery alone group, the patients received the same surgery procedure directly, and the excision extension was also defined 1 cm outside the primary lesion. Postoperative therapy was jointly determined by the surgeons, radiation oncologists and medical oncologists, as well as the patient's choice.

Follow-up and outcomes

The primary outcome of interest was overall survival (OS), and the secondary outcome of interest was disease-free survival (DFS). Overall survival was defined as the time from the start of treatment to the time of death from OSCC. Disease-free survival referred to the time from treatment to the time of tumor relapse or metastasis, as confirmed by the oral and maxillofacial surgeons.

Assessment of chemotherapy response

Clinical response was determined by clinical examination or imaging studies according to the response evaluation criteria in solid tumors v. 1.1 (RECIST 1.1): complete response – all target lesions including the primary lesions and any lymph nodes disappeared; partial response – the sum of the diameters of the target lesions decreased at least 30% compared to the baseline; progressive disease – the sum of the diameters of the target lesions increased at least 20% compared to the baseline; and stable disease – no significant tumor regression or increase.[18] Patients with complete or partial response were defined as clinical responders, while patients who had stable or progressive disease were classified as clinical non-responders. All patients underwent radical resection and pathological examination in our study, and patients with no remaining viable tumor cells were enrolled in the pathological complete response (pCR) group. Those with the presence of viable tumor cells were enrolled in the non-pCR group.

Statistical analyses

Pearson's χ^2 test or Fisher's exact test (if $n < 5$ in ≤20% of cells) were conducted for categorical data, and Student's t-test was used for continuous variables (Table 1). The normality of continuous variables was assessed using the Shapiro–Wilk test ($p > 0.05$) (Supplementary Fig. 1), and the homogeneity of variances was evaluated using Levene's test ($p > 0.05$). Survival analysis and survival curves were performed using the Kaplan–Meier (KM) method, with differences analyzed using the log-rank test. Multicollinearity was assessed using the variance inflation factor (VIF). All VIF values were below the widely accepted threshold of 10, indicating a lack of multicollinearity among the predictors (Supplementary Tables 1 and 2).

The proportional hazards assumption was tested using Schoenfeld residuals (Supplementary Fig. 2), and residual plots were generated to examine and confirm the absence of discernible trends between the log-hazard function and predictor variables (Supplementary Fig. 3). A Cox proportional hazard model was performed to estimate the hazard

Table 1. Demographic and clinical characteristics of neoadjuvant chemotherapy and surgery alone groups

Demographic and clinical characteristics		NAC and surgery (n = 81)	Surgery alone (n = 75)	p-value
Sex	male	63 (77.8%)	47 (62.7%)	0.058[a]
	female	18 (22.2%)	28 (37.3%)	–
Age [years]	mean ±SD	61.1 ±1.2	63.6 ±1.3	0.120[c]
	<64	41 (50.6%)	34 (45.3%)	0.617[a]
	≥64	40 (49.4%)	41 (54.7%)	–
Tumor location	tongue	31 (38.3%)	30 (40.0%)	<0.001[a]
	buccal mucosa	7 (8.6%)	26 (34.7%)	–
	floor of mouth	18 (22.2%)	5 (6.7%)	–
	hard palate and upper gum	9 (11.1%)	3 (4.0%)	–
	lower gum	16 (19.8%)	11 (14.7%)	–
cT stage	T2	4 (4.9%)	5 (6.7%)	0.351[b]
	T3	50 (61.7%)	53 (70.7%)	–
	T4a	27 (33.3%)	17 (22.7%)	–
cN stage	N0	35 (43.2%)	29 (38.7%)	0.236[a]
	N1	30 (37.0%)	37 (49.3%)	–
	N2	16 (19.8%)	9 (12.0%)	–
cTNM	II	46 (56.8%)	52 (69.3%)	0.136[a]
	IVA	35 (43.2%)	23 (30.7%)	–
Pathology differentiation	moderate-to-well	69 (85.2%)	69 (92.0%)	1[b]
	poor	6 (7.4%)	6 (8.0%)	–
	unknown	6 (7.4%)	0 (0%)	–
Postoperative treatment	none	31 (38.3%)	35 (46.7%)	<0.001[a]
	RT	11 (13.6%)	24 (32.0%)	–
	CT	22 (27.2%)	3 (4.0%)	–
	both	17 (21.0%)	13 (17.3%)	–

SD – standard deviation; [a] Pearson's χ^2 test; [b] Fisher's exact test; [c] Student's t-test; NAC – neoadjucant chemotherapy; cT – clinical T stage; cN – clinical N stage; cTNM – clinical TNM stage; RT – radiotherapy; CT – chemotherapy.

ratio (HR) with 95% confidence intervals (95% CIs) and to identify prognostic factors associated with survival. All hypothesis-generating tests with a $p < 0.05$ were considered statistically significant. All analyses were performed using the R statistical software v. 4.1.2 (R Foundation for Statistical Computing, Vienna, Austria).

Results

Baseline characteristics

Between 2017 and 2020, 156 eligible patients with untreated locally advanced OSCC received surgical treatment at our center. Eighty-one patients received preoperative chemotherapy followed by radical surgery, and 75 patients received surgery alone. The median follow-up duration was 36 months (range: 3.7–58.9 months). Table 1 presents the baseline characteristics of the patients included in our study for both the surgery alone and NAC groups. Statistical analysis showed no significant differences in sex, age, clinical TNM stage, or pathological grade between the 2 groups despite differences in tumor location and postoperative treatment.

Survival outcomes

Patients with or without preoperative chemotherapy had comparable OS at 3 years (78.3% vs 79.8%, log-rank test: $p = 0.76$) (Fig. 2A). However, the surgery alone group had better 3-year DFS when compared with the NAC group (59.2% vs 42.4%, log-rank test: $p = 0.048$) (Fig. 2B).

Kaplan–Meier survival analyses in the prespecified substrata of pathological T stage and N stage are presented in Fig. 3. Patients with pT0–2 OSCC after NAC and surgery exhibited similar survival patterns to patients with pT0–2 OSCC after surgery alone (Fig. 3A,B). Inferior 3-year DFS was detected in patients with pT3–4 stage after NAC and surgery when compared to patients with the same stage after surgery alone (40.2% vs 58%, log-rank test: $p = 0.033$), but OS rates were comparable in the 2 groups (Fig. 3C,D). There were no significant differences in OS or DFS rates when patients were stratified by pathologic nodal status (Fig. 2E–H).

Response to NAC

According to RECIST 1.1, 50 (61.7%) of 81 patients showed a favorable clinical response, consisting of complete response in 6 patients (7.40%) and partial response in 44 patients (54.3%). Twenty-nine patients (35.8%) had stable disease and 2 patients (2.50%) had progressive disease after preoperative chemotherapy. Pathological complete response was observed in 12 patients (14.8%), while viable tumor cell residue of varying degrees was observed in most patients. Clinical responders had a significantly higher 3-year OS compared to clinical non-responders (82.4% vs 60.7%, log-rank test: $p = 0.023$; Fig. 4A). The 3-year DFS also presented similar results (54.3% vs 18.7%, log-rank test: $p = 0.005$; Fig. 4B). There was a slight survival advantage for patients with pCR compared to patients without pCR, but the difference was not significant (Fig. 3C,D).

Cox regression

Tables 2,3 show the results of univariate Cox regression models for patients in both the NAC and surgery alone groups. For patients who received NAC and surgery, pathological T stage (pT) and clinical response to NAC were important predictors of OS in univariate analysis. Pathological tumor stage and clinical response, as well as pathological grade, were significant predictors of DFS. However, no clinical factors were found to be significant in the multivariate analysis for either OS or DFS. For patients who underwent surgery alone, pT stage was associated with lower OS, but no predictor of DFS was detected.

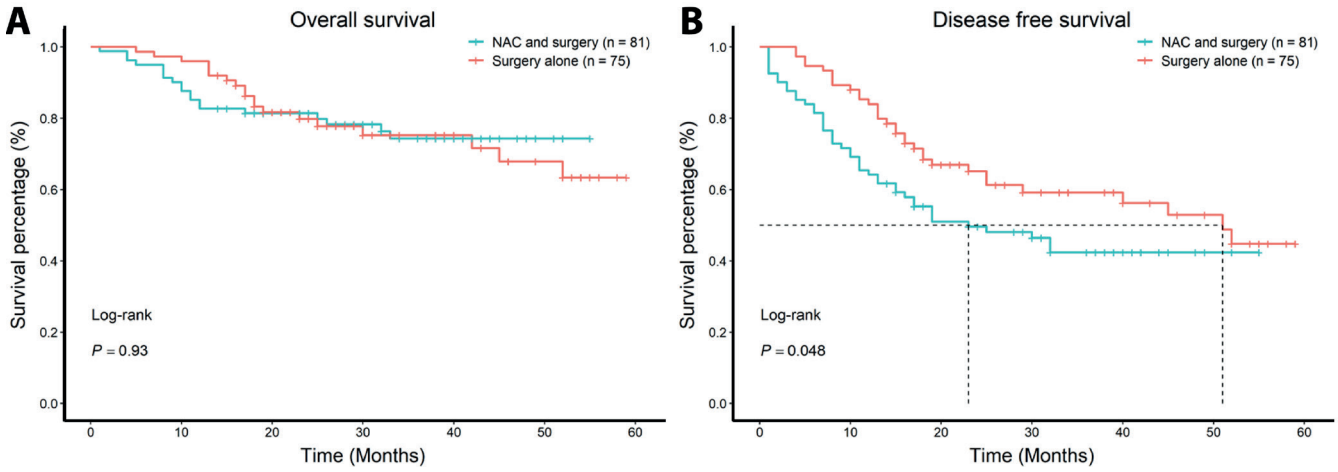


Fig. 2. Overall survival (OS) and disease-free survival (DFS) between neoadjuvant chemotherapy (NAC) and surgery alone groups

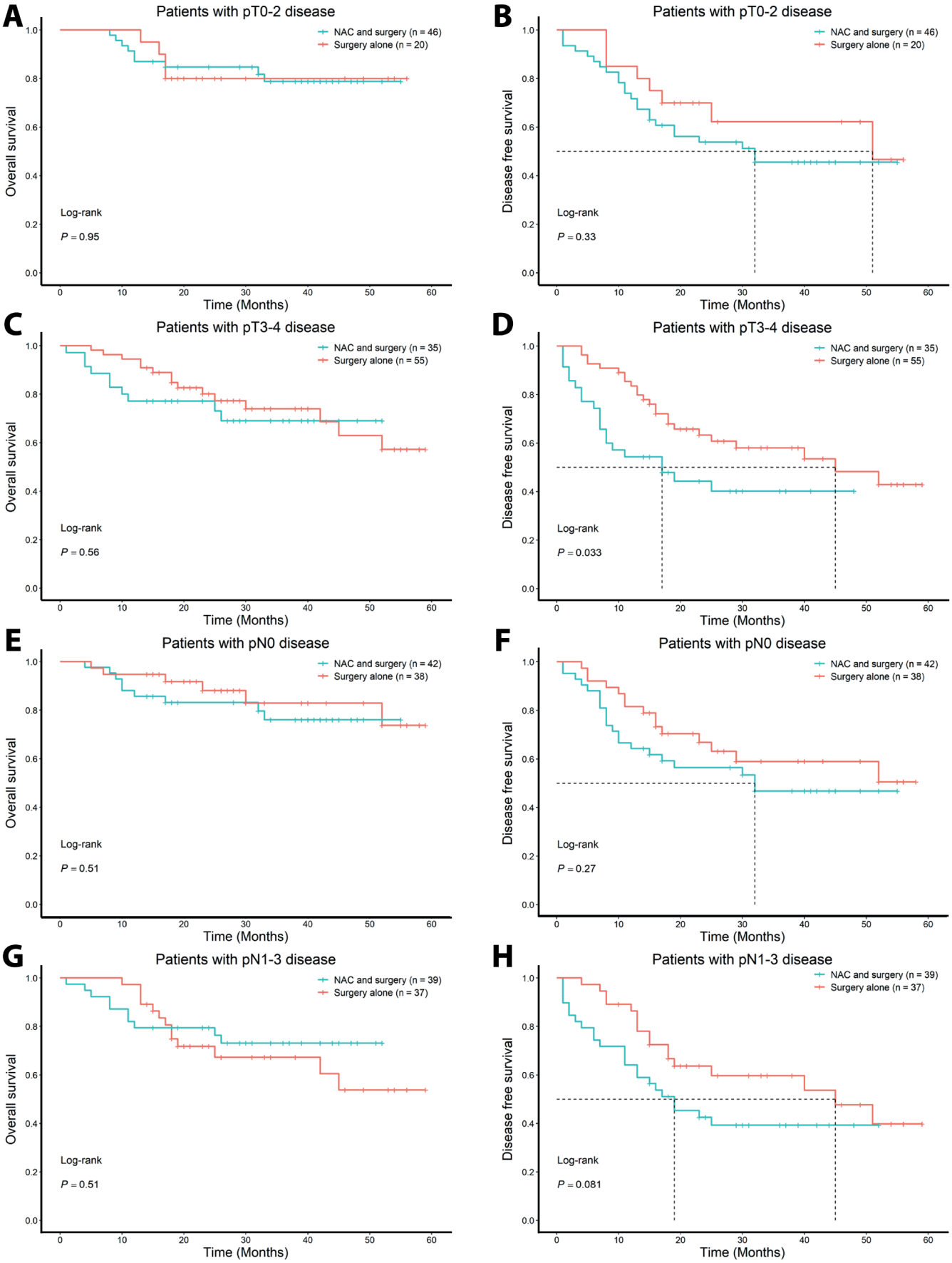


Fig. 3. Kaplan–Meier estimation in the prestratified substrata of pathological results

NAC – neoadjuvant chemotherapy.

Table 2. Cox regression analysis for disease-free survival (DFS) and overall survival (OS) of the neoadjuvant chemotherapy (NAC) group (n = 81)

Variables	OS		DFS	
	HR (95% CI)	p-value	HR (95% CI)	p-value
Sex: female vs male	1.25 (0.45–3.48)	0.665	1.26 (0.64–2.50)	0.506
Age: <64 years vs ≥64 years	1.13 (0.46–2.78)	0.790	1.14 (0.63–2.06)	0.669
BMI: abnormal vs normal	0.79 (0.27–2.27)	0.659	1.85 (0.96–3.58)	0.066
Comorbidity: present vs absent	0.47 (0.18–1.24)	0.129	1.40 (0.78–2.54)	0.264
Clinical T stage: T4 vs T2/T3	1.64 (0.66–4.09)	0.285	1.19 (0.64–2.22)	0.590
Clinical N stage: N2/N3 vs N0/N1	1.10 (0.37–3.33)	0.863	1.41 (0.71–2.80)	0.333
Pathologic T stage: T2–T4 vs T0/T1	**3.60 (1.05–12.36)**	**0.042**	**2.06 (1.06–4.01)**	**0.034**
Pathologic N stage: N2/N3 vs N0/N1	1.61 (0.65–4.00)	0.308	1.67 (0.92–3.03)	0.090
Tumor differentiation: poor vs moderate-to-well	1.27 (0.29–5.52)	0.751	**2.97 (1.25–7.06)**	**0.014**
Site: others vs tongue	0.71 (0.29–1.74)	0.450	0.76 (0.42–1.38)	0.368
Reconstruction type: yes vs no	1.16 (0.34–4.01)	0.810	0.84 (0.39–1.82)	0.667
Pathological response's CR vs non-CR	3.74 (0.50–28.09)	0.199	1.61 (0.63–4.10)	0.315
Clinical response: SD/PD vs PR/CR	**2.76 (1.11–6.88)**	**0.029**	**2.29 (1.26–4.16)**	**0.006**
Smoking status: current/former vs never	0.84 (0.33–2.15)	0.721	0.82 (0.44–1.52)	0.527
Alcohol use: current/former vs never	0.77 (0.31–1.90)	0.574	0.89 (0.48–1.63)	0.700
Postoperative therapy				
None	Ref.	Ref.	Ref.	Ref.
Radiotherapy	0.55 (0.12–2.00)	0.451	0.74 (0.28–2.00)	0.556
Chemotherapy	0.80 (0.27–2.40)	0.697	1.41 (0.70–2.83)	0.341
Both	0.57 (0.16–2.12)	0.404	0.62 (0.26–1.48)	0.282

T – tumor; N – lymph node; CR – complete response; SD – stable disease; PD – progressive disease; PR – partial response; 95% CI – 95% confidence interval; HR – hazard ratio.

Table 3. Cox regression analysis for disease-free survival (DFS) and overall survival (OS) of the surgery alone group (n = 75)

Variables	OS		DFS	
	HR (95% CI)	p-value	HR (95% CI)	p-value
Sex: female vs male	1.80 (0.73–4.44)	0.199	1.21 (0.60–2.44)	0.592
Age: <64 years vs ≥64 years	0.90 (0.36–2.23)	0.821	0.90 (0.45–1.79)	0.756
BMI: abnormal vs normal	1.36 (0.48–3.85)	0.557	0.92 (0.41–2.06	0.842
Comorbidity: present vs absent	0.82 (0.33–2.02	0.665	0.82 (0.41–1.65)	0.578
Clinical T stage: T4 vs T2/T3	1.50 (0.57–3.97)	0.410	0.71 (0.29–1.74)	0.456
Clinical N stage: N2/N3 vs N0N1	1.92 (0.56–6.67)	0.300	1.31 (0.46–3.76)	0.613
Pathologic T stage: T3/T4 vs T2	**3.19 (1.15–8.90)**	0.026	1.07 (0.38–3.07)	0.894
Pathologic N stage: N2/N3 vs N0N1	2.23 (0.87–5.70)	0.093	1.38 (0.64–2.99)	0.415
Tumor differentiation: poor vs moderate-to-well	1.89 (0.55–6.52)	0.311	0.094 (0.29–3.1)	0.924
Site: others vs tongue	0.64 (0.26–1.59)	0.337	0.58 (0.29–1.16)	0.124
Reconstruction type: yes vs no	0.69 (0.09–5.16)	0.714	1.27 (0.17–9.34)	0.814
Smoking status: current/former vs never	0.76 (0.31–1.84)	0.750	1.58 (0.91–2.75)	0.105
Alcohol use: current/former vs never	0.75 (0.32–1.77)	0.750	1.58 (0.91–2.75)	0.105
Postoperative therapy				
None	Ref.	Ref.	Ref.	Ref.
Radiotherapy	1.57 (0.62–3.96)	0.342	1.50 (0.70–3.20)	0.295
Chemotherapy	Inf	Inf	Inf	Inf
Both	0.36 (0.05–2.84)	0.331	1.28 (0.46–3.58)	0.633

T – tumor; N – lymph node; Ref. – reference group; Inf – infinity; 95% CI – 95% confidence interval; HR – hazard ratio.

Discussion

Neoadjuvant chemotherapy treatment strategies for locally advanced OSCC patients

Preserving tissue function and maintaining the patient's quality of life are fundamental criteria in the management of treatment for patients with locally advanced OSCC.[1] Advancements in flap tissue repair and reconstruction have expanded the indications for surgery.[19] The question of whether tumor volume reduction prior to surgery is necessary in OSCC remains a topic of debate.

Neoadjuvant chemotherapy has been discussed for decades; whether OSCC patients benefit from it is controversial. Supporters argue that NAC can reduce tumor volume, make margins clearer, increase the success rate of complete resection, reduce the difficulty of tissue reconstruction, and improve survival rates and quality of life. However, opponents believe that for patients with locally advanced OSCC, the tumor progresses rapidly, and non-response to NAC may delay the timing of treatment and increase the surgical risks. A study on the timing of NAC has shown that when the delayed time to surgery is over 34 days, the 3-year DFS rate is significantly worse.[20]

To evaluate the influence of NAC on survival in patients with locally advanced OSCC and compare the risk factors among patients with different treatment regimens, we retrospectively analyzed 2 groups of stage III or stage IVA OSCC patients with comparable baseline characteristics. Our data showed that NAC had no positive impact on the survival outcomes of OSCC patients, which suggests that upfront surgery could be more appropriate for patients with locally advanced OSCC in current practice. Theoretically, NAC can cause a reduction in tumor volume and improve long-term clinical outcomes by pretreating possible micrometastasis.[21] Despite a few studies demonstrating the benefits of NAC on survival,[22,23] many clinical trials have proved that neoadjuvant administration does not prolong the survival of patients with locally advanced OSCC.[13] A clinical trial in 2013 involving 256 patients with locally advanced OSCC demonstrated that patients who received 2 cycles of paclitaxel,

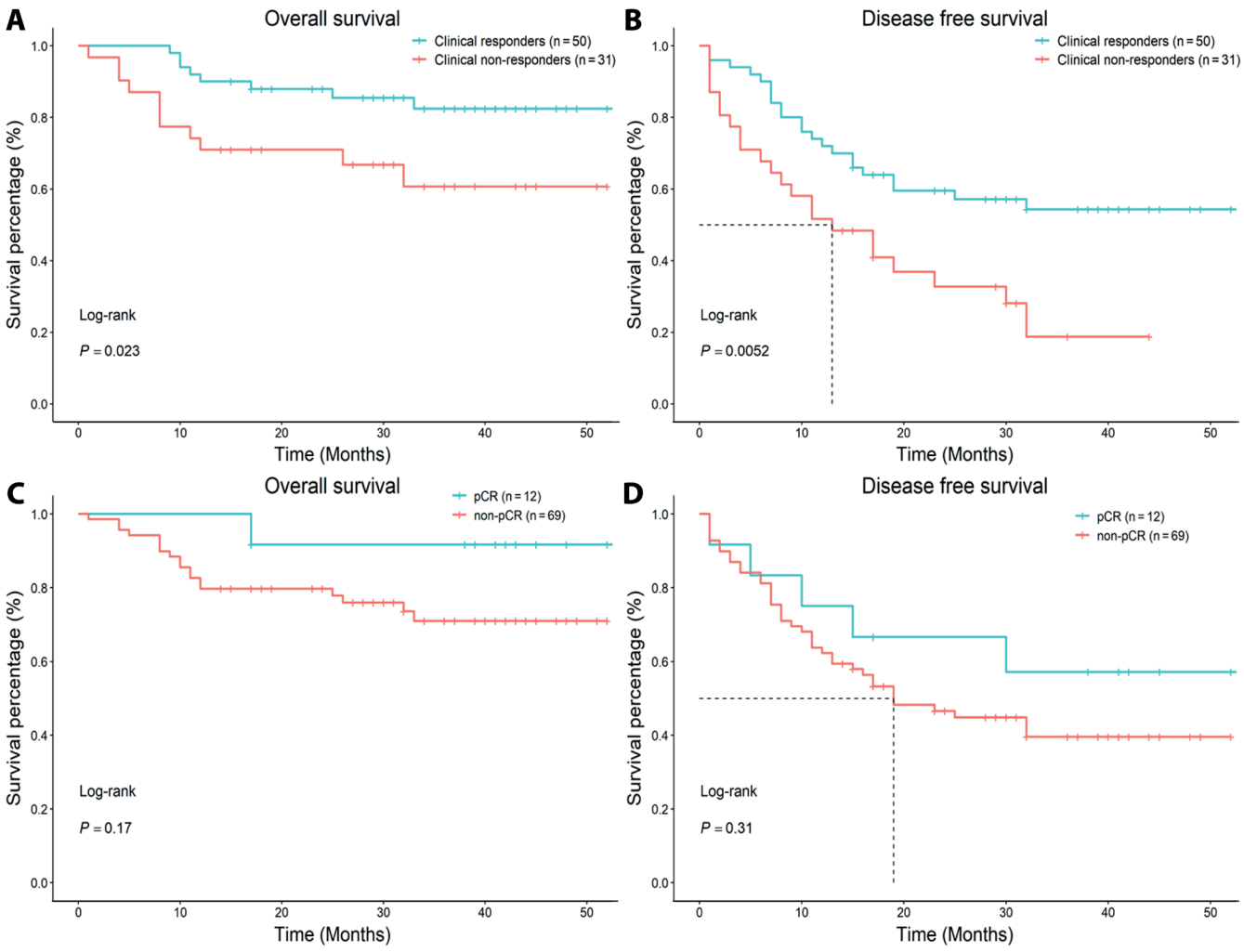


Fig. 4. Survival outcomes for patients with different responses to chemotherapy

pCR – pathological complete response.

cisplatin and 5-fluorouracil (TPF) regimen as NAC before surgery did not achieve better survival outcomes compared to those who underwent radical surgery directly.[13] Another randomized clinical trial involving 198 patients with OSCC showed that NAC with cisplatin and fluorouracil (PF) regimen before surgery did not significantly improve survival outcomes after 11.5 years of follow-up compared to direct surgery.[24] A meta-analysis on locally advanced HNSCC concluded that the addition of adjuvant chemotherapy or NAC on top of platinum-based chemoradiotherapy did not provide survival benefits for patients.[25] A recent meta-analysis including 1,373 patients indicated that there was no statistically significant difference between treatment groups in terms of OS, DSF, locoregional recurrence, and distant metastasis.[26] In this study, we also found no improvement in OS for patients with OSCC that were treated with NAC and radical surgery. However, worse DFS was observed in the NAC group, which indicated that more local recurrence and distant metastasis occurred in patients who received chemotherapy before radical surgery. Another retrospective study showed similar results.[15]

A possible reason we assumed for the inferior DFS in the NAC group was that worse locoregional control resulted from the challenge of the surgical margin after chemotherapy. The tumor can be less palpable after chemotherapy, which makes it more difficult to determine the extent of surgical resection. Furthermore, tumor regression was proven to be irregular and non-centripetal, leading to residual tumor cells being located away from the main tumor bed, which may result in false negative margins in frozen section examination and routine pathological examination.[27,28] On the other hand, the factors contributing to our research findings may also encompass a diminished chemotherapy response rate. The chemotherapy regimen, margin status, extranodal extension (ENE) status, and tumor differentiation level may be important factors influencing NAC. Within our study, the favorable prognostic implications observed in patients attaining a pCR did not result in an OS advantage for the entire cohort undergoing induction chemotherapy. This discrepancy could be ascribed to the relatively restricted number of patients achieving pCR, which may potentially dilute the cumulative survival benefit. The improved survival outcomes observed in pCR patients may be attributed to the beneficial effects of chemotherapy or could indicate an inherent positive prognosis in responsive individuals. Subsequent investigations should prioritize the identification of predictive biomarkers for response to induction chemotherapy to facilitate the optimized use of preoperative medications in chemosensitive patients while mitigating toxicities in nonresponsive cases.

Possible risk factors for failure of NAC

To identify patients with a higher risk of treatment failure and guide the choice of appropriate treatment modality, we conducted a KM analysis in subgroups stratified by pathological features. The results showed that the survival pattern was similar in patients with early-stage tumors (pT0/2) in the NAC group. However, patients with pT3/4 stage after upfront surgery had better DFS than patients who remained in stage pT3/4 after NAC. No significant difference in survival was found when we stratified the patients according to lymph node status. Local–regional recurrence has been proven to be the main failure pattern for OSCC patients both with and without preoperative treatment,[13,29] suggesting that patients with pT3/T4 stage after chemotherapy may have a higher risk of locoregional relapse than patients with the same stage after surgery alone. More to the point, the optimal postoperative administration for patients receiving NAC remains unclear.[30] Referring to postoperative therapy for patients without NAC, pT3/4 is only a relative indication for radiotherapy recommended by National Comprehensive Cancer Network (NCCN) guidelines. Given our results that patients who remained in pT3/4 stage after NAC faced a higher risk of locoregional failure, we believe that aggressive postoperative treatment is necessary to realize better local control for these patients, including radiotherapy or chemoradiotherapy. The benefits of enhanced locoregional control in the survival of patients pretreated with NAC further substantiate this view. In a clinical trial by Zhong et al.,[13] equivalent survival outcomes were achieved between the TPF induction arm and the upfront surgery arm, as all patients in both groups underwent postoperative radiotherapy. Nevertheless, more research is required to confirm this speculation, since our present study did not involve the decision-making of adjuvant administration directly.

Our analysis tried to identify the risk factors for survival in patients with different treatment regimens using Cox proportional hazards regression models. Pathologic tumor stage and clinical response to NAC were important factors in predicting survival outcomes after pretreated chemotherapy and surgery, but neither was an independent predictor, as the 2 factors interact strongly. For patients treated with upfront surgery, pathologic tumor stage exhibited a consistent effect on predicting OS, as a previous study reported.[31] The histologically confirmed tumor stage after NAC is usually considered invalid for prognosis.[32] However, our findings suggest that pathologic stage plays a similar prognostic role for patients both with and without NAC in whom advanced pathological stage was a predictor of worse survival. The degree of pathological differentiation is an independent prognostic factor for DFS, with patients of lower pathological differentiation being at a higher risk of regional recurrence and distant metastasis compared to those of moderate-to-high differentiation. Due to the higher microvessel density in histologically poorly differentiated SCC, it is believed that poorly differentiated SCC may be more sensitive to chemotherapy.[33] A retrospective analysis by Kina et al.[34] suggested that compared to well-differentiated OSCC, moderately-to-poorly

differentiated OSCC exhibits higher chemotherapy sensitivity and benefits from sequential neoadjuvant therapy (bleomycin regimen). However, our data did not reveal chemotherapy sensitivity in poorly differentiated patients. Similar to studies in the non-NAC population,[35,36] our results indicated that patients with histologically poorly differentiated oral cancer in the NAC + radical surgery group had worse DFS compared to those with moderate-to-high differentiation, possibly due to the higher invasiveness of poorly differentiated OSCC.

In this study, patients in the NAC group had a clinical response rate of 61.7% and a pCR rate of 14.8%, which are comparable to previous reports.[20,37] It is noteworthy that in patients with a favorable clinical response, survival was significantly improved compared to those with an unfavorable clinical response. Pathologic response was considered to be a more important predictor of survival than clinical response, which was determined imprecisely by image examination.[38] However, in this study, we failed to demonstrate a significant improvement in survival for patients with pCR due to a relatively small sample number. The identification of chemotherapy response as a prognostic factor for prolonged survival underscores the importance of identifying the potential chemosensitive subgroup of OSCC before determining the treatment regimen. Neoadjuvant chemotherapy before tumor excision should be avoided in patients who may have a poor response to chemotherapy to prevent chemotherapy complications and unnecessary surgical delays.[20] Recently, a few attempts have been made to solve this problem. For example, the expression levels of GDF15[39] and Annexin A1[40] have been reported to be potential predictive biomarkers for benefitting from TPF NAC for OS in patients with OSCC who were treated with NAC and radical surgery. Tumor blood flow assessed using perfusion computed tomography,[22] body mass index (BMI)[41] and preoperative mean platelet volume[42] have also been reported to be helpful in predicting NAC outcomes. Unfortunately, no universally available biomarker is currently in clinical use. For future studies, further investigations are necessary to identify the subgroups of patients who are sensitive to preoperative chemotherapy and thereby contribute to the advancement of personalized medicine practice.

Simultaneously, our results underscore the importance of postoperative adjuvant therapy. There are no established postoperative treatment guidelines for patients who have previously undergone NAC. Some patients who have received NAC may overlook postoperative adjuvant therapy due to issues such as tumor stage downgrading after surgery, poor economic conditions and decreased quality of life. However, several studies[43,44] have demonstrated the significance of postoperative radiotherapy/chemotherapy in improving DFS, and emphasis should be placed on postoperative adjuvant therapy for patients who have undergone NAC. Of course, this conclusion requires further confirmation through large-scale clinical studies.

The challenges and future of NAC for OSCC patients

Although studies on different chemotherapy regimens have shown some variations in their impact on DFS and OS rates in different research reports, there is still no traditional chemotherapy drug that has consistently demonstrated excellent efficacy. In current clinical practice, the TPF regimen is considered the standard induction chemotherapy regimen for advanced oral cancer patients due to its higher response rates.[45] However, fluorouracil has been associated with stronger toxic reactions, such as mucositis, gastrointestinal toxicity, hematologic toxicity, and cardiac toxicity,[46] prompting researchers to explore alternative neoadjuvant regimens in hopes of achieving higher response rates and lower toxicity. A 2014 retrospective study by Herman et al. [47] included 143 patients who received induction TPF or cisplatin plus paclitaxel (CT) prior to definitive chemoradiotherapy. The study results indicated that the CT regimen showed similar or even better progression-free survival and local control rates compared to the TPF regimen, with lower renal toxicity. Response rates for the CT regimen reported in other studies ranged from 50% to 85%.[46,48–50] A large-scale clinical study on borderline resectable oral cancer has demonstrated that using more than 2 drugs in combination increases the survival rate of patients compared to using only 2 drugs.[6]

Several meta-analyses have shown consistent results, indicating that NAC does not confer a survival or response rate benefit.[26] However, the efficacy of NAC in the context of surgical margin clearance remains inadequately investigated. At this juncture, surgery should be upheld as the primary treatment modality for locally advanced OSCC. Furthermore, for patients requiring neoadjuvant therapy, it should adhere closely to the principles of comprehensive cancer care, including postoperative adjuvant radiotherapy or chemotherapy. Although various studies have reported differences in DFS and OS rates with different chemotherapy regimens, no traditional chemotherapy agent has consistently demonstrated superior efficacy. In recent years, novel neoadjuvant regimens incorporating immune checkpoint inhibitors, such as anti-PD-1/PD-L1, anti-KIR, anti-Tim3, and anti-CTLA-4, collectively known as neoadjuvant immunotherapy, have shown promising results in terms of survival outcomes.[37,51] When conditions permit, immunotherapy may be combined to enhance the rate of response to neoadjuvant therapy.

Further research is warranted to validate the efficacy of neoadjuvant immunotherapy. For example, the expression of PDL1 in tumors and tumor-infiltrating immune cells can be utilized to predict the response rate to PD1/PDL1 immune checkpoint inhibitor therapy. However, the unknown expression patterns of immune checkpoints in tumor cells during NAC treatment pose challenges in predicting treatment efficacy based on protein

expression and gene mutations. In the context of OSCC, there remains a significant lack of broadly effective immune checkpoint inhibitors for the majority of patients with OSCC. Therefore, neoadjuvant immunotherapy may entail dual risks, including the potential side effects of immune checkpoint inhibitors and a high financial burden.

It is challenging to definitively classify NAC as entirely inconsequential solely based on the outcomes of a single clinical study. With stringent control over indications, our objective is to augment the response rate to chemotherapy and lengthen patients' DFS through a combination of diverse medications and immunotherapy. We maintain the belief that NAC remains advantageous for responsive patients. Furthermore, NAC plays a critical role in the management of patients with locally advanced unresectable oral cancer. We believe that, alongside exploring evolving chemotherapy combinations, investigating the patient's clinical characteristics and the genetic molecular markers that influence treatment response represents a promising avenue for future research in the field of NAC.

Limitations

As a retrospective study, this research faced challenges in controlling for patients' baseline data and was limited to a cohort of 156 patients with advanced OSCC from a single center. Furthermore, there were some missing clinical baseline data, complicating efforts to mitigate the bias introduced by clinical decision-making in the NAC group through methods such as matched grouping. Moreover, patients requiring NAC, even within the same advanced stage, may present with more severe conditions and higher disease grades. The absence of randomization introduced multiple factors that contribute to the uncertainty of the study results. While local recurrence and distant metastasis represent 2 patterns of treatment failure in OSCC patients, this study lacked the statistical power to differentiate between the two.

Conclusions

Patients with advanced pathological stages after NAC may be at a higher risk of treatment failure, and upfront surgery is recommended for locally advanced OSCC patients in current clinical practice.

Supplementary data

The Supplementary materials are available at https://doi.org/10.5281/zenodo.13373456. The package includes the following files:

Supplementary Fig. 1. Normality test of age.

Supplementary Fig. 2. Schoenfeld residuals plots for each covariate.

Supplementary Fig. 3. Residual plot of age.

Supplementary Table 1. Assessment of multicollinearity using the VIF.

Supplementary Table 2. Assessment of multicollinearity using the VIF.

Data availability

The datasets generated and/or analyzed during the current study are available from the corresponding author on reasonable request.

Consent for publication

Not applicable.

ORCID iDs

Xiaotong He https://orcid.org/0000-0001-7939-8768
Xiaoyue Lei https://orcid.org/0000-0002-9862-8159
Yangxi Cheng https://orcid.org/0009-0001-4603-1860
Huiyong Zhu https://orcid.org/0000-0003-0883-5355

References

1. Cramer JD, Burtness B, Le QT, Ferris RL. The changing therapeutic landscape of head and neck cancer. *Nat Rev Clin Oncol*. 2019;16(11):669–683. doi:10.1038/s41571-019-0227-z
2. Chinn SB, Myers JN. Oral cavity carcinoma: Current management, controversies, and future directions. *J Clin Oncol*. 2015;33(29):3269–3276. doi:10.1200/JCO.2015.61.2929
3. Bozec A, Culié D, Poissonnet G, Dassonville O. Current role of primary surgical treatment in patients with head and neck squamous cell carcinoma. *Curr Opin Oncol*. 2019;31(3):138–145. doi:10.1097/CCO.0000000000000531
4. Nair D, Singhvi H, Mair M, et al. Outcomes of surgically treated oral cancer patients at a tertiary cancer center in India. *Indian J Cancer*. 2017;54(4):616. doi:10.4103/ijc.IJC_445_17
5. Liao C, Chang JT, Wang H, et al. Surgical outcome of T4a and resected T4b oral cavity cancer. *Cancer*. 2006;107(2):337–344. doi:10.1002/cncr.21984
6. Noronha V, Dhanawat A, Patil VM, et al. Long-term outcomes of neoadjuvant chemotherapy on borderline resectable oral cavity cancers: Real-world data of 3266 patients and implications for clinical practice. *Oral Oncol*. 2024;148:106633. doi:10.1016/j.oraloncology.2023.106633
7. Siegel RL, Miller KD, Wagle NS, Jemal A. Cancer statistics, 2023. *CA Cancer J Clin*. 2023;73(1):17–48. doi:10.3322/caac.21763
8. Kitamura N, Sento S, Yoshizawa Y, Sasabe E, Kudo Y, Yamamoto T. Current trends and future prospects of molecular targeted therapy in head and neck squamous cell carcinoma. *Int J Mol Sci*. 2020;22(1):240. doi:10.3390/ijms22010240
9. He L, Jin M, Jian D, et al. Identification of four immune subtypes in locally advanced rectal cancer treated with neoadjuvant chemotherapy for predicting the efficacy of subsequent immune checkpoint blockade. *Front Immunol*. 2022;13:955187. doi:10.3389/fimmu.2022.955187
10. Pavese F, Capoluongo ED, Muratore M, et al. BRCA mutation status in triple-negative breast cancer patients treated with neoadjuvant chemotherapy: A pivotal role for treatment decision-making. *Cancers (Basel)*. 2022;14(19):4571. doi:10.3390/cancers14194571
11. Haddad R, O'Neill A, Rabinowits G, et al. Induction chemotherapy followed by concurrent chemoradiotherapy (sequential chemoradiotherapy) versus concurrent chemoradiotherapy alone in locally advanced head and neck cancer (PARADIGM): A randomised phase 3 trial. *Lancet Oncol*. 2013;14(3):257–264. doi:10.1016/S1470-2045(13)70011-1

12. Cohen EEW, Karrison TG, Kocherginsky M, et al. Phase III randomized trial of induction chemotherapy in patients with N2 or N3 locally advanced head and neck cancer. *J Clin Oncol*. 2014;32(25):2735–2743. doi:10.1200/JCO.2013.54.6309
13. Zhong LP, Zhang CP, Ren GX, et al. Randomized phase III trial of induction chemotherapy with docetaxel, cisplatin, and fluorouracil followed by surgery versus up-front surgery in locally advanced resectable oral squamous cell carcinoma. *J Clin Oncol*. 2013;31(6):744–751. doi:10.1200/JCO.2012.43.8820
14. Geoffrois L, Martin L, De Raucourt D, et al. Induction chemotherapy followed by cetuximab radiotherapy is not superior to concurrent chemoradiotherapy for head and neck carcinomas: Results of the GORTEC 2007-02 phase III randomized trial. *J Clin Oncol*. 2018; 36(31):3077–3083. doi:10.1200/JCO.2017.76.2591
15. Su X, Liu Q, Li J, et al. The oncological outcome and influence of neoadjuvant chemotherapy on the surgery in the resectable and locally advanced oral squamous cell carcinoma. *Cancer Manag Res*. 2019; 11:7039–7046. doi:10.2147/CMAR.S204961
16. Chaukar D, Prabash K, Rane P, et al. Prospective phase II open-label randomized controlled trial to compare mandibular preservation in upfront surgery with neoadjuvant chemotherapy followed by surgery in operable oral cavity cancer. *J Clin Oncol*. 2022;40(3):272–281. doi:10.1200/JCO.21.00179
17. Uppaluri R, Campbell KM, Egloff AM, et al. Neoadjuvant and adjuvant pembrolizumab in resectable locally advanced, human papillomavirus-unrelated head and neck cancer: A multicenter, phase II trial. *Clin Cancer Res*. 2020;26(19):5140–5152. doi:10.1158/1078-0432.CCR-20-1695
18. Eisenhauer EA, Therasse P, Bogaerts J, et al. New response evaluation criteria in solid tumours: Revised RECIST guideline (version 1.1). *Eur J Cancer*. 2009;45(2):228–247. doi:10.1016/j.ejca.2008.10.026
19. Quadri P, McMullen C. Oral cavity reconstruction. *Otolaryngol Clin North Am*. 2023;56(4):671–686. doi:10.1016/j.otc.2023.04.002
20. Kiong KL, Yao CMKL, Lin F, et al. Delay to surgery after neoadjuvant chemotherapy in head and neck squamous cell carcinoma affects oncologic outcomes. *Cancer*. 2021;127(12):1984–1992. doi:10.1002/cncr.33471
21. Reddavid R, Sofia S, Chiaro P, et al. Neoadjuvant chemotherapy for gastric cancer: Is it a must or a fake? *World J Gastroenterol*. 2018;24(2): 274–289. doi:10.3748/wjg.v24.i2.274
22. Ning Y, Yang H, Qin S, et al. Prognostic value of preoperative mean platelet volume and a predictive nomogram in oral squamous cell carcinoma patients based on real-world data. *Cancer Manag Res*. 2021;13:8495–8509. doi:10.2147/CMAR.S323117
23. Lau A, Li KY, Yang W fa, Su YX. Induction chemotherapy for squamous cell carcinomas of the oral cavity: A cumulative meta-analysis. *Oral Oncol*. 2016;61:104–114. doi:10.1016/j.oraloncology.2016.08.022
24. Bossi P, Lo Vullo S, Guzzo M, et al. Preoperative chemotherapy in advanced resectable OCSCC: Long-term results of a randomized phase III trial. *Ann Oncol*. 2014;25(2):462–466. doi:10.1093/annonc/mdt555
25. Jerzak KJ, Delos Santos K, Saluja R, Lien K, Lee J, Chan KKW. A network meta-analysis of the sequencing and types of systemic therapies with definitive radiotherapy in locally advanced squamous cell carcinoma of the head and neck (LASCCHN). *Oral Oncol*. 2017;71:1–10. doi:10.1016/j.oraloncology.2017.05.011
26. Kende P, Mathur Y, Varte V, Tayal S, Patyal N, Landge J. The efficacy of neoadjuvant chemotherapy as compared to upfront surgery for the management of oral squamous cell carcinoma: A systematic review and meta-analysis. *Int J Oral Maxillofac Surg*. 2024;53(1):1–10. doi:10.1016/j.ijom.2023.03.007
27. Ling DC, Sutera PA, Iarrobino NA, et al. Is multifocal regression a risk factor for ipsilateral breast tumor recurrence in the modern era after neoadjuvant chemotherapy and breast conservation therapy? *Int J Radiat Oncol Biol Phys*. 2019;104(4):869–876. doi:10.1016/j.ijrobp.2019.03.012
28. Kiong KL, Bell D, Yao CM, Ferrarotto R, Lewis CM. Multifocal regression and pathologic response predicts recurrence after neoadjuvant chemotherapy in head and neck squamous cell carcinoma. *Oral Oncol*. 2021;122:105520. doi:10.1016/j.oraloncology.2021.105520
29. Chai AWY, Lim KP, Cheong SC. Translational genomics and recent advances in oral squamous cell carcinoma. *Semin Cancer Biol*. 2020; 61:71–83. doi:10.1016/j.semcancer.2019.09.011
30. Verma M, Chakrabarti D. Are the classical indications of postoperative chemoradiotherapy in head and neck squamous cell cancers valid in the era of neoadjuvant chemotherapy? *Oral Oncol*. 2020; 107:104838. doi:10.1016/j.oraloncology.2020.104838
31. Monteiro LS, Delgado ML, Ricardo S, et al. EMMPRIN expression in oral squamous cell carcinomas: Correlation with tumor proliferation and patient survival. *Biomed Res Int*. 2014;2014:905680. doi:10.1155/2014/905680
32. Levenson G, Voron T, Paye F, et al. Tumor downstaging after neoadjuvant chemotherapy determines survival after surgery for gastric adenocarcinoma. *Surgery*. 2021;170(6):1711–1717. doi:10.1016/j.surg.2021.08.021
33. Kina S, Kinjo T, Liang F, Nakasone T, Yamamoto H, Arasaki A. Targeting EphA4 abrogates intrinsic resistance to chemotherapy in well-differentiated cervical cancer cell line. *Eur J Pharmacol*. 2018;840:70–78. doi:10.1016/j.ejphar.2018.09.031
34. Kina S, Kawabata-Iwakawa R, Miyamoto S, Arasaki A, Sunakawa H, Kinjo T. A molecular signature of well-differentiated oral squamous cell carcinoma reveals a resistance mechanism to metronomic chemotherapy and novel therapeutic candidates. *J Drug Target*. 2021; 29(10):1118–1127. doi:10.1080/1061186X.2021.1929256
35. Arun P, Arun I, Jain P, Manikantan K, Sharan R. Determinants of prognosis in patients with oral squamous cell carcinoma metastasizing to a single cervical lymph node. *Oral Oncol*. 2021;123:105586. doi:10.1016/j.oraloncology.2021.105586
36. Lindenblatt RDCR, Martinez GL, Silva LE, Faria PS, Camisasca DR, Lourenço SDQC. Oral squamous cell carcinoma grading systems: Analysis of the best survival predictor. *J Oral Pathol Med*. 2012;41(1): 34–39. doi:10.1111/j.1600-0714.2011.01068.x
37. Masarwy R, Kampel L, Horowitz G, Gutfeld O, Muhanna N. Neoadjuvant PD-1/PD-L1 inhibitors for resectable head and neck cancer: A systematic review and meta-analysis. *JAMA Otolaryngol Head Neck Surg*. 2021;147(10):871. doi:10.1001/jamaoto.2021.2191
38. Hirakawa H, Hanai N, Suzuki H, et al. Prognostic importance of pathological response to neoadjuvant chemotherapy followed by definitive surgery in advanced oral squamous cell carcinoma. *Jpn J Clin Oncol*. 2017;47(11):1038–1046. doi:10.1093/jjco/hyx097
39. Yang CZ, Ma J, Zhu DW, et al. GDF15 is a potential predictive biomarker for TPF induction chemotherapy and promotes tumorigenesis and progression in oral squamous cell carcinoma. *Ann Oncol*. 2014;25(6):1215–1222. doi:10.1093/annonc/mdu120
40. Zhu DW, Liu Y, Yang X, et al. Low annexin A1 expression predicts benefit from induction chemotherapy in oral cancer patients with moderate or poor pathologic differentiation grade. *BMC Cancer*. 2013;13(1):301. doi:10.1186/1471-2407-13-301
41. Singh K, Sunku R, Rathi A, Pradhan G. Predicting outcome of advanced head-and-neck cancer by measuring tumor blood perfusion in patients receiving neoadjuvant chemotherapy. *J Cancer Res Ther*. 2020;16(8):34. doi:10.4103/jcrt.JCRT_195_18
42. Zhao TC, Liang SY, Ju WT, et al. Normal BMI predicts the survival benefits of inductive docetaxel, cisplatin, and 5-fluorouracil in patients with locally advanced oral squamous cell carcinoma. *Clin Nutr*. 2020; 39(9):2751–2758. doi:10.1016/j.clnu.2019.11.037
43. Tian Q, Jiang L, Dai D, et al. Impact of postoperative radiotherapy on the prognosis of early-stage (pT1-2N0M0) oral tongue squamous cell carcinoma. *J Clin Oncol*. 2024;42(15):1754–1765. doi:10.1200/JCO.23.01106
44. Knochelmann HM, Horton JD, Liu S, et al. Neoadjuvant presurgical PD-1 inhibition in oral cavity squamous cell carcinoma. *Cell Rep Med*. 2021;2(10):100426. doi:10.1016/j.xcrm.2021.100426
45. Keil F, Hartl M, Altorjai G, et al. Docetaxel, cisplatin and 5-FU compared with docetaxel, cisplatin and cetuximab as induction chemotherapy in advanced squamous cell carcinoma of the head and neck: Results of a randomised phase II AGMT trial. *Eur J Cancer*. 2021; 151:201–210. doi:10.1016/j.ejca.2021.03.051
46. Yen C, Tsou H, Hsieh C, et al. Sequential therapy of neoadjuvant biochemotherapy with cetuximab, paclitaxel, and cisplatin followed by cetuximab-based concurrent bioradiotherapy in high-risk locally advanced oral squamous cell carcinoma: Final analysis of a phase 2 clinical trial. *Head Neck*. 2019;41(6):1703–1712. doi:10.1002/hed.25640

47. Herman LC, Chen L, Garnett A, et al. Comparison of carboplatin–paclitaxel to docetaxel–cisplatin-5–flurouracil induction chemotherapy followed by concurrent chemoradiation for locally advanced head and neck cancer. *Oral Oncol*. 2014;50(1):52–58. doi:10.1016/j.oraloncology.2013.08.007
48. Jelinek MJ, Foster NR, Zoroufy AJ, et al. A phase I trial adding poly(ADP-ribose) polymerase inhibitor veliparib to induction carboplatin-paclitaxel in patients with head and neck squamous cell carcinoma: Alliance A091101. *Oral Oncol*. 2021;114:105171. doi:10.1016/j.oraloncology.2020.105171
49. Airoldi M, Gabriele P, Gabriele AM, et al. Induction chemotherapy with carboplatin and taxol followed by radiotherapy and concurrent weekly carboplatin + taxol in locally advanced nasopharyngeal carcinoma. *Cancer Chemother Pharmacol*. 2011;67(5):1027–1034. doi:10.1007/s00280-010-1399-5
50. Chung CH, Rudek MA, Kang H, et al. A phase I study afatinib/carboplatin/paclitaxel induction chemotherapy followed by standard chemoradiation in HPV-negative or high-risk HPV-positive locally advanced stage III/IVa/IVb head and neck squamous cell carcinoma. *Oral Oncol*. 2016;53:54–59. doi:10.1016/j.oraloncology.2015.11.020
51. Amin N, Maroun CA, El Asmar M, et al. Neoadjuvant immunotherapy prior to surgery for mucosal head and neck squamous cell carcinoma: Systematic review. *Head Neck*. 2022;44(2):562–571. doi:10.1002/hed.26935

Clinical and radiological assessment of the Polish modification of the Ilizarov external fixator for the treatment of intra-articular calcaneal fractures

Piotr Morasiewicz[1,A–F], Marcin Pelc[2,A,B,D–F], Łukasz Tomczyk[3,C,D], Joanna Kochanska-Bieri[4,C,D], Andrzej Bobiński[1,C,D], Daniele Pili[5,C,D], Paweł Reichert[6,C,D]

[1] Department of Orthopedic and Trauma Surgery, Institute of Medical Sciences, University of Opole, Poland
[2] Institute of Medical Sciences, University of Opole, Poland
[3] Department of Food Safety and Quality Management, Poznan University of Life Sciences, Poland
[4] Bern Rehabilitation Center Heiligenschwendi, Switzerland
[5] Orthopedic and Trauma Department, G.B. Mangioni Hospital, Lecco, Italy
[6] Department of Orthopedics, Traumatology and Hand Surgery, Wroclaw Medical University, Poland

A – research concept and design; B – collection and/or assembly of data; C – data analysis and interpretation; D – writing the article; E – critical revision of the article; F – final approval of the article

Advances in Clinical and Experimental Medicine, ISSN 1899–5276 (print), ISSN 2451–2680 (online) *Adv Clin Exp Med*. 2025;34(8):1321–1329

Address for correspondence
Piotr Morasiewicz
E-mail: morasp@poczta.onet.pl

Funding sources
None declared

Conflict of interest
None declared

Received on March 26, 2024
Reviewed on May 28, 2024
Accepted on August 29, 2024

Published online on October 16, 2024

Cite as
Morasiewicz P, Pelc M, Tomczyk Ł, et al. Clinical and radiological assessment of the Polish modification of the Ilizarov external fixator for the treatment of intra-articular calcaneal fractures. *Adv Clin Exp Med*. 2025;34(8):1321–1329. doi:10.17219/acem/192772

DOI
10.17219/acem/192772

Copyright
Copyright by Author(s)
This is an article distributed under the terms of the Creative Commons Attribution 3.0 Unported (CC BY 3.0) (https://creativecommons.org/licenses/by/3.0/)

Abstract

Background. There is currently no established gold standard for the treatment of calcaneal fractures.

Objectives. To conduct a clinical and radiological evaluation of patients following intra-articular calcaneal fractures treated with the Polish modification of the Ilizarov method.

Materials and methods. This was a 2-center retrospective study. We evaluated 27 patients (2 women and 25 men) aged 28–73 years (mean age 50.5 years) after treatment of intra-articular calcaneal fractures with the Polish modification of the Ilizarov method. We assessed pain using a visual analogue scale (VAS), American Orthopedic Foot and Ankle Society (AOFAS) scores, patient satisfaction with treatment, use of analgesics, duration of Ilizarov treatment, length of hospital stay, duration of surgery, patient's declared willingness to choose the same treatment again, complications, degenerative changes, Böhler angle, inflection angle, and Gissane angle.

Results. The mean follow-up period was 3 years and 2 months. Following treatment, the mean VAS pain score was 2.3. Prior to surgery, all patients were taking analgesics in comparison with only 2 patients (7.4%) at long-term follow-up. The treatment was rated as satisfactory by 11 patients, with 16 patients rating it as highly satisfactory. The mean post-treatment AOFAS score was 76.6 points. The Ilizarov fixator was removed after a mean period of 88 days. The mean duration of hospital stay was 7.4 days. The mean duration of the procedure was 44 min. All patients would choose the same treatment again. Complications were observed in 5 patients. The long-term follow-up visit revealed degenerative changes in the talocalcaneal joint in 8 patients. The median Böhler angle was 5.5° preoperatively and 28.5° postoperatively, $p < 0.001$. The median preoperative inflection angle of 160° decreased to 145°, $p < 0.001$. The median preoperative Gissane's angle of 119° increased significantly to a median postoperative value of 143°, $p < 0.001$.

Conclusions. The patients achieved good clinical and radiological outcomes.

Key words: external fixator, Ilizarov method, radiological assessment, clinical assessment, calcaneal fractures

Background

Calcaneal fractures account for 1–2% of all fractures.[1–4] These fractures are predominantly intra-articular and displaced (75%).[1,4] Comminuted and intra-articular calcaneal fractures have been a serious orthopedic challenge for years.[1–13] There is no gold standard for the treatment of fractures of this type.[1–4,6,7,10–13]

The development of external fixation devices, particularly the Ilizarov method, enabled their use in the treatment of calcaneal fractures, even comminuted and/or intra-articular ones.[2–4,6–15] The use of the Ilizarov method in calcaneal fracture management has been reported to yield good outcomes, often even better than those achieved with internal fixation.[2,6] However, most authors who used the Ilizarov method did it with an open access approach to reducing the calcaneal fracture, which may have been responsible for complications in the form of infections, delayed wound healing, or skin and soft tissue necrosis.[2,3,6–10,12,13]

The Polish modification of the Ilizarov method enables closed reduction and fixation of the calcaneal bone fragments without an open access approach and allows stabilization of the foot with only 1 Kirschner wire.[4,15] There is only 1 study presenting the clinical and radiological results of closed reduction and Ilizarov fixation of calcaneal fractures with 1 Kirschner wire.[4] The authors of that paper evaluated 11 patients with calcaneal fractures treated with the Ilizarov method and analyzed selected clinical and radiological parameters (Rowe's score, Olerud–Molander Ankle score, Böhler angle, inflection angle).[4] Both the clinical and radiological parameters improved after treatment.[4] In another article, the authors assessed the balance and load distribution of the lower limbs after treatment of calcaneal fractures using the modified Ilizarov method.[15]

Those who have analyzed the treatment outcomes following calcaneal fracture management with the Ilizarov method usually assessed only selected clinical and radiological parameters.[2,3,6,9,13]

The reported peri-implant infection rates following calcaneal fracture treatment with the Ilizarov method were 16–33%.[2,3,6,10,12] There have also been reports of degenerative changes developing after this treatment; however, the authors did not assess the exact rates.[3,4]

We proposed the hypothesis that the Polish modification of the Ilizarov external fixator may help achieve good outcomes in the treatment of calcaneal fractures.

Objectives

The purpose of our study was to conduct a comprehensive clinical and radiological evaluation of patients following intra-articular calcaneal fractures treated with the Polish modification of the Ilizarov method.

Materials and methods

Study design

Our study was retrospective in nature. Thirty patients with intra-articular calcaneal fractures were treated with the Polish modification of the Ilizarov method (Fig. 1,2) in the years 2018–2021 in 2 academic level I trauma centers.

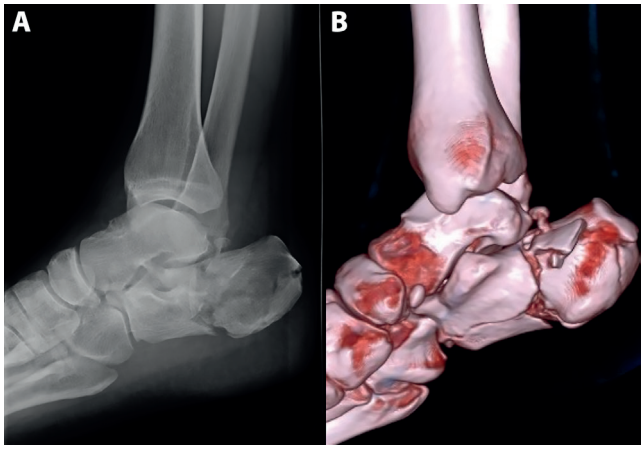


Fig. 1. The patient before treatment on (A) lateral X-ray and (B) computed tomography (CT) scan

Participants

The study inclusion criteria were a Sanders type II, III or IV calcaneal fracture treated with the Polish modification of the Ilizarov method, patient consent to participate in the study, complete medical and radiological records, a follow-up period of over 2 years, and no lower limb comorbidities. The exclusion criteria were a follow-up period under 2 years, incomplete medical records and incomplete radiological records. All patients were informed of the voluntary nature of their participation in this study. The study was approved by the Bioethics Committee of the University of Opole, Poland (protocol code UO/0023/KB/2023).

Interventions

All patients were diagnosed with a calcaneal fracture based on X-rays (anteroposterior and lateral views and the calcaneal axial view) and computed tomography (CT). The analyzed cases included 4 Sanders type II, 6 Sanders type III and 17 Sanders type IV calcaneal fractures. On arrival to the emergency room, all fractures were initially immobilized in a short leg cast. In the case of compound fractures (3 in the study population), the wounds were thoroughly rinsed, revised, cleaned, and sutured, and the limb was immobilized in a short leg cast on day 1. Patients with compound fractures received antibiotic therapy (600 mg clindamycin 3 times a day for 14 days, administered intravenously in the ward and orally for outpatient treatment). Fracture reduction and fixation with the Ilizarov method

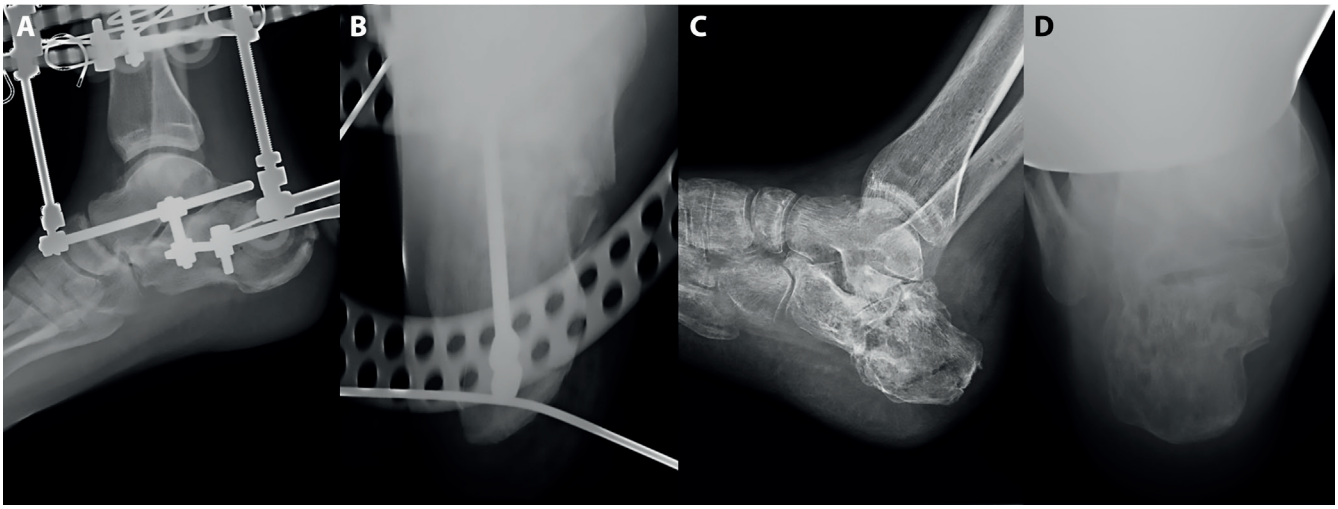


Fig. 2. The patient during (A, B), and after (C, D) treatment of an intra-articular calcaneal fracture with the Polish modification of the Ilizarov method

were conducted on days 3–5 after injury, depending on operating room and operator availability (all patients were operated on by the same orthopedic surgeon). Patients received perioperative antibiotic prophylaxis in the form of 1 dose of Biofazolin (1 g; BIOTON, Warsaw, Poland) administered intravenously.

The Polish modification of the Ilizarov external fixator was introduced for the treatment of calcaneal fractures in Wrocław, Poland, in the 1990s,[4,15] and personal communication: P. Koprowski and L. Morasiewicz. This modified external fixator comprised 2 rings, each fixed to the tibia and fibula with 2 or 3 Kirschner wires, and a semi-ring fixed with a single Kirschner wire inserted into the calcaneus (Fig. 3). The distal leg ring was attached to the calcaneal semi-ring with 2 connectors. The connectors were 2 threaded rods, attached perpendicularly to each other, enabling distraction and dorsal reposition of the calcaneal bone fragments (Fig. 3).

The procedure was performed in the supine position under spinal anesthesia. First, the 2 rings were attached with Kirschner wires to the tibia and fibula. Subsequently, a 2-mm Kirschner wire was inserted (under fluoroscopy) medially into the calcaneal tuberosity and into the most proximal and posterior bone fragment (Fig. 3). Then, a calcaneal semi-ring was attached to the Kirschner wire inserted into the calcaneus. The next step of the procedure involved joining the calcaneal semi-ring with the distal leg ring with 2 connectors (2 perpendicular threaded rods). Then, calcaneal fracture reduction was performed, under fluoroscopy, along the connectors between the calcaneal semi-ring and the distal leg ring (bone fragment distraction and dorsal repositioning were performed). The bone fragments were repositioned via closed reduction, under fluoroscopy, without opening the site surgically. This modified spatial arrangement of an Ilizarov external fixator and the effect of ligamentotaxis enabled an indirect correction of the calcaneal bone fragment's positioning. Thanks to an indirect alignment of the calcaneal bone fragments



Fig. 3. The Polish modification of the Ilizarov external fixator

in the sagittal plane, the modified arrangement of the fixator also enables the correction of the varus or valgus position of the calcaneal bone fragments (distraction or compression in the sagittal plane along 1 connector only).

The patients were allowed to walk with 2 elbow crutches and bear partial weight on the limb from the 1st postoperative day onward. A gradual increase in weight bearing was allowed as the pain subsided. If the wounds were healing well, the patient was discharged home on postoperative day 1. Follow-up radiographs were taken on the day of surgery, then 2 weeks and 6 weeks after surgery, and every 4 weeks thereafter until union. Bone union was determined based on radiological (callus, bone trabeculae crossing

the fracture line, or cortical continuity) and clinical evidence (no pain on physical examination, no pathological mobility of the bone fragments, painless weight bearing). If clinical and radiological evidence of union was present, the fixator was loosened at the connectors between the calcaneal semi-ring and the distal leg ring. The patient was allowed to walk, bearing full weight on the operated limb, and another follow-up radiograph was taken 7 days later. If there was no secondary displacement of the bone fragments and there was clinical and radiographic evidence of union, the Ilizarov external fixator was removed.

Variables

In this study, we assessed the following clinical and radiological parameters: pain severity using a visual analogue scale (VAS), American Orthopedic Foot and Ankle Society (AOFAS) scores, patient satisfaction with treatment, use of analgesics, period of time that the Ilizarov fixator was maintained on the lower limb, length of hospital stay, duration of surgery, patient's declared willingness to choose the same treatment again, complications, degenerative changes, Böhler angle, inflection angle, and Gissane's angle. The evaluated parameters were analyzed based on the available medical and radiological records and questionnaires completed by patients and doctors during a long-term follow-up visit.

Measurement

Pain severity was assessed with a 10-point VAS. Functional aspects were assessed with a 100-point AOFAS scale.[16] This tool helps evaluate ankle pain, range of motion, stability, and function.

The level of satisfaction with treatment was assessed on a 4-point scale: highly satisfied, satisfied, moderately satisfied, and dissatisfied.

We also assessed how many patients would choose the same treatment method again and how many patients were taking analgesic medications (tramadol, non-steroidal anti-inflammatory drugs (NSAIDs) and paracetamol) prior to surgery and at the time of their final long-term follow-up visit. The duration of Ilizarov treatment was expressed in days. The length of hospital stay was also measured in days. The duration of surgery was measured from the beginning to the end of the procedure and was expressed in minutes. The following complications were considered in our analysis: superficial pin-site infections, deep infections, skin and subcutaneous tissue necrosis, delayed wound healing, edema, necessity for reoperation, need for other procedures (arthrodesis, osteotomy or amputation), vascular injury, nerve injury, need for orthopedic footwear or shoe inserts following treatment, destabilization of the fixation, implant breakage, secondary displacement of the bone fragments, and nonunion. Possible degenerative changes were assessed based on radiographs taken at the long-term follow-up visit. The joints assessed for degenerative changes were the ankle joint, the talocalcaneal joint, the talonavicular joint, and the calcaneocuboid joint.[17] The Böhler angle, defined as the angle between a line joining the highest point of the anterior process of the calcaneus and the highest point of the posterior articular facet and a line joining the highest point of the posterior articular facet with the highest point of the calcaneal tuberosity, was assessed on lateral radiographs of the foot; normal values are 20–40°. The inflection angle, also assessed on lateral radiographs of the foot, was defined as the angle formed by the calcaneal tuberosity, the cuboid bone and the metatarsal heads (normal values: 145–150°). Gissane's angle, defined as the angle between the downward and upward slopes of the calcaneal superior surface, was also assessed on a lateral radiograph of the foot; normal values are 120–145°.

Bias

To avoid any source of bias, the measurements were recorded separately for every patient.

Study size

Application of the inclusion and exclusion criteria yielded 27 patients: 2 women and 25 men aged 28–73 years (mean age 50.5 years) included in our analysis.

Statistical analyses

The data were statistically analyzed using Statistica v. 13.1 (StatSoft Inc., Tulsa, USA). The Shapiro–Wilk test was used to check for normality of distribution. The Wilcoxon signed-rank test was used to compare quantitative variables. Bonferroni correction was used for multiple comparisons. The significance level was set at $p < 0.016$.

Results

Follow-up

The follow-up period ranged from 2 years to 5 years and 2 months (mean follow-up 3 years and 2 months).

Visual analogue scale

Following treatment, the mean VAS pain score was 2.3 (0–6). Prior to surgery, all patients were taking analgesics in comparison with only 2 patients (7.4%) at their long-term follow-up appointment. Eleven patients (40.7%) were satisfied with the treatment, and 16 patients (59.3%) were very satisfied.

American Orthopedic Foot and Ankle Society score

The mean post-treatment AOFAS score was 76.6 points (60–100). The Ilizarov fixator was removed after a mean period of 88 days (67–105 days) after surgery. The mean duration of hospital stay was 7.4 days (3–20 days). The mean duration of the procedure was 44 min (40–55 min). All patients would choose the same treatment again.

Complications

Complications were observed in 5 patients (18.5%). In all cases, these complications were superficial pin-site infections. In all patients, these infections were successfully treated with oral antibiotics and wound dressings. We observed no cases of deep tissue infections, skin or subcutaneous tissue necrosis, delayed wound healing, edema, necessity for reoperation, necessity for other procedures (arthrodesis, osteotomy or amputation), vascular injury, nerve injury, necessity for orthopedic footwear or shoe inserts following treatment, destabilization of the fixation, implant breakage, secondary displacement of the bone fragments, or nonunion.

The long-term follow-up visit revealed degenerative changes in the talocalcaneal joint in 8 patients (29.6%). There was no evidence of degenerative changes in the ankle, talonavicular or calcaneocuboid joints.

Böhler angle

The median Böhler angle was 5.5° preoperatively and 28.5° postoperatively. This difference was statistically significant ($Z = -4.461$, $p < 0.001$) (Table 1,2, Fig. 4).

Inflection angle

The median preoperative inflection angle of 160° decreased to 145° by the time of the long-term follow-up visit.

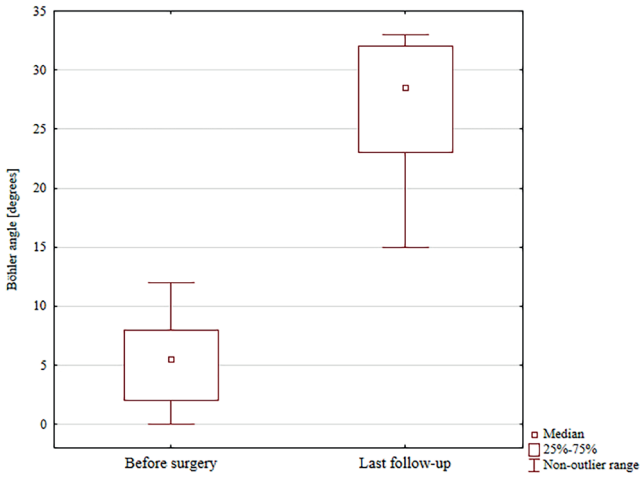


Fig. 4. Böhler angle values before and after surgery (Wilcoxon signed-rank test was used to determine significant differences)

Table 1. Detailed results before surgery and at the last follow-up

Analyzed variable		Value		p-value*
		before treatment	last follow-up	
Böhler angle [°]	Q1	2	23	<0.001
	median	5.5	28.5	
	Q3	8	32	
Gissane's angle [°]	Q1	113	137	<0.001
	median	119	143	
	Q3	131	157	
inflection angle [°]	Q1	150	140	<0.001
	median	160	145	
	Q3	170	150	

* Wilcoxon signed-rank test; Q1 – 1st quartile, Q3 – 3rd quartile

Table 2. The results of checking the normality of the data distribution (Shapiro–Wilk test) of the difference in values variables before and after surgery presented in Fig. 4–6.

Variables	W	p-value
Böhler angle [°]	0.83553	0.01
Gissane's angle [°]	0.85691	0.033
Inflection angle [°]	0.84071	0.014

W – the test value.

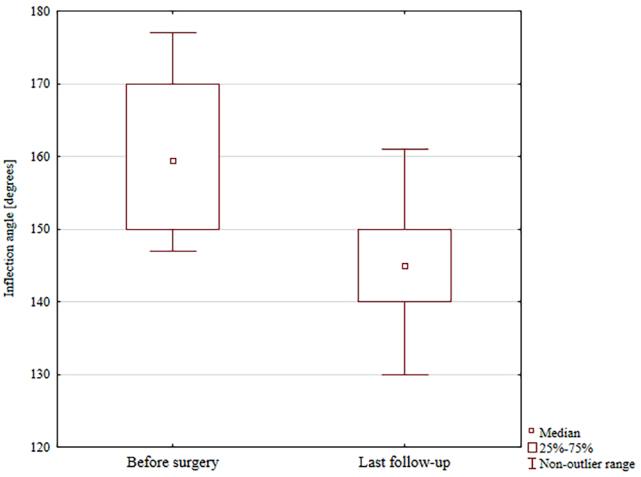


Fig. 5. Inflection angle before and after surgery (Wilcoxon signed-rank test was used to determine significant differences)

This difference was significant ($Z = -3.9101$, $p < 0.001$) (Table 1,2, Fig. 5).

Gissane's angle

The median preoperative Gissane's angle of 119° increased significantly to a mean postoperative value of 143° ($Z = -4.384$, $p < 0.001$) (Table 1,2, Fig. 6).

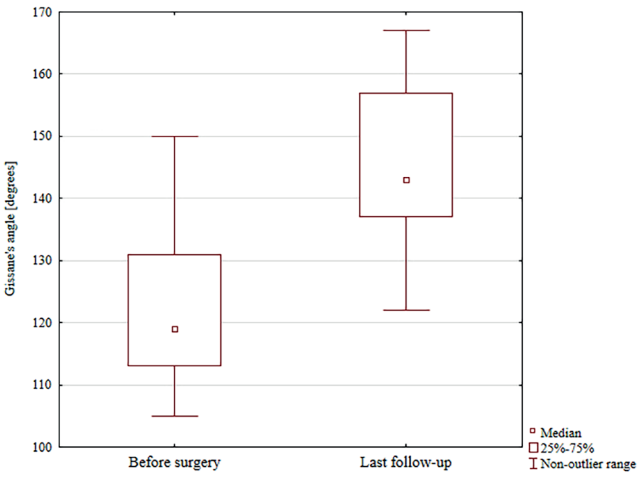


Fig. 6. Gissane's angle before and after surgery (Wilcoxon signed-rank test was used to determine significant differences)

Discussion

We conducted a detailed assessment of the clinical and radiological outcomes of using a modified Ilizarov fixator for the treatment of intra-articular calcaneal fractures. We observed good clinical outcomes and improved postoperative radiological parameters, such as the Böhler angle, the inflection angle and Gissane's angle, which supports our research hypothesis.

Most orthopedic surgeons use an open surgical approach for the treatment of intra-articular calcaneal fractures, which may be associated with high rates of complications, particularly superficial and deep tissue infections, delayed wound healing, and skin and subcutaneous tissue necrosis.[2–4,6–9,12–14,18–20] Using an open approach for the treatment of intra-articular calcaneal fractures is controversial due to high rates of limited range of motion, development of post-traumatic arthritis, infections, and delayed wound healing.[7] The Polish modification of the Ilizarov method for the treatment of intra-articular calcaneal fractures enables closed reduction, which is an advantage of this technique. Closed reduction lowers the risk of complications, shortens the duration of surgery and makes the procedure easier to perform.

Previous reports of calcaneal fracture management with the Ilizarov method mentioned the insertion of at least 3 Kirschner wires into the foot.[2,3,5–9,12–14,18–20] A higher number of implants inserted into the bones of the foot may further increase the risk of complications.[2,4] The modified Ilizarov method evaluated in our study requires only 1 Kirschner wire to be inserted into the calcaneus. The spatial configuration of Ilizarov external fixators presented by other authors for the treatment of calcaneal fractures is often complicated, bulky and burdensome for patients.[2,3,5–7,9] Usually, the Ilizarov external fixators seem to be arranged this way to improve bone fragment stability and achieve good fracture reduction.[2,3,5–7,9] Normal, anatomical repositioning of the bone fragments is believed to be the key factor for achieving good treatment outcomes in calcaneal fractures.[1,2,4–7] A normally shaped calcaneus determines the normal course of the pre-swing phase of gait.[4] Anatomical repositioning of the bone fragments and calcaneus reconstruction helps recreate normal anatomical relations of the foot structures and restores normal biomechanics.[1,2,4,6]

Our study shows that the evaluated modified Ilizarov external fixator, which requires only 1 Kirschner wire to be inserted into the calcaneus, is sufficient to achieve good clinical and radiological outcomes in the treatment of calcaneal fractures. This Polish modification of the Illizarov method ensures sufficient bone fragment stability to achieve union and correct bone fragment alignment and to restore calcaneal shape and structure. This is achieved through ligamentotaxis and the appropriate arrangement of the connectors joining the foot semi-ring and the distal leg ring (which allows for bone fragment distraction and dorsal repositioning). The corrected position and traction exerted by the most proximal and dorsal fragments of the calcaneus fixated using 1 Kirschner wire indirectly repositioned all the remaining bone fragments. The joint distraction, or arthrodiastasis, of the ankle joint and the talocalcaneal joint enabled by the Ilizarov fixator, may reduce the development of degenerative changes and reduce pain, which may result from arthrodiastasis-stimulated chondrocyte regeneration.[2,4,7]

There have been no studies assessing VAS pain scores following the treatment of calcaneal fractures using the Ilizarov method. Muir et al., who conducted a systematic review to analyze the treatment of calcaneal fractures with an external fixator, reported persistent pain in 36.7% of patients following treatment.[2] In our study, the mean post-treatment VAS pain intensity was rated at 2.3, which is a good outcome.

The systematic review by Muir et al. yielded a mean AOFAS score of 77.5.[2] In an 18-patient study conducted by McGarvey et al., the mean AOFAS score was 66.[3] Emara and Allam evaluated 12 patients after calcaneal fractures treated with the Ilizarov method and reported a mean AOFAS score of 88.2.[6]

Ali reported a mean AOFAS score of 68 in a group of 25 patients.[9] A group of 10 patients assessed by Li et al. had a mean AOFAS score of 80.[10] The 16 patients evaluated by Mauffrey et al. had a mean AOFAS score of 80.[13] In our study, the mean post-treatment AOFAS score was 76.6, which is consistent with the data found in the literature[2,3,6,9,10,13] and indicates good clinical and functional outcomes of managing calcaneal fractures with the Polish modification of the Ilizarov method.

There are no available literature reports on the level of patient satisfaction with calcaneal fracture treatment with the Ilizarov method. In our study, 40.7% of the patients were satisfied with their treatment, and the remaining 59.3% were very satisfied with their treatment. The Polish modification of the Ilizarov fixator requires

the insertion of a single Kirschner wire into the calcaneal bone and attaching it to the semi-ring, which leaves the midfoot and forefoot wire free. The Ilizarov external fixators used by other authors often take up more space, involve the entire foot, and require the insertion of at least 3 Kirschner wires into the foot.[2,3,5–9,12–14] The Polish modification to the fixator structure is the most advantageous spatial configuration in comparison with prior ones; it is also better tolerated by patients and less burdensome, and it produces higher levels of patient satisfaction with treatment.

There are no studies assessing the use of analgesics after Ilizarov treatment of calcaneal fractures. In our study, all patients had been taking analgesics before surgery, whereas by the time of their long-term follow-up visit, only 2 patients (7.4%) required analgesic treatment, indicating good long-term outcomes.

In the group of 33 patients evaluated by McGarvey et al., the Ilizarov external fixator was removed after a mean of 3 months after surgery.[3] In the group of 11 patients evaluated by Koprowski et al., the fixator was used for a mean of 3 months.[4] Emara and Allam, who evaluated 12 patients, removed the Ilizarov fixator after 3 months.[6] In our study, the Ilizarov fixator was removed after a mean of 88 days after surgery, which is consistent with the duration of Ilizarov treatment reported by other authors.[3,4,6]

In the study by Koprowski et al., the mean duration of hospital stay was 14.3 days in the younger age group and 7–10 days in the older age group of patients.[4] The patients in our study were hospitalized for a mean of 7.4 days, which is better than the duration of hospital stay reported by other authors.[4]

There have been no studies assessing the duration of surgery in the treatment of calcaneal fractures with the Ilizarov method. In our group of patients, the mean duration of surgery was 44 min, which is a good result that indicates a swift procedure. Nonetheless, some authors have described calcaneal fracture reduction and fixation with the Ilizarov method as a long and complex procedure.[2,3,5–7,9] The Polish modification of this method of calcaneal fracture treatment involves the insertion of a single implant into the foot, as opposed to the multiple implants typically required in other techniques. Furthermore, it does not necessitate an open surgical approach. This helps shorten the time of surgery and makes the method less complicated than what tends to be described in the literature.[2,3,5–7,9]

No other authors have evaluated patient willingness to choose the same method of treatment again after undergoing calcaneal fracture treatment with the Ilizarov method. All our patients declared their willingness to choose the same treatment method again if presented with a choice.

Muir et al., who conducted a systematic review of calcaneal fracture treatment with external fixators, reported persistent post-treatment pain in 36.7% of patients, limited mobility in 81% of patients, pin-site infection in 22.6% of patients, and the need to use orthopedic footwear or shoe inserts by 13.9% of patients after treatment.[2] In another study, McGarvey et al. reported limited range of motion in 80% of patients, with other post-treatment complications affecting 33.3% of patients; none of the patients required any additional procedures (arthrodesis, osteotomy or amputation).[3] Out of the 12 patients treated with the Ilizarov method and evaluated by Emara and Allan, 66.6% of the patients developed complications, which were pin-site infections in 16.6% of cases.[6] In the group of 10 patients assessed by Li et al., pin-site infections were reported in 20% of the patients.[10] Paley et al. reported pin-site infections in 14.3% out of the 7 evaluated patients, and the total proportion of patients who developed complications was 57.1%.[12] In our study, 5 patients (18.5%) developed complications; however, none of our patients required any additional procedures (arthrodesis, osteotomy or amputations). Superficial pin-site infections affected 18.5% of our patients, which is consistent with the data reported in the literature.[2,6,10,12] None of the patients in our study developed deep infections, skin or subcutaneous tissue necrosis, delayed wound healing, edema, vascular injury, nerve injury, or the need for orthopedic footwear or shoe inserts after treatment. The patients in our study underwent closed reduction, which may have lowered the complication rates in comparison with those reported by other authors.[2,3,6,10,12] The modified method of calcaneal fracture fixation used in our study allowed for walking and partial weight bearing on the operated limb as early as the 1st postoperative day. There were no cases of destabilization of the fixation, wire breakage, secondary displacement of the bone fragments, nonunion, or the necessity for reoperation. These results indicate good bone fragment stability. However, some authors, despite the use of at least 3 Kirschner wires for foot fixation, recommend bearing no weight on the operated foot for 3–10 weeks,[6,8,9,13] which may negatively affect treatment outcomes by restricting joint mobility, increasing the rates of edema, degenerative changes, and lowering the level of satisfaction with treatment.[2–4] A long period of reduced weight bearing on the operated limb may limit patient rehabilitation and lead to pain.[4]

Some authors have reported the development of degenerative changes after treatment of calcaneal fractures with the Ilizarov method; however, they did not specify the exact proportion of patients affected.[3,4] The possibly altered shape of the calcaneus leads to asymmetric load distribution through the ankle joint and the talocalcaneal joint and may result in the development of arthritis.[4] Evidence of osteoarthritis has been reported in 44–68% of patients after calcaneal fracture treatment.[2,9] Out of the 25 patients analyzed by Ali et al., 44% developed degenerative changes in the talocalcaneal joint and 24% in the calcaneocuboid joint.[9] In our study, 29.6% of the patients developed degenerative changes, within a mean period of 3 years and 2 months after treatment. In all cases, the degenerative

changes developed in the talocalcaneal joint. There was no evidence of degenerative changes in the ankle joint, talonavicular joint or calcaneocuboid joint. The Polish modification in the Ilizarov treatment of calcaneal fractures makes it possible to perform arthrodiastasis of the talocalcaneal and ankle joints,[4] which may limit the development of degenerative changes.[4,7] A long period of immobilization and reduced weight bearing in the treatment of calcaneal fractures is associated with an increased risk of complications, joint degeneration and stiffness, and poor treatment outcomes.[1,3] Our patients were allowed to bear weight on the operated limb very early, which may have limited the development of degenerative changes.

One study found that following open reduction and fixation with cannulated screws or a plate, the Böhler angle values improved by 16–30° in comparison with their preoperative values.[1] A systematic review of studies involving calcaneal fracture treatment with external fixators revealed the mean postoperative Böhler angle to be 24.8°.[2] In a group of 11 patients treated with the Polish modification of the Ilizarov method, the mean Böhler angle was 4° after injury and 27° after treatment.[4] In the evaluated group of 25 patients, Ali et al. observed an increase in the mean Böhler angle values from 11° before surgery to 24° after treatment.[9] The group of 10 patients assessed by Li et al. showed the mean Böhler angle value was 17.3° preoperatively and 25.9° postoperatively.[10] In 16 patients assessed by Mauffrey et al., the mean Böhler angle was 16° after the injury and 17° after treatment.[13] In our study, the median Böhler angle was 5.5° before surgery and increased significantly to reach 28.5° after surgery. The value of the Böhler angle achieved in our study is consistent with those reported by other authors.[1,2,4,9,10,13]

In the group of 11 patients assessed by Koprowski et al., the mean inflection angle was 154° prior to treatment and 147° after treatment.[4] We noted a median inflection angle of 160° before surgery, which decreased to 145° at long-term follow-up; these values are similar to those reported earlier.[4]

In the group of 10 patients evaluated by Li et al., the mean Gissane's angle was 100.5° before surgery and 109.5° after surgery.[10] Mauffrey et al., who evaluated 16 patients, reported a mean Gissane's angle of 115° before surgery and 106° after the operation.[13] In our study, the median preoperative Gissane's angle was 119°, and its value increased significantly to 143° after surgery.

The use of the Ilizarov method in the treatment of calcaneal fractures helps align the bone fragments during surgery and gradually correct their position afterwards in the case of failure to achieve normal alignment during surgery.[3,4,7] This helps achieve good radiological outcomes and reconstruction of the calcaneus. Reconstructing the normal shape of the calcaneus following a fracture helps restore normal load distribution in the foot and lowers the risk of degenerative changes.[4] The values of the evaluated radiological parameters in our group of patients were similar to those reported by other authors. The Polish modification of the Ilizarov method helps recreate the normal shape of the calcaneus and, depending on the nature of the fracture and the three-dimensional course of the fracture lines, its articular surfaces as well,[4] which is consistent with our findings. The radiographs obtained in our study showed the three-dimensional structure of the foot to be similar to normal.

The use of Ilizarov external fixators is particularly indicated in the case of calcaneal fracture with concomitant soft tissue injury, compound fractures, multiple trauma, and bilateral calcaneal fractures.[2,4,6,7]

The advantages of the Polish modification of the Ilizarov method in the management of intra-articular calcaneal fractures are the facts that it is easy to use, better tolerated by patients and minimally invasive, which minimizes soft tissue injury and reduces the risk of complications. The Polish modification of the Ilizarov method helps restore the shape and architecture of the calcaneus, which leads to normal load distribution in the foot and limits the development of post-traumatic arthritis.

Limitations

The limitations of our study include its retrospective character, which is due to the lack of possibility to assess clinical parameters prior to treatment in patients with calcaneal injury due to pain and pathological mobility of the injured calcaneus and the impossibility of predicting injury in advance. We would like to emphasize that other studies evaluating the treatment of calcaneal fractures were also retrospective in nature.[3–6,8–10,12–15,18–20] Another limitation of our study is the relatively low sample size, which was a result of several factors. One factor is the relative rarity of intra-articular calcaneal fractures; moreover, some patients lived far away from the study center and were unable to return for their final follow-up appointment. However, most other studies evaluating clinical and radiological parameters following calcaneal fractures also included similar, if not smaller, groups of patients.[3–6,8–10,12–15,18–20] Another limitation of our work is the lack of comparison of the results to patients with calcaneal fractures who underwent different treatment methods. Most available articles that describe the clinical or radiological results of the treatment of calcaneal fractures using the Ilizarov method[2–5,8–10,12–15,18–20] analyze the results of treatment only with the Ilizarov method, without a control group with different treatment methods. Another limitation of our study is the inclusion of patients with concomitant injuries. This was dictated by our eagerness to demonstrate the use of this modified Ilizarov method in the management of patients with calcaneal fractures and multiple other injuries and to increase the overall number of patients included in the study. Other authors also evaluated patients with calcaneal fractures, some of whom (30%) had concomitant musculoskeletal injuries.[4]

Another limitation of our work may be the disproportion in male/female distribution.

The strengths of our study are the uniform surgery protocol, the fact that the same orthopedic surgeon conducted all surgeries, the uniform rehabilitation protocol, and the fact that multiple clinical and radiographic parameters were assessed. We are currently planning a study in a larger patient population with a longer follow-up period. We also intend to prepare an article comparing the results of treating calcaneal fractures using the Polish modification of the Ilizarov method with those of a different treatment method, such as internal fixation.

Conclusions

The Polish modification of intra-articular calcaneal fracture treatment with the Ilizarov method helps achieve good stabilization of the bone fragments and restores the shape and architecture of the calcaneus.

The patients in our study exhibited lower rates of complications and degenerative changes than those reported by other authors who evaluated calcaneal fracture treatment with the Ilizarov method.

All patients in our study were satisfied or very satisfied with the treatment they received.

The patients achieved good clinical and radiological outcomes with the assessed Polish modification of the Ilizarov method for the management of intra-articular calcaneal fractures.

Data availability

The datasets generated and/or analyzed during the current study are available from the corresponding author on reasonable request.

Consent for publication

Not applicable.

ORCID iDs

Piotr Morasiewicz https://orcid.org/0000-0002-7587-666X
Marcin Pelc https://orcid.org/0009-0006-3889-0223
Łukasz Tomczyk https://orcid.org/0000-0002-4644-0111
Joanna Kochanska-Bieri https://orcid.org0009-0001-1502-1483
Andrzej Bobiński https://orcid.org/0009-0002-6641-5711
Daniele Pili https://orcid.org/0009-0005-9625-2919
Paweł Reichert https://orcid.org/0000-0002-0271-4950

References

1. Fan B, Zhou X, Wei Z, et al. Cannulated screw fixation and plate fixation for displaced intra-articular calcaneus fracture: A meta-analysis of randomized controlled trials. *Int J Surg*. 2016;34:64–72. doi:10.1016/j.ijsu.2016.08.234
2. Muir RL, Forrester R, Sharma H. Fine wire circular fixation for displaced intra-articular calcaneal fractures: A systematic review. *J Foot Ankle Surg*. 2019;58(4):755–761. doi:10.1053/j.jfas.2018.11.030
3. McGarvey WC, Burris MW, Clanton TO, Melissinos EG. Calcaneal fractures: Indirect reduction and external fixation. *Foot Ankle Int*. 2006;27(7):494–499. doi:10.1177/107110070602700703
4. Koprowski P, Kulej M, Romaszkiewicz P, Dragan S, Krawczyk A, Prastowski A. Assessment of Ilizarov's method in intraarticular calcaneal fractures. *Ortop Traumatol Rehabil*. 2004;6(4):423–432. PMID:17675969.
5. Ramanujam CL, Capobianco CM, Zgonis T. Ilizarov external fixation technique for repair of a calcaneal avulsion fracture and Achilles tendon rupture. *Foot Ankle Spec*. 2009;2(6):306–308. doi:10.1177/1938640009350983
6. Emara KM, Allam MF. Management of calcaneal fracture using the Ilizarov technique. *Clin Orthop Relat Res*. 2005;439:215–220. doi:10.1097/00003086-200510000-00037
7. Zgonis T, Roukis TS, Polyzois VD. The use of Ilizarov technique and other types of external fixation for the treatment of intra-articular calcaneal fractures. *Clin Podiatr Med Surg*. 2006;23(2):343–353. doi:10.1016/j.cpm.2006.01.011
8. Takahashi M, Noda M, Saegusa Y. A new treatment for avulsion fracture of the calcaneus using an Ilizarov external fixator. *Injury*. 2013;44(11):1640–1643. doi:10.1016/j.injury.2013.04.019
9. Ali AM, Elsaied MA, Elmoghazy N. Management of calcaneal fractures using the Ilizarov external fixator. *Acta Orthop Belg*. 2009;75(1):51–56. PMID:19358399.
10. Li D, Yin S, Wu P, et al. Management of calcaneus fractures by a new "below-the-ankle" Ilizarov frame: A series of 10 cases. *Niger J Clin Pract*. 2022;25(7):1143. doi:10.4103/njcp.njcp_1762_21
11. Paley D, Hall H. Calcaneal fracture controversies Can we put Humpty Dumpty together again? *Orthop Clin North Am*. 1989;20(4):665–677. PMID:2797756.
12. Paley D, Fischgrund J. Open reduction and circular external fixation of intraarticular calcaneal fractures. *Clin Orthop Relat Res*. 1993;290:125–131. PMID:8472439.
13. Mauffrey C, Klutts P, Seligson D. The use of circular fine wire frames for the treatment of displaced intra-articular calcaneal fractures. *J Orthopaed Traumatol*. 2009;10(1):9–15. doi:10.1007/s10195-008-0037-z
14. Gupta V, Kapoor S, Clubb S, Davies M, Blundell C. Treatment of bilateral open calcaneal fractures with Ilizarov frames. *Injury*. 2005;36(12):1488–1490. doi:10.1016/j.injury.2005.08.024
15. Pelc M, Kazubski K, Urbański W, et al. Balance and weight distribution over the lower limbs following calcaneal fracture treatment with the Ilizarov method. *J Clin Med*. 2024;13(6):1676. doi:10.3390/jcm13061676
16. Kitaoka HB, Alexander IJ, Adelaar RS, Nunley JA, Myerson MS, Sanders M. Clinical rating systems for the ankle-hindfoot, midfoot, hallux, and lesser toes. *Foot Ankle Int*. 1994;15(7):349–353. doi:10.1177/107110079401500701
17. Morasiewicz P, Dejnek M, Urbański W, Dragan SŁ, Kulej M, Dragan SF. Radiological evaluation of ankle arthrodesis with Ilizarov fixation compared to internal fixation. *Injury*. 2017;48(7):1678–1683. doi:10.1016/j.injury.2017.04.013
18. Heinig O, Feicht E, Mahamid A, Liberson R, Picard C, Liberson A. Treatment of a compound calcaneus fracture Sanders IV with an external circular fixator and calcaneal osteotomy. *Trauma Case Rep*. 2023;46:100850. doi:10.1016/j.tcr.2023.100850
19. Talarico LM, Vito GR, Zyryanov SY. Management of displaced intraarticular calcaneal fractures by using external ring fixation, minimally invasive open reduction, and early weightbearing. *J Foot Ankle Surg*. 2004;43(1):43–50. doi:10.1053/j.jfas.2003.11.010
20. Osman S. Early experience in the management of fractures of the calcaneus by Ilizarov external fixation. *Med J Cairo Univ*. 2009;77:279–285.

Effect of reduced saturation and elevated D-dimer and interleukin 6 levels on vessel density and foveal avascular zone in patients with COVID-19 bilateral pneumonia

Magdalena Kal[1,2,A–F], Michał Brzdęk[3,1,D–F], Elżbieta Cieśla[4,C,E,F], Piotr Rzymski[5,E,F], Izabella Karska-Basta[6,A,D–F], Antonio Pinna[7,A,E,F], Jerzy Mackiewicz[8,A,D–F], Mateusz Winiarczyk[8,A,D–F], Dominik Odrobina[2,9,A,E,F], Dorota Zarębska-Michaluk[1,3,A,E,F]

[1] Collegium Medicum of Jan Kochanowski University in Kielce, Poland
[2] Ophthalmic Clinic of the Voivodeship Hospital in Kielce, Poland
[3] Department of Infectious Diseases and Allergology, Jan Kochanowski University in Kielce, Poland
[4] Institute of Health Sciences, Jan Kochanowski University in Kielce, Poland
[5] Department of Environmental Medicine, Poznan University of Medical Sciences, Poland
[6] Department of Ophthalmology, Clinic of Ophthalmology and Ocular Oncology, Faculty of Medicine, Jagiellonian University Medical College, Cracow, Poland
[7] Department of Medicine, Surgery, and Pharmacy, Ophthalmology Unit, University of Sassari, Italy
[8] Department of Vitreoretinal Surgery, Medical University of Lublin, Poland
[9] Insitute of Medical Science, Jan Kochanowski University in Kielce, Poland

A – research concept and design; B – collection and/or assembly of data; C – data analysis and interpretation;
D – writing the article; E – critical revision of the article; F – final approval of the article

Advances in Clinical and Experimental Medicine, ISSN 1899–5276 (print), ISSN 2451–2680 (online) *Adv Clin Exp Med*. 2025;34(8):1331–1342

Address for correspondence
Michał Brzdęk
E-mail: michal.brzdek@gmail.com

Funding sources
None declared

Conflict of interest
None declared

Received on October 23, 2023
Reviewed on March 16, 2024
Accepted on July 29, 2024

Published online on November 7, 2024

Cite as
Kal M, Brzdęk M, Cieśla E, et al. Effect of reduced saturation and elevated D-dimer and interleukin-6 levels on vessel density and foveal avascular zone in patients with COVID-19 bilateral pneumonia. *Adv Clin Exp Med*. 2025;34(8):1331–1342. doi:10.17219/acem/191774

DOI
10.17219/acem/191774

Copyright
Copyright by Author(s)
This is an article distributed under the terms of the Creative Commons Attribution 3.0 Unported (CC BY 3.0) (https://creativecommons.org/licenses/by/3.0/)

Abstract

Background. Severe acute respiratory syndrome coronavirus 2 (SARS-CoV-2) infection can affect multiple organs, including the eyes.

Objectives. This study aimed to identify associations between vascular density (VD) and the foveal avascular zone (FAZ), assessed using optical coherence tomography angiography (OCTA), and baseline levels of D-dimers and interleukin 6 (IL-6) in patients with bilateral COVID-19 pneumonia, depending on oxygen saturation (SpO_2) on admission.

Materials and methods. The study included patients with COVID-19 bilateral pneumonia due to SARS-CoV-2 infection who were hospitalized between March and May 2021. Ophthalmological examination was performed 2 months after hospitalization. Optical coherence tomography angiography was used for the automatic assessment of the central retinal VD and the manual assessment of FAZ.

Results. A significant monotonic negative relationship was observed between $SpO_2 \leq 90\%$ and VD in some areas of the superficial capillary plexus (SCP) ($p = 0.048$) and choriocapillaris ($p = 0.021$), and the mean VD in the deep capillary plexus (DCP) ($p = 0.048$). No significant monotonic negative relationship was noted between $SpO_2 \leq 90\%$ and the FAZ in the SCP ($p = 0.075$). However, there was a significant monotonic positive relationship between VD in the nasal choriocapillaris and D-dimer levels in patients with $SpO_2 \leq 90\%$ ($p = 0.003$, respectively). Finally, a monotonic negative relationship was identified between foveal VD in the DCP and IL-6 levels in patients with $SpO_2 \leq 90\%$ ($p = 0.027$).

Conclusions. An OCTA study conducted 2 months after hospitalization for COVID-19 bilateral pneumonia showed reduced VD in those with $SpO_2 \leq 90\%$ and elevated levels of D-dimers and IL-6 during hospitalization. Optical coherence tomography angiography testing can provide monitoring of ocular status in patients following SARS-CoV-2 infection, especially those who report visual disturbances.

Key words: vessel density, oxygen saturation, COVID-19, optical coherence tomography angiography, foveal avascular zone

Background

Severe acute respiratory syndrome coronavirus 2 (SARS-CoV-2) is a virus that was initially identified in the airway epithelium of patients with pneumonia in Wuhan, China, in 2019. In March 2020, SARS-CoV-2 infection grew into a global pandemic. The virus causes coronavirus disease 2019 (COVID-19) with a wide spectrum of clinical pictures. Disease severity ranges from mild to fatal, depending on the virus itself and the patient's immune response.

Immune hyperreactivity leads to a cytokine storm with extensive vascular endothelial damage, increased blood clotting and overproduction of inflammatory factors.[1] The lungs are the main site of the clinical manifestation of COVID-19, but other organs are also involved, including the kidneys, intestines, brain, heart, and eyes.[2–7] One of the main cytokines participating in the pathogenesis of cytokine storm is interleukin 6 (IL-6).[8]

SARS-CoV-2 infection is mediated by the viral protein binding to the angiotensin-converting enzyme 2 (ACE2) receptor, which is responsible for the viral cellular entry. After attaching to ACE2, transmembrane serine protease 2 cleaves and stimulates the receptor-bound viral spike protein, thereby mediating the fusion of the viral envelope with the membrane of the target cell in the host.[9] The ACE2 is found on the surface of almost all vascular endothelial cells (VECs). When bound to SARS-CoV-2, it activates the rennin–angiotensin system, which reduces ACE2 expression and increases angiotensin II levels. Angiotensin II causes vasoconstriction and elevates the levels of tissue factor and plasminogen activator inhibitor, resulting in thrombosis. Angiotensin also participates in complement activation by generating reactive oxygen species (ROS) and downregulating C1 inhibitors. This, in turn, leads to increased vessel permeability and the release of cytokines, thereby increasing the thrombotic effects of angiotensin.[10] Patients with COVID-19 show generalized microvascular thrombosis and elevated D-dimer levels.[11]

Optical coherence tomography angiography (OCTA) is a useful tool for a noninvasive assessment of the microvasculature in the central retina and choroid of the eye. It enables the measurement of such parameters as vascular density (VD) and foveal avascular zone (FAZ) in patients with various systemic disorders such as anemia, carotid stenosis and SARS-CoV-2 infection.[12–14] Our previous studies showed differences in OCTA parameters between healthy controls and COVID-19 patients hospitalized for bilateral pneumonia. These differences persisted for at least 6 months.[15,16]

Objectives

This study aimed to identify associations of the OCTA parameters VD and FAZ with baseline oxygen saturation (SpO_2), D-dimer levels and IL-6 levels in patients with COVID-19 bilateral pneumonia.

Materials and methods

Study design

This prospective study was conducted in the Department of Infectious Diseases and the Ophthalmology Clinic of the Provincial Hospital in Kielce, Poland, from March to May 2021. The study was approved by the Bioethics Committee of the Collegium Medicum of Jan Kochanowski University in Kielce (study code 54; July 1, 2021). It was conducted in accordance with the Declaration of Helsinki, and all patients gave their informed consent.

Setting

While under SARS-CoV-2 infection, all patients were treated in the Department of Infectious Diseases. Two months after hospital discharge, they were examined in the Ophthalmology Clinic. In all patients, COVID-19 bilateral pneumonia was caused by the B.1.1.7 variant of SARS-CoV-2. The infection was determined by a positive polymerase chain reaction (PCR) test or a COVID-19 antigen rapid test device (Abbott, Lake Country, USA) Pneumonia was confirmed based on the presence of typical lesions on computed tomography (CT). The current study reports the outcomes of patients with COVID-19 bilateral pneumonia at 2 months after hospital discharge. The in-hospital outcomes of the study have been reported previously.[15]

Participants

The following exclusion criteria were applied: myopia higher than –3 diopters, hyperopia higher than +3 diopters, retinal diseases, optic neuropathies, previous eye surgery, uveitis, ocular injury, opaque media affecting OCTA scan or image quality, and diabetes mellitus.

Of the 94 patients (188 eyes) initially enrolled in the study, we excluded those with age-related macular degeneration (n = 10), diabetes mellitus (n = 13), glaucoma (n = 2), high hyperopia (n = 1), high myopia (n = 3), previous cataract surgery (n = 2), and poor-quality OCTA images (n = 1). Among the remaining 62 patients (124 eyes), we excluded 2 eyes with hyperopia >3 diopters, 1 eye with myopia >3 diopters, 1 eye after ocular trauma, and 1 eye after uveitis.

Variables

Baseline patient characteristics included demographic and clinical data: sex, age, body mass index (BMI), visual acuity, reading vision, spherical equivalent, axial length,

and oxygen saturation (SpO_2). Baseline laboratory parameters included serum alanine transaminase (ALT) activity, concentrations of C-reactive protein (CRP), procalcitonin (PCT), IL-6, D-dimer, white blood cell count (WBC), lymphocyte count, neutrophil count, and platelet count. In this study, we gathered crucial data pertaining to COVID-19 treatment, including the administration of low-molecular-weight heparin (LMWH) in both prophylactic and therapeutic doses; administration of tocilizumab, dexamethasone and remdesivir; and the need for continuous oxygen therapy. We conducted an assessment of VD and FAZ using OCTA.

Measurement

Optical coherence tomography angiography was performed using a TopconSwept Source DRIOCT Triton device (Topcon Inc., Tokyo, Japan). The images were captured using the 4.5 × 4.5 mm and 6 × 6 mm scanning protocols. Central retinal parameters were obtained using the Early Treatment Diabetic Retinopathy Study (ETDRS) grid consisting of 3 concentric circles with diameters of 1, 3 and 6 mm.

Vascular density was assessed in the superficial capillary plexus (SCP), deep capillary plexus (DCP) and choriocapillaris (CC), using the EDTRS grid subfield to define the areas of interest. The 5 areas of VD were defined as foveal VD, superior VD, nasal VD, inferior VD, and temporal VD. The VD values obtained in the parafoveal area (superior, nasal and inferior) were added together, and the average value was calculated to obtain mean VD.

The FAZ area is the central part of the macula without visible vessels (Fig. 1). Two independent ophthalmologists delineated the FAZ manually on the SCP and the DCP. Optical coherence tomography angiography scans with a quality of over 65% were eligible for examination.

Oxygen saturation, D-dimer levels and IL-6 levels assessed on admission for COVID-19 bilateral pneumonia were retrospectively obtained from hospital records. We assessed the correlations of baseline D-dimer, IL-6 and SpO_2 levels with the OCTA parameters VD and FAZ.

Statistical analyses

We calculated the frequencies (n) and percentages (%) for qualitative variables such as gender, use of drugs and the need for continuous oxygen therapy. Distributions were estimated for quantitative variables such as saturation, D-dimers, IL-6, and VD in the SCP, DCP, CC, and FAZ areas (Supplementary Fig. 1–82). Subsequently, the arithmetic mean and standard deviation (SD) or median (Me) and interquartile range (IQR) were calculated, depending on the distribution of the variables. Calculations were performed for the entire group and within groups for saturation ($SpO_2 \leq 90\%$, 91–95% and >95%), IL-6 (≤1.8 pg/mL and >1.8 pg/mL) and D-dimers (>500 µg/land and ≤500µg/L). Depending on whether data met the assumptions of Gaussian distribution and homogeneity of variance, the parametric Student's t-test or the non-parametric Mann–Whitney U test was used to assess differences in groups distinguished by IL-6 and D-dimers. Similarly, the parametric analysis of variance (ANOVA) test or the non-parametric Kruskal–Wallis ANOVA wasemployed to assess differences in means in saturation groups. Bonferroni corrections were applied to any multiple comparisons

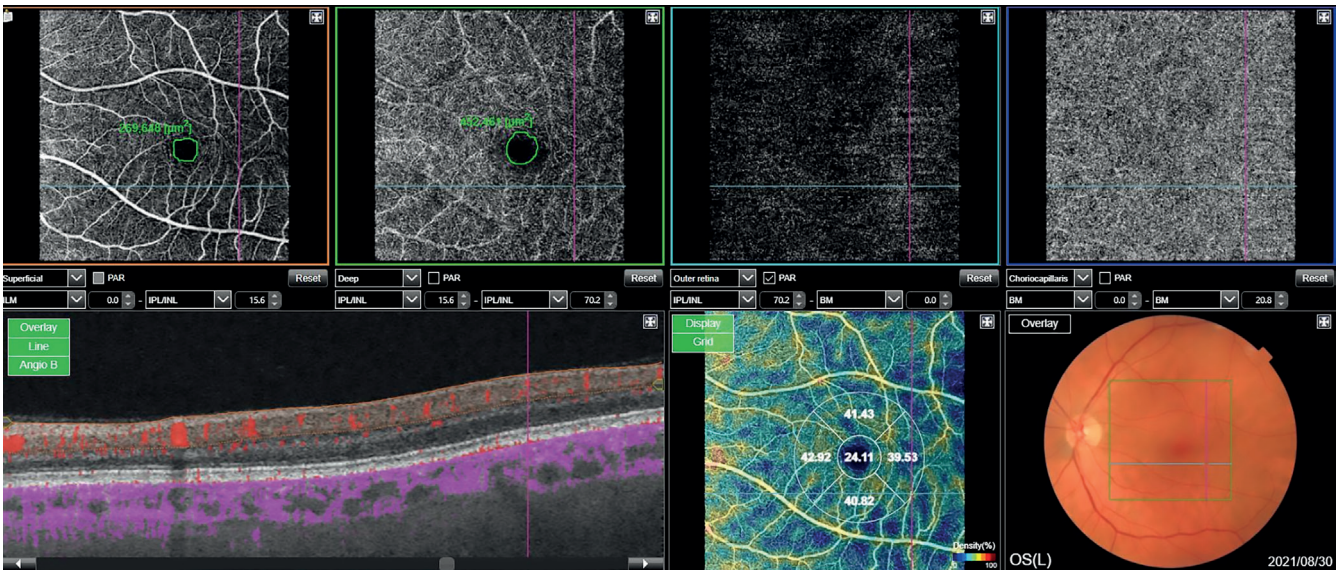


Fig. 1. The image of the foveal avascular zone (FAZ) was obtained using optical coherence tomography angiography (OCTA) manually: in the superficial capillary plexus (SCP) (left, superior corner) and in the deep capillary plexus (DCP) (the image next to the image of SCP) in the left eye. The map of the vessel density (VD) in the left eye was assessed automatically with OCTA using the early treatment diabetic retinopathy (ETDRS) grid situated in the fovea by fixation (right, lower corner) The automatic map of central VD is divided into 5 areas: the foveal VD (F VD = 24.11%), the superior area (S VD = 41.43%), the inferior VD (I VD = 40.82%), the temporal VD (T VD = 39.53%), and the nasal VD (N VD = 42.92%)

to account for alpha inflation and limit the probability of type 1 error (Supplementary Tables 1–3). The linearity was assessed based on scatter plots between saturation values, D-dimers, IL-6, and ocular parameters (Supplementary Fig. 83–143). Spearman rank correlation coefficients were used to assess the significance, direction and strength of the monotonic component of the relationship with VD in the SCP, DCP, CC, and FAZ areas based on OCTA and levels of D-dimers and IL-6 according to the saturation groups: $SpO_2 \leq 90\%$, 91–95% and >95%. Correlations were interpreted using Guilford's classification. The assumptions of the Student's t-tests were verified (testing the normality of distributions within groups with the Shapiro–Wilk test and the homogeneity of variances with Levene'stest). The same procedure was applied for the ANOVA. In case of heterogeneity of variances, Welch's F test was employed (Supplementary Table 1). Additionally, the difference (d) between individual means was calculated, and effect size was computed for all parameters in the saturation and D-dimer groups. For the Kruskal–Wallis ANOVA test, the following formula was used: eta2[H] = (H –k + 1)/(n – k), where H represents the value obtained in the Kruskal–Wallis test, k is the number of groups and n is the total number of observations. For the Student's t-test, Cohen's D was calculated according to the formula D = (mean1 – mean2)/sd_pooled. For the Mann–Whitney test, the Wendt formula was applied: It computes the rank-biserial correlation from U and from the sample size (n) of the 2 groups: r = 1 – (2U)/(n1×n2). Here, U denotes the value of the U parameter, n1 is the number for the 1st group, and n2 is the number for the 2nd group. In the parametric ANOVA test, eta square was employed as the measure of effect size; it was calculated according to the formula Eta squared = SSeffect/SStotal. The qualitative variables were presented as frequencies and percentages. A p-value of less than 0.05 was considered significant. Statistical analyses were done using Statistica v. 13.3 (StatSoft Poland, Cracow, Poland).

Results

Study group

The final study group included 119 eyes of 62 patients (42 men (67.7%) and 20 women (32.3%); mean age, 51.33 ±1.30 years). Patients were classified into 3 groups depending on SpO_2 at baseline: >95% (n = 22), 91–95% (n = 29) and ≤90% (n = 11). The demographic and ocular characteristics of patients are presented in Table 1.

Table 1. Demographic and ocular characteristics of patients with COVID-19 bilateral pneumonia

Variable		Value
Men, n (%)		42 (68.25)
Women, n (%)		20 (31.75)
Age [years][a]	mean (SD)	51.33 (1.30)
BMI [kg/m^2][b]	mean (SD)	28.41 (4.07)
Visual acuity*[,c]	median (IQR)	0.5 (0.0)
Reading vision*[,d]	median (IQR)	0.3 (0.0)
Spherical equivalent [diopters][e]	mean (SD)	0.13 (0.13)
Axial length [mm][f]	mean (SD)	23.55 (0.8)
	median (IQR)	23.45 (1.05)

*Based on the LogMar scale. BMI – body mass index; SD – standard deviation; IQR – interquartile range; [a]Shapiro–Wilk-test: p = 0.127; [b]Shapiro–Wilk-test: p = 0.817; [c]Shapiro–Wilk-test: p < 0.001; [d]Shapiro–Wilk-test: p < 0.001; [e]Shapiro–Wilk-test: p = 0.171; [f]Shapiro–Wilk-test: p = 0.514.

Visual acuity and laboratory and imaging tests on admission

Visual acuity and reading vision were assessed using the LogMar scale. The means for visual acuity and reading vision at 2 months after discharge are presented in Table 1.

Laboratory test results on admission, including mean SpO_2, CRP, PCT, WBC, lymphocytes, neutrophils, platelets, IL-6, D-dimers, and ALT, are presented in Table 2. Bilateral

Table 2. Baseline laboratory parameters in COVID-19 patients

Variable	Mean (SD)	Q1–Q3	Reference range
SpO_2 [%]	93.34 (3.68)	92.0–96.0	>95%
CRP [mg/dL]	63.99 (65.20)	14.58–93.42	<1.0
PCT [ng/mL]	0.17 (0.25)	0.04–0.18	0.05–0.1
WBC [µL]	5,723.23 (2312.33)	4,332.50–6,337.50	4,000–10,000
Lymphocytes [µL]	1,222.26 (416.43)	910.0–1,472.50	1,000–5,000
Neutrophils [µL]	3,997.26 (2,078.68)	2,532.5–4666.0	1,800–8,000
Platelets [µL]	205,411.29 (68,271.24)	150,500.0–231,000.0	150,000–400,000
IL-6 [pg/mL]	35.79 (27.75)	13.02–48.48	1.22 ±0.706
D-dimer [µg/L]	1,095.29 (3,435.20)	387.5–700.5	<500
ALT [U/L]	56.45 (37.45)	26.25–73.25	5–40

SD – standard deviation; Q – quartile; SpO_2 – oxygen saturation; CRP – C-reactive protein; PCT – procalcitonin; WBC – white blood cells count; IL-6 – interleukin 6.

lung lesions were confirmed with chest CT as ground glass opacities in 26 patients during hospitalization.

Treatment of COVID-19 patients during hospitalization

Study participants hospitalized due to SARS-CoV-2 infection were treated in line with applicable recommendations.[17] Oxygen supplementation was used in 23 patients for a median (Q1–Q2) (Table 3). In 59 patients, LMWH was administered at a prophylactic dose depending on body weight according to the summary of product characteristics. During the viral phase of COVID-19, 26 subjects were treated with intravenous remdesivir. The initial dose was 200 mg on the 1st day, followed by 100 mg for the next 4 days. Patients with hyperinflammatory syndrome were treated with immunosuppressive drugs. Dexamethasone was used on 22 patients (4 mg/day orally or 8 mg/day intravenously for 7–10 days). Intravenous tocilizumab was given to 3 patients at a single dose of 600–800 mg, depending on the patient's weight, according to the summary of product characteristics and national recommendations. Tocilizumab was administered in patients with elevated IL-6 levels.[18]

Table 3. Systemic treatment for COVID-19

Treatment	Value
Low-molecular-weight heparin, prophylactic dose, n (%)	59 (95.16)
Low-molecular-weight heparin, prophylactic dose, number of days: median (Q1–Q3)	9 (6.25–12)
Low-molecular-weight heparin, therapeutic dose, n (%)	2 (3.23)
Tocilizumab, n (%)	3 (4.84)
Dexamethasone, n (%)	22 (35.48)
Remdesivir, n (%)	26 (41.94)
Need for continuous oxygen therapy, n (%)	23 (37.10)
Need for continuous oxygen therapy, number of days, median (Q1–Q3); min–max	5 (4–10); 1–26

Q – quartile.

Structural OCTA outcomes depending on oxygen saturation and D-dimer and IL-6 levels

Differences in ocular parameters were observed in the OCTA scans depending on saturation levels. Post hoc analysis indicated significant differences between saturation groups 1 and 3, and between groups 2 and 3. Less frequent were differences based on the D-dimer and IL-6 groups (Supplementary Tables 1–3).

At 2 months, a significant monotonic negative relationship was found between SpO_2 of 90% or lower and VD in the foveal area of the SCP and the temporal area of the choriocapillaris (CC) and mean VD in the DCP (Table 4). Furthermore, there was a significant monotonic positive relationship between D-dimer levels in patients with SpO_2 of 90% or lower and VD in the nasal choriocapillaris CC (Table 4). Lastly, a monotonic negative relationship was identified between foveal VD in the DCP and IL-6 levels in patients with SpO_2 of 90% or lower (Table 4).

Safety

In the study group, hypertension was reported in 20 patients, ischemic heart disease in 3, fatty liver disease in 5, hyperlipidemia in 3, previous stroke in 2, previous myocardial infarction in 2, cancer in 5, degenerative spine disease in 2, hyperthyroidism in 2, and hysterectomy in 2. Asthma, epilepsy, delusional disorder, rheumatoid arthritis, chronic kidney disease (CKD), nephrolithiasis, chronic hepatitis C, cholelithiasis, thyroidectomy, and alcohol dependence were reported in 1 patient each. No patients reported any symptoms during the ophthalmological examination.

Discussion

The SARS-CoV-2 infection primarily affects the respiratory tract, but it also causes inflammation in the vascular endothelium with strong cytokine involvement, resulting in enhanced clotting in the microcirculation.[19]

Numerous papers have described fundus lesions caused by COVID-19.[20–23] These abnormalities, including hemorrhages and cotton wool spots, are typical for central retinal vein occlusion with subsequent macular edema. This indicates that the disease is vascular in nature. Noninvasive tests such as OCTA have been repeatedly used to diagnose the above conditions.

To demonstrate the effect of systemic hypoxia on retinal and choroidal microvasculature assessed using OCTA, we followed the same approach as our previous study: We divided COVID-19 patients into subgroups according to SpO_2 on admission.[24]

In the present study, we assessed correlations between SpO_2, D-dimer and IL-6 levels and ocular parameters such as VD and FAZ area as obtained using OCTA in patients with SARS-CoV-2 infection, at 2 months after hospital discharge. The aim of the study was to evaluate whether hypoxia, inflammation and hypercoagulability affect the retinal and choroidal microvasculature.

Correlations between SpO_2 and VD

Our study showed a significant monotonic negative relationship between SpO_2 of 90% or lower and VD in the foveal SCP and temporal CC, and the mean VD in the DCP.

Hommer et al.[25] evaluated the effects of hypoxia in 24 healthy subjects (mean age 26 years) on vasculature parameters in the central retina obtained with

Table 4. Correlations between vessel density in the superficial capillary plexus (SCP), deep capillary plexus (DCP), and choriocapillaris (CC) and foveal avascular zone (FAZ) in the SCP and DCP and oxygen saturation (SpO_2), interleukin 6 (IL-6) levels and D-dimer levels

OCTA	SpO_2	D-dimer	IL-6
Foveal VD in the SCP	r = –0.22; p = 0.048	r = –0.06; p = 1	r = –0.06; p = 1
Foveal VD in the DCP	r = –0.13; p = 0.513	r = –0.06; p = 1	r = –0.10; p = 0.786 for $SpO_2 \leq 90\%$ r = –0.57, p = 0.027
Foveal VD in the CC	r = –0.11; p = 0.645	r = 0.04; p = 1 for $SpO_2 \leq 90\%$ r = 0.33; p = 0.06	r = 0.17; p = 0.216
Superior VD in the SCP	r = 0.08; p = 1	r = –0.13; p = 0.486	r = 0.01; p = 1
Superior VD in the DCP	r = –0.01; p = 1	r = –0.11; p = 0.729	r = –0.06; p = 1
Superior VD in the CC	r = –0.01; p = 1	r = 0.08; p = 1	r = –0.01; p = 1
Nasal VD in the SCP	r = 0.11; p = 0.624	r = –0.11; p = 0.72	r = 0.08; p = 1
Nasal VD in the DCP	r = 0.01; p = 1	r = –0.17; p = 0.183 for $SpO_2 \leq 90\%$ r = –0.32; p = 0.288	r = 0.10; p = 0.906
Nasal VD in the CC	r = –0.05; p = 1	r = –0.07; p = 1 for $SpO_2 \leq 90\%$ r = 0.49; p = 0.003	r = 0.03; p = 1
Inferior VD in the SCP	r = 0.13; p = 0.525	r = 0.05; p = 1	r = –0.05; p = 1
Inferior VD in the DCP	r = –0.08; p = 1	r = –0.05; p = 1	r = 0.15; p = 0.321
Inferior VD in the CC	r = –0.08; p = 1	r = 0.16; p = 0.237 for $SpO_2 \leq 90\%$ r = –0.36; p = 0.054	r = –0.06; p = 1
Temporal VD in the SCP	r = 0.07; p = 1	r = –0.04; p = 1	r = –0.14; p = 0.396
Temporal VD in the DCP	r = –0.16; p = 0.255 for $SpO_2 \leq 90\%$ r = –0.47; p = 0.135	r = 0.07; p = 1	r = 0.06; p = 1
Temporal VD in the CC	r = –0.12; p = 0.543 for $SpO_2 \leq 90\%$ r = –0.59; p = 0.021	r = 0.04; p = 1	r = 0.12; p = 0.618
Mean VD in the SCP	r = 0.02; p = 1	r = –0.09; p = 1	r = –0.01; p = 1
Mean VD in the DCP	r = –0.15; p = 0.339 for $SpO_2 \leq 90\%$ r = –0.55; p = 0.048	r = –0.12; p = 0.546	r = 0.01;p = 1
Mean VD in the CC	r = –0.14; p = 0.345	r = 0.17; p = 0.174	r = 0.08; p = 1
FAZ in the SCP	r = –0.20; p = 0.075	r = –0.01; p = 1	r = –0.06; p = 1
FAZ in the DCP	r = 0.13; p = 0.414	r = 0.09; p = 0.921	r = –0.08; p = 1

p for Sp – Spearman rank correlation; values were statistically significant at $p < 0.05$; optical coherence tomography angiography (OCTA); VD – vascular density.

OCTA while breathing a mixture of nitrogen (88%) and oxygen (12%). Perfusion density in the superficial vascular density was significantly elevated and was stable in the DCP. Retinal vessel diameter was also significantly increased. Moreover, significantly elevated perfusion density in the DCP was observed in patients breathing 100% oxygen. At the same time, a significant reduction in vessel diameter was noted in the major retinal arteries and veins.[25]

For proper function, the retina requires an adequate oxygen supply. Retinal vessels can regulate blood circulation in response to hypoxia and hyperoxia. Hyperoxia reduces the caliber of retinal vessels. This regulatory mechanism helps avoid the oversupply of oxygen to the retina, which can induce retinal nerve fiber toxicity. The risk of hyperoxygenation and oxidative stress is reduced by the vasospasm of the vessels in the DCP.[26,27]

Correlations between SpO_2 and FAZ area

The large number of cones and the absence of retinal vessels in the FAZ area allow the best vision. Therefore, this area is particularly sensitive to hypoxia. The CC layer under the retina is responsible for supplying oxygen and nutrients to the cones that are located here. The enlargement of the FAZ area may indicate abnormalities associated with vascular disorders such as diabetic retinopathy or retinal veinocclusion.[28,29] However, in our study, there was no significant monotonic negative relationship between SpO_2 of 90% or lower and the FAZ area in the SCP and the DCP.

Correlations between D-dimer levels and VD

Our study showed a significant monotonic positive relationship between VD in the CC and D-dimer levels, but

only in patients with SpO_2 of 90% or lower in the nasal area of the CC.

Guemez-Villahoz et al.[30] reported reduced mean blood flow (19.6 ±9.3 vs 14.7 ±8.0, p = 0.018) and reduced VD in the SCP (8.8 ±4.0 vs 6.6 ±3.6, p = 0.013) 30 days after the diagnosis of COVID-19 in patients with elevated D-dimer levels of 500 ng/mL or higher. They hypothesized that the subclinical changes in the retinal microcirculation in these patients were secondary to increased blood clotting and intense inflammatory response due to COVID-19.[30]

In a subsequent paper, Guemez-Villahoz et al.[31] described OCTA outcomes at 12 weeks after the acute stage of COVID-19 in patients divided according to the presence of thrombotic events. They also compared OCTA findings between patients with COVID-19 and healthy controls. They found significantly reduced VD in patients with COVID-19 compared with controls in several areas of the macula, including the central macula, outer ring and full ring. Perfusion density was significantly reduced in the full ring and full area. Optical coherence tomography angiography parameters did not differ between the groups with and without thrombotic events. According to the authors, retinal vascular involvement in SARS-CoV-2 infection does not depend on the presence of thrombotic events at other levels. In addition, there were no retinal vascular incidents in COVID-19 patients with thrombotic events.[31]

Correlations between Il-6 levels and VD

In our study, there was a significant monotonic negative relationship between VD in some areas of the DCP and IL-6 levels in patients with SpO_2 of 90% or lower.

To our knowledge, no previous studies have described correlations between OCTA parameters and interleukin levels in patients with SARS-CoV-2 infection. Nevertheless, IL-6 is known to be one of the main mediators in retinal vasculitis.[32] Mesquida et al.[33] studied the effects of IL-6 on the retinal endothelium and retinal pigment epithelium (RPE) in vitro using human RPE cells and endothelial cells of the retinal vessels to show that this is the most important additional mediator of macular edema in numerous retinal diseases. Interleukin 6 impairs barrier function in RPE cells and retinal VECs.[33]

Park et al.[34] used human monocytes to investigate the relationship between elevated D-dimer levels, immune complexes and inflammatory processes in patients with COVID-19. They showed that D-dimers stimulate prostaglandin E2 (PGE2) and inflammatory cytokines such as IL-6, IL-8 and IL-1β in healthy monocytes. The monocytes were incubated with D-dimers and immune complexes of SARS-CoV-2 particles, resulting in a significant increase in PGE2 levels and cytokine production.[34] This confirmed the findings of other investigators who have emphasized the importance of the thrombolytic-inflammatory concept as a key phenomenon in the pathomechanism of COVID-19.[35,36]

Limitations

Several limitations of this study should be acknowledged. First, for organizational and logistical reasons, patients were assessed 2 months after hospitalization for COVID-19 bilateral pneumonia and not during the hospitalization itself. Second, the study did not include critically ill patients who required intensive care admission due to progressive hypoxia, which is associated with releasing proinflammatory and prothrombotic factors that could affect retinal and choroidal microvascular parameters. Finally, the study group was relatively small. Further research on a larger group of patients should be conducted to provide more information on the effect of COVID-19 on the microvasculature of the retina and choroid.

Conclusions

Patients with COVID-19 bilateral pneumonia with reduced SpO_2 and elevated D-dimer and IL-6 levels present with decreased VD in some areas assessed by OCTA. These patients require particular attention during anatomical and functional evaluation of posterior ocular structures. Optical coherence tomography angiography is a useful and widely available tool for the diagnosis of vascular disorders in the central retina and choroid in patients with previous SARS-CoV-2 infection.

Supplementary data

The Supplementary materials are available at https://doi.org/10.5281/zenodo.12745888. The package includes the following files:

Supplementary Table 1. Means, SD, median and IQR for OCTA parameters in 3 groups saturation (group 1: ≤90; group 2: 90–95; group 3: >95).

Supplementary Table 2. Characteristic of OCTA parameters according to D-dimers level group (>500 ng – group 0).

Supplementary Table 3. Characteristic of OCTA parameters according to IL-6 level (group 0: ≤1.8, group 1: >1.8).

Supplementary Fig. 1. The diagram for the correlation between VD F SCP (foveal vascular density in superficial capillary plexus) and saturation.

Supplementary Fig. 2. The diagram for the correlation between VD F DCP (foveal vascular density of deep capillary plexus) and saturation

Supplementary Fig. 3. The diagram for the correlation between VD F CC (foveal vascular density of choriocapillaris) and saturation.

Supplementary Fig. 4. The diagram for the correlation between VD S SCP (temporal vascular density of superficial capillary plexus) and saturation.

Supplementary Fig. 5. The diagram for the correlation between VD S DCP (superior vascular density of deep capillary plexus) and saturation.

Supplementary Fig. 6. The diagram for the correlation between VD S CC (superior vascular density of choriocapillaris) and saturation.

Supplementary Fig. 7. The diagram for the correlation between VD N SCP (nasal vascular density of superficial capillary plexus) and saturation.

Supplementary Fig. 8. The diagram for the correlation between VD N DCP (nasal vascular density of deep capillary plexus) and saturation.

Supplementary Fig. 9. The diagram for the correlation between VD N CC (nasal vascular density of choriocapillaris) and saturation.

Supplementary Fig. 10. The diagram for the correlation between VD I SCP and (inferior vascular density of superficial capillary plexus) and saturation.

Supplementary Fig. 11. The diagram for the correlation between VD I DCP (inferior vascular density of deep capillary plexus) and saturation.

Supplementary Fig. 12. The diagram for the correlation between VD I CC (inferior vascular density of choriocapillaris) and saturation.

Supplementary Fig. 13. The diagram for the correlation between VD T SCP (temporal vascular density of superficial capillary plexus) and saturation.

Supplementary Fig. 14. The diagram for the correlation between VD T DCP (temporal vascular density of deep capillary plexus) and saturation.

Supplementary Fig. 15. The diagram for the correlation between VD T CC (temporal vascular density of choriocapillaris) and saturation.

Supplementary Fig. 16. The diagram for the correlation between mean VD SCP (vascular density of superficial capillary plexus) and saturation.

Supplementary Fig. 17. The diagram for the correlation between mean VD DCP (vascular density of deep capillary plexus) and saturation.

Supplementary Fig. 18. The diagram for the correlation between mean VD CC (vascular density of choriocapillaris) and saturation.

Supplementary Fig. 19. The diagram for the correlation between FAZs (μm^2) (superficial foveal avascular zone) and saturation.

Supplementary Fig. 20. The diagram for the correlation between FAZd (μm^2) (deep foveal avascular zone) and saturation.

Supplementary Fig. 21. The diagram for the correlation between VD F SCP (foveal vascular density of superficial capillary plexus) and IL-6 level.

Supplementary Fig. 22. The diagram for the correlation between VD F DCP (foveal vascular density of deep capillary plexus) and IL-6 level.

Supplementary Fig. 23. The diagram for the correlation between VD F CC (foveal vascular density of choriocapillaris) and IL-6 level.

Supplementary Fig. 24. The diagram for the correlation between VD S SCP (superior vascular density of superficial capillary plexus) and IL-6 level.

Supplementary Fig. 25. The diagram for the correlation between VD S DCP (superior vascular density of deep capillary plexus) and IL-6 level.

Supplementary Fig. 26. The diagram for the correlation between VD N SCP (nasal vascular density of superficial capillary plexus) and IL-6 level.

Supplementary Fig. 27. The diagram for the correlation between VD S CC (superior vascular density of choriocapillaris) and IL-6 level.

Supplementary Fig. 28. The diagram for the correlation between VD N DCP (nasal vascular density of deep capillary plexus) and IL-6 level.

Supplementary Fig. 29. The diagram for the correlation between VD N CC (nasal vascular density of choriocapillaris) and IL-6 level.

Supplementary Fig. 30. The diagram for the correlation between VD I SCP (inferior vascular density of superficial capillary plexus) and IL-6 level.

Supplementary Fig. 31. The diagram for the correlation between VD I DCP (inferior vascular density of deep capillary plexus) and IL-6.

Supplementary Fig. 32. The diagram for the correlation between VD I CC (inferior vascular density of choriocapillaris) and IL-6 level.

Supplementary Fig. 33. The diagram for the correlation between VD T SCP (temporal vessel density of superficial capillary plexus) and IL-6 level.

Supplementary Fig. 34. The diagram for the correlation between VD T DCP (temporal vessel density of deep capillary plexus) and IL-6 level.

Supplementary Fig. 35. The diagram for the correlation between VD T CC (temporal vessel density of choriocapillaris) and IL-6 level.

Supplementary Fig. 36. The diagram for the correlation between mean VD SCP (vessel density of superficial capillary plexus) and IL-6 level.

Supplementary Fig. 37. The diagram for the correlation between mean VD DCP (vessel density of deep capillary plexus) and IL-6 level.

Supplementary Fig. 38. The diagram for the correlation between mean VD CC (vessel density of choriocapillaris) and IL-6 level.

Supplementary Fig. 39. The diagram for the correlation between FAZs (superficial foveal avascular zone) and IL-6 level.

Supplementary Fig. 40. The diagram for the correlation between FAZd (deep foveal avascular zone) and IL-6 level.

Supplementary Fig. 41. The diagram for the correlation between VD F SCP (foveal vessel density of superficial capillary plexus) and D-dimers level.

Supplementary Fig. 42. The diagram for the correlation between VD F DCP (foveal vessel density of deep capillary plexus) and D-dimers level.

Supplementary Fig. 43. The diagram for the correlation between VD F CC (foveal vessel density of choriocapillaris) and D-dimers level.

Supplementary Fig. 44. The diagram for the correlation between VD S SCP (vessel density of superficial capillary plexus) and D-dimers level.

Supplementary Fig. 45. The diagram for the correlation between VD S DCP (superior vessel density of deep capillary plexus) and D-dimers level.

Supplementary Fig. 46. The diagram for the correlation between VD S CC (superior vessel density of choriocapillaris) and D-dimers level.

Supplementary Fig. 47. The diagram for the correlation between VD N SCP (nasal vessel density of superficial capillary plexus) and D-dimers level.

Supplementary Fig. 48. The diagram for the correlation between VD N DCP (nasal vessel density of deep capillary plexus) and D-dimers level.

Supplementary Fig. 49. The diagram for the correlation between VD N CC (nasal vessel density of choriocapillaris) and D-dimers level.

Supplementary Fig. 50. The diagram for the correlation between VD I SCP (inferior vessel density of superficial capillary plexus) and D-dimers level.

Supplementary Fig. 51. The diagram for the correlation between VD I DCP (inferior vessel density of deep capillary plexus) and D-dimers level.

Supplementary Fig. 52. The diagram for the correlation between VD I CC (inferior vessel density of choriocapillaris) and D-dimers level.

Supplementary Fig. 53. The diagram for the correlation between VD T SCP (temporal vessel density of superficial capillary plexus) and D-dimers level.

Supplementary Fig. 54. The diagram for the correlation between VD T DCP (temporal vessel density of deep capillary plexus) and D-dimers level.

Supplementary Fig. 55. The diagram for the correlation between VD T CC (temporal vessel density of choriocapillaris) and D-dimers level.

Supplementary Fig. 56. The diagram for the correlation between mean VD SCP (vessel density of superficial capillary plexus) and D-dimers level.

Supplementary Fig. 57. The diagram for the correlation between mean VD DCP (vessel density of deep capillary plexus) and D-dimers level.

Supplementary Fig. 58. The diagram for the correlation between mean VD CC (vessel density of choriocapillaris) and D-dimers level.

Supplementary Fig. 59. The diagram for the correlation between FAZs (superficial foveal avascular zone) and D-dimers level.

Supplementary Fig. 60. The diagram for the correlation between FAZd (deep foveal avascular zone) and D-dimers level.

Supplementary Fig. 61. Histogram of IL-6 level.

Supplementary Fig. 62. Histogram of D-dimers level.

Supplementary Fig. 63. Histogram of saturation.

Supplementary Fig. 64. Histogram of VD F SCP (foveal vessel density of superficial capillary plexus).

Supplementary Fig. 65. Histogram of VD F DCP (foveal vessel density of deep capillary plexus).

Supplementary Fig. 66. Histogram of VD F CC (foveal vessel density of choriocapillaris).

Supplementary Fig. 67. Histogram of VD S SCP (superior vessel density of superficial capillary plexus).

Supplementary Fig. 68. Histogram of VD S DCP (superior vessel density of deep capillary plexus).

Supplementary Fig. 69. Histogram of VD S CC (superior vessel density of choriocapillaris).

Supplementary Fig. 70. Histogram of VD N SCP (nasal vessel density of superficial capillary plexus).

Supplementary Fig. 71. Histogram of VD N DCP (nasal vessel density of deep capillary plexus).

Supplementary Fig. 72. Histogram of VD N CC (nasal vessel density of choriocapillaris).

Supplementary Fig. 73. Histogram of VD I SCP (inferior vessel density of superficial capillary plexus).

Supplementary Fig. 74. Histogram of VD I DCP (inferior vessel density of deep capillary plexus).

Supplementary Fig. 75. Histogram of VD I CC (inferior vessel density of choriovcapillaris).

Supplementary Fig. 76. Histogram of VD T SCP (temporal vessel density of superficial capillary plexus).

Supplementary Fig. 77. Histogram of VD T DCP (temporal vessel density of deep capillary plexus).

Supplementary Fig. 78. Histogram of VD T CC (temporal vessel density of choriocapillaris).

Supplementary Fig. 79. Histogram of Mean VD SCP (vessel density of superficial capillary plexus).

Supplementary Fig. 80. Histogram of Mean VD DCP (vessel density of deep capillary plexus).

Supplementary Fig. 81. Histogram of Mean VD CC (vessel density of choriocapillaris).

Supplementary Fig. 82. Histogram of FAZs (superficial foveal avascular zone).

Supplementary Fig. 83. Histogram of FAZd (deep foveal avascular zone).

Supplementary Fig. 84. Normality distribution of VD F SCP in the category of saturation (foveal vessel density of superficial capillary plexus).

Supplementary Fig. 85. Normality distribution of VD F DCP in the category of saturation (foveal vessel density of deep capillary plexus).

Supplementary Fig. 86. Normality distribution of VD F CC in the category of saturation (foveal vessel density of choriocapillaris).

Supplementary Fig. 87. Normality distribution of VD S SCP in the category of saturation (superior vessel density of superficial capillary plexus).

Supplementary Fig. 88. Normality distribution of VD S DCP in the category of saturation (superior vessel density of deep capillary plexus).

Supplementary Fig. 89. Normality distribution of VD S CC in the category of saturation (superior vessel density of choriocapillaris).

Supplementary Fig. 90. Normality distribution of VD N SCP in the category of saturation (nasal vessel density of superficial capillary plexus).

Supplementary Fig. 91. Normality distribution of VD N DCP in the category of saturation (nasal vessel density of deep capillary plexus).

Supplementary Fig. 92. Normality distribution of VD N CC in the category of saturation (nasal vessel density of choriocapillaris).

Supplementary Fig. 93. Normality distribution of VD N DCP in the category of saturation (nasal vessel density of deep capillary plexus).

Supplementary Fig. 94. Normality distribution of VD I SCP in the category of saturation (inferior vessel density of superficial capillary plexus).

Supplementary Fig. 95. Normality distribution of VD I DCP in the category of saturation (inferior vessel density of deep capillary plexus).

Supplementary Fig. 96. Normality distribution of VD I CC in the category of saturation (inferior vessel density of choriocapillaris).

Supplementary Fig. 97. Normality distribution of VD T SCP in the category of saturation (temporal vessel density of superficial capillary plexus).

Supplementary Fig. 98. Normality distribution of VD T DCP in the category of saturation (temporal vessel density of deep capillary plexus).

Supplementary Fig. 99. Normality distribution of VD T CC in the category of saturation (temporal vessel density of choriocapillaris).

Supplementary Fig. 100. Normality distribution of mean VD SCP in the category of saturation (vessel density of superficial capillary plexus).

Supplementary Fig. 101. Normality distribution of mean VD DCP in the category of saturation (vessel density of deep capillary plexus).

Supplementary Fig. 102. Normality distribution of FAZs (superficial foveal avascular zone) in the category of saturation.

Supplementary Fig. 103. Normality distribution of FAZd (deep foveal avascular zone) in the category of saturation.

Supplementary Fig. 104. Normality distribution of VD F SCP (foveal vessel density of superficial capillary plexus) in the category of D-dimers level.

Supplementary Fig. 105. Normality distribution of VD F DCP (foveal vessel density of deep capillary plexus) in the category of D-dimers level.

Supplementary Fig. 106. Normality distribution of VD F CC (foveal vessel density of choriocapillaris) in the category of D-dimers level.

Supplementary Fig. 107. Normality distribution of VD F DCP (foveal vessel density of deep capillary plexus) in the category of D-dimers level.

Supplementary Fig. 108. Normality distribution of VD S DCP (superior vessel density of deep capillary plexus) in the category of D-dimers level.

Supplementary Fig. 109. Normality distribution of VD S CC (superior vessel density of choriocapillaris) in the category of D-dimers level.

Supplementary Fig. 110. Normality distribution of VD N SCP (nasal vessel density of superficial capillary plexus) in the category of D-dimers level.

Supplementary Fig. 111. Normality distribution of VD N DCP (nasal vessel density of deep capillary plexus) in the category of D-dimers level.

Supplementary Fig. 112. Normality distribution of VD N CC (nasal vessel density of choriocapillaris) in the category of D-dimers level.

Supplementary Fig. 113. Normality distribution of VD I SCP (inferior vessel density of superficial capillary plexus) in the category of D-dimers level.

Supplementary Fig. 114. Normality distribution of VD I DCP (inferior vessel density of deep capillary plexus) in the category of D-dimers level.

Supplementary Fig. 115. Normality distribution of VD I CC (inferior vessel density of choriocapillaris) in the category of D-dimers level.

Supplementary Fig. 116. Normality distribution of VD T SCP (temporal vessel density of superficial capillary plexus) in the category of D-dimers level.

Supplementary Fig. 117. Normality distribution of VD T DCP (temporal vessel density of deep capillary plexus) in the category of D-dimers level.

Supplementary Fig. 118. Normality distribution of VD T CC (temporal vessel density of choriocapillaris) in the category of D-dimers level.

Supplementary Fig. 119. Normality distribution of mean VD SCP (vessel density of superficial capillary plexus) in the category of D-dimers level.

Supplementary Fig. 120. Normality distribution of mean VD DCP (vessel density of deep capillary plexus) in the category of D-dimers level.

Supplementary Fig. 121. Normality distribution of mean VD CC (vessel density of choriocapillaris) in the category of D-dimers level.

Supplementary Fig. 122 Normality distribution of FAZs (superficial foveal avascular zone) in the category of D-dimers level.

Supplementary Fig. 123. Normality distribution of FAZd (deep foveal avascular zone) in the category of D-dimers level.

Supplementary Fig. 124. Histogram for VD F SCP (foveal vessel density of superficial capillary plexus) in 2 groups of IL-6 level.

Supplementary Fig. 125. Histogram for VD F DCP (foveal vessel density of deep capillary plexus) in 2 groups of IL-6 level.

Supplementary Fig. 126. Histogram for VD F CC (vessel density of choriocapillaris) in 2 groups of IL-6 level.

Supplementary Fig. 127. Histogram for VD S SCP (foveal vessel density of superficial capillary plexus) in 2 groups of IL-6 level.

Supplementary Fig. 128. Histogram for VD S DCP (superior vessel density of deep capillary plexus) in 2 groups of IL-6 level.

Supplementary Fig. 129. Histogram for VD S CC (superior vessel density of choriocapillaris) in 2 groups of IL-6 level.

Supplementary Fig. 130. Histogram for VD N SCP (nasal vessel density of superficial capillary plexus) in 2 groups of IL-6 level.

Supplementary Fig. 131. Histogram for VD N DCP (nasal vessel density of deep capillary plexus) in 2 groups of IL-6 level.

Supplementary Fig. 132. Histogram for VD N CC (nasal vessel density of choriocapillaris) in 2 groups of Interleukin 6 (IL 6).

Supplementary Fig. 133. Histogram for VD I SCP (inferior vessel density of superficial capillary plexus) in 2 groups of IL-6 level.

Supplementary Fig. 134. Histogram for VD I DCP (inferior vessel density of deep capillary plexus) in 2 groups of IL-6 level.

Supplementary Fig. 135 Histogram for VD I CC (inferior Vessel density of choriocapillaris) in 2 groups of IL-6 level.

Supplementary Fig. 136. Histogram for VD T SCP (temporal vessel density of superficial capillary plexus) in 2 groups of IL-6 level.

Supplementary Fig. 137. Histogram for VD T DCP (temporal vessel density of deep capillary plexus) in 2 groups of IL-6 level.

Supplementary Fig. 138. Histogram for VD T CC (temporal vessel density of choriocapillaris) in 2 groups of IL-6 level.

Supplementary Fig. 139. Histogram for mean VD SCP (mean vessel density of superficial capillary plexus) in 2 groups of IL-6 level.

Supplementary Fig. 140. Histogram for mean VD DCP (mean vessel density of deep capillary plexus) in 2 groups of IL-6 level.

Supplementary Fig. 141. Histogram for mean VD CC (mean vessel density of choriocapillaris) in 2 groups of IL-6 level.

Supplementary Fig. 142. Histogram for FAZs (superficial foveal avascular zone) in 2 groups of IL-6 level.

Supplementary Fig. 143. Histogram for FAZd (deep foveal avascular zone) in 2 groups of IL-6 level.

Data availability

The datasets generated and/or analyzed during the current study are available from the corresponding author on reasonable request.

Consent for publication

Not applicable.

ORCID iDs

Magdalena Kal https://orcid.org/0000-0003-1090-1542
Michał Brzdęk https://orcid.org/0000-0002-1180-9230
Elżbieta Cieśla https://orcid.org/0000-0001-6090-9900
Piotr Rzymski https://orcid.org/0000-0002-4713-0801
Izabella Karska-Basta https://orcid.org/0000-0001-7927-6277
Antonio Pinna https://orcid.org/0000-0003-3052-2662
Jerzy Mackiewicz https://orcid.org/0000-0003-0984-8908
Mateusz Winiarczyk https://orcid.org/0000-0001-9704-3848
Dominik Odrobina https://orcid.org/0009-0005-1613-5529
Dorota Zarębska-Michaluk https://orcid.org/0000-0003-0938-1084

References

1. Perico L, Benigni A, Casiraghi F, Ng LFP, Renia L, Remuzzi G. Immunity, endothelial injury and complement-induced coagulopathy in COVID-19. *Nat Rev Nephrol*. 2021;17(1):46–64. doi:10.1038/s41581-020-00357-4
2. Patel A, Charani E, Ariyanayagam D, et al. New-onset anosmia and ageusia in adult patients diagnosed with SARS-CoV-2 infection. *Clin Microbiol Infect*. 2020;26(9):1236–1241. doi:10.1016/j.cmi.2020.05.026
3. Romero-Sánchez CM, Díaz-Maroto I, Fernández-Díaz E, et al. Neurologic manifestations in hospitalized patients with COVID-19: The ALBACOVID registry. *Neurology*. 2020;95(8):e1060–e1070. doi:10.1212/WNL.0000000000009937
4. Dockery DM, Rowe SG, Murphy MA, Krzystolik MG. The ocular manifestations and transmission of COVID-19: Recommendations for prevention. *J Emerg Med*. 2020;59(1):137–140. doi:10.1016/j.jemermed.2020.04.060
5. Suresh Kumar VC, Mukherjee S, Harne PS, et al. Novelty in the gut: A systematic review and meta-analysis of the gastrointestinal manifestations of COVID-19. *BMJ Open Gastroenterol*. 2020;7(1):e000417. doi:10.1136/bmjgast-2020-000417
6. Jin X, Lian JS, Hu JH, et al. Epidemiological, clinical and virological characteristics of 74 cases of coronavirus-infected disease 2019 (COVID-19) with gastrointestinal symptoms. *Gut*. 2020;69(6):1002–1009. doi:10.1136/gutjnl-2020-320926
7. Shi S, Qin M, Shen B, et al. Association of cardiac injury with mortality in hospitalized patients with COVID-19 in Wuhan, China. *JAMA Cardiol*. 2020;5(7):802. doi:10.1001/jamacardio.2020.0950
8. Wang X, Tang G, Liu Y, et al. The role of IL-6 in coronavirus, especially in COVID-19. *Front Pharmacol*. 2022;13:1033674. doi:10.3389/fphar.2022.1033674
9. Hoffmann M, Kleine-Weber H, Schroeder S, et al. SARS-CoV-2 cell entry depends on ACE2 and TMPRSS2 and is blocked by a clinically proven protease inhibitor. *Cell*. 2020;181(2):271–280.e8. doi:10.1016/j.cell.2020.02.052
10. Banderas García S, Aragón D, Azarfane B, et al. Persistent reduction of retinal microvascular vessel density in patients with moderate and severe COVID-19 disease. *BMJ Open Ophthalmol*. 2022;7(1):e000867. doi:10.1136/bmjophth-2021-000867
11. Zhou F, Yu T, Du R, et al. Clinical course and risk factors for mortality of adult inpatients with COVID-19 in Wuhan, China: A retrospective cohort study. *Lancet*. 2020;395(10229):1054–1062. doi:10.1016/S0140-6736(20)30566-3
12. Kal M, Winiarczyk M, Głuszek S, Mackiewicz J. Choroidal thickness in lamellar macular holes. *Graefes Arch Clin Exp Ophthalmol*. 2021;259(3):653–659. doi:10.1007/s00417-020-04922-2
13. Marinho PM, Marcos AAA, Romano AC, Nascimento H, Belfort R. Retinal findings in patients with COVID-19. *Lancet*. 2020;395(10237):1610. doi:10.1016/S0140-6736(20)31014-X
14. Schnichels S, Rohrbach JM, Bayyoud T, Thaler S, Ziemssen F, Hurst J. Can SARS-CoV-2 infect the eye? An overview of the receptor status in ocular tissue. *Ophthalmologe*. 2021;118(Suppl 1):81–84. doi:10.1007/s00347-020-01281-5
15. Kal M, Winiarczyk M, Cieśla E, et al. Retinal microvascular changes in COVID-19 bilateral pneumonia based on optical coherence tomography angiography. *J Clin Med*. 2022;11(13):3621. doi:10.3390/jcm11133621
16. Kal M, Winiarczyk M, Zarębska-Michaluk D, et al. Long-term effect of SARS-CoV-2 infection on the retinal and choroidal microvasculature. *J Clin Med*. 2023;12(7):2528. doi:10.3390/jcm12072528

17. Flisiak R, Parczewski M, Horban A, et al. Management of SARS-CoV-2 infection: Recommendations of the Polish Association of Epidemiologists and Infectiologists. Annex No. 2 as of October 13, 2020. *Pol Arch Intern Med*. 2020;130(10):915–918. doi:10.20452/pamw.15658
18. Flisiak R, Horban A, Jaroszewicz J, et al. Diagnosis and therapy of SARS-CoV-2 infection: Recommendations of the Polish Association of Epidemiologists and Infectiologists as of November 12, 2021. Annex No. 1 to the Recommendations of April 26, 2021. *Pol Arch Intern Med*. 2021; 131(11):16140. doi:10.20452/pamw.16140
19. López Reboiro ML, Suárez Fuentetaja R, Gutiérrez López R, et al. Role of lupus anticoagulant and von Willebrand factor in chronic reactive endotheliitis in COVID-19. *J Infect*. 2021;82(6):e27–e28. doi:10.1016/j.jinf.2021.03.006
20. Padhy SK, Dcruz RP, Kelgaonkar A. Paracentral acute middle maculopathy following SARS-CoV-2 infection: The D-dimer hypothesis. *BMJ Case Rep*. 2021;14(3):e242043. doi:10.1136/bcr-2021-242043
21. Virgo J, Mohamed M. Paracentral acute middle maculopathy and acute macular neuroretinopathy following SARS-CoV-2 infection. *Eye*. 2020;34(12):2352–2353. doi:10.1038/s41433-020-1069-8
22. Naughton A, Ong AY, Gkika T, Downes S. Bilateral paracentral acute middle maculopathy in a SARS-CoV-2-positive patient. *Postgrad Med J*. 2022;98(e2):e105–e106. doi:10.1136/postgradmedj-2021-140500
23. Ozsaygılı C, Bayram N, Ozdemir H. Cilioretinal artery occlusion with paracentral acute middle maculopathy associated with COVID-19. *Indian J Ophthalmol*. 2021;69(7):1956. doi:10.4103/ijo.IJO_563_21
24. Kal M, Winiarczyk M, Mackiewicz J, et al. The effect of reduced oxygen saturation on retinal microvascularization in COVID-19 patients with bilateral pneumonia based on optical coherence tomography study. *J Pers Med*. 2022;12(11):1824. doi:10.3390/jpm12111824
25. Hommer N, Kallab M, Sim YC, et al. Effect of hyperoxia and hypoxia on retinal vascular parameters assessed with optical coherence tomography angiography. *Acta Ophthalmol*. 2022;100(6):e1272–e1279. doi:10.1111/aos.15077
26. Werkmeister RM, Schmidl D, Aschinger G, et al. Retinal oxygen extraction in humans. *Sci Rep*. 2015;5(1):15763. doi:10.1038/srep15763
27. Hagag AM, Pechauer AD, Liu L, et al. OCT angiography changes in the 3 parafoveal retinal plexuses in response to hyperoxia. *Ophthalmol Retina*. 2018;2(4):329–336. doi:10.1016/j.oret.2017.07.022
28. Conrath J, Giorgi R, Ridings B, Raccah D. Metabolic factors and the foveal avascular zone of the retina in diabetes mellitus. *Diabetes Metab*. 2005;31(5):465–470. doi:10.1016/S1262-3636(07)70217-3
29. Samara WA, Say EAT, Khoo CTL, et al. Correlation of foveal avascular zone size with foveal morphology in normal eyes using optical coherence tomography angiography. *Retina*. 2015;35(11):2188–2195. doi:10.1097/IAE.0000000000000847
30. Guemes-Villahoz N, Burgos-Blasco B, Vidal-Villegas B, et al. Reduced retinal vessel density in COVID-19 patients and elevated D-dimer levels during the acute phase of the infection. *Med Clin (Barc)*. 2021; 156(11):541–546. doi:10.1016/j.medcli.2020.12.006
31. Guemes-Villahoz N, Burgos-Blasco B, Vidal-Villegas B, et al. Reduced macular vessel density in COVID-19 patients with and without associated thrombotic events using optical coherence tomography angiography. *Graefes Arch Clin Exp Ophthalmol*. 2021;259(8):2243–2249. doi:10.1007/s00417-021-05186-0
32. Glass J, Robinson R, Lee TJ, Sharma A, Sharma S. Interleukin-6 transsignaling mediated regulation of paracellular permeability in human retinal endothelial cells. *Int J Transl Med*. 2021;1(2):137–153. doi:10.3390/ijtm1020010
33. Mesquida M, Drawnel F, Lait PJ, et al. Modelling macular edema: The effect of IL-6 and IL-6R blockade on human blood–retinal barrier integrity in vitro. *Trans Vis Sci Tech*. 2019;8(5):32. doi:10.1167/tvst.8.5.32
34. Park YJ, Acosta D, Vassell R, et al. D-dimer and CoV-2 spike-immune complexes contribute to the production of PGE2 and proinflammatory cytokines in monocytes. *PLoS Pathog*. 2022;18(4):e1010468. doi:10.1371/journal.ppat.1010468
35. Levi M, Van Der Poll T, Büller HR. Bidirectional relation between inflammation and coagulation. *Circulation*. 2004;109(22):2698–2704. doi:10.1161/01.CIR.0000131660.51520.9A
36. Gris JC, Perez-Martin A, Quéré I, Sotto A. COVID-19 associated coagulopathy: The crowning glory of thrombo-inflammation concept. *Anaesth Crit Care Pain Med*. 2020;39(3):381–382. doi:10.1016/j.accpm.2020.04.013

Assessment of the physical fitness status of patients with hematological malignancies qualified for hematopoietic stem cell transplantation

Michał Chmielewski[1,A–E], Agnieszka Szeremet[2,A,B,D–E], Paula Jabłonowska-Babij[2,A,B,D–E], Maciej Majcherek[2,E,F], Anna Czyż[2,E,F], Natalia Bursiewicz[1,A,E,F], Tomasz Wróbel[2,E,F], Iwona Malicka[3,A,C–F]

[1] Active Recovery, Wrocław, Poland
[2] Department and Clinic of Hematology, Blood Neoplasms and Bone Marrow Transplantation, Wroclaw Medical University, Poland
[3] Department of Physiotherapy, Wroclaw University of Health and Sport Sciences, Poland

A – research concept and design; B – collection and/or assembly of data; C – data analysis and interpretation; D – writing the article; E – critical revision of the article; F – final approval of the article

Advances in Clinical and Experimental Medicine, ISSN 1899–5276 (print), ISSN 2451–2680 (online) *Adv Clin Exp Med*. 2025;34(8):1343–1352

Address for correspondence
Agnieszka Szeremet
E-mail: agnieszka.szeremet@umw.edu.pl

Funding sources
This research was funded by the DKMS Foundation.

Conflict of interest
None declared

Acknowledgements
The authors thank Dr. Justyna Hanuszkiewicz for helping to coordinate the study in the control group.

Received on October 30, 2023
Reviewed on March 27, 2024
Accepted on September 27, 2024

Published online on March 18, 2025

Cite as
Chmielewski M, Szeremet A, Jabłonowska-Babij P, et al. Assessment of the physical fitness status of patients with hematological malignancies qualified for hematopoietic stem cell transplantation. *Adv Clin Exp Med*. 2025;34(8):1343–1352. doi:10.17219/acem/193825

DOI
10.17219/acem/193825

Copyright
Copyright by Author(s)
This is an article distributed under the terms of the Creative Commons Attribution 3.0 Unported (CC BY 3.0) (https://creativecommons.org/licenses/by/3.0/)

Abstract

Background. Hematopoietic stem cell transplantation (HSCT) is a procedure commonly used in the treatment of various hematological disorders with the aim of curing the patient or prolonging life. The vast majority of patients must have antineoplastic therapy before HSCT, which can result in weight loss, sarcopenia or cachexia. Additionally, there is a high risk of malnutrition and physical deterioration during HSCT. By assessing physical fitness prior to HSCT, a physical therapist can individualize an exercise program, which in turn may speed up recovery after HSCT.

Objectives. The aim of the study was to assess the physical fitness of patients with hematological malignancies qualified for HSCT as an indication for prehabilitation.

Materials and methods. The study included 65 patients with hematological malignancies who were qualified for HSCT between September 1, 2022, and September 1, 2023. The reference group consisted of 219 healthy adults. The clinical study protocol involved participants performing 3 tests: the 6-minute walk test (6MWT), the timed-up and go test (TUG) and the 30-second chair-stand test (30CST).

Results. Patients with hematological malignancies were characterized by significantly lower endurance capacity (median (Me) = 420.50 (IQR 110.25) vs Me = 580.00 (IQR 133.00); $p < 0.001$) and significantly lower body strength (Me = 11.00 (IQR 6.00) vs Me = 15.00 (IQR 5.00); $p < 0.001$). There was also a statistically significant difference in the diagnosis and in the number of lines of systemic therapy. Additionally, a statistically significant difference was observed between the outcomes of the physical fitness level, particularly for TUG and 30CST, and the time from diagnosis to transplantation.

Conclusions. The presented results suggest a negative consequence of hematological disease and its treatment on the functional status of patients qualified for HSCT and indicate the need for individualized rehabilitation management depending on the type of diagnosis, the number of lines of systemic therapy, and the time between diagnosis and transplantation.

Key words: hematology, prehabilitation, physical fitness status, hematopoietic stem cell transplant

Background

Hematopoietic stem cell transplant (HSCT) refers to any procedure where hematopoietic stem cells (HSCs) of any donor type and any source are given to a recipient with the intention of repopulating and replacing the hematopoietic system in total or in part. Donor type is categorized as autologous, human leukocyte antigen (HLA)-identical sibling donor or matched unrelated donor (MUD). A haploidentical donor is defined as a family member where only 1 HLA haplotype is genetically identical to the patient. Depending on the source of HSCs, the following transplantations are distinguished: autologous-HSCT (auto-HSCT), allogeneic-HSCT-sibling (allo-HSCT-Sib), allogeneic-HSCT-matched unrelated donor (allo-HSCT-MUD), and haploidentical-HSCT (haplo-HSCT).[1]

Hematopoietic stem cell transplant is a procedure commonly used in the treatment of various hematological disorders and is associated with significantly improved survival rates. Auto-HSCT is characterized by the reinfusion of the patient's HSCs after treatment with high doses of chemotherapy, which exhibit high anticancer potential while causing irreversible damage to the hematopoietic function of the bone marrow.

According to the recommendations of the European Society for Blood and Marrow Transplantation (EBMT), high-dose chemotherapy followed by auto-HSCT is generally considered a standard treatment option in patients with plasma cell myeloma (PCM) in the consolidation of response to first-line therapy, in patients with relapsed or primary refractory lymphoma in the consolidation of response to salvage therapy, and in addition, in some subtypes of clinically aggressive lymphomas, such as mantle cell lymphoma (MCL) or T-cell lymphomas (TCLs), in the consolidation of response to first-line therapy.[1]

Allo-HSCT is a treatment with curative potential that is used in transplant-eligible patients with high-risk malignancies or other serious hematologic disorders. The most common indications for allo-HSCT include intermediate and high-risk acute myeloid leukemia (AML) and myelodysplastic syndromes (MDS), acute lymphoblastic leukemia (ALL) with adverse prognostic factors, and myeloproliferative neoplasms (MPN) with a high risk of disease progression according to international prognostic scoring systems.[1] However, one of the drawbacks of allo-HSCT is the possibility of the development of serious post-transplant complications, including acute and chronic graft-versus-host disease (GvHD), which result in significant non-relapse mortality after transplant. Therefore, the patient's eligibility for transplantation is determined individually, taking into account the patient's performance status, the presence of comorbidities, the adequate function of vital organs, and the patient's age.[2]

The latest Poltransplant data indicates that in 2022, 1,135 auto-HSCTs and 798 allo-HSCTs, including 108 haplo-HSCTs, were performed in Poland.[3]

Systemic symptoms of hematological malignancies such as fever, weight loss, weakness, or excessive night sweating are associated with various mediators derived from cancer cells and cells within the tumor microenvironment, including inflammatory and immune cells.[4] In addition to the discomforts associated with the disease, the treatment entails adverse effects. The mucosa of the gastrointestinal tract is damaged after the administration of chemotherapy. As a result, taste disorders, anorexia, nausea, vomiting, diarrhea, and weight loss are observed. Chronic leukopenia has been identified as a contributing factor in the development of bacterial, fungal and viral infections.[5] During treatment, there are side effects, including deterioration in muscle strength and lung function, deterioration in cardiovascular function, and a decrease in lean body mass, which translates into poorer function.[6]

Yoshida et al. have reported that approx. 2/3 of the study patients low muscle mass before HSCT. In any case, we should be aware that there were many patients who had already shown low skeletal muscle mass prior to highly invasive HSCT.[7] Morishita et al. have presented that up to 50% of cancer patients suffer from cachexia associated with sarcopenia before allo-HSCT.[8]

Considering the severe course of the disease and intensive treatment fraught with a wide spectrum of complications, while at the same time increasing the survival and life expectancy of patients, it becomes very important to support cancer patients. There is a high risk of malnutrition and physical deterioration during HSCT. Mohammed et al. identified pre-transplant physical assessment of the patient as an important part of the process for monitoring patient improvement and deterioration. They also pointed out that patients with hematological malignancies did not always receive the required, appropriate rehabilitation.[9]

While there is no one-size-fits-all protocol that can help physiotherapists achieve optimal benefit for patients with hematological malignancies, studies show that patients who engage in thoughtful exercise programs are able to better manage activities of daily living and require less involvement from their caregivers. By assessing physical fitness prior to treatment, a physical therapist can design an exercise program, which can speed up recovery.[9]

In addition, baseline functional assessment results can be helpful not only for guiding hospital rehabilitation but also for planning exercises to return to daily functioning and work after HSCT.[10]

Due to the subsequent stages of transplantation (chemotherapy, additional immunosuppressive treatment in allo-HSCT and early and late treatment-related complications, including GvHD), fitness assessment can be helpful in identifying high-risk patients to implement prehabilitation.[11]

Objectives

The aim of the study was to assess the physical fitness of patients with hematologic malignancies qualified for HSCT in the context of an indication for prehabilitation.

Materials and methods

A total of 65 consecutive patients qualified for HSCT in the Department of Hematology, Blood Neoplasm and Bone Marrow Transplantation of Wroclaw Medical University (Poland) between September 1, 2022, and September 1, 2023, who met the inclusion criteria (see below) and signed the patient's informed consent form (ICF), were included in the study. The reference group consisted of healthy adults matched by sex and age to the study group who met the inclusion criteria for healthy volunteers and signed the participant's ICF (see below). Patients' baseline characteristics and treatment details are presented in Table 1.

Table 1. Patients' characteristics and treatment details

Characteristic		Value
Age, Me (Q1–Q3) [years]		57.00 (45.00–64.00)
Sex [n]	male	26
	female	39
Indication for hematopoietic stem cell transplantation [n]	AL	20
	MDS	3
	MPN	8
	HL+NHL	13
	PCM	18
	SAA	3
Previous treatment [n]	chemotherapy	58
	antineoplastic treatment excluding chemotherapy	7
Number of previous therapy lines [n]	0–1	34
	2	19
	3 or more	12

Me – median; Q1–Q3 – 1st quartile–3rd quartile; AL – acute leukemia (acute myeloid leukemia and acute lymphoblastic leukemia); MDS – myelodysplastic neoplasm; MPN – myeloproliferative neoplasm; HL + NHL – Hodgkin lymphoma and non-Hodgkin lymphoma; PCM – plasma cell myeloma; SAA – severe aplastic anemia.

Inclusion and exclusion criteria

The study was assessed based on specific inclusion and exclusion criteria. Inclusion criteria for the study group were as follows: 1) age between 18 and 75 years at the time of signing the ICF; 2) understanding and voluntarily signing an ICF prior to any study-related assessments or procedures being conducted; 3) confirmed diagnosis of hematological malignancy; 4) being qualified for HSCT. Inclusion criteria for a reference group were as follows: 1) age between 18 and 75 years at the time of signing the ICF; 2) understanding and voluntarily signing an ICF prior to any study-related assessments or procedures being conducted; 3) never treated for cancer; 4) no concomitant diseases; 5) no concomitant therapies or medications. Exclusion criteria for both groups were as follows: 1) significant medical condition or psychiatric condition that would prevent participation in the study; 2) condition, including the presence of laboratory abnormalities, that would place the study participant at unacceptable risk if they were to participate in the study; 3) condition that would interfere with the ability to interpret the data from the study.

Research methods

The detailed clinical study protocol involved participants performing 3 tests: the 6-minute walk test (6MWT), the timed-up and go test (TUG) and the 30-second chair-stand test (30CST).

The 6MWT was used to determine endurance capacity; the TUG was used to assess agility and dynamic balance, which is important in activities that require quick maneuvers or quick movement decisions; and the 30CST was used to assess lower body strength.

All 3 tests in the study group were performed on patients after signing the ICF within 3 days prior to the transplant conditioning regimen.

The 6MWT was performed in an enclosed space on a flat surface 30 m long. Participants had to walk as far as possible in 6 min. They were instructed to move at a walking pace, were not allowed to run or trot, and had to turn around at the beginning and end of the corridor, maintaining continuity and a walking pace. Before and immediately after the test, all participants had their blood pressure and heart rate checked. If necessary, the participants were allowed to slow down or rest during the test by sitting down in a chair, but the time was not stopped. We measured the distance (in meters) the study participant walked during the test.

The TUG required the study participants to perform a sequence of tasks relevant to independent mobility. These included getting up from a chair, walking a distance of 3 m, turning around, taking the same route back to the chair, and sitting down. The result of the TUG was the total time (in seconds) required to complete this sequence. No loss of balance was allowed during the test. The study participant started the TUG in a seated position on the chair. At the command "start", they would get up from the chair and walked the designated distance of 3 m at the fastest possible pace, then turned around and returned to the chair and sat down in the starting position. Then they heard the command "stop".

The 30CST began in an active sitting position on a chair (without support). The study participant had their arms

crossed. On the "start" command they hey alternated between standing up to a full standing position and sitting down in the chair within 30 s. The tester counted the number of full repetitions performed. Prior to the test, the study participants performed 2–3 test repetitions.

The above tests show high predictive value. They can be used to plan, conduct and control the effects of exercises and physical activity.[12,13]

Statistical analyses

Continuous variables were described as mean with standard deviation (SD) or median with minimum and maximum values. Categorical variables were provided as numbers with frequencies. Normal distribution was tested using the Shapiro–Wilk test. The Mann–Whitney U test was used to compare outcomes between 2 groups (study vs reference). The Kruskal–Wallis test was performed with post hoc Dunn–Bonferroni depending on the type of diagnosis and the number of lines of systemic therapy. The monotonicity of the relationship between time from diagnosis to transplantation and fitness test scores was checked using 2W scatter plots. The variable of time from diagnosis to transplantation was divided into ranges and the new variable was used as the grouping variable, and Kruskal–Wallis test was performed with post hoc Dunn–Bonferroni. The characteristics of the groups and the results were presented using descriptive statistics. All the statistical analyses were performed using STATISTICA v. 13.3 (StatSoft Poland, Cracow, Poland) and PQ Stat v. 1.8.2 (PQStat Software, Poznan/Plewiska, Poland). The results were considered statistically significant at $p < 0.05$.

Ethics

This study complies with the Declaration of Helsinki and was approved by the Wroclaw Medical University Ethics Committee (approval No. KB-843/2021, date of approval: October 28, 2021).

Results

The study group consisted of 65 patients (26 men and 39 women) with a mean age of 53.14 ±14.01) (range: 22–74 years). The reference group consisted of 219 individuals (112 men and 107 women) with a mean age of 53.29 ±15.13 (range: 20–75 years). Prior to the physical fitness assessment, the height and weight of each participant (study and reference group) were measured and used to calculate body mass index (BMI). The results were compared between groups and no differences were found (all $p > 0.05$). The results are summarized in Table 2.

Results of physical fitness level

In the 2 tests used, the 6MWT and the 30CST, the mean score in the reference group was statistically higher than the mean score in the study group. Patients with hematological malignancies had significantly lower endurance capacity and significantly lower body strength Assessment of dynamic agility and balance, important for activities requiring rapid maneuvering, showed no statistically significant differences. (Table 3).

For all tests used, a statistically significant difference was shown depending on the diagnosis (Fig. 1, Table 4).

A statistically significant difference was observed between the outcomes of the 6MWT and 30CST tests and the number of lines of systemic treatment (Fig. 2, Table 5).

In addition, the monotonicity of the relationship between the time from diagnosis to transplantation and the results of the physical fitness status was checked (Fig. 3). As an alternative approach, due to the non-monotonic relationship, the variable time from diagnosis to transplantation was divided into ranges and the new variable was used as a grouping variable. A statistically significant difference was observed between the outcomes of the physical fitness level, particularly for TUG and 30CST and the time from diagnosis to transplantation (Fig. 4, Table 6).

Table 2. Demographic and clinical results (Mann–Whitney U test; study group vs reference group)

Group	n	Age [years] Me (Q1–Q3)	Body height [m] Me (Q1–Q3)	Body weight [kg] Me (Q1–Q3)	BMI Me (Q1–Q3)
All (both groups)	284	56.00 (48.00–63.00)	1.70 (1.64–1.76)	76.00 (66.00–86.50)	26.03 (23.36–29.38)
Study group	65	57.00 (45.00–64.00)	1.70 (1.63–1.76)	79.00 (63.00–90.00)	27.14 (23.35–29.76)
Reference group	219	56.00 (49.00–63.00)	1.70 (1.64–1.76)	76.00 (66.00–85.00)	26.02 (23.37–29.29)
Z (study group vs reference group)		0.14	0.77	–0.35	–0.97
p-value		0.881	0.438	0.723	0.328

Me – median; Q1–Q3 – 1st quartile–3rd quartile 3; BMI – body mass index; *$p < 0.05$.

Table 3. Results of physical fitness level (study vs reference group). Mann–Whitney U test

Group	n	6MWT [m] Me (Q1–Q3)	TUG [s] Me (Q1–Q3)	30CST [n] Me (Q1–Q3)
All (both groups)	284	535.00 (437.00–620.00)	6.04 (5.00–7.17)	15.00 (12.00–18.00)
Study group	65	420.50 (379.00–490.00)	6.39 (5.50–7.24)	11.00 (9.00–15.00)
Reference group	219	580.00 (499.00–632.00)	6.00 (5.00–7.07)	15.00 (13.00–18.00)
Z (study group vs reference group)		7.68	–1.53	6.68
p-value		<0.001*	0.124	<0.001*

Me – median; Q1–Q3 – 1st quartile–3rd quartile; 6MWT – the 6-minute walk test; TUG – the timed-up and go test; 30CST – the 30-second chair-stand test; n – number of repetitions; *p < 0.05.

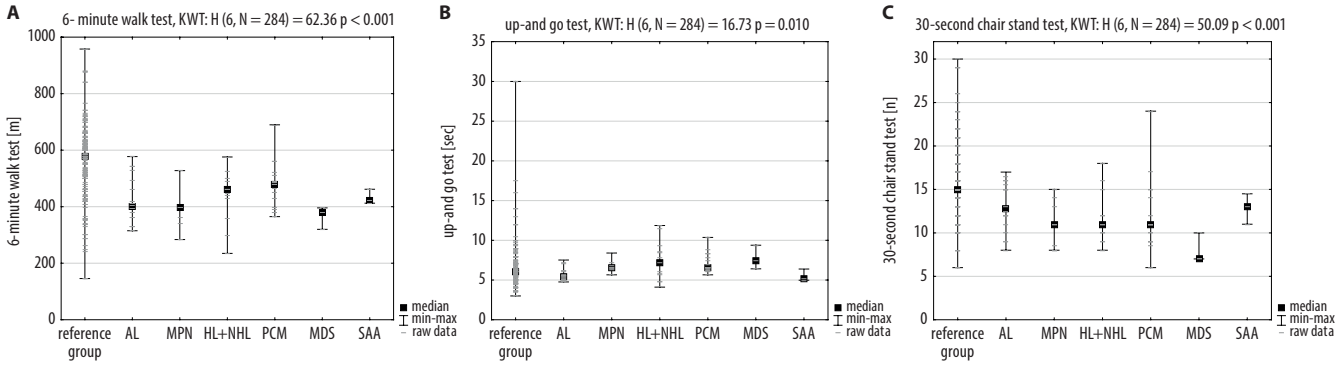


Fig. 1. Results of 6MWT (A), TUG (B) and 30CST (C) in groups divided by diagnosis (study group) vs reference group

KWT – Kruskal–Wallis test; 6MWT – the 6-minute walk test; TUG – the timed-up and go test; 30CST – the 30-second chair-stand test.

Table 4. The statistical significance of the effect of diagnosis type on physical fitness level in the overall Kruskal–Wallis test with post hoc Dunn–Bonferroni test

Physical fitness level test	Overall test	Post hoc test					
		group	Ref	AL	HL + NHL	MDS	MPN	PCM
6MWT	<0.001	AL	<0.001*	–	–	–	–	–
		HL+NHL	0.007*	1.000	–	–	–	–
		MDS	0.130	1.000	1.000	–	–	–
		MPN	0.005*	1.000	1.000	1.000	–	–
		PCM	0.024*	1.000	1.000	1.000	1.000	–
		SAA	0.936	1.000	1.000	1.000	1.000	1.000
TUG	0.010*	AL	1.000	–	–	–	–	–
		HL+NHL	1.000	0.507	–	–	–	–
		MDS	1.000	0.602	1.000	–	–	–
		MPN	1.000	0.700	1.000	1.000	–	–
		PCM	0.267	0.043*	1.000	1.000	1.000	–
		SAA	1.000	1.000	1.000	1.000	1.000	1.000
30CST	<0.001*	AL	0.176	–	–	–	–	–
		HL+NHL	0.005*	1.000	–	–	–	–
		MDS	0.043*	1.000	1.000	–	–	–
		MPN	0.025*	1.000	1.000	1.000	–	–
		PCM	0.001*	1.000	1.000	1.000	1.000	–
		SAA	1.000	1.000	1.000	1.000	1.000	1.000

6MWT – the 6-minute walk test; TUG – the timed-up and go test; 30CST – the 30-second chair-stand test; AL – acute leukemia (acute myeloid leukemia and acute lymphoblastic leukemia); HL + NHL – Hodgkin lymphoma and non-Hodgkin lymphoma; MDS – myelodysplastic neoplasm; MPN – myeloproliferative neoplasm; PCM – plasma cell myeloma; SAA – severe aplastic anemia; Ref – reference group; * p < 0.05.

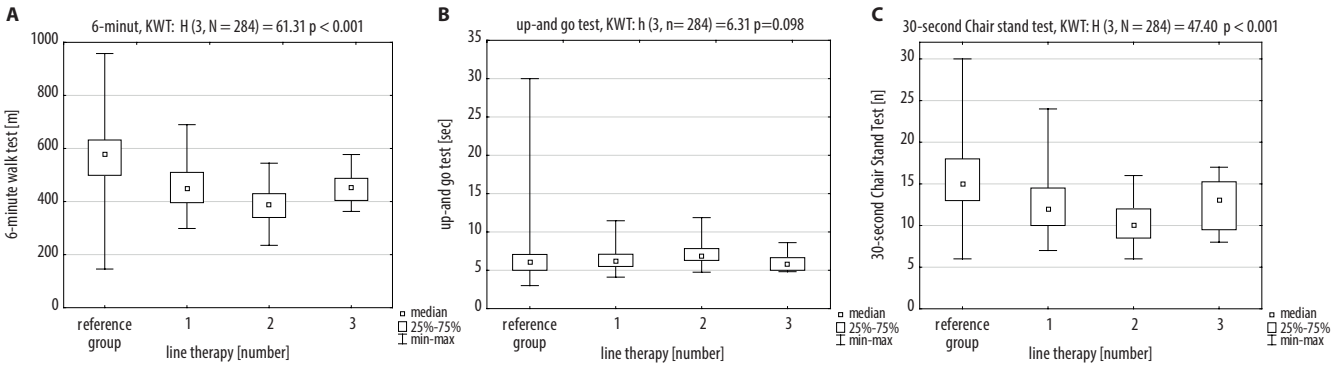


Fig. 2. Results of 6MWT (A), TUG (B) and 30CST (C) in groups divided by the number of lines of treatment (study group) vs reference group

KWT – Kruskal–Wallis test; 6MWT – the 6-minute walk test; TUG – the timed-up and go test; 30CST – the 30-second chair-stand test.

Table 5. The statistical significance of the effect of the number of treatment lines on physical fitness level in the overall Kruskal–Wallis test with post hoc Dunn–Bonferroni test

Physical fitness level test	Overall test	Post hoc test			
		treatment lines	1	2	3
6MWT	<0.001*	2	0.884	–	1.000
		3	1.000	1.000	–
		Ref	<0.001*	<0.001*	0.006*
TUG	0.097	2	0.791	–	–
		3	1.000	0.366	–
		Ref	1.000	0.103	1.000
30CST	<0.001*	2	1.000	–	–
		3	1.000	1.000	–
		Ref	<0.001*	<0.001*	0.062

6MWT – the 6-minute walk test; TUG – the timed-up and go test; 30CST – the 30-second chair-stand test; 1–3 – the number of lines of treatment; Ref – reference group; * p < 0.05.

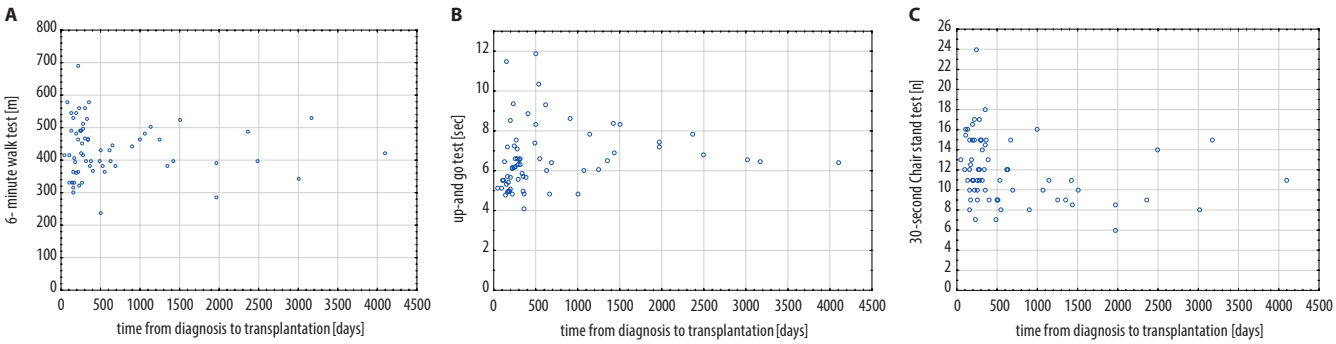


Fig. 3. Relationship between time from diagnosis to transplantation and 6MWT (A), TUG (B) and 30CST (C)

KWT – Kruskal–Wallis test; 6MWT – the 6-minute walk test; TUG – the timed-up and go test; 30CST – the 30-second chair-stand test.

Discussion

Prehabilitation is the multidirectional preparation of the patient for treatment. All activities undertaken are intended to prevent the emergence of functional limitations that may occur in the patient during and after treatment. Its implementation has been shown to reduce the incidence of complications, shorten the duration of hospitalization, and have a positive impact on patients' quality of life. However, there are few prehabilitation pathways for cancer patients, especially those who are not qualified for surgical treatment.[14] The lack of prehabilitation standards also applies to patients with hematological malignancies. At the same time, many publications contain information on the negative effects of cancer and anticancer treatment on the body, primarily on the deterioration of functional parameters, a decrease in muscle strength or cardiovascular fitness or general fatigue.[6,15–17]

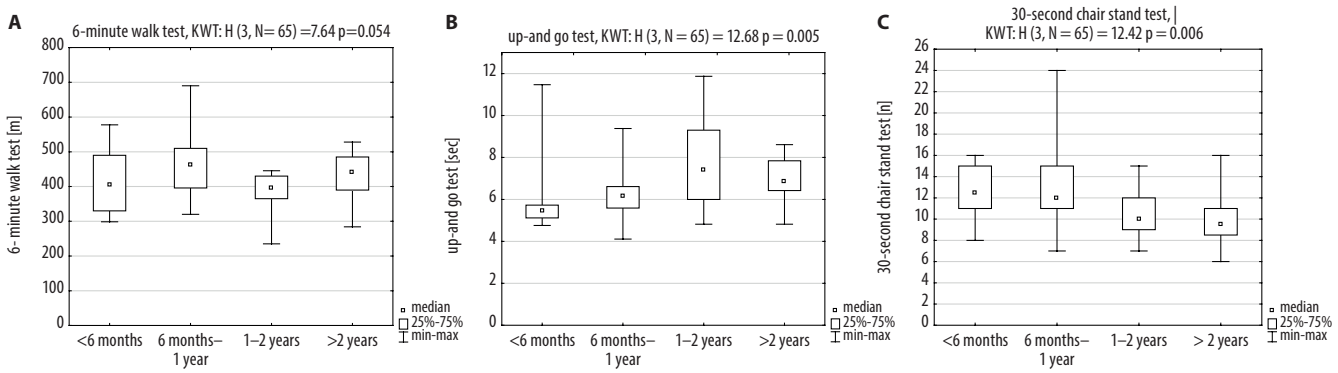


Fig. 4. Results of the 6WMT, TUG and 30CST in groups divided by the time of diagnosis to transplantation in the study group

KWT – Kruskal–Wallis test ; 6MWT – the 6-minute walk test; TUG – the timed-up and go test; 30CST – the 30-second chair-stand test.

Table 6. The statistical significance of the effect of the time from diagnosis to transplantation on physical fitness level in the overall Kruskal–Wallis test with post hoc Dunn–Bonferroni test

Physical fitness level test	Overall test	Post hoc test			
		time to transplantation	<6 months	6 months–1 year	1–2 years
6MWT	0.054	6 months–1 year	0.421	–	–
		1–2 years	1.000	0.066	–
		> 2 years	1.000	1.000	0.656
TUG	0.005*	6 months–1 year	1.000	–	–
		1–2 years	0.024*	0.223	–
		> 2 years	0.024*	0.252	1.000
30CST	0.006*	6 months–1 year	1.000	–	–
		1–2 years	0.414	0.121	–
		> 2 years	0.121	0.016*	1.000

6MWT – the 6-minute walk test; TUG – the timed-up and go test; 30CST – the 30-second chair-stand test; * $p < 0.05$.

The TUG test used in the study is one of the tools for assessing frailty, the identification of which is important because it is considered a very strong predictor of morbidity, disability and death, especially in elderly patients.[18] Frailty is characterized by decreased physiological function due to reduced muscle strength and endurance, and the prognosis of frailty syndrome can inform the evaluation of several invasive therapies, including chemotherapy.[19] In addition, according to a study by Nascimento et. al., the occurrence of complications due to frailty can be prevented by implementing physical exercise that is properly adapted to the patient's general condition.[18] Hedge and Murthy showed that traditionally used risk stratification parameters such as chronological age, comorbidity and performance status may not fully capture physical function and physiological fitness, highlighting the need for improvement in pre-transplant assessment (PTA).[20]

Patients in the study group compared to healthy subjects in the reference group performed statistically significantly worse in the 30CST, which assessed lower limb muscle strength. Similar results in post-transplant patients were presented by Morishita et al.,[8] who found that the decrease in knee joint extensor strength was independent of gender. In contrast, a study by Ishikawa et al. showed that lower limb extensor strength at the knee joint before transplantation was a significant factor in reduced extensor strength after transplantation.[21] At the same time, the function of the quadriceps muscle of the thigh is considered to be representative and predictive of other skeletal muscles. As a result, it can be used to assess the patient's functional status.[22] The fact that the strength of the quadriceps femoris muscle is reduced in patients with hematological malignancies prior to treatment was also highlighted by Granger, who suggested possible reasons for this condition. This situation may be explained by cancer-related factors such as decreased protein synthesis with increased protein catabolism and increased tumor necrosis factor, leading to muscle atrophy and contractile dysfunction.[23] A 2015 study by Fiuza-Luces et al highlighted that the loss of muscle mass and strength caused by therapy is a challenge to recovery, even up to 5 years after HSCT.[24] Consequently, prehabilitation targeting muscular strength and mass growth seems to be significant. Early exercise may help reduce the decline in strength and muscle mass, according to research by Liang et al.[25]

Significant differences were also observed in the 6MWT results. Patients with hematological malignancies were able to walk a shorter distance compared to healthy participants, indicating poorer endurance performance. Similar findings were reported by Potiaumpai et al., who compared the results of the 6MWT in transplant-eligible patients with those of healthy subjects of a similar age. The results for healthy adults ranged from 417.76 m to 582.22 m for women and from 416.69 m to 713.94 m for men. In comparison, patients achieved significantly lower results, with women ranging from 91.44 m to 487.68 m and men ranging from 243.84 m to 655.32 m.[26] Some patients with hematological malignancies have also been shown to have poorer endurance and lower limb strength at the time of diagnosis, several months before treatment.[23] A meta-analysis by Liang et al. showed that exercise had a beneficial effect on patients' lower muscle strength, fatigue and quality of life. It is recommended that patients begin exercise as soon as possible after diagnosis.[25]

The type of diagnosis also appears to be important. Compared with the reference group, significantly lower scores were observed for MPN, lymphoma and PCM on the 6MWT and 30CST, for AL on the 6MWT and for MDS on the 30CST. Hematological malignancies are a group of diseases with different symptom profiles. With this in mind, prehabilitation planning would need to take into account the expected condition of the patient, depending on the diagnosis and the time between diagnosis and transplantation.

In the 1990s, some patients were still advised to adopt a sedentary lifestyle.[27] For patients with hematological disorders, rest and avoidance of strenuous exercise are often recommended because of the frequent occurrence of cytopenias.[28] But is this the right approach? This study clearly showed that in 2 of 3 tests, patients with hematological neoplasms performed statistically significantly worse than the healthy group. This means that patients are already impaired before starting treatment. As many authors have pointed out, the introduction of heavy treatment, with its many complications, has led to a further deterioration in patients' fitness.[8,29,30] Therefore, it is reasonable that patients should be advised at the time of diagnosis to exercise according to their capabilities to maintain physical fitness and minimize treatment side effects. Wiskemann et al. showed that exercise is beneficial at all stages of treatment.[31] It seems most appropriate to use exercise and proper nutrition in patients after diagnosis to prepare them for treatment.[32] Hegde and Murthy also emphasized early involvement in physical training to avoid a lack of physical mobility.[20]

Only in certain cases should exercise be avoided. Absolute contraindications to physical training include: acute phase of infection; fever; severe pain and increased pain due to movement; platelet count below 10,000/μL; acute bleeding; and hemoglobin level below 8 g/dL with oxygen deficiency. At the same time, the contraindications listed do not preclude participation in activities of daily living.[27]

Limitations

The study has the advantage of presenting fitness results between a group of healthy volunteers and patients with hematological malignancies. Thanks to this comparison, we know the importance of both prehabilitation and rehabilitation in patients with hematological disorders prior to treatment. One of the biggest limitations of this study is the size of the study group. Ultimately, we plan to expand the number of people studied so that we can determine functional status with greater accuracy, depending at least on the diagnosis and/or age and sex.

Conclusions

The significant discrepancy in functional performance between the groups confirms the impact of hematological disorders on the deterioration of patients' fitness and indicates the need for individualized rehabilitation management depending on the type of diagnosis and time between diagnosis and transplantation. At the same time, poorer pre-treatment physical fitness may affect functional status post-treatment. This highlights the need for rehabilitation support for patients with hematological malignancies both before and during treatment.

Future research directions

It seems important to create a protocol for the prehabilitation and rehabilitation management of patients with hematological malignancies in order to help specialists select appropriate parameters for patients to exercise. To achieve this objective, it is necessary to study the impact of different types of training on the functional status of patients in the pre- and peri-transplant periods. With reference to information from the available literature, it is also necessary to study the impact of prehabilitation on the treatment process, taking into account changes in patients' functional status.

Supplementary data

The Supplementary materials are available at https://doi.org/10.5281/zenodo.13989751. The package includes the following files:

Supplementary Fig. 1. Assessment of age (years) normality using the Shapiro–Wilk test.

Supplementary Fig. 2. Assessment of body height (m) normality using the Shapiro–Wilk test.

Supplementary Fig. 3. Assessment of body weight (kg) normality using the Shapiro–Wilk test.

Supplementary Fig. 4. Assessment of BMI normality using the Shapiro–Wilk test.

Supplementary Fig. 5. Assessment of 6MWT results normality using the Shapiro–Wilk test.

Supplementary Fig. 6. Assessment of TUG results normality using the Shapiro–Wilk test.

Supplementary Fig. 7. Assessment of 30CST results normality using the Shapiro–Wilk test.

Data availability

The datasets generated and/or analyzed during the current study are available from the corresponding author on reasonable request.

Consent for publication

Not applicable.

Use of AI and AI-assisted technologies

Not applicable.

ORCID iDs

Michał Chmielewski https://orcid.org/0009-0003-6724-1888
Agnieszka Szeremet https://orcid.org/0000-0002-1897-3180
Paula Jabłonowska-Babij https://orcid.org/0000-0001-6984-2116
Maciej Majcherek https://orcid.org/0000-0001-6064-296X
Anna Czyż https://orcid.org/0000-0001-6641-0182
Natalia Bursiewicz https://orcid.org/0000-0002-2037-0100
Tomasz Wróbel https://orcid.org/0000-0002-6612-3535
Iwona Malicka https://orcid.org/0000-0002-7668-001X

References

1. Snowden JA, Sánchez-Ortega I, Corbacioglu S, et al. Indications for haematopoietic cell transplantation for haematological diseases, solid tumours and immune disorders: Current practice in Europe, 2022. *Bone Marrow Transplant*. 2022;57(8):1217–1239. doi:10.1038/s41409-022-01691-w
2. Carreras E, Dufour C, Mohty M, Kröger N, eds. *The EBMT Handbook: Hematopoietic Stem Cell Transplantation and Cellular Therapies*. Cham, Switzerland: Springer International Publishing; 2019. doi:10.1007/978-3-030-02278-5
3. Poltransplant. Rejestr przeszczepień komórek krwiotwórczych szpiku, krwi obwodowej oraz krwi pępowinowej. *Biuletyn Informacyjny Poltransplant*. 2023;1(32):59–71. https://files.poltransplant.org.pl/Biuletyn_2023_www.pdf. Accessed October 27, 2023.
4. Sharma R, Cunningham D, Smith P, Robertson G, Dent O, Clarke SJ. Inflammatory (B) symptoms are independent predictors of myelosuppression from chemotherapy in non-Hodgkin lymphoma (NHL) patients: Analysis of data from a British National Lymphoma Investigation phase III trial comparing CHOP to PMitCEBO. *BMC Cancer*. 2009;9(1):153. doi:10.1186/1471-2407-9-153
5. Hansen BA, Wendelbo Ø, Bruserud Ø, Hemsing AL, Mosevoll KA, Reikvam H. Febrile neutropenia in acute leukemia: Epidemiology, etiology, pathophysiology and treatment. *Mediterr J Hematol Infect Dis*. 2019;12(1):e2020009. doi:10.4084/mjhid.2020.009
6. Hayes S, Davies PSW, Parker T, Bashford J, Newman B. Quality of life changes following peripheral blood stem cell transplantation and participation in a mixed-type, moderate-intensity, exercise program. *Bone Marrow Transplant*. 2004;33(5):553–558. doi:10.1038/sj.bmt.1704378
7. Yoshida S, Sakurai G, Yahata T. Prevalence of low skeletal muscle quantity and quality and their associated factors in patients before allogeneic hematopoietic stem cell transplantation. *Intern Emerg Med*. 2022;17(2):451–456. doi:10.1007/s11739-021-02828-3
8. Morishita S, Kaida K, Tanaka T, et al. Prevalence of sarcopenia and relevance of body composition, physiological function, fatigue, and health-related quality of life in patients before allogeneic hematopoietic stem cell transplantation. *Support Care Cancer*. 2012;20(12):3161–3168. doi:10.1007/s00520-012-1460-5
9. Mohammed J, Smith SR, Burns L, et al. Role of physical therapy before and after hematopoietic stem cell transplantation: White paper report. *Biol Blood Marrow Transplant*. 2019;25(6):e191–e198. doi:10.1016/j.bbmt.2019.01.018
10. De Boer AGEM, Taskila T, Ojajärvi A, Van Dijk FJH, Verbeek JHAM. Cancer survivors and unemployment: A meta-analysis and meta-regression. *JAMA*. 2009;301(7):753. doi:10.1001/jama.2009.187
11. Mohammed J, AlGhamdi A, Hashmi SK. Full-body physical therapy evaluation for pre- and post-hematopoietic cell transplant patients and the need for a modified rehabilitation musculoskeletal specific grading system for chronic graft-versus-host disease. *Bone Marrow Transplant*. 2018;53(5):625–627. doi:10.1038/s41409-017-0075-3
12. Accogli MA, Denti M, Costi S, Fugazzaro S. Therapeutic education and physical activity are feasible and safe in hematologic cancer patients referred to chemotherapy: Results of a randomized controlled trial. *Support Care Cancer*. 2023;31(1):61. doi:10.1007/s00520-022-07530-4
13. Silva TC, Silva PO, Morais DS, et al. Functional capacity, lung function, and muscle strength in patients undergoing hematopoietic stem cell transplantation: A prospective cohort study. *Hematol Oncol Stem Cell Ther*. 2021;14(2):126–133. doi:10.1016/j.hemonc.2020.08.004
14. Wade-Mcbane K, King A, Urch C, Jeyasingh-Jacob J, Milne A, Boutillier CL. Prehabilitation in the lung cancer pathway: A scoping review. *BMC Cancer*. 2023;23(1):747. doi:10.1186/s12885-023-11254-x
15. Weis J, Wirtz MA, Tomaszewski KA, et al. Sensitivity to change of the EORTC quality of life module measuring cancer-related fatigue (EORTC QlQ-Fa12): Results from the international psychometric validation. *Psychooncology*. 2019;28(8):1753–1761. doi:10.1002/pon.5151
16. Goswami P, Oliva EN, Ionova T, et al. Quality-of-life issues and symptoms reported by patients living with haematological malignancy: A qualitative study. *Ther Adv Hematol*. 2020;11:204062072095500. doi:10.1177/2040620720955002
17. Yang YP, Pan SJ, Qiu SL, Tung TH. Effects of physical exercise on the quality-of-life of patients with haematological malignancies and thrombocytopenia: A systematic review and meta-analysis. *World J Clin Cases*. 2022;10(10):3143–3155. doi:10.12998/wjcc.v10.i10.3143
18. Nascimento CM, Ingles M, Salvador-Pascual A, Cominetti MR, Gomez-Cabrera MC, Viña J. Sarcopenia, frailty and their prevention by exercise. *Free Radic Biol Med*. 2019;132:42–49. doi:10.1016/j.freeradbiomed.2018.08.035
19. Morley JE, Vellas B, Abellan Van Kan G, et al. Frailty consensus: A call to action. *J Am Med Dir Assoc*. 2013;14(6):392–397. doi:10.1016/j.jamda.2013.03.022
20. Hegde A, Murthy HS. Frailty: The missing piece of the pre- hematopoietic cell transplantation assessment? *Bone Marrow Transplant*. 2018;53(1):3–10. doi:10.1038/bmt.2017.192
21. Ishikawa A, Otaka Y, Kamisako M, et al. Factors affecting lower limb muscle strength and cardiopulmonary fitness after allogeneic hematopoietic stem cell transplantation. *Support Care Cancer*. 2019;27(5):1793–1800. doi:10.1007/s00520-018-4433-5
22. Malicka I, Pawłowska K, Stefańska M. Wpływ ćwiczeń w wodzie na parametry siłowo-prędkościowe mięśni kobiet po leczeniu raka piersi – doniesienie wstępne. *Fizjoterapia*. 2006;14(2):57–63.
23. Granger CL. Physiotherapy management of blood cancers. *J Physiother*. 2023;69(2):70–78. doi:10.1016/j.jphys.2023.02.015
24. Fiuza-Luces C, Garatachea N, Simpson RJ, Berger NA, Ramírez M, Lucia A. Understanding graft-versus-host disease: Preliminary findings regarding the effects of exercise in affected patients. *Exerc Immunol Rev*. 2015;21:80–112. PMID:25826127.
25. Liang Y, Zhou M, Wang F, Wu Z. Exercise for physical fitness, fatigue and quality of life of patients undergoing hematopoietic stem cell transplantation: A meta-analysis of randomized controlled trials. *Jap J Clin Oncol*. 2018;48(12):1046–1057. doi:10.1093/jjco/hyy144
26. Potiaumpai M, Cutrono S, Medina T, et al. Multidirectional walking in hematopoietic stem cell transplant patients. *Med Sci Sports Exerc*. 2021;53(2):258–266. doi:10.1249/MSS.0000000000002474
27. Zoth N, Böhlke L, Theurich S, Baumann FT. Physical activity and exercise therapy in oncology [in German]. *Inn Med (Heidelb)*. 2023;64(1):19–24. doi:10.1007/s00108-022-01450-5
28. Knips L, Bergenthal N, Streckmann F, Monsef I, Elter T, Skoetz N. Aerobic physical exercise for adult patients with haematological malignancies. *Cochrane Database Syst Rev*. 2019;1(1):CD009075. doi:10.1002/14651858.CD009075.pub3

29. Fioritto AP, Oliveira CC, Albuquerque VS, et al. Individualized in-hospital exercise training program for people undergoing hematopoietic stem cell transplantation: A feasibility study. *Disabil Rehabil*. 2021; 43(3):386–392. doi:10.1080/09638288.2019.1626493
30. Matsugaki R, Ohtani M, Mine Y, Saeki S, Fushimi K, Matsuda S. Pre-transplant rehabilitation to decrease the post-transplant length of stay for hematological malignancy patients undergoing allo-HSCT. *Prog Rehabil Med*. 2021;6:20210020. doi:10.2490/prm.20210020
31. Wiskemann J, Dreger P, Schwerdtfeger R, et al. Effects of a partly self-administered exercise program before, during, and after allogeneic stem cell transplantation. *Blood*. 2011;117(9):2604–2613. doi:10.1182/blood-2010-09-306308
32. Prins MC, Van Hinte G, Koenders N, Rondel AL, Blijlevens NMA, Van Den Berg MGA. The effect of exercise and nutrition interventions on physical functioning in patients undergoing haematopoietic stem cell transplantation: A systematic review and meta-analysis. *Support Care Cancer*. 2021;29(11):7111–7126. doi:10.1007/s00520-021-06334-2

Renal protection by acacetin in streptozotocin-induced diabetic nephropathy via TLR4/NF-κB pathway modulation in rats

Hangying Yu[1,A,B,E,F], Min Guo[2,A–D]

[1] Department of Nephrology, Chunan Campus of Hangzhou Traditional Chinese Medicine Hospital, Chunan County Hospital of Traditional Chinese Medicine, Hangzhou, China
[2] Department of Acupuncture and Rehabilitation, Chunan Campus of Hangzhou Traditional Chinese Medicine Hospital, Chunan County Hospital of Traditional Chinese Medicine, Hangzhou, China

A – research concept and design; B – collection and/or assembly of data; C – data analysis and interpretation;
D – writing the article; E – critical revision of the article; F – final approval of the article

Advances in Clinical and Experimental Medicine, ISSN 1899–5276 (print), ISSN 2451–2680 (online) *Adv Clin Exp Med*. 2025;34(8):1353–1363

Address for correspondence
Hangying Yu
E-mail: yhy18768158205@outlook.com

Funding sources
Science and Technology Program of Traditional Chinese Medicine in Zhejiang Province (grant No. 2019ZQ040).

Conflict of interest
None declared

Received on February 9, 2024
Reviewed on March 26, 2024
Accepted on August 11, 2024

Published online on January 3, 2025

Abstract

Background. Diabetic nephropathy (DN), the most severe microvascular consequence of diabetes mellitus (DM), is the precursor to end-stage renal disease (ESRD). The development of problems linked to DN involves both oxidative damage and inflammation. Natural flavone acacetin (AC) has anti-inflammatory, antioxidant and anti-cancer properties. However, the effect of AC on DN is not clear.

Objectives. To investigate potential nephroprotective effects of AC caused by reducing inflammation and oxidative stress via the TLR4/NF-κB pathway in rats with streptozotocin (STZ)-induced DN.

Materials and methods. In this study, we investigated the nephroprotective effect of AC compared to that of a positive control therapy of irbesartan (IRB) in DN induced with STZ. In this model, rats were given an intraperitoneal injection of STZ (180 mg/kg body weight (BW)), along with daily doses of AC (10 mg/kg BW) or IRB (180 mg/kg BW) to induce DN. Histopathology, albumin, blood glucose (Bg), BW, oxidative stress indicators, and western blot of inflammatory signaling pathways in the kidney were examined.

Results. Reduction of blood glucose, proteinuria, serum malondialdehyde (MDA), serum creatinine, and blood urea nitrogen (BUN), as well as the inhibition of toll-like receptor 4 (TLR4), high mobility group box 1 (HMGB1) and nuclear factor kappa B (NF-κB) protein expression were observed. These data demonstrated that AC could improve BW, antioxidant enzyme and renal histopathology in rats with STZ-induced DN.

Conclusions. Results from the rat model highlight how AC-suppressed inflammation and oxidative stress can attenuate STZ-induced DN by downregulating the TLR4/NF-κB pathway in rats.

Key words: inflammation, diabetic nephropathy, oxidative stress, acacetin, TLR4/NF-κB signaling

Cite as
Yu H, Guo M. Renal protection by acacetin in streptozotocin-induced diabetic nephropathy via TLR4/NF-κB pathway modulation in rats. *Adv Clin Exp Med*. 2025;34(8):1353–1363. doi:10.17219/acem/192225

DOI
10.17219/acem/192225

Copyright
Copyright by Author(s)
This is an article distributed under the terms of the Creative Commons Attribution 3.0 Unported (CC BY 3.0) (https://creativecommons.org/licenses/by/3.0/)

Background

Diabetes mellitus (DM) is an endocrine illness caused by an acquired or inherited deficit of insulin formation.[1] Nearly 537 million adults suffered from DM in 2021, and it is predicted to affect 783 million by 2045.[2] Diabetes nephropathy (DN) is one of the severe enduring complications of DM resulting in hyperglycemia, proteinuria and reduced glomerular filtration rate (GFR). Diabetes nephropathy has an average occurrence of almost 3% per year throughout the initial 10–20 years after the onset of DM.[3,4] Around 30–40% of DM patients develop DN that advances to renal injury,[5] which can lead to chronic kidney failure and end-stage renal disease (ESRD). Characteristic pathogenesis related to DN resulting in kidney failure and ESRD comprises hypertrophy, glomerular hyperfiltration, basement membrane hardening, nodular glomerulosclerosis, mesangial matrix accretion, and proteinuria.[6] Advanced kidney damage can result in lipid disorders, inflammation, hemodynamic abnormalities, oxidative stress, apoptosis, and the release of inflammatory mediators and cytokines,[7] all of which can trigger inflammation, hyperproduction of reactive oxygen species (ROS) and mitochondrial impairment.[8] The pathogenesis of DN is not fully understood owing to its complex nature,[9] and existing therapeutic approaches cannot efficiently prevent the progression of DN, warranting further in-depth research.

Generally, DN has been regarded as an endocrine and metabolic disorder that, through hyperglycemia, worsens inflammation and triggers the stimulation and discharge of numerous chemokines, cytokines, growth factors, and cell adhesion molecules.[10,11] It has been established that toll-like receptor 4 (TLR4)/nuclear factor kappa B (NF-κB) is a central signaling pathway that plays a critical role in DN by facilitating immune-inflammatory reactions.[12,13] High mobility group box 1 protein (HMGB1) is a vastly nonhistone conserved protein that belongs to a highly migratory protein family.[14] The HMGB1 pathway is mostly intermediated by glycation end-product receptors and toll-like receptors (TLRs). The HMGB1 extracellular domain and its receptors trigger monocytes/macrophages, ultimately leading to NF-κB stimulation and production of pro-inflammatory mediators. The NF-κB is a ubiquitous and significant nuclear transcription element that facilitates numerous inflammatory pathways.[15] Stimulation of NF-κB may induce the expression of HMGB1 and its receptors, liberating cytokines that promote monocyte and macrophage stimulation. In the innate immune system, pattern recognition receptors of conserved families of TLRs stimulate inflammatory downstream signaling in reaction to microbial exogenous agents.[16] Triggering of TLRs signal is connected with the stimulation of NF-κB activity and results in elevated chemokine and cytokine release, including monocyte chemoattractant protein 1 (MCP1), interleukin (IL)-1β and IL-6, which sequentially induce native inflammation and accretion of the leukocyte.[17,18] Specifically, TLR4 has been shown to be involved in the pathogenesis of severe kidney damage, the incidence of DN and prolonged kidney illnesses.[19] The downstream effector of the TLR4 signaling is NF-κB, and it is widely thought that activation of NF-κB has a fundamental role in inflammation in the kidney during DN progression.[16] Hence, we hypothesize that TLR4/NF-κB signaling pathway suppression is capable of reducing the renal inflammatory responses associated with DN.

Acacetin (AC) is an O-methylated flavone sequestered from many herbal plants, including *Betula pendula*, *Robinia pseudoacacia*, *Carthamus tinctorius*, and *Turneradiffusa*.[20,21] Acacetin has displayed numerous neuroprotective, antioxidant, anti-peroxidative, and anti-inflammatory effects, and has shown activity against prostate, lung, skin, and breast carcinomas.[22–26] Acacetin exerts a protective influence in assorted cardiovascular diseases, including atherosclerosis, atrial fibrillation, doxorubicin-induced cardiomyopathy, and ischemia/reperfusion (I/R) heart injury.[27–31] Recently, it has been documented that AC mitigates the PPAR-α/AMPK pathway in streptozotocin (STZ)-induced diabetic cardiomyopathy by constraining energy metabolism and oxidative stress.[32] Acacetin repressed E-selectin manifestation by the MAPK signaling and NF-κB stimulation in human umbilical vein endothelial cells (HUVECs).[33] Acacetin has also demonstrated the ability to avert cyclooxygenase-2 (COX-2) and inducible nitric oxide synthase (iNOS) inflammatory mRNA levels in RAW 264.7 cells by suppressing NF-κB triggering via involving with the MAPK and PI3K/Akt/IKK signaling.[34] Furthermore, a prior study reported that AMPK-facilitated Nrf2 triggering by AC is included in cardiomyocyte defense counter to re-oxygenation and hypoxic harm by its anti-inflammatory, anti-oxidative and anti-apoptotic actions.[29] Together, these results illustrate the contribution of AC in inflammation-related disorders and oxidative stress. However, the effect of AC on DN has not been completely explored.

Streptozotocin is an effective experimental model for inducing DN, as it selectively abolishes pancreatic β-cells by producing ROS, which affects insulin secretion.[35] Streptozotocin produces an inflammatory reaction by discerningly abolishing islets of β-cells through manifold consecutive injections, which cause additional impairment of β-cell function that leads to decreased insulin and high glucose levels.[36] Consequently, multiple consecutive injections of the STZ are generally employed for creating experimental DM animal models.[35,36]

Objectives

Our research aims to examine the possible nephroprotective mechanisms of AC using an STZ-induced DN model in rats and confirm the hypothesis that AC ameliorates oxidative stress and inflammation through the regulation of the TLR4/NF-κB pathway.

Materials and methods

Chemicals

Acacetin and biochemicals were purchased from Ruicong Ltd (Shanghai, China). Streptozotocin was obtained from Novartis (Beijing, China). Irbesartan (IRB) was delivered by Sun Pharmaceutical Industries Ltd (Shanghai, China). Antibodies for western blot analysis were bought from Ese-Bio (Shanghai, China). Analytical-grade biochemicals and solvents were used.

Experimental animals

A total of 40 adult male Sprague Dawley rats aged 8–10 weeks and weighing between 180–200 g were selected 1 week prior to trials. Animals were preserved in aseptic polypropylene cages under specified laboratory environment, and nourished with a regular pellet diet ad libitum. All treatment protocols were piloted according to the animal ethical committee of the ChunanCounty Traditional Chinese Medicine Hospital, Hangzhou, China (approval No. 024).

Induction of diabetes mellitus

Animals were starved overnight and then STZ (180 mg/kg body weight (BW))[37] dissolved in 0.1 M citrate buffer (pH 4.5) was injected intraperitoneally (i.p.). After the 3rd day of STZ administration, sample blood was collected by tail puncture, and blood glucose (BG) levels were tested using a glucometer (LifeScan Inc., Malvern, USA).. Animals with BG levels above 300 mg/dL were identified as the diabetic controls.[38]

Investigational protocol

Rats were separated into a normal control group and 3 diabetic groups, with 10 rats in each. They were divided into 4 sets: normal control (NC); diabetic control (DC), DC+IRB (180 mg/kg/day); and DC+AC (10 mg/kg/day) for 8 weeks. On completion of the experimental period, animals were starved for 12 h and sedated with pentobarbital sodium (i.p., 45 mg/kg).[39] Blood samples were collected through cardiac puncturing of the retro-orbital and various biochemical parameters were estimated after sacrificing the animals. Centrifugation was performed at 10 × g rpm for 15 min for the separation of serum, and the separated serum sample was kept at –80°C for future use. The kidney was weighed, sliced and fixed in a 10% formalin-neutral buffer for histopathological examination.

Estimation of body weight and blood glucose level

Body weight and BG were determined at 2-week intervals using blood samples taken by tail puncture in the lateral vein. Blood glucose levels were tested using a glucometer (LifeScan Inc.)

Biochemical analysis

The levels of blood urea nitrogen (BUN) and creatinine (Cr) in urine and serum were estimated spectrophotometrically using the commercial assay kits cat. No. ab83362 (Jiancheng Bioengineering Institute, Nanjing, China) in an Olympus AU 600 Autoanalyzer (Olympus Corp., Tokyo, Japan). Malondialdehyde (MDA) and total superoxide dismutase activity (T-SOD) in serum and kidney were measured with commercial assay kits cat. No. ab118907 provided by Biomed (Badr City, Egypt). The quantity of microalbuminuria (m-ALB) was assayed by commercial kit cat. No. E-TSEL-H0005 (Elabscience Biotechnology, Wuhan, China) as per the manufacturer's protocol.

Histopathological analysis of kidney

For histopathological examination, the kidney was separated, tissues fixed with formalin (10%) and paraffin-embedded. To evaluate histopathological variations in the kidneys, 5-µm sections were cut using rotary microtome (HV-HSMA-1090A; Hoverlabs, Ambala, India) stained with hematoxylin and eosin (H&E), and observed through a microscope (BS-2074T; Beijing BestScope Technology Co., Ltd., Beijing, China).

Analysis of western blot

Total proteins were isolated from the rat's kidney tissue homogenate for the assessment of the role of AC and IRB on the signaling of TLR4/NF-κB. Kidney tissues were prepared by adding lysis buffer in ice-cold conditions for western blot analysis. Briefly, total protein was estimated using the Protein Assay Kit (Pierce Chemical Co, Rockford, USA), quantified, electrophoretically dispersed, and transferred to a polyvinylidene difluoride (PVDF) film. It was blocked by using a probe at room temperature for 1 h with treated primary antibodies TLR4, interleukin 1 receptor-associated kinase 4 (IRAK4), tumor necrosis factor receptor-associated factor 6 (TRAF6), inhibitory kappa B kinase beta (IKKβ), nuclear factor kappa-light-chain-enhancer of activated B cells (NF-κBp65), and HMGB1. in 1:1,000 dilutions, and kept at 4°C overnight. Then, horseradish peroxidase (HRP)-conjugated secondary antibodies were administered. The protein bands were stained and imaged for protein recognition. Protein bands were quantified through densitometry with ImageJ (National Institutes of Health (NIH), Bethesda, USA) and normalized to glyceraldehyde 3-phosphate dehydrogenase (GAPDH) expression.

Statistical analyses

The data from each group were analyzed statistically using GraphPad Prism v. 8.0.2 (GraphPad Software, San Diego, USA) and IBM SPSS v. 25 (IBM Corp., Armonk,

USA). The measurement data were reported as the median (min–max). The normality of the distribution was tested using the Kolmogorov–Smirnov test. Since all the distributions were normal, the Brown–Forsythe test was used to establish the equality of variances. Significant differences between multiple groups were analyzed using the Kruskal–Wallis test, and Dunn's post hoc test was used for multiple comparisons. If $p < 0.05$, the data divergence was considered statistically notable. All tests in this study were bilateral.

Results

The results of the Kruskal–Wallis test and Dunn's post hoc test are presented in Tables 1,2.

Influence of acacetin on body weight and blood glucose levels

The body weight (BW) gain was considerably reduced ($p < 0.05$) in DC rats, whereas the BG level was substantially elevated ($p < 0.01$) against NC (Table 1, Fig. 1,2). Administration of IRB (180 mg/kg) and AC (10 mg/kg) considerably ($p < 0.05$) enhanced BW gain; however, they reduced the level of BG during the experiment period. The effect was higher in IRB-treated DC rats than in AC-treated rats.

Influence of acacetin on microalbuminuria and diabetic nephropathy factors

As shown in Table 1, and Fig. 3A, STZ administration expressively ($p < 0.01$) increased the level of microalbuminuria (m-ALB), BUN and Cr in serum, whereas the levels of Cr and BUN were significantly ($p < 0.05$) lower in urine, confirming that STZ-administration could cause DN in rats (Table 1, Fig. 3B). Irbesartan and AC may inverse this inclination significantly ($p < 0.05$), as revealed by a reduced level of BUN, m-ALB, and Cr in serum, while elevated BUN and Cr were significant in urine. On the other hand, IRB and AC considerably ($p < 0.05$) reduced the m-ALB contained in the 24-h urine sample. These results established that IRB and AC could relieve STZ-induced renal impairments.

Table 1. Comparison of groups

Variables	Group I (n = 6)	Group II (n = 6)	Group III (n = 6)	Group IV (n = 6)	Test value (H)**	p-value*
BW week-2	27.11 (24.66–29.54)	26.36 (23.98–28.72)	25.38 (23.09–27.65)	25.20 (22.92–27.46)	2.26	0.519
BW week-4	31.26 (28.44–34.06)	23.81 (21.66–5.94)	22.43 (20.40–24.44)	21.30 (19.37–23.21)	15.62	0.001
BW week-6	35.12 (31.94–38.26)	25.20 (22.92–27.46)	27.61 (25.12–30.08)	24.19 (22.00–26.36)	16.66	0.001
BW week-8	41.27 (37.54–44.96)	29.18 (26.54–31.80)	34.76 (31.62–37.88)	30.24 (27.51–32.95)	17.87	<0.001
BG week-2	4.74 (4.31–5.17)	14.73 (13.40–16.06)	13.30 (12.10–14.50)	13.50 (12.29–14.72)	16.67	0.001
BG week-4	4.91 (4.47–5.35)	19.77 (17.98–21.54)	11.35 (10.33–12.37)	12.05 (10.97–13.13)	19.68	<0.001
BG week-6	5.13 (4.67–5.59)	20.82 (18.94–22.68)	14.51 (13.20–15.82)	15.11 (13.74–16.46)	19.68	<0.001
BG week-8	6.35 (5.78–6.92)	22.12 (20.12–24.10)	8.40 (7.64–9.16)	11.24 (10.23–12.25)	21.60	<0.001
mALB	51.27 (46.64–55.86)	99.79 (90.76–108.72)	55.33 (50.32–60.28)	61.96 (56.36–67.50)	18.62	<0.001
Urine-Cr	220.61 (200.66–240.35)	68.12 (61.96–74.22)	140.42 (127.72–152.98)	170.48 (155.06–185.74)	21.60	<0.001
Serum-Cr	81.79 (74.39–89.11)	241.07 (219.26–262.64)	87.54 (79.63–95.38)	160.38 (145.87–174.73)	19.68	<0.001
Urine-BUN	999.40 (909.00–1088.80)	535.52 (487.08–583.42)	850.47 (773.55–926.55)	740.47 (673.49–806.71)	20.007	<0.001
Serum-BUN	12.60 (11.47–13.73)	35.19 (32.00–38.34)	23.06 (20.98–25.12)	26.16 (23.80–28.50)	20.74	<0.001
Serum-T-SOD	315.36 (286.83–343.57)	115.96 (105.47–126.33)	230.91 (210.03–251.57)	208.50 (189.64–227.16)	20.74	<0.001
Kidney-T-SOD	740.52 (673.54–806.76)	610.83 (555.58–665.48)	651.07 (592.18–709.32)	625.71 (569.11–681.69)	11.12	0.011
Serum-MDA	15.92 (14.48–17.34)	129.33 (117.64–140.90)	31.36 (28.53–34.17)	57.43 (52.23–62.57)	21.60	<0.001
Kidney-MDA	43.97 (39.99–47.91)	37.06 (33.71–40.37)	41.77 (37.99–45.51)	40.53 (36.86–44.16)	9.54	0.023
TLR4	1.00 (0.91–1.09)	1.74 (1.58–1.90)	0.86 (0.78–0.94)	1.07 (0.97–1.17)	18.53	<0.001
IRAK4	1.00 (0.91–1.09)	1.61 (1.47–1.75)	0.92 (0.84–1.00)	1.12 (1.02–1.22)	19.12	<0.001
TRAF6	1.00 (0.91–1.09)	2.04 (1.86–2.22)	0.73 (0.66–0.80)	1.20 (1.09–1.31)	21.52	<0.001
Iκκβ	1.00 (0.91–1.09)	2.19 (1.99–2.39)	1.05 (0.96–1.14)	1.32 (1.20–1.44)	19.71	<0.001
NF-κBp65	1.00 (0.91–1.09)	1.59 (1.45–1.73)	0.58 (0.53–0.63)	0.73 (0.66–0.80)	21.65	<0.001
HMGB1	1.00 (0.91–1.09)	1.41 (1.28–1.54)	0.57 (0.52–0.62)	0.94 (0.86–1.02)	19.74	<0.001

Data were present as median (min and max); *p-value was generated from Kruskal–Wallis test with Dunn's test; **degrees of freedom is equal to 3.
BW – body weight; BG – blood glucose; mALB – microalbuminuria; Cr – creatinine; BUN – blood urea nitrogen; T-SOD – total superoxide dismutase; MDA – melanaldehyde; TLR4 – toll-like receptor 4; IRAK4 – interleukin 1 receptor-associated kinase 4; TRAF6 – tumor necrosis factor receptor-associated factor 6; IKKβ –inhibitory kappa B kinase beta; NF-κBp65 – nuclear factor kappa-light-chain-enhancer of activated B cells; HMGB1 – high mobility group box 1.

Table 2. Results of the Dunn's post hoc test

Explained variable	1 vs 2	1 vs 3	3 vs 2	4 vs 1	4 vs 2	4 vs 3
BW week-2	0.519	0.519	0.519	0.519	0.519	0.519
BW week-4	0.203	0.020	1.000	0.001	0.615	1.000
BW week-6	0.009	0.362	1.000	0.001	1.000	0.362
BW week-8	0.001	0.668	0.148	0.008	1.000	0.615
BG week-2	0.000	0.202	0.362	0.042	1.000	1.000
BG week-4	0.000	0.300	0.086	0.086	0.300	1.000
BG week-6	0.000	0.300	0.086	0.086	0.300	1.000
BG week-8	0.000	0.850	0.020	0.020	0.850	0.850
mALB	0.000	1.000	0.008	0.120	0.615	0.668
Urine-Cr	0.000	0.020	0.850	0.850	0.020	0.850
Serum-Cr	0.001	1.000	0.004	0.086	0.850	0.300
Urine-BUN	0.000	0.991	0.022	0.048	0.615	1.000
Serum-BUN	0.000	0.615	0.033	0.033	0.615	1.000
Serum-T-SOD	0.000	0.615	0.033	0.033	0.615	1.000
Kidney-T-SOD	0.010	0.273	1.000	0.068	1.000	1.000
Serum-MDA	0.000	0.850	0.020	0.020	0.850	0.850
Kidney-MDA	0.020	1.000	0.133	1.000	0.615	1.000
TLR4	0.054	0.613	0.000	1.000	0.299	0.133
IRAK4	0.011	1.000	0.000	0.845	0.610	0.085
TRAF6	0.021	0.815	0.000	0.916	0.815	0.021
Ικκβ	0.001	1.000	0.004	0.085	0.848	0.299
NF-κBp65	0.847	0.019	0.000	0.847	0.019	0.847
HMGB1	0.298	0.085	0.000	1.000	0.085	0.298

BW – body weight; BG – blood glucose; mALB – microalbuminuria; Cr – creatinine; BUN – blood urea nitrogen; T-SOD – total superoxide dismutase; MDA – melanaldehyde; TLR4 – toll-like receptor 4; IRAK4 – interleukin 1 receptor-associated kinase 4; TRAF6 – tumor necrosis factor receptor-associated factor 6; IKKβ – inhibitory kappa B kinase beta; NF-κBp65 – nuclear factor kappa-light-chain-enhancer of activated B cells; HMGB1 – high mobility group box 1.

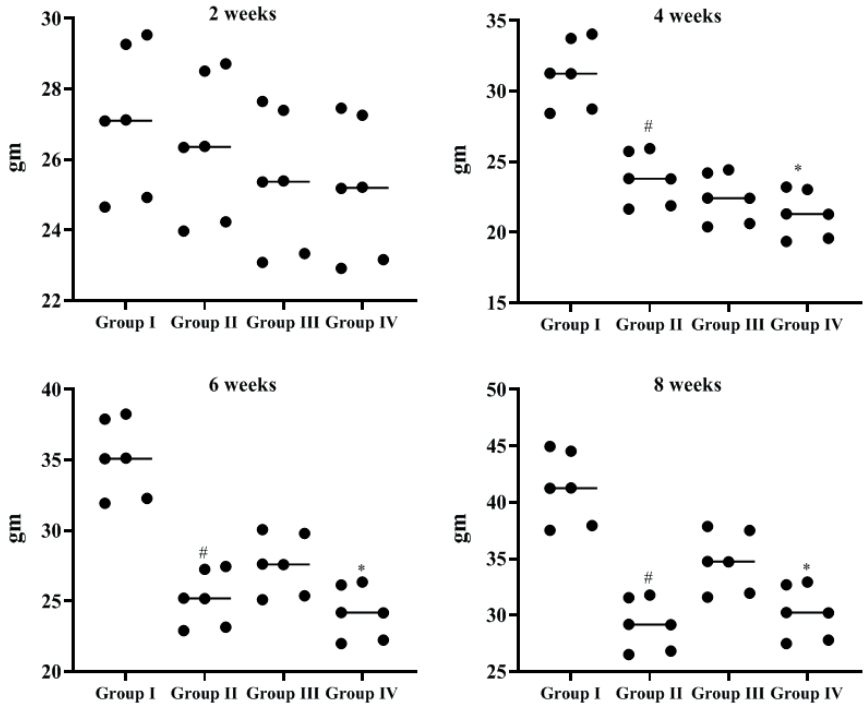


Fig. 1. Effect of acacetin (AC) on body weight (BW) level in control and diabetic control (DC) rats. Results were described as median (min–max) of 6 observations, and the significance was considered as $^{\#}p < 0.01$ and $^{*}p < 0.05$ against normal control (NC)

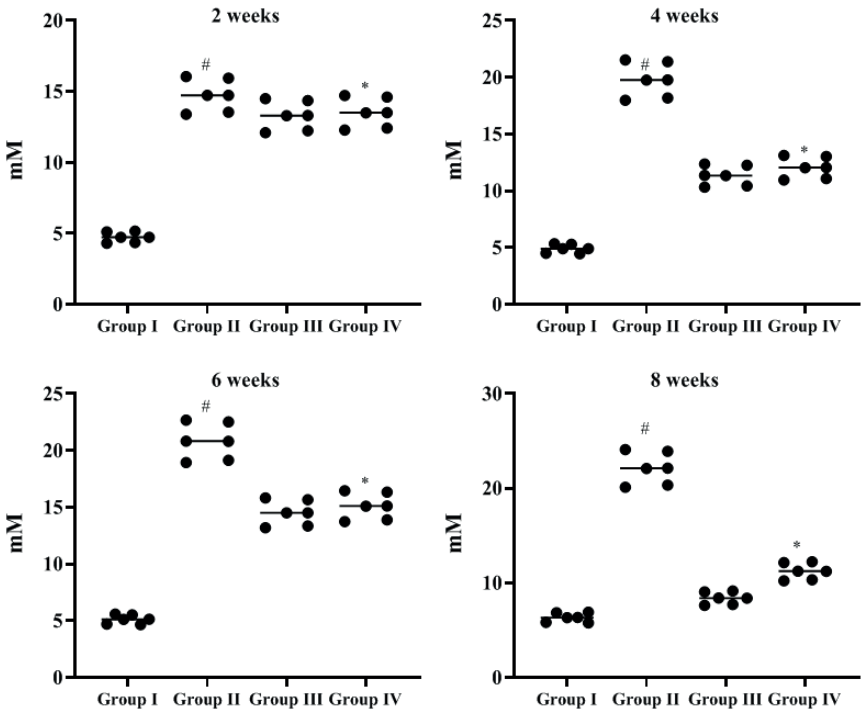


Fig. 2. Effect of acacetin (AC) on blood glucose (BG) level of control and diabetic control (DC) rats. Results were described as median (min–max) of 6 observations, and the significance was considered as $^{\#}p < 0.01$ and $^{*}p < 0.05$ against normal control (NC)

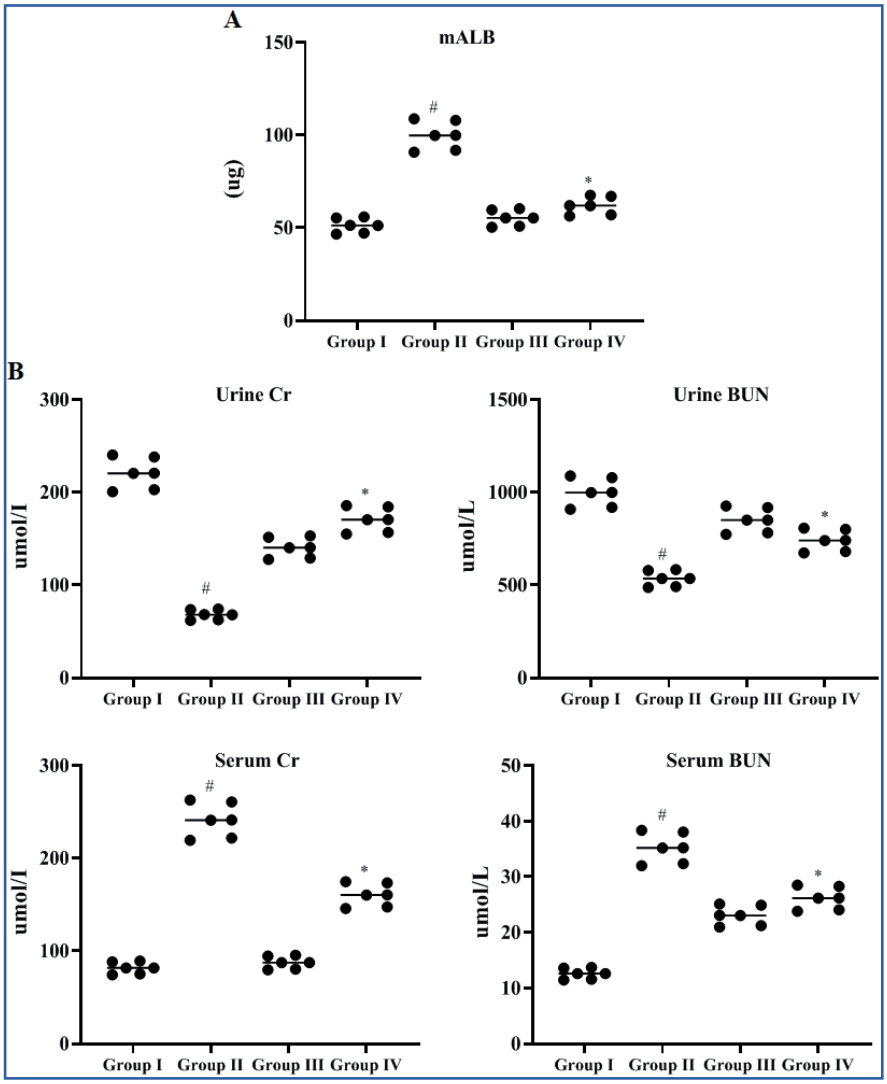


Fig. 3. Effect of acacetin (AC) on 24 h micro-albuminuria (m-ALB) and diabetic nephropathy (DN) factors in urine and serum on diabetic control (DC) rats. The level of urine (A) microalbuminuria (m-ALB) and (B) creatinine (Cr) urine blood urea nitrogen (BUN), serum Cr and serum BUN. Results were described as median (min–max) of 6 observations, and the significance was considered as $^{\#}p < 0.01$ and $^{*}p < 0.05$ against normal control (NC)

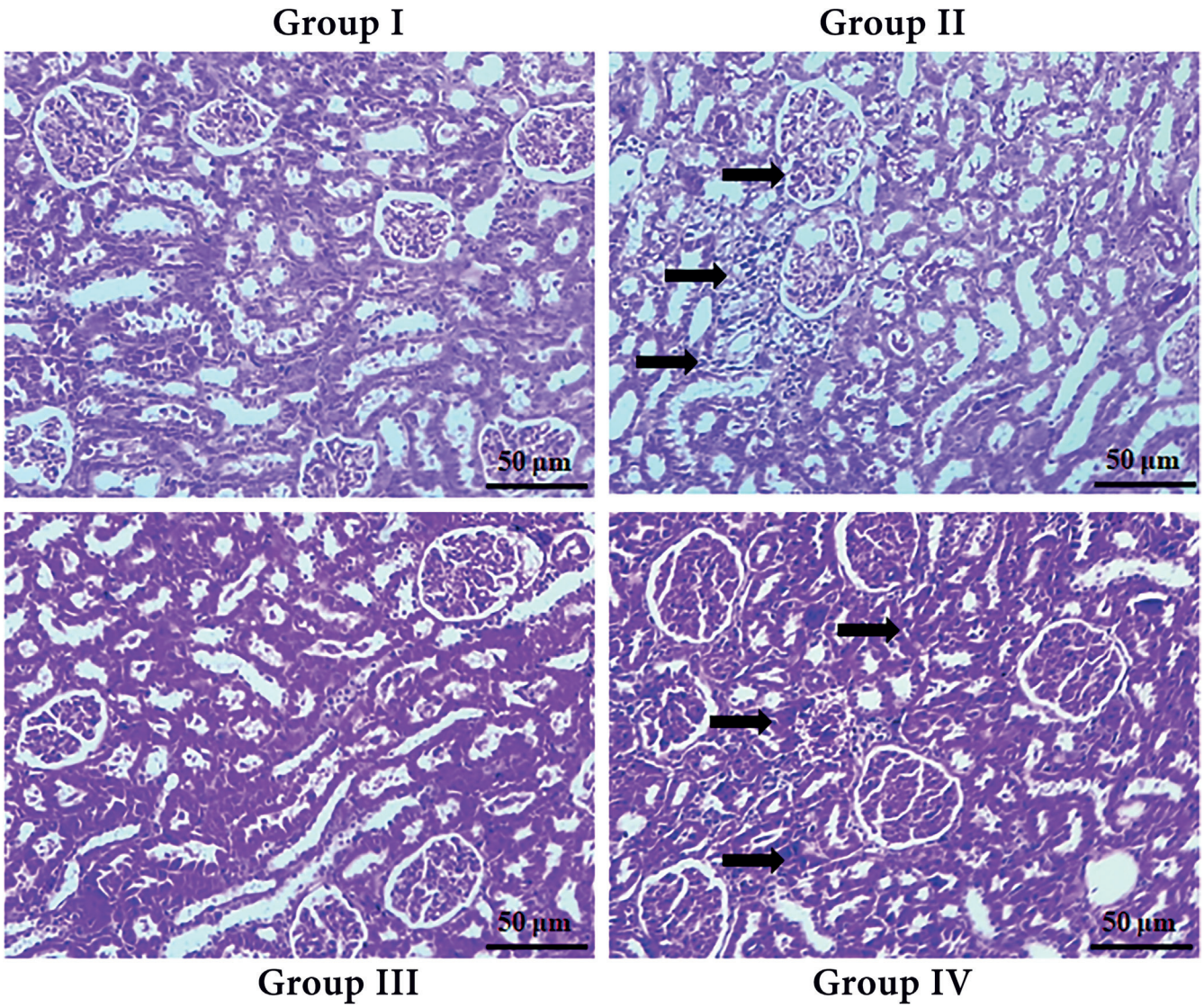


Fig. 4. Effect of acacetin (AC) on the histopathology of kidney in control and diabetic control (DC) rats. Kidney portions were stained with hematoxylin & eosin (H&E). Scale bar = 50 µm. Group I – normal control (NC) group depicting normal histology of the kidney cells. Group II – DC rats displayed apparent glomerulus hypertrophy, proliferation of mesangial cells, expanded Bowman's capsule, hyperplasia, hardening of basement tissue, and glycogen deposition. Group III and IV – rats administered with irbesartan (IRB) (180 mg/kg) and AC (10 mg/kg) demonstrated an absence of palpable extension of the glomerulus, slight thickening of mesangial cells, relief of the Bowman's capsule expansion, and reduced glycogen level

Histopathological investigation of kidney

Histopathological analysis of the kidney of DC rats depicted apparent glomerulus hypertrophy, mesangial cells proliferation, expanded Bowman's capsule, hyperplasia, basement tissue thickening, infiltration of inflammatory cells, and a few vacuolar tubular cells collapse with glycogen accumulation, in contrast to NC rats (Fig. 4). Conversely, the rats administered with IRB and AC demonstrated less Bowman's capsule expansion, slight thickening of mesangial cells, absence of palpable extension of the glomerulus, and mild glycogen accumulation due to their nephroprotective effects.

Effects of acacetin on oxidative markers in serum and kidney

Oxidative markers in DC rats revealed that T-SOD status in serum was reduced substantially, while there was no apparent alteration in the contents of T-SOD in renal cells (Table 1, Fig. 5). In DC model rats, the T-SOD content was expressively ($p < 0.01$) less in serum than that in the NC, whereas the IRB and AC group had significantly ($p < 0.05$) elevated T-SOD level. The concentration of serum MDA was considerably elevated ($p < 0.01$) in DC rats, whereas the MDA dropped to near ordinary levels in STZ-induced rats administered IRB and AC. No statistical difference ($p < 0.05$) was noted in the MDA level of the kidneys between groups. These results suggest that IRB and AC could attenuate oxidative stress and improve the antioxidant status in the STZ-induced DN rat model.

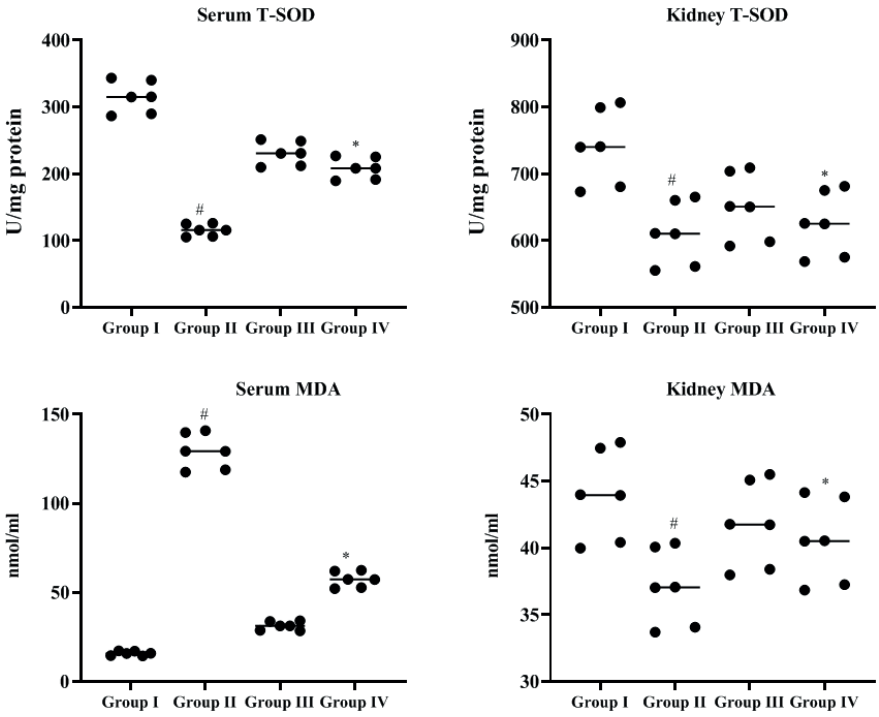


Fig. 5. Effect of acacetin (AC) on oxidative markers of control and diabetic control (DC) rats. The levels of serum total superoxide dismutase activity (T-SOD), malondialdehyde (MDA) and T-SOD, and MDA levels in kidney tissue. Results were described as median (min–max) of 6 observations, and the significance was considered as $^{\#}p < 0.01$ and $^{*}p < 0.05$ against normal control (NC)

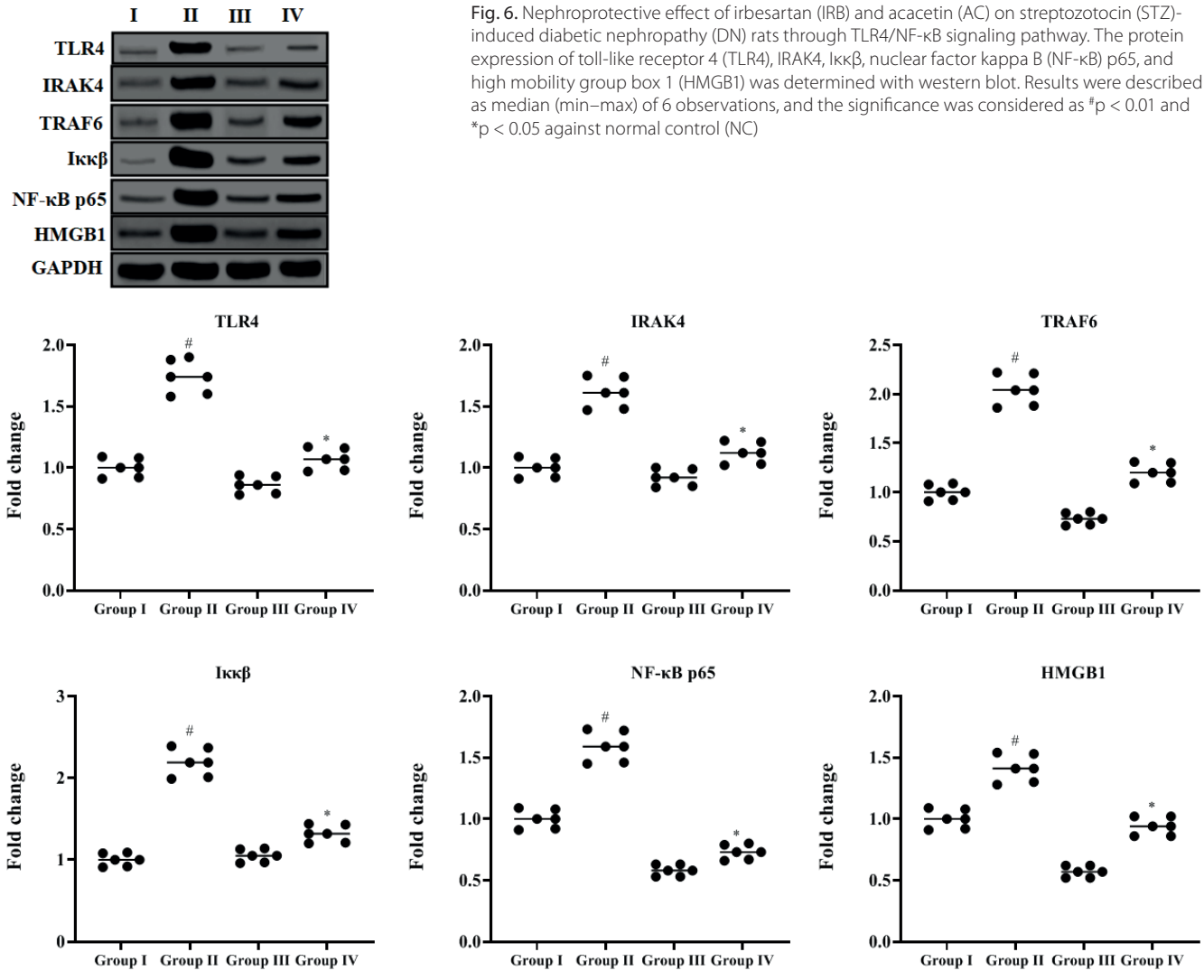


Fig. 6. Nephroprotective effect of irbesartan (IRB) and acacetin (AC) on streptozotocin (STZ)-induced diabetic nephropathy (DN) rats through TLR4/NF-κB signaling pathway. The protein expression of toll-like receptor 4 (TLR4), IRAK4, Iκκβ, nuclear factor kappa B (NF-κB) p65, and high mobility group box 1 (HMGB1) was determined with western blot. Results were described as median (min–max) of 6 observations, and the significance was considered as $^{\#}p < 0.01$ and $^{*}p < 0.05$ against normal control (NC)

Analysis of TLR4/NF-κB pathway

Streptozotocin-induced DC rats were seen to expressively upregulate HMGB1 ($p < 0.01$) and TLR4/NF-κB compared to the NC group, signifying that the TLR4/NF-κB pathway was triggered in the STZ-induced DN rats (Table 1, Fig. 6). These proteins were considerably ($p < 0.05$) downregulated after treatment with IRB and AC, suggesting that AC can avert the pathway of TLR4/NF-κB in DN rats by exhibiting nephroprotective action against renal inflammation.

Discussion

Streptozotocin-induced DM affects the β-cells damage in the islets of Langerhans due to depleted insulin secretion, which further induces diabetes-associated complications, particularly DN.[35,36] In the present research, STZ-induced rats exhibited characteristic features of DM, such as loss of BW and high glucose levels, along with enhanced renal tissue impairment. Diabetic nephropathy, as a severe microvascular complication, shows histologically significant renal injury, including glomerulosclerosis, mesangial dilatation, renal tubule interstitial fibrosis, and hardening of the glomerular basement membrane, progressively diminishing the normal function of the kidneys.[5,6] This persistent disorder is mostly related to a constant elevation of proteinuria and a severe decline in the GFR. Throughout the course of DM, BW reduction is a main complication of DN, and our results also showed reduced BW in STZ-prompted DN in rats. It has been previously reported that dehydration and catabolism of protein, as well as fats, lead to the loss of BW after STZ administration.[40] In DN progression, proteinuria is a vital index, as it directly reveals kidney function through GFR and renal tubular reabsorption.[3,4] This study demonstrated that AC not only effectively attenuated renal histopathological damage and BG levels, but also increased serum Cr, BUN and m-ALB 24-h urinary protein. Acacetin treatment considerably increases BW owing to its potential effect in preventing the wasting of muscle. Streptozotocin can affect the function of the β-cells of the islets of Langerhans, subsequently restraining insulin discharge, which in turn forms hyperglycemia and DM-allied complications, including DN. Our research aimed to assess the protective mechanism of AC against oxidative stress and inflammation and its ability to exert nephron protection from STZ-incited DN in rats. To the best of our knowledge, this study offers the first evidence for the potential of AC against kidney impairment in the STZ-prompted DN model.

Hyperglycemia is the key mark of DM, which generates extreme ROS within the body and leads to elevated levels of cytokines formation, hastening renal cell destruction. The joint action of inflammation and oxidative stress has a precise, crucial role in the pathogenesis and progression of renal impairment in DM. In DM, extreme ROS generation can lessen the activity of the antioxidant defense mechanism that causes the oxidation of DNA, proteins and lipids after DN.[7,8] Furthermore, high BG is susceptible to oxidative stress-prompted cell injury caused by attenuation of antioxidant capability in glycation of scavenging enzymatic antioxidants comprising glutathione peroxide (GPx) and superoxide dismutase activity (SOD). This may be attributed to the connection of glucose with proteins to form advanced glycation end products (AGEs), which deactivate enzymatic antioxidants by blocking receptors.[15] In STZ-induced DM in rat models, inflammation and oxidative stress have a crucial role in the progression of DN. In our research, STZ-induced DN exhibited elevated levels of MDA; conversely, T-SOD levels were considerably lower ($p < 0.05$) than in the control. The administration of AC (10 mg/kg BW) lowered the MDA levels while elevating the T-SOD level significantly ($p < 0.05$) in contrast to STZ-induced DN control rats. These findings support the theory that the ROS foraging by AC may be moderately connected to the enhanced action of enzymatic antioxidants and anti-inflammatory effects.[22–26] Lipid peroxidation products, such as MDA, are used as a marker of tissue impairment due to increased ROS formation. Streptozotocin is recognized to enhance MDA levels in tissues of several organs, particularly kidneys.[22,23] Acacetin was reported to attenuate kidney damage by suppressing oxidative stress and apoptosis in mice models.[41] An earlier study has recognized that AC mitigates STZ-induced diabetic cardiomyopathy by averting oxidative stress and energy metabolism via PPAR-α/AMPK signaling.[32] Another study concluded that AC could diminish the inflammatory reaction of myocardial tissue by constraining the levels of IL-6 and TLR4 signaling. Myocardial cell apoptosis results from multiple elements, including myocardial I/R inflammation and oxidative stress.[42] The above data suggest that the addition of AC lessens oxidative stress and inflammation, inhibiting nephropathy development in STZ-induced DM rats.

TLR4/NF-κB signaling is a typical inner inflammatory signal transduction pathway and the NF-κB pathway can be triggered by TLR4.[12,13] The TLR4 initiation successively activates the NF-κB allied pathway via the MyD88-reliant pathway, which mediates the discharge of inflammatory chemokines and cytokines responsible for leukocyte accumulation and innate inflammation (MCP-1, IL-6, IL-1β, and tumor necrosis factor alpha (TNF-α)).[10,11] The NF-κB controls the expression level of cellular genes responsible for inflammation as a significant transcription factor in DN pathogenesis. Under standard physiological conditions, NF-κB and IκB associate to form an inactive complex, which is confined in the cytoplasm. Then, IκB is degraded once phosphorylation occurs, and this is followed by ubiquitylation while the cells are in reaction to the peripheral stimuli. Successively, NF-κB arrives at the nucleus to affix to target genes that facilitate inflammation. The NF-κB activation is frequently stimulated by oxygen free radicals, cytokines, hyperglycemia, and

even viruses. Moreover, proteinuria connected with DN also plays a significant role in its stimulation.[3,4,7] There is strong evidence that NF-κB activation is integral in the progression of nephritis and fibrosis resulting in DN.[16,17] Several studies have established that DN in rats was reduced by constraining the NF-κB stimulation and subsequently reducing other inflammatory mediators.[18,19] The elevated levels of inflammatory mediators indicate inflammation in the body. These results established that AC expressively ameliorated kidney dysfunction and oxidative stress in DN rats. Furthermore, a recent study has substantiated that AC inhibited phosphorylation of NF-κB, and IκB degradation, ultimately leading to the inhibition of NF-κB nuclear translocation,[43] consistent with our findings. In the current experiments, AC attenuated the HMGB1 and TLR4 in the DN rat's kidney tissue simultaneously and downregulated the TLR4 downstream proteins, including IRAK4, TRAF6 and Iκκβ, to facilitate further reduction of NF-κB stimulation.

High mobility group box 1 is a highly conserved nonhistone DNA binding protein, which is extensively dispersed between numerous body parts, including the brain, lung, heart, kidney, and liver, and it can be discharged from necrotic cells through active discharge or passive release, causing inflammation.[14] It is discharged from inflammatory or necrotic cells, comprising dendritic cells, macrophages and monocytes, as a strong pro-inflammatory cytokine, and interacts with several cell-surface receptors such as TLR2, TLR4 and receptor for advanced glycation end products (RAGE).[15] Hence, HMGB1 is known as the endogenous ligand of TLR4, and the communication of HMGB1 with TLR4 marks an auxiliary translocation of NF-κB from the cytoplasm into the nucleus, prompting an inflammatory reaction.[14,15] In agreement with these results, HMGB1 plays a vital action in the pathogenesis of renal illness and DN. Previously, hyperglycemia-prompted release of HMGB1 was tested as a cause of kidney damage in DM rats. The pathogenic action of this HMGB1 is dependent on TLR4, with further stimulation of NF-κB. Thus, HMGB1/TLR4/NF-κB is a significant inflammatory pathway in kidney syndromes and recent literature showed an analogous enhancement in TLR4, HMGB1 and NF-κB in DN.[15–18] Similarly, our research suggests that AC administration could increase amounts of HMGB1 and TLR4 in DM rats, emphasizing the possible nephron-protective influence of AC through reducing inflammation in DN. The present study demonstrates that the nephroprotective effect of AC in STZ-activated DN in rats encompasses cell signaling pathways, including HMGB1, TLR4 and NF-κB.

Limitations

Altogether, the nephroprotective effect of acacetin in streptozotocin-induced diabetic nephropathy was revealed in rats. TLR4, IRAK4, TRAF6, IkkB, NF-KB p65, and HMGB1 were studied only in proteins levels; the function of the nuclear level needs to be further verified.

Conclusions

This study revealed that AC mitigated kidney damage in STZ-stimulated DN rats by suppressing oxidative stress and inflammation through suppression of the TLR4/NF-κB pathway. These findings propose that AC might be a potential nephroprotective agent for the treatment of DN. However, further molecular mechanisms require investigation to fully understand the renoprotective efficacy of AC.

Supplementary data

The supplementary materials are available at https://doi.org/10.5281/zenodo.13148016. The package includes the following files:

Supplementary Fig. 1. Results of Kruskal–Wallis test as presented in Fig. 1.

Supplementary Fig. 2. Results of Kruskal–Wallis test as presented in Fig. 2.

Supplementary Fig. 3. Results of Kruskal–Wallis test as presented in Fig. 3.

Supplementary Fig. 4. Results of Kruskal–Wallis test as presented in Fig. 5.

Supplementary Fig. 5. Results of Kruskal–Wallis test as presented in Fig. 6.

Data availability

The datasets generated and/or analyzed during the current study are available from the corresponding author on reasonable request.

Consent for publication

Not applicable.

ORCID iDs

Hangying Yu https://orcid.org/0009-0001-3460-4617
Min Guo https://orcid.org/0009-0002-6264-5093

References

1. Nasiry D, Khalatbary AR, Ahmadvand H, Talebpour Amiri F, Akbari E. Protective effects of methanolic extract of *Juglans regia* L. leaf on streptozotocin-induced diabetic peripheral neuropathy in rats. *BMC Complement Altern Med*. 2017;17(1):476. doi:10.1186/s12906-017-1983-x
2. Sun H, Saeedi P, Karuranga S, et al. IDF Diabetes Atlas: Global, regional and country-level diabetes prevalence estimates for 2021 and projections for 2045. *Diabetes Res Clin Pract*. 2022;183:109119. doi:10.1016/j.diabres.2021.109119
3. Sever B, Altıntop MD, Demir Y, et al. A new series of 2,4-thiazolidinediones endowed with potent aldose reductase inhibitory activity. *Open Chem*. 2021;19(1):347–357. doi:10.1515/chem-2021-0032
4. Sulaiman MK. Diabetic nephropathy: Recent advances in pathophysiology and challenges in dietary management. *Diabetol Metab Syndr*. 2019;11(1):7. doi:10.1186/s13098-019-0403-4
5. Martínez-Castelao A, Navarro-González J, Górriz J, De Alvaro F. The concept and the epidemiology of diabetic nephropathy have changed in recent years. *J Clin Med*. 2015;4(6):1207–1216. doi:10.3390/jcm4061207

6. DeFronzo RA, Reeves WB, Awad AS. Pathophysiology of diabetic kidney disease: Impact of SGLT2 inhibitors. *Nat Rev Nephrol*. 2021;17(5): 319–334. doi:10.1038/s41581-021-00393-8
7. Jing D, Bai H, Yin S. Renoprotective effects of emodin against diabetic nephropathy in rat models are mediated via PI3K/Akt/GSK-3β and Bax/caspase-3 signaling pathways. *Exp Ther Med*. 2017;14(5): 5163–5169. doi:10.3892/etm.2017.5131
8. Shati AA. Salidroside ameliorates diabetic nephropathy in rats by activating renal AMPK/SIRT1 signaling pathway. *J Food Biochem*. 2020; 44(4):e13158. doi:10.1111/jfbc.13158
9. Demir Y, Ceylan H, Türkeş C, Beydemir Ş. Molecular docking and inhibition studies of vulpinic, carnosic and usnic acids on polyol pathway enzymes. *J Biomol Struct Dyn*. 2022;40(22):12008–12021. doi:10.1080/07391102.2021.1967195
10. Demir Y, Köksal Z. Some sulfonamides as aldose reductase inhibitors: Therapeutic approach in diabetes. *Arch Physiol Biochem*. 2022;128(4): 979–984. doi:10.1080/13813455.2020.1742166
11. Akdağ M, Özçelik AB, Demir Y, Beydemir Ş. Design, synthesis, and aldose reductase inhibitory effect of some novel carboxylic acid derivatives bearing 2-substituted-6-aryloxo-pyridazinone moiety. *J Mol Struct*. 2022;1258:132675. doi:10.1016/j.molstruc.2022.132675
12. Jiang T, Shen S, Wang L, Zhao M, Li Y, Huang S. *Grifola frondosa* polysaccharide ameliorates early diabetic nephropathy by suppressing the TLR4/NF-κB pathway. *Appl Biochem Biotechnol*. 2022;194(9): 4093–4104. doi:10.1007/s12010-022-03976-8
13. Qi MY, He YH, Cheng Y, et al. Icariin ameliorates streptozocin-induced diabetic nephropathy through suppressing the TLR4/NF-κB signal pathway. *Food Funct*. 2021;12(3):1241–1251. doi:10.1039/D0FO02335C
14. Kang R, Chen R, Zhang Q, et al. HMGB1 in health and disease. *Mol Aspects Med*. 2014;40:1–116. doi:10.1016/j.mam.2014.05.001
15. Navarro-González JF, Mora-Fernández C, De Fuentes MM, García-Pérez J. Inflammatory molecules and pathways in the pathogenesis of diabetic nephropathy. *Nat Rev Nephrol*. 2011;7(6):327–340. doi:10.1038/nrneph.2011.51
16. Lin M, Yiu WH, Wu HJ, et al. Toll-like receptor 4 promotes tubular inflammation in diabetic nephropathy. *J Am Soc Nephrol*. 2012;23(1): 86–102. doi:10.1681/ASN.2010111210
17. Faure E, Equils O, Sieling PA, et al. Bacterial lipopolysaccharide activates NF-κB through toll-like receptor 4 (TLR-4) in cultured human dermal endothelial cells. *J Biol Chem*. 2000;275(15):11058–11063. doi:10.1074/jbc.275.15.11058
18. Shimamoto A, Chong AJ, Yada M, et al. Inhibition of toll-like receptor 4 with eritoran attenuates myocardial ischemia-reperfusion injury. *Circulation*. 2006;114(1 Suppl):I270-4. doi:10.1161/CIRCULATIONAHA.105.000901
19. Kaur H, Chien A, Jialal I. Hyperglycemia induces toll-like receptor 4 expression and activity in mouse mesangial cells: Relevance to diabetic nephropathy. *Am J Physiol Renal Physiol*. 2012;303(8):F1145–F1150. doi:10.1152/ajprenal.00319.2012
20. Han DG, Cha E, Joo J, et al. Investigation of the factors responsible for the poor oral bioavailability of acacetin in rats: Physicochemical and biopharmaceutical aspects. *Pharmaceutics*. 2021;13(2):175. doi:10.3390/pharmaceutics13020175
21. Zhang Q, Zhu L, Gong X, et al. Sulfonation disposition of acacetin: In vitro and in vivo. *J Agric Food Chem*. 2017;65(24):4921–4931. doi:10.1021/acs.jafc.7b00854
22. Shendge AK, Chaudhuri D, Mandal N. The natural flavones, acacetin and apigenin, induce Cdk-Cyclin mediated G2/M phase arrest and trigger ROS-mediated apoptosis in glioblastoma cells. *Mol Biol Rep*. 2021;48(1):539–549. doi:10.1007/s11033-020-06087-x
23. Kim HR, Park CG, Jung JY. Acacetin (5,7-dihydroxy-4′-methoxyflavone) exhibits in vitro and in vivo anticancer activity through the suppression of NF-κB/Akt signaling in prostate cancer cells. *Int J Mol Med*. 2014;33(2):317–324. doi:10.3892/ijmm.2013.1571
24. Singh S, Gupta P, Meena A, Luqman S. Acacetin, a flavone with diverse therapeutic potential in cancer, inflammation, infections and other metabolic disorders. *Food Chem Toxicol*. 2020;145:111708. doi:10.1016/j.fct.2020.111708
25. Singh S, Meena A, Luqman S, Meena A. Acacetin and pinostrobin as a promising inhibitor of cancer-associated protein kinases. *Food Chem Toxicol*. 2021;151:112091. doi:10.1016/j.fct.2021.112091
26. Wei Y, Yuan P, Zhang Q, et al. Acacetin improves endothelial dysfunction and aortic fibrosis in insulin-resistant SHR rats by estrogen receptors. *Mol Biol Rep*. 2020;47(9):6899–6918. doi:10.1007/s11033-020-05746-3
27. Li GR, Wang HB, Qin GW, et al. Acacetin, a natural flavone, selectively inhibits human atrial repolarization potassium currents and prevents atrial fibrillation in dogs. *Circulation*. 2008;117(19):2449–2457. doi:10.1161/CIRCULATIONAHA.108.769554
28. Liu H, Yang L, Wu HJ, et al. Water-soluble acacetin prodrug confers significant cardioprotection against ischemia/reperfusion injury. *Sci Rep*. 2016;6(1):36435. doi:10.1038/srep36435
29. Wu WY, Li YD, Cui YK, et al. The natural flavone acacetin confers cardiomyocyte protection against hypoxia/reoxygenation injury via AMPK-mediated activation of Nrf2 signaling pathway. *Front Pharmacol*. 2018;9:497. doi:10.3389/fphar.2018.00497
30. Wu W, Cui Y, Hong Y, et al. Doxorubicin cardiomyopathy is ameliorated by acacetin via Sirt1-mediated activation of AMPK/Nrf2 signal molecules. *J Cell Mol Med*. 2020;24(20):12141–12153. doi:10.1111/jcmm.15859
31. Wu Y, Song F, Li Y, et al. Acacetin exerts antioxidant potential against atherosclerosis through Nrf2 pathway in apoE$^{-/-}$ mice. *J Cell Mol Med*. 2021;25(1):521–534. doi:10.1111/jcmm.16106
32. Song F, Mao YJ, Hu Y, et al. Acacetin attenuates diabetes-induced cardiomyopathy by inhibiting oxidative stress and energy metabolism via PPAR-α/AMPK pathway. *Eur J Pharmacol*. 2022;922:174916. doi:10.1016/j.ejphar.2022.174916
33. Tanigawa N, Hagiwara M, Tada H, et al. Acacetin inhibits expression of E-selectin on endothelial cells through regulation of the MAP kinase signaling pathway and activation of NF-κB. *Immunopharmacol Immunotoxicol*. 2013;35(4):471–477. doi:10.3109/08923973.2013.811596
34. Pan MH, Lai CS, Wang YJ, Ho CT. Acacetin suppressed LPS-induced up-expression of iNOS and COX-2 in murine macrophages and TPA-induced tumor promotion in mice. *Biochem Pharmacol*. 2006;72(10): 1293–1303. doi:10.1016/j.bcp.2006.07.039
35. Bellenger J, Bellenger S, Bataille A, et al. High pancreatic n-3 fatty acids prevent STZ-induced diabetes in Fat-1 mice: Inflammatory pathway inhibition. *Diabetes*. 2011;60(4):1090–1099. doi:10.2337/db10-0901
36. Zhu D, Zhang X, Niu Y, et al. Cichoric acid improved hyperglycaemia and restored muscle injury via activating antioxidant response in MLD-STZ-induced diabetic mice. *Food Chem Toxicol*. 2017;107:138–149. doi:10.1016/j.fct.2017.06.041
37. Zhang H, Yang Y, Wang Y, Wang B, Li R. Renal-protective effect of thalidomide in streptozotocin-induced diabetic rats through anti-inflammatory pathway. *Drug Des Devel Ther*. 2018;12:89–98. doi:10.2147/DDDT.S149298
38. Seedevi P, Ramu Ganesan A, Moovendhan M, et al. Anti-diabetic activity of crude polysaccharide and rhamnose-enriched polysaccharide from *G. lithophila* on streptozotocin (STZ)-induced in Wistar rats. *Sci Rep*. 2020;10(1):556. doi:10.1038/s41598-020-57486-w
39. Laferriere CA, Pang. Erratum: Review of intraperitoneal injection of sodium pentobarbital as a method of euthanasia in laboratory rodents. *J Am Assoc Lab Animal*. 2024;63(3):343. doi:10.30802/AALAS-JAALAS-19-000081
40. Kumar V, Sharma K, Ahmed B, Al-Abbasi FA, Anwar F, Verma A. Deconvoluting the dual hypoglycemic effect of wedelolactone isolated from *Wedelia calendulacea*: Investigation via experimental validation and molecular docking. *RSC Adv*. 2018;8(32):18180–18196. doi:10.1039/C7RA12568B
41. Shiravi A, Jalili C, Vaezi G, Ghanbari A, Alvani A. Acacetin attenuates renal damage-induced by ischemia-reperfusion with declining apoptosis and oxidative stress in mice. *Int J Prev Med*. 2020;11(1):22. doi:10.4103/ijpvm.IJPVM_512_18
42. Wang J, Xue Z, Lin J, et al. Proline improves cardiac remodeling following myocardial infarction and attenuates cardiomyocyte apoptosis via redox regulation. *Biochem Pharmacol*. 2020;178:114065. doi:10.1016/j.bcp.2020.114065
43. Kanarek N, London N, Schueler-Furman O, Ben-Neriah Y. Ubiquitination and degradation of the inhibitors of NF-B. *Cold Spring Harb Perspect Biol*. 2010;2(2):a000166. doi:10.1101/cshperspect.a000166

Eupatorin modulates BCPAP in thyroid cancer cell proliferation via suppressing the NF-κB/P13K/AKT signaling pathways

Weiqi Song[1,A,B,D], Rongyue Yao[2,A–C], Annamalai Vijayalakshmi[3,A,B,D], Yuan An[1,A–C,F]

[1] Department of Head and Neck Oncology, Shaanxi Provincial Cancer Hospital Affiliated to Xi'an Jiaotong University, China
[2] School of Ophthalmology & Optometry (School of Biomedical Engineering), Wenzhou Medical University, China
[3] Department of Biochemistry, Rabiammal Ahamed Maideen College for Women, Thiruvarur, India

A – research concept and design; B – collection and/or assembly of data; C – data analysis and interpretation;
D – writing the article; E – critical revision of the article; F – final approval of the article

Advances in Clinical and Experimental Medicine, ISSN 1899–5276 (print), ISSN 2451–2680 (online) *Adv Clin Exp Med*. 2025;34(8):1365–1374

Address for correspondence
Yuan An
E-mail: 15389233663m@sina.cn

Funding sources
None declared

Conflict of interest
None declared

Received on March 16, 2024
Reviewed on June 21, 2024
Accepted on July 24, 2024

Published online on January 3, 2025

Abstract

Background. Thyroid carcinoma (TC), the most prevalent endocrine cancer worldwide, has become progressively more common, especially in women. Most TCs are epithelial-derived differentiated TCs, specifically papillary thyroid cancer (PTC). Although there are many therapeutic drugs available, curing TC is a difficult task.

Objectives. A flavone called eupatorin (EUP) obtained from herbs can prevent the growth of many types of cancerous cells. Nonetheless, the mechanisms of EUP's actions against PTC are still unknown.

Materials and methods. The goal of our work was to evaluate the mechanisms of EUP (20 and 30 μM/mL) and examine its antiproliferative and apoptotic effects on human PTC cells BCPAP. The MTT test; dual acridine orange/ethidium bromide (AO/EB), rhodamine-123 (Rh-123), and 4′,6-diamidino-2-phenylindole (DAPI) staining; adherence assays; and western blot analyses were used to evaluate the antiproliferative and apoptotic properties of EUP on BCPAP cells.

Results. Our research showed that the quantity-dependent administration of EUP inhibited the proliferation of BCPAP cells, which in turn caused apoptosis through the increase in caspase-9 and p53 protein expression and the reduction of proliferating cell nuclear antigen (PCNA) levels. Additionally, when P13K/AKT signaling is inhibited by nuclear factor kappa B (NF-κB), EUP reduces inflammation and BCPAP proliferation.

Conclusions. By blocking the NF-κB and P13K/AKT pathways, EUP can reduce the growth of BCPAP cells and promote cell death.

Key words: thyroid cancer, papillary thyroid cancer, apoptosis, P13K/AKT signaling, eupatorin

Cite as
Song W, Yao R, Vijayalakshmi A, An Y. Eupatorin modulates BCPAP in thyroid cancer cell proliferation via suppressing the NF-κB/P13K/AKT signaling pathways. *Adv Clin Exp Med*. 2025;34(8):1365–1374. doi:10.17219/acem/191595

DOI
10.17219/acem/191595

Copyright
Copyright by Author(s)
This is an article distributed under the terms of the Creative Commons Attribution 3.0 Unported (CC BY 3.0) (https://creativecommons.org/licenses/by/3.0/)

Background

Thyroid cancer (TC) is a fatal tumor of the endocrine system, and its prevalence has been progressively increasing over the past 30 years.[1,2] The major etiology of TC is environmental factors, radiation exposure, gender, family history, and lifestyle choices.[3] A recent study documented that intense living environments accompanied by working with gravitational variations may impair the function of the thyroid and affect various carcinomas.[4] The frequently occurring form of malignant TC is papillary thyroid carcinoma (PTC), which accounts for 80–85% of all human TCs.[5] Currently, the available treatments of TC rely on radioiodine ablation, suppression of thyroid-stimulating hormone and surgery.[6] These remedies are generally effective for the majority of TCs. However, advanced TC, including recurrent, 131I-refractory and metastatic or medullary TCs, remains a therapeutic challenge. Therefore, it is crucial to develop an effective therapeutic agent for these patients.

Herbal-based natural bioactive components have anticancer efficacy in numerous tumors, which can also be combined with traditional chemotherapy medications to enhance their anticancer properties.[7,8] Eupatorin (EUP) is a natural flavone isolated from several herbal plants.[9] Eupatorin has been established as an antiproliferative agent in numerous carcinoma cells, including gastric neoplasms, cervical adenocarcinoma, breast neoplasm cells, melanoma, and colon cancer cells.[10–12] Eupatorin activates apoptosis and concurrently inhibits the angiogenesis, invasion and migration of MCF-7 and MDAMB-231 cells by inactivation of the p-Akt pathway.[13] It has been documented that co-administring EUP with DOX in colon cancer triggered mitochondrial-facilitated apoptosis with an elevated ratio of Bax/Bcl-2, increased levels of caspase-3 and increased PARP cleavage.[14] An earlier study recognized that EUP halts the cell cycle at the G2–M stage in leukemia cells and prompts apoptosis by the stimulation of numerous caspases, discharge of cytochrome-c (cyt-c), and subsequently PARP cleavage through the instigation of the MAPK signaling. It was proposed that EUP-induced leukemia cell apoptosis is facilitated by the extrinsic and intrinsic apoptotic pathways.[15] Currently, no report is available on the apoptotic and cytotoxic efficacy of EUP on PTC cells.

Apoptosis is a specific kind of programmed cell death, which is characterized by variations in cellular morphology and nuclear alterations that commonly occur without inflammation. The crucial events that occur in the development of tumor progression are the inhibition of apoptotic cell death and organized de-restricted cellular propagation.[16] Malignant cells exhibit numerous systems that allow them to evade apoptosis triggered by chemotherapeutic medications, including p53 mutations, which is an important status.[17] Enhancing responses might be beneficially achieved by either growing a p53-self-regulating, pro-apoptotic target or altering the appearance and transcriptional function of p53 to chemotherapy agents.[18] Nuclear factor kappa-light-chain-enhancer of activated B cells (NF-κB) dynamically functions in many cancer cells and controls a sequence of essential proceedings in cancer progression including cell proliferation, cell survival, invasion, and angiogenesis.[19] The triggered NF-κB signalosome complex primes downstream signaling, which stimulates the transcription of proinflammatory intermediaries, including cyclooxygenase-2 (COX-2), inducible nitric oxide synthase (iNOS), interleukin 6 (IL-6), and tumor necrosis factor alpha (TNF-α).[20] These mediators triggered various immune reactions that are critical for carcinoma initiation in tissues.[21] For cell existence, NF-κB generally represses cell death by enhancing the transcription of anti-apoptotic genes encoding proteins such as Bcl-2 and Bcl-XL.[22] Hence, inhibition of NF-κB may be efficient in triggering apoptosis of neoplasms. The PI3K/Akt signaling has been shown to play a crucial role in cell proliferation, cell adhesion, invasion, migration, and apoptosis in diverse human cancers. The overexpression of the PI3K/AKT pathway appears to be linked to malignancies and poor prognosis in numerous human carcinomas.[23] Also, the PI3K/AKT pathway has been determined to be a characteristic of follicular carcinomas and ATCs, but it is less prevalent in PTC.[24] Furthermore, targeting the PI3K/AKT pathway has been supported to be an effective medicinal approach for treating both solid human tumors and TC.[25,26]

Objectives

In the current research, we inspected the efficacy of EUP on apoptosis and the inhibition of PTC cell BCPAP proliferation and explored the molecular mechanism of the anticancer effects through an analysis of the regulation of NF-κB and P13K/AKT pathways.

Materials and methods

Chemicals

Eupatorin (purity: ≥98%), antibiotics, phosphate-buffered saline (PBS), RPMI 1640 medium, fetal bovine serum (FBS), MTT (3-(4,5-dimethylthiazol-2-yl)-2,5-diphenyltetrazolium bromide) assay, acridine orange/ethidium bromide (AO/EB), dimethyl sulfoxide (DMSO), Rh-123, and DAPI(4′,6-diamidino-2-phenylindole) were purchased from Gibco (Waltham, USA). The primary and secondary antibodies were bought from Abcam (Cambridge, UK).

Cell culture

BCPAP human PTC cells were bought from the Peking Union Cell Resource Centre (Beijing, China). Cultured the BCPAP cells using RPMI 1640 media along with FBS (10%), penicillin/streptomycin antibiotics (1%) at 37°C, in a 5% CO_2 environment, and humidified air below 95%.

Cell proliferation assay

Human BCPAP cell proliferation was performed according to MTT assay.[27] The BCPAP cells were disseminated into 96 wells and cultured at 37°C using a 5% CO_2 wet incubator. After an overnight incubation period, the BCPAP cells were cultured for 24 h with various quantities of EUP (5–50 μM/mL). Later, the sustained BCPAP human PTC cells underwent MTT (10 μL) testing and maintained for an extra 4 h to allow MTT conversion into insoluble crystals of formazan. The DMSO (150 μL) was then used to dissolve the resultant insoluble crystals. The estimated viability was performed at 490 nm using Agilent BioTek Synergy Neo2 hybrid multimode reader (BioTek Instruments, Colmar, France). Cell cytotoxicity was determined as the ratio of viability compared to control DMSO (150 μL) cells (100%). The value of IC50 was obtained using the below equation:

$$\text{cell viability inhibition (\%)} = (\text{control OD} - \text{test OD}) \times 100,$$

where OD is optical density.

BCPAP cell apoptosis was evaluated by AO/EB staining

Human BCPAP cell morphology of apoptosis was assessed with AO/EB staining.[28] BCPAP cells were exposed to 20 and 30 μM/mL of EUP and incubated for 24 h. All groups were administered AO/EB dye (100 μg/mL of each dye) and preserved for 30 min at room temperature under dark conditions. The remaining unbound dye was removed with PBS washing and viewed through a fluorescence microscope (Nikon Eclipse TS100; Nikon Corp., Tokyo, Japan).

Assessment of BCPAP cell apoptosis

Apoptosis is a functional form of cell death that is distinguished by significant DNA fragmentation and physical features.[29] Human BCPAP cells were dispersed in well plates and kept in a humidified CO_2 (5%) incubator at 37°C for 24 h. Various amounts (control, 20 μM/mL and 30 μM/mL) of EUP were administered to the cells. Subsequent control and treated cells were washed twice with PBS, fixed by paraformaldehyde (4%), rinsed, DAPI-stained, and then incubated for 20 min. Then, DAPI-treated BCPAP cells were exposed to staining with Rh-123 and incubated at 37°C for 30 min. The stained cells were methanol washed 2-fold to eliminate extra dyes and immersed with PBS, and the mitochondrial membrane potential (MMP) variant was viewed using a fluorescence microscope (Nikon Eclipse TS100; Nikon Corp.).

Assay for cell adhesion analysis

Human BCPAP cells were immersed in RPMI 1640 culture media and pre-treated with EUP (control, 20 μM/mL and 30 μM/mL) and sowed in a 24-well fibronectin-coated (500 μL/well) plate. The whole well plate was preserved at 37°C for 60–100 min; then, non-adherent cells were removed and taken apart evenly twice with PBS cleaning. Next, 94% paraformaldehyde fixation in each well was kept at 4°C incubation for 5 min. After incubation, TB (0.4%) staining of the adherent cells was counted using fluorescence microscopy (Nikon Eclipse TS100; Nikon Corp.).[29]

Western blotting assay

Untreated BCPAP cells and 20 and 30 μM/mL of EUP-treated human BCPAP cells that had been cultured for 24 hours were used to create the cellular lysates for Western blot analysis. To guarantee protease inhibitory activity, lysis buffer was employed in extremely cold temperatures. Briefly, the entire protein was estimated by consuming the protein BCA Assay Kit (Pierce Chemical Co, Rockford, USA). Subsequently, quantified proteins were dispersed electrophoretically and moved to a polyvinylidene difluoride (PVDF) film. It was blocked by using a probe at room temperature for 1 h using the primary antibodies (PCNA, P53, caspase-3, TNF-α, NF-κB, COX-2, iNOS, IL-6, PI3K, p-PI3K, Akt, and p-Akt) in 1:1,000 dilutions and kept at 4°C overnight. Then, horseradish peroxidase (HRP)-conjugated secondary antibodies were administered. Afterward, the protein bands were stained and imagined for protein identification, quantifying the protein bands through densitometry with ImageJ software (National Institutes of Health (NIH), Bethesda, USA) and homogeneous to β-actin expression.

Statistical analyses

The data from each group were analyzed statistically using GraphPad Prism v. 8.0.2 (GraphPad Software, San Diego, USA) and IBM SPSS software v. 25 (IBM Corp., Armonk, USA). The measurement data were reported as medians (min–max). The normality of the distribution was tested using the Kolmogorov–Smirnov test. Since all the distributions were normal, the Brown–Forsythe test was used to establish the equality of variances, and then significant differences between multiple groups were analyzed using the Kruskal–Wallis test, and Dunn's post hoc test was used for multiple comparisons. If the p-value was <0.05, the data divergence was statistically notable. All tests in this study were bilateral tests.

Results

The Results of the Kruskal–Wallis test and Dunn's post hoc test are presented in Table 1 and Table 2.

Antiproliferative efficacy of EUP on BCPAP cells

The antiproliferative assay of BCPAP cells was estimated using the MTT experiment in a dose-dependent manner

Table 1. Comparison of the groups regardig MTT assay results

Variables	Control	5 µM	10 µM	20 µM	30 µM	40 µM	50 µM	Test value (H)**	p-value*
MTT	100.03 (90.98–108.98)	87.34 (79.44–95.16)	73.56 (66.91–80.15)	60.74 (55.25–66.17)	51.77 (47.0–56.41)	39.19 (35.64–42.70)	26.21 (23.84–28.56)	39.53	<0.001

Data were present as median (min–max); *p-value was generated from Kruskal–Wallis test with Dunn's post hoc test; **degrees of freedom (df) = 5.

Table 2. Groups compared with each other regarding other parameters

Variables	Control	20 µM	30 µM	Test value (H)**	p-value*
PCNA	1.00 (0.91 to 1.09)	0.74 (0.67 to 0.81)	0.49 (0.45 to 0.53)	15.23	<0.001
P53	1.00 (0.91 to 1.09)	1.25 (1.14 to 1.36)	2.10 (1.91 to 2.29)	15.20	<0.001
Caspase-3	1.00 (0.91 to 1.09)	1.02 (0.93 to 1.11)	1.97 (1.79 to 2.15)	11.82	0.003
TNF-α	1.00 (0.91 to 1.09)	0.69 (0.63 to 0.75)	0.46 (0.42 to 0.50)	15.26	<0.001
NF-κB	1.00 (0.91 to 1.09)	0.58 (0.53 to 0.63)	0.41 (0.37 to 0.45)	15.23	<0.001
COX-2	1.00 (0.91 to 1.09)	0.60 (0.55 to 0.65)	0.37 (0.34 to 0.40)	15.26	<0.001
iNOS	1.00 (0.91 to 1.09)	0.54 (0.49 to 0.59)	0.39 (0.35 to 0.43)	15.26	<0.001
IL-6	1.00 (0.91 to 1.09)	0.75 (0.68 to 0.82)	0.48 (0.44 to 0.52)	15.26	<0.001
PI3K/p-PI3K	1.00 (0.91 to 1.09)	0.81 (0.74 to 0.88)	0.53 (0.48 to 0.58)	15.22	<0.001
AKT/p-AKT	1.00 (0.91 to 1.09)	0.76 (0.69 to 0.83)	0.47 (0.43 to 0.51)	15.22	<0.001

Data was present as median (min and max). * p-value was generated from Kruskal–Wallis test with Dunn's post hoc test. ** degrees of freedom (df) is equal to 2. TNF-α – tumor necrosis factor alpha; PCNA – proliferating cell nuclear antigen; NF-κB – nuclear factor kappa-light-chain-enhancer of activated B cells; COX-2 – cyclooxygenase-2; iNOS – inducible nitric oxide synthase; IL-6 – interleukin 6.

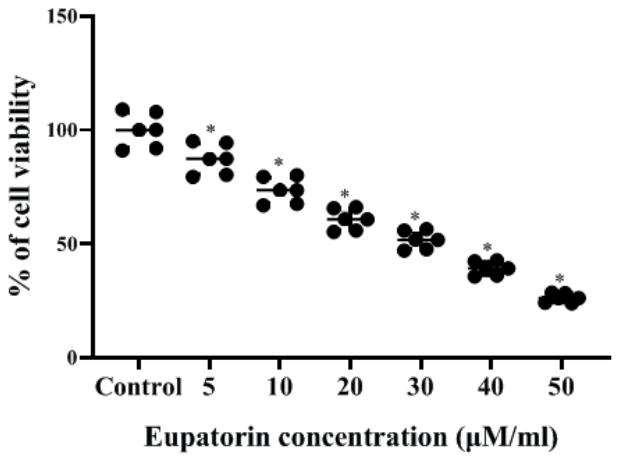


Fig. 1. Eupatorin inhibits human BCPAP cell proliferation. BCPAP human papillary thyroid cancer (PTC) cells were administered with different quantities (5–50 µM/mL) of flavone called eupatorin (EUP) for 1 day. Cell cytotoxicity was estimated using the MTT test. Data were displayed as medians (min–max), and the statistical significance was measured as *p < 0.05 against controls

(5–50 µM/mL) of EUP. Results showed that EUP diminished cell proliferation through its antiproliferative and cytotoxic deeds on BCPAP cells in a dosage-dependent way. Administration of EUP at a quantity less than 15 µM did not considerably amend BCPAP cell proliferation. However, moderate dosages of EUP (20 and 30 µM/mL) significantly decreased ($p < 0.05$) BCPAP cell viability compared to controls. A high dose of EUP (50 µM) impaired the BCPAP cells. After the MTT test, the IC_{50} assessment of EUP was 30 µM for BCPAP cells. The inhibitory concentration values of 20 and 30 µM/mL of EUP have been obtained for additional examination (Table 1, Fig. 1).

Effect of EUP on BCPAP cell apoptosis presented using the AO/EB dual method

Human BCPAP cell apoptosis was envisioned as distinct aberrations in morphology attributed to the AO/EB staining method. Untreated BCPAP control cells were visible as consistently live green-stained cells. Administration of EUP (control, 20 µM/mL and 30 µM/mL) in the BCPAP cells caused significant ($p < 0.05$) cell apoptosis in a quantity-reliant manner. Eupatorin (20 µM) treatment revealed primary apoptotic cells comprised of condensation of chromatin and membrane eruption, depicted as dots of light greenish and yellow. Supplementation of EUP (30 µM) exposed late apoptotic cells presenting an orange color because of ethidium bromide co-stain (Fig. 2).

Effect of EUP on the BCPAP cells, MMP loss and nuclear morphology

The effect of EUP on human BCPAP cells' morphological features, membrane integrity, nuclear condensation, nuclear fragmentation, and MMP were evaluated. The technique of DAPI staining can be utilized to identify DNA fragmentation in apoptotic bodies. Supplementation of the EUP (20 and 30 µM/mL) to the BCPAP cells triggers apoptosis, developing nuclear condensation and disintegration of nuclear bodies compared to controls. This outcome exposed the antiproliferative efficacy

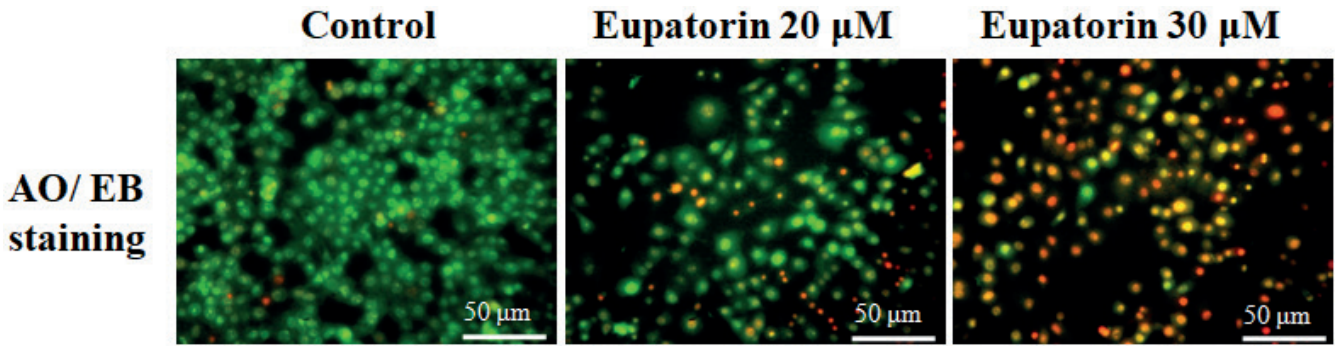


Fig. 2. Eupatorin-activated human BCPAP cell apoptosis. Scale bar = 50 µm. Human BCPAP papillary thyroid cancer (PTC) cells with 20 and 30 µM/mL of flavone called eupatorin (EUP) for 1 day. The apoptosis was assessed with the dual staining of acridine orange/ethidium bromide (AO/EB) and observed under a fluorescence microscope

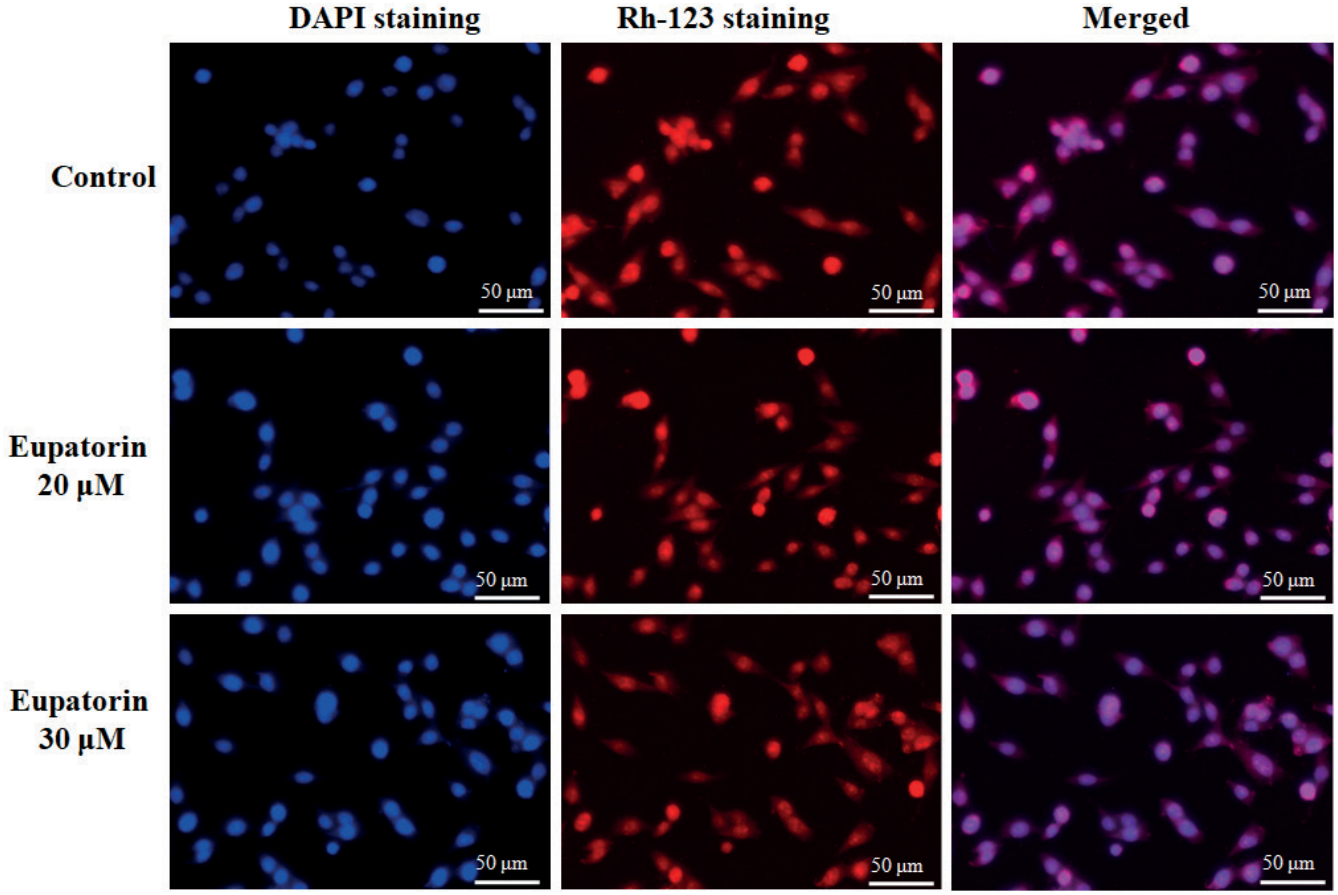


Fig. 3. Eupatorin induces apoptosis in human BCPAP cells. Scale bar = 50 µm. BCPAP human papillary thyroid cancer (PTC) cells were administered a control, 20, and 30 µM/mL of flavone called eupatorin (EUP) for 1 day. Cell death was determined through the application of DAPI (4',6-diamidino-2-phenylindole) and Rh-123 staining. Image of DAPI (blue) and Rh-123 (red) staining combined (pink) on the EUP preserved BCPAP cells and images photographed using a fluorescence microscope

of EUP on BCPAP cells in a quantity-dependent way. The MMP is permeable to ions and yields a promising electrical abnormality. Fluorescence microscopic images showed the accumulation of Rh-123 fluorescence dye from orange red to green compared in vehicle control and the accumulation found to be decreased in EUP treated BCPAP cells at various concentrations (20 µM/mL and 30 µM/mL). Rh-123 staining exhibited mitochondrial strength in apoptotic cell death with an intensified MMP. The untreated BCPAP exhibited higher fluorescence intensity due to the Rh-123 red accumulation. The fluorescence mass of Rh-123 was reduced when EUP (20 and 30 µM) was administered in a concentration-dependent way. These outcomes show that EUP-administered human BCPAP cells avert the MMP, thus increasing the mitochondrial-mediated apoptosis (Fig. 3).

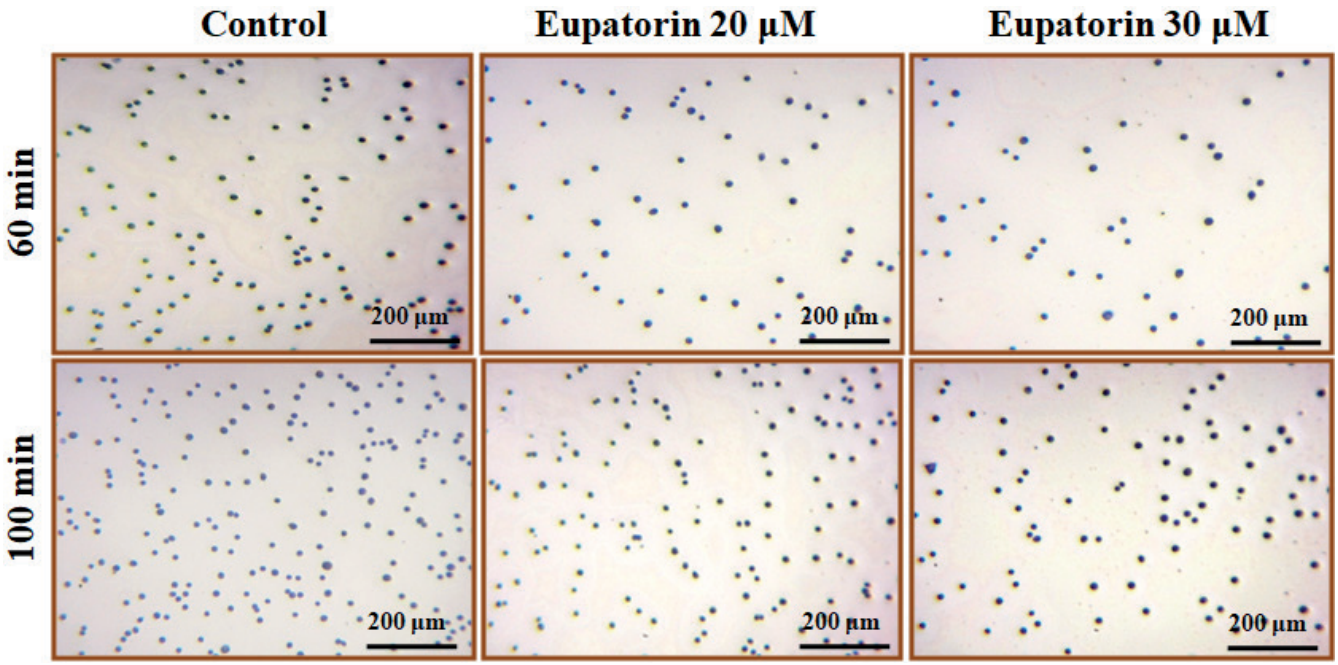


Fig. 4. Eupatorin reduced BCPAP cell adherence. Scale bar = 200 µm. Human BCPAP cell adherence force was assessed with an adherence assay after 60 and 100 min. The attached cells were fixed, stained and counted in 10 random fields

Influence of EUP on BCPAP cell adhesion

Extracellular matrix (ECM) and BCPAP cell adhesion played a substantial action in initiating cancer cell metastasis (Fig. 4). BCPAP cell adhesion and cell signaling are controlled by the ECM protein integrin. This cell adhesion assay analyzes the action of EUP silencing on BCPAP cell adhesion to the proteins present in the ECM. When EUP inhibition was administered for 60 or 100 min, the number of BCPAP adherent cells decreased in comparison to controls. The modulatory influences of cell adherence generated with EUP silencing might provide the suppression of cancer cell propagation and metastasis.

Effect of EUP on PCNA, caspase-3 and p53 protein levels in BCPAP cells

Administration of EUP (control, 20 µM/mL and 30 µM/mL) on BCPAP cells presented an extreme ($p < 0.05$) repression of PCNA while upregulating p53 and caspase-3 protein expression in a quantity-reliant way. These findings specified that EUP inhibited BCPAP cells during cell proliferation and elevated apoptosis via these signaling pathways (Table 2, Fig. 5).

Influence of EUP on apoptotic protein expression levels

Human BCPAP cells treated with EUP (control, 20 µM/mL and 30 µM/mL) attenuated TNF-α, NF-κB, COX-2, iNOS, and IL-6 protein expression. Our findings documented the anti-inflammatory action of EUP on human PTC cells BCPAP in a dose-dependent manner (Table 2, Fig. 6).

EUP attenuates the signaling of the P13K/AKT pathway

Our results show that PI3K/AKT signaling is involved in EUP-associated prevention of BCPAP cell metastasis. Our outcomes revealed that PI3K/AKT protein level expressions were remarkably ($p < 0.05$) alleviated in the BCPAP cancer cells treated with EUP (control, 20 µM/mL and 30 µM/mL) in a concentration-dependent way. These findings indicated that EUP triggered BCPAP cancer cell apoptosis through the suppression of the PI3K/AKT activation in the cell survival pathway (Table 2, Fig. 7).

Discussion

Thyroid carcinoma is an endocrine malignancy, of which PTC accounts for nearly 80% of all TCs that have been well differentiated by the variation of distinct protein kinases.[2,5] Phytochemicals are substances of plant origin with biological activity, which have beneficial effects on human health.[30] Two studies proposed that flavones and flavonoids exert powerful actions of anti-proliferation on TC cells and suggested it as a healing agent for controlling TC.[7,8] Other studies reported that EUP has antiproliferative and apoptotic effects in numerous tumor cells.[10–12] However, the anticancer potential of EUP and its corresponding apoptotic latent mechanisms of TC are still unknown. In this investigation, we proved the repressive

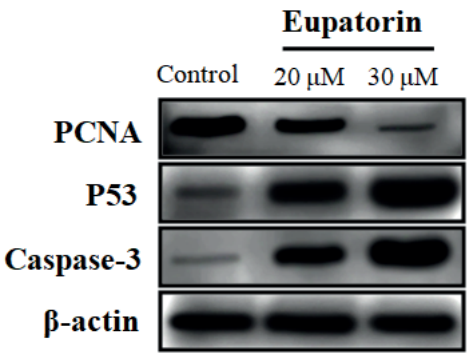
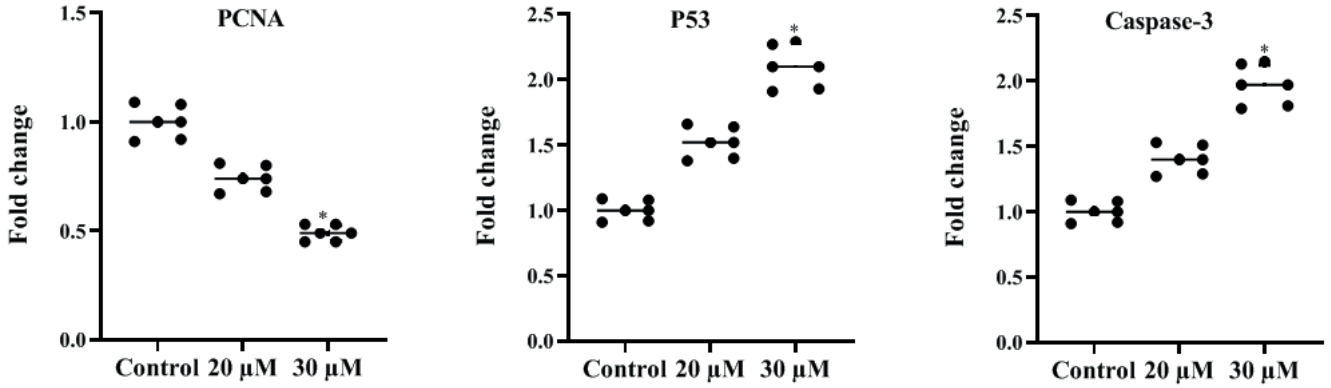
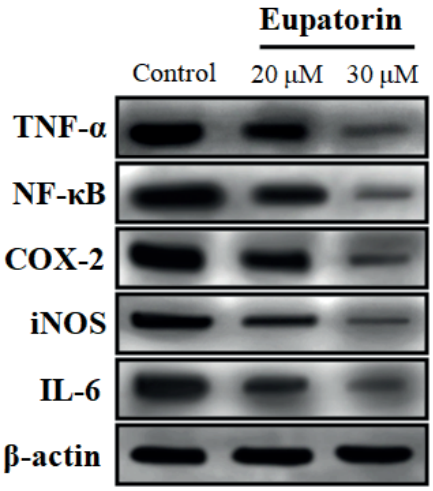


Fig. 5. The effect of flavone called eupatorin (EUP) on the protein expression levels of PCNA, p53 and caspase-3. BCPAP human papillary thyroid cancer (PTC) cells were tested with control, 20, and 30 μM/mL of EUP for 1 day. PCNA, p53 and caspase-mediated mitochondrial apoptosis cascade protein caspase-3 were measured using western blot. The depicted graph shows the relative protein expression using immunoblot. Data were displayed as medians (min–max), and the statistical significance was measured as *p < 0.05 against the control





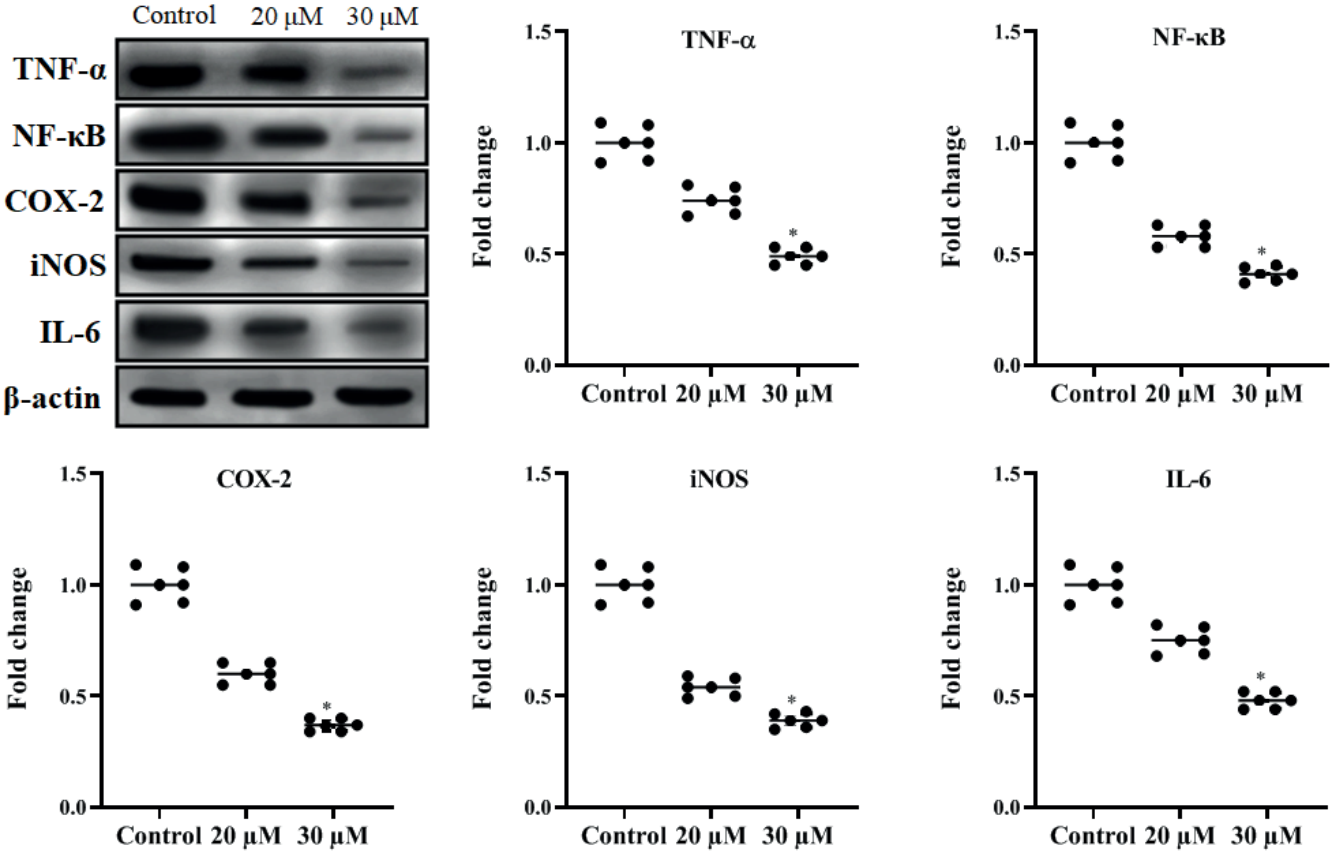


Fig. 6. Eupatorin alleviates nuclear factor kappa-light-chain-enhancer of activated B cells (NF-κB) mediated inflammatory pathways. BCPAP human papillary thyroid cancer (PTC) cells were administered a control, 20, and 30 μM/mL of flavone called eupatorin (EUP) for 1 day. The protein expression of proinflammatory mediators such as cyclooxygenase-2 (COX-2), inducible nitric oxide synthase (iNOS), interleukin-6 (IL-6), tumor necrosis factor alpha (TNF-α), and NF-κB were measured using western blot. The graph shows the relative protein expression of fold changes using immunoblot. Data are presented as medians (min–max), and the statistical significance was measured as *p < 0.05 against controls

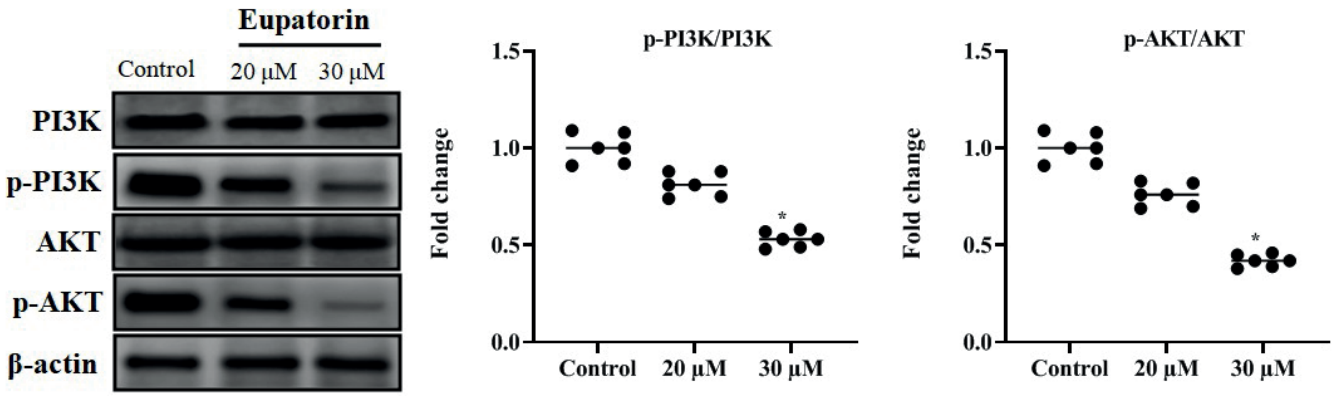


Fig. 7. Eupatorin repressed the PI3K/AKT signaling pathway. BCPAP human papillary thyroid cancer (PTC) cells were administered a control, 20, and 30 μM/mL of flavone called eupatorin (EUP) for 1 day. The protein expression of P13K, p-P13K, AKT, and p-AKT were measured with western blot. The graph shows the relative protein expression of fold changes using immunoblot. Data are presented as medians (min–max), and the statistical significance was measured as *$p < 0.05$ against the control

influence of cell growth displayed by apoptosis at various concentrations of EUP on BCPAP malignant cells. This research also explored the EUP activity on the regulation of NF-κB and P13K/AKT pathways in BCPAP human PTC cells.

One of the main ways that anti-tumor drugs work is by using their cytotoxic properties to stop tumor cells from proliferating. Cytotoxicity is distinguished as a cell necrotizing function of a compound relieved from the pathways of cell death.[31] The MTT assay is an appropriate method for testing innovative bioactive compounds to establish cytotoxicity on malignant cells over a short duration.[32] The MTT analysis implied that EUP reduced the BCPAP cell's growth in a quantity-dependent mode. Earlier studies illustrated that EUP inhibits many tumor cell proliferation involving gastric cancer, cervical adenocarcinoma cells, breast neoplasm cells, melanoma, and colon carcinoma.[10–12] It has been reported that EUP inhibits cancer cell viability and concurrently curbs the invasion, migration and angiogenesis of MCF-7 and MDAMB-231 mammary carcinoma cells through the attenuation of the p-Akt signaling.[13] In our study, EUP exhibited substantial inhibitory growth potential with IC50 values of 20 μM, which is within the range value stated for many flavonoids. As per our data, this is the primary report directing that EUP (20 and 30 μM/mL) greatly averts BCPAP cell proliferation in a dosage-dependent way.

Apoptosis is the main type of automated cell death that has a profound action in eliminating peculiar cells, which can be morphologically depicted by cell shrinkage, fragmentation of DNA and nuclear bodies, and, accordingly, being swallowed by macrophages.[16] A typical anti-tumor agent should target cancer cells without affecting normal cells. Hence, numerous anti-tumor agents rely on commencing apoptosis to generate malignant cell death.[17] An earlier study has investigated that co-administration of EUP with DOX on colon cancer triggered mitochondrial-facilitated apoptosis with an elevated ratio of Bax/Bcl-2, level of caspase-3, and poly(ADP-ribose) polymerase (PARP) cleavage.[14] It has been recognized that EUP halts the G2–M stage of the cell cycle in leukemia cells and prompts apoptosis in the stimulation of numerous caspases, cytochrome-c (cyto-c) discharge and PARP cleavage over the activation of the MAPK pathway. It has been suggested that EUP-induced leukemia cell apoptosis is facilitated by both extrinsic and intrinsic apoptotic pathways.[15]

Cell proliferation is involved in a multistep process of typical cell development, and unrestrained cell growth is the main hallmark of tumors.[33] A known proliferative marker, PCNA, shows a significant function in DNA replication, repair, cell cycle regulation, chromatin remodeling, and epigenetic conservation.[34] Proliferating cell nuclear antigen overexpression was observed in the genetic outcome of numerous tumors.[35] We showed that EUP can reduce the PCNA protein expression in human PTC cells BCPAP in a dose-dependent manner. The p53 wild type is efficient in initiating cell apoptosis under stress conditions.[17] Conversely, inactivation, mutation or depletion of the p53 gene leads to the failure to respond to radiotherapy and chemotherapy in several tumors.[17,18] There is evidence to support the idea that cancer cells bear the responsibility for apoptotic cell death when p53 function is restored.[21] In the current study, p53 and caspase-3 were upregulated by EUP in BCPAP human PTC cells. Anti-tumor medication-facilitated apoptosis in tumor cells is mostly regulated by intrinsic (mitochondrial) or extrinsic (death receptor) pathways through the activation of caspases. Caspase-3 triggers the mitochondrial-mediated intrinsic apoptosis, as observed in this work, which was enabled by the morphological examination of fluorescence microscopy images using DAPI, Rh-123 and AO/EB staining. These results indicate that EUP might be effective for the suppression and remedy for TC.

Chemotherapeutic agents targeting a reduction in pro-inflammatory mediators to explore novel strategies to avert the inflammatory disorders involved with malignant tumors.[19] The hyperactivation of NF-κB has a critical role in cancer pathogenesis, letting malignant cells persist

and offering a favorable target for the improvement of chemotherapeutic drugs.[19,20] During inflammation, several cytokines such as iNOS, IL-6, TNF-α, and COX-2, which are hyper-expressed in tumor cells, contribute to the malignant pathogenesis.[20,21] However, a stimulated NF-κB signaling pathway creates high levels of nitric oxide (NO) and prostaglandin E2 (PGE2) for an extended period, which influences tumor progression and inflammation. In this study, EUP administered to the BCPAP cells effectively reduced pro-inflammatory mediators, including iNOS, IL-6, TNF-α, NF-κB, and COX-2 protein expression measured using western blot examination, which specifies that EUP may deactivate NF-κB signaling in BCPAP cells.

Adhesion of cancer cells to the ECM has a crucial function in metastasis development.[36] Inhibiting and reducing the quantity of adhering BCPAP cells, the EUP modulates cell adhesion and represses metastasis, which is in line with our results from the apoptosis analysis. The number of adherent cells was noticeably reduced after BCPAP cell suppression of cell metastasis. The PI3K/Akt signaling pathway has been demonstrated to exert a vital function in cellular proliferation, cell adhesion, migration, invasion, metastasis, and apoptosis in several human cancers.[23] The PI3K-Akt pathway is directly linked to tumor cell proliferation.[37] The overexpression of the PI3K/AKT pathway figures to be linked to malignancies and a poor prognosis in numerous human carcinomas.[23] Furthermore, targeting the PI3K/AKT pathway has been confirmed to be effective for treating both human solid tumors and TC.[25,26] For instance, the antioxidant rutin has an antiproliferative effect on hepatic carcinoma by regulating the PI3K/Akt signaling pathway.[38] Another bioactive compound, quercetin, can modulate the PI3K/Akt pathway, thus showing anti-tumor efficacy on liver, gastric and oral carcinomas.[39,40] Likewise, phloretin can induce apoptosis in prostate cancer and mammary carcinoma cells through the PI3K/Akt signaling pathway.[41,42] In this study, EUP treatment reduces the PI3K/Akt and NF-κB pathways related to PTC cells that interrupt their communication, favoring BCPAP cell proliferation. Hence, EUP exerts its antiproliferative, anti-metastatic and apoptotic activity through the NF-κB and PI3K/Akt signaling pathways.

Limitations

The current study investigated EUP on human PTC cell proliferation, apoptotic and inflammatory pathways in a cancer cell line model. An in vivo experimental study in a mouse or rat model is preferred to analyze the molecular mechanism and correct route signaling.

Conclusions

Our report explores the efficacy of EUP against BCPAP human PTC cells and has elucidated its molecular actions involving cell proliferation, inflammation, cell adhesion, and apoptosis. It was noticed that EUP stimulated mitochondrial-facilitated apoptosis and a loss of MMP. The suppression of BCPAP cell proliferation and metastasis occurred in a concentration-dependent mode. Furthermore, it inhibited proliferation, inflammation and metastasis that triggered apoptosis through the NF-κB/COX-2 and PI3k/Akt signaling pathways. Our data show that EUP can inhibit the BCPAP human PTC cells. However, more studies are required on EUP for its clinical use in the therapy for TC patients.

Supplementary data

The supplementary materials are available at https://doi.org/10.5281/zenodo.12683722. The package includes the following files:

Supplementary Fig. 1. Results of Kruskal–Wallis test as presented in Fig. 1.

Supplementary Fig. 2. Results of Kruskal–Wallis test as presented in Fig. 5.

Supplementary Fig. 3. Results of Kruskal–Wallis test as presented in Fig. 6.

Supplementary Fig. 4. Results of Kruskal–Wallis test as presented in Fig. 7.

Data availability

The datasets generated and/or analyzed during the current study are available from the corresponding author on reasonable request.

Consent for publication

Not applicable.

ORCID iDs

Weiqi Song https://orcid.org/0009-0001-0786-304X
Rongyue Yao https://orcid.org/0009-0001-7126-8720
Annamalai Vijayalakshmi https://orcid.org/0000-0002-2436-8956
Yuan An https://orcid.org/0009-0000-4304-1679

References

1. Konturek A, Barczyński M, Stopa M, Nowak W. Trends in prevalence of thyroid cancer over three decades: A retrospective cohort study of 17,526 surgical patients. *World J Surg*. 2016;40(3):538–544. doi:10.1007/s00268-015-3322-z
2. Siegel RL, Miller KD, Wagle NS, Jemal A. Cancer statistics, 2023. *CA Cancer J Clin*. 2023;73(1):17–48. doi:10.3322/caac.21763
3. Liu FC, Lin HT, Lin SF, Kuo CF, Chung TT, Yu HP. Nationwide cohort study on the epidemiology and survival outcomes of thyroid cancer. *Oncotarget*. 2017;8(45):78429–78451. doi:10.18632/oncotarget.19488
4. Albi E, Krüger M, Hemmersbach R, et al. Impact of gravity on thyroid cells. *Int J Mol Sci*. 2017;18(5):972. doi:10.3390/ijms18050972
5. Xing M, Haugen BR, Schlumberger M. Progress in molecular-based management of differentiated thyroid cancer. *Lancet*. 2013;381(9871):1058–1069. doi:10.1016/S0140-6736(13)60109-9
6. Handkiewicz-Junak D, Czarniecka A, Jarząb B. Molecular prognostic markers in papillary and follicular thyroid cancer: Current status and

future directions. *Mol Cell Endocrinol*. 2010;322(1–2):8–28. doi:10.1016/j.mce.2010.01.007
7. Yin SY, Wei WC, Jian FY, Yang NS. Therapeutic applications of herbal medicines for cancer patients. *Evid Based Complement Alternat Med*. 2013;2013:302426. doi:10.1155/2013/302426
8. Ye R, Dai N, He Q, et al. Comprehensive anti-tumor effect of Brusatol through inhibition of cell viability and promotion of apoptosis caused by autophagy via the PI3K/Akt/mTOR pathway in hepatocellular carcinoma. *Biomed Pharmacother*. 2018;105:962–973. doi:10.1016/j.biopha.2018.06.065
9. González-Cortazar M, Salinas-Sánchez DO, Herrera-Ruiz M, et al. Eupatorin and salviandulin-A, with antimicrobial and anti-inflammatory effects from *Salvia iavanduloides* Kunth leaves. *Plants*. 2022;11(13):1739. doi:10.3390/plants11131739
10. Tezuka Y, Stampoulis P, Banskota AH, et al. Constituents of the Vietnamese medicinal plant *Orthosiphon stamineus*. *Chem Pharm Bull (Tokyo)*. 2000;48(11):1711–1719. doi:10.1248/cpb.48.1711
11. Nagao T, Abe F, Kinjo J, Okabe H. Antiproliferative constituents in plants. 10. Flavones from the leaves of *Lantana montevidensis* Briq. and consideration of structure-activity relationship. *Biol Pharm Bull*. 2002;25(7):875–879. doi:10.1248/bpb.25.875
12. Androutsopoulos V, Arroo RR, Hall JF, Surichan S, Potter GA. Antiproliferative and cytostatic effects of the natural product eupatorin on MDA-MB-468 human breast cancer cells due to CYP1-mediated metabolism. *Breast Cancer Res*. 2008;10(3):R39. doi:10.1186/bcr2090
13. Razak NA, Abu N, Ho WY, et al. Cytotoxicity of eupatorin in MCF-7 and MDA-MB-231 human breast cancer cells via cell cycle arrest, anti-angiogenesis and induction of apoptosis. *Sci Rep*. 2019;9(1):1514. doi:10.1038/s41598-018-37796-w
14. Namazi Sarvestani N, Sepehri H, Delphi L, Moridi Farimani M. Eupatorin and salvigenin potentiate doxorubicin-induced apoptosis and cell cycle arrest in HT-29 and SW948 human colon cancer cells. *Asian Pac J Cancer Prev*. 2018;19(1):131–139. doi:10.22034/APJCP.2018.19.1.131
15. Estévez S, Marrero MT, Quintana J, Estévez F. Eupatorin-induced cell death in human leukemia cells is dependent on caspases and activates the mitogen-activated protein kinase pathway. *PLoS One*. 2014;9(11):e112536. doi:10.1371/journal.pone.0112536
16. Evan GI, Vousden KH. Proliferation, cell cycle and apoptosis in cancer. *Nature*. 2001;411(6835):342–348. doi:10.1038/35077213
17. Bykov VJ, Wiman KG. Novel cancer therapy by reactivation of the p53 apoptosis pathway. *Ann Med*. 2003;35(7):458–465. doi:10.1080/07853890310017152
18. Amundson SA, Myers TG, Fornace AJ. Roles for p53 in growth arrest and apoptosis: Putting on the brakes after genotoxic stress. *Oncogene*. 1998;17(25):3287–3299. doi:10.1038/sj.onc.1202576
19. Aggarwal BB. Nuclear factor-κB. *Cancer Cell*. 2004;6(3):203–208. doi:10.1016/j.ccr.2004.09.003
20. Chen J, Chen ZJ. Regulation of NF-κB by ubiquitination. *Curr Opin Immunol*. 2013;25(1):4–12. doi:10.1016/j.coi.2012.12.005
21. He G, Karin M. NF-κB and STAT3: Key players in liver inflammation and cancer. *Cell Res*. 2011;21(1):159–168. doi:10.1038/cr.2010.183
22. Karin M. Nuclear factor-κB in cancer development and progression. *Nature*. 2006;441(7092):431–436. doi:10.1038/nature04870
23. Franke TF, Hornik CP, Segev L, Shostak GA, Sugimoto C. PI3K/Akt and apoptosis: Size matters. *Oncogene*. 2003;22(56):8983–8998. doi:10.1038/sj.onc.1207115
24. Robbins HL, Hague A. The PI3K/Akt pathway in tumors of endocrine tissues. *Front Endocrinol (Lausanne)*. 2016;6:188. doi:10.3389/fendo.2015.00188
25. Pons-Tostivint E, Thibault B, Guillermet-Guibert J. Targeting PI3K signaling in combination cancer therapy. *Trends Cancer*. 2017;3(6):454–469. doi:10.1016/j.trecan.2017.04.002
26. Yi H, Ye X, Long B, et al. Inhibition of the AKT/mTOR pathway augments the anticancer effects of sorafenib in thyroid cancer. *Cancer Biother Radiopharm*. 2017;32(5):176–183. doi:10.1089/cbr.2017.2187
27. Mosmann T. Rapid colorimetric assay for cellular growth and survival: Application to proliferation and cytotoxicity assays. *J Immunol Methods*. 1983;65(1–2):55–63. doi:10.1016/0022-1759(83)90303-4
28. Kasibhatla S, Amarante-Mendes GP, Finucane D, Brunner T, Bossy-Wetzel E, Green DR. Acridine orange/ethidium bromide (AO/EB) staining to detect apoptosis. *Cold Spring Harb Protoc*. 2006;2006(3):pdb.prot4493. doi:10.1101/pdb.prot4493
29. Vijayalakshmi A, Sindhu G. Umbelliferone arrest cell cycle at G0/G1 phase and induces apoptosis in human oral carcinoma (KB) cells possibly via oxidative DNA damage. *Biomed Pharmacother*. 2017;92:661–671. doi:10.1016/j.biopha.2017.05.128
30. Surguchov A, Bernal L, Surguchev AA. Phytochemicals as regulators of genes involved in synucleinopathies. *Biomolecules*. 2021;11(5):624. doi:10.3390/biom11050624
31. Ling T, Lang WH, Maier J, Quintana Centurion M, Rivas F. Cytostatic and cytotoxic natural products against cancer cell models. *Molecules*. 2019;24(10):2012. doi:10.3390/molecules24102012
32. Al-Qubaisi M, Rozita R, Yeap SK, Omar AR, Ali AM, Alitheen NB. Selective cytotoxicity of goniothalamin against hepatoblastoma HepG2 cells. *Molecules*. 2011;16(4):2944–2959. doi:10.3390/molecules16042944
33. Fouad YA, Aanei C. Revisiting the hallmarks of cancer. *Am J Cancer Res*. 2017;7(5):1016–1036. PMID:28560055. PMCID:PMC5446472.
34. Kowalska E, Bartnicki F, Fujisawa R, et al. Inhibition of DNA replication by an anti-PCNA aptamer/PCNA complex. *Nucl Acids Res*. 2018;46(1):25–41. doi:10.1093/nar/gkx1184
35. Kato K, Kawashiri S, Tanaka A, et al. Predictive value of measuring p53 labeling index at the invasive front of oral squamous cell carcinomas. *Pathol Oncol Res*. 2008;14(1):57–61. doi:10.1007/s12253-008-9022-3
36. Kumar KV, Hema K. Extracellular matrix in invasion and metastasis of oral squamous cell carcinoma. *J Oral Maxillofac Pathol*. 2019;23(1):10. doi:10.4103/jomfp.JOMFP_97_19
37. Liu Q, Liu G, Zhu Y, Chao Y. Study on the mechanism of houttuynin inducing apoptosis of MCF-7 cells by inhibiting PI3K/AKT signaling pathway. *Food Sci Technol*. 2022;42:e18721. doi:10.1590/fst.18721
38. Yu Y, Velu P, Ma Y, Vijayalakshmi A. Nerolidol induced apoptosis via PI3K/JNK regulation through cell cycle arrest in MG-63 osteosarcoma cells. *Environ Toxicol*. 2022;37(7):1750–1758. doi:10.1002/tox.23522
39. Asgharian P, Tazekand AP, Hosseini K, et al. Potential mechanisms of quercetin in cancer prevention: Focus on cellular and molecular targets. *Cancer Cell Int*. 2022;22(1):257. doi:10.1186/s12935-022-02677-w
40. Almatroodi SA, Alsahli MA, Almatroudi A, et al. Potential therapeutic targets of quercetin, a plant flavonol, and its role in the therapy of various types of cancer through the modulation of various cell signaling pathways. *Molecules*. 2021;26(5):1315. doi:10.3390/molecules26051315
41. Kang D, Zuo W, Wu Q, Zhu Q, Liu P. Inhibition of specificity protein 1 is involved in phloretin-induced suppression of prostate cancer. *Biomed Res Int*. 2020;2020:1358674. doi:10.1155/2020/1358674
42. Roy S, Mondru AK, Chakraborty T, Das A, Dasgupta S. Apple polyphenol phloretin complexed with ruthenium is capable of reprogramming the breast cancer microenvironment through modulation of PI3K/Akt/mTOR/VEGF pathways. *Toxicol Appl Pharmacol*. 2022;434:115822. doi:10.1016/j.taap.2021.115822

The effect of downregulation of ARL9 expression on the proliferation, metastasis and biological behavior of AGS gastric cancer cell lines

Caihua Sun[1,B,C], Hongliang Yao[1,E,F], Jipan Liu[1,A,D], Shuai Wang[2,A,D]

[1] Department of General Surgery, Hengshui People's Hospital, China
[2] Department of Gynecology, Hengshui People's Hospital, China

A – research concept and design; B – collection and/or assembly of data; C – data analysis and interpretation;
D – writing the article; E – critical revision of the article; F – final approval of the article

Advances in Clinical and Experimental Medicine, ISSN 1899–5276 (print), ISSN 2451–2680 (online) *Adv Clin Exp Med*. 2025;34(8):1375–1382

Address for correspondence
Shuai Wang
E-mail: wang-shuai2023@outlook.com

Funding sources
None declared

Conflict of interest
None declared

Received on October 22, 2023
Reviewed on August 30, 2024
Accepted on September 14, 2024

Published online on January 8, 2025

Abstract

Background. Some ADP ribosylation factors (ARF) and ADP ribosylation factor-like (ARL) family are involved in the regulation of certain cancers, but the role of ADP ribosylation factor-like 9 (ARL9) in gastric tumorigenesis remains elusive.

Objectives. The main aim of this study was to evaluate the ARL9 expression within stomach cancer cells and elucidate its influence on the modulation of cancer cell behavior.

Materials and methods. Differential ARL9 protein expression in normal stomach and stomach cancer tissue was ascertained through data sourced from the University of Alabama at Birmingham Cancer Data Analysis Portal (UALCAN). Quantitative analysis of ARL9 expression in gastric cancer tissue and its association with clinicopathological features was performed using quantitative polymerase chain reaction (qPCR) and western blot analysis (WB). Small interfering RNA (siRNA) was employed to suppress ARL9 protein expression in the human stomach gastric adenocarcinoma human gastric adenocarcinoma cells (AGS) cell line. Assessment of AGS gastric cancer (GC) cell proliferation, invasion and migration was performed using the 3-(4,5-dimethylthiazol-2-yl)-2,5-diphenyl tetrazolium bromide (MTT) and transwell techniques.

Results. The expression of ARL9 protein exhibited a significant upregulation in GC tissue, and showed a close association between tumor dimensions ($p < 0.05$) and the presence of distant metastases ($p < 0.05$) among individuals diagnosed with GC. However, no significant link was observed with sex, age and tumor-node-metastasis (TNM) staging in gastric malignancy patients. After the introduction of si-ARL9 in the experimental set, there was a noteworthy decrease in ARL9 protein levels in AGS cells ($p < 0.01$). In contrast to the control cohort, the restraint of ARL9 expression significantly hampered the growth, mobility and infiltration abilities of the AGS GC cell line ($p < 0.01$).

Conclusions. The significant correlation of ARL9 with the biological behavior of GC indicates its potentially pivotal role in the pathophysiology of the malignancy.

Key words: gastric carcinoma, *ARL9*, cellular growth, SiRNA intervention, metastatic dissemination

Cite as
Sun C, Yao H, Liu J, Wang S. The effect of downregulation of ARL9 expression on the proliferation, metastasis and biological behavior of AGS gastric cancer cell lines. *Adv Clin Exp Med*. 2025;34(8):1375–1382. doi:10.17219/acem/193399

DOI
10.17219/acem/193399

Copyright
Copyright by Author(s)
This is an article distributed under the terms of the Creative Commons Attribution 3.0 Unported (CC BY 3.0) (https://creativecommons.org/licenses/by/3.0/)

Background

Gastric cancer (GC) is a malignant disease influenced by a variety of factors, primarily environmental and genetic.[1,2] Recent statistical data places GC as the 4th most prevalent cancer worldwide, characterized by a median survival rate of less than 12 months.[3] By 2023, the USA will have about 26,500 new cases of GC and about 11,130 deaths.[4] Gastric cancer, known for its high invasiveness and heterogeneity, persists as a global health challenge.[5] Notably, the majority of GC patients receive diagnoses at advanced stage, which often results in a poor prognosis. Simultaneously, the recurrence rate among GC patients remains elevated. Presently, the primary approach to treating GC involves surgical resection coupled with adjuvant chemotherapy or radiotherapy to attain curative outcomes.[6] However, a substantial proportion of patients still experience recurrent GC within 5 years post-surgery, often with poor postoperative recovery.[7] Consequently, it is essential to delve deeper into the molecular pathways responsible for the initiation and advancement of GC to discover innovative indicators for its diagnosis, prognosis and therapeutic objectives.

ADP ribosylation factor (ARF), a component of the RAS superfamily, has been confirmed to play a tumorigenic role in the development and spread of gliomas.[8,9] Previous reports highlight ARL2 and ARL3 as archetypal members within the ADP ribosylation factor-like (ARL) family, displaying reduced expression levels in gliomas. Research has revealed a negative association between the presence of these elements and the unfavorable survival outcomes and outlook for individuals with glioma.[10,11] Most importantly, ARF1 has been demonstrated to be upregulated in GC, which can be a novel prognostic marker for GC.[12] In addition, ARLs are significantly dysregulated in GC and are involved in several cancer-related pathways. Among them, ARL4C is 1 of the 2 most significant clinical indicators for GC. Furthermore, ARL4C silencing remarkably inhibits the growth and metastasis of GC cells both in vitro and in vivo.[13] Notably, ARL9, a newly recognized guanosine triphosphate (GTP)-binding protein, displays substantial preservation and broad distribution in eukaryotic organisms.[14] Given its recent inclusion in the ARF family, the clinical significance of ARL9 protein in gastric tumorigenesis remains to be elucidated.

Objectives

The current study attempted to compare the expression of ARL9 between normal gastric tissue and GC tissue, in order to examine its relationship with clinicopathological parameters such as tumor growth and distant metastasis, and to investigate the effects of ARL9 silencing by siRNA transfection on proliferation, invasion and migration in human gastric adenocarcinoma cells (AGS) GC cells. The novelty of this study was to elucidate the role and regulatory mechanism of ARL9 in GC and to uncover a promising prognostic biomarker in GC patients. Another aim of the study was to enhance our understanding of the mechanisms underlying GC onset and progression, and identify potential therapeutic targets.

Materials and methods

Tissue samples

The RNA expression of ARL9 in GC tissues (n = 415) and normal stomach tissues (n = 34) was selected from The University of Alabama at Birmingham Cancer Data Analysis Portal (UALCAN) database (http://ualcan.path.uab.edu/index.html). The pathology department of Hengshui People's Hospital (Hengshui, China) retained normal gastric tissue samples (n = 70), while clinical samples were collected from patients with GC who underwent surgical resection (n = 70).

Cell lines, chemicals and reagents

The AGS human GC cell line was obtained from the American Type Culture Collection (ATCC; Manassas, USA). Serum-free medium bovine serum and Roswell Park Memorial Institute-1640 (RPMI 1640) were purchased from Gibco (Waltham, USA). Immunohistochemistry utilized a universal EnVision two-step assay kit and diaminobenzidine (DAB) colorant acquired from Beijing Zhongshan Jinqiao Biotechnology Co. (Beijing, China). The rabbit anti-human ARL9 antibodies and mouse anti-human β-actin antibodies were purchased from Thermo Fisher Scientific (Waltham, USA). TransGen Biotech Co., Ltd. (Beijing, China) provided real-time fluorescence quantitative polymerase chain reaction (PCR) and RNA reverse transcription reagents. Six-well plates, transwell chambers, Lipofectamine 3000 transfection reagent, and TRIzol® reagent were acquired from Invitrogen (Waltham, USA). Throughout the experiment, the phosphate-buffered saline (PBS) served as a negative control. All cell experiments were performed in triplicate (n = 3).

UALCAN database

Using data from the UALCAN database, we analyzed RNA sequencing and clinical data from GC patients. The study involved examining ARL9 messenger RNA (mRNA) articulation in normal human stomach tissue, followed by statistical analysis and data visualization utilizing the information available in the record.

The inclusion and exclusion criteria

The inclusion criteria were as follows: 1) no age or sex bias; 2) patients undergoing surgical treatment; 3) a pathological diagnosis of GC; 4) complete survival information.

The exclusion criteria were as follows: 1) multiple tumors in situ; 2) distant metastasis; 3) incomplete tumor staging; 4) incomplete information.

Immunohistochemistry

Sections of GC tissue were cut into continuous pieces about 4-μm thick, fixed in paraffin and stored with a 10% formalin. According to the experimental guidelines, Beijing Zhongshan Jinqiao Company's universal EnVision two-step reagent kit and DAB kit were used to identify the expression of ARL9 protein in GC. Following that, the sections were divided into 3 groups according to the intensity of staining: cells with no staining received a score of 0; cells stained light yellow received a score of 1; and cells stained brownish yellow received a score of 2. Independent pathologists diagnosed every outcome.[15]

Cell culture

The human GC cell line AGS was kept alive in RPMI-1640 medium supplemented with 10% fetal bovine serum (FBS) and 1% penicillin-streptomycin. The cells were cultivated in a 37°C constant-temperature chamber with 5% CO_2, and the cell culture media was changed about every 1–2 days. Cell passaging was done when the cells in the culture dish reached 80% confluence or full confluence.

Cell transfection

Approximately 1.5×10^5 cells per well were achieved by seeding and cultivating AGS cell lines in a 6-well plate until they reached the logarithmic growth phase. Following an overnight culture, the cell status was monitored. The Lipofectamine 3000 transfection reagent handbook was followed for transfection once the cell density reached 80%. Cells were transfected with the NC-siRNA in a control group and with si-ARL9 in an experimental group, respectively. Cells were harvested and total protein was extracted 48 h after transfection. The cell state and density were examined under a microscope (IM-3; OPTIKA, Bergamo, Italy), and the culture media were quickly changed. Western blot (WB) and quantitative polymerase chain reaction (qPCR) were then used to evaluate the effectiveness of transfection. For ARL9, Shanghai Jima Biological Company provided the negative control and the si-RNA sequences (si-ARL9-1 and si-ARL9-2). Transfection efficiency was assessed with WB and qPCR 48 h after transfection.[16]

MTT assay for assessing GC cell proliferation capability

After the well-cultured GC cell line AGS was subcultured and injected, 6 parallel control wells were placed in each group of a 96-well plate. After seeding each well with about 1×10^3 cells, the remaining wells received an equivalent volume of PBS solution. Prior to testing, 96-well plates were first aspirated of their culture media. After that, each well received 100 μL of 3-(4,5-dimethylthiazol-2-yl)-2,5-diphenyl tetrazolium bromide (MTT) mixture, which was made by dividing culture medium and MTT solution in a 1:9 ratio. Each well was then incubated for 1 h at 37°C. Then, 100 μL of dimethyl sulfoxide (DMSO) solution was added and the mixture was discarded. The plate was stirred in the dark for 20 min. Finally, a microplate reader was used to measure and record the absorbance at optical density (OD) of 570 nm.[17]

Transwell assay for assessing the metastatic capability of GC cells

AGS, a well-cultured stomach cancer cell line, was counted and trypsinized. A serum-rich medium comprising 800 μL was put beneath every well. Above, a transwell chamber was placed, and 200 μL of serum-free media containing 6×10^4 stomach cancer cells were added. The chamber was then taken out of the setup and left in an incubator set at 37°C for 8 h. Following that, it was cleaned with a PBS solution, fixed for 1 h with a 90% ethanol solution, and then stained for 10 min with a crystal violet solution. Afterwards, a soft water stream was used to rinse the chamber, and a cotton swab was used to remove any leftover crystal violet solution from the edge of the chamber. Three randomly chosen visual fields from the microscope observation were chosen for statistical analysis and counting.[17]

Statistical analyses

Data analysis was conducted using IBM SPSS v. 22.0 (IBM Corp., Armonk, USA) and R (R Foundation for Statistical Computing, Vienna, Austria) software. The Pearson's χ^2 test was performed on clinical and demographic characteristics of the patients. The Shapiro–Wilk normality test was conducted to confirm that the distribution was acceptable, and the normality of the distribution was not checked for a very large group (using the central limit theorem for $n > 100$). For the data with a non-normal distribution, the median of Q1–Q3 was used to represent the data. Comparisons between the 2 groups were conducted using the Mann–Whitney U test, and multiple groups were compared using Kruskal–Wallis tests followed by post hoc Dunn's comparison tests. Non-parametric analysis of variance (ANOVA) test followed by Bonferroni post hoc test was chosen to analyze the proliferation ability. Pearson's χ^2 test of independence was used to test for a relationship between categorical variables. A p-value <0.05 was considered to be statistically significant. Main line of code from the WRS2 package for the nonparametric repeated measures ANOVA test into statistical analysis along with dedicated post hoc tests with Bonferroni correction is given below:

```
install.packages("readxl")
install.packages("WRS2")
library(readxl)
library(WRS2)
file_path<– "D:/data.xlsx"
data <– read_excel(file_path)
rm_anova_result<– aov(Score ~ Group * `Time Frame` * Replicate + Error(Group/`Time Frame`/Replicate), data = data)
summary(rm_anova_result)
kruskal_test_result<– kruskal.test(Score ~ Group, data = data)
print(kruskal_test_result)
wilcox_test_result<– pairwise.wilcox.test(data$Score, data$Group, paired = TRUE, p.adjust.method = "bonferroni")
print(wilcox_test_result)
```

Results

Analysis of ARL9 RNA and protein expression in normal gastric and GC tissues

Using the UALCAN database, the RNA expression of ARL9 was examined in 415 GC tissues and 34 normal stomach tissues. Figure 1 shows that there was a significantly higher RNA expression of ARL9 in GC tissues (Mann–Whitney U test (U) = 11,861.50, Z-score = 6.61, $p < 0.001$; see Supplementary Table 1). Later, we used WB to evaluate ARL9 protein expression in 70 GC tissues and 70 normal gastric tissues that were taken from clinical samples. The data demonstrated that the ARL9 protein was upregulated in GC tissues but downregulated in normal gastric tissues (Fig. 2). Five high-power visual fields were randomly selected for observation from each slice after immunohistochemical screening and evaluated semi-quantitatively.[18,19] The ARL9 protein expression differences between 70 GC tissues and 70 normal gastric tissues (degrees of freedom (df) = 1.00, χ^2 =48.04, $p < 0.001$) were statistically significant. Conclusively, out of 70 normal gastric tissues, 15 showed positive expression, while in 70 GC tissues, 56 showed positive expression (expected frequency is presented in Supplementary Table 2). Additionally, human GC tissues and normal gastric tissues were validated with hematoxylin and eosin (H&E) staining (Fig. 3).

The correlation between ARL9 protein expression and clinical pathological parameters in GC tissue

A strong association was found between the results of 70 normal and GC tissues from each group and clinical case data. Regarding age, gender, tumor-mode-metastasis (TNM) stage, or lymph node metastases, we found no compelling associations. On the other hand, Table 1 shows a strong correlation (expected frequency is presented in Supplementary Table 3) between ARL9 protein expression and both distant metastasis (df = 1.00, p = 0.011) and tumor size (df = 1.00, χ^2 = 11.50, p = 0.001).

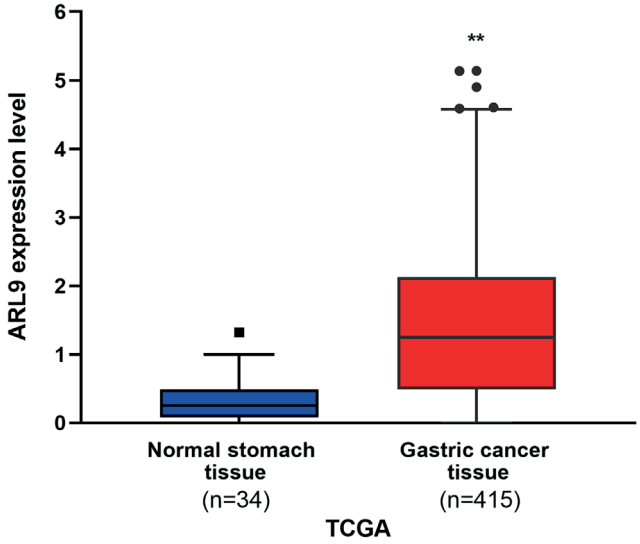


Fig. 1. The expression of ARL9 in 415 GC tissues and 34 normal gastric tissues in the University of Alabama at Birmingham Cancer Data Analysis Portal (UALCAN) database (**$p < 0.001$). The expression level in normal gastric tissue ranges from 0 to 1.32, median is 0.281, 1st quartile is 0.079, and 3rd quartile is 0.512. The expression level in GC tissue ranged from 0 to 5.14, mean was 1.605 and standard deviation (SD) was 1.371. The lower boundary was calculated using the formula: First quartile (Q1) –1.5 × interquartile range (IQR), and the upper boundary was calculated using the fomula: 3rd quartile (Q3) +1.5 × IQR. The upper boundary for normal gastric tissue was 1.162 and outliers for normal gastric tissue was 1.32. The upper boundary for GC tissue was 4.541, and outliers for GC tissue were 4.588, 4.607, 4.902, 5.138, and 5.140

GC – gastric cancer.

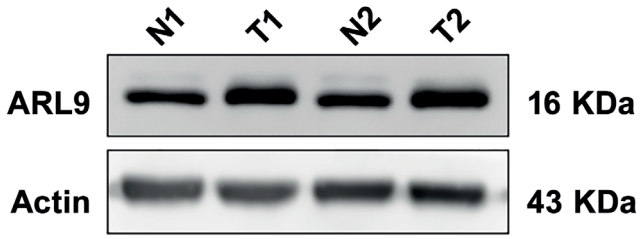


Fig. 2. Protein expression of ARL9 in 70 human GC tissues and 70 normal gastric tissues. Normal gastric tissue N1 and GC tissue T1 were from patient 1 (n = 3), and normal gastric tissue N2 and GC tissue T2 were from patient 2 (n = 3)

N1 – normal gastric tissue sample 1; T1 – GC tissue sample 1; N2 – normal gastric tissue sample 2; T2 – GC tissue sample 2; GC – gastric cancer.

Expression of ARL9 mRNA and protein in normal gastric and GC tissues

ARL9 expression in the GC cell line AGS was evaluated with reverse transcription qPCR (RT-qPCR), which measures ARL9 mRNA and protein levels after ARL9-specific NC, siARL9 #1 and siARL9 #2 are transfected. Figure 4A,B

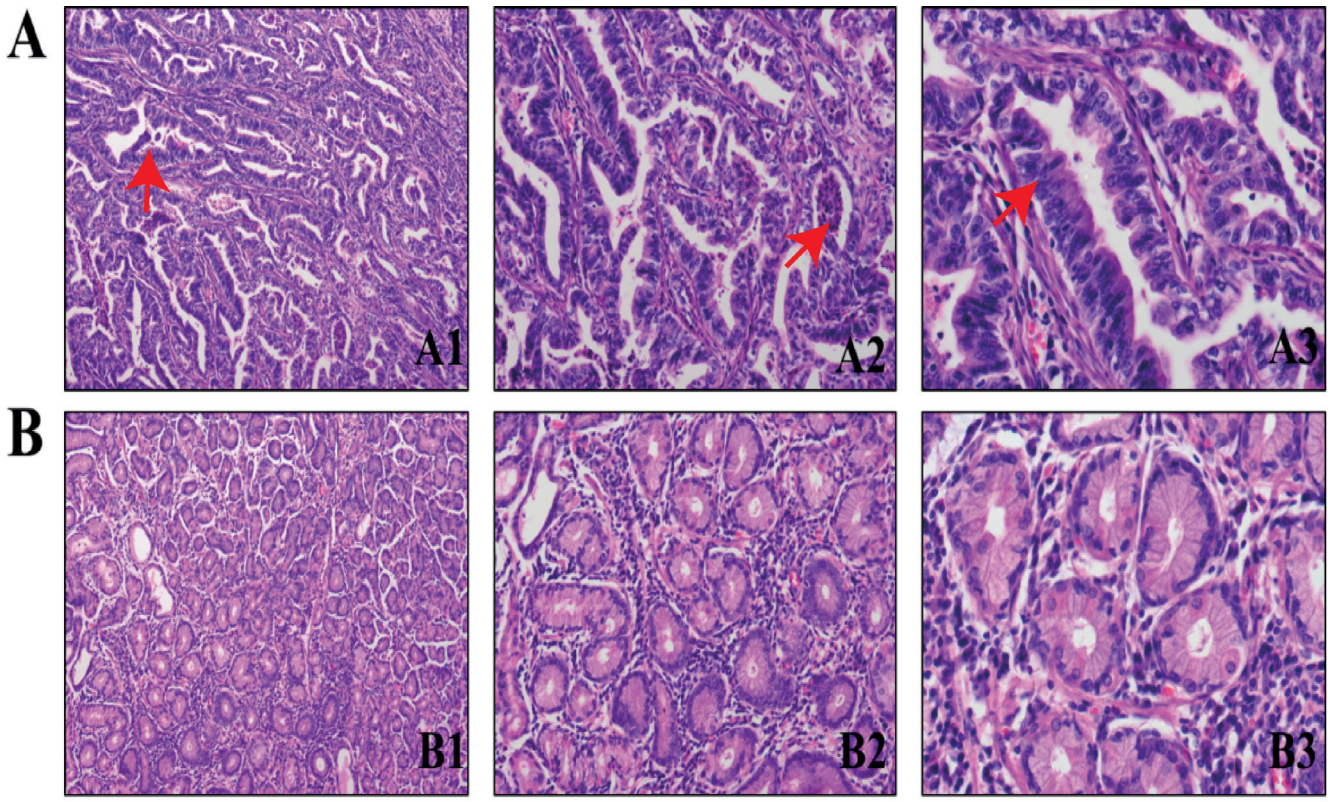


Fig. 3. Validation of human GC tissue and normal gastric tissue using hematoxylin and eosin (H&E) staining. A. GC tissue; A1. Microscope magnification of ×100 (n = 3); A2. Microscope magnification ×200 (n = 3); A3. Microscope magnification ×400 (n = 3); B. Normal gastric tissue; B1. Microscope magnification ×100 (n = 3); B2. Microscope magnification ×200 (n = 3); B3. Microscope magnification ×400 (n = 3). Compared to normal gastric tissue, gastric glands had disordered structures (arrow in A1), necrosis occurred in the glandular cavity (arrow in A2), and atypical glandular epithelium and increased nuclear division were also observed (arrow in A3) in GC tissue. One patient was selected in each group for representation

GC – gastric cancer.

Table 1. Relationship between the expression of ARL9 in GC tissue and clinical pathological characteristics. Pearson's χ^2 test of independence was used to analyze the relationship of ARL9 expression in GC tissues with clinicopathological characteristics

Clinical pathological parameters		n	ARL9 high expression [%]	Test name	df	χ^2	p-value
Gender	male	40	25	Pearson's χ^2 test of independence	1.00	0.13	0.719
	female	30	20				
Age [years]	>60	46	33	Pearson's χ^2 test of independence	1.00	3.25	0.072
	≤60	24	12				
Tumor size [cm]	<5	37	17	Pearson's χ^2 test of independence	1.00	11.50	0.001*
	≥5	33	28				
Metastasis	yes	10	10	Fisher's exact test	1.00	–	0.011*
	no	60	35				
Lymphatic metastasis	yes	15	8	Pearson's χ^2 test of independence	1.00	1.00	0.318
	no	55	37				
TNM stage	I–II	49	28	Pearson's χ^2 test of independence	1.00	3.63	0.057
	III–IV	21	17				

* $p < 0.05$; TNM – tumor-node-metastasis; n – number of cases; df – degrees of freedom; ARL9 – ADP-ribosylation factor-like 9; GC – gastric cancer.

shows a decline in ARL9 mRNA and protein expression levels in the GC cell line AGS after transfection (df = 2.00, Kruskal–Wallis statistic = 5.45, p = 0.071, NC vs siARL9#1, p = 0.130; NC vs siARL9#2, p = 0.130, siARL9#1 vs siARL9#2; p = 0.999).

Assessment of proliferation and invasion capabilities of ARL9 in the GC cell line AGS

At time points of 0, 24, 48, 72, and 96 h following transfection, the MTT assay was utilized to assess the impact

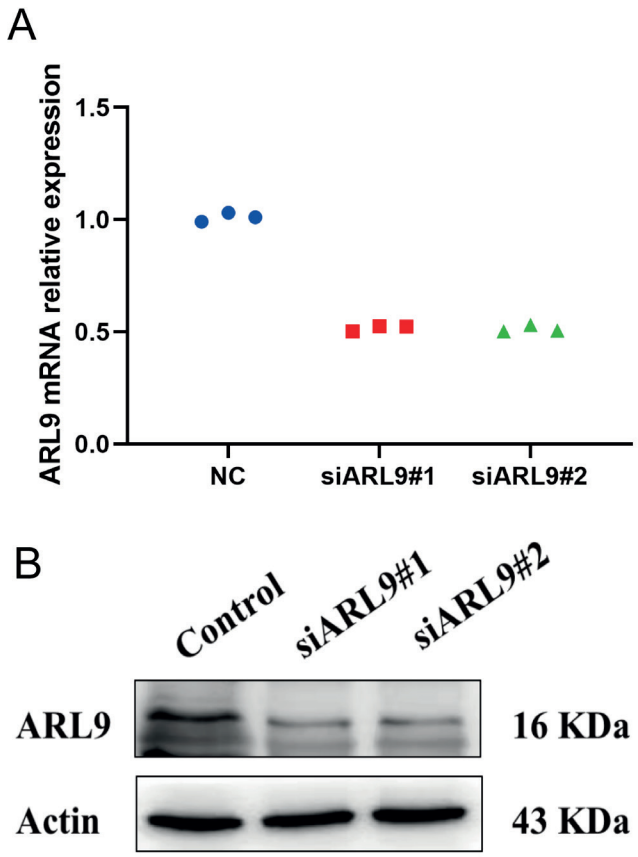


Fig. 4. Expression level of ARL9 in GC cells transfected with siARL9 by AGS GC cells. A. Quantitative polymerase chain reaction (qPCR) was used to detect mRNA expression in GC cell AGS after transfection with siARL9. B. Western blotting was used to detect protein expression in GC cells AGS after transfection with siARL9

NC (n = 3) – control human gastric adenocarcinoma cells (AGS); siARL9#1 (n = 3) – AGS transfected with siRNA sequence 1 targeting ARL9; siARL9#2 (n = 3) – AGS transfected with siRNA sequence 2 targeting ARL9; control – control AGC; GC – gastric cancer; NC – negative control.

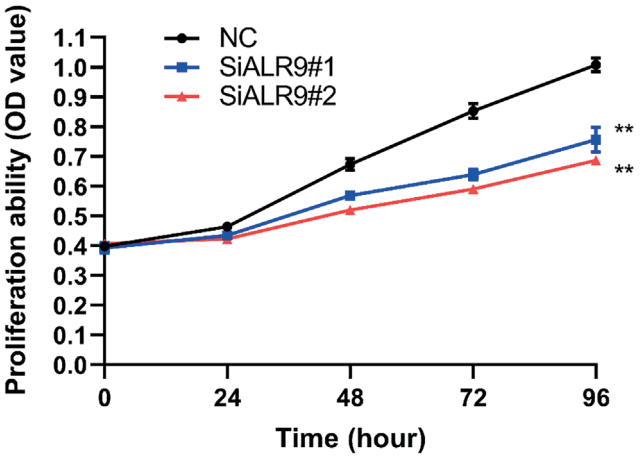


Fig. 5. MTT assay for detecting the effect of siARL9 transfection on the proliferation ability of AGS GC cells (**p < 0.01)

NC (n = 3) – human gastric adenocarcinoma cells (AGS); siARL9#1 (n = 3) – AGS transfected with siRNA sequence 1 targeting ARL9; siARL9#2 (n = 3) – AGS transfected with siRNA sequence 2 targeting ARL9; GC – gastric cancer; NC – negative control.

Table 2. Nonparametric repeated measures ANOVA test for Fig. 5

Statistical methods	Group	Statistic (n = 3)
Kruskal–Wallis multivariate ANOVA test	df	2.00
	H	3.37
	p-value	0.185
Pairwise comparisons (Wilcoxon test)	NC vs siARL9#1	p < 0.001
	NC vs siARL9#2	p < 0.001
	siARL9#1 vs siARL9#2	p = 0.013

ANOVA – analysis of variance; df – degrees of freedom; NC – negative control. p-value adjustment method: Bonferroni, where H represents test statistic.

of ARL9 on the capacity of GC cells AGS to multiply. The results demonstrated a statistically significant difference between the NC group and the siARL9 #1 and siARL9 #2 transfected groups in terms of the AGS cells' capacity to proliferate (Fig. 5; df = 2.00, Kruskal–Wallis statistic = 3.37, p = 0.185; NC vs siARL9#1, p < 0.001; NC vs siARL9#2, p < 0.001, siARL9#1 vs siARL9#2, p = 0.013; Table 2). The effect of the protein on the invasive and migratory capabilities of AGS cells was evaluated 48 h after ARL9 transfection using cell counts and the transwell method. Microscopic studies revealed significantly decreased invasion and migratory potentials of AGS cells in the siARL9 #2 transfected groups compared to the NC group (Fig. 6; for both invasion and migration: df = 2.00, Kruskal–Wallis statistic = 7.20, p = 0.027; NC vs siARL9#1, p = 0.539; NC vs siARL9#2, p = 0.022, siARL9#1 vs siARL9#2, p = 0.539).

Discussion

The precise mode of action and clinical significance of the *ARL9* gene in tumors remains unclear, although analogous oncogenes have been identified and documented in previous research.[20,21] A negative association has been established between gliomas[22] and the malignant growth of prostate tumors.[14] Tumor suppressor protein ARF controls apoptosis, ageing and cell proliferation, all of which are vital in halting the growth of cancer.[23] The fundamental function of ARF in inhibiting tumor growth has been thoroughly described. Its function as a suppressor of tumor growth is strongly associated with the p53 MDM2 axis, mostly because of its capacity to react to oncogenic cues like c-MYC and trigger p53 activation.[24] The biological significance of ARL9, which is a recent member of the ARF family, in relation to tumors is still unknown.

In this research, we meticulously examined ARL9 expression using the public database UALCAN and subsequently corroborated our findings at both the protein and mRNA levels.[25] In vitro experiments demonstrated a noteworthy downregulation of ARL9 protein and mRNA

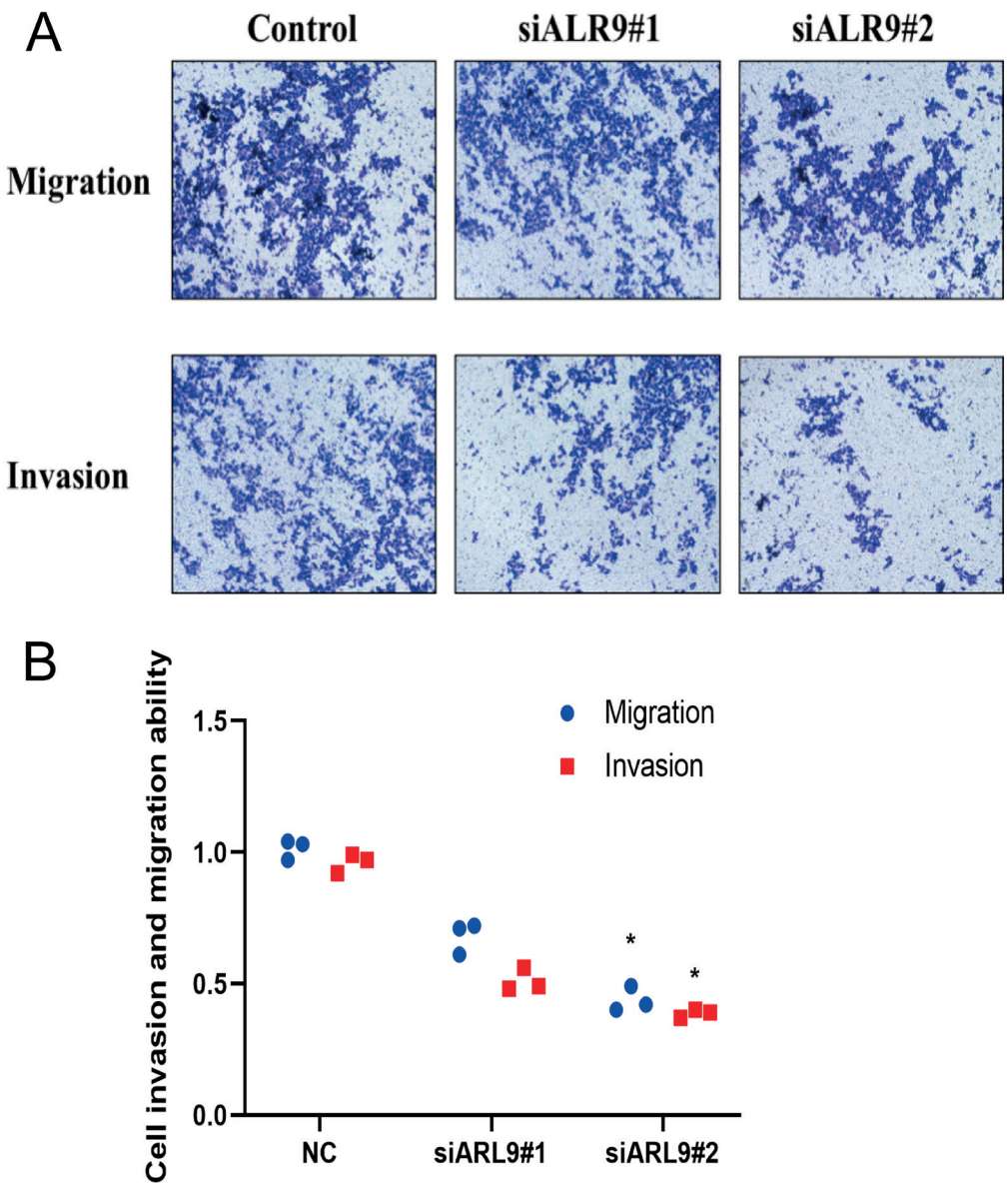


Fig. 6. Transwell method was used to detect the effect of siARL9 transfection on invasion and migration in human gastric adenocarcinoma cells (AGS)

NC or control (n = 3) – control AGS cells; siARL9#1 (n = 3) – AGS transfected with siRNA sequence 1 targeting ARL9; siARL9#2 (n = 3) – AGS transfected with siRNA sequence 2 targeting ARL9; * $p < 0.05$ for comparison with NC; GC – gastric cancer; NC – negative control.

expression following ARL9 siRNA transfection. This reduction significantly impaired ce l proliferation and migration. Gastric cancer cells with elevated ARL9 protein expression exhibited greater proclivity for proliferation and metastasis than those with lower ARL9 expression.[26] Additionally, ARL9 protein expression in GC tissues of patients with high ARL9 levels was confirmed by immunohistochemistry results to be highly associated with tumor growth and distant metastasis in patients with GC. However, $p > 0.05$ indicated no statistically significant correlation between TNM staging, age or gender of GC patients. Therefore, we draw the conclusion that the ARL9 protein is highly expressed in GC and may have the ability to promote the growth and migration of GC cells.

Limitations

Although our data suggest that ARL9 may play a role in the GC carcinogenesis, we must acknowledge that we have not thoroughly revealed the mechanisms of ARL9 protein in gastric tumorigenesis. This limitation highlights the need for further research to fully elucidate the role of ARL9 in GC, both in experimental settings and in complex molecular networks. In addition, a previous study reported that ARL9 was negatively regulated by *ARL9* DNA methylation in low-grade glioma,[22] so we should investigate the epigenetic regulatory mechanism of ARL9 expression in GC in future studies.

Conclusions

The study provides new insights into the *ARL9* gene and sheds light on how it relates to gastric cancer.[27] Given that ARL9 expression is downregulated in vitro after siRNA transfection and that this results in a decrease in cell migration and proliferation, it is highly probable that *ARL9* is an oncogene in stomach cancer. These findings correlates

with the previous research that demonstrated an inverse correlation between ARL9 and the development of malignancy in many cancer types.[22,28] For example,ARL9 as upregulated in colon adenocarcinoma and ARL9 silence reduced the proliferation and migration of colon adenocarcinoma cells.[28] According to these data, ARL9 may be helpful as a diagnostic and prognostic marker for stomach cancer.

Supplementary data

The Supplementary materials are available at https://doi.org/10.5281/zenodo.13765995. The package includes the following files:

Supplementary Table 1. Statistical analysis for Fig. 1.

Supplementary Table 2. Expected frequency for ARL9 protein expression.

Supplementary Table 3. Expected frequency for Table 1.

Data availability

The datasets generated and/or analyzed during the current study are available from the corresponding author on reasonable request.

Consent for publication

Not applicable.

ORCID iDs

Caihua Sun https://orcid.org/0000-0001-6624-8162
Hongliang Yao https://orcid.org/0000-0002-2900-3251
Jipan Liu https://orcid.org/0000-0002-5098-3653
Shuai Wang https://orcid.org/0009-0002-7506-5426

References

1. Yusefi AR, Bagheri Lankarani K, Bastani P, Radinmanesh M, Kavosi Z. Risk factors for gastric cancer: A systematic review. *Asian Pac J Cancer Prev*. 2018;19(3):591–603. doi:10.22034/APJCP.2018.19.3.591
2. Iwu CD, Iwu-Jaja CJ. Gastric cancer epidemiology: Current trend and future direction. *Hygiene*. 2023;3(3):256–268. doi:10.3390/hygiene3030019
3. Zhang XY, Zhang PY. Gastric cancer: Somatic genetics as a guide to therapy. *J Med Genet*. 2017;54(5):305–312. doi:10.1136/jmedgenet-2016-104171
4. Siegel RL, Miller KD, Wagle NS, Jemal A. Cancer statistics, 2023. *CA Cancer J Clin*. 2023;73(1):17–48. doi:10.3322/caac.21763
5. Park JY, Von Karsa L, Herrero R. Prevention strategies for gastric cancer: A global perspective. *Clin Endosc*. 2014;47(6):478. doi:10.5946/ce.2014.47.6.478
6. Guan WL, He Y, Xu RH. Gastric cancer treatment: Recent progress and future perspectives. *J Hematol Oncol*. 2023;16(1):57. doi:10.1186/s13045-023-01451-3
7. Spolverato G, Capelli G, Mari V, et al. Very early recurrence after curative-intent surgery for gastric adenocarcinoma. *Ann Surg Oncol*. 2022;29(13):8653–8661. doi:10.1245/s10434-022-12434-y
8. Zhong C, Shu M, Ye J, et al. Oncogenic Ras is downregulated by ARHI and induces autophagy by Ras/AKT/mTOR pathway in glioblastoma. *BMC Cancer*. 2019;19(1):441. doi:10.1186/s12885-019-5643-z
9. Yan Y, Jiang Y. RACK1 affects glioma cell growth and differentiation through the CNTN2-mediated RTK/Ras/MAPK pathway. *Int J Mol Med*. 2016;37(1):251–257. doi:10.3892/ijmm.2015.2421
10. Wang Y, Guan G, Cheng W, et al. ARL2 overexpression inhibits glioma proliferation and tumorigenicity via down-regulating AXL. *BMC Cancer*. 2018;18(1):599. doi:10.1186/s12885-018-4517-0
11. Wang Y, Zhao W, Liu X, Guan G, Zhuang M. ARL3 is downregulated and acts as a prognostic biomarker in glioma. *J Transl Med*. 2019;17(1):210. doi:10.1186/s12967-019-1914-3
12. Tsai M, Lin PY, Cheng W, et al. Overexpression of ADP-ribosylation factor 1 in human gastric carcinoma and its clinicopathological significance. *Cancer Sci*. 2012;103(6):1136–1144. doi:10.1111/j.1349-7006.2012.02243.x
13. Xie N, Bai Y, Qiao L, et al. ARL4C might serve as a prognostic factor and a novel therapeutic target for gastric cancer: Bioinformatics analyses and biological experiments. *J Cell Mol Med*. 2021;25(8):4014–4027. doi:10.1111/jcmm.16366
14. Louro R, Nakaya HI, Paquola ACM, et al. RASL11A, member of a novel small monomeric GTPase gene family, is down-regulated in prostate tumors. *Biochem Biophys Res Commun*. 2004;316(3):618–627. doi:10.1016/j.bbrc.2004.02.091
15. Zhao W, Cui M, Zhang R, et al. IFITM1, CD10, SMA, and h-caldesmon as a helpful combination in differential diagnosis between endometrial stromal tumor and cellular leiomyoma. *BMC Cancer*. 2021;21(1):1047. doi:10.1186/s12885-021-08781-w
16. Ran LW, Wang H, Lan D, Jia HX, Yu SS. Effects of RNA interference combined with ultrasonic irradiation and SonoVue microbubbles on expression of *STAT3* gene in keratinocytes of psoriatic lesions. *J Huazhong Univ Sci Technol Med Sci*. 2017;37(2):279–285. doi:10.1007/s11596-017-1728-6
17. Xu H, Lu G, Zhou S, Fang F. MicroRNA-19a-3p acts as an oncogene in gastric cancer and exerts the effect by targeting SMOC2. *Appl Biochem Biotechnol*. 2022;194(9):3833–3842. doi:10.1007/s12010-022-03944-2
18. Wang L, Zhang J, Yang X, et al. SOX4 is associated with poor prognosis in prostate cancer and promotes epithelial–mesenchymal transition in vitro. *Prostate Cancer Prostatic Dis*. 2013;16(4):301–307. doi:10.1038/pcan.2013.25
19. Jin M, Yang Z, Ye W, Yu X, Hua X. Prognostic significance of histone methyltransferase enhancer of zeste homolog 2 in patients with cervical squamous cell carcinoma. *Oncol Lett*. 2015;10(2):857–862. doi:10.3892/ol.2015.3319
20. Wang LM, Li Z, Piao YS, et al. Clinico-neuropathological features of isocitrate dehydrogenase 2 gene mutations in lower-grade gliomas. *Chin Med J (Engl)*. 2019;132(24):2920–2926. doi:10.1097/CM9.0000000000000565
21. Wu F, Zhao Z, Chai R, et al. Prognostic power of a lipid metabolism gene panel for diffuse gliomas. *J Cell Mol Med*. 2019;23(11):7741–7748. doi:10.1111/jcmm.14647
22. Tan Y, Zhang S, Xiao Q, et al. Prognostic significance of ARL9 and its methylation in low-grade glioma. *Genomics*. 2020;112(6):4808–4816. doi:10.1016/j.ygeno.2020.08.035
23. Ko A, Han SY, Song J. Regulatory network of ARF in cancer development. *Mol Cells*. 2018;41(5):381–389. PMID:29665672
24. Lindström MS, Wiman KG. Myc and E2F1 induce p53 through p14ARF-independent mechanisms in human fibroblasts. *Oncogene*. 2003;22(32):4993–5005. doi:10.1038/sj.onc.1206659
25. Sun C, Yuan Q, Wu D, Meng X, Wang B. Identification of core genes and outcome in gastric cancer using bioinformatics analysis. *Oncotarget*. 2017;8(41):70271–70280. doi:10.18632/oncotarget.20082
26. Xie N, Shu Q, Wang Z, et al. ARL11 correlates with the immunosuppression and poor prognosis in breast cancer: A comprehensive bioinformatics analysis of ARL family members. *PLoS One*. 2022;17(11):e0274757. doi:10.1371/journal.pone.0274757
27. Li C, Ge M, Yin Y, Luo M, Chen D. Silencing expression of ribosomal protein L26 and L29 by RNA interfering inhibits proliferation of human pancreatic cancer PANC-1 cells. *Mol Cell Biochem*. 2012;370(1–2):127–139. doi:10.1007/s11010-012-1404-x
28. Yang HD, Jin XX, Gu BB, Zhang Y, Li D, Yan LL. ARL9 is upregulated and serves as a biomarker for a poor prognosis in colon adenocarcinoma. *BMC Gastroenterol*. 2023;23(1):48. doi:10.1186/s12876-023-02677-8

Umbelliferone inhibits proliferation and metastasis via modulating cadherin/β-catenin complex-aided cell-cell adhesion in glioblastoma cells

Wei Ma[1,A–C], Hangyu Shi[2,C,D], Xinya Dong[2,B,C,E], Yongqiang Shi[2,B–D], Luyi Zhang[2,A,B,D], Bin Jiang[2,A,F]

[1] Department of Neurosurgery, The Second Affiliated Hospital of Air Force Medical University, Xi'an, China
[2] Department of Neurosurgery, The Affiliated Children's Hospital of Xi'an Jiaotong University, Xi'an Children's Hospital, China

A – research concept and design; B – collection and/or assembly of data; C – data analysis and interpretation;
D – writing the article; E – critical revision of the article; F – final approval of the article

Advances in Clinical and Experimental Medicine, ISSN 1899–5276 (print), ISSN 2451–2680 (online) *Adv Clin Exp Med*. 2025;34(8):1383–1392

Address for correspondence
Bin Jiang
E-mail: jiangbin1984@outlook.com

Funding sources
Natural Science Basic Research Program of Shaanxi Province (grant No. 2022JM-595).

Conflict of interest
None declared

Received on January 29, 2024
Reviewed on April 2, 2024
Accepted on August 22, 2024

Published online on January 10, 2025

Abstract

Background. Glioblastoma multiforme (GBM) is the most aggressive brain tumor malignancy in adults, accounting for nearly 50% of all gliomas. Current medications for GBM frequently lead to drug resistance.

Objectives. Umbelliferone (UMB) is found extensively in many plants and shows numerous pharmacological actions against inflammation, degenerative diseases and cancers. However, its anticancer effects on GBM cells have not yet been explored.

Materials and methods. This research intended to assess the antitumor efficacy of UMB and the molecular mechanism of cell–cell adhesion proteins in human U-87 GBM cells. The cytotoxicity assay, intracellular reactive oxygen species (ROS), cell adhesion proteins, and cell apoptosis actions of UMB were assessed using 3-[4, 5-dimethylthiazol-2-yl]-2, 5-diphenyl tetrazolium bromide (MTT), dichlorodihydrofluorescein diacetate (DCFH-DA), 4′,6-diamidino-2-phenylindole (DAPI), acridine orange/ethidium bromide (AO/EB), and western blot.

Results. The findings revealed that UMB reduced the proliferation of GBM cells and cell adhesion proteins, while augmenting apoptosis through the elevation of cellular ROS. Bcl-2 family protein levels of Bcl-2 and Bcl-XL were mitigated; conversely, the pro-apoptotic proteins Bad and Bim were elevated upon treatment with UMB in a quantity-dependent way. Furthermore, UMB-treated GBM cells suppressed N-cadherin, β-catenin, Slug, and matrix metalloproteinase 2 (MMP-2) expression, whereas they showed enhanced TIMP protein and E-cadherin levels.

Conclusions. Our findings suggest that UMB can prevent proliferation and metastasis and stimulate apoptosis in GBM cells.

Key words: glioblastoma, proliferation, apoptosis, umbelliferone, cell adhesion proteins

Cite as
Ma W, Shi H, Dong X, Shi Y, Zhang L, Jiang B. Umbelliferone inhibits proliferation and metastasis via modulating cadherin/β-catenin complex-aided cell-cell adhesion in glioblastoma cells. *Adv Clin Exp Med*. 2025;34(8):1383–1392. doi:10.17219/acem/192547

DOI
10.17219/acem/192547

Copyright
Copyright by Author(s)
This is an article distributed under the terms of the Creative Commons Attribution 3.0 Unported (CC BY 3.0) (https://creativecommons.org/licenses/by/3.0/)

Background

Gliomas are the predominant kind of malignancy in the central nervous system and are accountable for a significant number of human deaths.[1] Gliomas comprise 24.7% of all primary brain tumors and 74.6% of all malignancies, according to the American Brain Tumor Association (ABTA).[2] Glioma patients have an extremely low survival rate; with current treatments, the average survival duration for low-grade gliomas is less than 60 months, and for advanced phases, it is fewer than 15 months.[3] As a recurrent brain tumor in adults, glioblastoma multiforme (GBM) is an extremely aggressive malignancy owing to its highly invasive and vascularizing nature.[4] Currently, available standard therapy for GBM is surgical resection with subsequent radiotherapy and temozolomide chemotherapy.[5] Because of the level of distortion and chemoresistance, GBM certainly relapses despite recent advancements in these treatments.[6] Thus, it is urgently required to advance innovative therapeutic approaches for the management and improvement of GBM survival rates.

Reactive metabolic byproducts, such as reactive oxygen species (ROS), greatly influence both harmful and positive actions. Reactive oxygen species in cells act as secondary messengers in signaling cascades that are a threat to usual physiological actions, including development and differentiation.[7,8] Conversely, hypergeneration of ROS can impair biomolecules,[9] which leads to cell integrity harm followed by cell pathology. Recently, ROS have been shown to promote tumorigenesis, angiogenesis and metastasis.[10] However, extreme accumulation of ROS has been recognized to bring about apoptotic cell death.[11] Metastasis is the primary cause of cancer-associated mortality,[12] along with catastrophic organ dysfunction following the establishment and uncontrolled progression of exogenous cancer cells surrounded by normal tissue. Adhesion and cell–cell interaction are crucial tools for effective tissue function and homeostasis by describing compartmentalization and polarity in cells.[13] Among the numerous adhesion molecules, the key group is the cadherins superfamily, which are transmembrane proteins that are essential in the development of adherens junctions.[14] Matrix metalloproteinases (MMPs) are endopeptidases in a zinc-dependent family that are responsible for destroying constituents of the extracellular matrix (ECM),[15] tumor cell incursion, angiogenesis, and the subduing of antitumor immune surveillance.[16] There are natural endogenous secreted proteins comprising tissue inhibitors of metalloproteinases (TIMPs) that constrain the actions of MMPs.[17] Hence, TIMPs control cellular functions, including proliferation, movement and survival, by regulating ECM deprivation through communication with MMPs.[18]

Natural herbal constituents have been shown to be vital sources of medicines and models for drug design. The well-known 7-hydroxycoumarin umbelliferone (UMB) is extensively found in numerous popular plants from the Umbelliferae family comprising garden angelica, coriander, carrot, etc. It displays numerous pharmacological actions against microbial infections, inflammation, degenerative diseases, and cancers.[19] It employs anticancer activities against colon cancer,[20] laryngeal cancer[21] and liver cancer.[22]

Objectives

This report was intended to explore the anticancer efficacy of UMB in terms of cytotoxicity, apoptosis and metastasis in the most commonly studied GBM cells.

Materials and methods

Chemicals

Umbelliferone, Dulbecco's modified Eagle's medium (DMEM), foetal bovine serum (FBS), antibiotics, 3-(4,5-dimethylthiazol-2-yl)-2,5-diphenyltetrazolium bromide (MTT), 2′–7′-dichlorodihydrofluorescein diacetate (DCFH-DA), 6-diamidino-2-phenylindole (DAPI), sodium dodecyl sulphate (SDS), dimethyl sulphoxide (DMSO), and phosphate-buffered saline (PBS) were acquired from Gibco (Waltham, USA). The primary and secondary antibodies for Western blot analysis were purchased from Beyotime Biotechnology (Beijing, China). Analytical-grade biochemicals and solvents were used.

Cell culture

Human U-87 GBM cells were acquired from Shanghai Aiyan Biotechnology Co., Ltd (Shanghai, China) and cultured in DMEM medium, which contained 10% FBS, streptomycin (100 µg/mL) and penicillin (100 U/mL) in a 5% CO_2 atmosphere with below 95% humidity at 37°C.

Cell proliferation assay

Human glioma cell viability was evaluated using the MTT test.[23] Briefly, U-87 GBM cells were sowed into 96-well plates (1×10^5 cells/well) and cultured at 37°C in a 5% CO_2 wet incubator. Once they were incubated overnight, the medium was separated, washed with PBS in the cells and incubated through different concentrations of UMB (5–60 µM/mL) for 1 day. Then, a 10 µL solution of MTT was supplemented to the treated cells and sustained for another 4 h. Subsequently, crystals of formazan were dissolved by treating with DMSO (150 µL). The optical density (OD) was determined at 490 nm using a multifunctional plate reader (BD Biosciences, Franklin Lakes, USA). Cell proliferation was measured as a percentage of viability against control GBM cells (100%). The IC50 value was determined using the method shown below:

cell viability inhibition (%) = (control OD – test OD) × 100.

Determination of intracellular ROS

Human glioma cells were sowed in 6-well plates each and kept for 1 day; then, different concentrations of UMB (30 or 40 μM/mL) were added. Next, the control and treated cells were stained with 10 μM of DCFH-DA and preserved for 30 min at 37°C. The stained cells were washed with ice-cold PBS twice to remove any excess dye. The excitation and emission fluorescence were measured using a PR 4100 microplate reader, which is a next-generation 8-channel absorbance microplate reader (Bio-Rad Laboratories India Pvt. Ltd., Gurgaon, India), as described previously.[24]

Evaluation of apoptosis using dual staining with AO/EB

The apoptotic morphology of the human U87 cells after exposure to UMB was evaluated using acridine orange/ethidium bromide (AO/EB) staining.[25] Glioblastoma multiforme cells were supplemented with different concentrations of UMB (30 or 40 μM/mL) and kept for 1 day. The UMB-supplemented and control cells were treated with an AO/EB (100 μg/mL each dye) mixture. All groups were kept in the dark at room temperature for 20 min, ensuring unattached dye was separated using PBS and detected using a fluorescence microscope (model BX51; Olympus Corp., Tokyo, Japan).

Apoptosis assessed using DAPI staining

Human GBM cells were sowed at 1×10^5 cells per plate and added to UMB (30 or 40 μM/mL) and then fixed with 4% paraformaldehyde for 10 min at 37°C. These preserved GBM cells underwent DAPI staining to evaluate the nucleus changes related to apoptotic cell death using a method described previously.[26] Then, all samples were fixed on a glass slip and examined through a BX51 fluorescence microscope (Olympus Corp.).

Western blotting analysis

Human GBM cells were supplemented with 30 or 40 μM/mL of UMB and cultivated for 1 day. The cell lysates were set with lysis buffer in ice-cold conditions, ensuring protease inhibitors, and western blot analysis was performed. Concisely, protein measurement was achieved using a Protein BCA Assay Kit (Pierce Chemical Co., Rockford, USA). After these were quantified, they were electrophoretically dispersed and moved into a polyvinylidene fluoride (PVDF) film. At that point, the film was blocked with a probe preserved at room temperature for 1 h, treated with primary antibodies in a 1:1,000 dilution (Bcl-XL, Bcl-2, Bim, Bad, N-cadherin, E-cadherin, β-catenin, MMP-2, Slug, TIMP-1, and TIMP-2), and set aside overnight at 4°C. Then, horseradish peroxidase (HRP)-conjugated secondary antibodies were added. The protein bands were successively stained and then visualized. The protein band quantification was determined using densitometry with ImageJ software (National Institutes of Health (NIH), Bethesda, USA) and normalized to GAPDH expression.

Statistical analyses

The statistical analysis of the data from each group was conducted using GraphPad Prism v. 8.0.2 (GraphPad Software, San Diego, USA) and IBM SPSS v. 25.0 (IBM Corp., Armonk, USA). Measurement data were presented as medians (min–max). As the sample size was too small to verify normal data distribution, the differences between the groups were analyzed using the nonparametric Kruskal–Wallis test with Dunn's post hoc test. Subsequently, significant differences among multiple groups were examined using the Kruskal–Wallis test, and Dunn's post hoc test was employed for multiple comparisons. A statistically significant data divergence was considered when $p < 0.05$. All tests in this study were bilateral.

Results

Tables 1–3 show the results of comparing variables among groups.

Antiproliferative and cytotoxic effects of UMB on glioma cells

Human U-87 GBM cell viability was assessed using the MTT test with different concentrations (5–60 μM/mL) of UMB. The data revealed that UMB reduced viability through its cytotoxic and antiproliferative actions on GBM cells in a dose-dependent way. Umbelliferone treatment at a concentration of less than 10 μM did not expressly alter the antiproliferation and cytotoxicity results for GBM cells. Conversely, higher concentrations of UMB (30 and 40 μM/mL) substantially reduced ($p < 0.05$) the viability of both U-87 cells compared to an untreated control. Using MTT assay, we detected the IC50 values of the GBM cells. Recognized based on the figure of the inhibitory concentration data of 30 and 40 μM/mL, UMB was taken for further trials (Table 1, Fig. 1).

Impact of UMB on intracellular ROS accumulation in human GBM cells

The formation of intracellular ROS is related to numerous stimuli, and it can trigger cell death and cell cycle arrest. Intracellular ROS levels were elevated in U-87 cells after being supplemented with 30 or 40 μM/mL UMB in an amount-dependent way, in contrast to the control. To clearly distinguish the accumulation of ROS, the DCFH-DA-labeled cells were examined under a BX51 fluorescence microscope (Olympus Corp.). The intensity

Table 1. Groups compared with each other regarding MTT results

Variables	Control	5 μM	10 μM	20 μM	30 μM	40 μM	50 μM	60 μM	Test value (H)**	p-value*
MTT	99.96 (90.95–108.95)	89.82 (81.73–97.89)	78.61 (71.53–85.67)	70.55 (64.17–76.87)	61.04 (55.54–66.52)	52.17 (47.46–56.84)	37.72 (34.33–41.11)	28.21 (25.66–30.74)	45.08	0.005

Data were presented as median (min–max); *p-value was generated from Kruskal–Wallis test with Dunn's post hoc test; **degrees of freedom (df) = 7.
MTT – 5-diphenyl tetrazolium bromide; H – total test values.

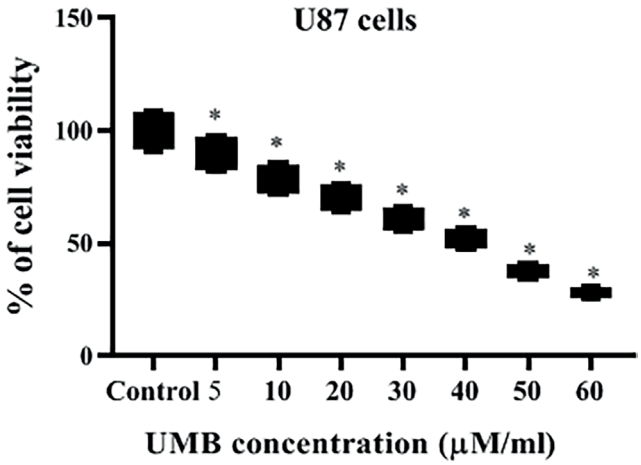


Fig. 1. Umbelliferone inhibits human GBM cell proliferation. Human U-87 GBM cells were supplemented with various concentrations (5–60 μM/mL) of UMB for 1 day. Cell viability was determined using an MTT assay. Results are presented as medians (min–max) for triplicate trials. Significant differences compared to the untreated control are denoted by *($p < 0.05$). The p-value was generated from the Kruskal–Wallis test with Dunn's post hoc test

GBM – glioblastoma multiforme; UMB – umbelliferone; MTT – 3-(4,5-dimethylthiazol-2-yl)-2,5-diphenyltetrazolium bromide.

of ROS was greatly augmented with 40 μM/mL of UMB (Table 2,3, Fig. 2).

Umbelliferone-induced apoptosis of human GBM cells revealed using dual staining with AO/EB

Apoptotic alterations in U-87 cells were visualized using dual staining with AO/EB. The GBM control cells exhibited evenly stained viable green cells (Table 2,3, Fig. 3A). The UMB-treated GBM cells presented higher apoptosis variations compared to the controls in a dose-dependent mode. Umbelliferone-treated (30 or 40 μM/mL) U-87 cells revealed apoptotic cells, chromatin condensation and membrane blebbing in what seemed like light greenish-yellow dots. Supplementation with UMB at a dose of 40 μM/mL exposed late apoptotic alterations in GBM cells, which presented as an orange-red color.

Table 2. Groups compared with each other regarding other parameters

Variables	Control (n = 6)	30 μM (n = 6)	40 μM (n = 6)	Test value (H)**	p-value*
ROS	7.03 (6.40–7.66)	23.40 (21.29–25.51)	34.90 (31.76–38.04)	15.15	<0.001
AO/EB staining	1.75 (1.59–1.91)	34.19 (31.11–37.27)	50.49 (45.95–55.03)	15.17	<0.001
DAPI staining	3.90 (3.55–4.25)	35.02 (31.87–38.17)	51.07 (46.47–55.67)	15.17	<0.001
Bcl-2	1.00 (0.91–1.09)	0.62 (0.56–0.68)	0.47 (0.43–0.51)	15.23	<0.001
Bcl-XL	1.00 (0.91–1.09)	0.68 (0.62–0.74)	0.50 (0.46–0.55)	15.22	<0.001
Bad	1.00 (0.91–1.09)	1.36 (1.24–1.48)	2.25 (2.05–2.45)	15.20	<0.001
Bim	1.00 (0.91–1.09)	1.40 (1.27–1.53)	1.96 (1.78–2.14)	15.20	<0.001
E-cadherin	1.00 (0.91–1.09)	1.37 (1.25–1.49)	2.15 (1.96–2.34)	15.20	<0.001
N-cadherin	1.00 (0.91–1.09)	0.80 (0.73–0.87)	0.65 (0.59–0.71)	15.20	<0.001
β-catenin	1.00 (0.91–1.09)	0.62 (0.56–0.68)	0.45 (0.41–0.49)	15.23	<0.001
MMP-2	1.00 (0.91–1.09)	0.80 (0.73–0.87)	0.53 (0.48–0.58)	15.20	<0.001
Slug	1.00 (0.91–1.09)	0.65 (0.59–0.71)	0.37 (0.34–0.40)	15.23	<0.001
TIMP-1	1.00 (0.91–1.09)	1.58 (1.44–1.72)	2.30 (2.09–2.51)	15.20	<0.001
TIMP-2	1.00 (0.91–1.09)	1.20 (1.09–1.31)	2.01 (1.83–2.19)	15.01	<0.001

Data were presented as median (min–max); *p-value was calculated using Kruskal–Wallis test with Dunn's post hoc test; **degrees of freedom (df) = 2; ROS – reactive oxygen species; AO/EB – acridine orange/ethidium bromide; DAPI – 4',6-diamidino-2-phenylindole; Bcl-2 – B-cell leukemia/lymphoma 2 proteins; Bcl-XL – B-cell lymphoma-extra-large; Bad – BCL2-associated death promoter; Bim – BCL-2-interacting mediator of cell death; MMP-2 – matrix metalloproteinases 2; Slug – SNAIL family of transcriptional repressors; TIMP-1 – tissue inhibitor of metalloproteinase-1; TIMP-2 – tissue inhibitor of metalloproteinase-2.

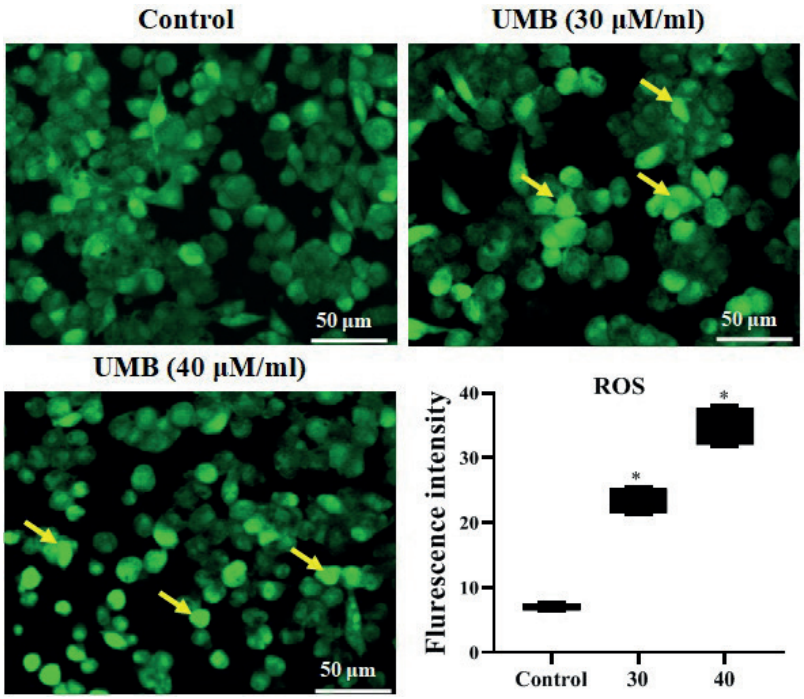


Fig. 2. Umbelliferone enhances the accumulation of ROS in glioma cells. Scale bar = 50 µm. U-87 cells with untreated control (green florescence) showing weak background florescence; arrow mark represents clearly visible DCF fluorescence. Cells treated with UMB (30 or 40 µM/mL) for 1 day showing bright DCF florescence. Results are presented as medians (min–max) for triplicate trials. Significant differences compared to the untreated control are denoted by *($p < 0.05$). The p-value was calculated using the Kruskal–Wallis test with Dunn's post hoc test

ROS – reactive oxygen species; DCFH – DA – 2'–7'-dichlorodihydrofluorescein diacetate; UMB – umbelliferone.

Table 3. The results of the Dunn's post hoc test

Explained variable	C vs 30 µM	C vs 40 µM	30 µM vs 40 µM
ROS	$p < 0.155$	$p < 0.001$	$p < 0.155$
AO/EB staining	$p < 0.154$	$p < 0.001$	$p < 0.154$
DAPI staining	$p < 0.154$	$p < 0.001$	$p < 0.154$
Bcl-2	$p < 0.154$	$p < 0.001$	$p < 0.154$
Bcl-XL	$p < 0.153$	$p < 0.001$	$p < 0.153$
Bad	$p < 0.154$	$p < 0.001$	$p < 0.154$
Bim	$p < 0.154$	$p < 0.001$	$p < 0.154$
E-cadherin	$p < 0.154$	$p < 0.001$	$p < 0.154$
N-cadherin	$p < 0.154$	$p < 0.001$	$p < 0.154$
β-catenin	$p < 0.153$	$p < 0.001$	$p < 0.153$
MMP-2	$p < 0.154$	$p < 0.001$	$p < 0.154$
Slug	$p < 0.153$	$p < 0.001$	$p < 0.153$
TIMP-1	$p < 0.154$	$p < 0.001$	$p < 0.154$
TIMP-2	$p < 0.174$	$p < 0.001$	$p < 0.174$

ROS – reactive oxygen species; AO/EB – acridine orange/ethidium bromide; DAPI – 4',6-diamidino-2-phenylindole; Bcl-2 – B-cell leukemia/lymphoma 2 proteins; Bcl-XL – B-cell lymphoma-extra-large; Bad – BCL2-associated death promoter; Bim – BCL-2-interacting mediator of cell death; MMP-2 – matrix metalloproteinases 2; Slug – SNAIL family of transcriptional repressors; TIMP-1 – tissue inhibitor of metalloproteinase-1, TIMP-2 – tissue inhibitor of metalloproteinase-2.

Umbelliferone-triggered apoptosis of human GBM cells displayed using DAPI staining

Human U-87 GBM cells stained with DAPI revealed typical viable cells with normal nuclei (Table 2,3, Fig. 3B). Treatment of the glioma cells with UMB stimulated apoptosis that intensified the nuclear morphology and fragmentation of the nuclear bodies compared to the control cells. When UMB (30 or 40 µM/mL) was added to the glioma cells, they exhibited chromatin reduction, membrane blebbing, destruction of the nuclear envelope, and cellular collapse. These effects underlined that UMB-triggered apoptosis occurs in a quantity-dependent way.

Studies on the effects of UMB on Bcl-2 family protein expression

In human GBM cells supplemented with UMB (30 or 40 µM/mL), pro-apoptotic Bad and Bim levels were elevated, whereas anti-apoptotic Bcl-2 and Bcl-XL mitigated their protein levels. These results established the apoptotic action of UMB in a quantity-dependent way (Table 2,3, Fig. 4).

Influence of UMB on metastatic protein expression

For U-87 human GBM cells supplemented with UMB (30 or 40 µM/mL), E-cadherin protein expression was elevated, whereas N-cadherin, β-catenin, MMP-2, and Slug showed attenuated protein expression. These results confirmed the apoptotic action of UMB in a concentration-dependent way (Table 2,3, Fig. 5).

Protein expression analysis of TIMP-1 and TIMP-2

TIMP-1 and TIMP-2 expressions were downregulated in untreated glioma cells. The GBM cells supplemented

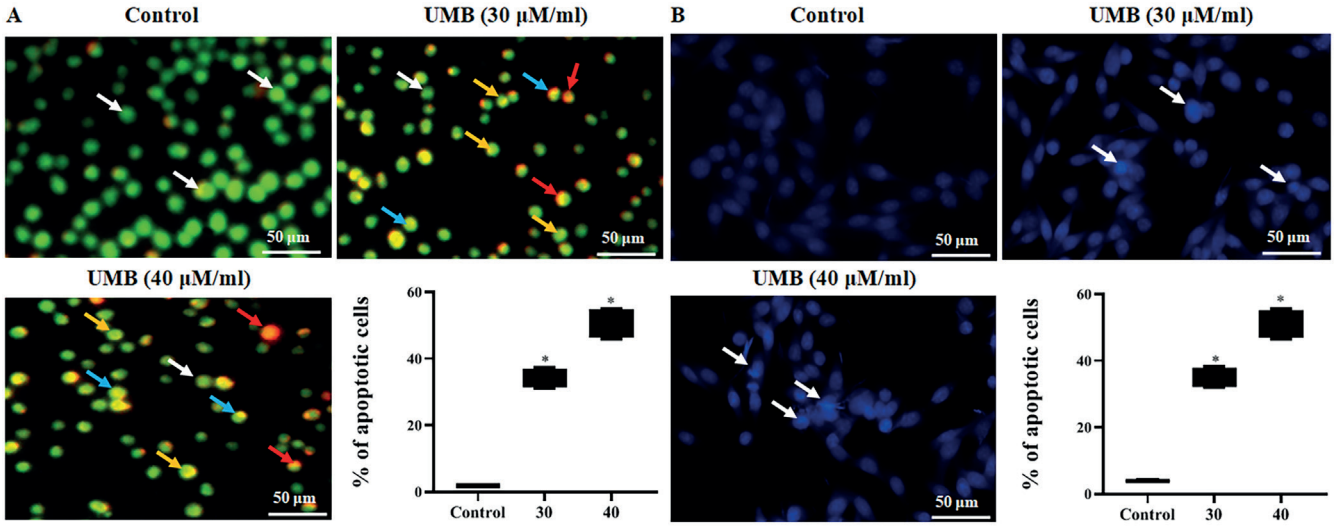


Fig. 3. Umbelliferone triggered apoptosis in glioma cells. U-87 cells were either untreated controls or U-87 cells treated with 30 or 40 μM/mL UMB for 24 h. Scale bar = 50 μm. The evaluation of apoptosis was performed using the dual staining of: (A) AO/EB staining; white arrow indicates green florescence, the orange arrow indicates apoptotic bodies, the blue arrow indicates apoptotic cells, and the yellow arrow indicates necrotic cells; (B) DAPI staining examined under a fluorescence microscope. The control cells showed a dark background as normal cells, but for the UMB-treated cells, the white arrow indicates bright fluorescence. Results are presented as medians (min–max) for triplicate trials. Significant differences compared to the untreated control are denoted by *($p < 0.05$). The p-value was calculated using the Kruskal–Wallis test with Dunn's post hoc test

ROS – reactive oxygen species; DCFH DA – 2'–7'- dichlorodihydrofluorescein diacetate; UMB – umbelliferone.

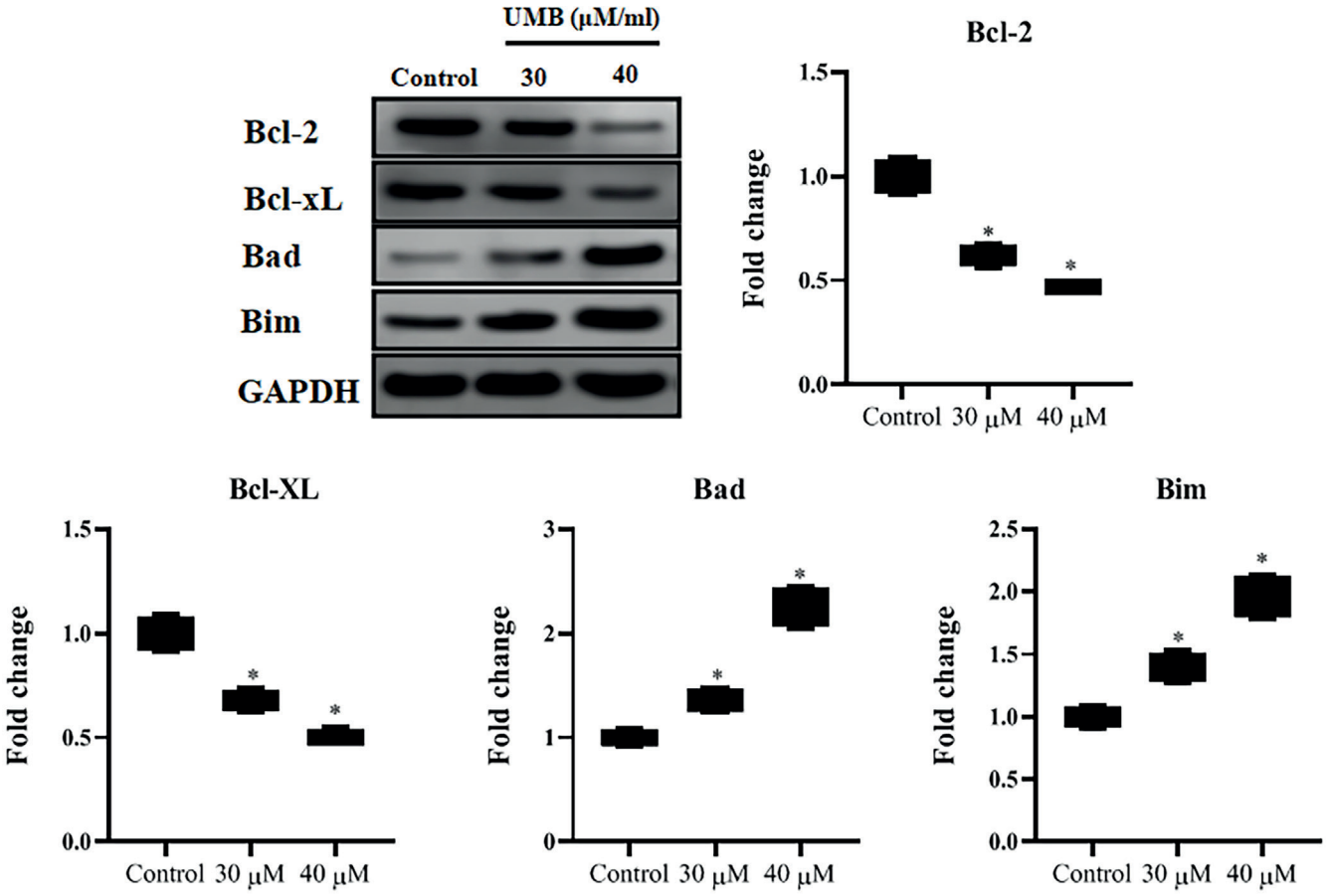


Fig. 4. Influence of UMB on the Bcl-2 family protein expression in human GBM cells. Umbelliferone (30 or 40 μM/mL) was added to the U-87 cells for 24 h, and protein levels were studied using western blot. Results are presented as medians (min–max) for triplicate trials. Significant differences compared to the untreated control are denoted by *($p < 0.05$). The p-value was calculated using the Kruskal–Wallis test with Dunn's post hoc test

GBM – glioblastoma multiforme; UMB – umbelliferone.

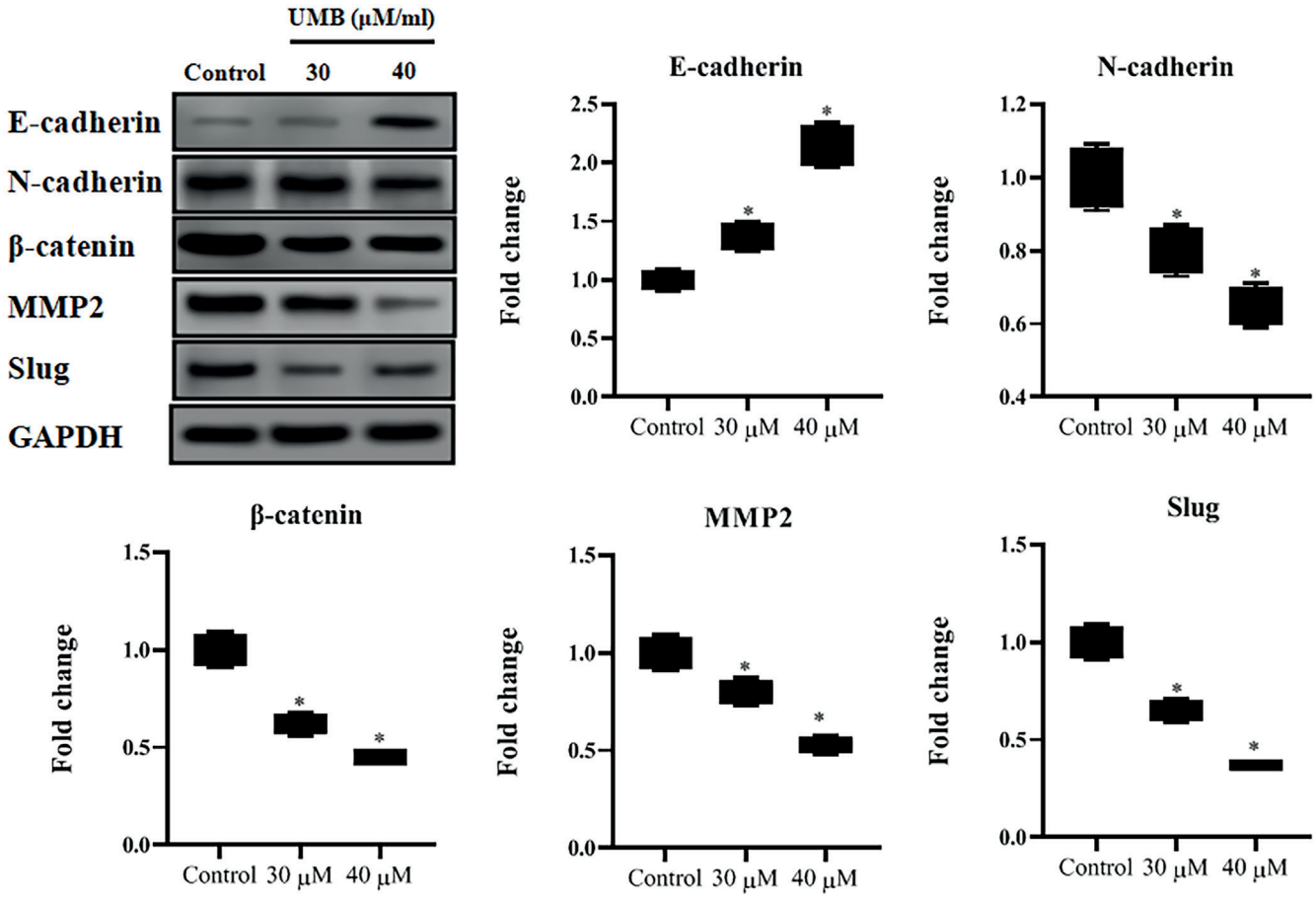


Fig. 5. Influence of UMB on metastatic protein expression in human GBM cells. Umbelliferone (30 or 40 μM/mL) was added to glioma cells for 1 day. Results are presented as medians (min–max) for triplicate trials. Significant differences compared to the untreated control are denoted by *($p < 0.05$). The p-value was calculated using the Kruskal–Wallis test with Dunn's post hoc test

GBM – glioblastoma multiforme; UMB – umbelliferone.

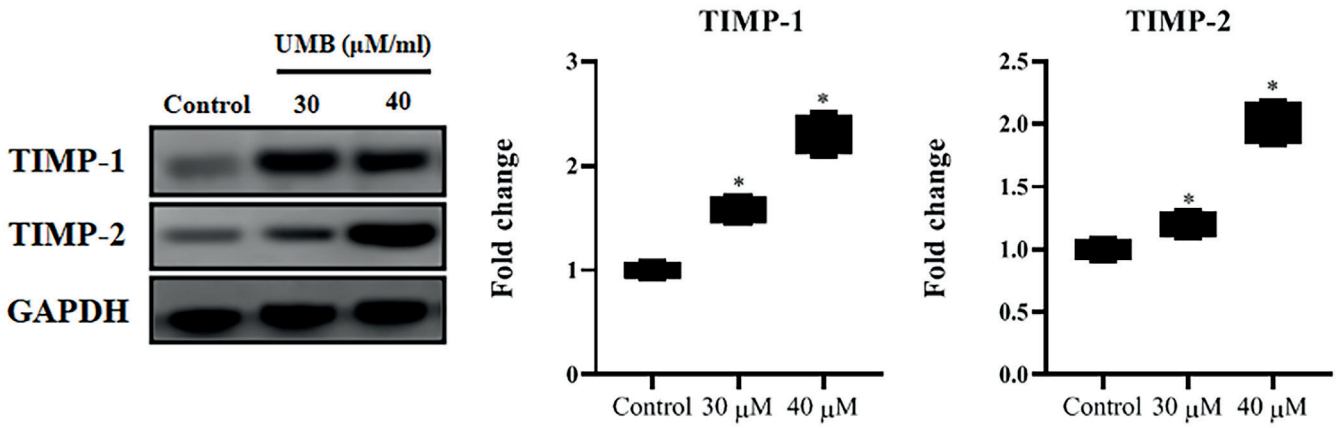


Fig. 6. Influence of UMB on TIMP-1 and TIMP-2 protein levels in human GBM cells. Umbelliferone (30 or 40 μM/mL) was added to U-87 cells for 24 h. Results are presented as medians (min–max) for triplicate trials. Significant differences compared to the untreated control are denoted by *($p < 0.05$). The p-value was calculated using the Kruskal–Wallis test with Dunn's post hoc test

GBM – glioblastoma multiforme; UMB – umbelliferone; TIMP-1 – tissue inhibitor of metalloproteinase-1; TIMP-2 – tissue inhibitor of metalloproteinase-2.

with 30 or 40 μM/mL UMB upregulated TIMP-1 and TIMP-2 protein expression in a quantity-dependent way (Table 2,3, Fig. 6).

Discussion

Malignant carcinomas are a growing problem in the medical community due to delayed diagnosis, elevated metastasis, augmented resistance, and the massive

complexity of currently existing medications. The GBM is the most common glioma, with the highest grade of malignancy among brain tumors, the least-favorable prognosis and the greatest likelihood of metastasis and recurrence.[1,3] Temozolomide is the most beneficial medication accepted for GBM treatment, but its drawback is drug resistance, which frequently happens in medical use, eventually causing treatment failure.[5] At present, several treatments are available for GBM; however, their effectiveness is partly owing to their broad ramifications. As such, researchers are mainly focused on the development of innovative medications with reduced complications. Over 50% of cancer medicines are produced from natural ingredients.

Umbelliferone, also known as 7-hydroxycoumarin, is an extensive natural component of the coumarin family. It has been documented to have analgesic, anti-inflammatory, antinociceptive, and bronchodilatory actions.[27,28] Umbelliferone has been demonstrated to display anticancer and immunomodulatory actions by constraining tumor progression of sarcoma 180 in mice models.[29] Kielbus et al.[21] stated that UMB repressed laryngeal cancer cell proliferation and migration. They reported that UMB mitigated the proliferation and migration of laryngeal RK33 malignant cells in a quantity-dependent way.[21] Umbelliferone has also been tested for anticancer activities against 7,12-dimethylbenz(a)anthracene-prompted mammary carcinomas in rats.[30] To the best of our knowledge, the current study is the first report to exhibit the cytotoxic, apoptotic and antimetastatic prompting actions of UMB in human U-87 GBM cells in vitro. The MTT assay showed that treatment with UMB mitigated cell proliferation in a dose-dependent way in glioma cells, which indicates that UMB might be an active antitumor candidate, as shown in this research.

It has been stated that stable levels of ROS are vital for preserving typical physiological roles.[7,8] The generation of intracellular ROS accompanies oxidative stress, which ultimately leads to the process of apoptosis. Additional ROS production in a biological system is harmful to proteins and DNA, which may eventually cause cell death. When there are upsurges in ROS generation, morphological variations occur and cause late apoptotic modifications, as evidenced by the dual staining of AO/EB in the current research. Next, to confirm that UMB triggered apoptosis, DAPI staining was performed. The fluorescent dye DAPI attaches to the A-T-rich DNA section. U-87-stained cells were examined under a fluorescent microscope, and the images presented fragmented DNA after treatment with UMB. Our findings revealed that elevated ROS generation occurred following UMB administration at different concentrations (30 or 40 μM/mL), in contrast to the control GBM cells, in a quantity-dependent manner. This finding also confirmed the ROS-stimulating action of UMB on U-87 cells.

To clarify the outcomes, we assessed the level of apoptotic protein expression following supplementation of glioma cells with UMB. The proportion of pro-apoptotic and anti-apoptotic proteins is vital during cell destiny determination. Our findings revealed that UMB attenuated the level of anti-apoptotic (Bcl-XL and Bcl-2) proteins and elevated the level of pro-apoptotic (Bad and Bim) proteins in a dose-dependent way. Anti-apoptotic and pro-apoptotic proteins also offer the creation of discrete channels for the permeabilization of the mitochondrial membrane.[31] Finally, we showed that the mediator molecules for cell death by UMB are Bim and Bad, which are involved in the crucial mechanisms of cell apoptosis in the mitochondrial pathway.

The current study revealed that UMB-treated glioma cells enhanced E-cadherin and TIMPs while mitigating the protein levels of N-cadherin, β-catenin, MMP-2, and Slug, compared to untreated GBM control cells. Numerous researchers have assessed the arrays of classical cadherin expression in GBM. The expression of N-cadherin in GBM has been examined in different patient cohorts, with nearly 60–80% of cases.[32] E-cadherin levels have been further showed as rare or lacking in gliomas.[33] Slug protein is a well-considered transcriptional repressor, which can directly attach to and curb the E-cadherin promoter and other cell–cell adhesion within epithelial cells.[34] The cytoplasmic domain of cadherin also contributes to cell–cell adhesion by alleviating the cadherin/catenin complex and binding this complex to the actin cytoskeleton at the membrane. It controls an extensive variety of typical physiological developments, comprising embryo enlargement, cell propagation, differentiation, gene expression, and apoptosis.[35] Preceding reports have established that the TIMP gene family members are differentially expressed in numerous tumors.[36,37] As MMPs are greatly associated with the prognosis of multiple cancers, TIMPs, at least theoretically, may affect diagnosis in a few malignancy cases as precise inhibitors. In brain tumors, including GBM, several reports have explored the disparity in the expression of TIMPs.[38] In the current study, UMB enhanced the protein expression levels of TIMP-1 and TIMP-2 in GBM cells in a dosage-dependent way.

Limitations

As a limitation, microRNA interference level molecular studies were not performed.

Conclusions

This report showed that UMB subdues the proliferation of human U-87 GBM cells through the stimulation of ROS-mediated apoptosis and its cytotoxic effects. Additionally, it could also suppress metastasis of the GBM cells by modulating the cadherin/β-catenin complex-mediated cell–cell adhesion in human glioblastoma cells. These outcomes suggest that UMB may prove to be a key component of antitumor agents or antitumor lead molecules. However, further research endeavors involving the precise molecular mechanisms of its antimetastatic effects are urgently required.

Supplementary data

The supplementary materials are available at https://doi.org/10.5281/zenodo.12804976. The package includes the following files:

Supplementary Fig. 1. Results of Kruskal–Wallis test as presented in Fig. 1.

Supplementary Fig. 2. Results of Kruskal–Wallis test as presented in Fig. 2.

Supplementary Fig. 3. Results of Kruskal–Wallis test as presented in Fig. 3.

Supplementary Fig. 4. Results of Kruskal–Wallis test as presented in Fig. 4.

Supplementary Fig. 5. Results of Kruskal–Wallis test as presented in Fig. 5.

Supplementary Fig. 6. Results of Kruskal–Wallis test as presented in Fig. 6.

Data availability

The datasets generated and/or analyzed during the current study are available from the corresponding author on reasonable request.

Consent for publication

Not applicable.

ORCID iDs

Wei Ma https://orcid.org/0009-0000-2793-1065
Hangyu Shi https://orcid.org/0009-0005-8832-1646
Xinya Dong https://orcid.org/0009-0008-9413-8663
Yongqiang Shi https://orcid.org/0009-0009-7240-0488
Luyi Zhang https://orcid.org/0009-0008-8173-1468
Bin Jiang https://orcid.org/0000-0001-8438-0001

References

1. Molinaro AM, Taylor JW, Wiencke JK, Wrensch MR. Genetic and molecular epidemiology of adult diffuse glioma. *Nat Rev Neurol*. 2019;15(7):405–417. doi:10.1038/s41582-019-0220-2
2. Souza TKF, Nucci MP, Mamani JB, et al. Image and motor behavior for monitoring tumor growth in C6 glioma model. *PLoS One*. 2018;13(7):e0201453. doi:10.1371/journal.pone.0201453
3. Delgado-Martín B, Medina MÁ. Advances in the knowledge of the molecular biology of glioblastoma and its impact in patient diagnosis, stratification, and treatment. *Adv Sci (Weinh)*. 2020;7(9):1902971. doi:10.1002/advs.201902971
4. Bleeker FE, Molenaar RJ, Leenstra S. Recent advances in the molecular understanding of glioblastoma. *J Neurooncol*. 2012;108(1):11–27. doi:10.1007/s11060-011-0793-0
5. Stupp R, Hegi ME, Mason WP, et al. Effects of radiotherapy with concomitant and adjuvant temozolomide versus radiotherapy alone on survival in glioblastoma in a randomised phase III study: 5-year analysis of the EORTC-NCIC trial. *Lancet Oncol*. 2009;10(5):459–466. doi:10.1016/S1470-2045(09)70025-7
6. Furnari FB, Fenton T, Bachoo RM, et al. Malignant astrocytic glioma: Genetics, biology, and paths to treatment. *Genes Dev*. 2007;21(21):2683–2710. doi:10.1101/gad.1596707
7. Sena LA, Chandel NS. Physiological roles of mitochondrial reactive oxygen species. *Mol Cell*. 2012;48(2):158–167. doi:10.1016/j.molcel.2012.09.025
8. Covarrubias L, Hernández-García D, Schnabel D, Salas-Vidal E, Castro-Obregón S. Function of reactive oxygen species during animal development: Passive or active? *Dev Biol*. 2008;320(1):1–11. doi:10.1016/j.ydbio.2008.04.041
9. Bellance N, Lestienne P, Rossignol R. Mitochondria: From bioenergetics to the metabolic regulation of carcinogenesis. *Front Biosci (Landmark Ed)*. 2009;14(11):4015–4034. doi:10.2741/3509
10. Sullivan LB, Chandel NS. Mitochondrial reactive oxygen species and cancer. *Cancer Metab*. 2014;2(1):17. doi:10.1186/2049-3002-2-17
11. Redza-Dutordoir M, Averill-Bates DA. Activation of apoptosis signalling pathways by reactive oxygen species. *Biochim Biophys Acta Mol Cell Res*. 2016;1863(12):2977–2992. doi:10.1016/j.bbamcr.2016.09.012
12. Bacac M, Stamenkovic I. Metastatic cancer cell. *Annu Rev Pathol Mech Dis*. 2008;3(1):221–247. doi:10.1146/annurev.pathmechdis.3.121806.151523
13. Coopman P, Djiane A. Adherens junction and E-cadherin complex regulation by epithelial polarity. *Cell Mol Life Sci*. 2016;73(18):3535–3553. doi:10.1007/s00018-016-2260-8
14. Hulpiau P, Van Roy F. Molecular evolution of the cadherin superfamily. *Int J Biochem Cell Biol*. 2009;41(2):349–369. doi:10.1016/j.biocel.2008.09.027
15. Lu P, Takai K, Weaver VM, Werb Z. Extracellular matrix degradation and remodeling in development and disease. *Cold Spring Harb Perspect Biol*. 2011;3(12):a005058. doi:10.1101/cshperspect.a005058
16. Ahir BK, Engelhard HH, Lakka SS. Tumor development and angiogenesis in adult brain tumor: Glioblastoma. *Mol Neurobiol*. 2020;57(5):2461–2478. doi:10.1007/s12035-020-01892-8
17. Arpino V, Brock M, Gill SE. The role of TIMPs in regulation of extracellular matrix proteolysis. *Matrix Biol*. 2015;44–46:247–254. doi:10.1016/j.matbio.2015.03.005
18. Ries C. Cytokine functions of TIMP-1. *Cell Mol Life Sci*. 2014;71(4):659–672. doi:10.1007/s00018-013-1457-3
19. Mazimba O. Umbelliferone: Sources, chemistry and bioactivities review. *Bull Fac Pharm Cairo Univ*. 2017;55(2):223–232. doi:10.1016/j.bfopcu.2017.05.001
20. Muthu R, Thangavel P, Selvaraj N, Ramalingam R, Vaiyapuri M. Synergistic and individual effects of umbelliferone with 5-fluorouracil on the status of lipid peroxidation and antioxidant defense against 1,2-dimethylhydrazine induced rat colon carcinogenesis. *Biomed Prevent Nutr*. 2013;3(1):74–82. doi:10.1016/j.bionut.2012.10.011
21. Kielbus M, Skalicka-Wozniak K, Grabarska A, et al. 7-substituted coumarins inhibit proliferation and migration of laryngeal cancer cells in vitro. *Anticancer Res*. 2013;33(10):4347–4356. PMID:24123002.
22. Yu SM, Hu DH, Zhang JJ. Umbelliferone exhibits anticancer activity via the induction of apoptosis and cell cycle arrest in HepG2 hepatocellular carcinoma cells. *Mol Med Rep*. 2015;12(3):3869–3873. doi:10.3892/mmr.2015.3797
23. Mosmann T. Rapid colorimetric assay for cellular growth and survival: Application to proliferation and cytotoxicity assays. *J Immunol Methods*. 1983;65(1–2):55–63. doi:10.1016/0022-1759(83)90303-4
24. Gao H, Liu Z, Xu W, et al. Pterostilbene promotes mitochondrial apoptosis and inhibits proliferation in glioma cells. *Sci Rep*. 2021;11(1):6381. doi:10.1038/s41598-021-85908-w
25. Kasibhatla S, Amarante-Mendes GP, Finucane D, Brunner T, Bossy-Wetzel E, Green DR. Acridine orange/ethidium bromide (AO/EB) staining to detect apoptosis. *Cold Spring Harb Protoc*. 2006;2006(3):pdb.prot4493. doi:10.1101/pdb.prot4493
26. Zheng D, Zhu G, Liao S, et al. Dysregulation of the PI3K/Akt signaling pathway affects cell cycle and apoptosis of side population cells in nasopharyngeal carcinoma. *Oncol Lett*. 2015;10(1):182–188. doi:10.3892/ol.2015.3218
27. Leal LKAM, Ferreira AAG, Bezerra GA, Matos FJA, Viana GSB. Antinociceptive, anti-inflammatory and bronchodilator activities of Brazilian medicinal plants containing coumarin: A comparative study. *J Ethnopharmacol*. 2000;70(2):151–159. doi:10.1016/S0378-8741(99)00165-8
28. Lino CS, Taveira ML, Viana GSB, Matos FJA. Analgesic and antiinflammatory activities of *Justicia pectoralis* Jacq and its main constituents: Coumarin and umbelliferone. *Phytother Res*. 1997;11(3):211–215. doi:10.1002/(SICI)1099-1573(199705)11:3<211::AID-PTR72>3.0.CO;2-W
29. Stefanova TH, Nikolova NJ, Toshkova RA, Neychev HO. Antitumor and immunomodulatory effect of coumarin and 7-hydroxycoumarin against sarcoma 180 in mice. *J Exp Ther Oncol*. 2007;6(2):107–115. PMID:17407969.

30. Maucher A, Von Angerer E. Antitumour activity of coumarin and 7-hydroxycoumarin against 7, 12-dimethylbenz[a]anthracene-induced rat mammary carcinomas. *J Cancer Res Clin Oncol*. 1994;120(8):502–504. doi:10.1007/BF01191806
31. Youle RJ, Strasser A. The BCL-2 protein family: Opposing activities that mediate cell death. *Nat Rev Mol Cell Biol*. 2008;9(1):47–59. doi:10.1038/nrm2308
32. Noh MG, Oh SJ, Ahn EJ, et al. Prognostic significance of E-cadherin and N-cadherin expression in gliomas. *BMC Cancer*. 2017;17(1):583. doi:10.1186/s12885-017-3591-z
33. Howng SL, Wu CH, Cheng TS, et al. Differential expression of Wnt genes, β-catenin and E-cadherin in human brain tumors. *Cancer Lett*. 2002;183(1):95–101. doi:10.1016/S0304-3835(02)00085-X
34. Eger A, Aigner K, Sonderegger S, et al. DeltaEF1 is a transcriptional repressor of E-cadherin and regulates epithelial plasticity in breast cancer cells. *Oncogene*. 2005;24(14):2375–2385. doi:10.1038/sj.onc.1208429
35. Ratheesh A, Yap AS. A bigger picture: Classical cadherins and the dynamic actin cytoskeleton. *Nat Rev Mol Cell Biol*. 2012;13(10):673–679. doi:10.1038/nrm3431
36. Böckelman C, Beilmann-Lehtonen I, Kaprio T, et al. Serum MMP-8 and TIMP-1 predict prognosis in colorectal cancer. *BMC Cancer*. 2018;18(1):679. doi:10.1186/s12885-018-4589-x
37. Azevedo Martins JM, Rabelo-Santos SH, Do Amaral Westin MC, Zeferino LC. Tumoral and stromal expression of MMP-2, MMP-9, MMP-14, TIMP-1, TIMP-2, and VEGF-A in cervical cancer patient survival: A competing risk analysis. *BMC Cancer*. 2020;20(1):660. doi:10.1186/s12885-020-07150-3
38. Guo H, Sun Z, Wei J, et al. Expressions of matrix metalloproteinases-9 and tissue inhibitor of metalloproteinase-1 in pituitary adenomas and their relationships with prognosis. *Cancer Biother Radiopharm*. 2019;34(1):1–6. doi:10.1089/cbr.2018.2589

Improving sepsis mortality prediction with machine learning: A comparative study of advanced classifiers and performance metrics

*Puyu Zhou[1,A–F], *Jiazheng Duan[2,A–F], Jianqing Li[1,A–F]

[1] Macau University of Science and Technology, China
[2] Dongguan Yumei Photoelectric Co., Ltd., China

A – research concept and design; B – collection and/or assembly of data; C – data analysis and interpretation;
D – writing the article; E – critical revision of the article; F – final approval of the article

Advances in Clinical and Experimental Medicine, ISSN 1899–5276 (print), ISSN 2451–2680 (online) *Adv Clin Exp Med*. 2025;34(8):1393–1402

Address for correspondence
Jianqing Li
E-mail: jqli@must.edu.mo

Funding sources
None declared

Conflict of interest
None declared

* Puyu Zhou and Jiazheng Duan contributed equally to this work.

Received on January 22, 2024
Reviewed on August 9, 2024
Accepted on October 15, 2024

Published online on February 11, 2025

Abstract

Background. High sepsis mortality rates pose a serious global health problem. Machine learning is a promising technique with the potential to improve mortality prediction for this disease in an accurate and timely manner.

Objectives. This study aimed to develop a model capable of rapidly and accurately predicting sepsis mortality using data that can be quickly obtained in an ambulance, with a focus on practical application during ambulance transport.

Materials and methods. Data from the Medical Information Mart for Intensive Care-IV (MIMIC-IV) dataset were used to compare the performance of 11 machine learning algorithms against the widely utilized quick Sequential Organ Failure Assessment (qSOFA) score. A dynamic updating model was implemented. Performance was evaluated using area under the curve (AUC) and precision-recall area under the curve (PRAUC) scores, and feature importance was assessed with SHapley Additive exPlanations (SHAP) values.

Results. The light gradient boosting machine (LightGBM) model achieved the highest AUC (0.79) and PRAUC (0.44) scores, outperforming the qSOFA score (AUC = 0.76, PRAUC = 0.40). The LightGBM also achieved the highest PRAUC (0.44), followed by Optuna_LightGBM (0.43) and random forest (0.42). The dynamically updated and tuned model further improved performance metrics (AUC = 0.79, PRAUC = 0.44) compared to the base model (AUC = 0.76, PRAUC = 0.39). Feature importance analysis offers clinicians insights for prioritizing patient assessments and interventions.

Conclusions. The LightGBM-based model demonstrated superior performance in predicting sepsis-related mortality in an ambulance setting. This study underscores the practical applicability of machine learning models, addressing the limitations of previous research, and highlights the importance of real-time updates and hyperparameter tuning in optimizing model performance.

Key words: machine learning, LightGBM, hyperparameter tuning, sepsis-related mortality, dynamic updating

Cite as
Zhou P, Duan J, Li J. Improving sepsis mortality prediction with machine learning: A comparative study of advanced classifiers and performance metrics. *Adv Clin Exp Med*. 2025;34(8):1393–1402. doi:10.17219/acem/194660

DOI
10.17219/acem/194660

Copyright
Copyright by Author(s)
This is an article distributed under the terms of the Creative Commons Attribution 3.0 Unported (CC BY 3.0) (https://creativecommons.org/licenses/by/3.0/)

Introduction

Sepsis is a critical global health issue, contributing significantly to worldwide morbidity and mortality. Rapid identification and intervention are crucial for improving patient outcomes because early interventions have been shown to increase survival rates. Developing accurate and efficient diagnostic tools for sepsis is, therefore, essential. Due to the limitations of current medical technologies in diagnosing sepsis from a biomarker perspective, statistics-driven machine learning techniques have gained increasing attention from medical diagnostic researchers. A growing volume of data, including laboratory results, vital signs, genetic, molecular, and clinical data, as well as patient health histories, is available in high resolution for high-risk individuals and sepsis patients.[1–5] Gradient boosting trees (GBT) are among the most widely used machine learning methods,[6] followed by logistic regression,[6,7] random forest (RF),[8] ridge regression,[9] lasso regression (LR),[10] naïve Bayes (NB),[11] K-nearest neighbors (KNN),[12–14] gated recurrent units,[15,16] and long short-term memory.[17] For hyperparameter tuning, 2 studies used grid search methods,[18,19] and 2 use Bayesian optimization methods.[20,21] Amrollahi et al.[22] and Zhang et al.[23] compared their algorithms to scoring systems used in clinical practice, such as systemic inflammatory response syndrome (SIRS), Sequential Organ Failure Assessment (SOFA), quick SOFA (qSOFA), Modified Early Warning System (MEWS), or targeted real-time Early Warning System (TREWScore).

However, the aforementioned papers have some shortcomings. Some studies have relatively small sample sizes, which may affect the generalizability of the results, such as the studies by Delahanty et al.[24] and Hammoud et al.[25] In some studies, the proposed models were not adequately validated. For example, the study by Culliton et al.[26] did not provide detailed information about the model's performance on an independent test set. Some studies used different feature selection methods, making it difficult to fairly compare the performance differences between methods, such as the studies by Goh et al.[3] and Qin et al.[27] In some studies, multiple algorithms were compared without explaining why these particular algorithms were chosen, such as in the studies by Horng et al.[28] and Apostolova and Velez.[29] When using machine learning methods, several papers did not provide detailed information about hyperparameter tuning, such as the study by Amrollahi et al.[22] Other publications compared their algorithms to existing clinical scoring systems but did not elaborate on the limitations of these scoring systems. For example, the study by Delahanty et al.[24] compared their algorithm to SIRS, SOFA, qSOFA, MEWS, and TREWScore, without discussing the shortcomings of these scoring systems in detail. Additionally, racial, age and sex differences in the study participants were not adequately considered in some research, which may affect the predictive ability of the model.

Differences exist among various populations. For example, in the study by Liu et al.,[30] natural language processing methods were used to predict sepsis, but the demographic characteristics of the study participants were not discussed in detail. Some studies do not fully address the feasibility and practicality of the models in clinical practice. For example, in the studies by Goh et al.[3] and Qin et al.,[27] although their models demonstrate high accuracy in predicting sepsis, challenges related to data acquisition, data processing and model deployment in actual clinical applications were not addressed. Additionally, some studies did not thoroughly discuss the handling methods and potential issues associated with different data types. For example, in the study by Johnson et al.,[31] various types of data (such as laboratory, vital signs, genetic, molecular, and clinical data) were mentioned, but detailed integration methods and potential problems were not discussed. Furthermore, some studies did not explicitly point out the advantages and areas for improvement of machine learning methods in sepsis prediction. For example, Hammoud et al.[25] used LR for prediction but did not discuss the advantages and limitations of this method compared to others. The choice of evaluation metrics may also affect the interpretation of results. For example, Horng et al.[28] used multiple evaluation metrics but did not discuss the relationships between these metrics and their applicability in assessing model performance. Finally, some studies did not consider the baseline risk characteristics of patients, which may influence the accuracy and applicability of model predictions. For example, Apostolova and Velez[29] did not discuss the patient's baseline risk characteristics and their impact on model predictions.

In this study, we aimed to develop a model that can quickly and accurately predict sepsis mortality using data that can be rapidly obtained during ambulance transport. Using the Medical Information Mart for Intensive Care (MIMIC)-IV dataset, we compared the performance of 11 machine learning algorithms and benchmarked our results against the widely used qSOFA score. To enhance the clinical applicability of our model, we carefully selected features that are feasible to collect during ambulance transport, addressed demographic differences among patients, and considered baseline risk characteristics that could impact predictive performance. Additionally, we emphasized the importance of the precision-recall area under the curve (PRAUC) metric for evaluating models on imbalanced datasets, a common challenge in sepsis research. To further improve the predictive capabilities of our clinical decision support system, we implemented a real-time updating model, leveraging both online and incremental learning approaches to dynamically incorporate new patient data.

Objectives

Our research contributes to the practical application of machine learning methods for predicting sepsis-related mortality.

Materials and methods

The data used in this study were derived from the MIMIC-IV database, a comprehensive de-identified database that provides intensive care data from Beth Israel Deaconess Medical Center (BIDMC; Boston, USA).[31] The database contains information on over 40,000 patients who were admitted to the intensive care units (ICUs) at BIDMC between 2008 and 2019. It adopts a modular approach to data organization, emphasizing data sources and enabling the separation and combination of different data types. The dataset includes 'hosp' modules and 'icu' modules. The 'hosp' module contains data from electronic health records throughout the hospital. These measurements are mainly recorded during hospitalization, though some tables also include data from outpatient sources (e.g., outpatient laboratory tests). Patient demographics (patients), hospitalizations (admissions) and within-hospital transfers (transfers) are recorded in the 'hosp' module. The 'icu' module contains data from BIDMC's clinical information system, MetaVision (iMDSoft).[31] Necessary training data samples have been completed, with a record ID of 49953233.

Ambulance measurable features

The features in the MIMIC-IV dataset (Table 1) can be rapidly measured during ambulance transport. Early assessment and intervention by ambulance teams are crucial for improving patient outcomes and minimizing complications. Real-time monitoring of vital signs and laboratory indicators allows emergency medical providers to assess the patient's condition promptly and administer appropriate treatment. This approach can improve patient survival rates, shorten hospital stays and reduce medical costs.[32,33]

Methods

Features

The features in the dataset are mainly divided into 2 types: numerical and categorical. Numerical features are represented by real numbers, such as age, heart rate (HR) and blood pressure, and usually require scaling (normalization or standardization). Categorical features consist of fixed categories, such as sex, ethnicity and marital status, and must usually be encoded (e.g., one-hot encoding) to convert them into numerical form. To distinguish between numerical and categorical features in the dataset, we defined 2 separate lists and applied different preprocessing steps to them. Missing values in numerical features were filled with the median, whereas missing values in categorical features were filled with the mode. For outlier handling, HR values were limited to the range of 30–200 bpm.

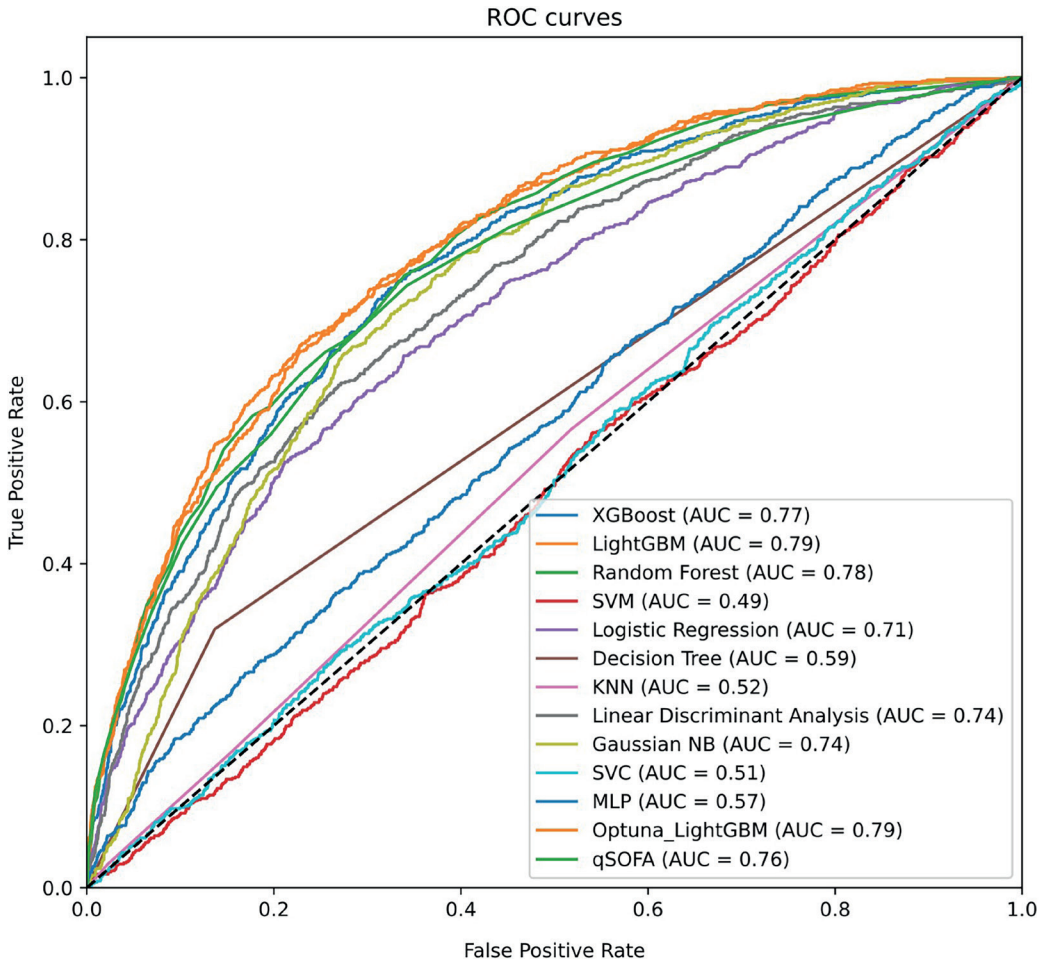
Although both feature and label values after one-hot encoding were represented as 0/1, their meanings differed. Features after one-hot encoding indicated the presence of a particular category, whereas label values represented the survival status of the patient. During model training, the algorithm attempts to combine all features to predict the target variable. If concerns arise about the potential negative impact of one-hot encoding on predictions, alternative encoding methods, such as ordinal encoding or target encoding, may be considered. However, in most cases, one-hot encoding is an effective method for encoding categorical features.

Statistical analyses

When the dataset contains many categorical features, each with multiple categories, one-hot encoding can result in a significant increase in data dimensionality. In such cases, dimensionality reduction methods (e.g., principal

Table 1. Features that can be measured quickly in an ambulance from the Medical Information Mart for Intensive Care-IV (MIMIC-IV) dataset

Category	Feature	Meaning
Vital signs	heart rate (HR)	An abnormal HR may indicate deterioration of the patient's condition.
	systolic blood pressure (SBP)	Abnormal blood pressure may be a sign of septic shock.
	diastolic blood pressure (DBP)	?
	respiratory rate (RR)	An increased RR may be a sign of complications such as hypoxemia.
	temperature (temp)	Abnormal temperature may be a sign of infection.
	oxygen saturation (SpO_2)	Low oxygen saturation may indicate hypoxemia.
Laboratory indicators	white blood cell count (WBC)	Abnormal WBC count may indicate infection.
	lactic acid	Elevated lactic acid levels may be associated with septic shock.
	C-reactive protein (CRP)	Elevated CRP levels during the acute-phase response may indicate infection.
	creatinine	Elevated creatinine levels may be a sign of renal impairment.
	liver function indicators (e.g., ALT, AST)	Abnormal liver function indicators may indicate liver damage.
Patient demographics	age	Age may be an important factor in determining the patient's health status.
	sex	Different sexes may have different risks for certain diseases, such as cardiovascular diseases or cancers.



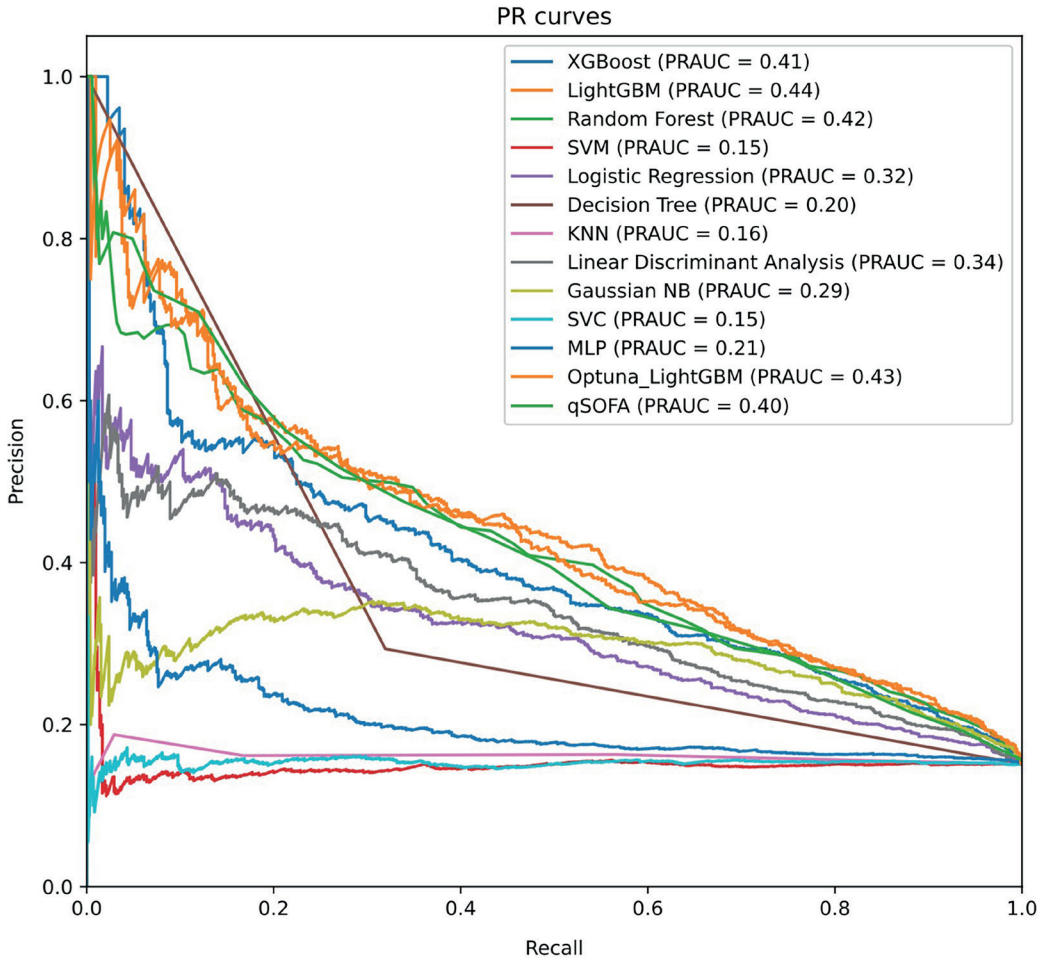


Fig. 1. Performance comparison of machine learning algorithms for sepsis-related mortality prediction. This figure presents the area under the curve (AUC) and precision-recall area under the curve (PRAUC) scores for 11 machine learning algorithms and the quick Sequential Organ Failure Assessment (qSOFA) score evaluated in our study. The LightGBM algorithm achieved the highest AUC score (0.79) and PRAUC score (0.44), outperforming both the qSOFA score (AUC = 0.76, PRAUC = 0.40) and other machine learning models. These results highlight the superior performance of the LightGBM-based model for predicting sepsis-related mortality in an ambulance setting

component analysis) or feature selection methods can be used to reduce the number of features.

In clinical applications, identifying minority samples is often more valuable than identifying majority samples, which is the focus of classifier construction. However, current machine learning models for predicting sepsis mortality are mainly designed to maximize overall classification accuracy, which limits their ability to effectively identify minority samples. Therefore, we included both PRAUC and area under the curve (AUC) as indicators to select the optimal algorithm.

We used several algorithms to classify the dataset, including XGBoost, light gradient boosting machine (LightGBM) (https://github.com/microsoft/LightGBM), RF, support vector machine, logistic regression, decision tree, KNN, linear discriminant analysis, Gaussian NB, support vector classification, and multilayer perceptron.

The purpose of this study was to analyze specific datasets. The chosen algorithm may not always be the one considered best for general use, but rather the most appropriate one for the specific data at hand. In addition to the aforementioned algorithms, we introduced an updating model strategy to improve the predictive performance of our clinical decision support system. We explored both online learning and incremental learning approaches to dynamically update the model as new patient data became available. This updating strategy enables the model to adapt to changes in patient physiological parameters, providing more accurate predictions for clinicians.

The updating model involves retraining the classifier with new data, which can be achieved by either retraining the model from scratch or updating the existing model with the new data. For algorithms that support incremental learning (e.g., XGBoost, LightGBM), we employed an incremental learning approach. For algorithms that do not support incremental learning, we used an online learning approach, which involves retraining the model from scratch using the updated dataset.

In summary, our methodology involved preprocessing the dataset, selecting the optimal algorithm based on PRAUC and AUC indicators, and implementing an updating model strategy to ensure the model's performance remains accurate and relevant in the face of changing patient data.

The underlying hypothesis for our methodology is the variance contribution hypothesis, which posits that the variance of the data is mainly contributed by a few principal components (i.e., most of the information can be summarized by a smaller number of composite variables). This hypothesis is tested by evaluating the cumulative variance contribution ratio.

Results

The LightGBM algorithm achieved the highest AUC score of 0.79, followed closely by RF (AUC = 0.78) and XGBoost (AUC = 0.77), as shown in Fig. 1, which provides a comprehensive comparison of the AUC and PRAUC scores for all evaluated models. The qSOFA score had an AUC of 0.76, demonstrating that the LightGBM-based model outperformed traditional methods in terms of discriminatory ability. In terms of PRAUC, LightGBM also achieved the highest score (0.44), followed by Optuna_LightGBM (0.43) and RF (0.42). The qSOFA score had a PRAUC of 0.40, demonstrating the advantage of our proposed model in detecting the positive class in the presence of class imbalance.

Despite involving hyperparameter tuning, the Optuna_LightGBM model did not outperform the default LightGBM model in terms of AUC and PRAUC scores.

By calculating the SHAP values of the LightGBM model, as shown in Fig. 2, we ranked the features by importance in descending order: maximum blood urea nitrogen, patient age at admission, maximum HR, minimum mean arterial pressure, minimum blood glucose, patient ethnicity, maximum blood sodium concentration, minimum respiratory rate, maximum respiratory rate, maximum blood creatinine, minimum blood urea nitrogen, minimum HR, minimum blood sodium concentration, minimum blood creatinine, minimum white blood cell count, minimum hematocrit, maximum blood glucose, maximum mean arterial pressure, maximum white blood cell count, and maximum hematocrit. These features are ranked according to their contribution to the model's predictions.

In this study, we implemented a real-time updating model to improve the predictive performance of our clinical decision support system. We explored both online learning and incremental learning approaches to dynamically update the model as new patient data became available. The incremental GBT, which was compatible with our current LightGBM model, was used as the incremental learning method.

To evaluate the performance of our dynamically updated model, we used sliding window validation and other time series validation methods. The results show that the dynamically updated model better adapts to changes in patient physiological parameters, providing more accurate predictions for clinicians.

We also addressed the issue of overfitting by incorporating regularization, reducing model complexity, employing early stopping, and utilizing additional data when available. These techniques help prevent overfitting while ensuring optimal model performance with the available data.

Additionally, we conducted hyperparameter tuning using grid search, focusing on key parameters such as "num_leaves", "feature_fraction", "bagging_fraction", "bagging_freq", and "learning_rate". We then compared the tuned model to the base model in terms of AUC and PRAUC.

The results showed that the tuned model with dynamic updating outperformed the base model, achieving an AUC of 0.79 (compared to 0.76 for the base model) and a PRAUC

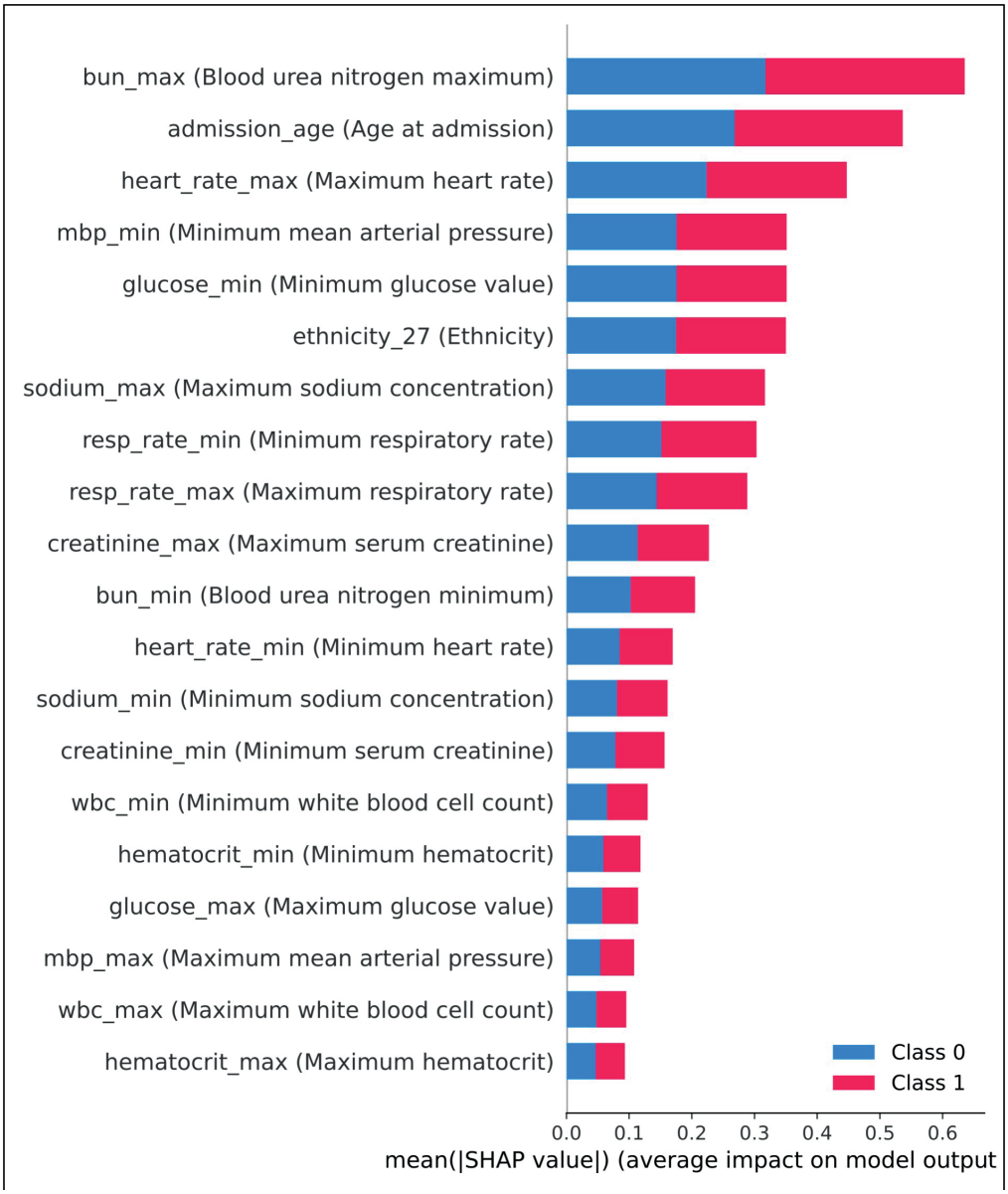


Fig. 2. Feature importance ranking for the LightGBM model using SHAP values. This figure presents a horizontal bar chart illustrating the relative importance of the top 20 features, ranked in descending order, for predicting sepsis-related mortality using the LightGBM model. The x-axis represents the SHAP (SHapley Additive exPlanations) values, reflecting each feature's contribution to the model's prediction. The y-axis lists the features, with the most important feature (maximum blood urea nitrogen) at the top and the least important feature (maximum hematocrit) at the bottom. This ranking helps healthcare professionals prioritize physiological indicators and focus on critical factors when assessing a patient's condition during ambulance transport

of 0.44 (compared to 0.39 for the base model), as illustrated in Fig. 3, which highlights the advantages of real-time updates and hyperparameter tuning.

Discussion

Addressing the challenges posed by imbalanced classification problems, this study applies machine learning algorithms to improve sepsis mortality prediction. Our results show that the LightGBM algorithm outperformed other classifiers in this context, largely due to its ability to handle imbalanced datasets and its efficient computational properties. Furthermore, we found that the PRAUC was a more appropriate evaluation metric for imbalanced classification problems because it better reflected the performance changes of the classifier at different thresholds and provided insight into the trade-off between precision and recall.

The Optuna_LightGBM did not outperform the default LightGBM model in terms of AUC and PRAUC scores. This may be because the default hyperparameters of LightGBM were already well optimized for this specific problem, and additional tuning did not result in a significant improvement. Moreover, hyperparameter tuning may introduce the risk of overfitting, which could potentially limit the generalizability of the model.

The superior performance of LightGBM over other classifiers can be attributed to its ability to handle large-scale data, high-dimensional features and class imbalance more effectively. As a gradient boosting framework, LightGBM is known for its efficiency and scalability, making it well-suited for the complex nature of sepsis-related mortality prediction.

These results are of great value for doctors using the LightGBM model to predict sepsis mortality in patients transported using ambulances. First, doctors can

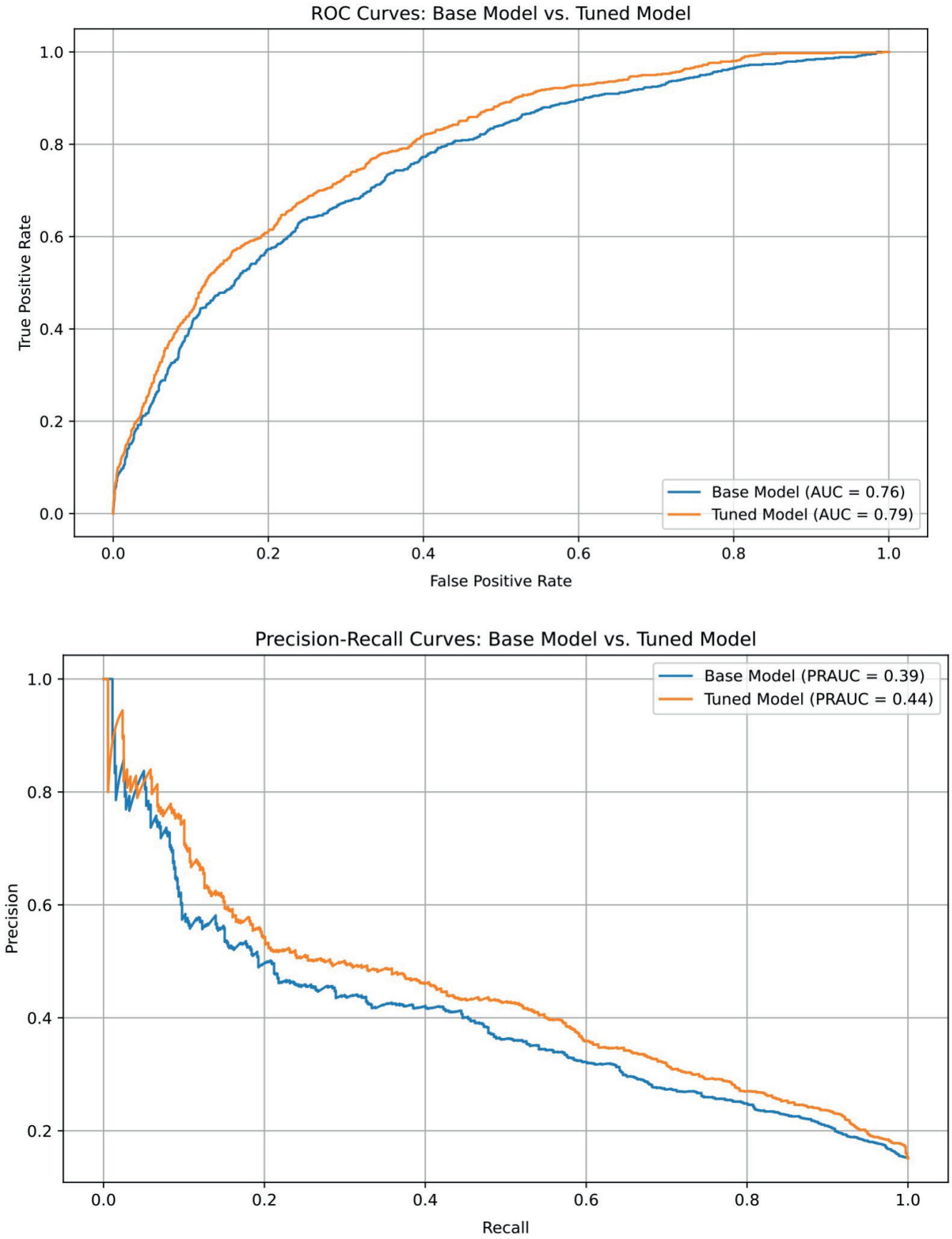


Fig. 3. Performance comparison of the dynamically updated model and the base model. The dynamically updated model achieves higher area under the curve (AUC) (0.79) and precision-recall area under the curve (PRAUC) (0.44) scores compared to the base model (AUC = 0.76, PRAUC = 0.39), demonstrating the advantages of real-time updates and hyperparameter tuning in improving the model's predictive performance for sepsis-related mortality in an ambulance setting

understand which physiological indicators play a more significant role in mortality prediction, based on feature rankings, allowing them to prioritize attention to these indicators. Second, the feature rankings help doctors quickly assess the patient's condition in the ambulance and take appropriate intervention measures based on the model's predictions.

The LightGBM demonstrates superior performance in our experiment for several reasons:

Data structure: As a gradient boosted trees-based algorithm, LightGBM employs an optimized feature histogram method that handles large-scale datasets and high-dimensional features more efficiently. Additionally, it incorporates gradient-based one-side sampling and exclusive feature bundling techniques to reduce memory consumption and computational complexity, enabling faster convergence while maintaining high accuracy.

Model structure: LightGBM uses a leaf-wise growth strategy that reduces the risk of overfitting compared to traditional level-wise growth strategies. This approach focuses on fitting the training data by splitting the leaf with the highest gain.

Regularization strategy: LightGBM implements effective regularization strategies, including L1 and L2 regularization, along with parameters for maximum tree depth, minimum leaf node weight and minimum split gain. These strategies control model complexity, prevent overfitting and enhance the classifier's generalization ability.

Ability to handle class imbalance: LightGBM includes built-in mechanisms for addressing class imbalance, such as automatic class weight adjustment using the class_weight parameter and adjusting the weights of positive and negative samples via the scale_pos_weight parameter. These mechanisms help the training process focus on improving the prediction performance of minority classes, resulting in better classification results.

The PRAUC is considered a more appropriate evaluation metric for imbalanced classification problems because it emphasizes the classifier's performance in predicting negative samples, such as deaths in sepsis mortality prediction. Compared to other metrics, such as AUC and F1 scores, PRAUC provides a more accurate and reliable assessment of the classifier's performance in imbalanced datasets. This is due to the following reasons:

Unaffected by the number of negative samples: PRAUC is not influenced by the number of negative samples, unlike the AUC of the receiver operating characteristic (ROC) curve, which considers both the true positive rate (recall) and false positive rate. The latter is heavily affected by the number of negative samples.

Focus on small probability events: PRAUC is more suited for cases where the main concern is correctly detecting positive samples, especially those with a small probability. Precision and recall rates provide a better reflection of model performance in these situations compared to other evaluation metrics.

Trade-off between precision and recall: PRAUC emphasizes both precision and recall, allowing for the identification of an optimal balance point to achieve the best trade-off between these 2 metrics.

In our study, we also explored the performance of updated models by incorporating additional features, fine-tuning hyperparameters and employing ensemble techniques. These updated models aim to further enhance prediction accuracy and generalization ability for sepsis mortality.

Additional features: By integrating relevant clinical data, such as laboratory test results, vital signs and comorbidities, our updated models can capture a more comprehensive view of the patient's condition, which may contribute to a better understanding of the underlying risk factors associated with sepsis mortality.

Hyperparameter tuning: We performed a systematic search for optimal hyperparameters using techniques such as grid search and random search. These methods help our updated models achieve better performance by optimizing their configurations.

Ensemble techniques: By combining predictions from multiple base models, we employed ensemble techniques such as bagging, boosting and stacking. These techniques aim to reduce overfitting, increase model stability and improve overall performance by leveraging the strengths of different base models.

Limitations

The updated models showed improved performance compared to the initial models, indicating that incorporating additional features, fine-tuning hyperparameters and using ensemble techniques can enhance the prediction accuracy of sepsis mortality. However, further research is needed to explore other potential factors influencing sepsis mortality predictions and to investigate novel machine learning algorithms and techniques for continuously improving model performance.

Conclusions

This study addressed the limitations and gaps in the existing literature on predicting sepsis-related mortality using machine learning models, focusing on their practical application in an ambulance setting. We demonstrated that the LightGBM-based model outperformed other classifiers and the qSOFA score. By implementing a dynamic updating model and fine-tuning hyperparameters, we further enhanced the model's performance, resulting in more accurate and reliable predictions for clinicians.

Our findings significantly contribute to the practical application of machine learning models in the medical field, particularly for predicting sepsis-related mortality

in an ambulance setting. The feature importance analysis provides valuable insights that help doctors prioritize patient assessment and interventions, ultimately improving patient outcomes. This research demonstrates the potential of real-time updating and hyperparameter tuning to further optimize the performance and clinical utility of sepsis-related mortality prediction models in real-world ambulance settings.

Supplementary data

The Supplementary materials are available at https://doi.org/10.5281/zenodo.14644757. The package includes the following files:

Supplementary Table 1. Training data for ASPII.
Supplementary Table 2. Training data for SOFA.
Supplementary Table 3. Testing data for sepsis.

Data availability

The datasets generated and/or analyzed during the current study are available from the corresponding author on reasonable request.

Consent for publication

Not applicable.

Use of AI and AI-assisted technologies

Not applicable.

ORCID iDs

Puyu Zhou https://orcid.org//0000-0002-2361-2101
Jiazheng Duan https://orcid.org/0009-0009-3805-3937
Jianqing Li https://orcid.org/0000-0002-6768-1483

References

1. Fleischmann C, Scherag A, Adhikari NKJ, et al. Assessment of global incidence and mortality of hospital-treated sepsis: Current estimates and limitations. *Am J Respir Crit Care Med*. 2016;193(3):259–272. doi:10.1164/rccm.201504-0781OC
2. Fleuren LM, Klausch TLT, Zwager CL, et al. Machine learning for the prediction of sepsis: A systematic review and meta-analysis of diagnostic test accuracy. *Intensive Care Med*. 2020;46(3):383–400. doi:10.1007/s00134-019-05872-y
3. Goh KH, Wang L, Yeow AYK, et al. Artificial intelligence in sepsis early prediction and diagnosis using unstructured data in healthcare. *Nat Commun*. 2021;12(1):711. doi:10.1038/s41467-021-20910-4
4. Valik JK, Ward L, Tanushi H, et al. Predicting sepsis onset using a machine learned causal probabilistic network algorithm based on electronic health records data. *Sci Rep*. 2023;13(1):11760. doi:10.1038/s41598-023-38858-4
5. Yong L, Zhenzhou L. Deep learning-based prediction of in-hospital mortality for sepsis. *Sci Rep*. 2024;14(1):372. doi:10.1038/s41598-023-49890-9
6. Brownlee J. A gentle introduction to the gradient boosting algorithm for machine learning. San Juan, Puerto Rico: Machine Learning Mastery; 2020. https://machinelearningmastery.com/gentle-introduction-gradient-boosting-algorithm-machine-learning. Accessed August 21, 2024.
7. Bonte C, Vercauteren F. Privacy-preserving logistic regression training. *BMC Med Genomics*. 2018;11(Suppl 4):86. doi:10.1186/s12920-018-0398-y
8. Wang L, ed. *Support Vector Machines: Theory and Applications*. Vol. 177. Studies in Fuzziness and Soft Computing. Berlin–Heidelberg, Germany: Springer Berlin Heidelberg; 2005. doi:10.1007/b95439
9. Rokem A, Kay K. Fractional ridge regression: A fast, interpretable reparameterization of ridge regression. *GigaScience*. 2020;9(12):giaa133. doi:10.1093/gigascience/giaa133
10. Lee JH, Shi Z, Gao Z. On LASSO for predictive regression. *J Econometrics*. 2022;229(2):322–349. doi:10.1016/j.jeconom.2021.02.002
11. Anand MV, KiranBala B, Srividhya SR, Kavitha C, Younus M, Rahman MH. Gaussian naïve Bayes algorithm: A reliable technique involved in the assortment of the segregation in cancer. *Mobile Information Systems*. 2022;2022:1–7. doi:10.1155/2022/2436946
12. Borgohain O, Dasgupta M, Kumar P, Talukdar G. Performance analysis of nearest neighbor, K-nearest neighbor and weighted K-nearest neighbor for the classification of Alzheimer disease. In: Borah S, Pradhan R, Dey N, Gupta P, eds. *Soft Computing Techniques and Applications*. Vol. 1248. Advances in Intelligent Systems and Computing. Singapore: Springer Singapore; 2021:295–304. doi:10.1007/978-981-15-7394-1_28
13. Negi A, Hajati F. Analysis of variants of KNN for disease risk prediction. In: Barolli L, Hussain F, Enokido T, eds. *Advanced Information Networking and Applications*. Vol. 451. Lecture Notes in Networks and Systems. Cham, Switzerland: Springer International Publishing; 2022:531–545. doi:10.1007/978-3-030-99619-2_50
14. Uddin S, Haque I, Lu H, Moni MA, Gide E. Comparative performance analysis of K-nearest neighbour (KNN) algorithm and its different variants for disease prediction. *Sci Rep*. 2022;12(1):6256. doi:10.1038/s41598-022-10358-x
15. Agarap AF. A neural network architecture combining gated recurrent unit (GRU) and support vector machine (SVM) for intrusion detection in network traffic data [preprint posted online September 10, 2017]. *arXiv*. doi:10.48550/ARXIV.1709.03082
16. Erichson NB, Lim SH, Mahoney MW. Gated recurrent neural networks with weighted time-delay feedback [preprint posted online December 1, 2022]. arXiv. doi:10.48550/arXiv.2212.00228. Accessed October 15, 2024.
17. Li Q, Kamaruddin N, Yuhaniz SS, Al-Jaifi HAA. Forecasting stock prices changes using long-short term memory neural network with symbolic genetic programming. *Sci Rep*. 2024;14(1):422. doi:10.1038/s41598-023-50783-0
18. Jiang X, Xu C. Deep learning and machine learning with grid search to predict later occurrence of breast cancer metastasis using clinical data. *J Clin Med*. 2022;11(19):5772. doi:10.3390/jcm11195772
19. Magalhães MMDC. Hyperparameter fine tuning for a time series forecasting model [doctoral thesis]. Carcavelos, Portugal: Nova School of Business and Economics. 2022.
20. Tomlinson G, Al-Khafaji A, Conrad SA, et al. Bayesian methods: A potential path forward for sepsis trials. *Crit Care*. 2023;27(1):432. doi:10.1186/s13054-023-04717-x
21. Zhao QY, Liu LP, Luo JC, et al. A machine-learning approach for dynamic prediction of sepsis-induced coagulopathy in critically ill patients with sepsis. *Front Med*. 2021;7:637434. doi:10.3389/fmed.2020.637434
22. Amrollahi F, Shashikumar SP, Razmi F, Nemati S. Contextual embeddings from clinical notes improves prediction of sepsis. *AMIA Annu Symp Proc*. 2020;2020:197–202. PMID:33936391. PMCID:PMC8075484.
23. Zhang Y, Xu W, Yang P, Zhang A. Machine learning for the prediction of sepsis-related death: A systematic review and meta-analysis. *BMC Med Inform Decis Mak*. 2023;23(1):283. doi:10.1186/s12911-023-02383-1
24. Delahanty RJ, Alvarez J, Flynn LM, Sherwin RL, Jones SS. Development and evaluation of a machine learning model for the early identification of patients at risk for sepsis. *Ann Emerg Med*. 2019;73(4):334–344. doi:10.1016/j.annemergmed.2018.11.036
25. Hammoud I, Ramakrishnan I, Henry M, Morley E. Multimodal early septic shock prediction model using LASSO regression with decaying response. In: *2020 IEEE International Conference on Healthcare Informatics (ICHI)*. Oldenburg, Germany: IEEE; 2020:1–3. doi:10.1109/ICHI48887.2020.9374377
26. Culliton P, Levinson M, Ehresman A, Wherry J, Steingrub JS, Gallant SI. Predicting severe sepsis using text from the electronic health record [preprint posted online November 30, 2017]. *arXiv*. doi:10.48550/ARXIV.1711.11536

27. Qin F, Madan V, Ratan U, et al. Improving early sepsis prediction with multimodal learning [preprint posted online July 23, 2021]. arXiv. doi:10.48550/arXiv.2107.11094. Accessed October 15, 2024.
28. Horng S, Sontag DA, Halpern Y, Jernite Y, Shapiro NI, Nathanson LA. Creating an automated trigger for sepsis clinical decision support at emergency department triage using machine learning. *PLoS One*. 2017;12(4):e0174708. doi:10.1371/journal.pone.0174708
29. Apostolova E, Velez T. Toward automated early sepsis alerting: Identifying infection patients from nursing notes [preprint posted online September 11, 2018] *arXiv*. doi:10.48550/arXiv.1809.03995
30. Liu R, Greenstein JL, Sarma SV, Winslow RL. Natural language processing of clinical notes for improved early prediction of septic shock in the ICU. In: *2019 41st Annual International Conference of the IEEE Engineering in Medicine and Biology Society (EMBC)*. Berlin, Germany: IEEE; 2019:6103–6108. doi:10.1109/EMBC.2019.8857819
31. Johnson AEW, Pollard TJ, Shen L, et al. MIMIC-III, a freely accessible critical care database. *Sci Data*. 2016;3(1):160035. doi:10.1038/sdata.2016.35
32. Báez AA, Hanudel P, Perez MT, Giraldez EM, Wilcox SR. Prehospital Sepsis Project (PSP): Knowledge and attitudes of United States advanced out-of-hospital care providers. *Prehosp Disaster Med*. 2013;28(2):104–106. doi:10.1017/S1049023X12001744
33. Studnek JR, Artho MR, Garner CL, Jones AE. The impact of emergency medical services on the ED care of severe sepsis. *Am J Emerg Med*. 2012;30(1):51–56. doi:10.1016/j.ajem.2010.09.015

The consequences of cardiac autonomic nervous system modulation during pulmonary vein isolation: A review

Piotr Brzozowski[1,2,A–F], Piotr Niewiński[1,2,A,D–F], Stanisław Tubek[1,2,A,E,F], Krzysztof Nowak[1,2,A,E,F], Piotr Ponikowski[1,2,E,F]

[1] Institute of Heart Diseases, Wroclaw Medical University, Poland
[2] Clinical Cardiology Ward, University Teaching Hospital, Wrocław, Poland

A – research concept and design; B – collection and/or assembly of data; C – data analysis and interpretation;
D – writing the article; E – critical revision of the article; F – final approval of the article

Advances in Clinical and Experimental Medicine, ISSN 1899–5276 (print), ISSN 2451–2680 (online) *Adv Clin Exp Med*. 2025;34(8):1403–1413

Address for correspondence
Piotr Brzozowski
E-mail: piotr.brzski@gmail.com

Funding sources
None declared

Conflict of interest
None declared

Received on May 29, 2024
Reviewed on June 29, 2024
Accepted on July 26, 2024

Published online on October 21, 2024

Abstract

Pulmonary vein isolation (PVI) is a well-established treatment modality for atrial fibrillation (AF). Apart from the desired effect regarding the arrhythmic substrate within the left atrium, PVI commonly leads to modulation of the intrinsic cardiac autonomic nervous system (ICANS). Using the available literature, this article presents the anatomy of ICANS and describes methods of assessing its function, mainly focusing on heart rate (HR) variability metrics. Then, we summarize the modern pathophysiological outlooks on the onset and recurrence of AF and explain how the arrhythmia and the activation of ICANS are intertwined. Further, the article discusses the extent, dynamics and persistence of ICANS modulation during PVI, accounting for various modalities and procedural strategies. Both the potential benefits and pitfalls of such modulation are explored, considering AF recurrence, HR and HR variability changes, as well as the unclear effect on ventricular arrhythmias and nerve remodeling. Finally, the article aims to outline further directions of research necessary to improve our understanding of ICANS and its modulation.

Key words: atrial fibrillation, catheter ablation, pulmonary veins, autonomic ganglia, autonomic denervation

Cite as
Brzozowski P, Niewiński P, Tubek S, Nowak K, Ponikowski P. The consequences of cardiac autonomic nervous system modulation during pulmonary vein isolation: A review. *Adv Clin Exp Med*. 2025;34(8):1403–1413. doi:10.17219/acem/191684

DOI
10.17219/acem/191684

Copyright
Copyright by Author(s)
This is an article distributed under the terms of the Creative Commons Attribution 3.0 Unported (CC BY 3.0) (https://creativecommons.org/licenses/by/3.0/)

Introduction

Atrial fibrillation (AF) is the most common arrhythmia in adult patients worldwide. Its estimated prevalence is 7.7% among individuals aged 55 and above, with an observed increase in prevalence with age. Projections indicate a potential rise in the number of cases in the near future.[1,2] Catheter ablation has been established as a reliable method of treatment and prevention of AF recurrence, and it holds a strong position in the European Society of Cardiology (ESC) guidelines.[3] Pulmonary vein isolation (PVI) is regarded as a standard in AF catheter ablation, given that the role of the pulmonary veins (PVs) in AF pathophysiology has been widely researched and agreed upon.[4] Both well-established techniques, radiofrequency ablation (RFA) and cryoballoon ablation (CBA), have similar safety profiles and provide a similar reduction in AF burden and freedom from AF recurrence.[5] A recently developed method, pulse field ablation (PFA), is showing comparable results as well.[6]

It has been postulated that the intrinsic cardiac autonomic nervous system (ICANS) plays a pivotal role in the triggering and recurrence of AF.[7] The ICANS is an intricate network of neurons and ganglionated plexi (GP) that regulates electrical and mechanical functioning of the heart. The GPs, which consist of parasympathetic neuronal bodies intertwined with sympathetic neuron axons, are located on the epicardial fat pads, with major GPs placed in close proximity to the PVs, atrioventricular node (AVN) and sinoatrial node (SAN). The intrinsic cardiac autonomic nervous system consists of both sympathetic and parasympathetic neurons, which in healthy patients assure that the heart rate (HR) and blood pressure are adequate to meet the demands of the organism. Several studies have shown that the PVI procedure, whether RFA or CBA, modulates ICANS noticeably, although the extent and permanence of this modulation remain disputed.[8–10] There is much disagreement regarding many aspects of targeted ICANS modification during PVI, including both efficacy and safety issues.[11] Considering that even the anatomical terminology is not uniform, we feel that a comprehensive review of the literature is needed to summarize what we already know and what directions are worth exploring.

Objectives

The aim of this article is to review the physiological, anatomical and procedural background of ICANS modulation during and after PVI, provide insight into its potential benefits and consequences, and indicate areas that need further exploration.

Anatomy of the atrial autonomic nervous system

The adult heart contains an average of 701 ganglia, and up to 84% of them are located on the surface of the atria, with most of them located on the posterior and superior surfaces.[12] While the terminology of ICANS anatomy remains inconsistent and varies between anatomists and electrophysiologists, we adapted the nomenclature of atrial GPs proposed by Aksu et al.,[13] which is based on older anatomical studies.[12,14,15] It postulates 5 major atrial GPs: superior right atrial (RSGP) – on the posterosuperior surface of the right atrium (RA) adjacent to the junction of the superior vena cava (SVC) and the RA; inferior right atrial (RIGP) – on the posterior surface of the RA adjacent to the interatrial groove; superior left atrial (LSGP) – on the posterosuperior surface of the left atrium (LA) between the PVs; posteromedial left atrial (PMLGP) – on the posteromedial surface of the LA; and posterolateral inferior left atrial (LIGP) – on the posterior lateral surface of the LA base on the atrial side of the atrioventricular groove (Fig. 1). Of these GPs, the most prominent (RIGP and PMLGP) and their extensions were shown to be merged to form the interatrial septal GP (ISGP), which contains the highest number of ganglia (average of 355) among ICANS.[14] Two vital structures of the heart's conductivity system are innervated by atrial GPs: RSGP extensions reach the SAN, while the AVN is innervated primarily by PMLGP.[12]

While historically it was thought that the intrinsic GPs consisted only of parasympathetic neurons synthesizing acetylcholine (ACh), histological studies proved that ICANS also contains neurons that have the potential to release noradrenaline (NA), although these were significantly more prominent in the ventricular ganglia.[16]

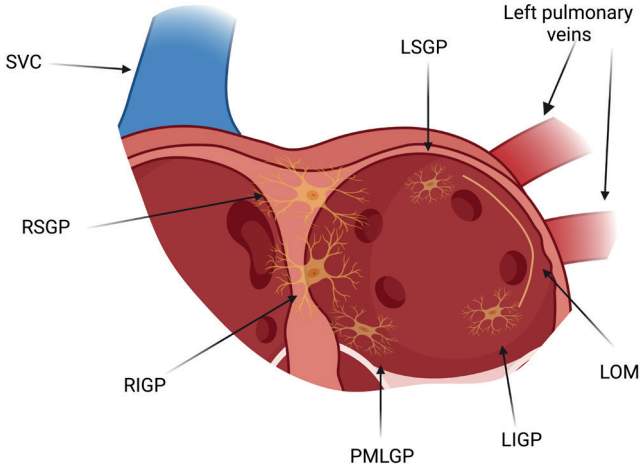


Fig. 1. A simplified overview of intrinsic cardiac autonomic nervous system (ICANS) anatomy in the human atria

SVC – superior vena cava; RSGP – superior right atrial ganglion plexus; RIGP – inferior right atrial ganglion plexus; PMLGP – posteromedial left atrial ganglion plexus; LIGP – inferior left atrial ganglion plexus; LOM – ligament of Marshall; LSGP – superior left atrial ganglion plexus.

In immunohistochemical studies of porcine and mouse hearts, a variety of other potent neurotransmitters, such as vasoactive intestinal peptide, neuropeptide Y, nitric oxide, synaptophysin, and calcitonin gene-related peptide, were found throughout ICANS.[17,18]

One crucial feature that differentiates sympathetic nerves from parasympathetic nerves is the location of their neural bodies. While the nuclei of parasympathetic neurons are located directly on the surface of the heart, the bodies of sympathetic neurons are located further away in the stellate and caudal cervical ganglia.[19] Thus, given the appropriate penetration of radiofrequency or cryoenergy originating from the intracardiac catheter, the effect toward the parasympathetic arm ought to be more permanent due to the ablation of neural bodies. On the contrary, sympathetic modulation would be transient because of isolated destruction of the long axons with spared sympathetic ganglia.

The autonomic innervation of the heart does not only involve the GPs. Parasympathetic neurons located on the surface of the heart operate under the control of the central nervous system. Said control is exerted through the longest cranial nerve in the human body, the vagus nerve, connecting the lower brainstem (mainly the nucleus ambiguus and the nucleus tractus solitarius) to the GPs of the heart.[20] The anatomical proximity of the vagus nerve and the internal jugular vein allows for transvenous stimulation, which is often utilized during cardioneuroablation (CNA) procedures. One cannot ignore the significance of the ligament of Marshall (LOM), which was described in 1850 as "a vestigial fold containing fibrous bands, small blood vessels and nervous filaments".[21] It is located above the left atrial appendage and lateral to the left superior PV and runs from the coronary sinus to insert itself into the LA free wall myocardium. The muscular fibers inside the LOM, called Marshall bundles, were shown to merge with the muscle tissue of both the coronary sinus and the LA and have been reported to be a potential source of arrhythmia.[22] Today, we also know that the structure contains abundant parasympathetic and sympathetic innervation, with parasympathetic ganglia located in the vicinity of the coronary sinus–LOM junction and sympathetic fibers concentrated in the part closer to the LA–LOM junction.[23]

Onset and recurrence of atrial fibrillation: A review of modern pathophysiological outlooks

The pathophysiology of AF is a very complex and still poorly understood matter. Modern hypotheses assume a conjunction of anatomical substrate,[24] focal triggers[25] and autonomic fluctuations[26] in inducing and sustaining AF. Studying each of these components and how they interact with each other is of vital importance in understanding the basis of this arrhythmia and how modern medicine can attempt to treat it.

Atrial fibrosis has been linked to the incidence and recurrence[27] of AF; however, there has been a disagreement on whether the extent of fibrosis is correlated to the type (paroxysmal/persistent) of AF.[27,28] At the same time, the presence of fibrous tissue facilitates arrhythmogenesis through providing a basis for re-entrant circuits that enable the induction of the arrhythmia.[29] Atrial fibrillation then propagates electrical and structural remodeling of the atria, which led to the emergence of the concept that "AF begets AF".[30]

Anatomical substrate alone would not initiate the arrhythmia on its own. It needs a trigger – a premature, most of the time ectopic beat – that will induce a re-entrant loop. These premature impulses can originate from any part of atria or even the aforementioned LOM,[22] but predominantly, up to 94% of the time, their source lies within the PVs.[31] This knowledge is the rationale behind PVI – isolating the source of the focal trigger from the LA prohibits the initiation of AF and prevents its recurrence.

The 3rd key factor in initiating and sustaining AF is autonomic regulation. Bettoni and Zimmermann[26] proved that there are significant variations in HR variability (HRV) parameters before the onset of paroxysmal AF, suggesting increased adrenergic modulation at least 20 min before initiation of the arrhythmia, with a subsequent shift toward parasympathetic dominance in the last minutes before the onset of AF. In a computational simulation study with models based on recordings of human atrial myocytes, Bayer et al.[32] showed that parasympathetic activation through heterogeneous ACh release promotes AF by creating unidirectional conduction blocks and re-entry loops, especially in fibrotic atria. Furthermore, in an experimental canine model, simultaneous adrenergic and cholinergic stimulation of the atria through NA and ACh infusions were shown to induce AF.[33] Similar results were obtained by Hou et al.,[34] who proposed that both ACh and NA excitatory effects on human atria were stronger when both transmitters acted simultaneously. Interestingly, adrenergic-mediated AF could not be induced if parasympathetic modulation was blocked by atropine. Conversely, cholinergic-mediated AF, while less likely to occur after propranolol infusion, still manifested despite total adrenergic blockade.[33] With that amount of evidence, it is clear that both the parasympathetic and sympathetic nervous systems play significant roles in the propagation of AF, which makes the topic of ICANS modulation even more important in regard to the long-term efficacy of PVI.

Assessment of cardiac autonomic nervous system function

Measurement of the regulatory functions of ICANS can be conducted both during and after the procedure. Intraoperatively, acute vagal responses (VRs), such as deep sinus bradycardia (<40 bpm), asystole or atrioventricular block, can be elicited using all contemporary PVI methods.[35–37] These responses are triggered by energy applications

at the locations of the GPs and are transient, although sometimes the use of atropine or temporary pacing is necessary. At the same time, after successful ablation, one can sometimes observe the elimination of VRs, which stems from vagal denervation.[38]

Further assessment of ICANS function is usually done through HR and HRV analyses of Holter recordings. Through the aforementioned vagal denervation, an increase in resting HR can be observed in many patients who underwent PVI.[9] While the measurement of average HR is a rather trivial task, analyses of HRV are more complex, as we can divide them into time domain analyses and frequency domain analyses.

Time domain analyses provide us with parameters that are derived from beat-to-beat changes in RR intervals. While relatively simple to calculate, they mostly reflect the parasympathetic influence on HRV. Examples of such parameters are as follows:

- SDNN – standard deviation of normal beat to normal beat (NN) interval;
- SDANN – standard deviation of average (taken from 5-min periods) NN intervals;
- RMSSD – root mean square of successive RR interval differences;
- pNN50% – percentage of successive RR intervals that differ by >50 ms.

Frequency domain analyses with the use of more complex calculations based on fast Fourier transform or autoregression modeling measure the power of HR fluctuations within 3 frequency bands:

- Very low frequency (VLF – spectrum between 0.01 and 0.04 Hz);
- Low frequency (LF – spectrum between 0.04 and 0.15 Hz) influenced by both sympathetic and parasympathetic activity;
- High frequency (HF – spectrum between 0.15 and 0.4 Hz) predominantly connected to respiratory arrhythmia and vagal activity.[39]

The ratio of power within the LF band to the HF band (LF/HF ratio) has been used as a measure of adrenergic tone toward the sinus node in many reports. However, its usefulness for the assessment of the sympathetic system is questionable.[40] It has to be noted that the aforementioned parameters are by no means the only ones used in HRV analyses. However, they are the most commonly used metrics in the reviewed literature.

The quantitative assessment of autonomic denervation might also be accomplished with atropine administration. When given in a sufficiently high dose (i.e., 0.04 mg/kg), atropine leads to complete vagal blockade.[41] The elimination of parasympathetic input by atropine leads to a situation in which HR is determined by only the 2 following factors: 1) sympathetic input and 2) intrinsic activity of the sinus node. Thus, given the unchanged intrinsic activity of the sinus node, the difference in HR on atropine before and after CNA reflects the change in sympathetic activity toward the sinus node. Hence, the atropine method gives us the opportunity for a more comprehensive insight into the consequences of CNA.

A method of intraprocedural assessment of parasympathetic denervation using a neurostimulator was developed by Pachon et al.[42] It involves electrical stimulation of the vagus nerve through a catheter positioned in the internal jugular vein, which results in an acute vagal response (mostly temporary asystole) in patients with unmodified ICANS. Conversely, after ablation of the GPs, vagal responses could not be induced through the identical mode of stimulation. A recent study suggested improved long-term efficacy of CNA procedures with the use of vagus nerve stimulation.[43] Another way to assess the extent of parasympathetic injury due to PVI is based on measuring the serum concentration of neuron-specific enolase, an enzyme released from damaged neurons, which was shown to significantly increase after PVI.[44]

Does pulmonary vein isolation modulate the autonomic system of the heart?

The effectiveness of PVI relies predominantly upon thorough isolation of the PVs from the LA myocardium. Ouyang et al.[45] showed that recovery of conduction in the PVs is found in approx. 80% of patients with AF recurrence. Successful isolation is achieved through applying a continuous line of transmural lesions. Due to the anatomical reasons outlined above, the proximity of ICANS and the PV ostia could lead to inadvertent damage of the autonomic neurons during PVI. Moreover, a strategy of purposeful atrial GP ablation as an addition to standard PVI has also been proposed.

Aksu et al.[46] conducted an interesting study in patients undergoing targeted CNA. By mapping the LA and presenting an electroanatomical map to a blinded observer, they showed that the designed lines for PVI, especially around the right PVs, exhibit a major overlap with the location of the atrial GPs. In fact, all of the patients in the study had some, although varied, degree of overlap, with approx. 80% of the cases showing overlap in 2 or 3 PVs, which gives us the reasoning for both the occurrence and variance of ICANS modulation throughout the population of patients undergoing PVI.

There is abundant evidence of autonomic modulation related to PVI. Modulation of ICANS can already be seen during the procedure. There are studies that describe coincidental acute VRs during RFA, CBA and PFA alike. These responses manifest as deep sinus bradycardia (<40 bpm), asystole or atrioventricular block.[47] The first experiments regarding HR changes after interventions within the PV ostia were performed in animal models as early as 1964.[48] One of the first reports regarding this topic in human study participants was made in 2004 when Pappone et al.[38] proved significant alterations in HR (72.4 ±8.4 bpm baseline vs 80.3 ±9.1 bpm after 1 week; $p < 0.001$) and HRV

(130.4 ±30.5 ms SDNN baseline vs 81.4 ±18.8 ms SDNN after 1 week) in patients undergoing radiofrequency PVI. Similarly, in 2006, Bauer et al.[49] showed significant changes in HR (65 ±7 bpm baseline vs 71 ±7 bpm after 12 months; p = 0.01) and HRV (SDNN 125 ±31 ms baseline vs 110 ±20 ms after 12 months; p = 0.01) after catheter radiofrequency PVI. That study also showed that autonomic modulation after RFA persists after 12 months. Interestingly, similar changes in HRV parameters were shown by Suwalski et al.[50] in patients after surgical PVI.

Periprocedural changes in HR after PVI are different from patient to patient; however, most of the reviewed literature shows a short-term increase in mean HR ranging from 4 to 12 bpm in PVI patients,[9,35,51–53] while targeted GP ablation can yield higher periprocedural increases, even up to 27 bpm.[54] At the same time, no significant changes in maximal HR during exertion have been described in PVI[38] and CNA[55] alike, and maximum metabolic equivalents on exercise treadmill testing remained stable.[56] Another marker of autonomic modulation – cardiac baroreflex sensitivity – was also significantly reduced in patients after PVI. This reduction, however, was only transient, as in the reviewed study, most metrics apart from Valsalva ratio returned to baseline after 6 months.[57]

Persistence and dynamics of ICANS modification after transcatheter ablation is still not an entirely clear matter. While analyzing the CIRCA-DOSE (Cryoballoon vs Irrigated Radiofrequency Catheter Ablation) study population, Tang et al. showed that HRV parameters change significantly not only right after PVI (both CBA and RFA), but also throughout the following 12 months.[9] In that study, patients were monitored using implantable loop recorders. Immediately after the procedure, a sizable drop in HRV (mean baseline SDANN 122.26 ±1.66 ms decreased by approx. 60 ms) was noted, with a partial reversal during the next 3 months (mean 100-day follow-up SDANN 103.0 ±1.7 ms), after which it remained stable throughout 12 months after the procedure (mean ΔSDANN of 2.2 ms, 3.7 ms, 4.7 ms for months 6, 9 and 12 vs month 3). An increase of approx. 5 bpm in daytime HR (from mean baseline DHR of 68.18 ±0.57 bpm) after the procedure was also recorded, with further augmentation in the 100-day follow-up (ΔDHR at 100 days post-PVI of 9.6 bpm; range: 7.4–11.8 bpm; p < 0.0001) and a slight downward, although statistically insignificant, trend in the following months. A similar trend of a peak and small gradual decline in HR can be observed in other studies regarding PVI; however, the decrease likewise failed to reach statistical significance.[58,59] In CNA, on the other hand, this trend seems to be exacerbated, with a higher peak and greater drop in HR in the months following the procedure, which suggests a greater degree of acute autonomic modulation.[60] The aforementioned HR and HRV changes spanning months after both PVI and CNA suggest at least some degree of reinnervation during the first months post-procedure. Pachon et al.[55] demonstrated that significant autonomic denervation lasted for at least 24 months (median HR 71.2 ±11 bpm at baseline vs 79.6 ±12 bpm 2 years after CNA; p < 0.0001; SDNN 134.3 ±32 ms at baseline vs. 88.3 ±30 ms 2 years after CNA; p < 0.0001) in patients undergoing targeted CNA. There were no significant differences in HR and HRV parameters comparing 12 to 24 months follow-up, which indicates that most reinnervation concludes in the first few months after the procedure, after which HRV parameters remain stagnant.

The differences in devices used could also potentially influence procedural outcomes regarding autonomic modulation. It is known that second-generation cryoballoons (CBs), compared to first-generation CBs improve procedural efficacy (procedural duration 128 ±27 min vs 98 ±30 min; p < 0.001; fluoroscopy exposure 19.5 ±7.4 min vs 13.4 ±5.3 min; p = 0.001)[61] and clinical outcomes (freedom from AF at 365 days follow-up 63.9% vs 83.6% of patients)[62] of PVI. It would also seem that second-generation CBs provide more definitive ICANS modulation. In the study conducted by Oswald et al.,[10] HRV metrics were back to baseline 3 months after PVI using first-generation CBs. In contrast, in more recent studies utilizing second-generation CBs, the effects of ICANS modulation were more permanent, lasting over 12 months,[9,53] which could be explained by the fact that second-generation CBs have a bigger ablation surface, providing a wider and more thorough line of lesions. Yorgun et al.[8] also hypothesized that the size of the CB might also influence the extent of ICANS modulation (Fig. 2).

However, not all PVI techniques carry the risk of autonomic nervous system neuronal damage. While CBA and RFA use thermal energy, a novel method with a different approach (PFA) has been developed recently and is rising in popularity. Using irreversible electroporation (IRE), PFA targets the myocardium while sparing the surrounding tissues, including nerves, which was confirmed both in preclinical[63] and clinical studies.[64] Considering the tissue specificity of PFA, it was not surprising that Musikantow et al.[37] proved that despite eliciting coincidental VRs in some patients, there was no significant change in resting HR after 3 months following PFA. In conclusion, PFA seems to have only minor and insignificant effects on ICANS.

Benefits of cardiac autonomic modulation during PVI

Having established that PVI utilizing CBA and RFA indeed has a significant impact on autonomic regulation of the heart, we have to assess whether such an impact is beneficial or detrimental in the scope of the cardiovascular system.

Importantly, Yorgun et al.[8] showed that patients developing intraprocedural VRs requiring atropine administration or temporary pacing during CBA had significantly less AF recurrence (16.20% vs 29.00%; p = 0.009), and such

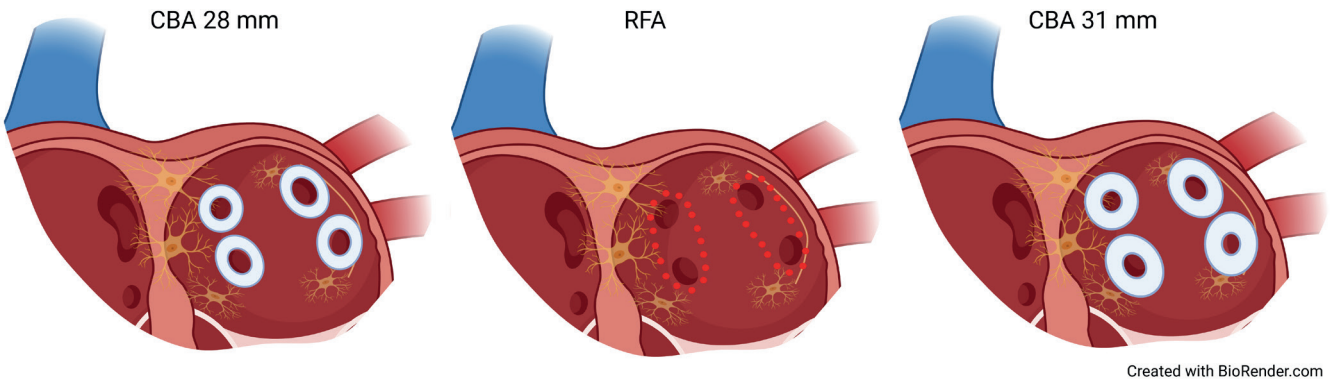


Fig. 2. Schematic view of potential differences in intrinsic cardiac autonomic nervous system (ICANS) modulation related to pulmonary vein isolation modality

RFA – radiofrequency ablation; CBA – cryoballoon ablation.

VRs were associated with decreased arrhythmia recurrence (hazard ratio (HR): 0.550, 95% confidence interval (95% CI): 0.331–0.915; p = 0.021). Moreover, Qin et al.[65] showed that identifying and eliminating those reactions by means of RFA can significantly reduce the recurrence of arrhythmia in comparison to the non-VR group (HR: 0.53, 95% CI: 0.22–0.89; log-rank = 15.3; p = 0.004).

In the CIRCA-DOSE[9] study, patients with no AF recurrence after PVI had a larger relative change in nighttime and daytime HR than those with recurrence (ΔDHR 11 ±11 bpm vs 8 ±12 bpm; p = 0.001; ΔNHR 8 ±9 bpm vs 6 ±8 bpm; p = 0.049). However, there was no difference in measured SDNN between the 2 groups. Conversely, the research conducted by Pappone et al.[38] showed that vagal denervation occurring at the time of PVI (expressed in transient changes in both HR and HRV parameters) was correlated with longer AF-free survival (adjusted HR: 0.101, 95% CI: 0.014–0.750; p = 0.025).

Interestingly, the strategy of anatomic atrial GP ablation in addition to classic PVI was found to yield better results in terms of arrhythmia recurrence than PVI or GP ablation alone in patients with paroxysmal AF.[66] At 2-year follow-up, patients in the PVI + targeted GP ablation group were significantly more often free from arrhythmia than those in the PVI or GP ablation groups (74% vs 56% vs 48%; p = 0.0036).[67] The aforementioned findings were confirmed in a meta-analysis performed by Yan et al.[68] that pooled together 5 studies comparing standalone catheter PVI vs PVI + GP ablation. A significant benefit of adjunct GP ablation was demonstrated in terms of freedom from AF (odds ratio (OR) [95% CI]: 1.79 [1.35, 2.37]; p < 0.001).

At the same time, while ICANS modulation may not be effective in the treatment of bradycardia–tachycardia syndrome (BTS), as the cause of BTS is often an organic dysfunction of the SAN, it can be beneficial in patients with both AF and vasovagal syncope. Targeted CNA is emerging as an alternative to traditional pacing, especially in young, otherwise healthy patients with vagally-mediated syncope,[69] and ICANS modulation employing PVI could have a similar therapeutic effect as proposed by Maj et al.[70]

Intrinsic cardiac autonomic nervous system modulation also exerts a significant effect on the physiological properties of the AVN. As reported by Wichterle et al.,[71] after targeted CNA, there was a significant increase in AVN conduction capabilities (shortening of AH interval by 15 ±31 ms, increase in Wenckebach point by 28 ±33 bpm). This, in conjunction with increased resting HR, could potentially open up the possibility of β-blocker and antiarrhythmic drug uptitration (if needed) in patients treated with PVI.[72] Moreover, Aksu et al. showed that CNA can also successfully treat an advanced atrioventricular block.[73] Such interventions, however, would only be effective in a case of functional block, rather than organic block, so careful identification of potential responders using preprocedural atropine challenge is mandatory.

Potential pitfalls of cardiac autonomic modulation during PVI

As discussed above, ICANS modulation during PVI commonly leads to a profound decrease in HRV. It was shown that decreased HRV following myocardial infarction was significantly correlated with mortality rates, as patients with SDNN <50 ms had a 5.3 times higher chance of death than those with SDNN >100 ms.[74] In fact, decreased HRV was the strongest Holter-derived predictor of mortality among patients in that study, even stronger than ventricular arrhythmias (VAs). The Framingham Heart Study analysis also showed that decreased HRV was significantly associated with all-cause mortality,[75] while the UK-Heart study described a correlation between SDNN < 100 ms and mortality due to progressive heart failure.[76]

While it is true that impaired HRV is correlated with increased mortality throughout multiple studies, we must keep in mind that correlation does not equal causation, and decreased HRV is most probably not the cause of death but merely a marker of potentially lethal coexisting conditions. Thus, HRV-increasing agents, such as scopolamine, failed to provide protection against fatal VAs, even though they significantly improved HRV metrics.[77] It is highly unlikely

that the iatrogenic HRV decrease caused by PVI increases the risk of death by itself, as there was no significant difference in mortality in studies comparing PVI to optimal medical therapy.[78]

Respiratory sinus arrhythmia (RSA), a phenomenon primarily mediated by cardiac vagal tone and predominantly responsible for HRV in high frequency domains, is an old evolutionary mechanism present not only in humans but also throughout the animal kingdom.[79] Through ICANS modulation, RSA was observed to be severely diminished in patients undergoing PVI.[80] Although seemingly unimportant, physiological RSA was shown to improve pulmonary gas exchange efficiency through a reduction in intrapulmonary shunting and pulmonary dead space to tidal volume ratio compared to abolished RSA.[81] Additionally, in a sheep model of heart failure, a special pacing protocol emulating RSA led to an improvement in cardiac output (1.4 ±0.5 L/min; $p < 0.001$) compared to both traditional pacing and non-paced groups.[82] Attenuation of RSA after PVI may then have a similar detrimental effect in humans, although studies investigating this matter have not yet been conducted.

The effect of ICANS modulation on VAs is still a matter of debate. In canines after myocardial infarction,[83] it was shown that ablation of atrial GPs and LOM caused increased inducibility of VAs, as programmed stimulation (S1S2S3) induced VAs in 30% of study participants in the control group compared to 90% in the post-ablation group ($p = 0.02$). Induced arrhythmias were also significantly faster in the GP ablation group (363 ±6 bpm vs 274 ±8 bpm; $p < 0.001$). Susceptibility to VAs was probably related to greater prolongation of the QTc interval at 8 weeks after the procedure compared to the control group (342 ±14 ms vs 356 ±12 ms; $p < 0.05$), larger dispersion of the effective refractory period (32 ±13 ms vs 24 ±10 ms; $p < 0.05$), and increased density of the immunohistochemical marker of adrenergic neurons (tyrosine hydroxylase) (582 ±301 $\mu m^2/mm^2$ vs 231 ±187 $\mu m^2/mm^2$; $p = 0.006$) and nerve growth factor (672 ±387 $\mu m^2/mm^2$ vs 266 ±20^2 $\mu m^2/mm^2$; $p = 0.009$). This suggests that there was promotion of ventricular sympathetic nerve remodeling. In a porcine model,[84] CNA was associated with QTc prolongation after sympathetic stimulation (11.23% ±4.0% vs 1.49% ±4.0%; $p < 0.001$), earlier occurrence (61.44 ±73.7 s vs 245.11 ±104.0 s; $p = 0.002$) and incidence of VA after left coronary artery ligation. In human studies, however, there is no conclusive evidence of arrhythmia propagation after ICANS modulation. There is a study that reported temporary QTc prolongation after the CNA procedure (QTcHodges 434 ±24 ms vs 409 ±23 ms 1 day after procedure; $p < 0.00001$).[85] However, this was not confirmed in other observations following CNA.[55,86] A similar discord can be found in studies on PVI and QTc. Chikata et al.[87] noticed a QTc prolongation after PVI (QTcHodges 400.7 ±22.8 ms vs 410.6 ±40.2 ms 1 day after procedure; $p < 0.05$), whereas Hermans et al.[88] did not produce such findings in their study. At the same time, Styczkiewicz et al.[57] observed decreased baroreflex sensitivity in patients after PVI, and research conducted by Garcia et al.[89] suggests an association between reduced cardiac baroreflex sensitivity and VAs.

One of the common side effects of ICANS modulation is inappropriate sinus tachycardia (IST). Van Deutekom et al.[90] showed that IST was not uncommon (4.1%) in patients undergoing PVI. In patients undergoing targeted CNA, however, this phenomenon was much more frequent, ranging from 7% to even 27% of patients,[91] which is an important factor to consider when deciding on a procedural strategy. The only identified risk factors for developing IST following CNA are higher baseline and post-atropine HR.[92] The issue of IST could be especially important in patients in which an increase in HR is known to be detrimental, as in, e.g., heart failure (as shown in the SHIFT trial[93]) or coronary artery disease (CAD).[94]

Further directions

Considering how important autonomic regulation is in the context of cardiovascular diseases and how complex its mechanisms are, further research on the topic of autonomic modulation is critical for a deeper understanding of this subject and the development of new treatments.

First, to gain certainty in the degree and effectiveness of ICANS modulation, appropriate and validated measurement techniques should be agreed upon. For example, throughout the reviewed literature, many different HRV metrics were used, which are often incomparable to each other and provide different information about the state of ICANS. Also, there is no consensus regarding which of the following modalities ought to be used to establish vagal modulation of the heart and serve as the periprocedural end-point: HR, HRV, intraprocedural VRs, or extracardiac vagal stimulation.[55]

Second, no trials have compared the influence of various sizes of CBs on the autonomic parameters after PVI, given that a greater ablation surface could equal a greater degree of autonomic modulation. The advent of adjustable 28–31 mm CBs[95] could be a logical starting point for further exploration in this area.

Third, a lack of long-term follow-up of autonomic function metrics after PVI should also be addressed by proper research initiatives to adequately assess the far-reaching implications of the intervention, especially now that operators in some cases can choose the degree of impact on ICANS (PFA vs CBA/RFA vs PVI + CNA). Larger studies, or perhaps thorough meta-analyses of certain issues (QT interval, AVN conduction, VA susceptibility, exercise tolerance, left ventricular contractility, autonomic remodeling, and reinnervation), would be beneficial for understanding the potential consequences of long-standing ICANS modulation.

Another point of consideration is: How should operators decide on the extent of ICANS modulation, taking into

account the availability of different modalities? What criteria should be taken into account to differentiate patients who will benefit from additional autonomic modulation from those who should be treated with myocardium-specific methods? At this point, we can only hypothesize that patients with sinus bradycardia, vasovagal syncope and functional atrioventricular block will benefit from adjunct CNA, while perhaps patients with heart failure or at risk of VAs could gain more by sparing the parasympathetic nerves.

Limitations

This review was limited by the available research. Drawing conclusions from studies with different methodologies, metrics of autonomic modulation or even anatomical nomenclature makes comparing their results challenging. A large share of the cited studies also had relatively small sample sizes, and some concepts were studied only in animal models. Only studies that were published in English were analyzed.

Conclusions

In summary, PVI, as a staple of AF treatment, is a well-studied method with regard to its safety and efficacy. However, the extent of its impact on ICANS remains disputed. While the benefits of ICANS modulation during PVI have been widely reported, the potential disadvantages of vagal denervation also require careful attention (Fig. 3).

We believe that all PVI modalities and adjunct CNA strategies have their place in the clinical setting. Ideally, however, the optimal method should be chosen through an individualized approach to maximize the benefits and avoid the potential pitfalls of autonomic modulation.

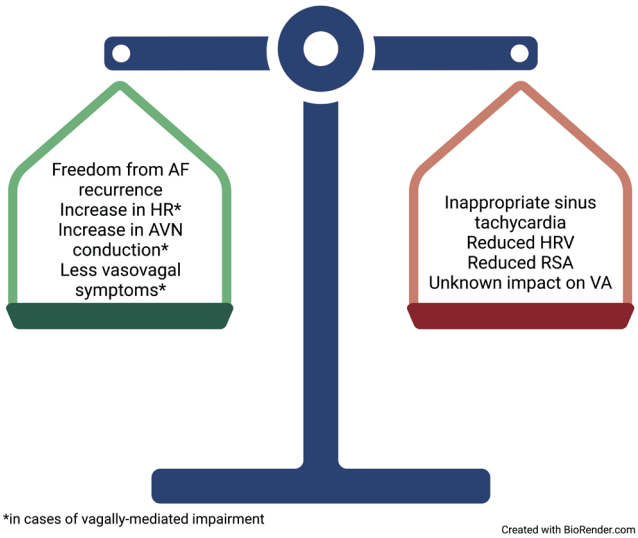


Fig. 3. Advantages and potential disadvantages of pulmonary vein isolation-related intrinsic cardiac autonomic nervous system (ICANS) modulation

Further research on larger groups with long-term follow-up might allow for the identification of the appropriate ablation modality tailored to the clinical and autonomic profile and needs of each patient.

ORCID iDs

Piotr Brzozowski https://orcid.org/0000-0003-0206-8124
Piotr Niewiński https://orcid.org/0000-0001-8148-071X
Stanisław Tubek https://orcid.org/0000-0002-0059-5150
Krzysztof Nowak https://orcid.org/0000-0001-9078-0087
Piotr Ponikowski https://orcid.org/0000-0002-3391-7064

References

1. Benjamin EJ, Muntner P, Alonso A, et al. Heart disease and stroke statistics: 2019 update. A report from the American Heart Association. *Circulation*. 2019;139(10):e56–e528. doi:10.1161/CIR.0000000000000659
2. Krijthe BP, Kunst A, Benjamin EJ, et al. Projections on the number of individuals with atrial fibrillation in the European Union, from 2000 to 2060. *Eur Heart J*. 2013;34(35):2746–2751. doi:10.1093/eurheartj/eht280
3. Hindricks G, Potpara T, Dagres N, et al. 2020 ESC Guidelines for the diagnosis and management of atrial fibrillation developed in collaboration with the European Association for Cardio-Thoracic Surgery (EACTS). *Eur Heart J*. 2021;42(5):373–498. doi:10.1093/eurheartj/ehaa612
4. Mahida S, Sacher F, Derval N, et al. Science linking pulmonary veins and atrial fibrillation. *Arrhythm Electrophysiol Rev*. 2015;4(1):40. doi:10.15420/aer.2015.4.1.40
5. Sørensen SK, Johannessen A, Worck R, Hansen ML, Hansen J. Radiofrequency versus cryoballoon catheter ablation for paroxysmal atrial fibrillation: Durability of pulmonary vein isolation and effect on atrial fibrillation burden. The RACE-AF randomized controlled trial. *Circ Arrhythm Electrophysiol*. 2021;14(5):e009573. doi:10.1161/CIRCEP.120.009573
6. Schipper J, Dittrich S, Erlhoefer S, et al. Comparison of pulsed field ablation and cryoballoon ablation in atrial fibrillation. *Europace*. 2023;25(Suppl 1):euad122.085. doi:10.1093/europace/euad122.085
7. Lim PB, Malcolme-Lawes LC, Stuber T, et al. Intrinsic cardiac autonomic stimulation induces pulmonary vein ectopy and triggers atrial fibrillation in humans. *J Cardiovasc Electrophysiol*. 2011;22(6):638–646. doi:10.1111/j.1540-8167.2010.01992.x
8. Yorgun H, Aytemir K, Canpolat U, Ahiner L, Kaya EB, Oto A. Additional benefit of cryoballoon-based atrial fibrillation ablation beyond pulmonary vein isolation: Modification of ganglionated plexi. *Europace*. 2014;16(5):645–651. doi:10.1093/europace/eut240
9. Tang LYW, Hawkins NM, Ho K, et al. Autonomic alterations after pulmonary vein isolation in the CIRCA-DOSE (Cryoballoon vs Irrigated Radiofrequency Catheter Ablation) study. *J Am Heart Assoc*. 2021;10(5):e018610. doi:10.1161/JAHA.120.018610
10. Oswald H, Klein G, Koenig T, Luesebrink U, Duncker D, Gardiwal A. Cryoballoon pulmonary vein isolation temporarily modulates the intrinsic cardiac autonomic nervous system. *J Interv Card Electrophysiol*. 2010;29(1):57–62. doi:10.1007/s10840-010-9491-7
11. Brignole M, Aksu T, Calò L, et al. Clinical controversy: Methodology and indications of cardioneuroablation for reflex syncope. *Europace*. 2023;25(5):euad033. doi:10.1093/europace/euad033
12. Pauza DH, Skripka V, Pauziene N, Stropus R. Morphology, distribution, and variability of the epicardiac neural ganglionated subplexuses in the human heart. *Anat Rec (Hoboken)*. 2000;259(4):353–382. doi:10.1002/1097-0185(20000801)259:4<353::AID-AR10>3.0.CO;2-R
13. Aksu T, Skeete JR, Huang HH. Ganglionic plexus ablation: A step-by-step guide for electrophysiologists and review of modalities for neuromodulation for the management of atrial fibrillation. *Arrhythm Electrophysiol Rev*. 2023;12:e02. doi:10.15420/aer.2022.37
14. Armour JA, Murphy DA, Yuan BX, MacDonald S, Hopkins DA. Gross and microscopic anatomy of the human intrinsic cardiac nervous system. *Anat Rec (Hoboken)*. 1997;247(2):289–298. doi:10.1002/(SICI)1097-0185(199702)247:2<289::AID-AR15>3.0.CO;2-L
15. Armour JA. Potential clinical relevance of the 'little brain' on the mammalian heart. *Exp Physiol*. 2008;93(2):165–176. doi:10.1113/expphysiol.2007.041178

16. Kawano H, Okada R, Yano K. Histological study on the distribution of autonomic nerves in the human heart. *Heart Vessels*. 2003;18(1):32–39. doi:10.1007/s003800300005
17. Wake E, Brack K. Characterization of the intrinsic cardiac nervous system. *Autonom Neurosci*. 2016;199:3–16. doi:10.1016/j.autneu.2016.08.006
18. Hanna P, Dacey MJ, Brennan J, et al. Innervation and neuronal control of the mammalian sinoatrial node: A comprehensive atlas. *Circ Res*. 2021;128(9):1279–1296. doi:10.1161/CIRCRESAHA.120.318458
19. Coote JH, Chauhan RA. The sympathetic innervation of the heart: Important new insights. *Autonom Neurosci*. 2016;199:17–23. doi:10.1016/j.autneu.2016.08.014
20. Hoffman HH, Kuntz A. Vagus nerve components. *Anat Rec (Hoboken)*. 1957;127(3):551–567. doi:10.1002/ar.1091270306
21. Marshall J. VI. On the development of the great anterior veins in man and mammalia, including an account of certain remnants of fætal structure found in the adult: A comparative view of these great veins the different mammalia, and an analysis of their occasional peculiarities in the human subject. *Phil Trans R Soc*. 1850;140:133–170. doi:10.1098/rstl.1850.0007
22. Hwang C, Wu TJ, Doshi RN, Peter CT, Chen PS. Vein of Marshall cannulation for the analysis of electrical activity in patients with focal atrial fibrillation. *Circulation*. 2000;101(13):1503–1505. doi:10.1161/01.CIR.101.13.1503
23. Makino M, Inoue S, Matsuyama T, et al. Diverse myocardial extension and autonomic innervation on ligament of Marshall in humans. *Cardiovasc Electrophysiol*. 2006;17(6):594–599. doi:10.1111/j.1540-8167.2006.00375.x
24. Kottkamp H. Human atrial fibrillation substrate: Towards a specific fibrotic atrial cardiomyopathy. *Eur Heart J*. 2013;34(35):2731–2738. doi:10.1093/eurheartj/eht194
25. Calkins H, Kuck KH, Cappato R, et al. 2012 HRS/EHRA/ECAS Expert Consensus Statement on Catheter and Surgical Ablation of Atrial Fibrillation: Recommendations for Patient Selection, Procedural Techniques, Patient Management and Follow-up, Definitions, Endpoints, and Research Trial Design. A report of the Heart Rhythm Society (HRS) Task Force on Catheter and Surgical Ablation of Atrial Fibrillation. Developed in partnership with the European Heart Rhythm Association (EHRA), a registered branch of the European Society of Cardiology (ESC) and the European Cardiac Arrhythmia Society (ECAS); and in collaboration with the American College of Cardiology (ACC), American Heart Association (AHA), the Asia Pacific Heart Rhythm Society (APHRS), and the Society of Thoracic Surgeons (STS). Endorsed by the governing bodies of the American College of Cardiology Foundation, the American Heart Association, the European Cardiac Arrhythmia Society, the European Heart Rhythm Association, the Society of Thoracic Surgeons, the Asia Pacific Heart Rhythm Society, and the Heart Rhythm Society. *Europace*. 2012;14(4):528–606. doi:10.1093/europace/eus027
26. Bettoni M, Zimmermann M. Autonomic tone variations before the onset of paroxysmal atrial fibrillation. *Circulation*. 2002;105(23):2753–2759. doi:10.1161/01.CIR.0000018443.44005.D8
27. Marrouche NF, Wilber D, Hindricks G, et al. Association of atrial tissue fibrosis identified by delayed enhancement MRI and atrial fibrillation catheter ablation: The DECAAF Study. *JAMA*. 2014;311(5):498. doi:10.1001/jama.2014.3
28. Kuppahally SS, Akoum N, Burgon NS, et al. Left atrial strain and strain rate in patients with paroxysmal and persistent atrial fibrillation: Relationship to left atrial structural remodeling detected by delayed-enhancement MRI. *Circ Cardiovasc Imaging*. 2010;3(3):231–239. doi:10.1161/CIRCIMAGING.109.865683
29. Hansen BJ, Zhao J, Csepe TA, et al. Atrial fibrillation driven by micro-anatomic intramural re-entry revealed by simultaneous sub-epicardial and sub-endocardial optical mapping in explanted human hearts. *Eur Heart J*. 2015;36(35):2390–2401. doi:10.1093/eurheartj/ehv233
30. Wijffels MCEF, Kirchhof CJHJ, Dorland R, Allessie MA. Atrial fibrillation begets atrial fibrillation: A study in awake chronically instrumented goats. *Circulation*. 1995;92(7):1954–1968. doi:10.1161/01.CIR.92.7.1954
31. Haïssaguerre M, Jaïs P, Shah DC, et al. Spontaneous initiation of atrial fibrillation by ectopic beats originating in the pulmonary veins. *N Engl J Med*. 1998;339(10):659–666. doi:10.1056/NEJM199809033391003
32. Bayer JD, Boukens BJ, Krul SPJ, et al. Acetylcholine delays atrial activation to facilitate atrial fibrillation. *Front Physiol*. 2019;10:1105. doi:10.3389/fphys.2019.01105
33. Sharifov OF, Fedorov VV, Beloshapko GG, Glukhov AV, Yushmanova AV, Rosenshtraukh LV. Roles of adrenergic and cholinergic stimulation in spontaneous atrial fibrillation in dogs. *J Am Coll Cardiol*. 2004;43(3):483–490. doi:10.1016/j.jacc.2003.09.030
34. Hou ZY, Lin CI, Vassalle M, Chiang BN, Cheng KK. Role of acetylcholine in induction of repetitive activity in human atrial fibers. *Am J Physiol Heart Circ Physiol*. 1989;256(1):H74–H84. doi:10.1152/ajpheart.1989.256.1.H74
35. Vesela J, Osmancik P, Herman D, Prochazkova R. Changes in heart rate variability in patients with atrial fibrillation after pulmonary vein isolation and ganglionated plexus ablation. *Physiol Res*. 2019;68(1):49–57. doi:10.33549/physiolres.933710
36. Aytemir K, Gurses KM, Yalcin MU, et al. Safety and efficacy outcomes in patients undergoing pulmonary vein isolation with second-generation cryoballoon. *Europace*. 2015;17(3):379–387. doi:10.1093/europace/euu273
37. Musikantow DR, Neuzil P, Petru J, et al. Pulsed field ablation to treat atrial fibrillation. *JACC Clin Electrophysiol*. 2023;9(4):481–493. doi:10.1016/j.jacep.2022.10.028
38. Pappone C, Santinelli V, Manguso F, et al. Pulmonary vein denervation enhances long-term benefit after circumferential ablation for paroxysmal atrial fibrillation. *Circulation*. 2004;109(3):327–334. doi:10.1161/01.CIR.0000112641.16340.C7
39. Shaffer F, Ginsberg JP. An overview of heart rate variability metrics and norms. *Front Public Health*. 2017;5:258. doi:10.3389/fpubh.2017.00258
40. Billman GE. The LF/HF ratio does not accurately measure cardiac sympatho-vagal balance. *Front Physiol*. 2013;4:26. doi:10.3389/fphys.2013.00026
41. Jose AD, Taylor RR. Autonomic blockade by propranolol and atropine to study intrinsic myocardial function in man. *J Clin Invest*. 1969;48(11):2019–2031. doi:10.1172/JCI106167
42. Pachon JCM, Pachon EIM, Santillana P. TG, et al. Simplified method for vagal effect evaluation in cardiac ablation and electrophysiological procedures. *JACC Clin Electrophysiol*. 2015;1(5):451–460. doi:10.1016/j.jacep.2015.06.008
43. Pachon JCM, Pachon-M EI, Pachon CTC, et al. Long-term outcomes of cardioneuroablation with and without extra-cardiac vagal stimulation confirmation in severe cardioinhibitory neurocardiogenic syncope. *Cardiovasc Electrophysiol*. 2024;35(4):641–650. doi:10.1111/jce.16188
44. Acibuca A, Vurgun VK, Gerede DM, et al. Serum neuron-specific enolase, a marker of neuronal injury, increases after catheter ablation of atrial fibrillation. *J Int Med Res*. 2018;46(11):4518–4526. doi:10.1177/0300060518767768
45. Ouyang F, Antz M, Ernst S, et al. Recovered pulmonary vein conduction as a dominant factor for recurrent atrial tachyarrhythmias after complete circular isolation of the pulmonary veins: Lessons from double LASSO technique. *Circulation*. 2005;111(2):127–135. doi:10.1161/01.CIR.0000151289.73085.36
46. Aksu T, Yalin K, Bozyel S, Gopinathannair R, Gupta D. The anatomical basis behind the neuromodulation effects associated with pulmonary vein isolation. *Cardiovasc Electrophysiol*. 2021;32(6):1733–1736. doi:10.1111/jce.15038
47. Mori H, Kato R, Ikeda Y, et al. Analysis of the heart rate variability during cryoballoon ablation of atrial fibrillation. *Europace*. 2018;20(8):1259–1267. doi:10.1093/europace/eux225
48. Ledsome JR, Linden RJ. A reflex increase in heart rate from distension of the pulmonary-vein-atrial junctions. *J Physiol*. 1964;170(3):456–473. doi:10.1113/jphysiol.1964.sp007343
49. Bauer A, Deisenhofer I, Schneider R, et al. Effects of circumferential or segmental pulmonary vein ablation for paroxysmal atrial fibrillation on cardiac autonomic function. *Heart Rhythm*. 2006;3(12):1428–1435. doi:10.1016/j.hrthm.2006.08.025
50. Suwalski G, Suwalski P, Kalisnik JM, et al. How does successful off-pump pulmonary vein isolation for paroxysmal atrial fibrillation influence heart rate variability and autonomic activity? *Innovations (Phila)*. 2008;3(1):1–6. doi:10.1097/imi.0b013e31816755c3
51. Fang P, Wang J, Wei Y, Wang X, Yang H, Zhang M. Vagal response during circumferential pulmonary vein isolation decreases the recurrence of atrial fibrillation in the short-term in patients with paroxysmal atrial fibrillation: A prospective, observational study. *J Electrocardiol*. 2021;69:145–150. doi:10.1016/j.jelectrocard.2021.10.007

52. Kim MY, Coyle C, Tomlinson DR, et al. Ectopy-triggering ganglionated plexuses ablation to prevent atrial fibrillation: GANGLIA-AF study. *Heart Rhythm*. 2022;19(4):516–524. doi:10.1016/j.hrthm.2021.12.010
53. Goff ZD, Laczay B, Yenokyan G, et al. Heart rate increase after pulmonary vein isolation predicts freedom from atrial fibrillation at 1 year. *Cardiovasc Electrophysiol*. 2019;30(12):2818–2822. doi:10.1111/jce.14257
54. Piotrowski R, Baran J, Sikorska A, Krynski T, Kulakowski P. Cardioneuroablation for reflex syncope. *JACC Clin Electrophysiol*. 2023;9(1):85–95. doi:10.1016/j.jacep.2022.08.011
55. Pachon JCM, Pachon EIM, Pachon CTC, et al. Long-term evaluation of the vagal denervation by cardioneuroablation using Holter and heart rate variability. *Circ Arrhythm Electrophysiol*. 2020;13(12):e008703. doi:10.1161/CIRCEP.120.008703
56. Mandsager KT, Phelan DM, Diab M, et al. Outcomes of pulmonary vein isolation in athletes. *JACC Clin Electrophysiol*. 2020;6(10):1265–1274. doi:10.1016/j.jacep.2020.05.009
57. Styczkiewicz K, Spadacini G, Tritto M, et al. Cardiac autonomic regulation in patients undergoing pulmonary vein isolation for atrial fibrillation. *J Cardiovasc Med*. 2019;20(5):297–305. doi:10.2459/JCM.0000000000000791
58. Marinković M, Mujović N, Vučićević V, Steffel J, Potpara TS. A square root pattern of changes in heart rate variability during the first year after circumferential pulmonary vein isolation for paroxysmal atrial fibrillation and their relation with long-term arrhythmia recurrence. *Kardiol Pol*. 2020;78(3):209–218. doi:10.33963/KP.15187
59. Wagner L, Darche FF, Thomas D, et al. Cryoballoon pulmonary vein isolation-mediated rise of sinus rate in patients with paroxysmal atrial fibrillation. *Clin Res Cardiol*. 2021;110(1):124–135. doi:10.1007/s00392-020-01659-0
60. Debruyne P, Rossenbacker T, Janssens L, et al. Durable physiological changes and decreased syncope burden 12 months after unifocal right-sided ablation under computed tomographic guidance in patients with neurally mediated syncope or functional sinus node dysfunction. *Circ Arrhythm Electrophysiol*. 2021;14(6):e009747. doi:10.1161/CIRCEP.120.009747
61. Fürnkranz A, Bordignon S, Schmidt B, et al. Improved procedural efficacy of pulmonary vein isolation using the novel second-generation cryoballoon. *Cardiovasc Electrophysiol*. 2013;24(5):492–497. doi:10.1111/jce.12082
62. Fürnkranz A, Bordignon S, Dugo D, et al. Improved 1-year clinical success rate of pulmonary vein isolation with the second-generation cryoballoon in patients with paroxysmal atrial fibrillation. *Cardiovasc Electrophysiol*. 2014;25(8):840–844. doi:10.1111/jce.12417
63. Koruth J, Kuroki K, Iwasawa J, et al. Preclinical evaluation of pulsed field ablation: Electrophysiological and histological assessment of thoracic vein isolation. *Circ Arrhythm Electrophysiol*. 2019;12(12):e007781. doi:10.1161/CIRCEP.119.007781
64. Reddy VY, Dukkipati SR, Neuzil P, et al. Pulsed field ablation of paroxysmal atrial fibrillation. *JACC Clin Electrophysiol*. 2021;7(5):614–627. doi:10.1016/j.jacep.2021.02.014
65. Qin M, Liu X, Jiang WF, Wu SH, Zhang XD, Po S. Vagal response during pulmonary vein isolation: Re-recognized its characteristics and implications in lone paroxysmal atrial fibrillation. *Int J Cardiol*. 2016;211:7–13. doi:10.1016/j.ijcard.2016.02.116
66. Katritsis DG, Pokushalov E, Romanov A, et al. Autonomic denervation added to pulmonary vein isolation for paroxysmal atrial fibrillation. *J Am Coll Cardiol*. 2013;62(24):2318–2325. doi:10.1016/j.jacc.2013.06.053
67. Katritsis DG, Giazitzoglou E, Zografos T, Pokushalov E, Po SS, Camm AJ. Rapid pulmonary vein isolation combined with autonomic ganglia modification: A randomized study. *Heart Rhythm*. 2011;8(5):672–678. doi:10.1016/j.hrthm.2010.12.047
68. Yan F, Zhao S, Wu W, Xie Z, Guo Q. Different effects of additional ganglion plexus ablation on catheter and surgical ablation for atrial fibrillation: A systemic review and meta-analysis. *Cardiovasc Electrophysiol*. 2019;30(12):3039–3049. doi:10.1111/jce.14258
69. Pachon JCM, Pachon EIM, Cunha Pachon MZ, Lobo TJ, Pachon M JC, Santillana PTG. Catheter ablation of severe neurally meditated reflex (neurocardiogenic or vasovagal) syncope: Cardioneuroablation long-term results. *Europace*. 2011;13(9):1231–1242. doi:10.1093/europace/eur163
70. Maj R, Osório TG, Borio G, et al. A novel strategy to treat vaso-vagal syncope: Cardiac neuromodulation by cryoballoon pulmonary vein isolation. *Indian Pac Electrophysiol J*. 2020;20(4):154–159. doi:10.1016/j.ipej.2020.03.008
71. Wichterle D, Stiavnicky P, Jansova H, et al. Anatomically-guided cardioneuroablation for recurrent neurally mediated syncope. *Europace*. 2022;24(Suppl 1):euac053.324. doi:10.1093/europace/euac053.324
72. Zarębski Ł, Futyma P, Sethia Y, Futyma M, Kułakowski P. Improvement in atrioventricular conduction using cardioneuroablation performed immediately after pulmonary vein isolation. *Healthcare (Basel)*. 2024;12(7):728. doi:10.3390/healthcare12070728
73. Aksu T, Gopinathannair R, Bozyel S, Yalin K, Gupta D. Cardioneuroablation for treatment of atrioventricular block. *Circ Arrhythm Electrophysiol*. 2021;14(9):e010018. doi:10.1161/CIRCEP.121.010018
74. Kleiger RE, Miller JP, Bigger JT, Moss AJ. Decreased heart rate variability and its association with increased mortality after acute myocardial infarction. *Am J Cardiol*. 1987;59(4):256–262. doi:10.1016/0002-9149(87)90795-8
75. Tsuji H, Venditti FJ, Manders ES, et al. Reduced heart rate variability and mortality risk in an elderly cohort: The Framingham Heart Study. *Circulation*. 1994;90(2):878–883. doi:10.1161/01.CIR.90.2.878
76. Nolan J, Batin PD, Andrews R, et al. Prospective study of heart rate variability and mortality in chronic heart failure: Results of the United Kingdom Heart Failure Evaluation and Assessment of Risk Trial (UK-Heart). *Circulation*. 1998;98(15):1510–1516. doi:10.1161/01.CIR.98.15.1510
77. Hull SS, Vanoli E, Adamson PB, De Ferrari GM, Foreman RD, Schwartz PJ. Do increases in markers of vagal activity imply protection from sudden death? The case of scopolamine. *Circulation*. 1995;91(10):2516–2519. doi:10.1161/01.CIR.91.10.2516
78. Packer DL, Mark DB, Robb RA, et al. Effect of catheter ablation vs antiarrhythmic drug therapy on mortality, stroke, bleeding, and cardiac arrest among patients with atrial fibrillation: The CABANA randomized clinical trial. *JAMA*. 2019;321(13):1261. doi:10.1001/jama.2019.0693
79. Elstad M, O'Callaghan EL, Smith AJ, Ben-Tal A, Ramchandra R. Cardiorespiratory interactions in humans and animals: Rhythms for life. *Am J Physiol Heart Circ Physiol*. 2018;315(1):H6–H17. doi:10.1152/ajpheart.00701.2017
80. Jungen C, Alken FA, Eickholt C, et al. Respiratory sinus arrhythmia is reduced after pulmonary vein isolation in patients with paroxysmal atrial fibrillation. *Arch Med Sci*. 2020;16(5):1022–1030. doi:10.5114/aoms.2019.83883
81. Hayano J, Yasuma F, Okada A, Mukai S, Fujinami T. Respiratory sinus arrhythmia: A phenomenon improving pulmonary gas exchange and circulatory efficiency. *Circulation*. 1996;94(4):842–847. doi:10.1161/01.CIR.94.4.842
82. Shanks J, Abukar Y, Lever NA, et al. Reverse re-modelling chronic heart failure by reinstating heart rate variability. *Basic Res Cardiol*. 2022;117(1):4. doi:10.1007/s00395-022-00911-0
83. Wu B, Xu S, Dai R, Hong M, Wu H, Lin R. Epicardial ganglionated plexi ablation increases the inducibility of ventricular tachyarrhythmias in a canine postmyocardial infarction model. *Cardiovasc Electrophysiol*. 2019;30(5):741–746. doi:10.1111/jce.13912
84. Chung WH, Masuyama K, Challita R, et al. Ischemia-induced ventricular proarrhythmia and cardiovascular autonomic dysreflexia after cardioneuroablation. *Heart Rhythm*. 2023;20(11):1534–1545. doi:10.1016/j.hrthm.2023.08.001
85. Wichterle D, Jansova H, Stiavnicky P, et al. Temporary prolongation of corrected QT interval after cardioneuroablation for functional bradyarrhythmias. *Eur Heart J*. 2021;42(Suppl 1):ehab724.0619. doi:10.1093/eurheartj/ehab724.0619
86. Aksu T, Guler TE, Bozyel S, et al. Medium-term results of cardioneuroablation for clinical bradyarrhythmias and vasovagal syncope: Effects on QT interval and heart rate. *J Interv Card Electrophysiol*. 2021;60(1):57–68. doi:10.1007/s10840-020-00704-2
87. Chikata A, Kato T, Usuda K, et al. Prolongation of QT interval after pulmonary vein isolation for paroxysmal atrial fibrillation. *Cardiovasc Electrophysiol*. 2020;31(9):2371–2379. doi:10.1111/jce.14625
88. Hermans BJM, Zink MD, Van Rosmalen F, et al. Pulmonary vein isolation in a real-world population does not influence QTc interval. *Europace*. 2021;23(Suppl 1):i48–i54. doi:10.1093/europace/euaa390

89. Garcia R, Degand B, Fraty M, et al. Baroreflex sensitivity assessed with the sequence method is associated with ventricular arrhythmias in patients implanted with a defibrillator for the primary prevention of sudden cardiac death. *Arch Cardiovasc Dis*. 2019;112(4):270–277. doi:10.1016/j.acvd.2018.11.009
90. Van Deutekom C, Mulder BA, Groenveld HF, et al. Heart rate increase and inappropriate sinus tachycardia after cryoballoon pulmonary vein isolation for atrial fibrillation. *Neth Heart J*. 2022;30(5):282–288. doi:10.1007/s12471-021-01645-9
91. Kulakowski P, Baran J, Sikorska A, et al. Cardioneuroablation for reflex asystolic syncope: Mid-term safety, efficacy, and patient's acceptance. *Heart Rhythm*. 2024;21(3):282–291. doi:10.1016/j.hrthm.2023.11.022
92. Stiavnicky P, Haskova J, Peichl P, et al. Prediction of sinus tachycardia after cardioneuroablation: The utility of atropine test. *Eur Heart J*. 2023;44(Suppl 2):ehad655.605. doi:10.1093/eurheartj/ehad655.605
93. Swedberg K, Komajda M, Böhm M, et al. Ivabradine and outcomes in chronic heart failure (SHIFT): A randomised placebo-controlled study. *Lancet*. 2010;376(9744):875–885. doi:10.1016/S0140-6736(10)61198-1
94. Ma R, Gao J, Mao S, Wang Z. Association between heart rate and cardiovascular death in patients with coronary heart disease: A NHANES-based cohort study. *Clin Cardiol*. 2022;45(5):574–582. doi:10.1002/clc.23818
95. Schiavone M, Fassini G, Moltrasio M, et al. Early clinical outcomes and advantages of a novel-size adjustable second-generation cryoballoon: A proof-of-concept study. *J Clin Med*. 2024;13(5):1259. doi:10.3390/jcm13051259